# Hemipiperazines - Novel Photochromic Cyclic Dipeptides for Bioactivity Photomodulation

Zur Erlangung des akademischen Grades eines

DOKTORS DER NATURWISSENSCHAFTEN

(Dr. rer. nat.)

von der KIT-Fakultät für Chemie und Biowissenschaften

des Karlsruher Instituts für Technologie (KIT)

vorgelegte

DISSERTATION

von

Susanne Kirchner

aus

Tübingen

Hiermit erkläre ich, die vorliegende Arbeit selbstständig angefertigt und keine anderen als die angegebenen Quellen und Hilfsmittel benutzt, sowie die wörtlich oder inhaltlich übernommenen Stellen als solche kenntlich gemacht und die Satzung der Universität Karlsruhe zur Sicherung guter wissenschaftlicher Praxis beachtet zu haben. Die Dissertation wurde bisher an keiner anderen Hochschule oder Universität eingereicht.

Susanne Kirchner

Teile dieser Dissertation wurden bereits veröffentlicht unter:

- S. Kirchner, A.-L. Leistner, P. Gödtel, A. Seliwjorstow, S. Weber, J. Karcher, M. Nieger, Z. L. Pianowski, *submitted*. *Hemipiperazines – novel molecular photoswitches with low-nanomolar cytotoxicity*.
- S. Kirchner, Z. Pianowski, *Int. J. Mol. Sci.* **2022**, *23(10), 5657. Photopharmacology of Antimitotic Agents*.

*"Man merkt nie, was schon getan wurde, man sieht immer nur, was noch zu tun bleibt."*

*"Człowiek nigdy nie ogląda się na to, co zrobione, ale na to patrzy, co ma przed sobą do zrobienia."*

*"One never notices what has been done; one can only see what remains to be done."*

Marie Salomea Skłodowska–Curie (physicist and chemist)

Meinen Eltern.

# Table of contents

# Kurzzusammenfassung

Nach Angaben der Internationalen Agentur für Krebsforschung, einer Einrichtung der Weltgesundheitsorganisation, wurden im Jahr 2020 schätzungsweise 19,3 Millionen Menschen Krebs diagnostiziert, von denen 9,96 Millionen den Kampf gegen diese Krankheit verlieren werden. Krebstherapien werden häufig durch schwere Nebenwirkungen beeinträchtigt, die die anwendbare Dosis einschränken und die Lebensqualität der Patienten stark einschränken können. Die Entwicklung neuer, effizienter Therapeutika, die selektiv wirken und weniger Nebenwirkungen haben, ist daher von großer Bedeutung. Die Photopharmakologie stellt ein vielversprechendes Forschungsgebiet dar, um diesen Anforderungen gerecht zu werden, indem neue Medikamente entwickelt werden, die lokal und bioorthogonal mit Licht aktiviert werden können.

In dieser Arbeit stelle ich die Identifizierung und Charakterisierung von 3-Aryliden-2,5-diketopiperazinen (Hemipiperazine, HPIs) als eine neue Klasse von molekularen Photoschaltern vor. Ein HPI ist in Plinabulin enthalten, einem zytotoxischen Wirkstoff, der auf Mikrotubuli abzielt und sich derzeit in einer Phase-III-Studie zur Krebsbehandlung befindet. Es wurde entdeckt, dass die Bioaktivität von Plinabulin mit sichtbarem Licht moduliert werden kann, was eine biorthogonale Aktivierung dieses Medikaments mit räumlicher und zeitlicher Präzision ermöglichen kann. Außerdem wurden Derivate mit verbesserten photophysikalischen und pharmakologischen Eigenschaften identifiziert.

Das photochrome Kernfragment von Plinabulin enthält ein zyklisches Dipeptid (2,5-Diketopiperazin, DKP), welches selbst ein wichtiges Pharmakophor darstellt und auch in zahlreichen biokompatiblen intelligenten Materialien zu finden ist. Der Photochromismus von HPIs und der Einfluss von elektronenziehenden und -schiebenden Gruppen auf die photophysikalischen Eigenschaften wurde systematisch untersucht.

Darüber hinaus wurde gezeigt, dass HPI-Photoschalter in andere molekulare Gerüste eingebaut werden können und eine reversible Photomodulation der Fluoreszenzintensität ermöglichen. Es wurde festgestellt, dass fluoreszierende Derivate von Zellen aufgenommen und mittels konfokaler Mikroskopie innerhalb dieser Zellen sichtbar gemacht werden können. Diese Ergebnisse könnten die Grundlage für die Entwicklung neuartiger photoschaltbarer Fluoreszenzmarker bilden.

# Abstract

According to the International Agency for Research of Cancer, an institution of the World Health Organization, in 2020 an estimate of 19.3 million humans were diagnosed with cancer, of which 9.96 million will lose the fight against this disease. Cancer therapy is often impaired by severe side effects that limit the applicable dose and can enormously diminish the patients' quality of life. The development of new, efficient therapeutics that act selectively and have fewer side effects is therefore of pronounced relevance. Photopharmacology represents a promising area of research for addressing these needs, by developing new drugs that can be activated locally and bioorthogonally with light.

In this thesis, I present the identification and characterization of 3-arylidene-2,5-diketopiperazines (Hemipiperazines, HPIs) as a novel class of molecular photoswitches. An HPI is found in plinabulin, a microtubule targeting cytotoxic agent currently in the $3^{rd}$ phase of clinical trials for cancer treatment. It was discovered that the bioactivity of plinabulin can be modulated with visible light, which can enable biorthogonal activation of this drug with spatial and temporal precision. Furthermore, derivatives with improved photophysical and pharmacological properties have been identified.

The core photochromic fragment of plinabulin contains a cyclic dipeptide core (2,5-diketopiperazine, DKP), which itself is an important pharmacophore and also found in numerous biocompatible smart materials. The photochromism of HPIs and influence of electron-withdrawing and -donating groups on the photophysical properties was investigated systematically.

It was additionally demonstrated that HPI photoswitches can be incorporated into other molecular scaffolds and enable reversible photomodulation of fluorescence intensity. Fluorescent derivatives were found to be taken up by cells and were visualized within these cells *via* confocal microscopy. These results might form the basis for the development of novel photoswitchable fluorescent labels.

# 1  Introduction

## 1.1  Photopharmacology

To enable the study or even the control of biochemical processes, it is of great interest to develop tools and protocols that allow precise manipulation of bioactivity in a biorthogonal and non-invasive manner. Given the complexity of biological systems, it is not possible to selectively target individual processes or species by altering parameters like temperature or pH without significantly affecting or even harming the surrounding species in cells or tissue. Photopharmacology, however, can overcome these barriers and allow external control of bioactivity with light.[1] Light as a trigger of drug activity does not lead to contamination, is not influenced by diffusion, can be applied reversibly, and can be varied by using different wavelengths. Additionally, it offers the unique advantage that it can be tuned in three dimensions: its location, timing and its intensity.[2] These properties even enable studies on systems that are not accessible to alternative methods like for example genetic manipulation.[3-7]

To enable light-mediated regulation of pharmacokinetic and pharmacodynamic properties, light-triggered molecular scaffolds are being introduced into biologically active compounds. Three approaches to light-dependent pharmacology have been investigated: photodynamic therapy (PDT), photouncaging and photopharmacology (Figure 1). Photosensitizers developed for PDT generate highly cytotoxic reactive oxygen species upon irradiation.[8] The disadvantage of this method is the lack of specificity in the activity due to general toxicity. This is not the case with photouncaging, where photolabile protecting groups are introduced, yielding biologically inactive compounds. These prodrugs are then activated through light-induced cleavage of a covalent bond.[9] A drawback of this method is its irreversibility, which allows for diffusion of bioactive compounds into non-targeted tissues and can also lead to excretion of bioactive substances, causing the emergence of resistances.[10] Additional disadvantages include the formation of potentially harmful byproducts as well as uncontrolled enzymatic hydrolysis of the photolabile bond. Another concept of photopharmacology is based on the implementation of molecular photoswitches by covalent attachment to or direct incorporation into a pharmacophore. The photoswitchable motif allows for reversible changes in shape and/or polarity, which can enable the design of a pharmaceutical with significantly different biological activities in the light-dependent structural states. Ideally, one photoisomer does not interfere with the drug's functionality, whereas switching to the corresponding isomer allows deactivation of the compound to reduce systemic side effects while maintaining specificity.[10]

Especially in the past decade, interdisciplinary research including the fields of chemistry, medicine, pharmacy, and molecular biology facilitated the rapid evolution of photopharmacology towards clinical applications.[1] The efficacy at the cellular level has already been reported for possible applications including the treatment of pain[11-14], microbial infections[15,16], diabetes[17-21], and cancer [6,7,22-30]. In some cases, the applicability has been demonstrated in live animals.[31]
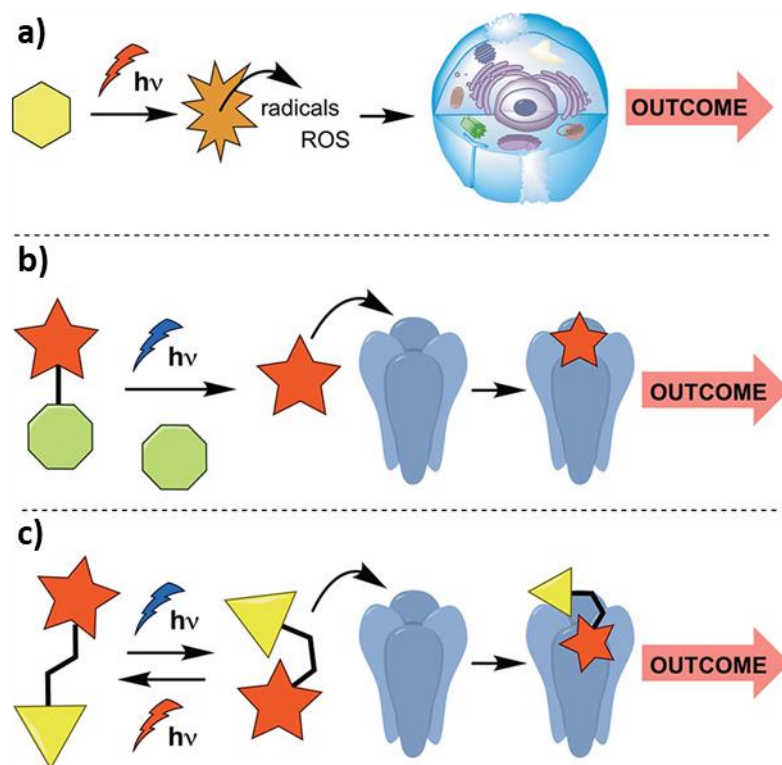


**Figure 1:** Principles of different approaches for light-dependent pharmacology: a) photodynamic therapy (ROS = reactive oxygen species), b) photouncaging, c) photopharmacology. Reprinted with permission from [32]. Copyright 2020 American Chemical Society.

However, further developments are necessary to address all the limitations of the currently known examples. One problem is the commonly observed decrease in overall bioactivity due to a significant change in the pharmacokinetic and pharmacodynamic properties upon introduction of the molecular photoswitch.[2,10] Additional properties like the polarity, solubility and metabolic stability may be altered and have to be evaluated and optimized for both photoisomers.[10]

To address these issues, the optimal position of the photoswitchable motif within the drug has to be identified in structure-activity relationship studies. As there are various molecular photoswitches with different photophysical properties available, it is also vital to choose one with characteristics that suit the intended application best.

## 1.2  Molecular Photoswitches

### 1.2.1  Characteristics of Molecular Photoswitches in the Context of Photopharmacology

Molecular photoswitches are molecules which can reversibly interconvert between two or more photoisomers upon irradiation with light. The photoisomers differ in their geometry and photophysical properties and, in some cases, also in their polarity.[33] In most cases, the photoconversion proceeds as *E*/*Z*-isomerization, which usually causes distinct structural modifications,[34] or as pericyclic reaction, which often leads to significant changes in electronic properties and/or polarity.[35] A distinction is made between T- and P-type photoswitches based on the relaxation process following photoexcitation, which can occur thermally (T) or photochemically (P). Additional classification concerns the observed change in color triggered by irradiation. Positive photochromism describes an increased intensity of color and negative photochromism the reversible color fading upon light irradiation.[36]

When aiming at photomodulation of bioactivity, it is crucial to develop a system that responds to light irradiation with high efficiency. Hence, a distinct difference in potency between the irradiated and non-irradiated forms is fundamental. And for efficient photoactivation, irradiation must result in accumulation of the bioactive species. To achieve this, it has to be ensured that the thermal stability of the more active species is on a timescale that allows to elicit the biological effect. Additionally, a sufficient photoswitching quantum yield is required to harness the limited amount of light reaching the targeted tissue effectively.[32,37]

Introducing a molecular photoswitch does not only influence the potency of a drug, but also its pharmacodynamic properties. Azobenzenes belong to the best studied molecular photoswitches and widely applied in photopharmacology. However, a serious drawback of azobenzene-based photoswitches is the metabolic instability of several derivatives. Especially electron-rich azobenzenes were found to be degraded by glutathione-catalyzed reduction of the N=N double bond in the cellular environment. This increases the required concentrations and – more importantly – yields mutagenic and cancerogenic arylhydrazines.[38]

When developing molecular photoswitches for pharmacological applications or medicinal research, one has to consider the wavelengths required for photoisomerization. Although highly energetic UV-light (365 nm) is very often applied, it is not well suited in a biological context due to its potential phototoxicity and inefficient penetration of soft tissues due to absorption by biomolecules and optical scattering in cells or tissues.[39,40] Since shortwave visible light normally only penetrates a few millimeters into tissue, an excitation in the range of 650 – 900 nm - the so-

called 'therapeutic window' - with the highest penetration depth of soft human tissues is aspired in photopharmacology.[1,2]

## 1.2.2    Visible Light-triggered Photoswitches

The scientific community working on organic photoswitches successfully developed a variety of different photoswitchable compounds reversibly photoisomerizable with visible light.

The aforementioned azobenzenes reversibly undergo *E*-to-*Z*-isomerization at the N=N double bond. Because UV-light is required for an efficient isomerization of unsubstituted azobenzenes, several structural modifications have been investigated to tune their photophysical properties. Numerous derivatives that allow for selective *E*-to-*Z*- and *Z*-to-*E*-photoisomerization within the visible range of the electromagnetic spectrum with high or, in some cases, even complete photoconversion have been identified. Selected examples are presented in Figure 2.[41-45]
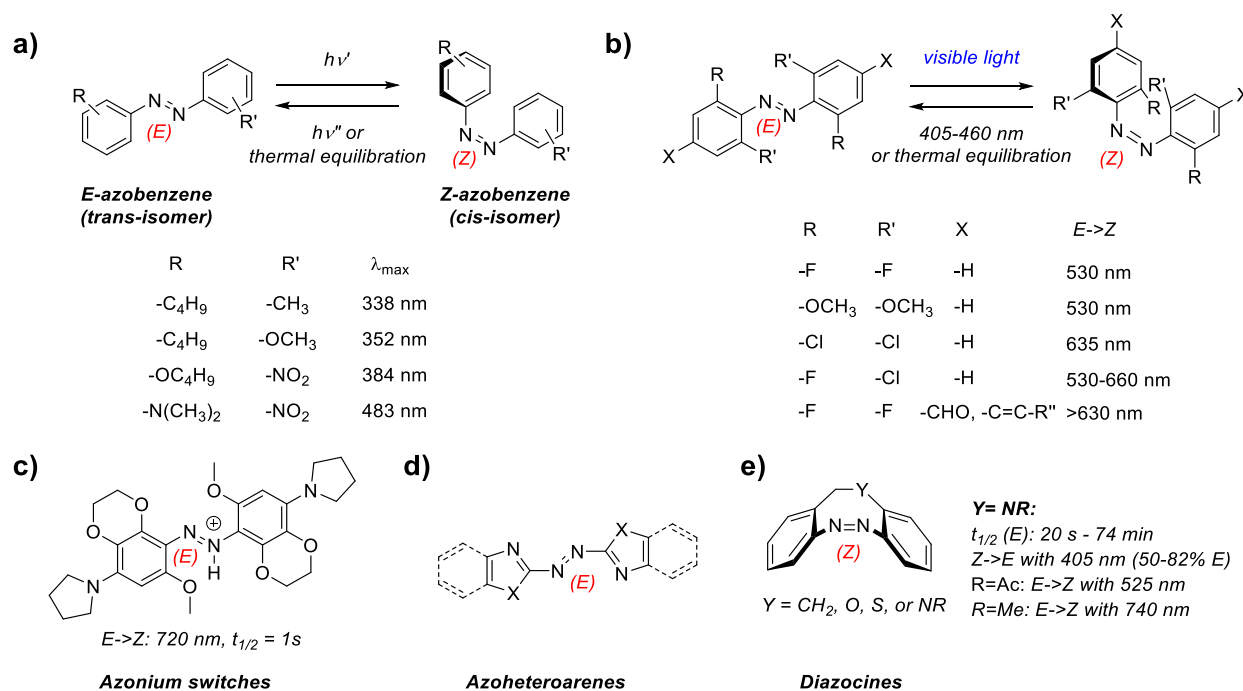


**Figure 2:** Structural modifications of azobenzenes that enable reversible photoisomerization with visible light. a) Push-pull azobenzenes and the corresponding absorption maxima ($\lambda_{max}$) determined in chloroform[46,47], b) *ortho*-substituted azobenzenes and the wavelengths required for *E*-to-*Z* switching[42-44,48,49], c) azonium switches[50], d) azoheteroarenes[51], e) diazocines[52,53]. In c)-e) the thermodynamically stable forms are depicted. Reproduced from reference [45].

Various examples of visible light-responsive photoswitches undergoing *E*/*Z*-photoisomerization are derived from the dye indigo (Figure 3). Intramolecular hydrogen bonding stabilizes the *E*-isomer of indigo and prevents photoisomerization.[54,55] Consequently, indigoid photoswitches were designed by introducing alkyl or aryl substituents that prevent hydrogen bond formation on the nitrogen atoms of indigo.[56] Other classes of indigoid photoswitches are obtained by combining

stilbene with indigo (hemiindigo)[55,57] or thioindigo (hemithioindigo)[58-61]. Optimization of the photophysical properties is feasible by installing electron-donating substituents (Figure 3b). [45,60]
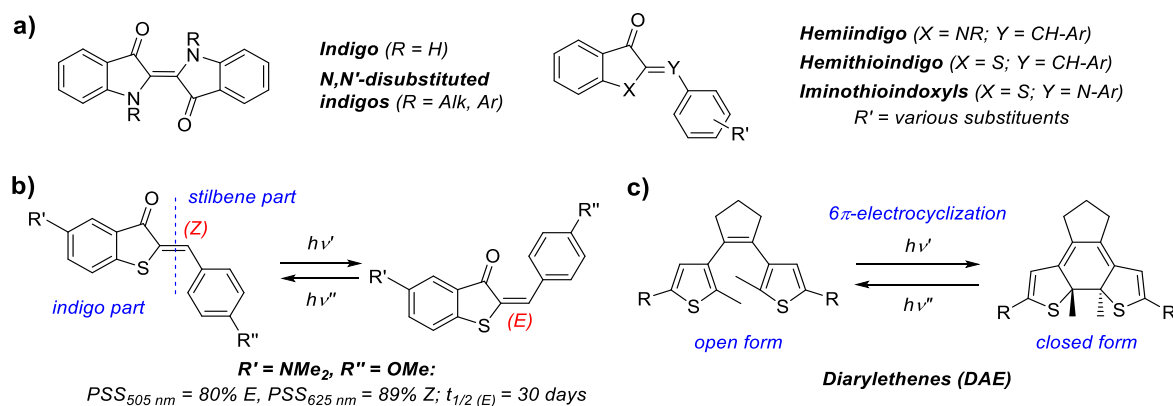


**Figure 3:** Indigoid and diarylethene photoswitches. a) Structural modifications of indigo yielding photochromic indigoids, b) By installing electron-donating substituents at both *para*-positions, visible-light responsive hemithioindigos with an increased lifetime of the respective *E*-isomer were obtained.[61] Reproduced from reference [45].

Diarylethenes are an established example for bistable molecular photoswitches undergoing reversible electrocyclization, which leads to considerable differences in the polarity of the respective photoisomers. Since photoisomerization of unsubstituted diarylethene requires UV-light, a variety of approaches, including extension of the conjugated $\pi$-system, have been investigated to shift the absorption spectrum bathochromically.[62-66]

Besides these more common examples, several other scaffolds, including spiropyrans[67], dihydropyrenes[68], norbornadienes[69-71] and donor-acceptor Stenhouse adducts[72-74], have been found to undergo visible light induced photoismerization.

## 1.3   Photoswitchable Antimitotic Agents

One of the most pursued applications for photopharmacology is cancer therapy, which is often impaired by severe side effects that limit the applicable dose and can enormously diminish the patients' quality of life.[75] This is frequently observed with pharmaceuticals that target microtubule dynamics, including clinically approved drugs such as vinca alkaloids, taxanes, and epothilone, which belong to the most important drug classes for cancer treatment.[76,77]

### 1.3.1   Microtubules: Structure and Dynamics

Microtubules are a major component of the eukaryotic cytoskeleton and involved in essential biological processes including intracellular transport, motility, and cell proliferation. These noncovalent polymers are composed of $\alpha/\beta$-tubulin heterodimers that first arrange head-to-tail to form long strands called protofilaments (Figure 4). Typically, 13 protofilaments assemble into

tube-like structures with a diameter of ~25 nm by lateral association.[78-81] The cellular microtubule network undergoes constant remodeling, required to fulfill the spatiotemporally-distinct functions of microtubules and is described as 'dynamic instability'.[82] The equilibrium between phases of dissociation ('catastrophe') and polymerization ('rescue') is guanosine triphosphate (GTP)-dependent and regulated by microtubule-associated proteins (MAPs).[77,83-85]
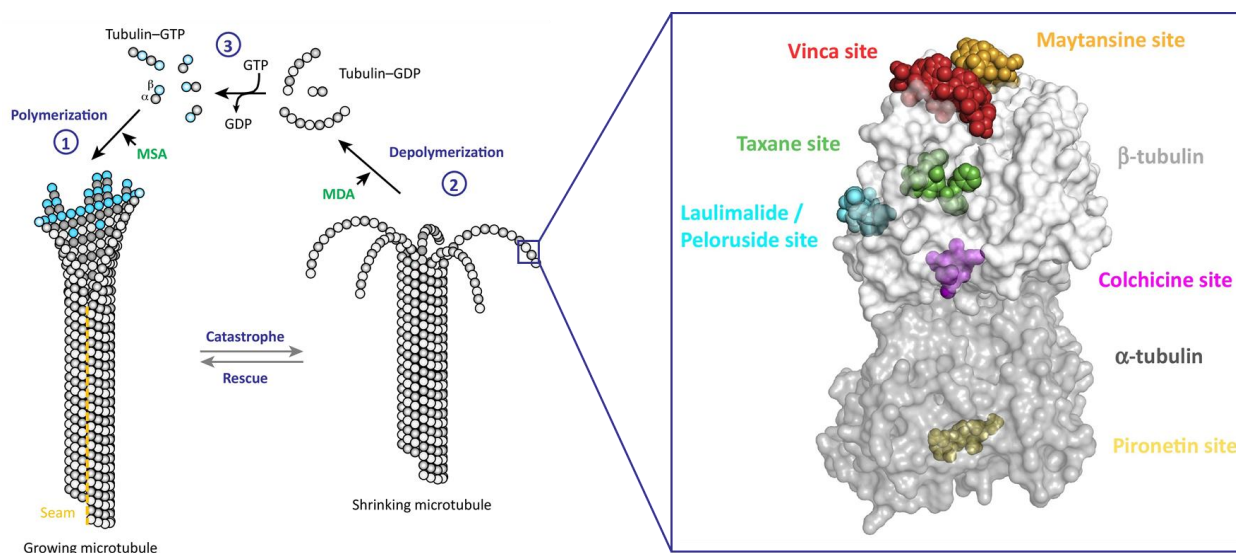


**Figure 4:** 'Dynamic instability' describes the GTP-dependent equilibrium of assembly and disassembly of α/β-tubulin heterodimers. Microtubule targeting agents either stabilize (microtubule stabilizing agents, MSAs) or destabilize microtubule polymers (microtubule destabilizing agents, MDAs). The identified binding sites have been named after the most prominent agents of classes of agents binding at this region. They are highlighted and assigned *via* color code. GTP = guanosine triphosphate, GDP = guanosine diphosphate. Adapted with permission from the reference [77]. Copyrights (2018) Elsevier.

### 1.3.2  Targeting the Microtubule Cytoskeleton

Microtubule-targeting agents interfere with the 'dynamic instability' of microtubules by promoting either microtubule polymerization (microtubule stabilizing agents, MSAs) or dissociation (microtubule destabilizing agents, MDAs) (Figure 4). Both classes of agents can severely impair cell viability by suppressing microtubule dynamics, which characteristically results in cell cycle arrest in the $G_2/M$ phase.[76,77,86,87] Six distinct ligand binding sites have been characterized by structural biology and assigned to the respective most prominent compound class that binds to this region, as presented in Figure 4.[77]

Due to their antiproliferative effect, these agents are promising candidates for cancer therapy. However, from several hundred compounds found to be capable of inducing mitotic arrest, only a few have been clinically approved. The suitability of these compounds as pharmaceuticals is diminished by their nonspecific mode of action. They affect vital processes in all cells and can cause systemic side effects and leads to a low therapeutic index of the drugs. Consequently, therapy

suffers a compromise with limited applicable doses reducing the desired effect and severe adverse effects including myelosuppression and neutropenia that have to be endured.[76]

Spatiotemporal control of the activity of these compounds could reduce side effects and allow for higher concentration in the targeted tissue. This goal is being pursued by developing photoswitchable analogues of these agents.

### 1.3.3   Photoswitchable Microtubule-Targeting Agents

A variety of photoswitchable microtubule-targeting agents based on different molecular photoswitches have been demonstrated as analogues of the naturally occurring alkaloid and microtubule-destabilizing agent colchicine (Figure 5 a).

Combretastatin A-4 (CA4) is a naturally occurring stilbene that acts as a microtubule-destabilizing agent. Whereas the thermodynamically less stable $Z$-isomer is structurally similar to colchicine, can bind efficiently to the colchicine binding site in tubulin, and is a very potent microtubule inhibitor, the corresponding $E$-isomer is 60-fold less potent.[88,89] Although $E$-to-$Z$-isomerization of this compound is possible, the intrinsic characteristics of stilbenes prevent successful applications. Photoactivation of this compound requires UV-light and is not entirely reversible due to photochemical electrocyclization.[90]

To enable reversible photoisomerization, a photopharmacological azologue of CA4 was designed by replacing the carbon atoms of the C=C double bond with nitrogen atoms, as independently reported by three groups (photostatin-1, PST-1, Figure 5).[7,22,23] The biologically less active but thermodynamically more stable $E$-isomer can be efficiently and reversibly transformed into the colchicine-like $Z$-isomer with light in the range of 380-410 nm. A significantly increased potency against various cell lines and light-triggered $G_2/M$ arrest were demonstrated. In addition, light-induced mitotic arrest in metaphase was shown *in vivo* with *C. elegans* embryos and it was found to be possible to target only selected single cells and reverse this process by green light-triggered $Z$-to-$E$-isomerization.[7] However, PST-1 was found to be unstable under reducing conditions and it was further observed that the more active $Z$-isomer is degraded considerably faster by cellular glutathione. As mentioned in chapter 1.2.1, this is a commonly observed phenomenon with azobenzene photoswitches and severely limits their applicability in biological environments.
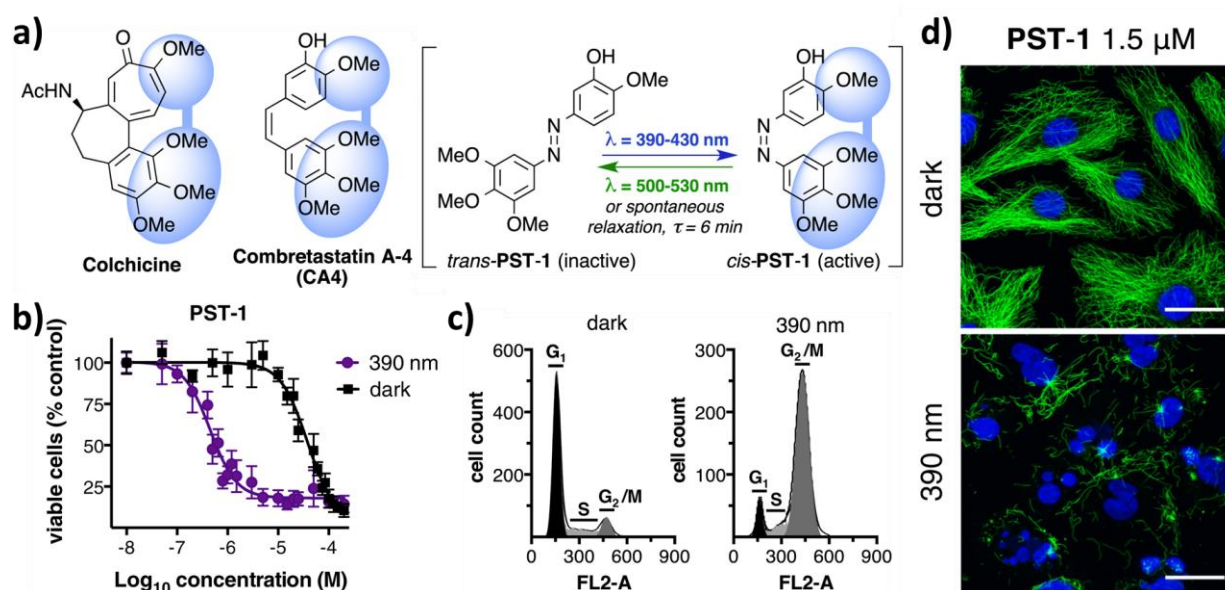
**Figure 5:** a) Photostatin-1 (PST-1) is a photoswitchable azologue of combretastatin A-4 (CA4), b) Viability assays demonstrate the light-tunable potency of PST-1, c) Light-dependent cell-cycle analysis illustrates that irradiated PST-1 leads to $G_2/M$ arrest, a characteristic observation for microtubule-targeting agents, d) PST-1 selectively causes disassembly of microtubules and nuclear fragmentation upon irradiation with 390 nm. Treatment with the same concentration but in the dark does not affect microtubule structure. (MDA-MB-231 cells; α-tubulin (green), DNA (blue); scale bars, 20 mm). Adapted with permission from reference [7]. Copyright 2015 Elsevier Inc.

The limitations of azobenzene photoswitches motivated scientists to expand the variety of photoswitchable colchicine-inspired designs, including alternative molecular photoswitches such as spiropyrans[91], benzodiazo *N*-substituted pyrrole[92], hemithioindigos[6,25], pyrrole hemithioindigos[28] and heterostilbenes[29,93].

Photoswitchable pyrrole hemithioindigos reported by Sailer *et al.* (e.g. PHTub-7, Figure 6) overcome two factors that limit the photoswitchability of azobenzenes in biological assays. In contrast to the previously reported azobenzenes, these photoswitches can be photoisomerized nearly quantitatively in both directions within the biologically compatible light spectrum. Moreover, high photostationary states (PSSs) can be reached by applying fixed-wavelength lasers available in confocal microscopes.[28] Complementary to this, another series of photoswitchable microtubule-destabilizing agents based on the heterostilbene styrylbenzothiazole was deleveloped, specifically designed to be orthogonal to common light frequencies applied for imaging with confocal microscopes. These compounds can be employed for photocontrol of microtubules in biological assays in combination with multichannel imaging. Fluorescence imaging of for example green fluorescent protein (GFP) labelled species is possible without affecting these photopharmacological agents. Further favorable characteristics of these compounds include their stability against degradation by cytoplasmic glutathione and the enhanced lifetime of the more

active species.[93] Two lead compounds, SBTub2M and SBTubA4 (Figure 6), with potencies in the mid-nanomolar range and 30- to 200-fold enhanced antimitotic activity in the lit state have been identified.[29] Unfortunately, photomodulation of styrylbenzothiazole-based photoswitches is limited due to the low band separation between the two respective photoisomers in combination with the high thermal stability of the *Z*-isomers. These characteristics prevent photoactivation from being reversed thermally or by irradiation with another wavelength. However, it was found that diffusion of the photoactivated species enables recovery of microtubule dynamics after photoactivation with half-lives of ca. 20 s in 2D cell culture and ca. 10 min in organoids and *in vivo*. It was further demonstrated that reversible and spatiotemporal control of mitotic progression in zebrafish *D. rerio* is possible in repeatable cycles with the water-soluble prodrug SBTubA4P (Figure 6).[29]
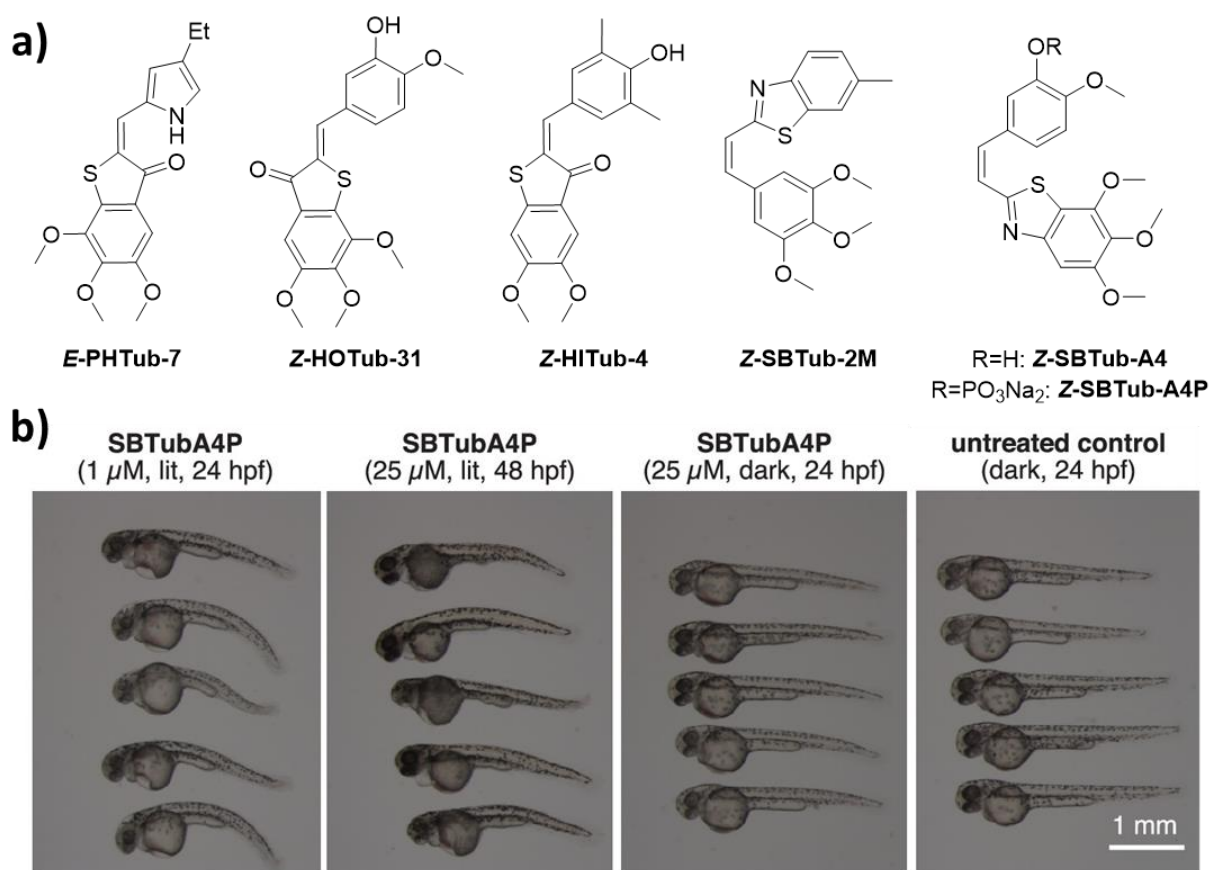


**Figure 6:** Examples of photoswitchable microtubule-destabilizing agents. a) Examples for active photoisomers of agents with photoswitchable antimitotic activity, b) Heterostilbene **SBTubA4P** (1 or 25 μM) causes morphological abnormalities in the development of *D. rerio* selectively in the lit state. hpf = hours post-fertilization. Reproduced and adapted with permission from reference [29].

Further possible applications were realized by designing photoswitchable analogues of the microtubule-stabilizing agents paclitaxel and epothilone B and D, which provide access to a further

spectrum of biological effects. Compared to microtubule-destabilizing agents, they differ in their pharmacological properties and stoichiometry.[26]

Müller-Deku *et al.* synthesized a library of 3'-azobenzamide-taxanes and identified AzTax3MP as the lead compound for which the structural alterations resulted in the smallest loss of overall potency and which was found to reach the highest dark/lit ratio of $EC_{50}$ values. In contrast to the previously described compounds, like for example PST-1, this compound does not inhibit but promotes tubulin polymerization with an enhanced potency in the lit state (Figure 7).[26]
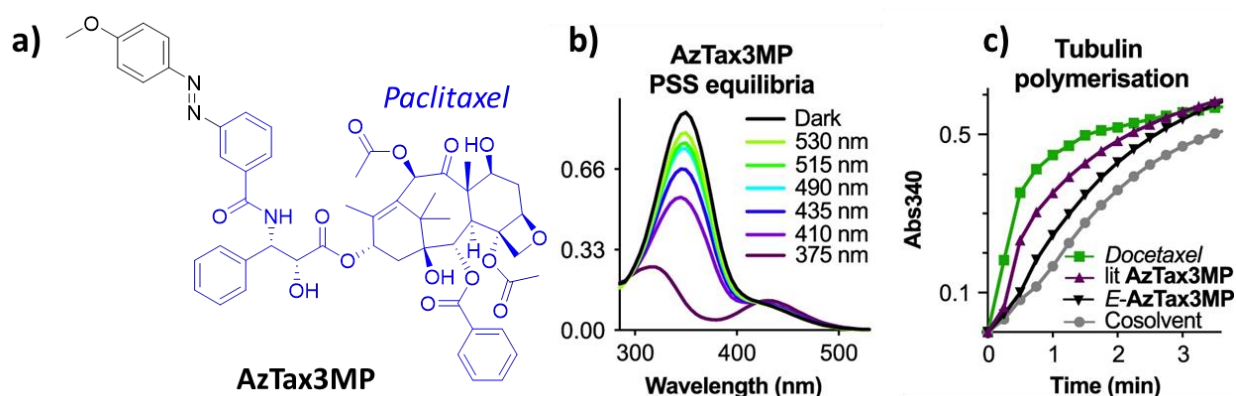


**Figure 7:** a) **AzTax3MP** was designed by installing a methoxy-substituted azobenzene on the microtubule stabilizing agent paclitaxel (marked in blue), b) UV–Vis absorption spectra of **AzTax3MP** in the photostationary states (PSSs) reached upon irradiation with selected wavelengths, c) Light-enhanced promotion of tubulin polymerization by Z-**AzTax3MP** was demonstrated in cell-free assays and compares to docetaxel. Panels b) and c) were reprinted under the terms of the Creative Commons CC BY license from reference [26].

In another study Gao *et al.* installed a photoswitchable styrylthiazole (ST) moiety on epothilone D by either expanding the molecular scaffold or connecting the ST to the macrolactone *via* the phenyl ring (Figure 8). Interestingly, they obtained light-activated derivatives (Figure 8 a) as well as an agent that loses potency upon irradiation (Figure 8 b). Because the absorption spectra of both photoisomers do not overlap with the commonly applied laser lines 488 nm and 561 nm, it was possible to monitor the disorganized microtubule networks caused by photoactivated STEpo2 *in situ*.[30]
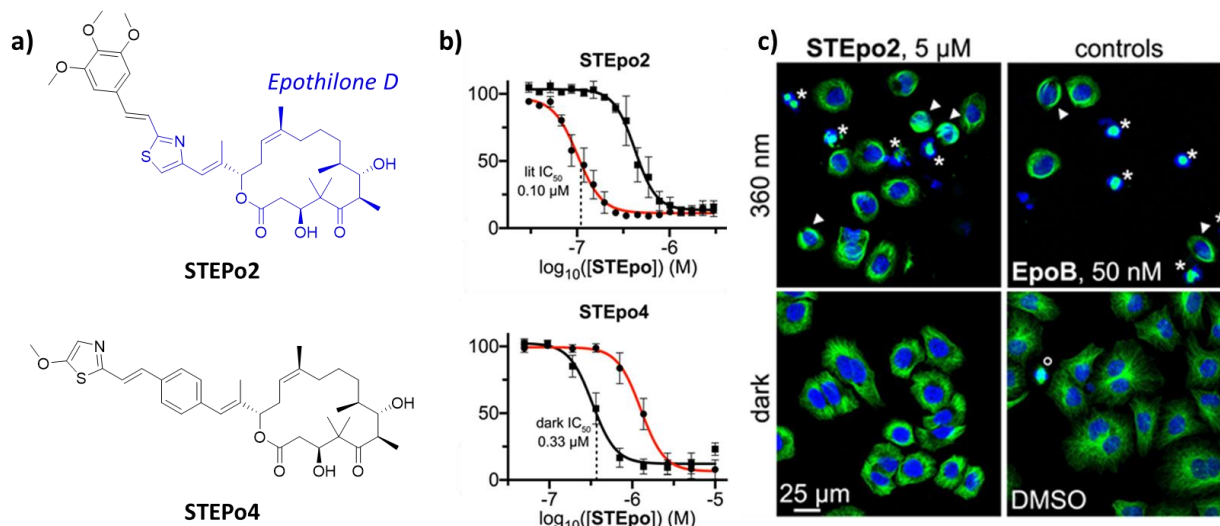
**Figure 8:** a) **STEpos** are photoswitchable microtubule-targeting agents derived from epothilone D (highlighted in blue) by either expanding the molecular scaffold (**STEpo2**) or inverting the introduced ST photoswitch (**STEpo4**), b) Photomodulation of the antiproliferative activity of **STEpo2** and **STEpo4** was investigated in cell viability assays. While **STEpo2** is activated under lit conditions, **STEpo4** loses potency upon irradiation, c) HeLa cells were treated with **STEpo2** (20 hours incubation) and imaged *via* fluorescence microscopy ($\alpha$-tubulin: green, DNA stained with DAPI: blue). Generation of a high population of the *Z*-isomer *via* 360 nm pulsing results in disorganized microtubule networks: spindle defects (asterisks) and bundled MTs (arrowheads). EpoB = epothilone B, DMSO = dimethyl sulfoxide, co-solvent control. Panels b) and c) were adapted from reference [30].

## 1.3.4   Plinabulin

Plinabulin is a microtubule-destabilizing agent with low-nanomolar activity and it is currently being investigated in a global phase 3 clinical trial as an agent for the treatment of non-small cell lung cancer[94-96] and chemotherapy-induced neutropenia.[97] It is a synthetic analogue of the natural product phenylahistin, discovered in cultures of the marine fungus *Aspergillus ustus* in 1997, which was found to induce cell cycle arrest in the $G_2M$ phase with a significantly higher potency of the (*S*)-enantiomer.[95,98-100] In systematic and extensive structure-activity relationship studies, plinabulin (also referred to as NPI-2358) was identified as a synthetically readily accessible derivative with optimized bioactivity.[100,101] Plinabulin binds to the colchicine binding site of $\beta$-tubulin but differs in the nature of binding compared to colchicine and CA4. This is a possible explanation for its effect against chemotherapy-induced neutropenia, which has not been observed for the other two compounds.[102]
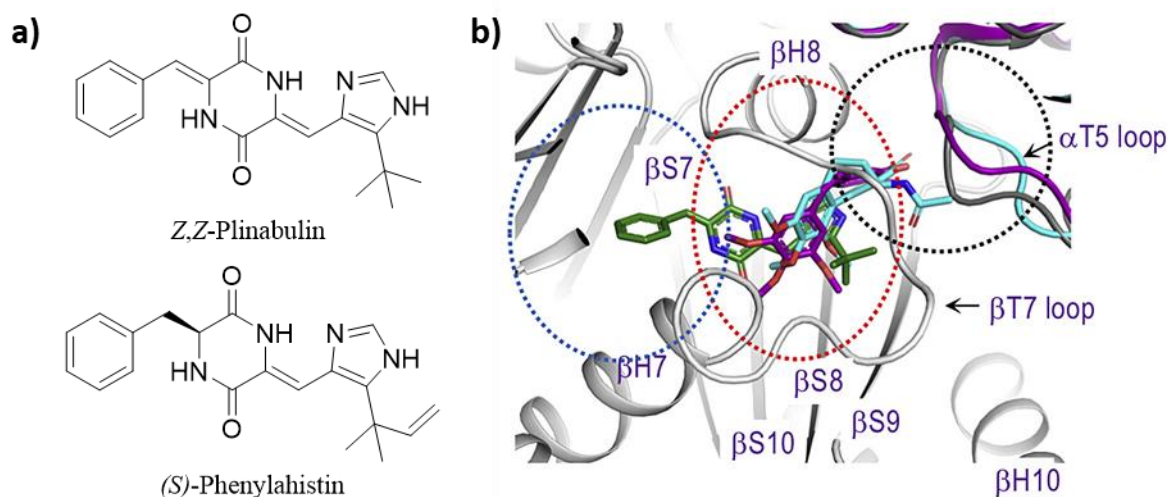
**Figure 9:** a) Plinabulin is a synthetic analogue of phenylahistin, which was isolated from the marine fungus *Aspergillus ustus*, b) An overlay of the X-ray crystal structure analyses revealed the different nature of binding of plinabulin (green sticks) compared to colchicine (cyan sticks) and CA4 (purple sticks). Panel b) was adapted from reference [102].

Plinabulin can be described as a cyclic dipeptide and consists of a 2,5-diketopiperazine (DKP) ring with two arylidene substituents. The pseudo-tricyclic structure of the DKP ring and the imidazole moiety highlighted in Figure 10 are essential for its biological activity and should not be altered when designing new derivatives of plinabulin. However, the installation of functional groups on the phenyl ring is tolerated in some cases and the two derivatives depicted in Figure 10 b were found to be even more potent than plinabulin.[100]
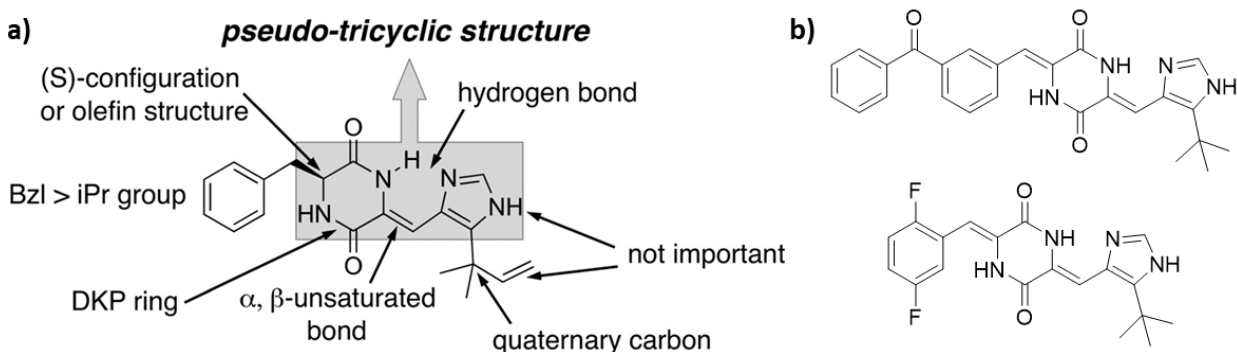


**Figure 10:** a) Structural features of plinabulin that are essential for its biological activity, b) Derivatives with an enhanced potency compared to plinabulin. Reproduced from. Panel a) was reprinted with permission from reference [100]. Copyright 2012 American Chemical Society.

Adverse effects of plinabulin include fever, tumor pain, transient hypertension, fever, fatigue, and nausea/vomiting.[96] To enable light-triggered release of this drug, plinabulin was encapsulated into DKP-based hydrogels and efficiently released upon irradiation with green light.[103] While working on this project, it was discovered that plinabulin itself can be reversibly photoisomerized with visible light.

## 2 Objective

The newly discovered photoswitchability of plinabulin constitutes a previously unexplored characteristic of a potent agent currently in the 3rd phase of clinical trials. This sets the basis for the qualification of plinabulin as an alternative to previously described photoswitchable antimitotic agents that suffer a dramatic loss in potency caused by the structural modifications made when introducing the respective molecular photoswitch.

This research work aims to gain an understanding on the nature of photoswitching of plinabulin and to introduce plinabulin and its derivatives as a new class of photopharmacological agents. For this purpose, first, the photoswitchable structural motif is identified by isolating and studying the respective photoisomers. To investigate possibilities for optimization of these agents, a series of derivatives is synthesized and investigated strategically with respect to their photophysical and photopharmacological properties.

The photochromism of plinabulin was never reported before. It also does not contain any established photoswitch within its structure. Therefore, the unexpected discovery in our group, that plinabulin can reversibly photoisomerize, opens up new interesting perspectives both in photopharmacology and in basic photochromism research. Consequently, the identified photoisomerizable structural motif – arylidene-2,5-dietopiperazine, abbreviated below as "hemipiperazine" or "HPI" - is studied systematically by installing electron-withdrawing and electron-donating substituents on a model compound. The photophysical properties are assessed and correlated with computational quantum mechanical modeling (applying the density-functional theory, DFT) calculations.

Finally, the new photoswitch – HPI - is introduced into another core structure to demonstrate the broader applicability and expand the scope of possible applications.
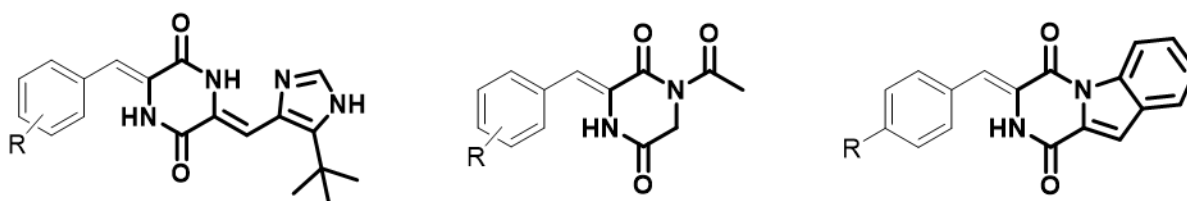
# 3 Results and Discussion

## 3.1 Plinabulin Derivatives

This work introduces plinabulin as a novel photoswitchable antimitotic agent that comprises a previously unidentified molecular photoswitch suitable for photopharmacological applications. A library of plinabulin derivatives was synthesized in order to identify the scope of photochromism and the optimization potential of the photophysical and photopharmacological properties - for future human therapeutic applications.

### 3.1.1 Synthesis

The syntheses of plinabulin (**6**) and the investigated derivatives were achieved according to literature procedures in eight reaction steps, starting with the formation of the molecular building blocks *N,N'*-diacetyl-2,5-piperazinedione (**2**) and aldehyde **4** (Scheme 1). These two compounds are synthetically accessible starting from the commercially available substrates glycine (**1**) and ethyl isocyanoacetate (**3**) in two and four synthetic steps, respectively. In a subsequent condensation reaction, they are coupled, yielding arylidenepiperazinedione **5**.[100,104-106]
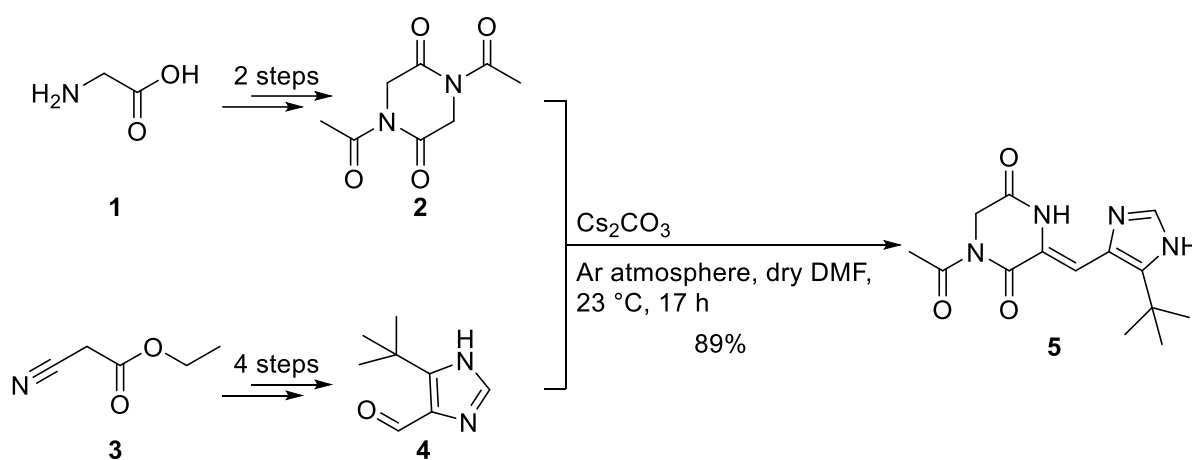


**Scheme 1:** The synthetic intermediate diketopiperazine (DKP) **5** is accessible *via* a seven-step synthesis route, starting from the commercially available substrates glycine (**1**) and ethyl isocyanoacetate (**3**).

In the final reaction step, a series of carbocyclic aromatic and heteroaromatic aldehydes were coupled with intermediate **5** in a second condensation reaction. This aldol-type condensation is a common reaction for introducing arylidene substituents on diketopiperazines (DKPs) (Figure 11).[107-112]
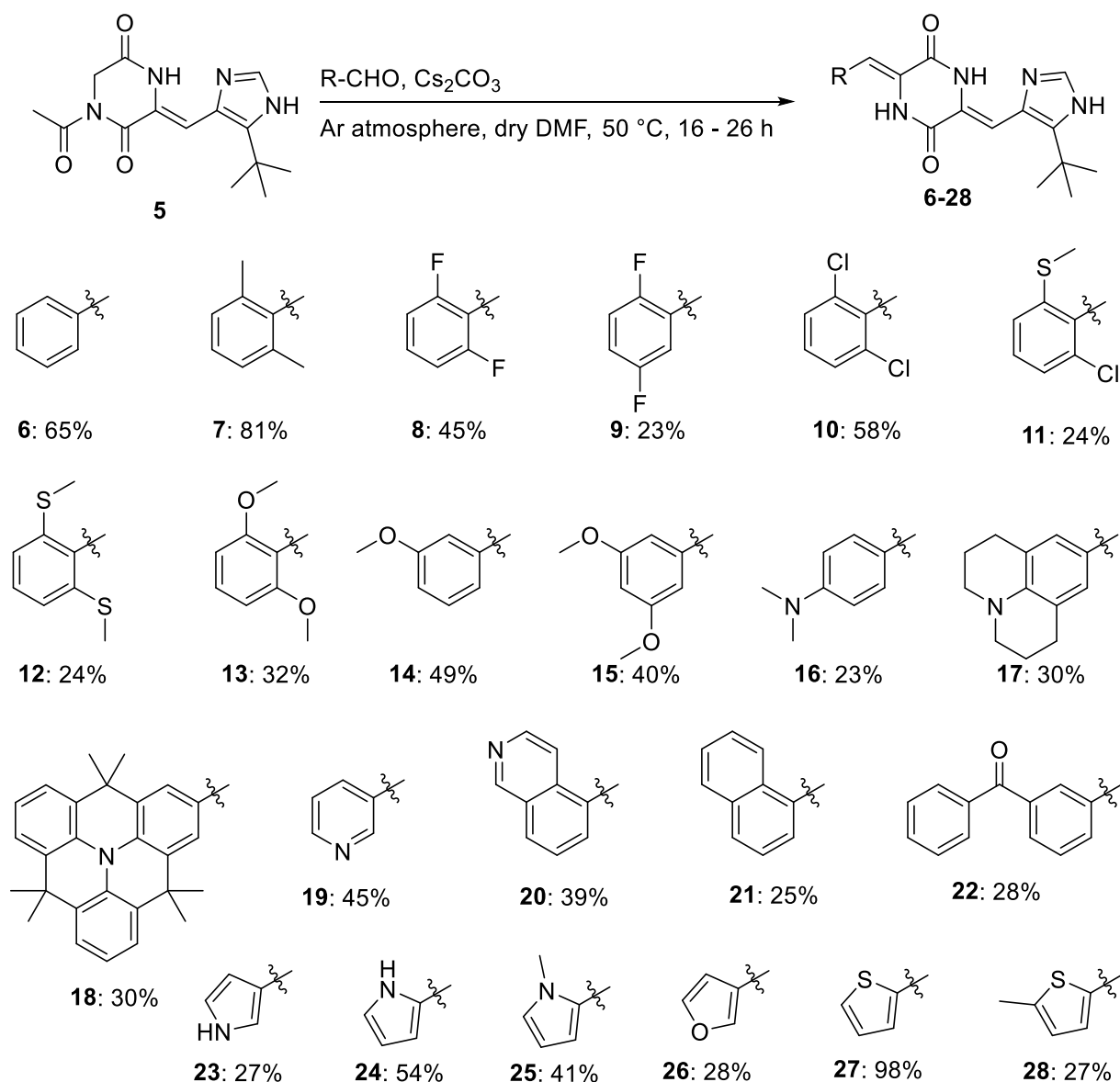
**Figure 11:** A library of plinabulin derivatives was synthesized by coupling carbocyclic aromatic and heteroaromatic aldehydes with intermediate **5** in an aldol condensation reaction.

The respective aldehydes were usually obtained commercially and only in a few cases synthesized in preparation for the respective condensation reaction (details in chapter 5.4.2). The aldehyde subjected to the reaction towards compound **23** (Figure 11) contained a *tert*-butyloxycarbonyl (Boc) protecting group which was removed in an additional, ninth reaction step.

As shown in Scheme 1, the condensation reactions were preceded by an activation of the diketopiperazine by an *N*-acetylation of the DKP. The acylated DKP can subsequently be subjected to aldol-type condensation reactions with aromatic and aliphatic aldehydes in the presence of a suitable base (e.g. triethylamine (Et$_3$N), caesium carbonate (Cs$_2$CO$_3$) or potassium *tert*-butoxide (KO$^t$Bu)). The enhanced reactivity of the acylated derivative was rationalized by a greater acidity of the vicinal methylene proton, which is cleaved off by a base and leads to the enolate formation

in the first step of the proposed mechanism (Scheme 2).[107,112] Yet, computational studies did not show a significant distance in the acidity of these protons in unsubstituted DKP (pK$_a$ = 24.0) and the acetylated analogue (pK$_a$ = 24.1).[113] However, the acetylation additionally supports the condensation reaction by enabling a kinetically favored intramolecular *N–O* shift of the acyl group (step 3, Scheme 2).[107,112]
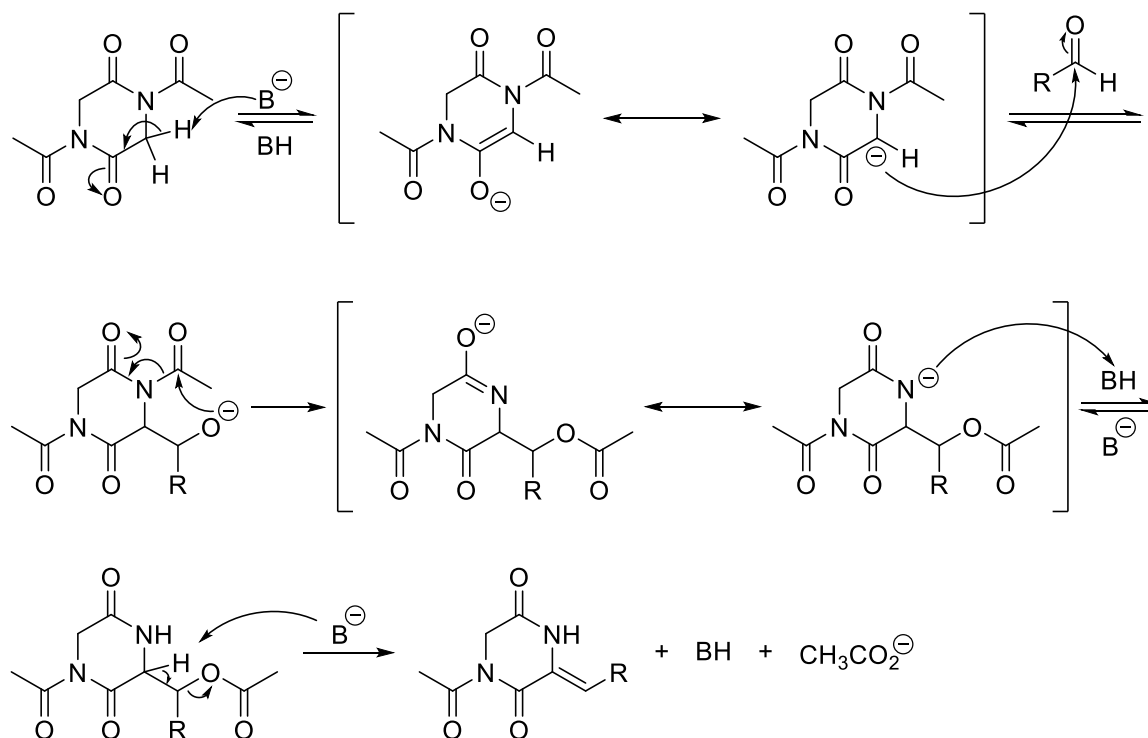
**Scheme 2:** General reaction mechanism of the aldol-type condensation of acylated DKP **2** and aromatic or aliphatic aldehydes proposed by Gallina and Liberatori in 1973.[107]

In the last step, the double bond is formed by elimination of acetate. The reaction is typically diastereoselective in favor of the respective *Z*-isomers, which may be explained by applying the Zimmermann-Traxler model to the second step of the mechanism, the aldol addition.[111,112] The two competing transition states proposed by Balducci *et al.* are shown in Figure 12. The reaction proceeds *via* the transition state in which the relative orientation of the aldehyde to the acetyl group causes less steric hindrance.[114]
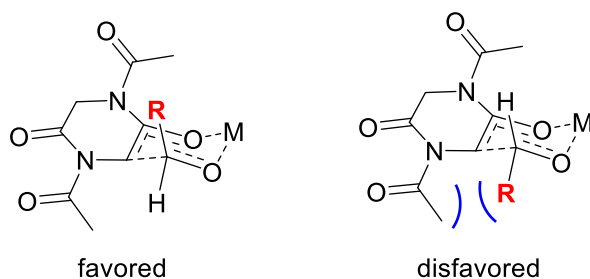
**Figure 12:** The diastereoselectivity of the aldol condensation can be rationalized by applying the Zimmermann-Traxler model to the aldol addition following the enolization of the DKP **2**. The reaction proceeds *via* the transition state depicted on the left with less steric hindrance. R = aliphatic or aromatic residue, M = Metal of the base applied in the reaction.[114]

When performing the aldol condensation with carbocyclic aromatic aldehydes the yield and/or the required reaction time is highly dependent on the substituents. In general, the reaction is significantly faster when coupling aldehydes bearing electron-withdrawing groups, which promote a nucleophilic attack of the intermediate enolate on the aldehyde group. The reaction conditions can be optimized by choosing a suitable combination of base and solvent.[112] During this work, it was studied whether the speed of the reaction with electron-rich aldehydes can be enhanced by raising the reaction temperature from room temperature to 50 °C when performing reactions. When monitoring these reactions *via* analytical HPLC, it was observed that an increased temperature lead to the formation of undesired side products which thus resulted in lower yields. Satisfactory yields were achieved when stirring at room temperature and prolonging the reaction up to several days.

For nine of the synthesized derivatives single crystals were grown successfully and subjected to single-crystal X-ray diffraction studies. The corresponding structures are shown in Figure 13. As expected, the *Z*-conformation of both C=C double bonds was confirmed for all these compounds, respectively.
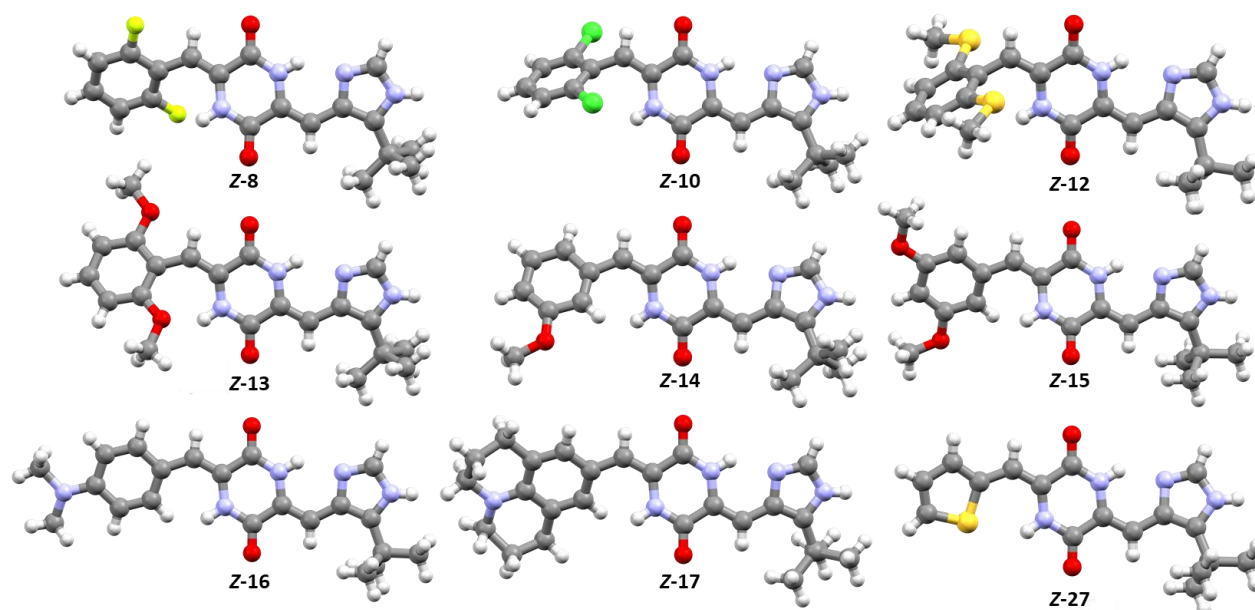
**Figure 13:** Single crystals of *Z*-**8**, *Z*-**10**, *Z*-**12-17** and *Z*-**27** were analyzed in single-crystal X-ray diffraction studies. The results were visualized with Mercury 2020.1 (CCDC). Additional atoms in the results of *Z*-**8**, *Z*-**13**, *Z*-**27** (H$_2$O), *Z*-**14** (disordered 3-methoxybenzylidene moiety) and *Z*-**17** (disordered *tert*-butyl and julolidine moieties) were removed in this visual presentation. Atoms of carbon are depicted in grey, hydrogen in white, oxygen in red, nitrogen in blue, sulfur in deep yellow, fluorine in bright yellow and chlorine in green.

Also, the pseudo-tricyclic structure described by Yamazaki et al. (see also chapter 1.3.3)[100] was confirmed. The imidazole ring was found to be in plane with the diketopiperazine ring, which is presumably supported by an intramolecular hydrogen bond between the lone electron pair of the nitrogen atom on the imidazole ring and the amide proton on the DKP ring. It was additionally observed that the introduction of substituents in *ortho* position on the phenyl ring leads to a twist of the aromatic ring out of plane, which can be rationalized by steric repulsion.

### 3.1.2 Investigation of the Photoswitching

In course of our research on encapsulation and light-induced plinabulin (**6**) release as a bioactive cargo from photoswitchable supramolecular hydrogels based on azobenzene[103], our group discovered that in absence of the azobenzene-containing hydrogelator the cargo molecule itself also exhibited reversible photochromic behavior. Because plinabulin (**6**) does not contain any previously investigated photoswitchable structural motifs, the first major goal was to determine the conformation of the less stable photoisomer of plinabulin (**6**) that is being formed upon irradiation. When assuming that photoconversion proceeds as *E/Z*-isomerization, there are two double bonds that could hypothetically isomerize, leading to four possible photoisomers in total,

which are depicted in Figure 14. However, all collected results of NMR and HPLC measurements suggest that only one additional photoisomer is formed during photoisomerization.
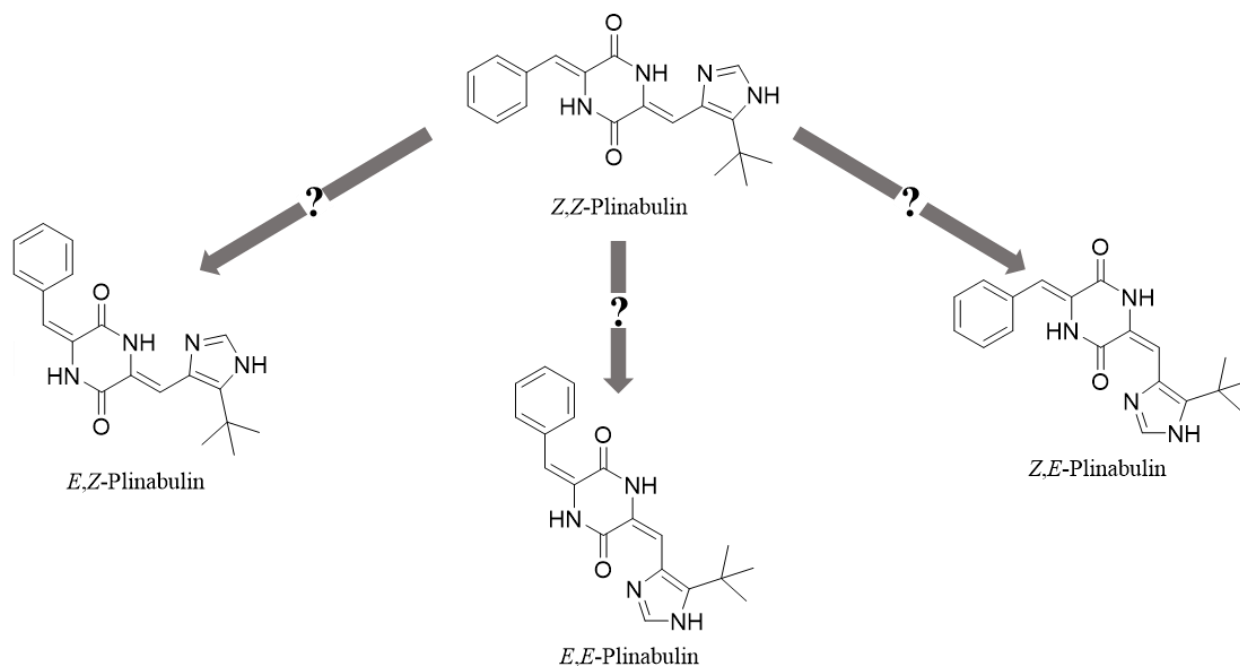


**Figure 14:** In theory, the thermally most stable *Z,Z*-isomer can be photoisomerized into the three other isomers when undergoing *E/Z*-isomerization.

To identify this photoisomer a method to separate the respective photoisomers *via* preparative HPLC was developed. It was found that both photoisomers are sufficiently stable to be analyzed *via* NMR spectroscopy. Sections of the respective $^1$H NMR spectra are presented in Figure 15 and selected signals were assigned to the corresponding protons *via* color code. One of the two signals assigned to the two vinylic protons (blue) is shifted significantly more into the high field than the other one (green). This allows the conclusion that the proton on the side of the phenyl residue is subjected to a greater change in its electronic surroundings, than the proton on the side of the heterocycle. This is a first indication that the depicted *E,Z*-isomer is formed.
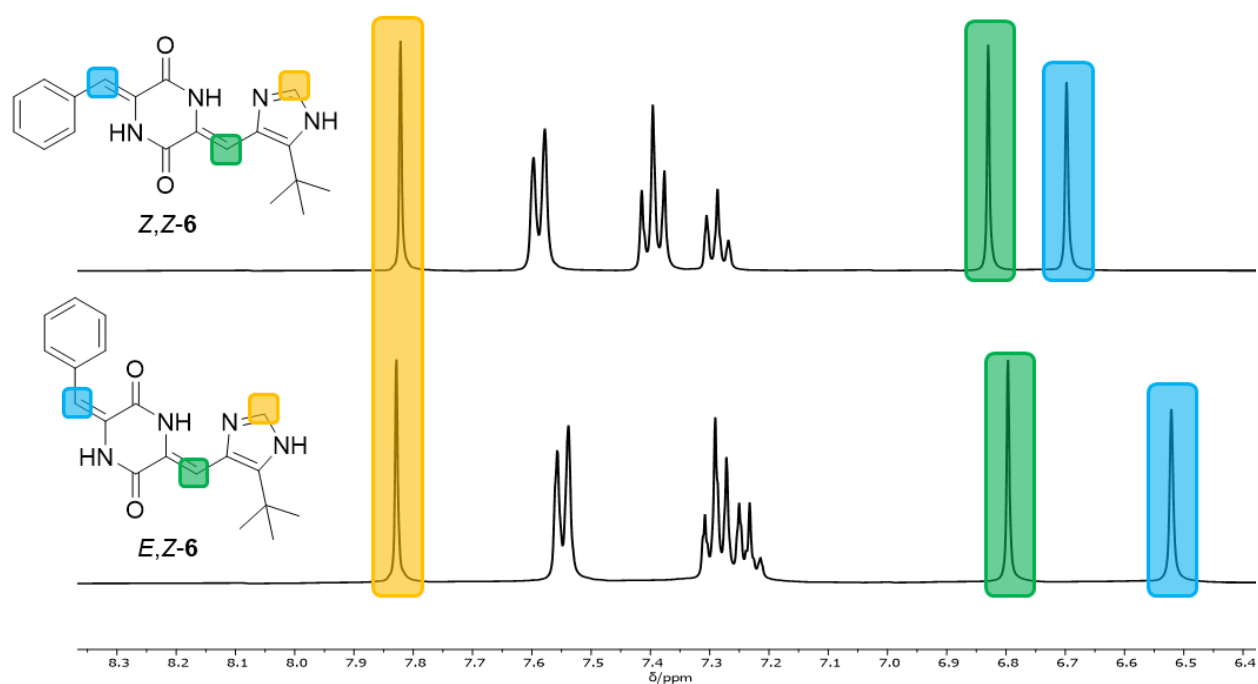
**Figure 15:** Comparison of sections of $^1$H NMR spectra (400 MHz) in deuterated dimethyl sulfoxide (DMSO-$d_6$) of the photoisomers of plinabulin (**6**). Selected signals are assigned to the respective proton *via* color code.

Additionally, NOESY NMR spectra of both photoisomers of plinabulin (**6**), 3-methoxyplinabulin **14** and 3,5-dimethoxyplinabulin **15** were measured and analyzed. Sections of these spectra are presented in Figure 16 and important signals are assigned to the respective protons *via* color code. It is evident that after photoisomerization the signal, assigned to interactions of the NH proton with aromatic protons (highlighted in yellow, not detected for *Z*-**6**) is replaced by a signal that indicates close proximity of the NH proton to the vinylic proton. These results also support the light-triggered formation of the respective *E,Z*-isomers.
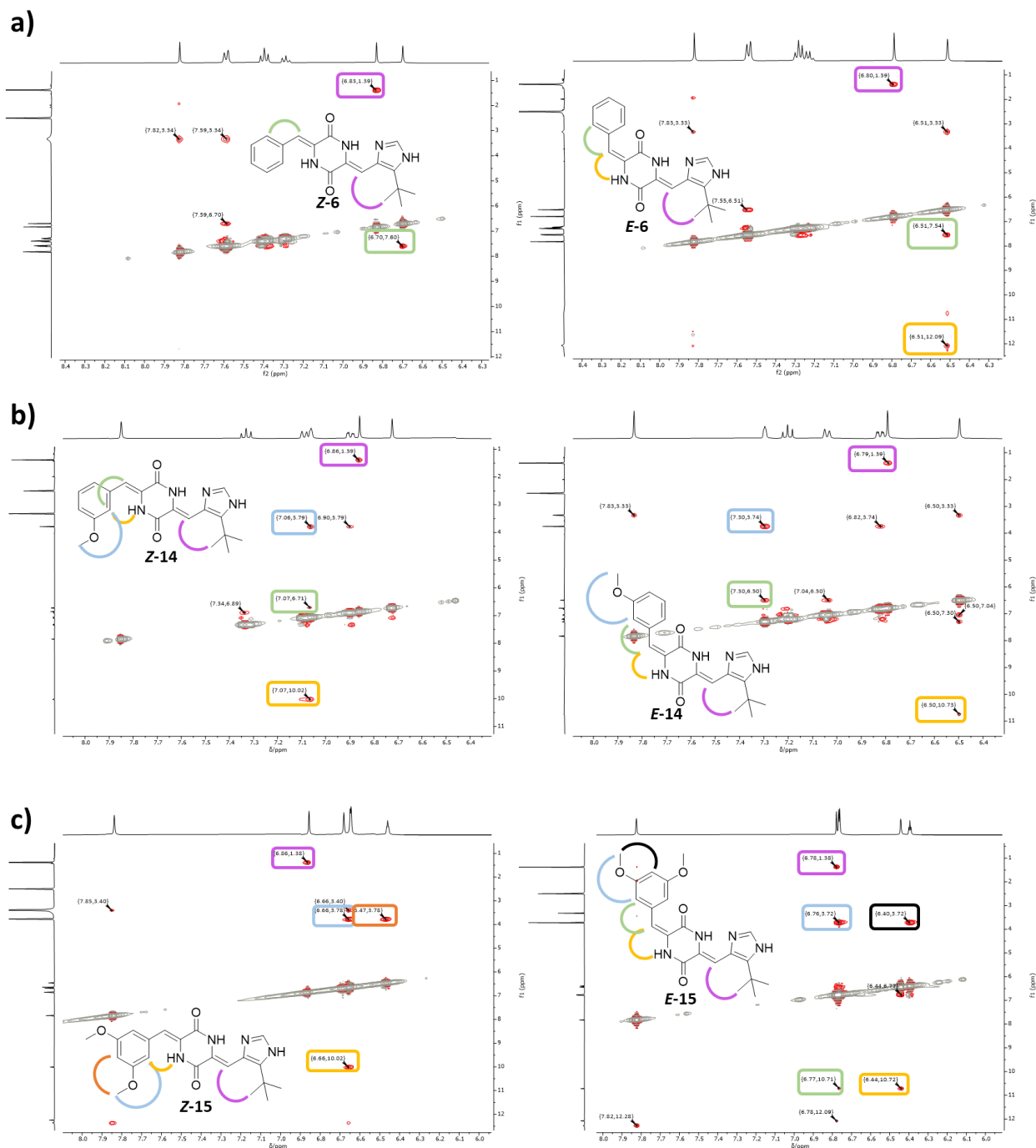
**Figure 16:** Sections NOESY NMR spectra in deuterated dimethyl sulfoxide (DMSO-$d_6$) of the two respective photoisomers of a) **6**, b) **14** and c) **15**. Selected signals are assigned to the respective protons *via* color code.

Furthermore, single crystals of both photoisomers of 2,6-dichloroplinabulin **10** were obtained and analyzed *via* X-ray diffraction analysis to determine their respective conformations. As depicted in Figure 17, the formation of the *E,Z*-isomer could be confirmed.
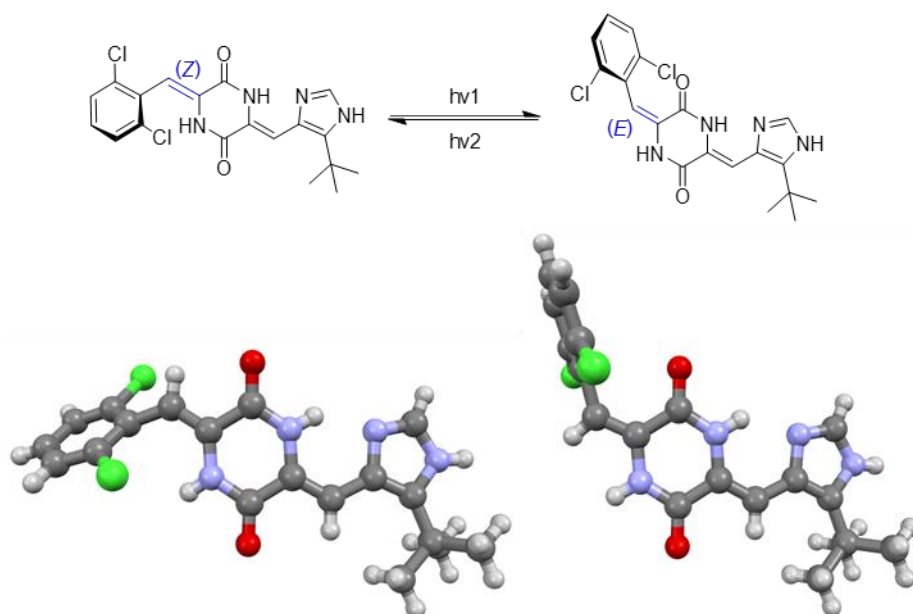
**Figure 17:** The conformations of the two photoisomers of 2,6-dichloroplinabulin **10** were determined *via* single-crystal X-ray diffraction analysis.

Based on the combined data it was concluded that the synthesized plinabulin derivatives undergo light-induced *E/Z*-isomerization of the carbocyclic arylidene group attached to the cyclic dipeptide. This *E/Z*-photoisomerization is analogous to the isomerization of arylidene substituents adjacent to heterocyclic five-membered-ring scaffolds of the previously described classes of molecular photoswitches indigoids[115], hydantoins[116], and isoindolinones[117]. The photosensitivity of arylidene groups attached to heterocyclic six-membered-rings has been mentioned in 1970[118] and 1982[119] and was also shortly described for an isolated natural product in a report that was published over the course of this work[120]. Although these studies do not include any characterization of photochromism, they support the hypothesis of an *E/Z*-isomerization of the proposed C=C double bond. This novel molecular photoswitch is a combination of a <u>hemi</u>stilbene and a 2,5-diketo<u>piperazine</u> and was thus named hemipiperazine (HPI).

Under the investigated conditions, no *Z/E*-photoisomerization of the C=C bond on the heterocyclic arylidene substituent of plinabulin (**6**), nor its derivatives, has been observed. Therefore, it was decided to split the original system on two halves – each with one arylidene-substituted DKP – in order to separately check if there is any inherent structural reason for such a behavior. The photochromism of two alternative monoarylidene synthetic intermediates of plinabulin (**6**) – the benzylidene-*N*-monoacetyl-DKP **29** and the imidazole-substituted *N*-monoacetyl-DKP **5** shown in Figure 18 were investigated. They both contain the rudimentary HPI motif. For compound **29**, the *Z*-configuration could be confirmed *via* single-crystal X-ray diffraction analysis (see chapter 5.5.11). Interestingly, both compounds were found to be reversibly photoswitchable with

UV- and violet light and the respective photoisomers were isolated successfully and analyzed *via* NMR spectroscopy. Sections of the respective NOESY NMR spectra are shown in Figure 18 and important signals are assigned to the respective protons *via* color code. In both cases, a signal that indicates close proximity of the NH proton on the DKP ring to the vinylic proton was identified in the spectrum of the respective thermodynamically less stable photoisomer formed upon irradiation.
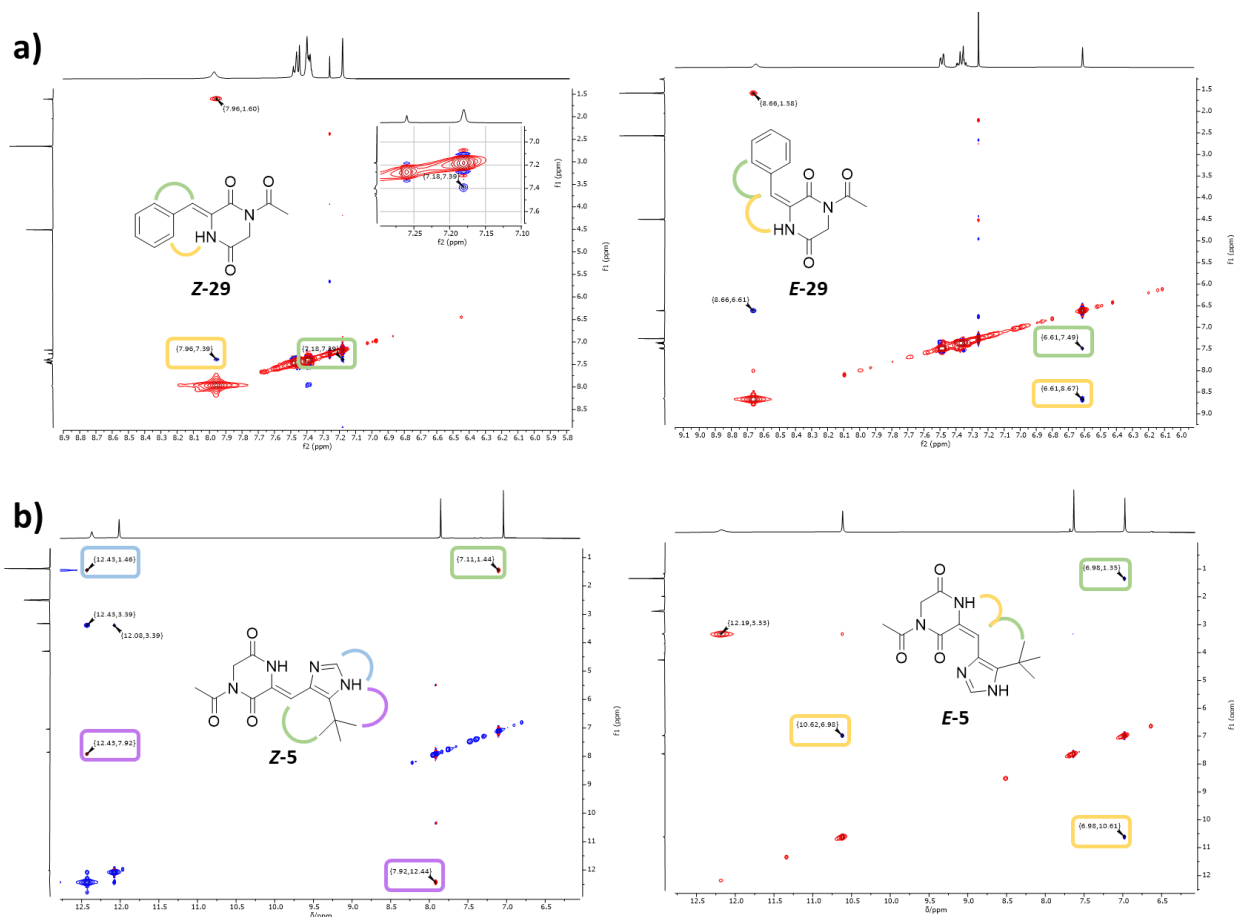


**Figure 18:** Sections NOESY NMR spectra in deuterated dimethyl sulfoxide (DMSO-$d_6$) of the two respective photoisomers of a) HPI **29** and b) HPI **5**. Selected signals are assigned to the respective protons *via* color code.

The collected data suggests that both intermediates – the carbocyclic aromatic **29** and the heteroaromatic **5** – are functional HPI photoswitches that separately undergo light-triggered *Z/E*-photoisomerization. This speaks against a preliminary working hypothesis, that it is the hydrogen bonding between the DKP amide bond and the imidazole nitrogen atom which stabilizes the *Z*-configuration of the heteroarylidene and prevents it from photoisomerization. Yet, in plinabulin (**6**), which comprises both a carbocyclic aromatic and a heteroaromatic HPI motif, the heterocyclic arylidene substituent is inert to light. Possible explanation for the stabilized *Z*-configuration is the particular relative geometric configuration of the two chromophores. A similar effect has been observed elsewhere for multiphotochromic azobenzenes.[121]

### 3.1.3   Photophysical and Photopharmacological Properties of Plinabulin (6)

When studying the photophysical properties of plinabulin (**6**), a minor solvatochromic effect was observed for both photoisomers. The absorption maxima of spectra measured in different solvents fluctuate between 355 and 371 nm (Figure 19). However, no direct correlation on the solvents' dipole moment and the shift of the absorption maxima was observed.
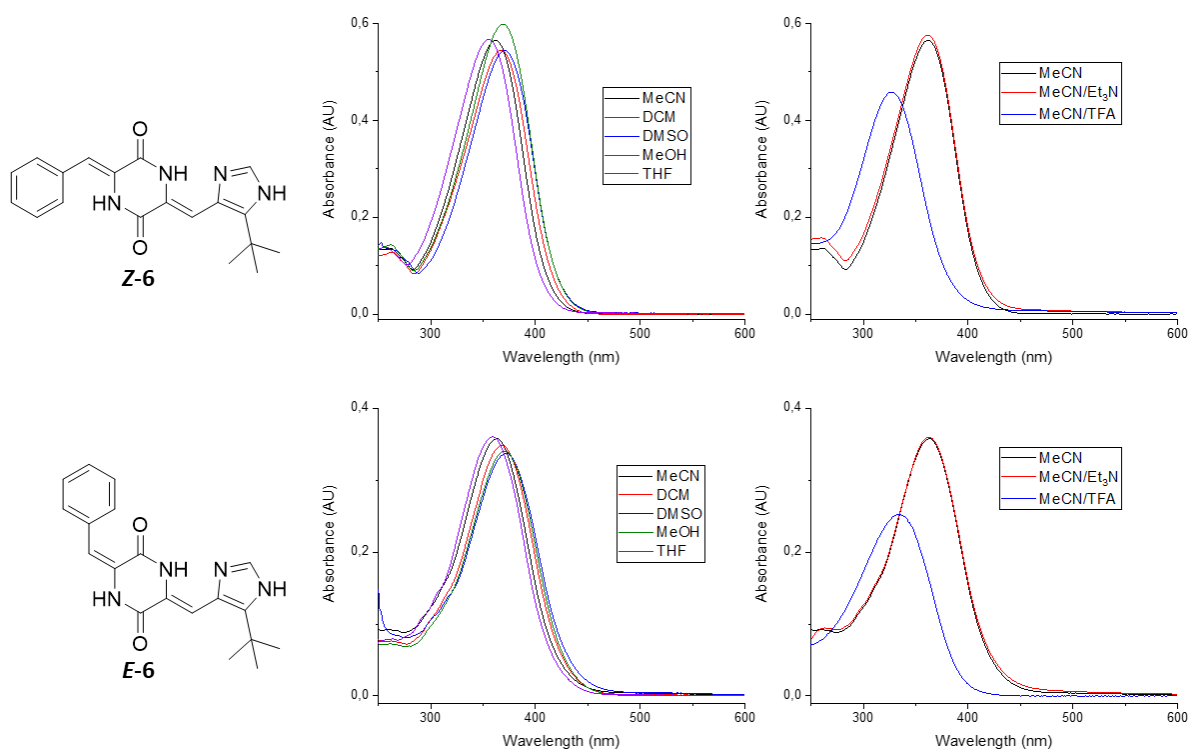


**Figure 19:** Solvatochromism and acidochromism was observed for both photoisomers *Z*-**6** (top) and *E*-**6** (bottom). Absorption spectra were measured (c = 80 µM, d = 2 mm) and spectra are assigned to the respective solvents *via* color code.

Additionally, absorption spectra measured in acetonitrile without any additive were compared with those of solutions with the same concentration but with 1% (v/v) of an acid (trifluoroacetic acid, TFA) and a base (triethylamine, Et$_3$N), respectively (Figure 19). While the addition of Et$_3$N had no significant influence on the absorption spectra, TFA addition was found to lead to a hypsochromic shift of the absorption maximum of 35 nm (*Z*-**6**) and 41 nm (*E*-**6**), respectively. The shift in the absorption spectra is assumed to be caused by protonation and can be tuned by adding different amounts of TFA whereby saturation is reached at 2.0 equivalents TFA (Figure 20). When investigating the two HPIs and synthetic intermediates of plinabulin **5** and **29**, no acidochromism was observed for the carbocyclic aromatic HPI **29** but TFA addition lead to a hypsochromic shift in the absorption maximum of 45 nm in the spectra of compound **5**. These results suggest that plinabulin (**6**) is protonated on the imidazole moiety when TFA (pKa in MeCN = 12.65)[122] is

added, which is in accordance with a pK$_a$ value of 15.07 for unsubstituted imidazole in MeCN.[123] In consequence of these findings, work-up after purification *via* preparative HPLC was adjusted: Because TFA was added to the mobile phase during purification all collected fractions were washed with saturated aqueous solution of sodium hydrogen carbonate to remove all TFA.
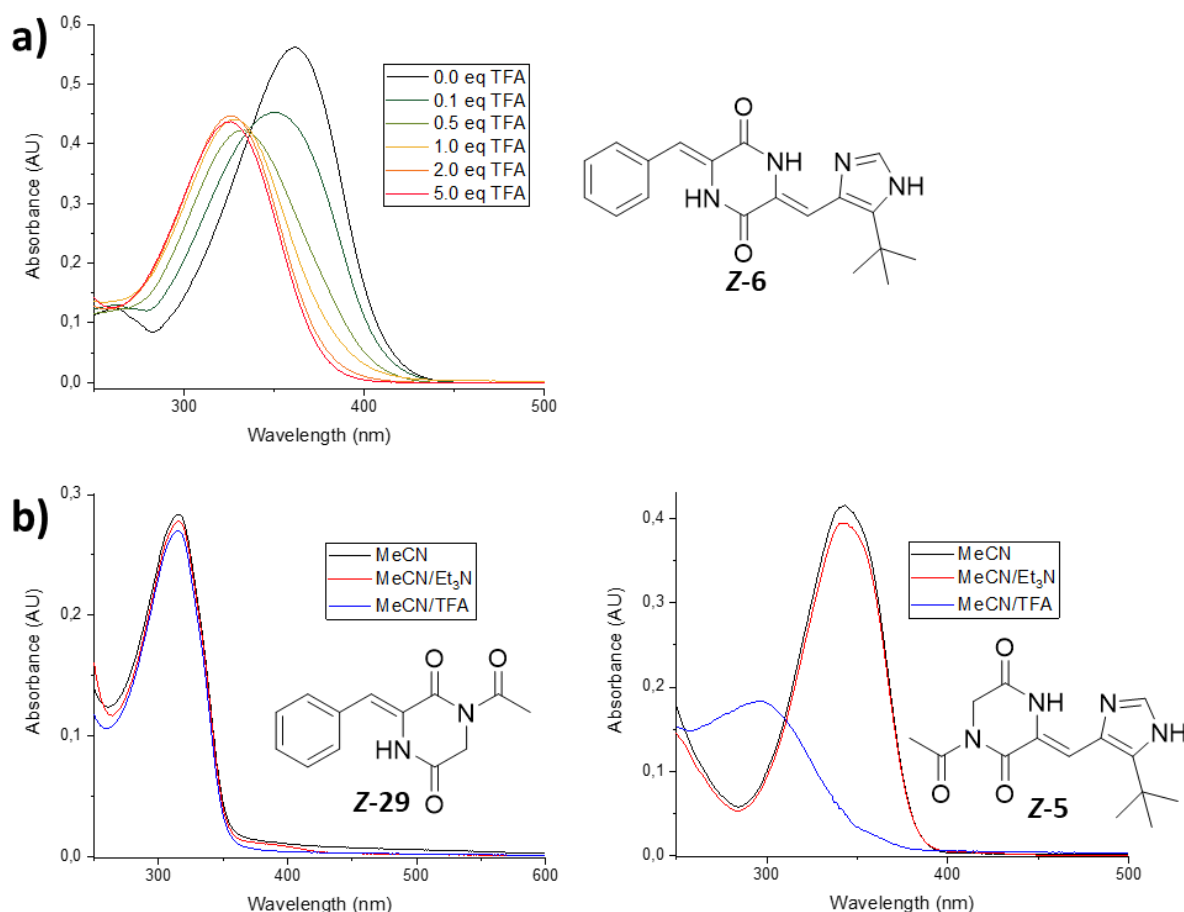


**Figure 20:** Results of investigations of the acidochromism of plinabulin (**6**) suggest a protonation on the imidazole ring. a) Absorption spectra of *Z*-**6** with different amounts of TFA, b) Compounds **29** (left) and **5** (right) were dissolved in pure MeCN and in mixtures of 1% (v/v) TFA in MeCN and 1% (v/v) Et$_3$N in MeCN, respectively. Acidochromism was not observed for *Z*-**29** but for *Z*-**5**. Absorption spectra (c = 80 µM, d = 2 mm) are assigned to the respective solvents and mixtures *via* color code.

After having assessed the photophysical properties of the isolated photoisomers the changes upon irradiation with selected wavelengths were investigated. The compositions of the photostationary states (PSSs) were determined *via* NMR spectroscopy in deuterated dimethyl sulfoxide (DMSO-*d$_6$*) (Figure 21).
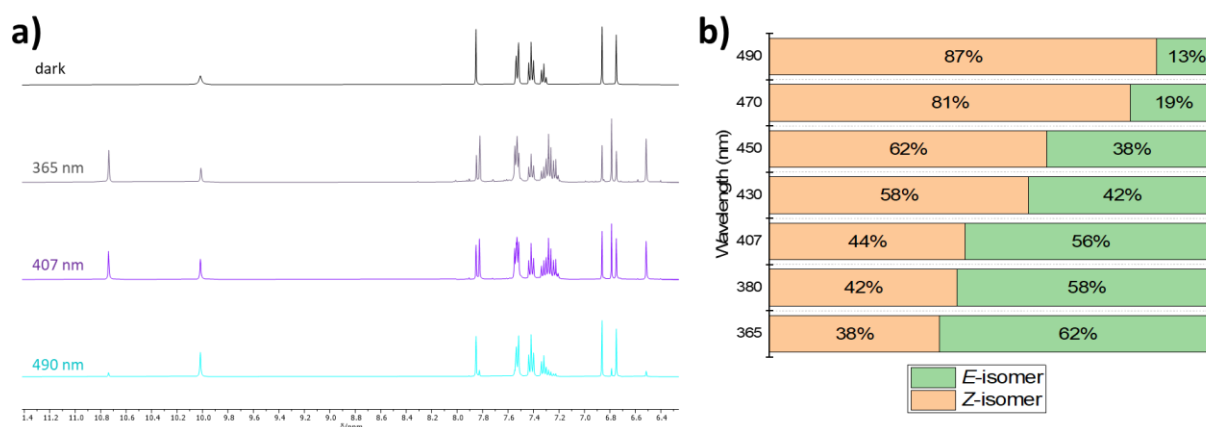
**Figure 21:** The compositions of the photostationary states (PSSs) of plinabulin (**6**) were determined *via* $^1$H NMR spectroscopy. Samples in deuterated dimethyl sulfoxide (DMSO-$d_6$) were irradiated with selected wavelengths and photoisomerization was monitored until prolonged irradiation did not lead to further changes in the relative integrals of the signals assigned to the two photoisomers. a) Sections of NMR spectra obtained after irradiation with selected wavelengths and the PSS was reached. The spectra are assigned to the respective wavelengths *via* color code, b) Compositions of the respective PSSs for all applied wavelengths.

A PSS is reached once further irradiation does no longer induce a change in the ratio of *E*- and *Z*-isomer. It was found that the thermodynamically more stable *Z*-isomer can be photoisomerized to up to 62% of the corresponding *E*-isomer with UV-light (365 nm) and efficient back-isomerization to 87% *Z*-isomer is achieved upon irradiation with cyan light (490 nm).

In diluted samples, slight photodegradation was noticed upon irradiation at and below 430 nm. In presence of blue or cyan light (450-490 nm) however, plinabulin (**6**) was found to be stable. To investigate the photostability of plinabulin (**6**) in details, ten subsequent switching cycles in DMSO were performed by first irradiating the sample with violet light (407 nm, 2 min per cycle), then with cyan light (490 nm, 35 min per cycle). The resulting mixtures were analyzed after every irradiation step *via* analytical HPLC (Figure 22).
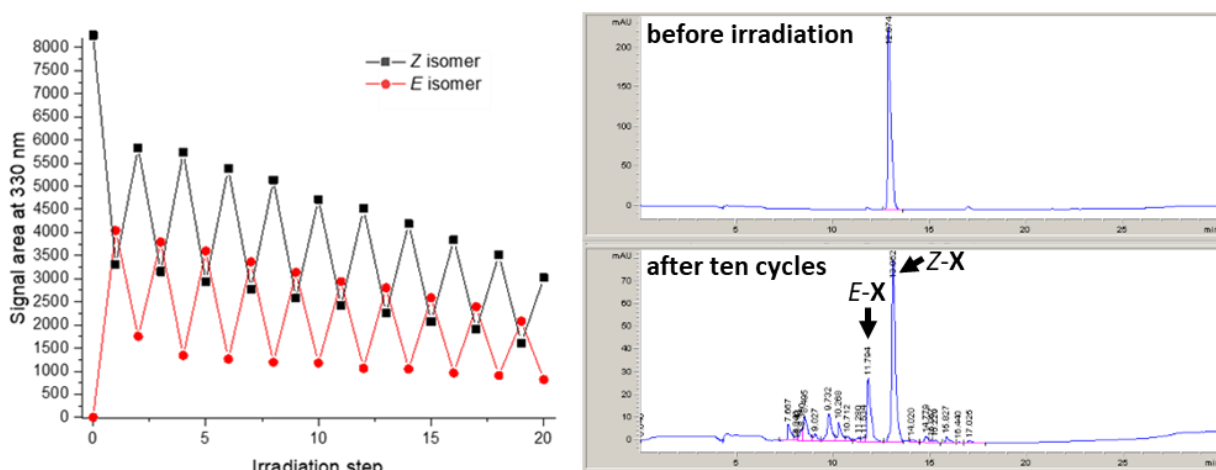
**Figure 22:** Photodegradation of plinabulin (**6**) in ten subsequent switching cycles. a) A solution of pure *Z*-**6** (1.0 mM) in DMSO was analyzed *via* analytical HPLC. The sample was first irradiated with 407 nm for 2 min, followed by with 490 nm for 35 min, respectively. The irradiation cycles were performed ten times and after every irradiation step the solution was analyzed *via* analytical HPLC, b) Two of the corresponding HPLC traces - before irradiation (top right) and after completing ten switching cycles (bottom right) - are depicted.

It was observed that the integrals of the signals assigned to both, the *E*- and the *Z*-isomer of plinabulin (**6**), continuously decrease with progressing irradiation time. After 20 irradiation steps, over ten additional signals besides those assigned to the photoisomers of plinabulin (**6**) were detected in the HPLC trace. This indicates a formation of multiple degradation products in reactions with low specificity and prevents the identification of a predominant degradation pathway. To investigate the influence of oxygen on the degradation, a 40 µM solution of plinabulin (**6**) in DMSO was split into three separate samples: Whereas one sample was kept under ambient atmosphere, the other two were purged for five minutes with gases, one sample with oxygen and the other with argon. Subsequently, absorption spectra of these samples were measured before and after irradiation with first 490 nm, followed by 407 nm (Figure 23).
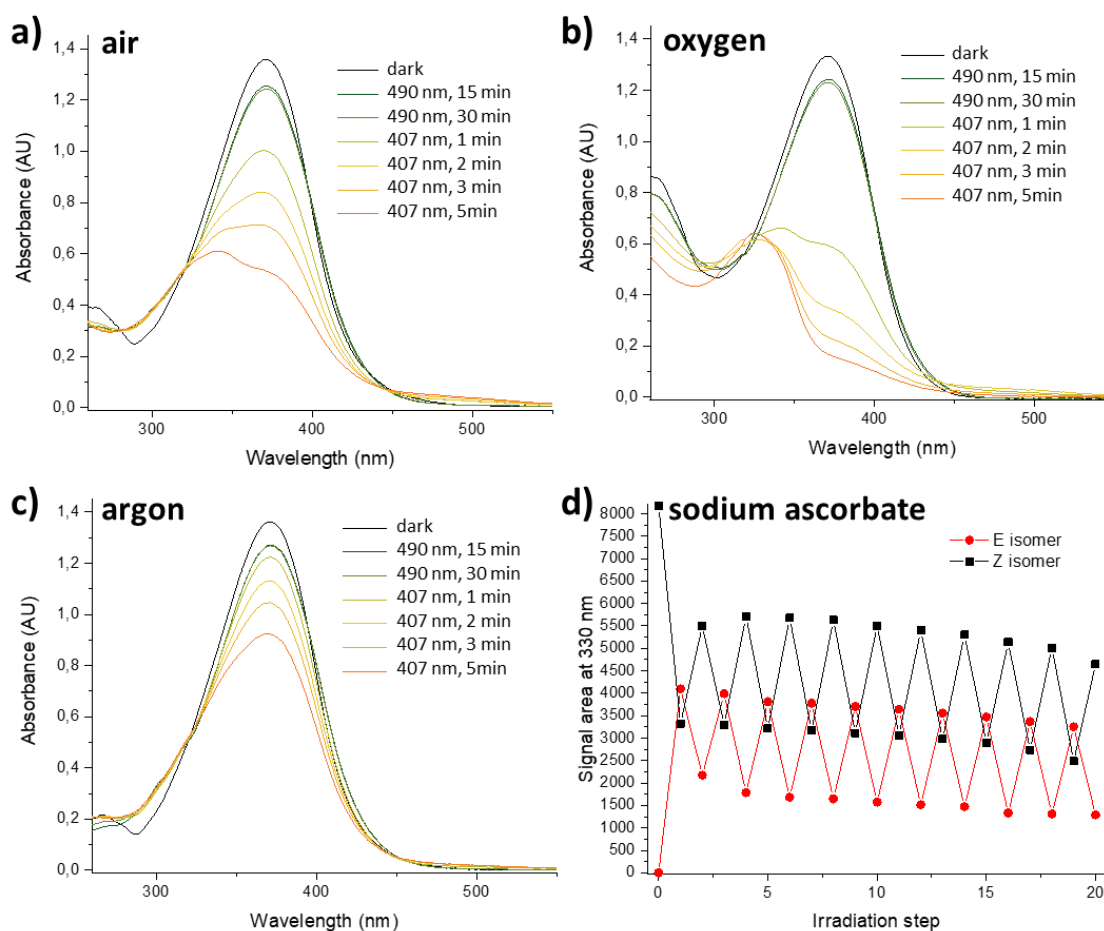
**Figure 23:** The photodegradation is promoted by oxygen and can be significantly reduced by the addition of the reactive oxygen species (ROS) quenchers, like sodium ascorbate. a)-c) A 40 µM solution of **6** in DMSO was prepared and split up into three samples. One sample a) was kept under ambient atmosphere, the other samples were purged for 5 min with b) oxygen or c) argon, respectively. Afterwards, the samples were first irradiated twice for 15 min with 490 nm and subsequently five times for 1 min with 407 nm. Absorption spectra were first recorded in the dark and then after each irradiation step. d) A solution of pure Z-**6** (1.0 mM) in a saturated solution of sodium ascorbate in DMSO was analyzed *via* analytical HPLC. The sample was irradiated with 407 nm for 2 min and with 490 nm for 35 min, respectively. The irradiation cycles were repeated ten times and after every irradiation step the solution was analyzed *via* analytical HPLC.

It was observed that irradiation with cyan light (490 nm) leads to a change in the absorption spectra, while doubling the irradiation time from 15 min to 30 min does not lead to further significant changes. Two isosbestic points are visible and it can be concluded that the PSS is reached after 15 min irradiation time and no photodegradation is detected. Subsequent irradiation with violet light (407 nm) induces changes in the absorption spectra of all three samples. Notably, already after 1 min irradiation time the spectra do not intersect at the isosbestic point anymore and further irradiation leads to a continuous decrease in the absorption maxima. This decrease in absorbance presumably correlates with progressing photodegradation. The enrichment of oxygen accelerates this process, while the degradation of the sample purged with argon is decelerated, which clearly indicates that the photoinduced degradation of plinabulin (**6**) is promoted by oxygen.

Therefore, it was concluded that the degradation products result from unspecific reactions with reactive oxygen species (ROS) formed upon irradiation. Consequently, sodium ascorbate – a known quencher of ROS[124] – was added to a sample to suppress the degradation process. It was found that this additive significantly slows down the decrease of the integrals of the signals assigned to both, the *E*- and the *Z*-isomer, when performing photoswitching cycles with indicates that it successfully reduces the amount of degradation (Figure 23).

The hypothesis of photodegradation caused by reaction with ROS is also supported by the known instability of natural products like guanosine or histidine against singlet oxygen. It has been reported by several groups that singlet oxygen attacks these compounds on the imidazole moiety and it is presumed that photooxidation of histidine is caused by singlet oxygen attacking the imidazole ring.[125,126] Furthermore, in this work it was observed that irradiation of the carbocyclic HPI **29** – a synthetic intermediate of plinabulin (**6**) without the imidazole substituent – does not lead to photodegradation. Ten switching cycles were performed without any additive, monitored *via* analytical HPLC and no decrease of the areas of the signals assigned to the two photoisomers and no formation of any additional signals was observed (Figure 24).
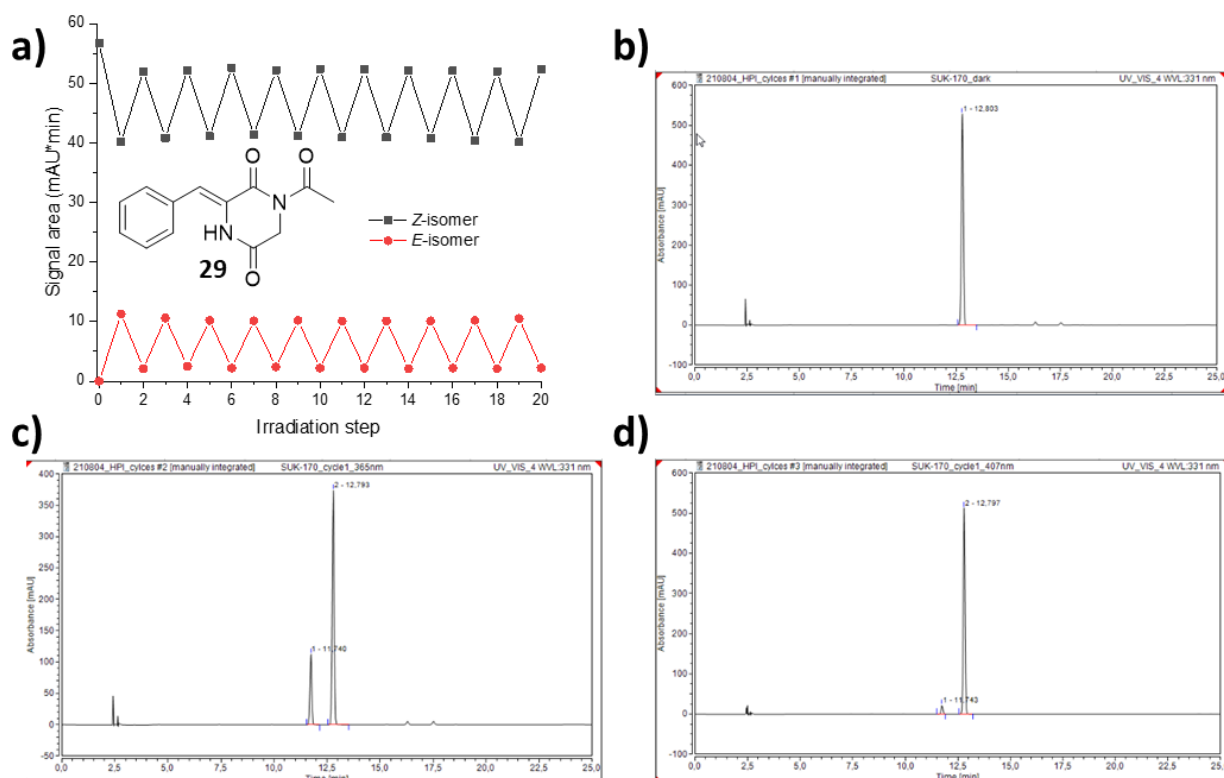


**Figure 24:** Switching stability of the carbocyclic HPI **29**. A solution of pure *Z*-**29** in DMSO (1.0 mM) were alternately irradiated with 365 nm for 2 min, followed by 407 nm for 10 min. a) After every irradiation step the solutions were analyzed *via* analytical HPLC. The corresponding HPLC traces b) before irradiation, c) after irradiation with 365 nm, and d) after irradiation with 407 nm are depicted.

Absorption spectra of PSSs of plinabulin (**6**) were recorded in presence of the ROS quencher sodium ascorbate (Figure 25 a), or alternatively in presence of the reducing agents glutathione and tris(2-carboxyethyl)phospine (TCEP) (Figure 25 b). The observed photoswitchablility of plinabulin (**6**) in presence of these reducing agents is an enormous benefit compared to azobenzene-based photopharmacophores known to be prone to degradation under intracellular reducing conditions.[38] Plinabulin (**6**) however, is stable in presence of a mixture of reduced glutathione (10 mM) with TCEP (5 mM) without any detectable degradation for 14 hours at 37 °C (see chapter 5.4.11).
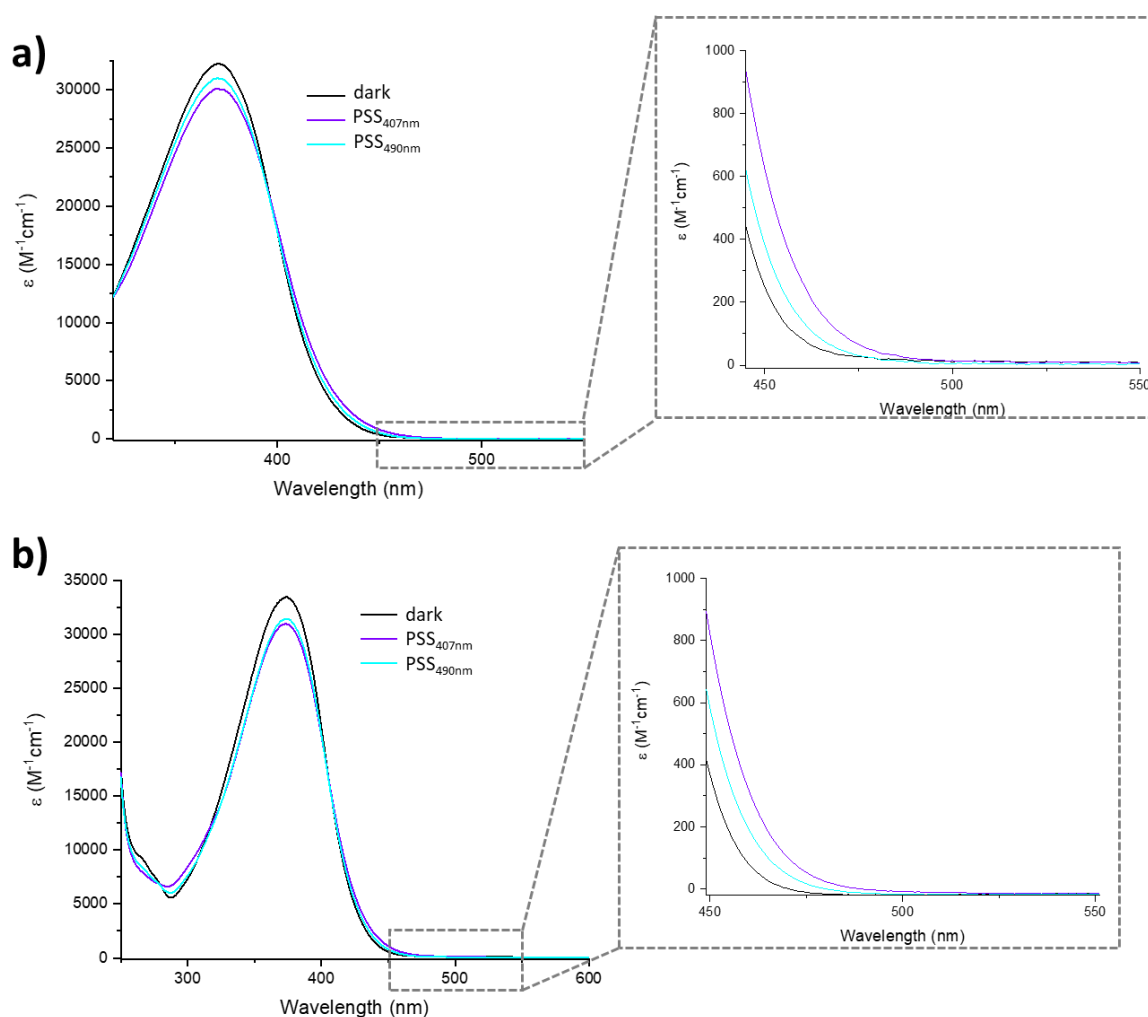


**Figure 25:** Absorption spectra of plinabulin (**6**) before and after irradiation in a) saturated solution of sodium ascorbate in DMSO and b) in 25% PBS in DMSO with 10 mM glutathione and 5.0 mM tris(2-carboxyethyl)phospine (TCEP).

The relatively small differences between the absorption spectra of plinabulin (**6**) before and after irradiation reveal a comparably low band separation between the two photoisomers. The spectrum obtained after irradiation with 407 nm corresponds to over 50% *E*-isomer, yet there is no noticeable shift in the absorption maximum. The observed differences in the extinction coefficients

in the absorption spectra caused by photoisomerization correlate with the composition of the photostationary states determined *via* NMR spectroscopy. The spectra intersect in an isosbestic point at 401 nm. At wavelengths in the range of 365 nm to 410 nm, a higher extinction coefficient was determined for the *Z*-isomer whereas above 401 nm the absorption coefficient of the *E*-isomer was found to be higher. This is a possible explanation for the effective *E*-to-*Z*-isomerization upon irradiation with cyan light.

It was additionally observed that solutions of plinabulin (**6**) exhibited isomer-dependent moderate yellow fluorescence emission. Compared to the *Z*-isomer (*Z*-**6**) the emission spectrum of *E*-plinabulin (*E*-**6**) is shifted bathochromically by 21 nm and the fluorescence quantum yield is lowered ( $\Phi_F(Z\text{-}\mathbf{6}) = 4.5\%$, $\Phi_F(E\text{-}\mathbf{6}) = 2.0\%$ ).

During the characterization of both photoisomers of plinabulin (**6**) under ambient conditions no significant thermal *E*-to-*Z*-isomerization was observed for at least one day. Therefore, the thermal stability was first investigated at 60 °C in MeCN (Figure 26) by monitoring a solution of *E*-plinabulin (*E*-**6**) *via* analytical HPLC. It was found that even at this elevated temperature less than 5% *E*-plinabulin (*E*-**6**) had been thermally relaxed after 25 hours.
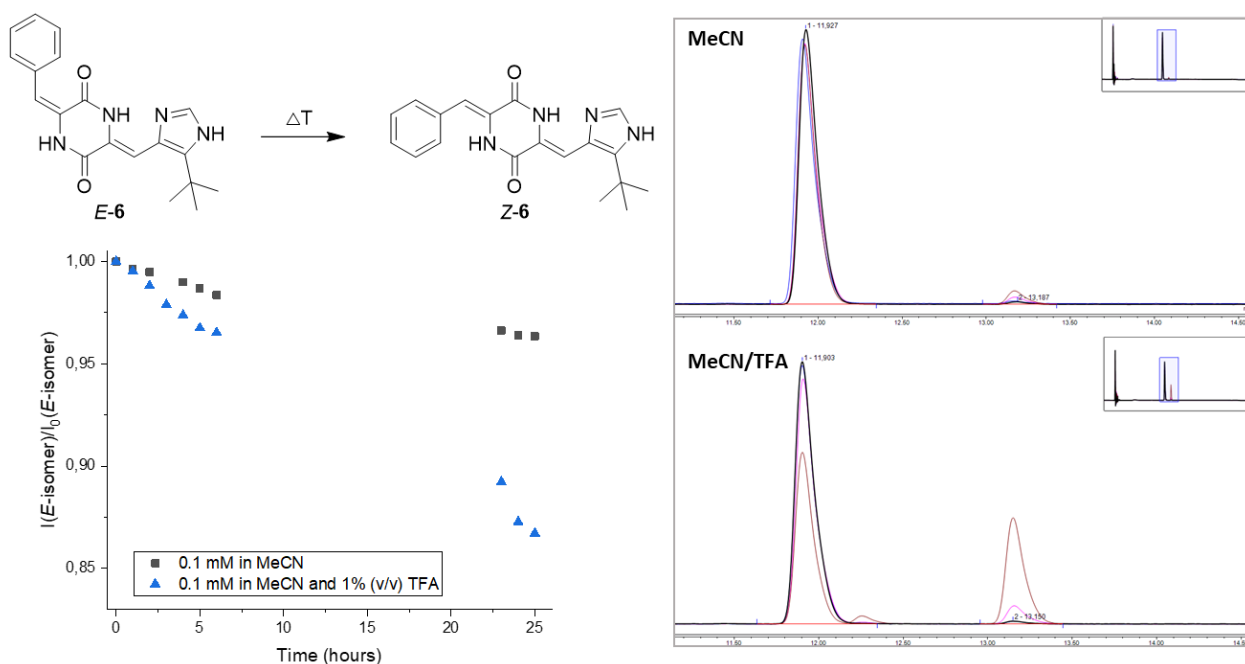


**Figure 26:** The thermal relaxation of *E*-plinabulin (*E*-**6**) in MeCN at 60 °C in absence and presence of TFA was monitored *via* analytical HPLC, respectively. The integrals of the signals assigned to the respective *E*-isomer were determined at 330 nm: $I_0$ = initial integral area, I = integral area at given point in time. A comparison of the overlays of the HPLC traces collected for the sample with TFA (bottom right) and without (top right) clearly demonstrate an accelerated backisomerization in an acidic medium.

Additionally, the thermal relaxation of the protonated species was followed by repeating the experiment with an acidified sample (1% (v/v) of TFA in MeCN). It was found that protonation significantly reduces the lifetime of *E*-plinabulin (**6**) and almost 15% of *E*-**6** was thermally isomerized to the *Z*-isomer after 25 hours. In preparation for biological assays, samples were dissolved in DMSO and – if needed – irradiated. It was found that these samples could be stored in a freezer for over two months without significant changes in the photoisomer composition.

After the photophysical properties had been successfully assessed, the cytotoxicity of both photoisomers was investigated by performing cell viability MTT assays against HT-29 human colon cancer cells with the isolated photoisomers in the dark. The results shown in Figure 27 clearly demonstrate that the geometry changes upon photoisomerization affect bioactivity and an >300-fold enhanced potency of the *Z*-isomer was determined ($IC_{50}$(*Z*-**6**) = 0.3 nM, vs. $IC_{50}$(*E*-**6**) = 92 nM). In summary, these results demonstrate the successful photomodulation of bioactivity by applying plinabulin (**6**) as a photopharmacological agent. The high thermal stability of the less active *E*-isomer allows for isolation and storage. It can be considered as a prodrug and photoactivation of *E*-plinabulin (*E*-**6**) by irradiation with cyan light (490 nm) gives a mixture with 87% *Z*-plinabulin (*Z*-**6**) with a 20-fold higher cytotoxicity against HT-29 cells.
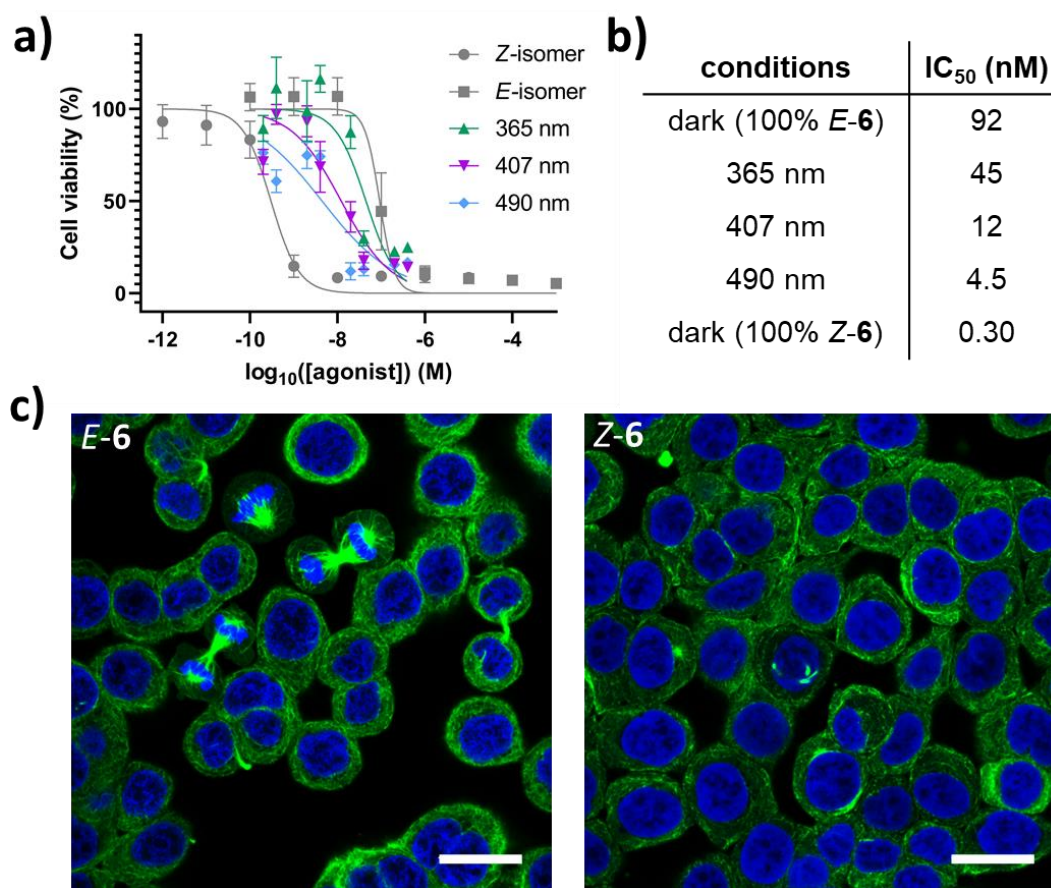
**Figure 27:** Photomodulation of the bioactivity of plinabulin (**6**). a) Viability of HT-29 cells after treatment with the HPLC-purified *Z-* and *E*-isomers of plinabulin (**6**) and with the respective mixtures of the isomers generated upon equilibration under 490 nm irradiation (cyan light), 407 nm (violet light) or 365 nm (UV-light) for 48 hours, b) Light-dependent $IC_{50}$ values for plinabulin (**6**) were determined *via* viability assays with HT-29 cells after treatment with the respective pure photoisomers and mixtures that resulted from irradiation with the listed wavelengths, c) HT-29 cells were treated for six hours with *E-* (left) or *Z*-plinabulin (right) at 2 nM concentrations, then fixed, and stained for α-tubulin (green) and DNA (blue). Scale bars, 20 µm.

Photoisomer dependent inhibition of microtubule dynamics was confirmed by immunofluorescence imaging of endogenous tubulin. HT-29 cells were treated separately with the same concentration of *E-* and *Z*-plinabulin (**6**) (2nM) and incubated for 6 hours. After six hours incubation time the microtubule networks were visualized *via* immunostaining. As expected, significant differences were observed because the applied concentration lies in between the respective $IC_{50}$ values of the two photoisomers. No cell proliferation was detected after treatment with *Z*-plinabulin (*Z*-**6**) whereas mitosis was proceeding in the sample treated with the same concentration of *E*-plinabulin (*E*-**6**) (Figure 27 c). This difference in activity supports that the potency of plinabulin (**6**) as an inhibitor of tubulin polymerization can be tuned by photoisomerization.

It was noticed that there was a reproducible discrepancy between the $IC_{50}$ value obtained for *Z*-plinabulin (**6**) (0.30 nM) and the $IC_{50}$ reported in literature (15 nM)[100] for the same cell type. To investigate this, a sample of the more active *Z*-isomer was – contrary to the usual procedure – not protected from daylight exposure one day before as well as during the viability assay. It was found that during this time 15% of the less active *E*-isomer had been formed and that this led to a decrease in activity ($IC_{50}$ = 1.08 nM, see also chapter 5.4.12). It was additionally observed that prolonged exposure to daylight resulted in an equilibrium containing 32% *E*-isomer in the sample mixture. These results support the assumption that the higher values reported in literature resulted from unintentional exposure to daylight before or while performing viability assays.

In summary, it was discovered that plinabulin (**6**) was a novel photoswitchable microtubule targeting agent. In contrast to previously reported compounds presented in chapter 1.3.3, it has not been synthetically modified, which in turn preserves its' potency completely. It can be reversibly photoisomerized within the visible light spectrum (by alternating 407 nm and 490 nm irradiation) and contrary to many azobenzene-based photopharmacological agents it is stable under reducing conditions. The photophysical properties are compatible with fixed wavelengths of lasers commonly applied in confocal microscopy. Violet (405 nm) and cyan (488 nm) light are expected to enable *in situ* photomodulation while light frequencies of the green (561 nm) and the red (642 nm) channel are not absorbed and can be applied for parallel imaging without affecting the photoswitchable compound.

### 3.1.4 Investigation of Plinabulin Derivatives 7-28

After having thoroughly investigated the characteristics of plinabulin (**6**), the identification of structural features that enable tuning the photophysical and/or the photopharmacological properties was pursued. Three main characteristics were aspired for enhancing applicability of the plinabulin (**6**) photopharmacophore: a bathochromic shift in the absorption spectrum – to enable photoswitching with green or even red light that enable deeper penetration of soft human tissues, a larger band separation between the two photoisomers to enable better photoconversions, and an increased difference in potency between the two photoisomers that would enlarge the therapeutic window.

A library of plinabulin analogues bearing various functional groups on the phenyl ring or heteroaromatic substituents instead of the phenyl ring were synthesized and characterized (see chapter 0, Figure 11).

First, various substituents were introduced in *ortho* position of the phenyl ring. This position was chosen for two reasons: many *ortho*-modifications are not detrimental for plinabulin (**6**) activity[100], and *ortho*-modifications of azobenzenes are known for substantial bathochromic shift combined with high thermal stability. Yet, the absorption spectra of *ortho*-substituted plinabulin derivatives are very similar to the original plinabulin (**6**). In that instance, they resemble much closer hemithioindigo switches.[127] The absorption maxima in MeCN are presented in Table 1 and differ only by a few nanometers, compared to plinabulin (**6**) and neither of them absorbs green light (> 500 nm). Thus, no substantial bathochromic shift in the absorption spectra was observed.

**Table 1:** Comparison of the absorption maximum of plinabulin (**6**) with those of derivatives **7**-**13** bearing functional groups in *ortho* position of the phenyl ring.

| **Compound** | **6** | **7** | **8** | **10** | **11** | **12** | **13** |
|---|---|---|---|---|---|---|---|
| $\lambda_{abs,max}$ **(MeCN)** | 362 | 351 | 362 | 358 | 358 | 359 | 366 |

The bioactivities of the respective photoisomers were – analogous to plinabulin (**6**) – evaluated in cell viability assays against HT-29 cells. For all *ortho* substituted derivatives a similar or lower potency of the *E*-isomers compared to the corresponding *Z*-isomers was assessed. A significant loss in potency of both photoisomers was observed for compounds bearing more bulky substituents (see chapter 5.4.12). It can be assumed that these substituents lead to steric repulsion in the

colchicine binding pocket and prevent efficient binding.[100] $Z$-2,6-Difluoroplinabulin **8**, however, showed an activity similar to that of $Z$-plinabulin ($IC_{50}(Z$-**8**$) = 0.27$ nM) and a 1555-fold difference in potency between the two photoisomers, which is considerably higher than for plinabulin (306-fold). As shown in Figure 28, irradiation of the isolated metastable $E$-**8** with cyan light (490 nm) gives a mixture containing 44% of $Z$-**8** and leads to a 107-fold enhanced potency. Unfortunately, a very low band separation between the two photoisomers of **8** results in negligible $E$/$Z$-isomer ratio differences upon irradiation with different wavelengths (maximal difference between 64% $E$-**8** at 380 nm and 56% $E$-**8** at 490 nm). Hence, efficient therapeutically conceivable photoactivation of $E$-2,6-difluoroplinabulin **8** is possible with cyan light, but practically irreversible.
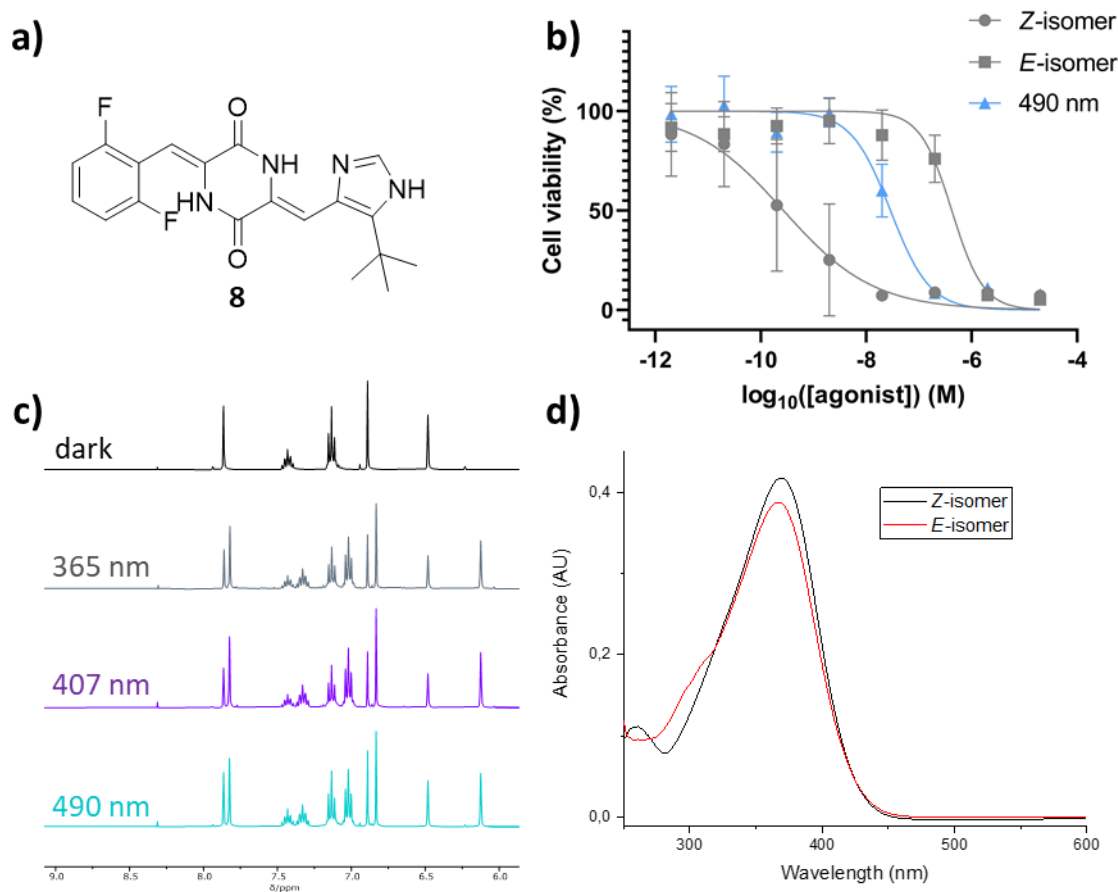


**Figure 28:** Photomodulation of bioactivity of $Z$-2,6-difluoroplinabulin **8**. a) After synthesis in the dark the thermodynamically more stable $Z$-**8** is obtained, b) Cell viability assays against HT-29 cells showed a 1555-fold higher potency of $Z$-**8** compared to $E$-**8** and a 107-fold enhanced potency after irradiation of $E$-**8** with cyan light (490 nm), c) The compositions of the photostationary states were determined by NMR spectroscopy and revealed a low difference between the applied wavelengths, d) The low band separation between the two photoisomers of **8** becomes apparent when comparing the corresponding absorption spectra.

An alternative substitution pattern was investigated by synthesizing and characterizing $Z$-2,5-difluoroplinabulin **8**. It was found that moving one fluorine substituent from *ortho* to *meta* position

leads to an overall loss in potency (IC$_{50}$(Z-**9**) = 5.47 nM) and a lower difference between the two photoisomers (13.8-fold). Consequently, even quantitative photoisomerization would not allow for improved photomodulation of bioactivity. In that case, significant reversible photoisomerization has been observed with alternating 407 and 490 nm irradiation with UV-Vis spectroscopy, but the exact composition of the respective photostationary states remains to be determined.

In contrast to its fluorinated analogue, 2,6-dichloroplinabulin **10** can be reversibly photoisomerized with significant differences in the *E*/*Z*-isomer ratios (62% *E*-**10** at 365 nm; 13% *E*-**10** at 490 nm). However, it is significantly less potent overall and a much lower difference in potency (27.5-fold) between the isolated photoisomers was determined.

As mentioned before, for the derivatives **11**-**13**, bearing more bulky substituents, the potency loss was even more significant (IC$_{50}$ >1 μM) and therefore they were not considered for further investigations as candidates for optimized plinabulin (**6**) analogues.

Considerable bathochromic shifts of the absorption spectra up to 62 nm were determined when electron-donating amino substituents (compounds **16**, **17** and **18**; Figure 29 and Figure 30) were introduced in *para* position of the phenyl ring. This effect was even more pronounced for the julolidine-bearing derivative **18**. The latter substituent was also embedded into the structure of hemithioindigo photoswitches with similar consequences (see Figure 29 a) and Table 2).[45,60] In contrast to plinabulin (**6**), all three compounds absorb green light (> 500 nm) and in case of *para*-(*N*,*N*-dimethylamino)-plinabulin (*p*-NMe$_2$-plinabulin) **16** irradiation with 523 nm yields 90 % *Z*-isomer. The corresponding NMR and absorbance spectra are shown in Figure 29.
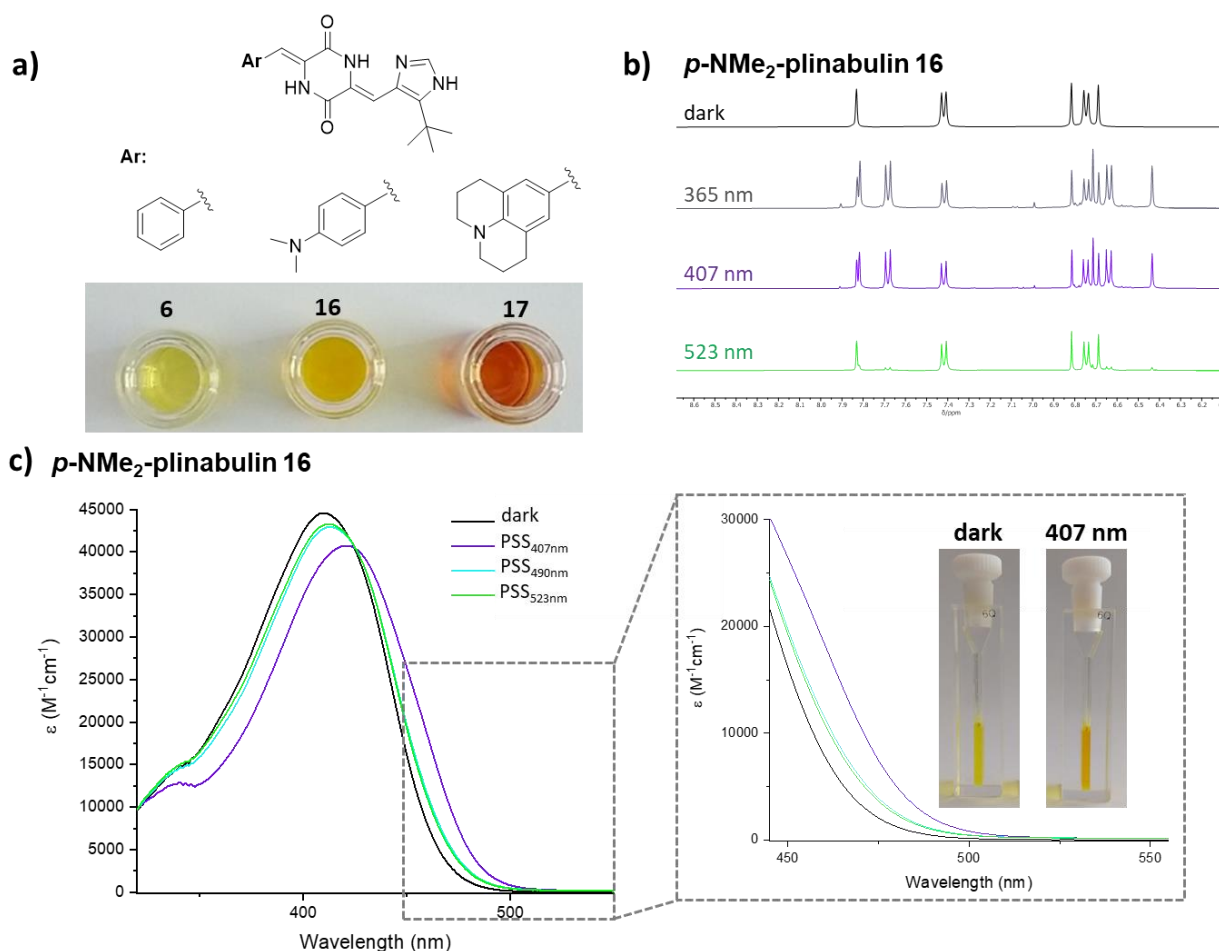
**Figure 29:** a) Electron-donating substituents in *para* position of plinabulin (**6**) lead to a distinctive bathochromic shift in the absorption spectra in DMSO visible with the bare eye, b) The bathochromic shift in the absorbance of **16** enables efficient photoisomerization with green light (523 nm). Photostationary states were characterized *via* $^1$H NMR spectroscopy in DMSO-$d_6$ (61% *E*-**16** at 365 nm; 55% *E*-**16** at 407 nm; 10% *E*-**16** at 523 nm), c) Absorption spectra of **16** a saturated solution of sodium ascorbate in DMSO (80 µM) reveal an enhanced band separation when compared to plinabulin (**6**). Irradiation of pure *Z*-**16** (dark) with violet light (407 nm) is accompanied by a visible change in color from yellow to orange.

It was furthermore observed that these electron-donating substituents lead to a bigger band separation, which is clearly visible in the absorption spectra as well as the pictures of *p*-NMe$_2$-plinabulin **16** in Figure 29 c and explains the efficient *E*-to-*Z*-isomerization with green light. While *p*-NMe$_2$-plinabulin **16** proved to be superior to plinabulin (**6**) in the aforementioned photophysical properties it does not meet requirements of an optimized photopharmacological agent due to a significantly shorter thermal half-life of the metastable stable *E*-isomer and – more importantly – an undesired pronounced loss in activity (also observed for compound **17**). The IC$_{50}$ values of *E*-**16** and *E*-**17** were not determined because the limited solubility in aqueous media prevented the application of the necessary, higher concentrations.

The derivatives bearing electron-donating amino substituents also include compound **18**, which comprises a planarized triphenylamine. The dimethylmethylene-bridges lead to an enhanced π-

conjugation and prevent twisting of the phenyl rings around the C–N bonds.[128] Besides the bathochromic shift, a significantly enhanced fluorescence quantum yield of 23.6% has been observed (Table 2).

**Table 2:** Electron-donating amino substituents lead to significant bathochromic shifts in absorption and emission spectra of the respective plinabulin (**6**) derivatives. Planarized triarylamine **18** additionally showed a strongly enhanced fluorescence intensity.

| Compound | 6 | 16 | 18 | 17 |
|---|---|---|---|---|
| $\lambda_{abs,max}$ **(MeCN)** | 362 nm | 400 nm | 413 nm | 424 nm |
| $\lambda_{em,max}$ **(MeCN)** | 512 nm | 534 nm | 554 nm | - |
| $\Phi_F$ **(MeCN)** | 4.5% | 2.7% | 23.6% | - |

Compared to plinabulin (**6**), the solvatochromism of **18** is slightly more pronounced with a maximal difference of 25 nm between the absorbance maxima (for plinabulin (**6**) 16 nm). A solvatochromic effect was additionally found to influence the fluorescence spectra considerably, causing a bathochromic shift in the emission maximum of 77 nm in MeOH when compared to the spectrum measured in tetrahydrofuran (THF) (Figure 30).
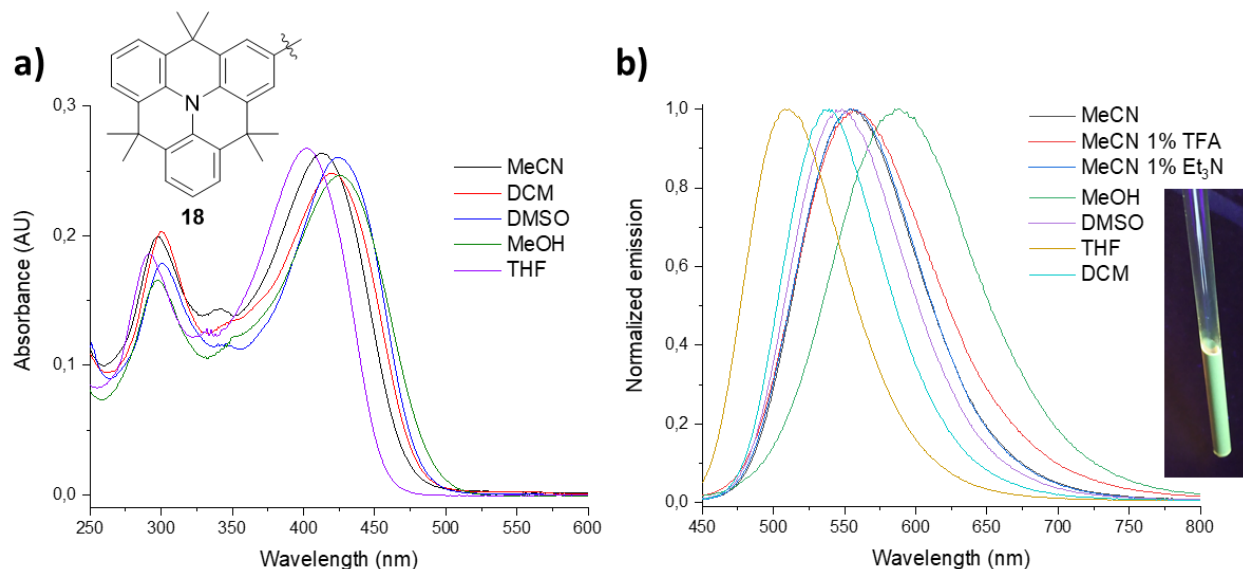


**Figure 30:** Photochromism of plinabulin derivative **18**. Compound *Z*-**18** was dissolved in different solvents (80 µM) and in mixtures of 1% (v/v) TFA in MeCN and 1% (v/v) Et₃N in MeCN, respectively. a) Absorption and b) emission spectra were measured (d = 2 mm). The spectra are assigned to the respective solvents *via* color code.

Eventually, two derivatives – 3-methoxyplinabulin **14** and 3,5-dimethoxyplinabulin **15** – with superior pharmacological properties were identified. The potencies of respective *Z*-isomers are similar but those of the *E*-isomers are significantly reduced compared to *E*-plinabulin (*E*-**6**). Since absorption spectra and band separation are also comparable to those of plinabulin (**6**) reversible

photoswitching is possible within the visible light spectrum. Consequently, the achievable photomodulation of bioactivity is considerably enhanced.

For 3,5-dimethoxyplinabulin **15** an over 2900-fold difference in potency between the two photoisomers was determined (Figure 31). The less active, metastable *E*-**15** was found to be stable in aqueous medium at 37 °C for at least 32 hours without any detectable thermal backisomerization. Photoactivation of cytotoxicity was demonstrated in cell viability assays. Irradiation of the less active *E*-**15** (IC$_{50}$ = 618 nm) with cyan light (490 nm) yields an over 1800-fold more potent mixture that contains 89% *Z*-**15**. It was additionally confirmed that irradiation with violet light generates a mixture with over 50% *E*-**15** and an over 100-fold lower potency.
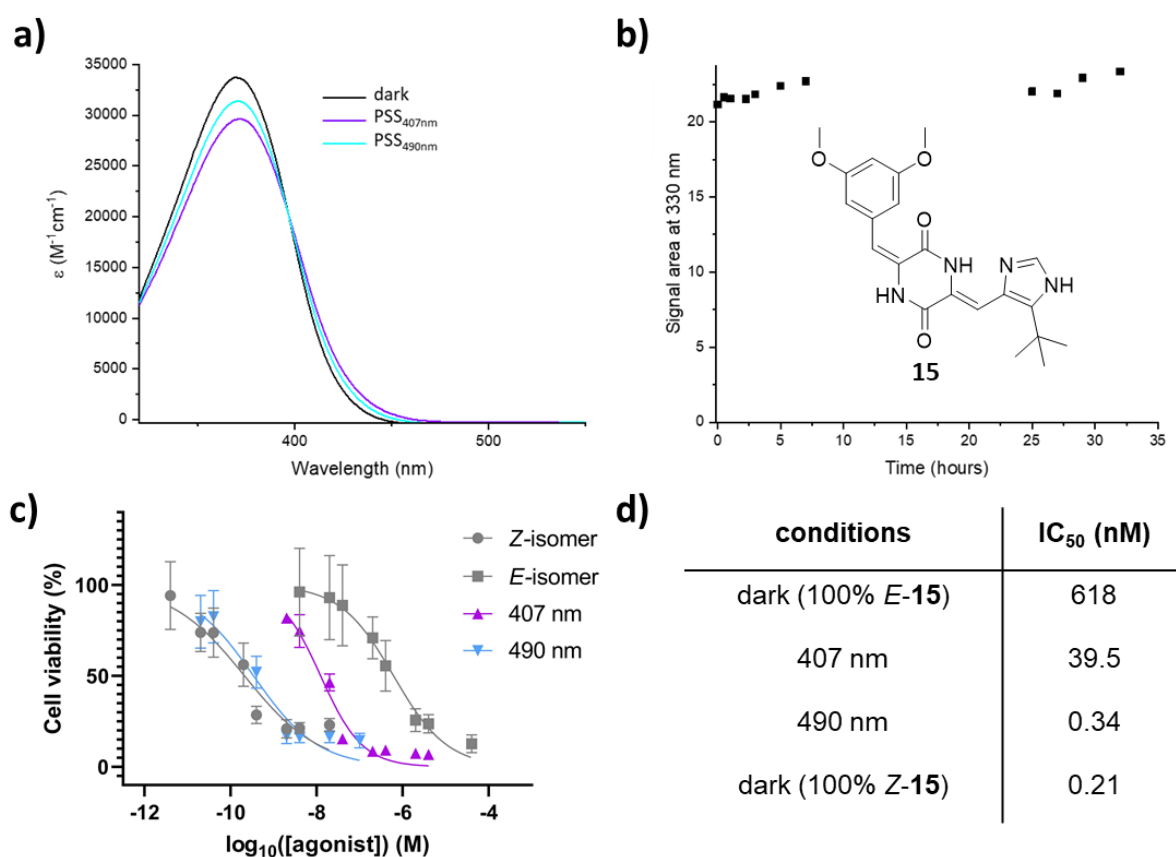


**Figure 31:** Characterization of 3,5-dimethoxyplinabulin **15** a) Compound **15** was dissolved in a saturated solution of sodium ascorbate in DMSO (80 µM). An absorption spectrum (d = 2 mm) was first measured in the dark. The sample was then first irradiated with 407 nm (2 min), then with 490 nm (15 min) and an absorption spectrum was measured after each irradiation step, b) Solutions of compounds *E*-**15** in PBS/DMSO (1:1) with a concentration of 33 µM were incubated at 37 °C for 32 hours. Samples were taken after certain time intervals and analyzed *via* analytical HPLC at 330 nm, c) Viability of HT-29 cells after treatment with the HPLC-purified *Z*- and *E*-isomers of **15** or with the respective mixtures of the *E*- and *Z*-isomers generated upon equilibration under 490 nm irradiation (cyan light) or 407 nm (violet light) for 48 hours, d) Light-dependent IC$_{50}$ values for **15** were determined *via* viability assays with HT-29 cells after treatment with the respective pure photoisomers or mixtures that resulted from irradiation with the listed wavelengths.

Further studies focused on design strategies towards plinabulin derivatives with bathochromically shifted absorption spectra with sufficient potency for photopharmacological applications. Because electron-donating groups in *para* position on the phenyl ring were found to lead to an almost complete loss in bioactivity, two alternative strategies were investigated: 1) Expanding the π-system, 2) replacing the phenyl ring with five-membered heterocycles. To ensure sufficient bioactivity the investigated compounds were selected from a previously reported library of compounds subjected to structure-activity-relationship studies by Yamazaki *et al.*.[100]

Three derivatives with an expanded π-system were synthesized and characterized (Figure 32). However, the pursued bathochromic shift in the absorption spectra was not observed. The absorbance maxima of these compounds vary only by 3 nm and all three compounds were not photoisomerizable with wavelengths above 500 nm. A stronger bathochromic shift of 14-36 nm was observed in the corresponding fluorescence spectra shown in Figure 32 ($\Phi_F$ of plinabulin (**6**) in DMSO = 521 nm).
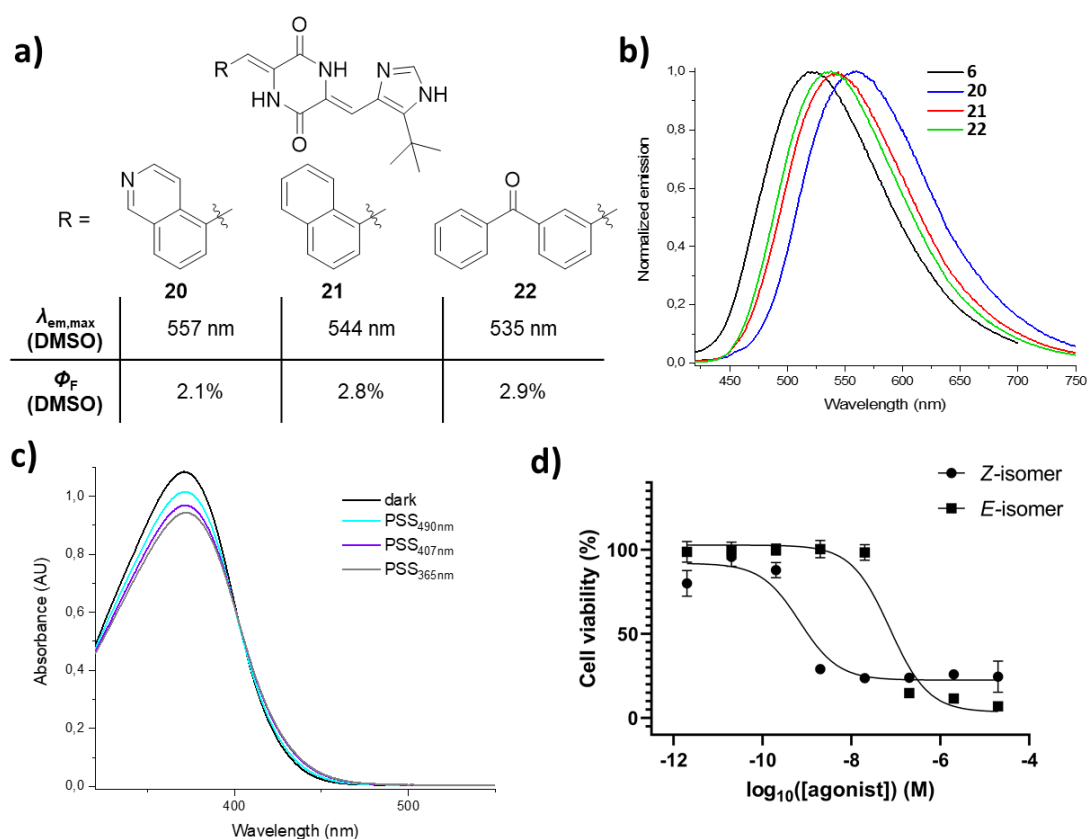


**Figure 32:** Characterization of plinabulin derivatives **20**-**22** with an expanded π-system. a), b) The emission maxima of the investigated compounds are shifted bathochromically compared to that of plinabulin (**6**) ($\Phi_F$ (DMSO) = 521 nm) with a slightly lower fluorescence quantum yield, c) Compound **22** was dissolved in a saturated solution of sodium ascorbate in DMSO (80 µM). An absorption spectrum (d = 2 mm) was first measured in the dark. The sample was then first irradiated with 407 nm (2 min), then with 490 nm (15 min) and an absorption spectrum was measured after each irradiation step, d) Viability of HT-29 cells after treatment with the HPLC-purified *Z*- and *E*-isomers of compound **22** for 48 hours.

When evaluating the cytotoxicity of both respective compounds *via* cell viability assays against HT-29 cells the best results were obtained for the benzophenone derivative **22**. In accordance with the literature, it was found to be highly potent in the *Z*-configuration (IC$_{50}$ = 0.68 nM) and a 108-fold difference in cytotoxicity between the two photoisomers was determined.

Following the second design strategy towards bathochromically shifted plinabulin derivatives, seven heterocyclic plinabulin derivatives were synthesized and investigated regarding their photophysical behavior. For five derivatives, bathochromically shifted absorbance maxima were determined with a maximal shift of 28 nm. However, the bathocromic shifts were lower than that of *p*-NMe$_2$-plinabulin **16** ($\lambda_{abs,max}$ (DMSO) = 410 nm) and none of these plinabulin analogues were photoswitchable with light above 500 nm (Table 3).

**Table 3:** Comparison of the absorption maximum of plinabulin (**6**) with those of analogues bearing a five-membered heterocyclic substituent.

| compound | 6 | 19 | 23 | 24 | 25 | 26 | 27 | 28 |
|---|---|---|---|---|---|---|---|---|
| $\lambda_{abs,max}$ (DMSO) | 371 nm | 369 nm | 374 nm | 398 nm | 399 nm | 368 nm | 387 nm | 387 nm |

When then phenyl ring in plinabulin (**6**) was replaced by 2-pyrrole or 2-thiophene substituents the most pronounced bathochromic shifts were determined. Additionally, the absorption spectra showed a larger band separation between the two respective photoisomers with the most pronounced separation for *N*-methyl-2-pyrrole-plinabulin **25** (Figure 33 a). This was found to enable almost quantitative *E*-to-*Z*-isomerization upon irradiation with cyan light (490 nm).
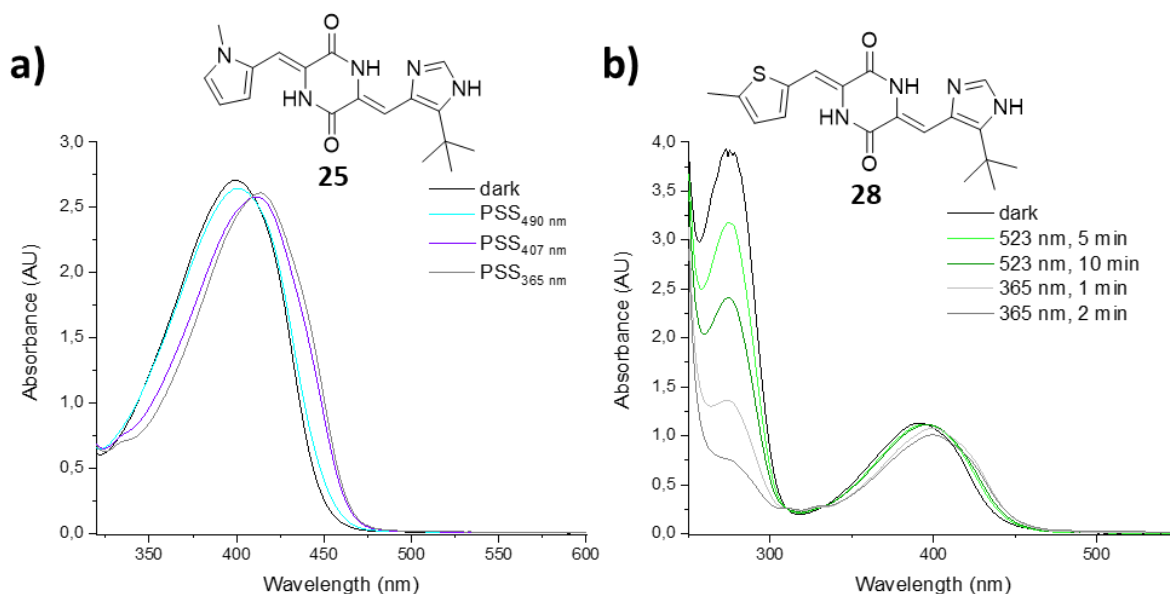
**Figure 33:** Absorption spectra of two plinabulin derivatives that contain a second five-membered heterocycle. a) *N*-Methyl-2-pyrrole-HPI **25** was dissolved in a saturated solution of sodium ascorbate in DMSO (81 µM) and purged with argon. An absorption spectrum (d = 10 mm) was first measured in the dark. The sample was then irradiated with 490 nm (15 min), 407 nm (2 min) and 365 nm (2 min) in succession and an absorption spectrum was measured after each irradiation step, b) 5-Methyl-2-thiophene-HPI **28** was dissolved in a saturated solution of sodium ascorbate in DMSO (160 µM). An absorption spectrum (d = 10 mm) was first measured in the dark. The sample was then first irradiated with 523 nm, then with 365 nm and an absorption spectrum was measured after each irradiation step. To demonstrate the photoinduced consumption of sodium ascorbate the spectra were not blanked to the solution of ascorbate.

However, an acceleration of the consumption of the added ROS quencher sodium ascorbate was observed when performing light-dependent absorption spectroscopy. This is clearly visible in the spectra of 5-methyl-2-thiophen **28** shown in the right panel in Figure 33. To demonstrate the continuous decrease of the absorption band of sodium ascorbate these spectra were not blanked to the solution of ascorbate. To obtain satisfactory spectra it was necessary to additionally purge the samples with argon before starting irradiation. It was concluded that the second heterocycle leads to an enhanced formation of singlet oxygen which is presumed to be the cause for photodegradation of plinabulin derivatives. Consequently, plinabulin derivatives bearing a second heterocycle were not considered for further investigations as candidates for optimized plinabulin analogues. Future studies should be started with investigations of the formation of singlet oxygen *via* colorimetric singlet oxygen detection assays, by monitoring the bicyclic ozonide formation from 2,5-diphenylfuran.[129,130]

After having investigated the whole library of compounds it was found that the thermal half-life, the composition of the photostationary states and the absorption spectra can be tuned by installing different substituents on the phenyl ring of plinabulin (**6**). 3,5-Dimethoxyplinabulin **15** was identified as a derivative with optimized photopharmacological characteristics allowing for efficient photomodulation of bioactivity.

## 3.2 Hemipiperazines: Model Compounds

3-Arylidene-2,5-diketopiperazines – abbreviated as hemipiperazines (HPIs) – are novel photoswitchable motifs first identified within the microtubule targeting compound plinabulin (**6**). To characterize this molecular photoswitch, the core photochromic fragment of plinabulin (**6**), which contains only one double bond and no heterocycle, was chosen to serve as a model system. A panel of derivatives were synthesized and characterized systematically to investigate the influence of electron-withdrawing and -donating groups on their photophysical properties.

### 3.2.1 Synthesis

A series of carbocyclic benzaldehyde derivatives were coupled with acetylated DKP **2** in aldol condensation reactions under basic conditions (Figure 34), also applied for the synthesis of the plinabulin derivatives discussed in the previous chapter. Usually, mild conditions were preferred and the reaction was performed with $Cs_2CO_3$ in DMF at room temperature. For the synthesis of compounds **36** and **38**, where electron-rich aldehydes are used, $Cs_2CO_3$ was replaced by the stronger base $KO^tBu$ in THF. In case of compound **38**, a Boc-protected aldehyde was subjected to the reaction and the protecting group was removed in a subsequent, additional reaction step (see chapter 5.5.1).
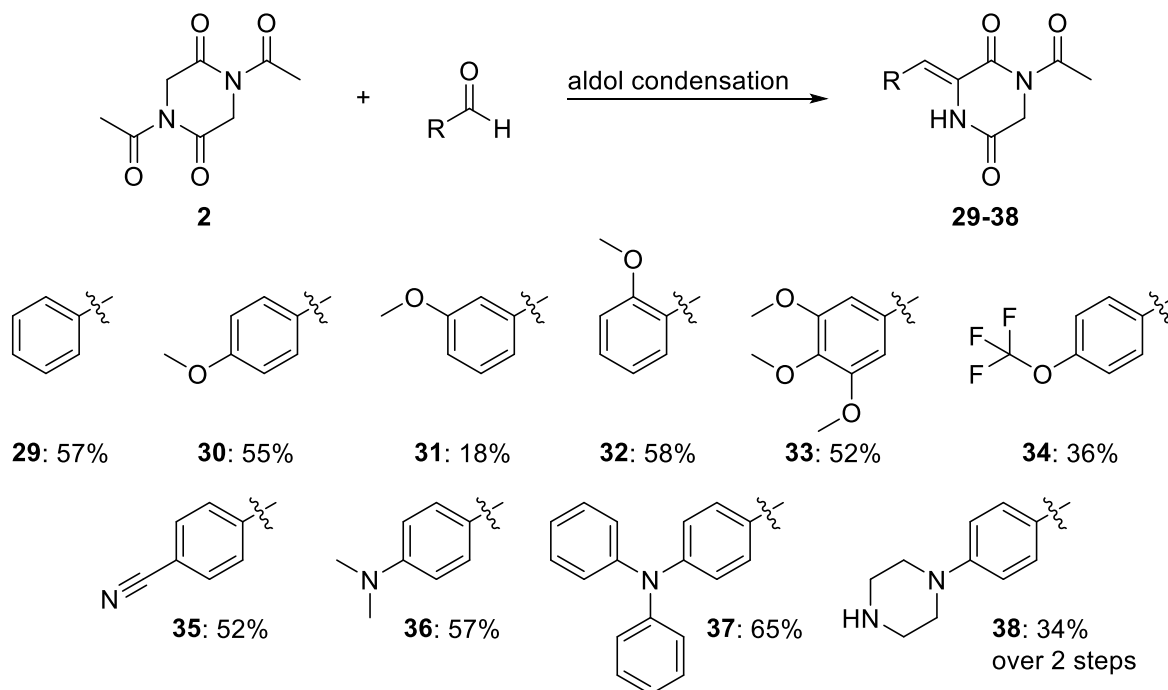


**Figure 34:** A library of HPIs was synthesized by coupling carbocyclic aldehydes with acetylated DKP **2** in a base aldol condensation reaction under basic conditions.

All compounds were isolated in the respective thermodynamically more stable Z-configuration, which was verified *via* NMR spectroscopy and for five derivatives additionally in single-crystal X-ray diffraction studies (Figure 35).
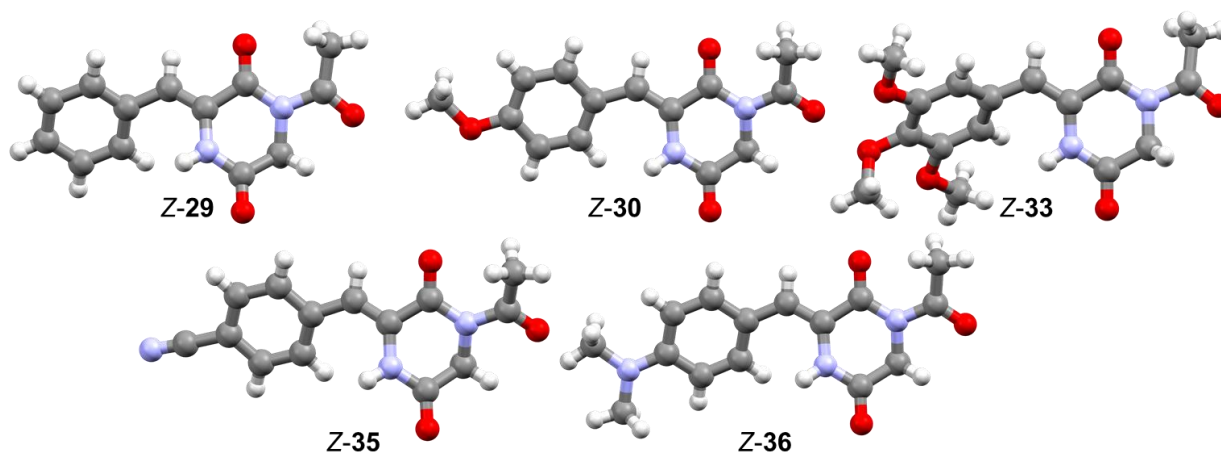


**Figure 35:** Single crystals of Z-**29**, Z-**30**, Z-**33**, Z-**35**, and Z-**36** were analyzed in single-crystal X-ray diffraction studies. The results were visualized with Mercury 2020.1 (CCDC). Additional atoms in the results of Z-**35** ($H_2O$) and Z-**29** (three additional crystallographic independent molecules, also in Z-configuration) were removed in this visual presentation. Atoms of carbon are depicted in grey, hydrogen in white, oxygen in red and nitrogen in blue.

### 3.2.2   Photophysical Properties

First, the absorption spectra of the respective Z-isomers in DMSO were compared. In general, most of the absorption spectra are shifted hypsochromically compared to those of the previously discussed plinabulin derivatives, which might be explained by a smaller expansion of the π-system due to the missing conjugation with the imidazole substituent. It was found that both, electron-withdrawing and electron-donating substituents in *para* position, cause a bathochromic shift relative to unsubstituted HPI **29** in the respective absorption spectra. The conjugated *ortho*-methoxy substituent (compound **32**, see resonance structures in Figure 36 b) also leads to a significantly bathochromically shifted absorbance maximum while the non-conjugated *meta*-substituted **31** only showed a slight bathochromic shift (Figure 36).
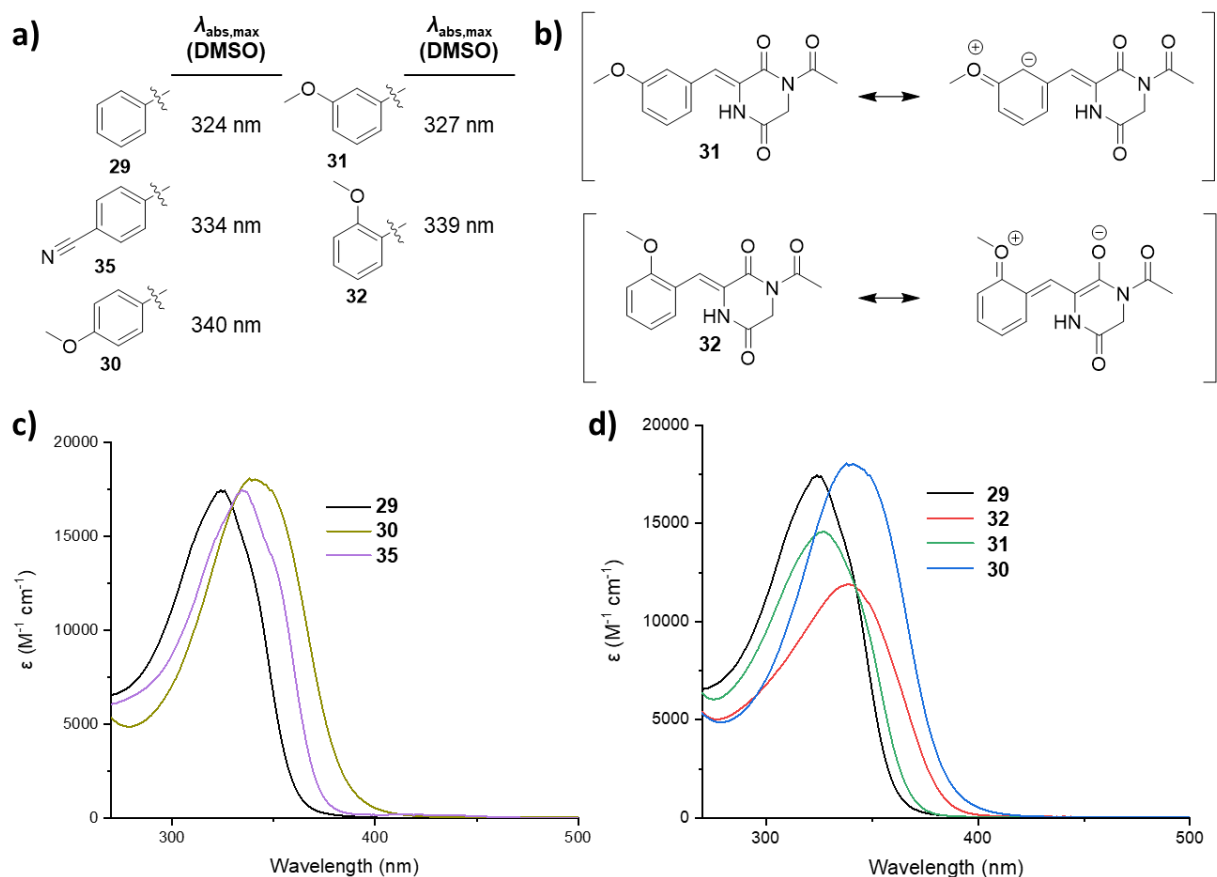
**Figure 36:** Installation of electron-withdrawing (compound **35**) and electron-donating (compounds **30**-**32**) substituents on the phenyl ring of carbocyclic aromatic HPI photoswitches causes a bathochromic shift in the absorbance spectra relative to unsubstituted HPI **29**. The respective *Z*-isomers were dissolved in DMSO (80 – 160 µM) and absorption spectra were measured in the dark. a) Absorbance maxima of compounds **29**-**32** and **35** on DMSO, b) A comparison of the resonance structures of HPIs **31** and **32** demonstrates that *ortho*-substituted **32** is additionally mesomerically stabilized, c) When comparing the same substitution pattern, the bathochromic shift of the absorbance maximum is generally more pronounced for electron-donating substituents (HPI **30**) than electron-donating substituents (HPI **35**), d) Comparison of the absorbance spectra in different substitution patterns of methoxy-substituted HPIs. The bathochromic shift is very low for non-conjugated *meta*-substituted **31** and most pronounced conjugated *para*-methoxy substituted **32**.

All the synthesized HPIs showed reversible photochromic behavior and for three compounds (**29**, **30** and **36**) the respective photoisomers were separated *via* flash column chromatography. Sections of the corresponding NOESY NMR spectra of **30** and **36** are shown in Figure 37 and important signals are assigned to the respective protons *via* color code. Analogous to the observations made for plinabulin derivatives, after *Z*-to-*E*-isomerization, the signals assigned to interactions of the NH proton with aromatic protons (highlighted in green) are replaced by signals that indicate close proximity of the NH proton to the vinylic proton. These results support again the light-triggered formation of the respective *E*-isomers.
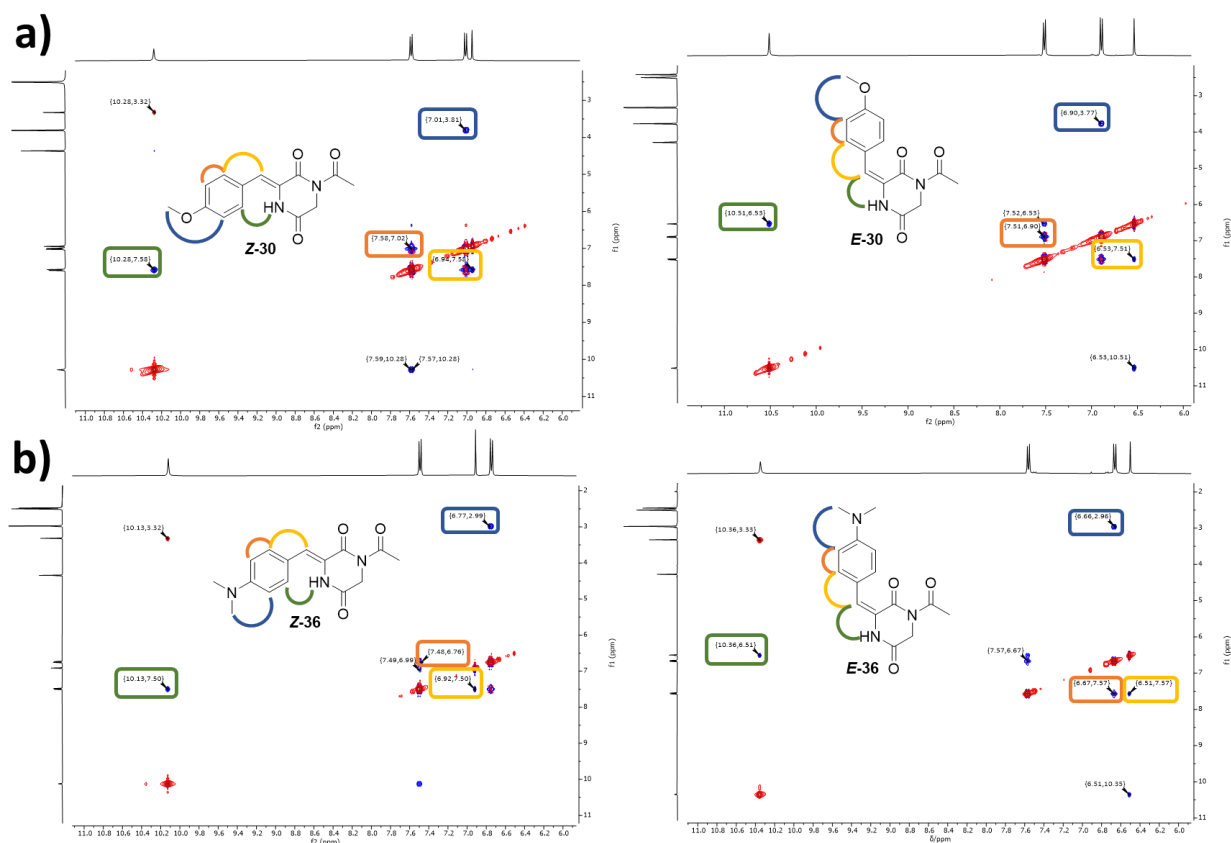
**Figure 37:** Sections of NOESY NMR spectra in DMSO-$d_6$ of the two respective photoisomers of a) **30** and b) **36**. Selected signals are assigned to the respective protons *via* color code.

All compounds were found to be photoswitchable and reversible photoisomerization without significant fatigue upon ten isomerization cycles was demonstrated (see e.g. Figure 38 and chapter 5.5.9). However, the photochromism of unsubstituted HPI **29** and the electron-poor cyano-substituted HPI **35** was low and irradiation with UV-light (365 nm) produced only 12% of *E*-**29** (in CD$_2$Cl$_2$) and 19% of *E*-**35** (in DMSO-$d_6$), respectively (Figure 38). However, it has to be noted that the absorbance maxima of these compounds could not be addressed with the available light-emitting diodes (LEDs) used for photoisomerization. Conceivably, irradiation with wavelengths in the range of 320 nm could result in the formation of higher amounts of the respective *Z*-isomers.
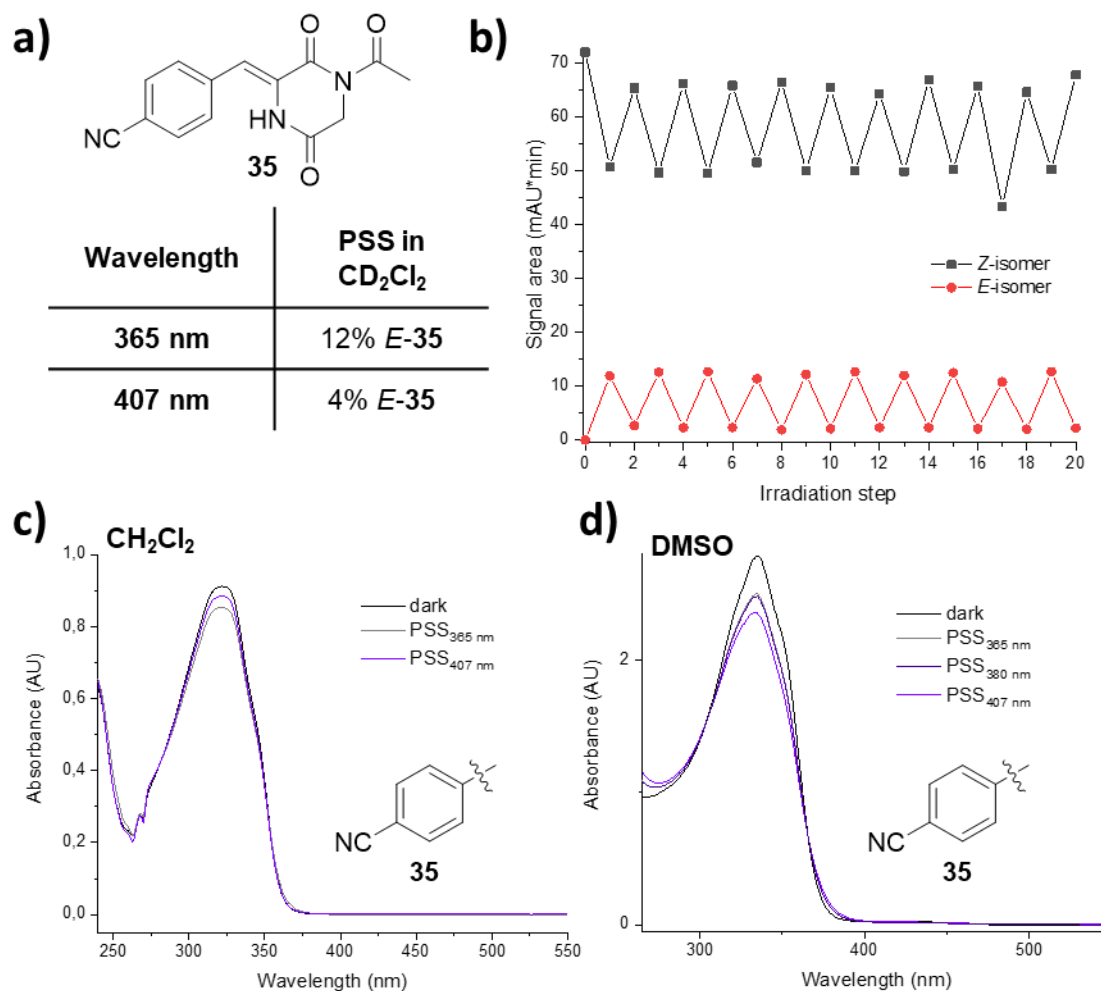
**Figure 38:** Reversible photoisomerization of electron-poor HPI **35**. a) PSS composition in $CD_2Cl_2$ determined by measuring $^1H$ NMR spectra of the respective compounds after irradiation. b) A solution of pure Z-**35** in DMSO (1.0 mM) was alternately irradiated with 365 nm for 4 min and with 430 nm for 45 min. After every irradiation step the solution was analyzed *via* analytical HPLC. c),d) Compound **35** was dissolved in $CH_2Cl_2$ (80 µM, c)) and DMSO (160 µM, d)), respectively. Absorption spectra (d = 10 mm) were first measured in the dark. The samples were then irradiated with 365 nm, 380 nm and 407 nm. An absorption spectrum was measured after each irradiation step until the PSS was reached, respectively.

Photoisomerization of *para*-methoxy substituted HPI **30** was investigated *via* absorption spectroscopy in $CH_2Cl_2$ and the compositions of the PSSs were determined *via* $^1H$ NMR spectroscopy in $CD_2Cl_2$ (Figure 39). Irradiation of this derivative with UV-light (365 nm) gave 29% of the corresponding *E*-isomer and irradiation with indigo light (430 nm) enabled quantitative backisomerization (<1% *E*-isomer). An interesting observation has been made when performing these measurements in DMSO. Here, a new isosbestic point at 410 nm occurred and the extinction coefficient of Z-**30** was found to be higher than that of *E*-**30** at wavelengths above this point. Whereas irradiation with light above 400 nm induced *E*-to-*Z*-isomerization in $CH_2Cl_2$, the reversed process was triggered when the compound was irradiated in DMSO. The progressing *Z*-to-*E*-

isomerization upon irradiation with blue light (470 nm) was followed by absorption spectroscopy (Figure 39). The photoisomerization process was relatively slow – presumably because of the low extinction coefficient at this wavelength – and the PSS was reached after one hour irradiation time.
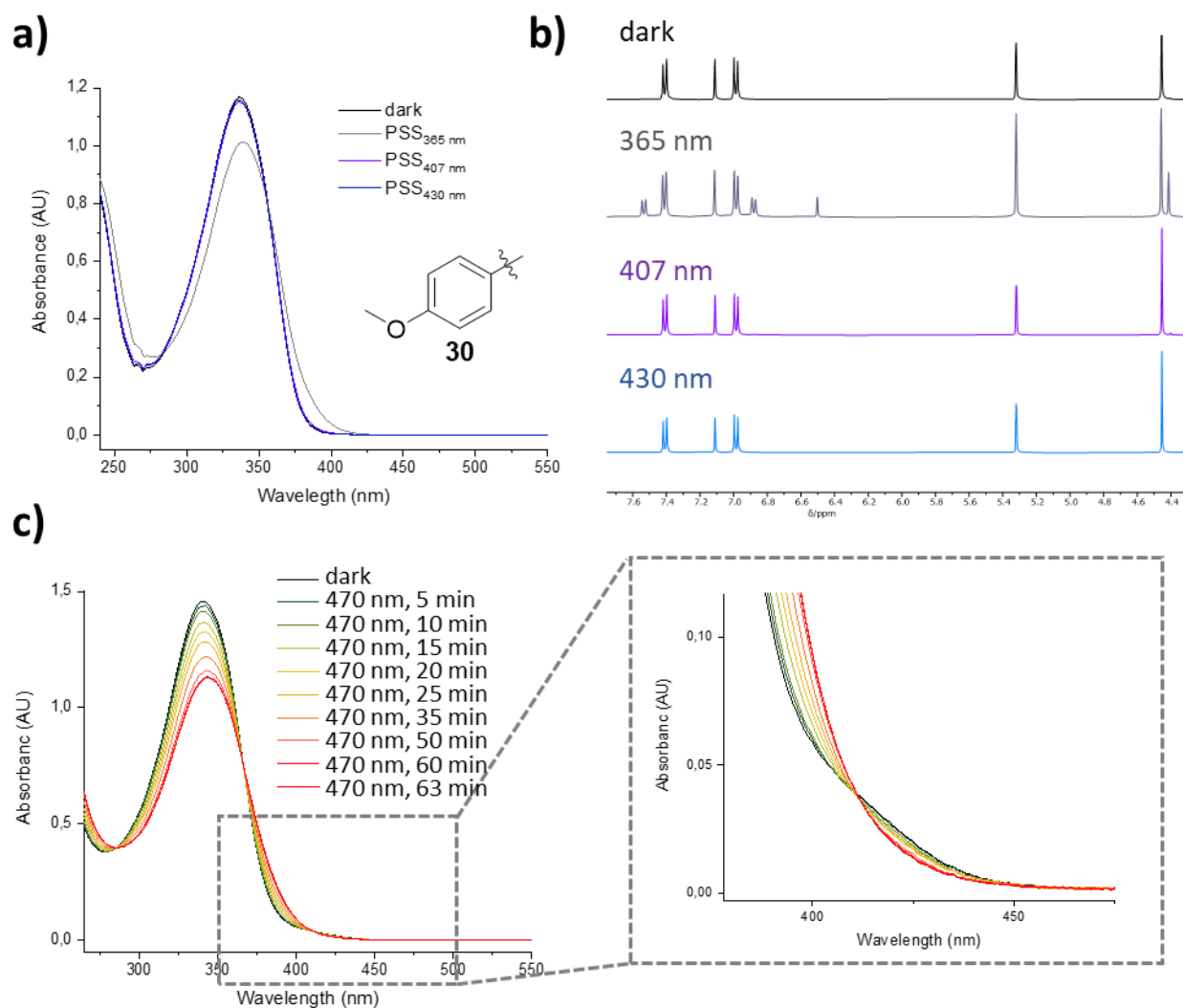


**Figure 39:** Photophysical properties of *para*-methoxy substituted HPI **30**. a) Compound **30** was dissolved in $CH_2Cl_2$ (80 µM) and an absorption spectrum (d = 10 mm) was measured. The sample was then irradiated with 365 nm, 407 nm and 430 nm and an absorption spectrum was measured after each irradiation step until the PSS was reached, respectively, b) Sections of $^1H$ NMR spectra of compound **30** in $CD_2Cl_2$ in the dark (top) and after reaching the PSS upon irradiation with 365 nm, 407 nm and 430 nm. The spectra are assigned to the corresponding irradiation wavelength *via* color code, c) Compound **30** was dissolved DMSO (80 µM) and an absorption spectrum (d = 10 mm) was first measured in the dark. The sample was then irradiated with 470 nm and photoisomerization over time was followed *via* absorption spectroscopy.

Unexpectedly, the shoulder in the absorption spectrum did not recover upon back-isomerization with shorter wavelengths and the isosbestic point at 410 nm was not retained. In consequence, a repetition of the switching cycle was not possible. With lower wavelengths however, photoisomerization was found to be repeatable over ten cycles and no photodegradation was

observed. The origin of this phenomenon has not yet been identified. DMSO and $CH_2Cl_2$ are both non-protic solvents that differ significantly in their respective dielectric constant ($\varepsilon_r$) ($\varepsilon_r$(DMSO) = 47 *versus* $\varepsilon_r$($CH_2Cl_2$) = 9.1[131]). It is conceivable that in DMSO a tautomer of *Z*-**30** with a higher dipole moment or even charge separation is stabilized (Scheme 3). Excitation with light might diminish this tautomer, which is not recovered within the timescale of subsequent backisomerization. However, further investigations are needed before reliable explanations for this phenomenon can be found.
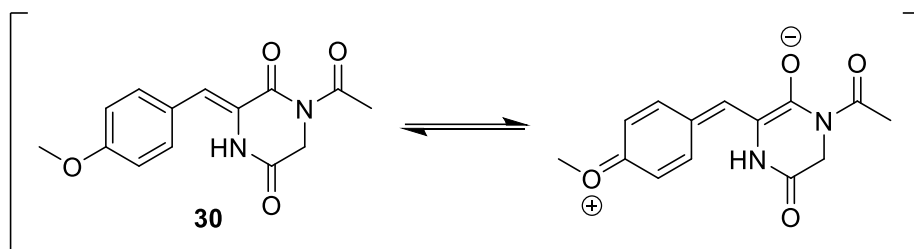


**Scheme 3:** A possible explanation for the solvent-dependent shoulder observed in the absorbance spectrum of **30** is the stabilization of a zwitterionic tautomer of HPI **30** in DMSO.

The highest bathochromic shifts in combination with high PSSs were achieved by introducing the strongly electron-donating dimethylamino ($NMe_2$) group in *para*-position on the phenyl ring (compound **36,** Figure 40). HPI **36** can be efficiently photoisomerized in DMSO within the range of 365-523 nm with PSSs up to 71% of *E*-**36** with UV light (365 nm), and as much as 97% *Z*-**36** with green light (523 nm). The results of ten subsequent switching cycles suggest that the presence of the $NMe_2$ group enables or promotes photodegradation, which was not observed for the unsubstituted compound (Figure 40). When dissolved in $CH_2Cl_2$, both *para*-amino-substituted HPIs **36** and **37** were found to be less photostable and degradation was observed upon irradiation with wavelengths below 450 nm (see chapter 5.5.4). However, an enhanced solubility in aqueous media – more of relevance for potential photopharmacological applications – allowed for reversible photoisomerization in phosphate-buffered saline (PBS, pH 7.4) doped with 25% DMSO without any detectable degradation (Figure 40).
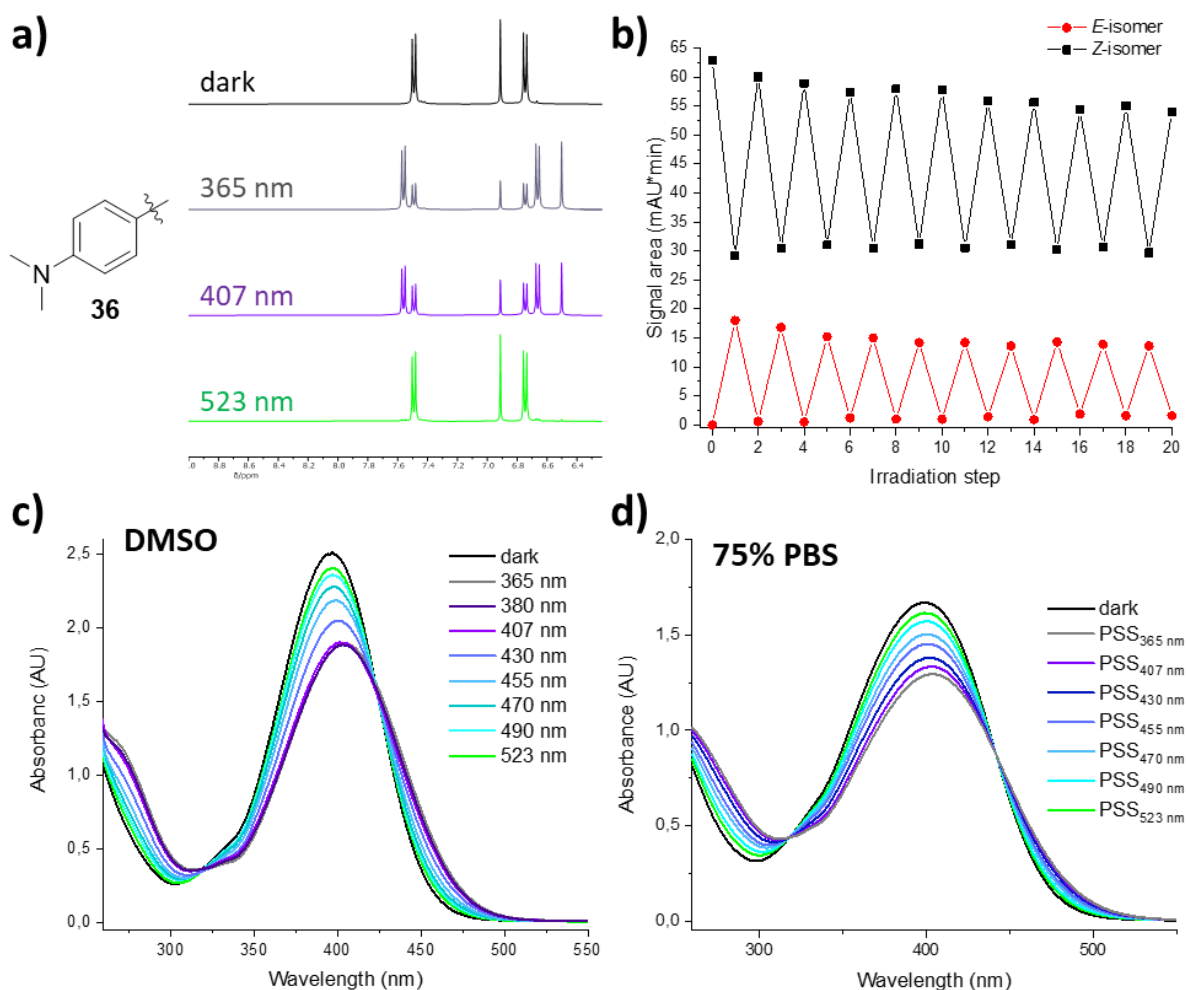
**Figure 40:** Reversible photoisomerization of electron-rich *p*-NMe$_2$ HPI **36** in different media. a) Sections of $^1$H NMR spectra (DMSO-*d*$_6$) of compound **36** in the dark (top) and after reaching the PSS upon irradiation with 365 nm, 407 nm and 523 nm. The spectra are assigned to the corresponding irradiation wavelength *via* color code, b) A solution of pure *Z*-**36** in DMSO (1.0 mM) was alternately irradiated with 407 nm for 4 min and with 523 nm for 10 min and after every irradiation step the solution was analyzed *via* analytical HPLC, c) Compound **36** was dissolved in DMSO (80 µM), as well as d) 75% PBS in DMSO (v/v) (80 µM), respectively. Absorption spectra (d = 10 mm) were first measured of the dark-state, then the samples were irradiated with 365 nm, 380 nm, 407 nm, 430 nm, 455 nm, 470 nm, 490 nm and with 523 nm. An absorption spectrum was measured after each irradiation step until the PSS at the respective wavelength was reached.

A second electron-rich HPI, the *para*-bisphenylamino (*p*-NPh$_2$)-substituted HPI **37**, was found to have very similar characteristics as HPI **36** in absorbance (Figure 41) as well as the compositions of the photostationary states (see also chapters 5.5.4 and 5.5.6). However, a bathochromic shift of 49 nm and significantly enhanced intensity was determined when comparing the fluorescence spectra of both compounds. A change from green fluorescence (HPI **36**: $\lambda_{em,max}$(DMSO) = 516 nm) with very low intensity (HPI **36**: $\Phi_F$(DMSO): 0.004) to a much brighter yellow fluorescence (HPI **37**: $\lambda_{em,max}$(DMSO) = 565 nm, $\Phi_F$(DMSO): 0.030) was observed (Figure 41).
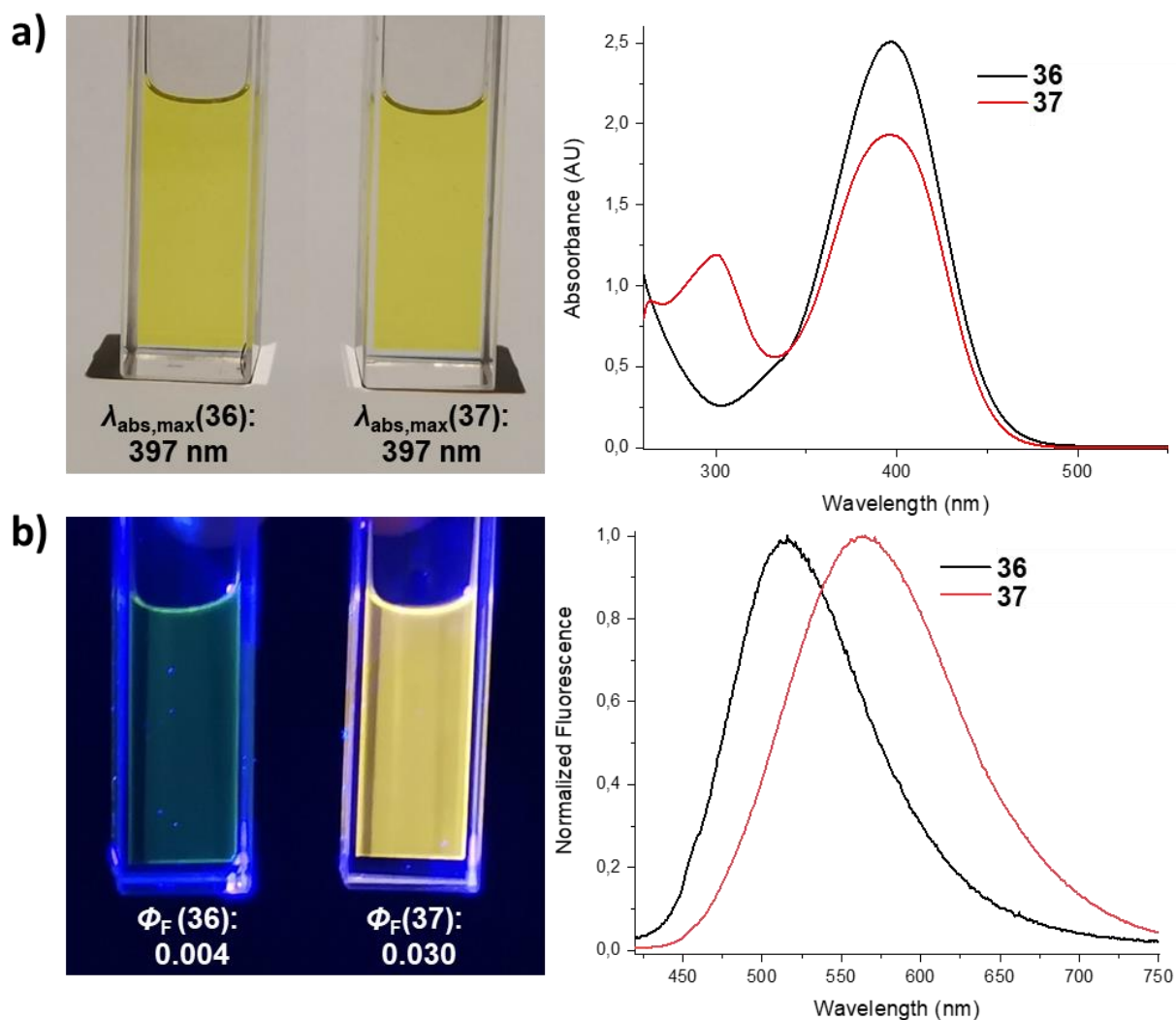
**Figure 41:** Comparison of the photophysical properties of the electron-rich HPIs **36** and **37**. a) The absorption spectra of both compounds in DMSO (80 µM, d = 10 mm) reveal a very similar absorption maximum at 397 nm. B) The fluorescence of *para*-diphenylamino-substituted HPI **37**, however, is bathochromically shifted compared to HPI **36** and a significantly increased fluorescence quantum yield was determined.

For *p*-NPh$_2$-substituted HPI **37** the photoisomerization quantum yields were determined using a setup developed by the group of Riedle (details in chapter 5.5.7).[132] The quantum yields were found to be comparable to those determined for hemithioindigo photoswitches[133] with values of $\Phi_{(Z \to E)} = 16 \pm 1$ % (398 nm) and $\Phi_{(E \to Z)} = 15 \pm 1$ % (520 nm). As the values were found to be in the same range for both directions of photoisomerization, it can be concluded that the different compositions of the photostationary states correspond to the differences in the extinction coefficients of both photoisomers.

The thermal stability of the *E*-isomers of all the investigated HPIs was found to be very high, analogous to the plinabulin derivatives discussed in the previous chapter. The thermal *E*-to-*Z*-isomerization was monitored *via* analytical HPLC and even at an elevated temperature of 60 °C in

MeCN only 0.8% to 12% of the respective *E*-isomers had been thermally relaxed to the corresponding *Z*-configuration within one week (Figure 42).
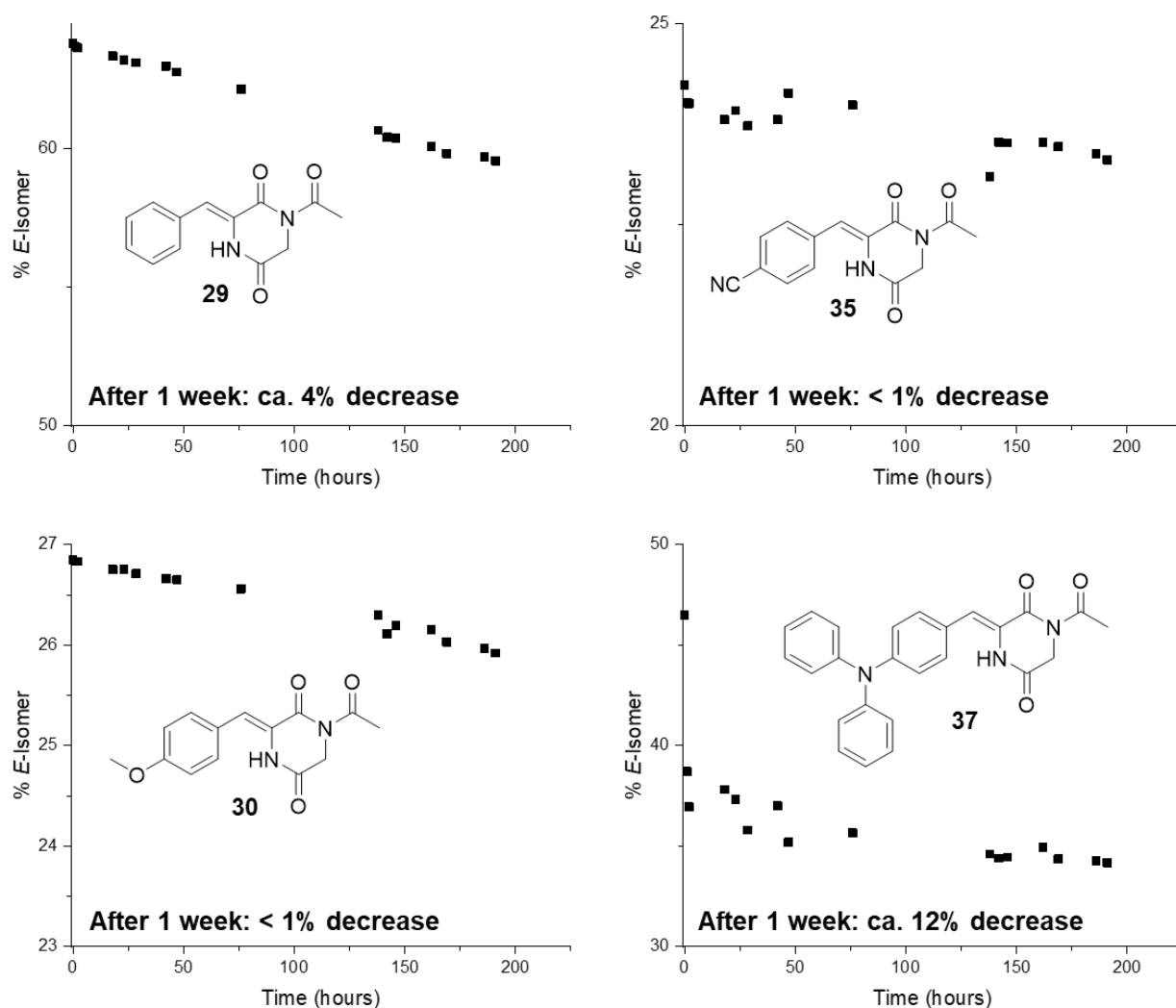


**Figure 42:** Thermal relaxation of the *E*-isomers of HPIs **29**, **30**, **35** and **37** in MeCN at 60 °C was monitored *via* analytical HPLC. The percentage of *E*-isomer was determined with the integrals of the signals assigned to the respective isomer.

One additional HPI bearing a piperazine ring in *para* position (compound **38**) was synthesized to further optimize HPI photoswitches for biomedical applications, by enhancing solubility in aqueous media while maintaining a significant bathochromic shift, compared to the unsubstituted HPI **29**. The characterization of this compound was not completed yet. However, a qualitative comparison of the absorbance spectra of *para*-piperazine-HPI **38** and *p*-NMe$_2$-HPI **36** obtained *via* analytical HPLC measurements indicates that the absorbance of **38** compound is in a similar range as those of the other two electron-rich *para*-amino derivatives (Figure 43). It was furthermore observed that after purification *via* preparative HPLC the compound was obtained as the corresponding TFA salt (pK$_a$ of piperazine in MeCN = 18.69)[134] and neutralization of this compound by washing with a saturated aqueous solution of sodium bicarbonate gave the neutral

compound and led to a color change from yellow to orange. Consequently, it can be presumed that the spectrum obtained from analytical HPLC corresponds to a protonated species and neutralization might lead to a more pronounced bathochromic shift in the absorption spectrum.
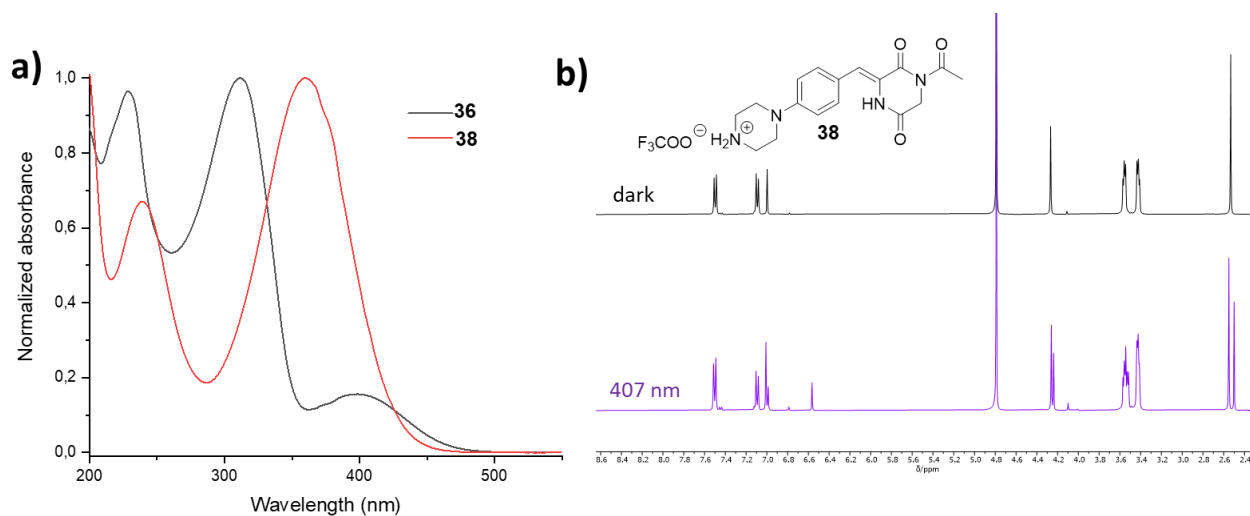


**Figure 43:** Results of first investigations of the photophysical properties of the water-soluble HPI **38**. a) Qualitative comparison of the normalized absorption spectra of *p*-NMe$_2$-substituted HPI **36** and *para*-piperazine-substituted HPI **38**. The spectra were obtained from the analytical HPLC and consequently measured in different mixtures of MeCN and H$_2$O containing 1% TFA (v/v), b) Sections of $^1$H NMR spectra (400 MHz, D$_2$O) of compound **38** in the dark (top) and after irradiation 407 nm for 15 min (bottom).

The piperazine-HPI **38** was found to be soluble in water and was characterized *via* NMR spectroscopy in D$_2$O. In first investigations it was furthermore demonstrated that this derivative can be photoisomerized in D$_2$O with violet light (407 nm) (Figure 34). These first results indicate that compound **38** is a promising candidate for *in vivo* switching and further investigations of its photomodulation in aqueous media will be done in the future.

### 3.2.3 Theoretical Calculations

To investigate HPI photoswitches further, theoretical calculations for HPIs **29**-**38** have been performed by employing the B3LYP-GD3BJ/6-311G(d,p) PCM(DMSO) level of theory, which previously proved to be suitable for modelling of hemithioindigo photoswitches.[135] First, theoretical calculations have been conducted to obtain structures and orbital energies for both respective photoisomers in the ground state. The resulting electron distribution of the highest occupied molecular orbitals (HOMOs) and lowest unoccupied molecular orbitals (LUMOs) for compounds *Z*-**29**, *Z*-**35** and *Z*-**36** are shown in Figure 44. The shapes of the calculated HOMOs and LUMOs are similar, but slight shifts that correspond with the electron-donating or -withdrawing properties of the substituents are observed.
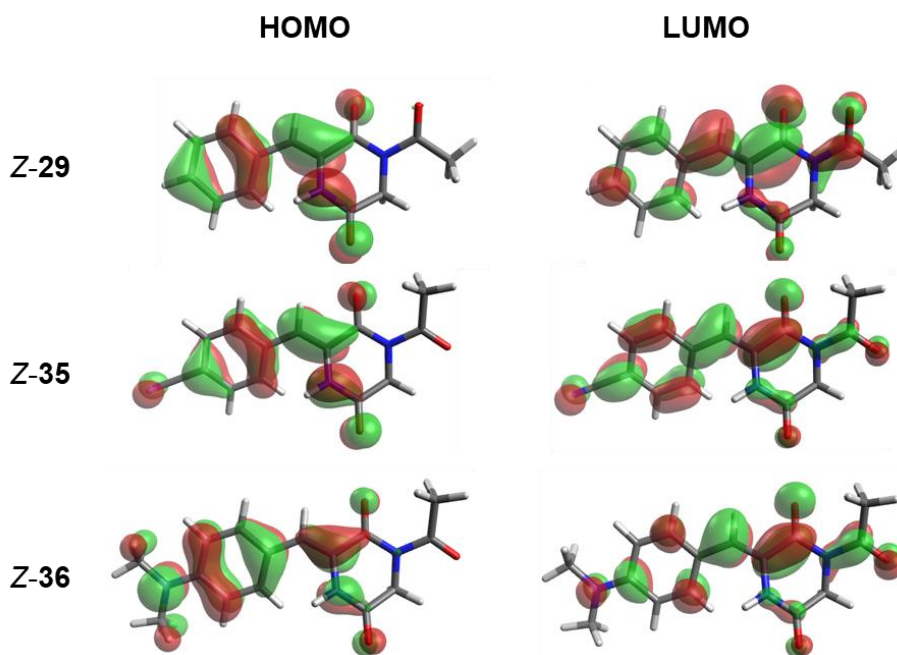
**Figure 44:** The electron distribution of HOMO and LUMO orbitals have been calculated for *Z*- and *E*-isomers of all discussed HPIs using B3LYP-GD3BJ/6-311G(d,p) PCM(DMSO) level of theory. The orbitals of the unsubstituted HPI *Z*-**29** are compared with those of the electron-poor HPI **35** and the electron-rich HPI **36**.

To investigate the differences between electron-rich and electron-poor HPIs the *p*-CN-substituted HPI **35** and *p*-NMe$_2$-substituted **36** have been selected and compared to the unsubstituted HPI **29** (Figure 45). It was found that an electron-withdrawing substituent in *para*-position leads to stabilization of both, the HOMO and the LUMO. Because the stabilization of the LUMO is less pronounced, the HOMO-LUMO gap is reduced. Also, a smaller band separation was determined for the electron-poor derivative. All these results are in agreement with an experimentally observed bathochromic shift in the absorption spectra and less pronounced changes in the absorbance spectra upon photoisomerization of *p*-CN-substituted HPI **35**. For the electron-rich derivative **36** a destabilization of both, the HOMO and the LUMO was observed. Here, the energy of the HOMO is significantly more increased compared to that of the LUMO and an even smaller HOMO-LUMO gap was determined. These results are again consistent with a more pronounced bathochromic shift determined for electron-rich HPIs observed *via* absorption spectroscopy. It was also found that based on the calculated HOMO-LUMO gaps the band separation between the two photoisomers of the unsubstituted HPI **29** is in the same range as for the electron-rich HPI **36**, which could be efficiently and reversibly photoisomerized. These results suggest, that also HPI **29** might be photoswitchable with high PSSs when irradiated with wavelengths below 365 nm.
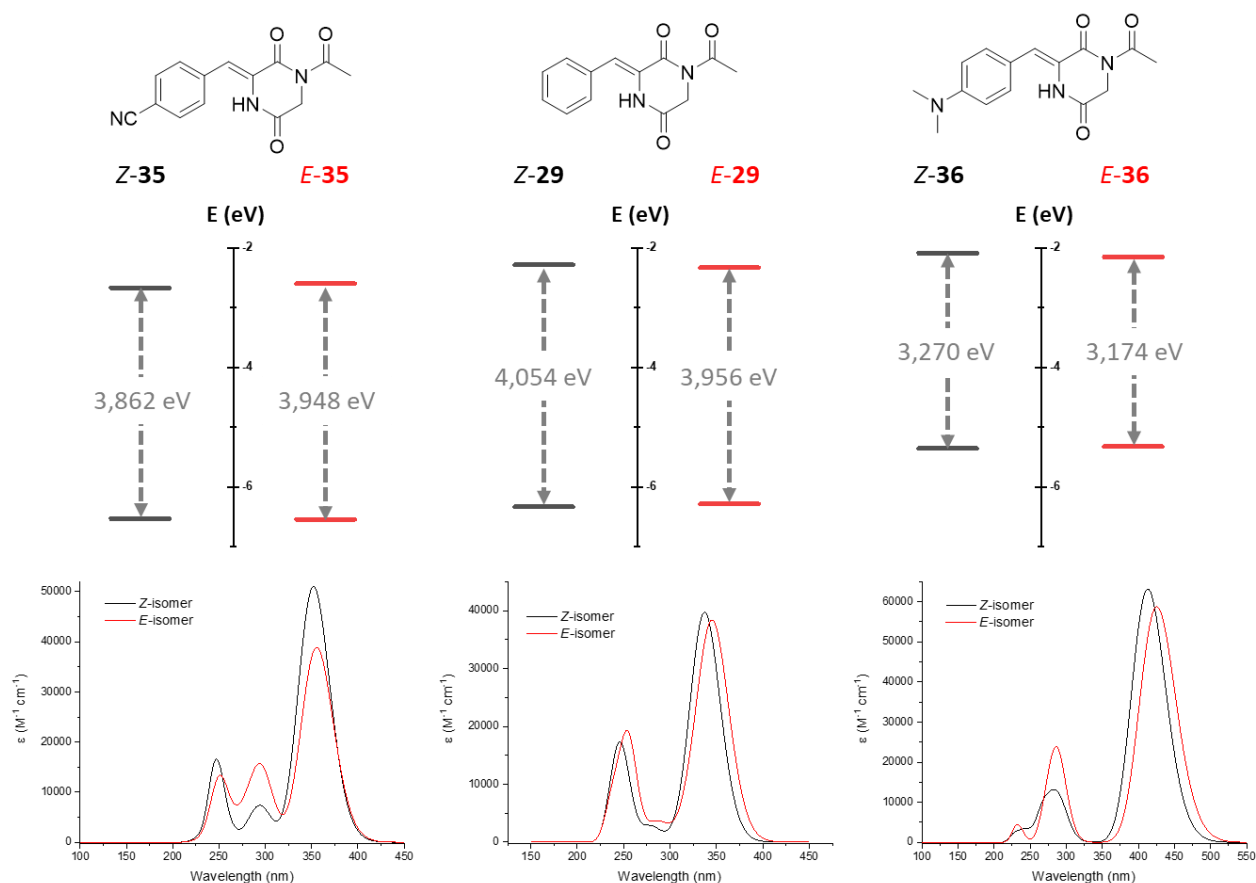
**Figure 45:** Theoretical description and comparison of electronic transitions of both respective photoisomers of HPIs **29**, **35** and **36**. Orbitals and associated energies were obtained at the B3LYP-GD3BJ/6-311 G(d,p) PCM(DMSO) level and corresponding absorption spectra on the TD-B3LYP-GD3BJ/6-311+G(d,p) PCM(DMSO) level of theory based on the optimized structures.

Furthermore, time-dependent B3LYP-GD3BJ/6-311G(d,p) calculations were performed based on the previously obtained structures. Solvent interactions were simulated using a polarizable continuum model (PCM), with parameters taken for DMSO. Absorption spectra were calculated based on these results (using 10 states) and were found to support the experimental data (Figure 45). In general, the calculated absorbance maxima are slightly higher compared to the results from absorption spectra measurements. However, the trend in the absorbance maxima matches the experimental data well (Table 4). Calculations for the not fully characterized water-soluble HPI **38** suggest that this compound – analogous to the other two amino-substituted HPIs **36** and **37** – absorbs green light (>500 nm).

**Table 4:** Comparison of calculated absorbance maxima (TD-B3LYP-GD3BJ/6-311+G(d,p) PCM(DMSO) level of theory) of selected HPIs with experimental data in measured in DMSO.

| Compound | 29 | 30 | 35 | 36 | 37 | 38 |
|---|---|---|---|---|---|---|
| Calculated $\lambda_{abs,max}$ (DMSO) | 337 nm | 362 nm | 352 nm | 413 nm | 449 nm | 409 nm |
| Experimental $\lambda_{abs,max}$ (DMSO) | 324 nm | 341 nm | 335 nm | 397 nm | 397 nm | n.d. |

In summary, all theoretical calculations are well in agreement with the experimental data and the applied level of theory was found to be suitable for describing and potentially predicting photophysical characteristics of HPI photoswitches.

## 3.3  'Locked' Plinabulin Analogue and Derivatives

To further clarify the initial observation, that the photoisomerization of plinabulin (**6**) and its derivatives occurs only at the carbocyclic arylidene C=C double bond but not on the heteroarylidene site, a synthesis route towards a plinabulin analogue with a 'locked' carbocyclic arylidene in Z-configuration was developed by adding another single bond in the *ortho*-position (highlighted in red, compound **40** in Scheme 4). The double bond formation between the DKP scaffold and the imidazole substituent was planned analogous to the synthesis of plinabulin (**6**) in an aldol condensation of the newly designed intermediate DKP **29** and imidazole aldehyde **4**.
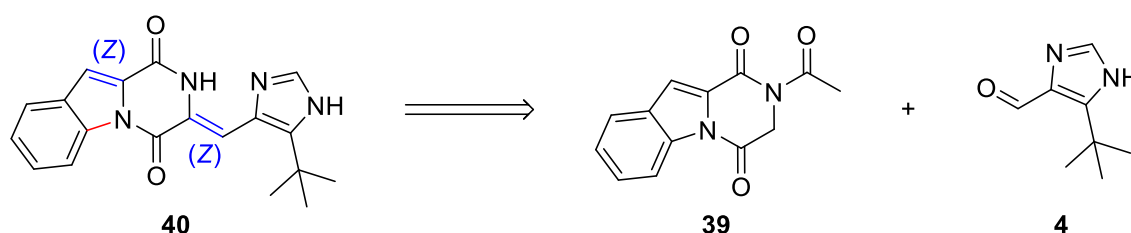


**Scheme 4:** Plinabulin analogue **40** with a 'locked' carbocyclic arylidene can be obtained by an aldol condensation of acetylated DKP **39** and imidazole aldehyde **4**.

### 3.3.1  Synthesis

The synthetic intermediate acetylated DKP **39** is a cyclic dipeptide that consist of the two amino acids 2-carboxyindole (**41**) and glycine (Scheme 5). The synthesis was started with a peptide bond formation, in which the coupling agent EDC·HCl and DMAP were applied successfully to couple carboxyindole **41** and methyl 2-aminoacetate hydrochloride (**42**).
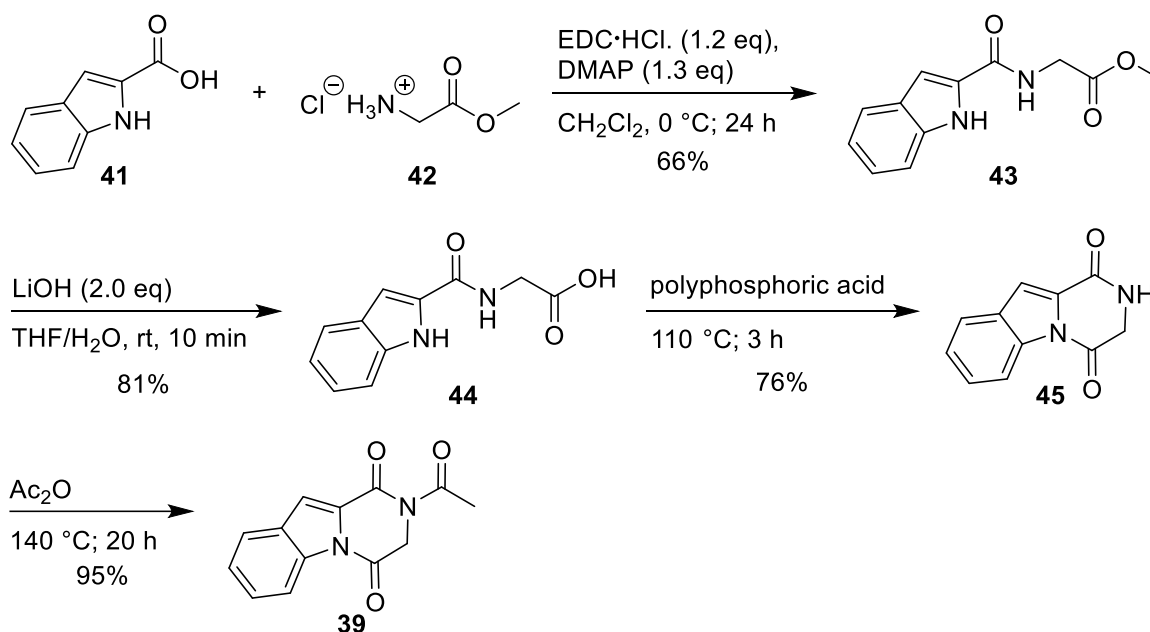


**Scheme 5:** Four-step synthesis route towards synthetic intermediate **39**.

After a subsequent ester saponification, the resulting dipeptide **44** was heated for three hours in polyphosphoric acid which promotes cyclization of *N*-(2-indoyl carbonyl)amino acids as previously reported by Pigulla and Röder.[136] Analogous to the synthesis of other HPI scaffolds, the resulting DKP **45** was then activated by acetylation and the synthesis of target compound **39** was achieved in a subsequent aldol condensation applying mild conditions by using Cs$_2$CO$_3$ in DMF (Scheme 6).
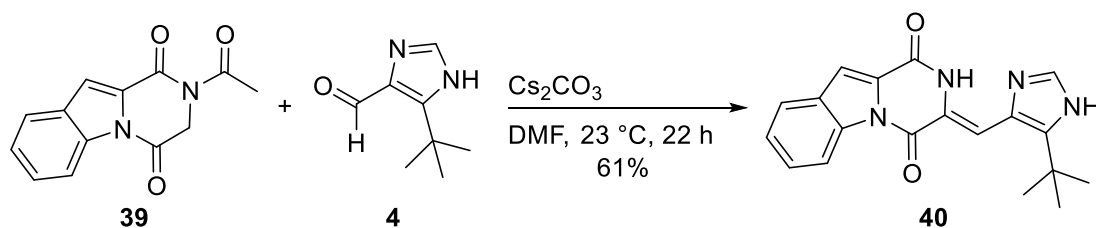


**Scheme 6:** 'Locked' plinabulin analogue **40** was synthesized by coupling acetylated DKP **39** and imidazole aldehyde **4** in an aldol condensation reaction.

Because of a lower solubility of plinabulin analogue **40** in aqueous solutions, the purification was more challenging than for plinabulin (**6**). Purification *via* preparative HPLC was successful with significantly reduced loading and 'locked' plinabulin analogue **40** was obtained in a satisfactory yield of 61% as a yellow solid. By single-crystal X-ray diffraction studies of intermediate **39** as well as derivative **40** (Figure 46) the planarity of these compounds was demonstrated. It was assumed that the decreased solubility is explained by the planar structure that facilitates intermolecular stacking forces of adjacent π-planes.
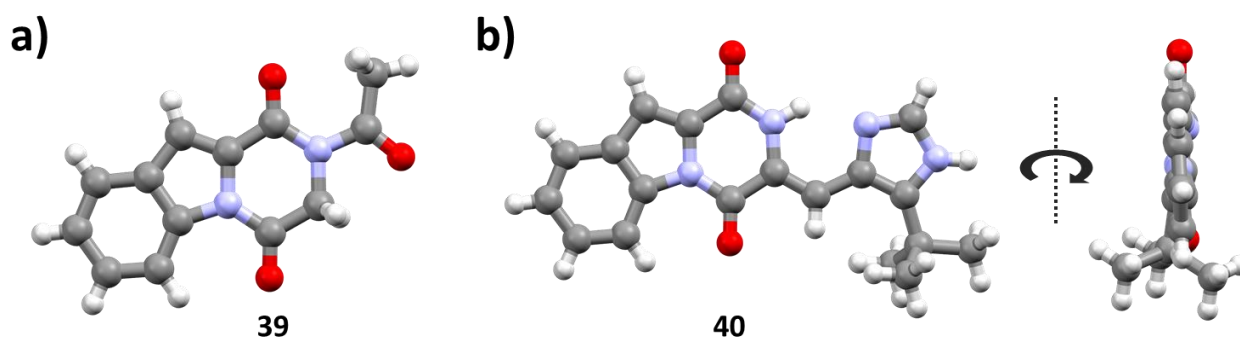


**Figure 46:** Single crystals of a) **39** and b) **40** were analyzed in single-crystal X-ray diffraction studies and the results were visualized with Mercury 2020.1 (CCDC). Atoms of carbon are depicted in grey, hydrogen in white, oxygen in red and nitrogen in blue.

### 3.3.2 Photophysical Properties of 'Locked' Plinabulin Analogue 40

When investigating the photophysical properties of compound **40**, it was found that the introduction of the single bond in the *ortho*-position leads to pronounced changes in the photophysical properties. In case of intermediate DKP **39**, the absorbance maximum was found to be shifted hypsochromically ($\lambda_{abs.max}$(MeCN) = 299 nm) compared to the analogue with a

photoswitchable C=C double bond, HPI **29** ($\lambda_{abs,max}$(MeCN) = 316 nm). However, for the 'locked' plinabulin analogue **40** a bathochromic shift of the absorbance maximum of 27 nm in MeCN (Figure 47 b) compared to plinabulin (**6**) was determined. A contrary trend was observed for the emission maximum, which was shifted 42 nm hypsochromically. Whereas a yellow fluorescence was observed for all previously discussed plinabulin derivatives, the 'locked' analogue **40** was found to emit cyan light (Figure 47 a). Interestingly, the fluorescence quantum yield of **40** ($\Phi_F$ = 24%) was significantly increased compared to plinabulin (**6**) ($\Phi_F$ = 4%) and most of the previously investigated derivatives.
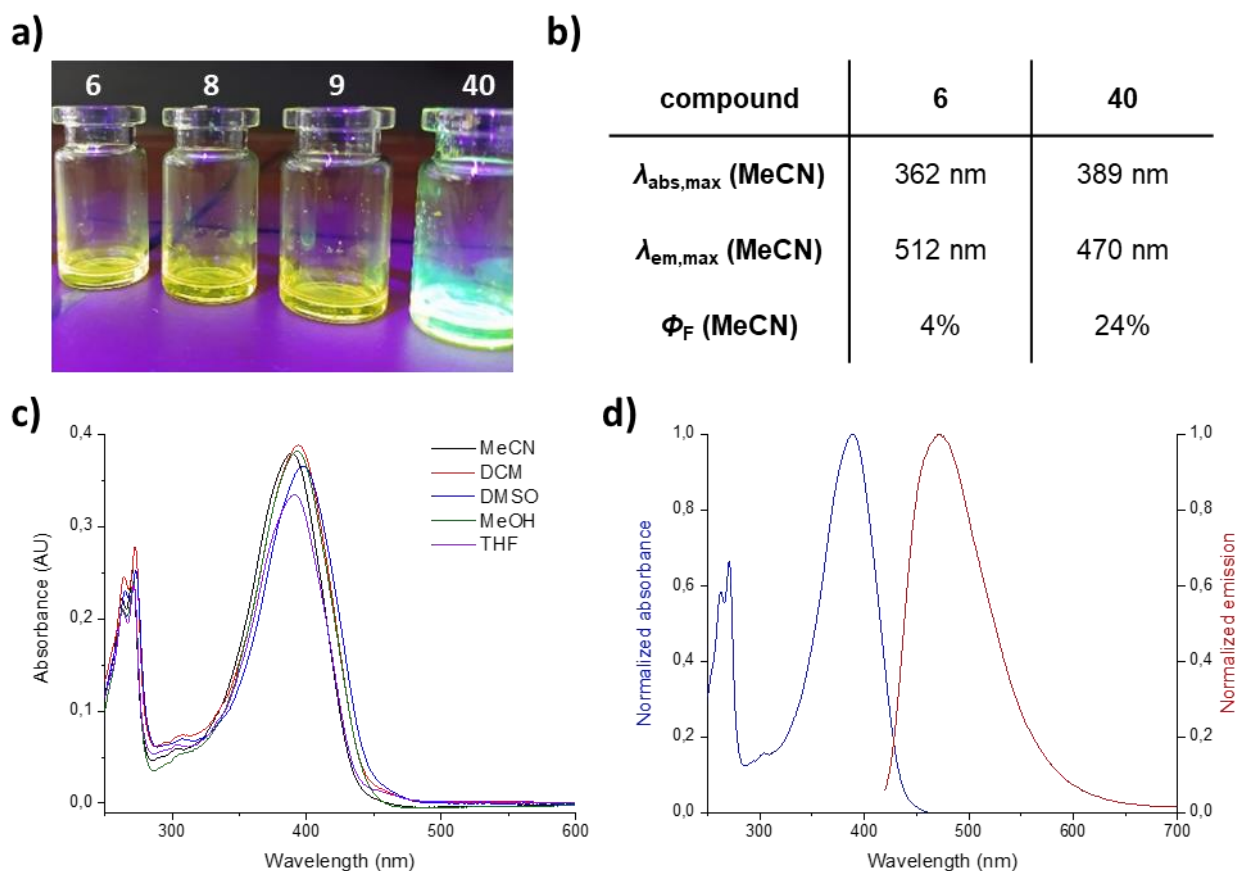


**Figure 47:** Photophysical properties of 'locked' plinabulin analogue **40**. a) A yellow fluorescence was observed for all previously discussed plinabulin derivatives, including compounds **6**, **8** and **9**. In contrast to that, the 'locked' plinabulin analogue **40** was found to emit cyan light, b) Comparison of the absorption and emission maxima as well as the fluorescence quantum yields determined for plinabulin (*Z*-**6**) and its analogue (*Z*-**40**), c) Compound *Z*-**40** was dissolved in different solvents (80 μM), respectively. Absorption spectra were measured (d = 2 mm) and the spectra are assigned to the respective solvents *via* color code, d) Normalized absorption (blue) and emission (red) spectra of solutions of *Z*-**40** in MeCN.

To investigate if the heteroarylidene group is undergoing *Z*-to-*E*-isomerization once the carbocyclic arylidene is 'locked' in *Z*-configuration, solutions of compound **40** in DMSO-$d_6$ were analyzed *via* NMR spectroscopy and analytical HPLC before and after irradiation. It was found that **40** can be photoisomerized and that under the applied conditions isomerization is accompanied

by photodegradation. In contrast to observations made with plinabulin (**6**), the formation of one primarily degradation product was observed: the corresponding ¹H NMR spectra and HPLC traces (Figure 48) clearly demonstrated the development of two additional species upon irradiation. Whereas the intensity of one of the signals reduced upon irradiation with longer wavelengths, the intensity of the second signal (highlighted in red) continuously increased upon prolonged irradiation. To date, the degradation product has not yet been isolated or identified.
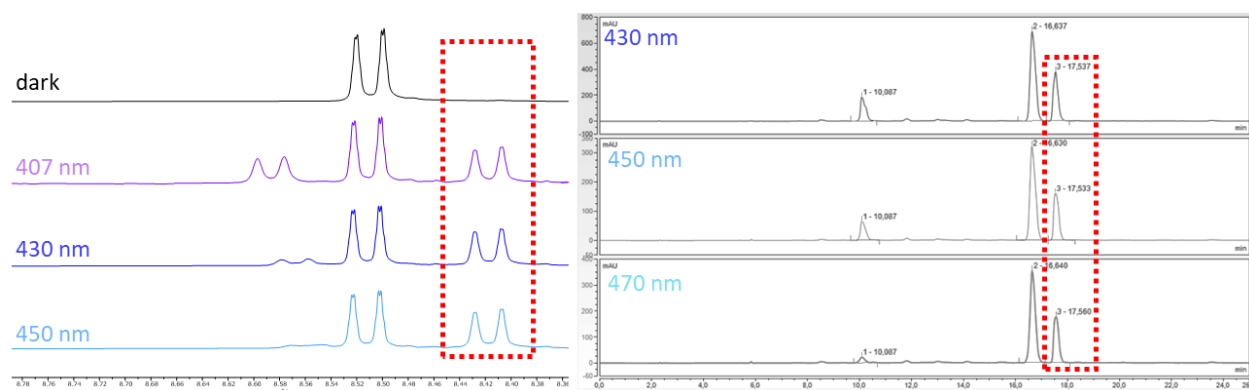


**Figure 48:** Irradiation of *Z*-**40** lead to the formation of two additional species that were detected in the corresponding a) ¹H NMR spectra and b) HPLC traces. Whereas the amount of one species decreased upon irradiation with longer wavelengths, the intensity of signals assigned to a second compound (highlighted in red) continuously increased.

Based on the observations made in previous studies on plinabulin derivatives (see chapter 3.1.2), ascorbic acid was used as an additive for all further investigations of 'locked' plinabulin analogue **40** to inhibit photodegradation. After the addition of ascorbic acid, a hypsochromic shift in the absorption spectrum was detected, accompanied by a fade of color of the solution (Figure 49 a,b). Reversible photoisomerization of **40** in presence of ascorbic acid was demonstrated by performing ten subsequent switching cycles while monitoring the absorbance spectra before and after every irradiation step (Figure 49 d). Only a slight decrease in absorbance was detected in the course of this experiment. In contrast to plinabulin (**6**), there is a pronounced change in the absorbance spectrum upon irradiation with violet light (410 nm), which enables efficient *Z*-to-*E*-isomerization resulting in a photoequilibrium with 93% *E*-**40** (see chapter 5.6.7). Backisomerization with cyan light (490 nm) however, was not as efficient and gave 33% *Z*-**40**.
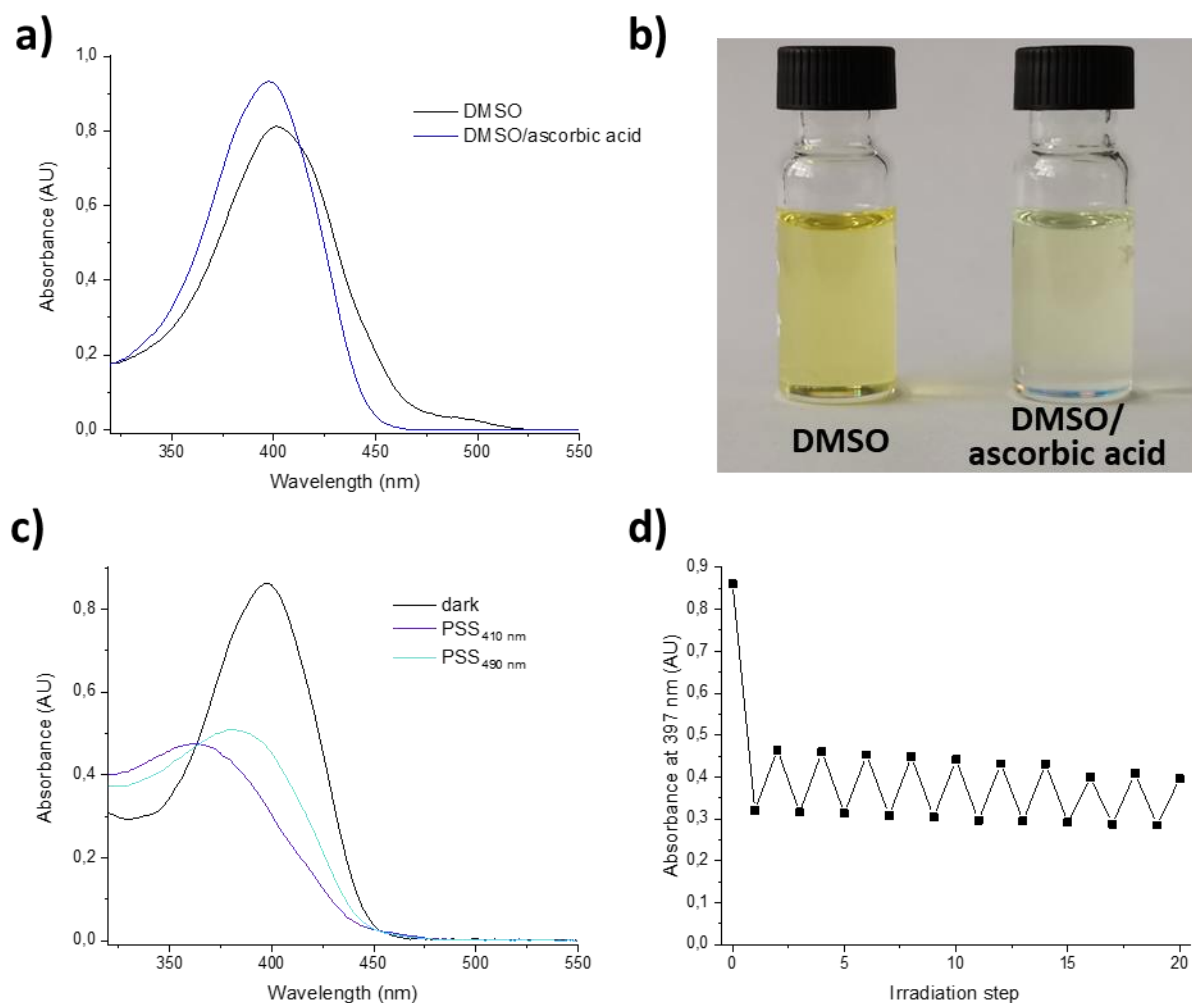
**Figure 49:** Reversible photoisomerization of **40** is possible in presence of ascorbic acid and was monitored *via* absorbance spectroscopy. a) Compound *Z*-**40** was dissolved in DMSO and in a saturated solution of ascorbic acid in DMSO (DMSO/ascorbic acid), respectively. Absorption spectra were measured in the dark (d = 2 mm). The spectra are assigned to the respective solvents *via* color code, b) The additive ascorbic acid leads to a hypsochromic shift in the absorbance of *Z*-**40** visible by a fade of yellow color, c) A solution of pure *Z*-**40** in a saturated solution of ascorbic acid in DMSO (200 µM) was irradiated and an absorption spectrum (d = 2 mm) was measured after each irradiation step until the PSS was reached, respectively, d) A solution of pure *Z*-**40** in a saturated solution of ascorbic acid in DMSO (200 µM) was irradiated with 410 nm for 30 s and with 490 nm for 12 min, respectively. The irradiation cycle was repeated ten times and after every irradiation step the absorbance at 397 nm was determined.

The photoisomerization of **40** was additionally followed *via* fluorescence spectroscopy. When analyzing the fluorescence spectra before and after irradiation with specific wavelengths (410 nm and 490 nm) it was found that the fluorescence intensity after excitation with UV-light (380 nm) can be modulated reversibly by irradiation with visible light (Figure 50). *Z*-to-*E*-Isomerization with violet light (410 nm) leads to a significant decrease in fluorescence intensity, which can be subsequently increased by *E*-to-*Z*-isomerization triggered with cyan light (490 nm). It was furthermore observed, that the PSS was reached more quickly upon irradiation with 410 nm, which

can be explained by a lower intensity of the 490 nm LED as well as a lower extinction coefficient of **40** at this wavelength.
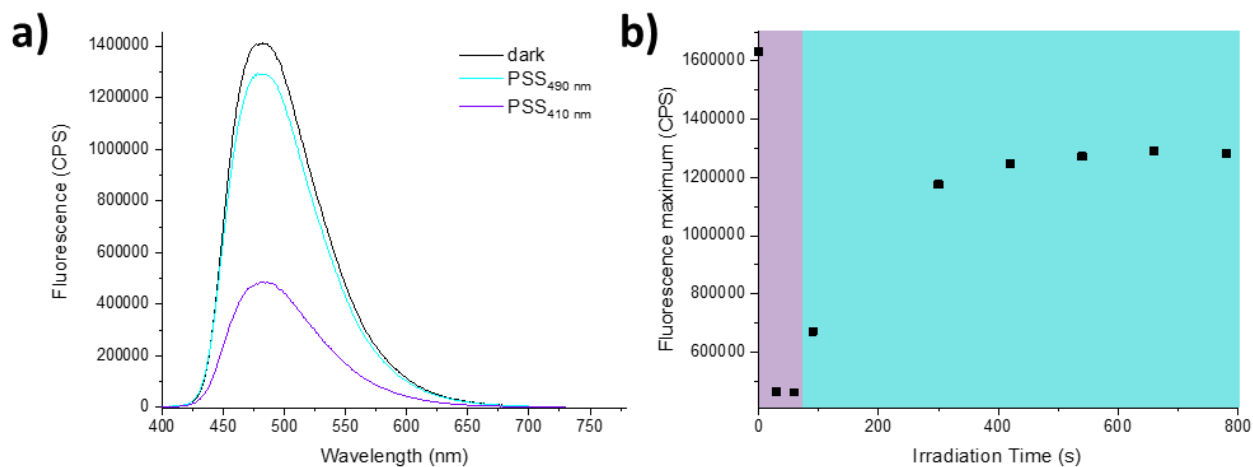


**Figure 50:** a) Fluorescence spectra of compound **40** (200 µM) in saturated solution of ascorbic acid in DMSO before and after irradiation (excitation at 380 nm). The spectra are assigned to the respective mixture *via* color code, b) Compound **40** (200 µM) in saturated solution of ascorbic acid in DMSO was analyzed *via* fluorescence spectroscopy before and after irradiation with first 410 nm and subsequently 490 nm (indicated by the color of the background). The maximal fluorescence was plotted against the irradiation time.

The thermal half-life of *E*-**40** at room temperature exceeds several days, which is in accordance with observations made for the *E*-isomers of the other investigated HPI photoswitches discussed in the previous chapters. The thermal relaxation of *E*-**40** in a mixture of water and DMSO (v/v = 1:1) at 37 °C was monitored *via* analytical HPLC. After 6 hours less than 1% of the isomer have undergone thermal backisomerization (Figure 51).
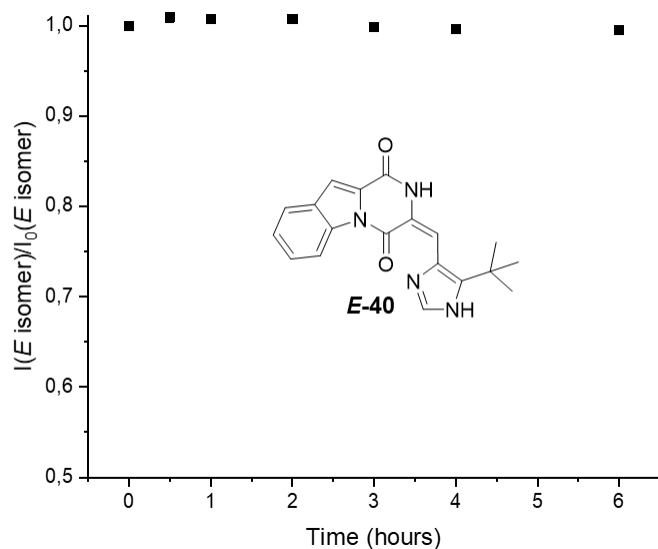


**Figure 51:** The thermal relaxation of *E*-**40** in $H_2O$/DMSO (1:1) at 37 °C was monitored *via* analytical HPLC. The integrals of the signals assigned to the respective *E*-isomer were determined at 330 nm: $I_0$ = initial integral, I = integral at given time point.

Further studies concentrated on the identification of the structural motif that is required for an enhanced fluorescence quantum yield compared to plinabulin (**6**). For this purpose, two new derivatives have been prepared with the same synthetic procedure as applied for 'locked' plinabulin analogue **40** in aldol condensation reactions with the suitable aldehydes (see also chapter 5.6.2): Compound **46** also contains an imidazole ring but without a *tert*-butyl substituent, whereas in compound **47** the imidazole substituent is replaced by a phenyl ring with a *tert*-butyl group in *para* position relative to the vinyl group (Figure 52).
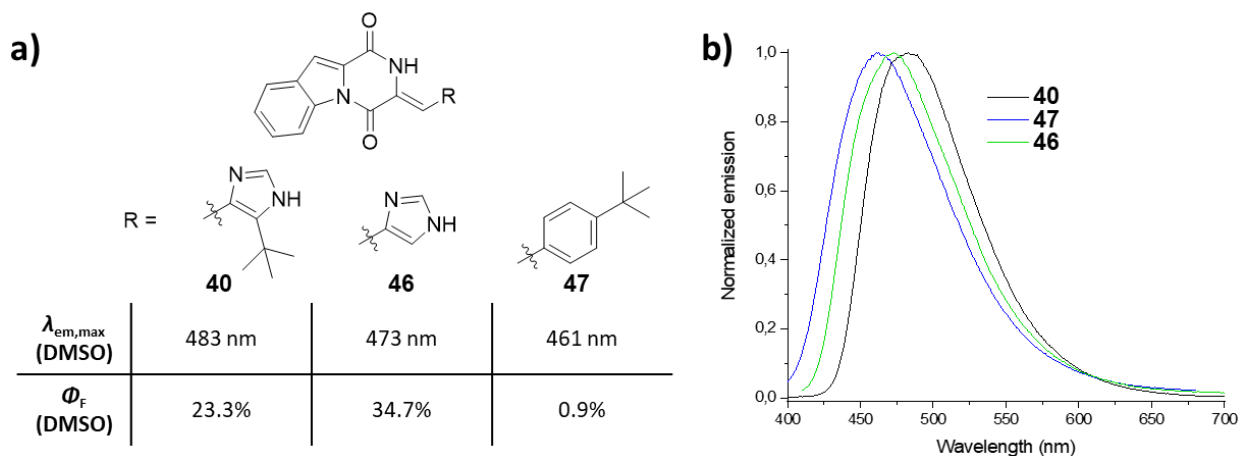


**Figure 52:** a) Comparison of the emission maxima and the fluorescence quantum yields of compounds **40**, **46** and **47** in DMSO, b) Normalized emission spectra of **40** in a saturated solution of ascorbic acid in DMSO and compounds **46** and **47** in DMSO. The spectra are assigned to the compounds *via* color code.

Compared to plinabulin analogue **40** the emission maxima of both of these compounds are shifted hypsochromically. Interestingly, it was found that the fluorescence quantum yield is significantly increased when the compounds contain an imidazole ring and the electron-donating *tert*-butyl group is removed (compound **46**) and below 1% for carbocyclic compound **47**. This trend might be explained by an increasing fluorescence intensity with more electron deficient substituents. Whereas imidazole substituents are known to have an electron-withdrawing character, phenyl substituents are slightly electron-donating substituents.[137,138] This leads to the assumption that the imidazole substituent is required for an enhanced fluorescence quantum yield.

### 3.3.3 Carbocyclic Analogous of 'Locked' Plinabulin 40

The 'locked' plinabulin analogue **40** represents a new structure that contains an HPI photoswitch. After having established and characterized HPIs within the plinabulin (**6**) scaffold as well as in a model system, it was now investigated whether the observed trends in photophysical properties can also be transferred to this third molecular scaffold. For this purpose, benzaldehyde and other, functionalized carbocyclic aromatic aldehydes were coupled to DKP **39** in an aldol condensation

reaction under basic conditions (Figure 53). In case of compound **55**, a Boc-protected aldehyde was subjected to the reaction and the protecting group was removed in a subsequent, additional reaction step (see chapter 5.6.2).
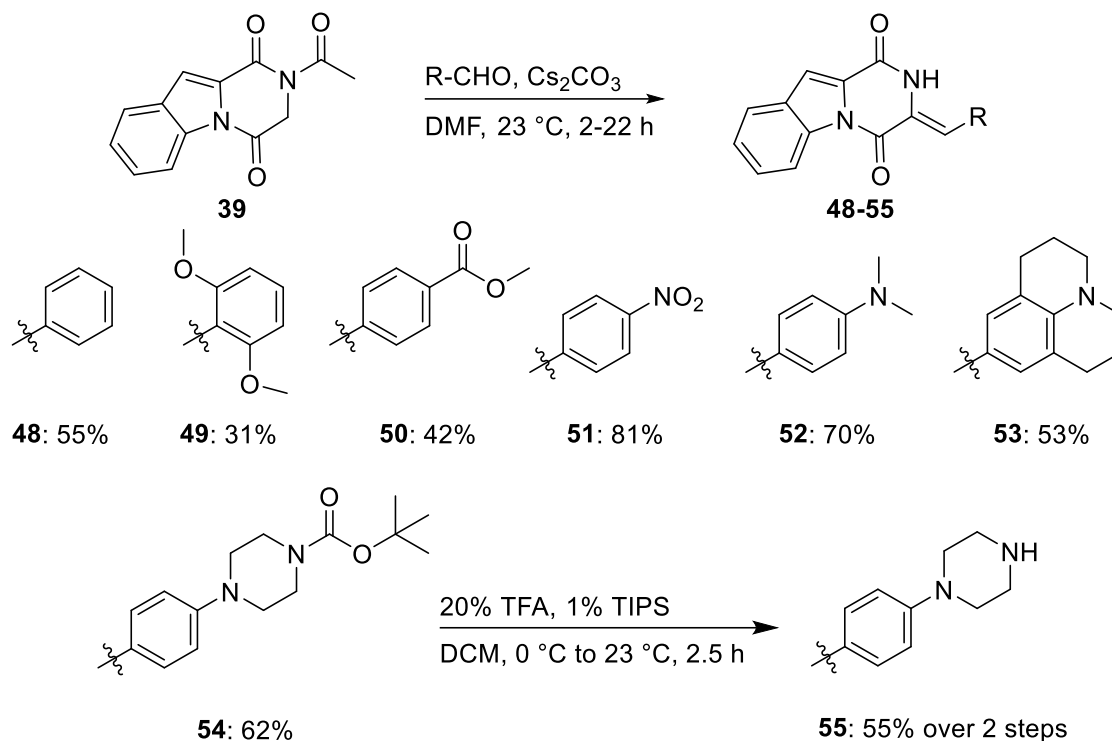


**Figure 53:** A short series of HPIs was synthesized by coupling carbocyclic aldehydes with acetylated DKP **39** in a base-catalyzed aldol condensation reaction.

In course of testing different methods for purifying these compounds, a generally low solubility in organic solvents was observed. It was found that the solubility can be significantly improved by installing substituents in *ortho* position relative to the vinyl bond. Whereas the concentration of saturated solutions of unsubstituted carbocyclic **48** in DMSO-$d_6$ was too low for $^{13}$C NMR measurements, the spectra from measurement with *ortho*-dimethoxy-substituted **49** were found to have a satisfactory signal-to-noise ratio. It can be presumed that the methoxy substituents prevent a planar arrangement of the phenyl ring and consequently an efficient π-π stacking of the molecules, which can limit solubilization of compound **48**. An enhanced solubility was also observed for compounds that contain other bulky substituents, such as a *tert*-butyl group (compound **54** as well as compound **47** presented in chapter 3.3.2) and the electron-rich *para*-amino substituted derivatives **52**, **53** and **55**.

First, absorption spectra of *ortho*-dimethoxy-substituted **49** were measured in various solvents and mixtures analogous to experiments performed with plinabulin derivatives (Figure 54). Similar to plinabulin (**6**), a minor solvatochromic effect was observed with absorbance maxima ranging from

364 nm in THF to 371 nm in DMSO. Analogous to the observations made in the previous chapters, TFA addition was found to lead to a hypsochromic shift of the absorption maximum of compound **46**, which bears an imidazole ring. However, only slight differences were observed when comparing absorption spectra of carbocyclic **49** measured in acetonitrile without any additives with those of solutions with the same concentration but with 1% (v/v) of TFA and Et$_3$N, respectively. The reversible photoisomerization of *ortho*-dimethoxy-substituted **49** was demonstrated *via* absorption spectroscopy in DMSO and no photodegradation was observed (Figure 54).
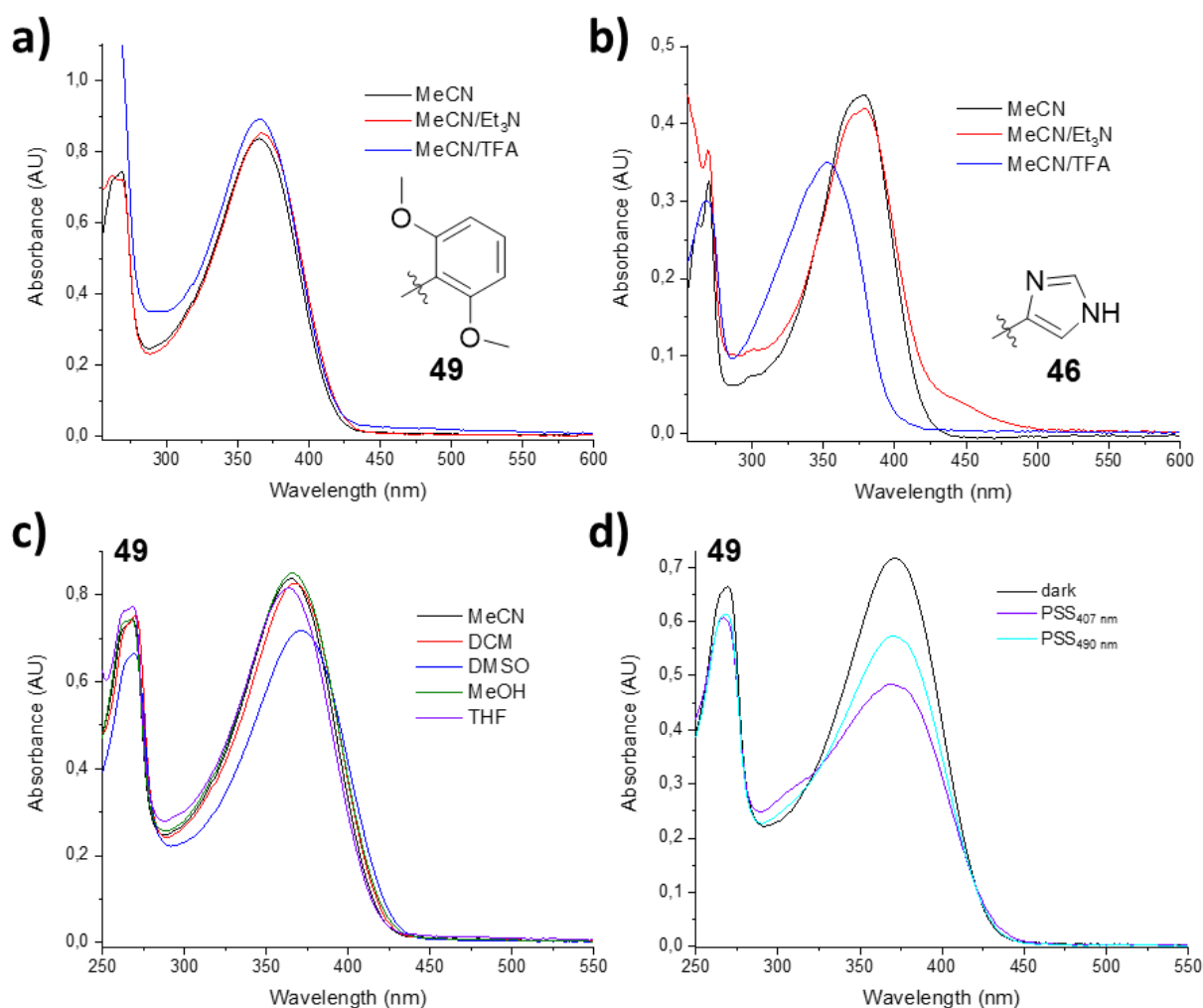


**Figure 54:** Photophysical properties of *ortho*-dimethoxy-substituted **49**. a) Compound *Z*-**49** was dissolved in MeCN and in mixtures of 1% (v/v) TFA in MeCN and 1% (v/v) Et$_3$N in MeCN, respectively and absorption spectra were measured (d = 2 mm), b) Compound *Z*-**46** was dissolved in MeCN and in mixtures of 1% (v/v) TFA in MeCN and 1% (v/v) Et$_3$N in MeCN, respectively and absorption spectra were measured (d = 2 mm). The spectra are assigned to the respective solvents *via* color code. c) Left: Compound *Z*-**49** was dissolved in different solvents (160 μM) and absorption spectra were measured in the dark (d = 2 mm). Right: Compound **49** was dissolved in DMSO (160 μM) and an absorption spectrum (d = 2 mm) was measured. The sample was then irradiated with 407 nm and 490 nm and an absorption spectrum was measured after each irradiation step until the PSS was reached, respectively.

Subsequently, the influence of electron-withdrawing (compounds **50** and **51**) and electron-donating (e.g. compound **52**) substituents in the *para* position on the photophysical properties of these derivatives were compared (Figure 55). Analogous to the model system and to the theoretical calculations discussed in chapter 3.2.3, the absorbance was found to be shifted bathochromically for all the functionalized derivatives, with a more pronounced effect for electron-donating substituents. It was additionally observed that the trends in bathochromic shifts are analogous to the hammett parameters of the substituents. For electron withdrawing substituents a higher hammett parameter ($\sigma$+(COOCH3) = +0.49, $\sigma$+(NO2) = +0.78) and for electron-donating substituents a lower hammett parameter ($\sigma$+(N(CH3)2) = −1.70, $\sigma$+(Julolidine) = −2.03) corresponds to a more pronounced bathochromic shift.[133,137,138] Furthermore, a lower band separation was observed for electron-poor derivatives, analogous to the one observed in theoretical calculations for simple mono-substituted HPIs, discussed in the previous chapter 3.2.3. Additionally, for compounds **50** and **51** significant photodegradation was observed, and no photoequilibria were reached upon irradiation with violet light (410 nm). It should be tested whether ascorbic acid could be added and enable reversible photoisomerization and determination of the composition of different PSSs.
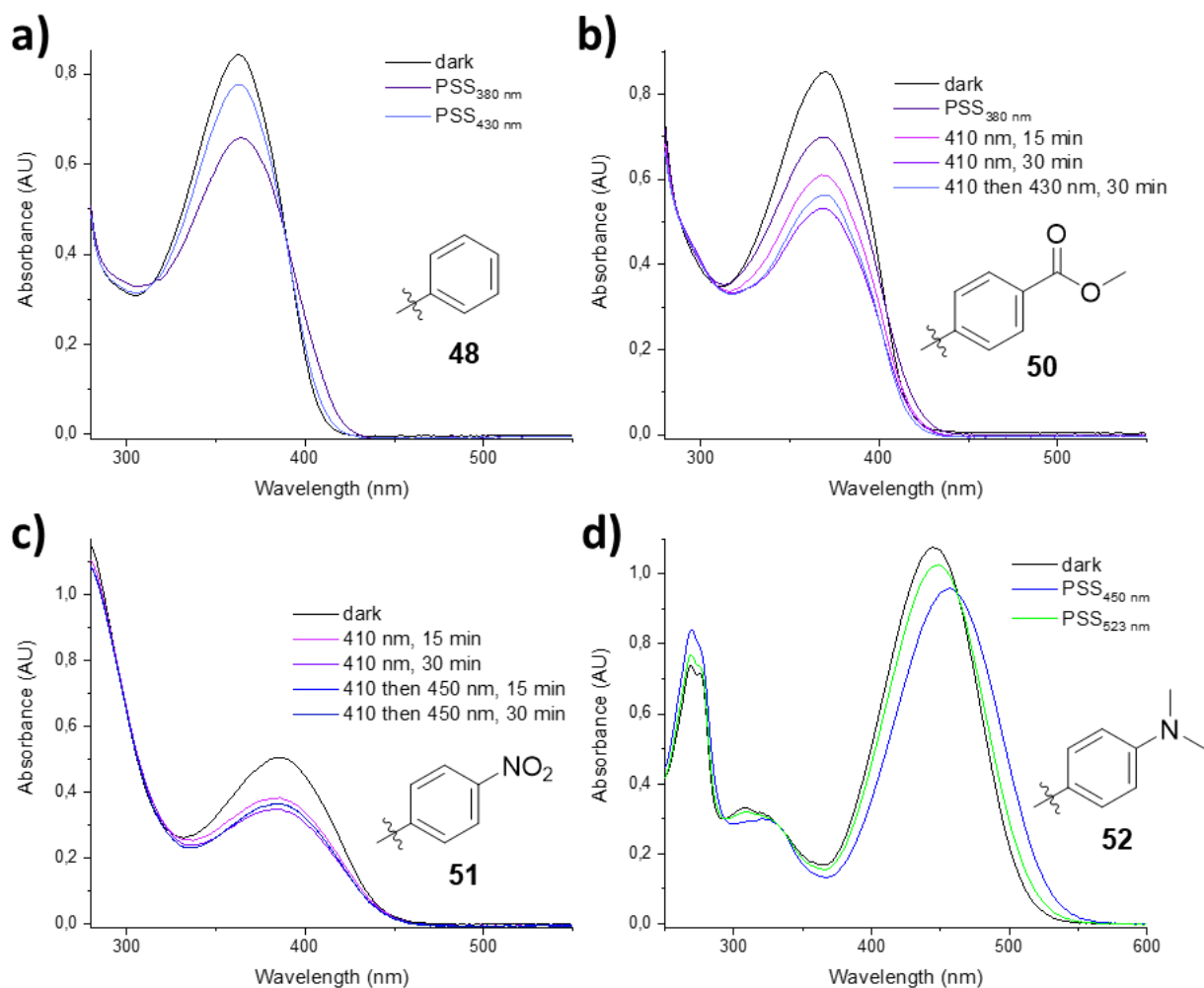
**Figure 55:** Compounds **48**-**52** were dissolved in DMSO (160 µM) and absorption spectra (d = 2 mm) were measured. The samples were then irradiated and an absorption spectrum was measured after each irradiation step until the PSS was reached, respectively. Photodegradation was observed for compounds **50** and **51** and consequently, no PSS was reached.

A noticeable bathochromic shift with an absorbance maximum at 444 nm was observed in the spectrum of *p*-NMe$_2$-substituted **52**. This shift is more pronounced than that of the model compound **36** ($\lambda_{abs,max}$(DMSO) = 397 nm) as well as the plinabulin derivative **16** ($\lambda_{abs,max}$(DMSO) = 410 nm), that both also contain electron-donating *p*-NMe$_2$ substituents. The composition of the PSS was determined *via* $^1$H NMR spectroscopy in DMSO-*d$_6$* after irradiation with selected wavelengths. It was found that the thermodynamically more stable *Z*-**52** can be isomerized to 64% *E*-isomer with indigo light (430 nm) and subsequent irradiation with green light (523 nm) resulted in 83% *Z*-isomer (see chapter 5.6.7).

Furthermore, the fluorescence spectra of the electron-rich and electron-poor derivatives were compared (Figure 56). Analogous to the trend observed in the absorbance spectra, a bathochromic shift was observed for all derivatives. The shift correlated with the hammett parameters (σ+) of

the respective functional groups and was generally more pronounced for electron-donating substituents.
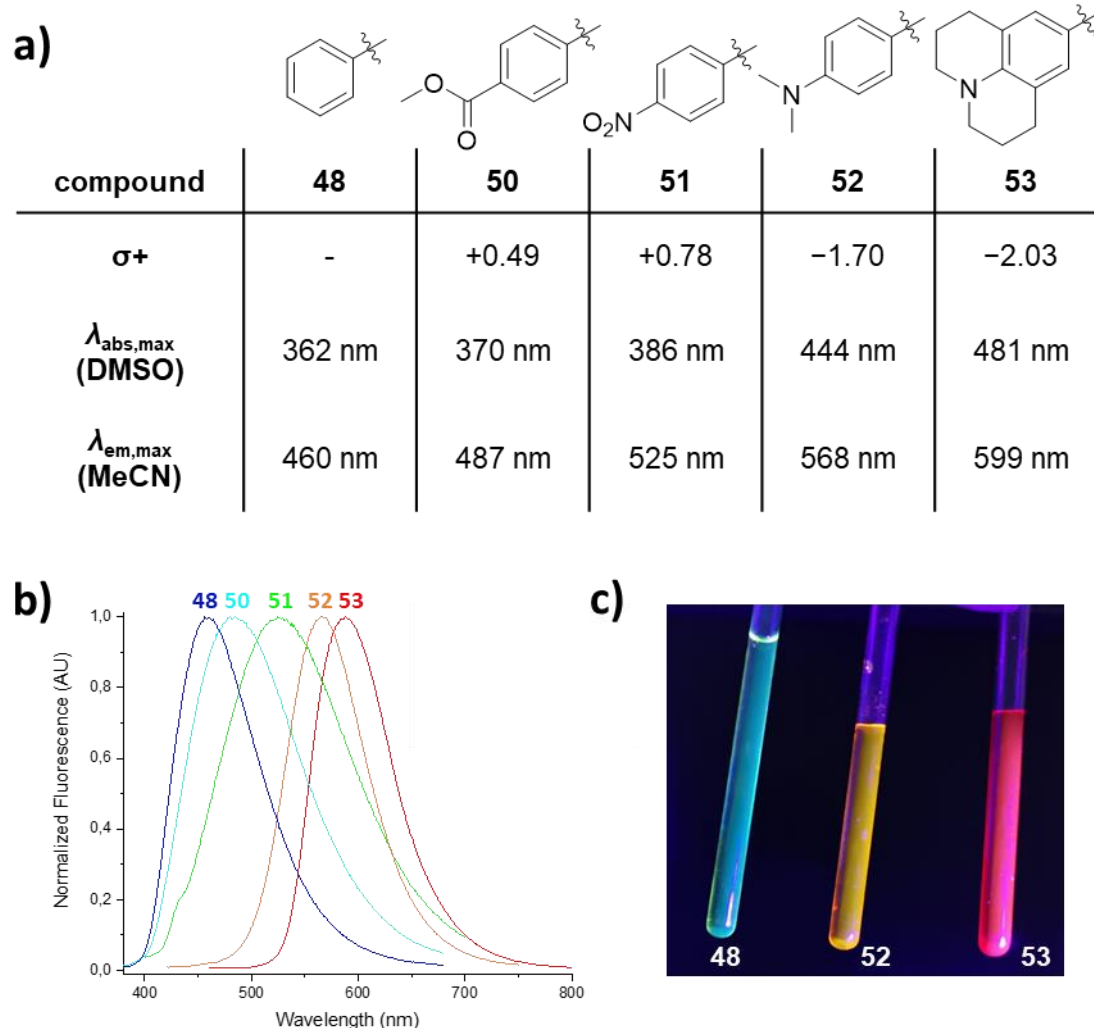


**Figure 56** a) Comparison of absorbance and fluorescence maxima of compounds bearing electron-withdrawing or -donating substituents. Bathochromic shifts were found to correlate with the hammett parameters (σ+) of the respective functional groups, b) Comparison of normalized emission spectra of the *Z*-isomers of compounds **48** and **50**-**53** in DMSO, c) Electron-donating substituents lead to a significant shift in the emission spectra from cyan (**48**) to orange (**52**) and even red (**53**). The compounds were dissolved in DMSO-$d_6$ and excited with 365 nm.

An impressive shift was observed for julolidine derivative **53**, which was the first HPI photoswitch found to be photoconverted with red light (623 nm), within the 'therapeutic window' (Figure 57). To investigate the compounds suitability for *in vivo* experiments, its behavior in aqueous media was investigated. It was found that an increasing amount of water in mixtures with DMSO led to a continuous bathochromic shift in the absorbance, which even could be observed with the bare eye. At 160 μM concentration the compound started to precipitate at a water content above 30%.
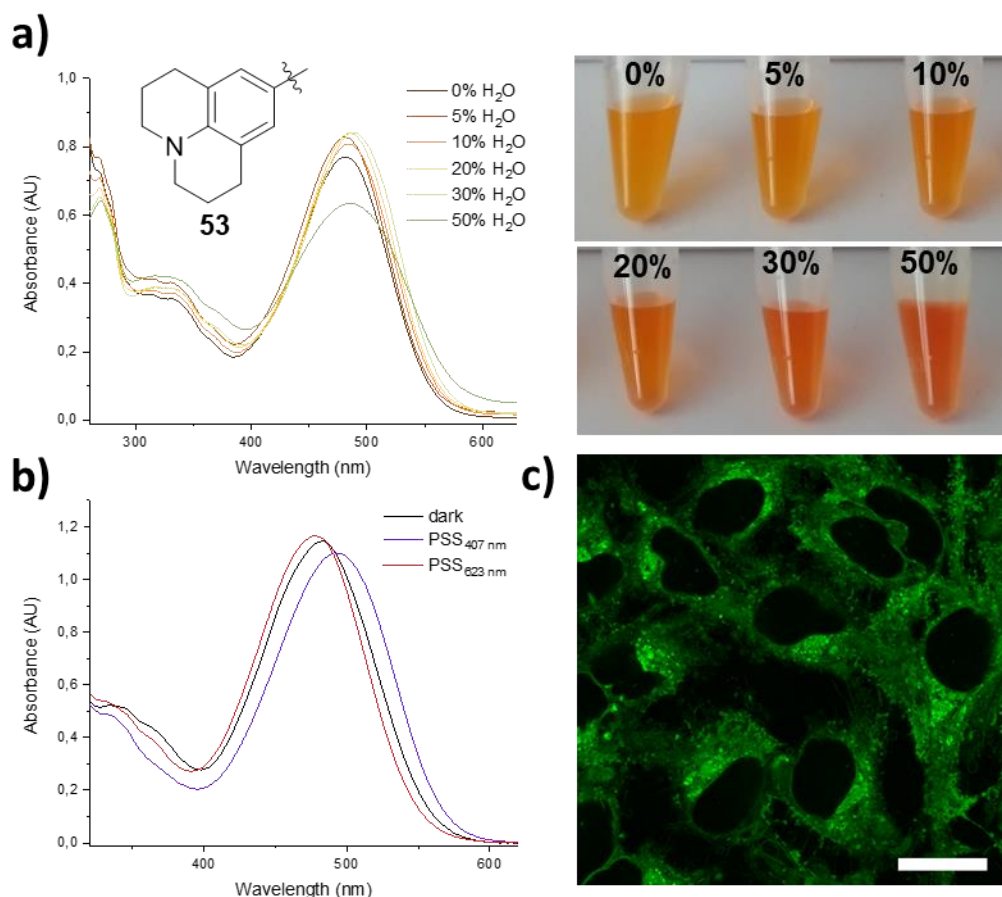
**Figure 57:** a) The absorption spectra of compound *Z*-**53** (160 μM) in DMSO and different mixtures of water and DMSO (d = 2 mm) were measured and a bathochromic shift was observed with an increasing amount of water in the mixture. The spectra are assigned to the corresponding solvent mixture *via* color code. A water content of 30% or higher resulted in precipitation of the compound, b) Compound **53** was dissolved in DMSO (80 µM) and an absorption spectrum (d = 2 mm) was first measured in the dark. The sample was then irradiated and an absorption spectrum was measured after each irradiation step until the PSS was reached, respectively. The spectra are assigned to the corresponding wavelength *via* color code. c) Imaging of compound **53** in HeLa cells *via* confocal microscopy (scale bars 20 µm, excitation laser line: 488 nm, 2.2% intensity, detection at 500-600 nm, gain 854) after 15 h treatment (8.0 µM). The results were processed and visualized with Leica Application Suite X 3.7.4.23463 from Leica Microsystems CMS GmbH.

Subsequently, it was tested whether julolidine derivative **53** has cell-penetrating properties. For this purpose, HeLa cells were incubated with **53** (8 µM) for 15 hours and then the cells were washed with PBS buffer and fixed. Afterwards, the fluorescent compound **53** was detected *via* confocal microscopy applying the selected laser wavelength of 488 nm (Figure 57). Fluorescence was detected in the cells, but not inside the nucleus. The fluorescence was not distributed homogeneously in the cytoplasm, but some line-shaped structures and round shaped fluorescent spots were detected with a higher concentration close to the nucleus. It was concluded that compound **53** can cross cell membranes of HeLa cells, but the exact localization within the cells has not been identified yet.

Because the solubility of julolidine derivative **53** in aqueous media was found to be limited, another derivative bearing a piperazine substituent in *para* position (compound **55**) was synthesized. When investigating HPI model compounds (chapter 3.2.2) this functional group was found to enhance solubility in aqueous media while maintaining a significant bathochromic shift in the absorbance compared to an unsubstituted analogue. After purification *via* preparative HPLC, the TFA salt of compound **55** was obtained (Figure 58). The salt was found to be significantly bathochromically shifted in absorbance and emission ($\lambda_{abs,max}$(DMSO) = 413 nm, $\lambda_{em,max}$(DMSO) = 543 nm) compared to the unsubstituted analogue **48** ($\lambda_{abs,max}$(DMSO) = 362 nm, $\lambda_{em,max}$(DMSO) = 460 nm). After addition of Et$_3$N a bathochromic shift in the absorbance spectrum in MeCN of 23 nm was detected, which is presumed to correspond to the formation of uncharged compound **55**. Reversible photoisomerization in DMSO with visible light was observed *via* absorbance spectroscopy without any detectable photodegradation (Figure 58). Cell penetration assays were performed analogous to the experiments with julolidine derivative **53** and it was found that also piperazine **55** can penetrated cell membranes of HeLa cells. However, the distribution of the detected fluorescence differed from the compound **53**. There was a more homogeneous distribution within the cytoplasm, which might be explained by an enhanced solubility in aqueous media. Additionally, fluorescent circles are found predominantly close to the cell membrane. It can be presumed that these structures are vesicles being transported to the cell membrane during exocytosis. Interestingly, fluorescence was also observed inside of the nuclei in round-shaped structures, which might correspond to a localization of piperazine **55** in the nucleoli. However, this is yet to be verified in co-staining experiments.
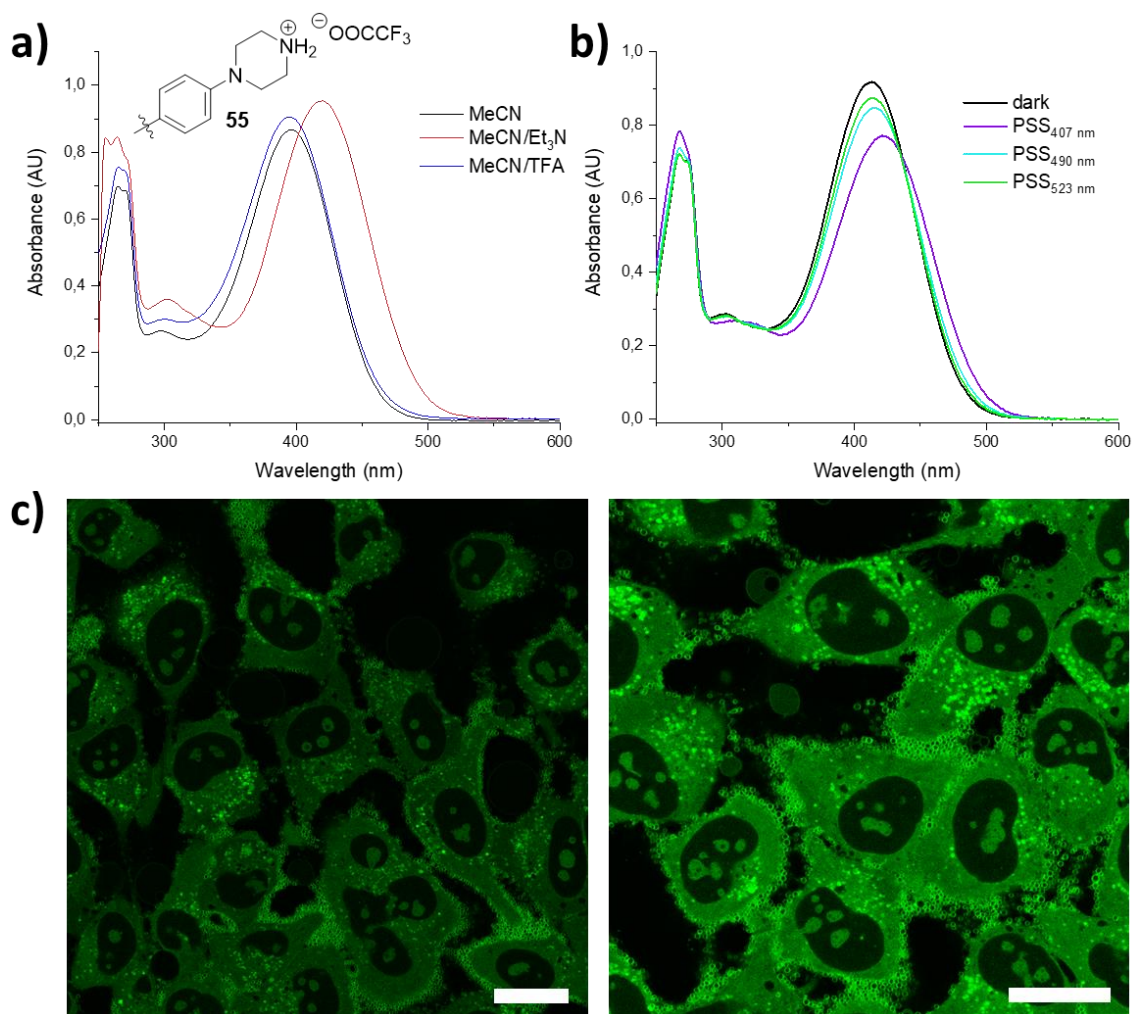
**Figure 58:** The TFA salt of compound *Z*-**55** was dissolved MeCN (160 µM) and mixtures of 1% (v/v) TFA in MeCN and 1% (v/v) Et₃N in MeCN, respectively. Absorption spectra were measured (d = 2 mm) and the spectra are assigned to the respective solvents *via* color code, b) the TFA salt of compound **55** was dissolved in DMSO (160 µM) and an absorption spectrum (d = 2 mm) was first measured, the sample was then irradiated and an absorption spectrum was measured after each irradiation step until the PSS was reached, respectively, c) Imaging of compound **55** in HeLa cells *via* confocal microscopy (scale bars 20 µm, excitation laser line: 488 nm, 2.2% intensity, detection at 530-603 nm, gain 1044) after 15 h treatment (8.0 µM). The results were processed and visualized with Leica Application Suite X 3.7.4.23463 from Leica Microsystems CMS GmbH.

These results set basis for further experiments that will be conducted in the future. First, the cytotoxicity of both respective photoisomers should be assessed *via* cell viability assays to determine the applicable concentration range. In co-staining experiments, the location of the photoswitches within the cells can be determined and parameters including the incubation time as well as the concentration of the fluorescent compounds should be screened. Further studies should be conducted to evaluate whether there is a difference in cell-penetrating activity or location within the cells between two photoisomers, which would enable photomodulation of these characteristics. Lastly, the structures can be further modified to enhance solubility in aqueous media by installing functional groups like e.g. a phosphate group.

# 4 Conclusion and Outlook

A novel molecular photoswitch was identified in the microtubule targeting agent plinabulin (**6**) and found to enable light-triggered activation of bioactivity as well as photomodulation of fluorescence intensity.

## 4.1 Plinabulin Derivatives

A panel of plinabulin derivatives (**6**-**28**) was synthesized successfully and characterized in respect to their photophysical and photopharmacological properties. Unmodified plinabulin (**6**) was found to be reversibly photoswitchable within the visible light spectrum and it was demonstrated that light-triggered *E*/*Z*-isomerization of plinabulin (**6**) enables the photomodulation of antimitotic bioactivity. In contrast to previously reported photoswitchable microtubule-targeting agents, it has not been synthetically modified, which in turn preserves its' potency completely and contrary to many azobenzene-based photopharmacological agents it is stable under reducing conditions. The photophysical properties are compatible with fixed wavelengths of lasers commonly applied in confocal microscopy. Violet (405 nm) and cyan (488 nm) light are expected to enable in situ photomodulation while light frequencies of the green (561 nm) and the red (642 nm) channel are not absorbed and can be applied for parallel imaging without affecting the photoswitchable compound. Furthermore, properties including the composition of the PSSs, the absorption spectra and the difference in potency between two photoisomers were tuned by installing different substituents on the phenyl ring of plinabulin (**6**).

By installing electron-donating amino substituents on the phenyl ring, considerable bathochromic shifts of the absorption maxima up to 62 nm were determined, which resulted in green light-responsive (> 500 nm) photoswitches. Additionally, and bigger band separation between the two respective photoisomers was observed for these derivatives allowing for efficient reversible photoisomerization within the visible light spectrum.

Furthermore, 3,5-dimethoxyplinabulin **15** (Figure 59) was found to possess superior pharmacological properties with an over 2900-fold difference in potency between the two photoisomers, which considerably enhanced the achievable photomodulation of bioactivity. The less active, metastable *E*-**15** can be isolated *via* preparative HPLC. *E*-**15** was found to be stable in aqueous medium at 37 °C for at least 32 hours and it could be stored in a freezer without any detectable thermal backisomerization. Photoactivation of cytotoxicity was demonstrated in cell viability assays. Irradiation of the less active *E*-**15** ($IC_{50}$ = 618 nm) with cyan light (490 nm) yields an over 1800-fold more potent mixture that contains 86% *Z*-**15**. It was additionally confirmed that

the mixture can be deactivated by irradiation with violet light, which generates a mixture with over 50% *E*-**15** and an over 100-fold lower potency.
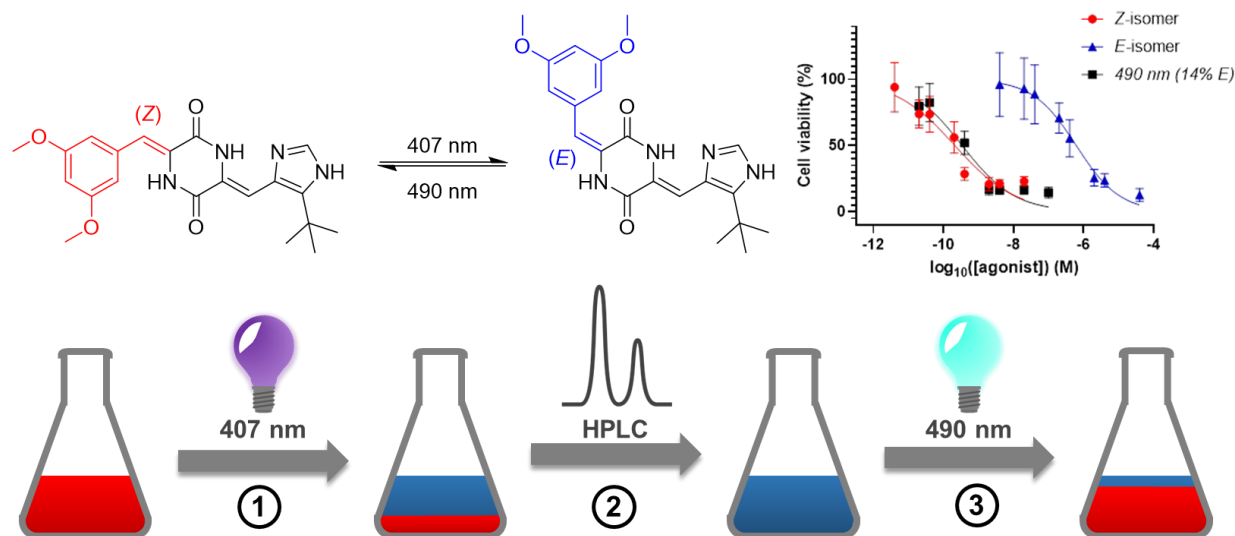


**Figure 59:** The photoswitchable 3,5-dimethoxyplinabulin **15** was found to possess superior pharmacological properties with an over 2900-fold difference in potency. Less active, metastable E-**15** is formed upon irradiation with violet light (407 nm) (①) and can be isolated *via* preparative HPLC (②) and stored in a freezer for at least two months. It can be considered as a prodrug, that can be activated by irradiation with cyan light (490 nm) (③), which gives a mixture with 89% Z-**15** (Z-**6**) with 1800-fold higher cytotoxicity against HT-29 cells.

Plinabulin derivatives consist of two arylidene residues attached to a cyclic dipeptide core (2,5-diketopiperazine, DKP). Because of structural analogies to linear peptides and appearance in numerous bioactive natural products, DKP became an important structural motif for drug design and discovery and a constitutive part of numerous biocompatible smart materials.[110,139-141] Consequently, the results of this work can be applied for designing photoswitchable analogues of other DKP-based drugs and materials.

## 4.2  Hemipiperazines: Model Compounds

3-Arylidene-2,5-diketopiperazines – abbreviated as hemipiperazines (HPIs) – are novel photoswitchable motifs first identified within the microtubule targeting compound plinabulin (**6**). These photoswitches are based on the cyclic dipeptide motif (DKP), which is also found in other bioactive compounds and biocompatible materials and may be applied in various applications in the field of photopharmacology. To clarify the scope and limitations of these novel molecular photoswitches, the core photochromic fragment of plinabulin (**6**), which contains only one double bond and no heterocycle, was chosen to serve as a model system. A panel of derivatives were synthesized and characterized systematically to investigate the influence of electron-withdrawing and -donating groups on their photophysical properties (examples shown in Figure 60).
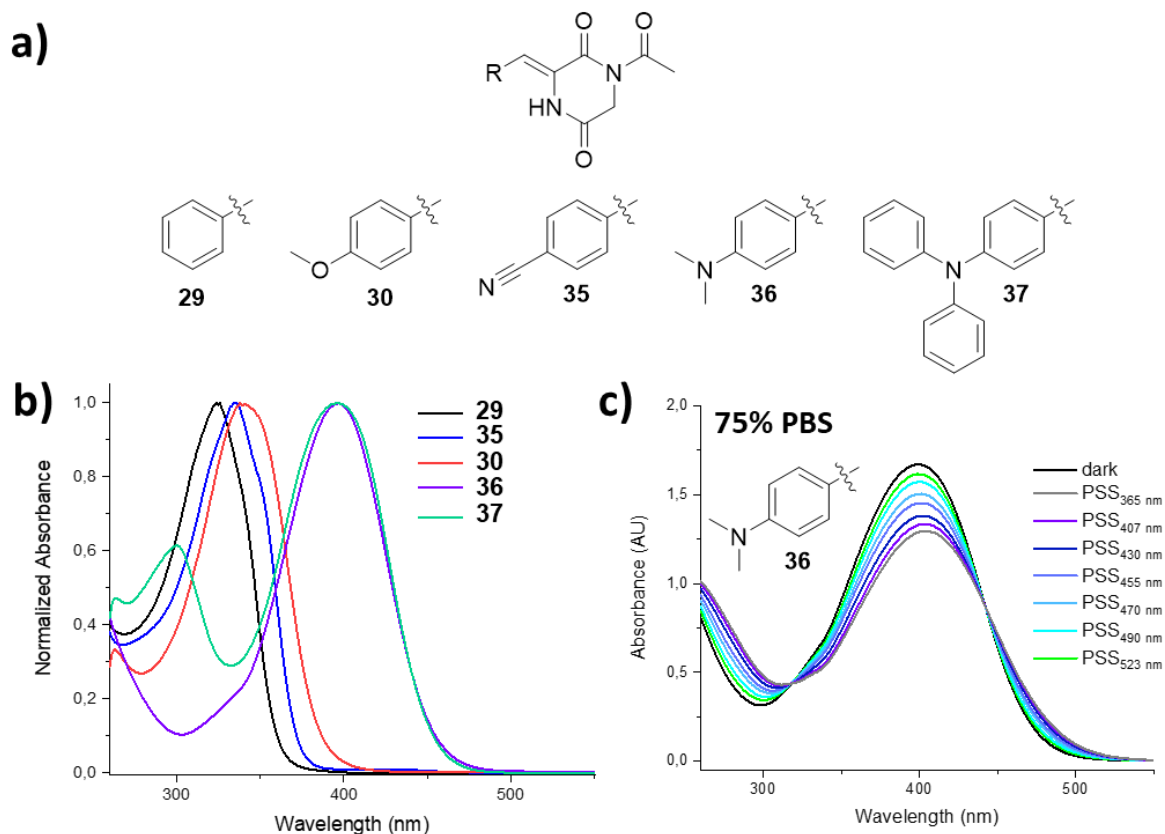
**Figure 60:** a) A panel of derivatives, including compounds **29**, **30**, and **35**-**37**, were synthesized and characterized systematically to investigate the influence of electron-withdrawing and -donating groups on their photophysical properties, b) Normalized absorbance spectra of compounds **29**, **30**, and **35**-**37** in DMSO, c) Electron-rich HPI **36** exhibits a bathochromically shifted absorbance and was found to be reversibly photoswitchable in aqueous media containing up to 75% PBS buffer.

Both, electron-withdrawing and -donating groups were found to lead to a bathochromic shift in absorbance, but this effect was much more pronounced for electron-donating substituents. Photochromism was observed for all derivatives, however with low photoconversion for unsubstituted HPI **29** as well as the electron-poor cyano-HPI **35**. The electron-rich HPIs **36** and **37** were found to be reversible photoisomerizable with visible light frequencies (green and violet light) in aqueous media. Furthermore, the switching quantum yields determined for **37** are comparable with established classes of photoswitches. Additionally, theoretical calculations were performed and found to be well in agreement with the experimental data. For future research, theoretical calculations can be applied to predict photophysical properties of HPI derivatives. The piperazine-HPI **38** was found to be soluble in water and was characterized *via* NMR spectroscopy in $D_2O$. In first investigations it was furthermore demonstrated that this derivative can be photoisomerized in $D_2O$ with violet light (407 nm). These preliminary results indicate that compound **38** is a promising candidate for *in vivo* switching and further investigations of its photomodulation in aqueous media will be done in the future.

## 4.3  'Locked' Plinabulin Analogue and Derivatives

To further clarify the initial observation, that the photoisomerization of plinabulin (**6**) and its derivatives occurs only at the carbocyclic arylidene C=C double bond but not on the heteroarylidene site, a plinabulin analogue **40** with a 'locked' carbocyclic arylidene in *Z*-configuration was synthesized (Figure 61). It was found that **40** exhibits a significantly enhanced fluorescence quantum yield can be reversibly photoisomerized with visible light frequencies. The fluorescence intensity can be modulated reversibly by irradiation with visible light. *Z*-to-*E*-Isomerization with violet light (410 nm) leads to a significant decrease in fluorescence intensity, which can be subsequently increased by *E*-to-*Z*-isomerization triggered with cyan light (490 nm) (Figure 61).
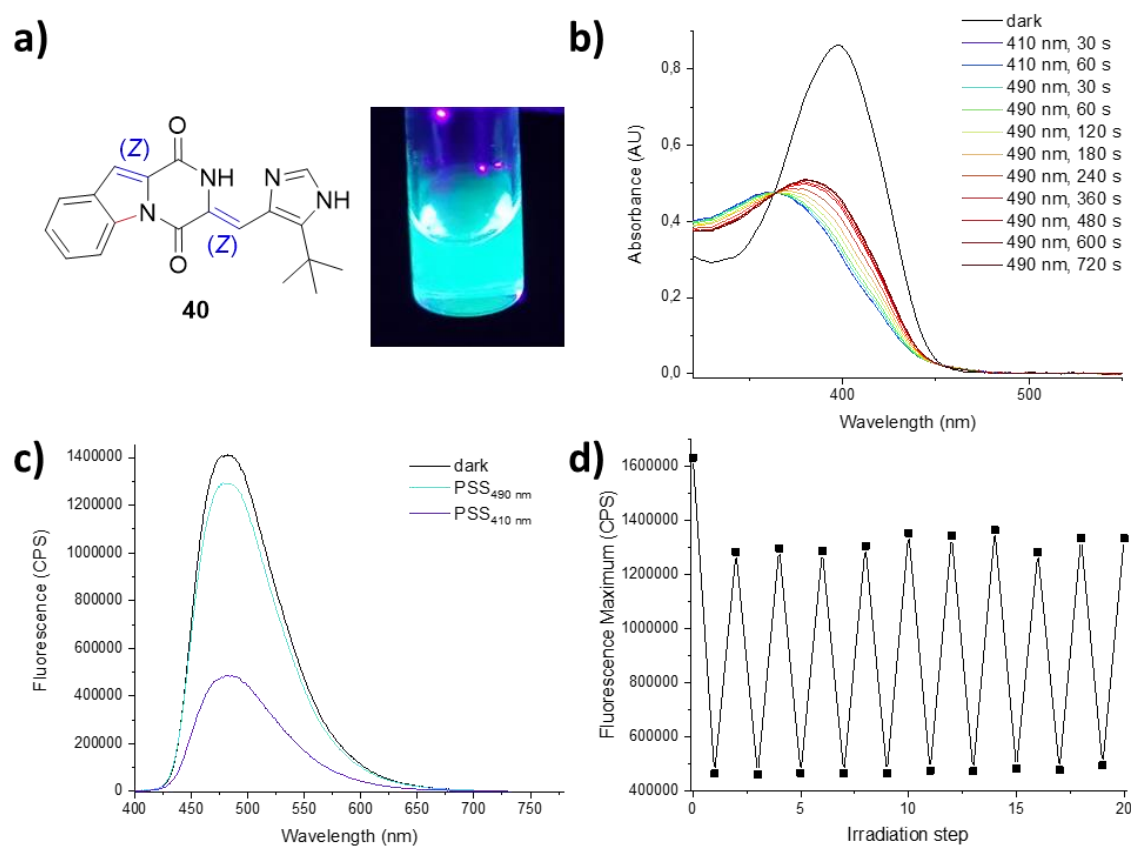


**Figure 61:** a) The emission of 'locked' plinabulin analogue **40** was found to be shifted hypsochromically and cyan fluorescence was observed with a fluorescence quantum yield of 24%, b) **40** in a saturated solution of ascorbic acid in DMSO (200 µM) can be photoisomerized reversibly with visible light frequencies. The solution was irradiated and an absorption spectrum (d = 2 mm) was measured after each irradiation step until the PSS was reached, respectively. The spectra are assigned to the irradiation wavelength and time *via* color code, c) Fluorescence spectra of compound **40** (200 µM) in saturated solution of ascorbic acid in DMSO before and after irradiation (excitation at 380 nm) The spectra are assigned to the irradiation wavelength *via* color code, d) A solution of pure *Z*-**40** in a saturated solution of ascorbic acid in DMSO (200 µM) was irradiated with 410 nm for 30 s and with 490 nm for 12 min, respectively. The irradiation cycle was repeated ten times and after every irradiation step the solution was analyzed *via* fluorescence spectroscopy.

The 'locked' plinabulin analogue **40** represents a new structure that contains an HPI photoswitch. After having established and characterized HPIs within the plinabulin (**6**) scaffold as well as in a model system, it was now investigated whether the observed trends in photophysical properties can also be transferred to this third molecular scaffold. For this purpose, carbocyclic aromatic derivatives (examples shown in Figure 62) were synthesized and characterized with respect to their photophysical properties.
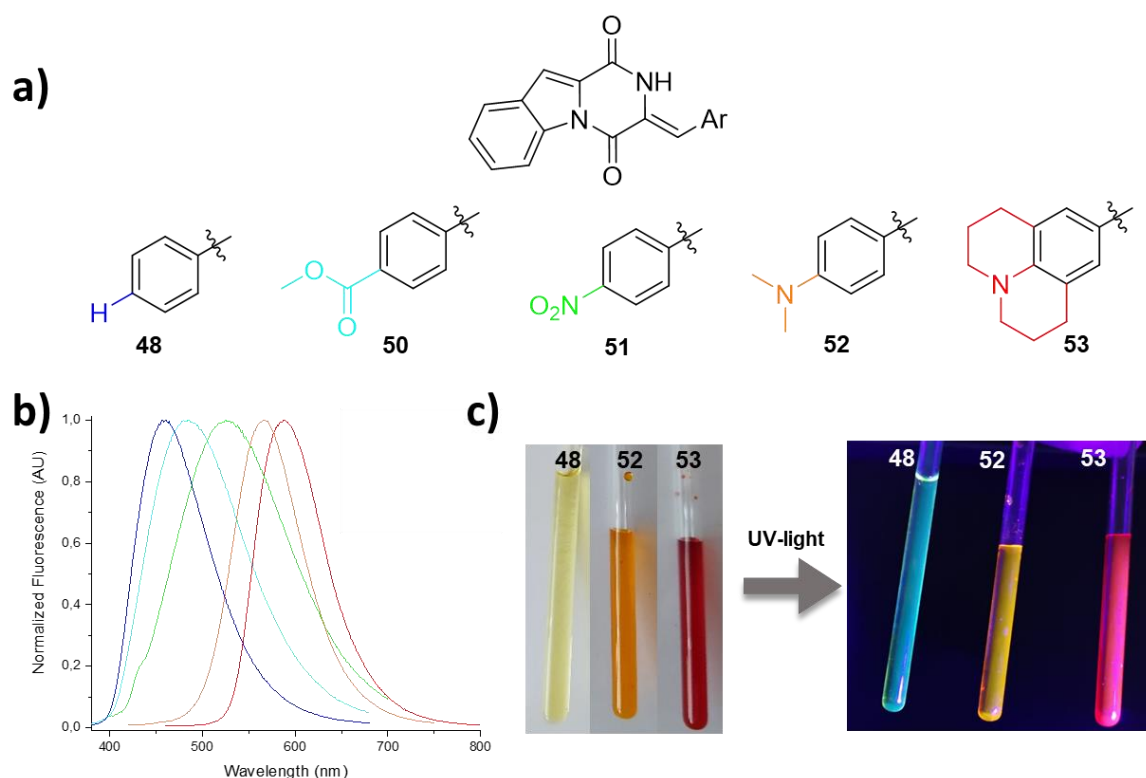


**Figure 62:** a) A panel of carbocyclic derivatives of 'locked' plinabulin analogue **40**, including compounds **48** and **50**-**53**, were synthesized and characterized systematically to investigate the influence of electron-withdrawing and -donating groups on their photophysical properties, b) Comparison of normalized emission spectra of the *Z*-isomers of compounds **48** and **50**-**53** in DMSO. The spectra are assigned to the compounds *via* color code (see panel a), c) Electron-donating substituents lead to a significant shift in the absorption (left) and emission (right) spectra. The observed fluorescence changes from cyan (**48**) to orange (**52**) and even red (**53**). The compounds were dissolved in DMSO-$d_6$ and excited with 365 nm.

Cell-penetrating properties of **53** and **55** were investigated *via* confocal microscopy. HeLa cells were incubated with the fluorescent compounds **53** and **55** and fluorescence was detected inside the cells after excitation at 488 nm (Figure 63). The distribution of the compounds inside the cells was found to differ between the two derivatives. **53** was not distributed homogeneously in the cytoplasm, but some line-shaped structures and round shaped fluorescent spots were detected with a higher concentration close to the nucleus. In contrast to that, there was a more homogeneous distribution of **55** within the cytoplasm, which might be explained by an enhanced solubility in aqueous media. Additionally, fluorescent round-shaped structures were observed inside of the

nuclei in, which might correspond to a localization of piperazine **55** in the nucleoli. However, the exact localization of both derivatives within the cells has not been identified yet and this is yet to be verified in co-staining experiments.
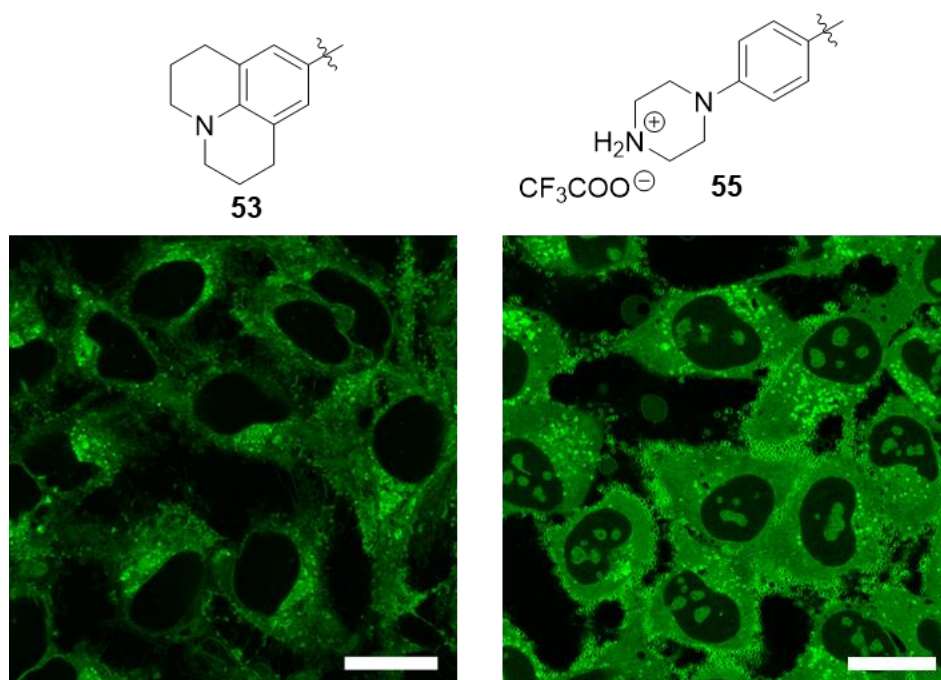


**Figure 63:** Imaging of compounds **53** (left) and **55** (right) in HeLa cells *via* confocal microscopy (scale bars 20 µm, excitation laser line: 488 nm, 2.2% intensity, **53**: detection at 500-600 nm, gain 854, **55**: detection at 530-603 nm, gain 1044) after 15 h treatment (8.0 µM). The results were processed and visualized with Leica Application Suite X 3.7.4.23463 from Leica Microsystems CMS GmbH.

Further investigations of these fluorescent cell-penetrating compounds will be conducted in the future. Fist, the cytotoxicity of both respective photoisomers should be assessed *via* cell viability assays to determine the applicable concentration range. In co-staining experiments the location of the photoswitches within the cells can be determined and parameters including the incubation time as well as the concentration of the fluorescent compounds should be screened. Further studies should be conducted to evaluate whether there is a difference in cell-penetrating activity or location within the cells between two photoisomers, which would enable photomodulation of these characteristics. Lastly, the structures can be further modified to enhance solubility in aqueous media by installing functional groups like e.g. a phosphate group.

# 5 Experimental Section

## 5.1 General Remarks

All reagents and starting materials are commercially available (Sigma-Aldrich, Fluorochem, chemPur, Alfa Aesar or BLDpharm) and were used as supplied unless otherwise indicated. Solvents of technical quality were distilled prior to use.

All experiments were conducted in air and in deionized water (Millipore) unless otherwise noted. In the experiments where physiological conditions were required, Dulbecco's Phosphate-Buffered Saline (DPBS) buffer pH 7.4, (-/-): no calcium, no magnesium, Gibco$^{TM}$ from Thermofisher, cat.#: 14190136, abbreviated below and in the thesis simply as "PBS buffer", was used.

All experiments with photoisomerizable molecules in the visible light spectrum were performed in absence of sunlight, for example with brown glassware, or colourless glassware wrapped with aluminium foil, working in a room with dimmed light. All experiments were conducted in air unless otherwise noted and all reactions containing air- and moisture-sensitive compounds were performed under argon using oven-dried glassware applying common Schlenk-techniques. Liquids were added *via* steel cannulas and solids were added directly in powdered shape. For the aqueous extraction, for all analytic samples and for the HPLC deionized water (diH$_2$O) from Millipore was used unless otherwise noted. For certain reactions, flat-bottom crimp neck vials from CHROMAGLOBE with aluminum crimp cap were used. Reactions at low temperatures were cooled using flat dewars produced by Isotherm (Karlsruhe) with water/ice or isopropanol/dry ice mixtures.

## 5.2 Methods and Instruments

### 5.2.1 Analytical Balance

Used devices: SARTORIUS Basic (0.001 g), METTLER TOLEDO AE163 or RADWAG AS220.X2 (0.0001 g) and Sartorius M2P Micro Balance (0.001 mg).

### 5.2.2 Thin Layer Chromatography (TLC)

Analytical thin layer chromatography was carried out using silica coated aluminum plates (silica 60, F$_{254}$, layer thickness: 0.25 mm) with fluorescence indicator by Merck. The TLC plates with a size of 20 × 20 cm were cut into pieces according to demand. UV active compounds were detected with a UV lamp at λ=254 nm and λ=365 nm. When required, ninhydrin (1.5 g in 100 mL ethanol and 3.0 mL acetic acid), potassium permanganate (0.45 g potassium permanganate and 2.35 g of

sodium carbonate in 90 ml of water) or 2,4-DNP (1.2 g 2,4-dinitrophenylhydrazin in 8.0 mL water, 20 mL ethanol and 6.0 mL conc. $H_2SO_4$) was used as TLC-stain.

### 5.2.3 Chromatography

Flash column chromatography was performed using Merck silica 60 ($0.040 \times 0.063$ mm, 230–400 mesh ASTM) and quartz sand (glowed and purified with hydrochloric acid).

### 5.2.4 High-Performance Liquid Chromatography (HPLC)

Analytical High Performance Liquid Chromatography (HLPC) was performed using two different instruments: (1) The 1200 Series from Agilent Technologies. The flow rate was 1.0 mL/min on an YMC C18-column JH08S04-2546WT with 250 mm length $\times$ 4.8 mm diameter and a column bead of 4 µm diameter. ChemStation for LC 3D systems (Agilent Technologies) was used for data extraction. (2) A Thermofisher UltiMate 3000 system containing a degasser, pump, autosampler, column compartment and diode array detector. The flow rate was 1 mL/min on a stationary PerfectSil Target (MZ-Analytik) C18 column (3-5 µm, 4.0 mm $\times$ 250 mm). Chromeleon 7 software was used for data extraction.

Preparative Reversed Phase High Performance Liquid Chromatography (RP-HPLC) was performed on the Puriflash™ 4125 system from Interchim. A VDSpher® C18-M-SE precolumn (10 µm, 40 x 16 mm) followed by a VDSPher® C18-M-SE separation column (10 µm, 250 x 20 mm, VDS Optilab) was used as the stationary phase. A linear gradient of acetonitrile and double distilled water, both supplemented with 0.1% trifluoroacetic acid (TFA), at a flow rate of 15 mL/min served as the mobile phase.

### 5.2.5 Nuclear Magnetic Resonance Spectroscopy (NMR)

NMR spectra were recorded using the following devices: $^1$H NMR: Bruker 300 (300 MHz), Bruker Avance 400 (400 MHz), Bruker Ascend 500 (500 MHz), $^{13}$C NMR: Bruker 300 (75 MHz), Avance 400 (101 MHz), Ascend 500 (126 MHz), $^{19}$F NMR: Avance 400 (377 MHz) or Ascend 500 (471 MHz). The following solvents from Eurisotop were used: $CDCl_3$, acetic acid-$d_4$, DMSO-$d_6$, and $D_2O$. Chemical shifts $\delta$ were expressed in parts per million (ppm) and referenced to $CDCl_3$ ($^1$H: $\delta = 7.26$ ppm, $^{13}$C: $\delta = 77.2$ ppm), acetic acid-$d_4$ ($^1$H: $\delta = 2.04$ ppm, $^{13}$C: $\delta = 179.0$ ppm), DMSO-$d_6$ ($^1$H: $\delta = 2.50$ ppm, $^{13}$C: $\delta = 39.5$ ppm) and $D_2O$ ($^1$H: $\delta = 4.79$ ppm).[142] $^{19}$F NMR were not referenced. For the characterization of centrosymmetric signals, the signal's median point was chosen, for multiplets the signal range. The signal structure is described as follows: s=singlet, d=doublet, t=triplet, q=quartet, quin=quintet, bs=broad singlet, m=multiplet, dt=doublet of

triplets. The spectra were analyzed according to the first order. All coupling constants are absolute values and expressed in Hertz (Hz). All NMR spectra were processed using MestReNova v14.1.2 (Mestrelab Research S.L.).

### 5.2.6 Mass Spectrometry (MS)

Mass spectra were recorded on a Finnigan MAT 95 mass spectrometer using electron ionization-mass spectrometry (EI-MS) or fast atom bombardment-mass spectroscopy (FAB-MS). For FAB measurements *m*-nitrobenzyl alcohol (3-NBA) was used as the matrix. The software used for FAB and EI measurements adds the mass of one electron. The molecular ion is abbreviated [M] for EI-MS and FAB-MS, the protonated molecular ion is abbreviated [M+H] for FAB-MS. Electrospray ionization-mass spectrometry (ESI-MS) spectra were recorded on a Thermo Fisher Scientific Q Executive mass spectrometer. Calibration was carried out using premixed calibration solutions (Thermo Fisher Scientific). The molecular fragments are stated as ratio of mass per charge *m/z*.

### 5.2.7 Infrared Spectroscopy (IR)

The infrared spectra were recorded with a Bruker, Alpha P instrument. All samples were measured by attenuated total reflection (ATR). The positions of the absorption bands are given in wavenumbers $\tilde{v}$ in cm$^{-1}$ and were measured in the range from 3600 cm$^{-1}$ to 500 cm$^{-1}$.

Characterization of the absorption bands was done in dependence of the absorption strength with the following abbreviations: vs (very strong, 0−9%), s (strong, 10−39%), m (medium, 40−69%), w (weak, 70−89%), vw (very weak, 90−100%).

### 5.2.8 Elemental Analysis (EA)

Elemental analysis was done on an Elementar vario MICRO instrument. The weight scale used was a Sartorius M2P. Calculated and found percentage by mass values for carbon, hydrogen, nitrogen, and sulfur are indicated in fractions of 100%.

### 5.2.9 LED Irradiation

Sample irradiation for photoisomerization and measurements of photostationary states was performed using LEDs with emission maxima of 523 nm, 407 nm and 365 nm from LED Engin, with 380 nm, 430 nm, 450 nm and 490 nm from Avonec and with 470 nm from OSRAM. For the time of irradiation, samples were maintained at constant temperature (22 ± 2 °C) using a metal cooling block. Irradiation intensities of the respective LEDs were determined using the PowerMax USB (type PS19Q) sensor device (Coherent®) in five independent measurements. The detector

(diameter 19 mm) was located at a distance of 55 mm from the light source, identical to the position of irradiated samples. The results are presented in Table 5.

**Table 5:** Irradiation intensities of the LEDs. The LEDs applied to irradiate the photoswitchable compounds were determined using the PowerMax USB (type PS19Q) sensor device (Coherent®).

| λ$_{max}$ of the LED diode [nm] | Max Power [mW/cm$^2$] | Max mean power measured [W] | Min Power [mW/cm$^2$] | Min mean power measured [W] |
|---|---|---|---|---|
| 365 nm | - | - | 5.61E-01 | 1.59E-03 |
| 380 nm | 8.67E-02 | 2.46E-04 | - | - |
| 407 nm | 9.39E+01 | 2.66E-01 | 8.59E+01 | 2.43E-01 |
| 430 nm | 1.85E+01 | 5.23E-02 | 1.19E+01 | 3.38E-02 |
| 450 nm | 1.13E+00 | 3.21E-03 | 8.86E-01 | 2.51E-03 |
| 470 nm | 1.69E+01 | 4.80E-02 | 1.59E+01 | 4.52E-02 |
| 490 nm | 7.64E+00 | 2.17E-02 | 4.98E+00 | 1.41E-02 |
| 523 nm | 7.08E+00 | 2.01E-02 | 6.56E+00 | 1.86E-02 |

### 5.2.10  Absorption Spectroscopy

UV-Vis absorption spectra between 200 nm and 800 nm were recorded on a Lambda 750 (PerkinElmer) UV-Vis spectrophotometer and an UV/Vis/NIR spectrometer Cary 500 (Varian), referenced against pure solvent. The spectra were measured in Quartz cuvettes of 10 mm or 2 mm optical path length at 20 °C. Baseline correction was performed manually to correct for solvent composition.

### 5.2.11  Fluorescence Spectroscopy

Fluorescence spectra were recorded on a Fluoromax-4 (Jobin Yvon - HORIBA) equipped with a Haake AC200 thermostat from Thermo Scientific at 20 °C. The spectra were recorded using FluorEssence v3.5.

### 5.2.12  Fluorescence Quantum Yield

Fluorescence quantum yield ($\Phi_F$) measurements (absolute values) were performed on a Hamamatsu Quantaurus-QY absolute PL quantum yield spectrometer C11347.

### 5.2.13 Photoswitching Quantum Yield

The maximum reaction quantum yields $\Phi_{max}$ for either isomerization direction (*Z*-isomer to *E*-isomer $\Phi_{Z\rightarrow E}$ and the reverse process $\Phi_{E\rightarrow Z}$) were determined, using the experimental setup previously published by the working group around Riedle (LMU). [132]

### 5.2.14 Crystal Structure Determinations

The single-crystal X-ray diffraction studies were carried out by Dr. Martin Nieger at the University of Helsinki (Finland) on a Bruker D8 Venture diffractometer with a PhotonII detector at 123(2) K, 173(2) K, or 298(2) K using Cu-Kα radiation ($\lambda$ = 1.54178 Å). Dual space methods (SHELXT) [143] were used for structure solution and refinement was carried out using SHELXL-2014 (full-matrix least-squares on F2) [144]. Hydrogen atoms were localized by difference electron density determination and refined using a riding model (H(N, O) free). Semi-empirical absorption corrections were applied. All measurement parameters and further details are presented in the chapters 5.4.14, 5.5.11 and 5.6.11.

### 5.2.15 Quantum Chemical Calculations

All calculations were performed with the GAUSSIAN09 program package [145], employing the B3LYPGD3BJ/6-311G(d,p) PCM(DMSO) level of theory (these parameters were successfully applied for calculations in another arylidene-substituted heterocyclic photochromic system – hemiindigos [135]). The global minima geometries were first optimized on the MPW1K/6-311G(d,p) and subsequently on the B3LYP-GD3BJ/6-311G(d,p). Frequency analysis confirmed all structures to be minimum structures since no imaginary frequencies have been found. Visualization of minimized structures, molecular orbitals, and calculated extinction spectra were done with GaussView 6.1.1. Excitation energies were calculated on TD-B3LYP-GD3BJ/6-311G(d,p) level of theory, using previously obtained structures. Solvent interactions were simulated using a polarizable continuum model (PCM), with parameters taken for DMSO. More detailed information and all results can be found in chapter 5.5.10.

## 5.3  Cell Experiments

All viability assays were performed by Anna-Lena Leistner and Angelika Seliwjorstow.

### 5.3.1  Cell Cultivation

HT-29 cells (Caucasian colon adenocarcinoma, ATCC HTB-38™) and HeLa cells (Human cervix carcinoma) were grown separately in DMEM (Dulbecco's Modified Eagle Medium) which was modified with 10% FCS (fetal calf serum) and 1% penicillin/streptomycin solution (10,000

units/mL of penicillin and 10,000 μg/mL of streptomycin) in a humid incubator at 37 °C with 5% $CO_2$. Cells were washed with PBS (Phosphate-Buffered Saline) from Gibco®. Cells were detached from the surfaces with Trypsin-EDTA (0.25%) from Gibco®. The cells were tested negative for mycoplasma contamination.

### 5.3.2   Viability Assays

Method A: HT-29 cells were seeded in 96-well plates at 3.000 cells/well and incubated overnight to ensure cell attachment to the well-bottom and cell growth. The tested compounds were added in the dark and the cells were incubated for 48 h (final well volume 100 μL, 0.25% DMSO; six technical replicates). To ensure the same treatment to the control rows, the DMEM was removed from the wells and 0.25% DMSO in DMEM (100 μL) was added to the corresponding wells. The positive control was treated with 5 μL of Triton™ X-100 detergent (10% solution (w/v)) per well for at least 5 min to induce cell death before adding 15 μL of MTT dye-solution (3-(4,5-dimethylthiazol-2-yl)-2,5-diphenyltetrazoliumbromid in water / CellTiter 96®Non-Radioactive Cell Proliferation Assay from Promega or Invitrogen™ CyQUANT™ MTT Cell Viability Assay) to all sample wells and incubating for 3 h in the dark. 100 μL of Solubilization Solution/Stop Mix (CellTiter 96®Non-Radioactive Cell Proliferation Assay from Promega / Invitrogen™ CyQUANT™ MTT Cell Viability Assay) were added after incubation to stop the reduction of MTT to formazan, therefore prevent overreaction and solubilize the formazan crystals. Alternatively, a freshly prepared stop solution (10% sodium dodecyl sulfate, 0.01 M HCl in water) was used. After 24 h of solubilization in the incubator, the plate was read out with a plate reader (SpectraMax® iD3, Molecular Devices) by measuring the absorption of each well at 570 nm or 590 nm. Data points were only excluded from the analysis when errors were observed during execution of the experiment (e.g. pipetting to a wrong well). In the experiment where a sample of compound **15** was irradiated at 490 nm, a complete row of wells (one concentration) was excluded. Otherwise only single wells were excluded. Absorbance data was averaged over the technical replicates, the positive control subtracted as background, then normalized to viable cell count from negative control cells (% control) as 100%. Three independent experiments were performed. Data were plotted against the log of agonist concentration (log10([agonist]) (M)) with mean and SD in GraphPad Prism Version 9.1.1 for Windows, GraphPad Software, San Diego, California USA, www.graphpad.com.

Method B: Following changes apply for viability assay with more detailed concentration range (compounds **14** and **15**): The tested photoisomers or irradiated mixtures were added in the dark

and the cells were incubated for 48 h (final well volume 100 µL, *E*-isomer: 0.5% DMSO / *Z*-isomer and 490 nm PSS: 0% DMSO; three to six technical replicates). To ensure the same treatment to the control rows, the DMEM was removed from the wells and *E*-isomer: 0.5% DMSO / *Z*-isomer and 490 nm PSS: 0% DMSO in DMEM (100 µL) was added to the corresponding wells. The positive control was treated with 5 µL of Triton™ X-100 detergent (10% solution (w/v)) per well for at least 5 min before adding 10 µL of MTT dye-solution (3-(4,5-dimethylthiazol-2-yl)-2,5-diphenyltetrazoliumbromid in water / Cell Proliferation kit I (MTT) from Roche) to all sample wells and incubating for 4 h in the dark. 100 µL of Solubilization Solution/Stop Mix (Cell Proliferation kit I (MTT) from Roche) were added after incubation to stop the reduction of MTT to formazan, therefore prevent overreaction and solubilize the formazan crystals.

### 5.3.3   Cell Penetration Assays

HeLa cells (Human cervix carcinoma cells, 4 x $10^4$ cells/well) were seeded in 8 well µ-slides (IBIDI® µ-Slide 8 well) with 200 µL Dulbecco's modified Eagle's medium (DMEM, 5 high glucose, Gibco) supplemented with 10% fetal calf serum (FCS, PAA) and 1 U/mL Penicillin/Streptomycin and incubated overnight at 37 °C, 5% CO2 and 95% humidity. The medium was replaced by 200 µL test solution per well, diluted in DMEM medium containing 0.25% (v/v) DMSO and incubated at 37 °C, 5% CO2 and 95% humidity for 15 hours.

Fixation was performed by removing the medium after the incubation time and each well washed with 200 µL PBS and 200 µL/well of a 4% *para*-formaldehyde solution in PBS were added. After incubation for 10 min the fixing solution was removed, the cells were washed ten times with PBS. 200 µL PBS/well were added and imaging was performed with a DMi8 inverted microscope (LEICA). The added compounds were excited at 488 nm and detected at wavelengths in the range of 500 - 650 nm. The results were processed and visualized with LEICA Application Suite X 3.7.4.23463 from LEICA Microsystems CMS GmbH.

### 5.3.4   Immunofluorescence Imaging

HT-29 cells were seeded in 8 well µ-slides from Ibidi and incubated overnight. The medium was replaced by 200 µL test solution per well, diluted in DMEM medium containing 0.25% DMSO. Based on the results of the viability assays, a concentration between the two IC50-values of the respective photoisomers was chosen: plinabulin (**6**): 2 nM; compound **8**: 20 nM; compound **10**: 200 nM. After 6 h of incubation in the dark, the medium was removed, each well washed with 200 µL PBS and 200 µL/well of a 4% *para*-formaldehyde solution in PBS were added. After incubation for 10 min the fixing solution was removed, the cells were washed with PBS and 200 µL of a 1%

Triton-X100 solution in PBS was added to each well and incubated for 4 min. Then the solution was removed, and the cells were washed again with PBS. To avoid false positive staining of the antibody, all binding sites were blocked by a CAS-Block™ histochemical reagent solution (ThermoFisher). For this purpose, PBS was removed and the CAS-Block™ solution was added (200 µL per well) and incubated for 30 min. For tubulin staining a fluorescein (FITC)-labeled monoclonal anti-α-tubulin antibody produced in mice (Sigma; F2168-2ML) was used. 200 µL of a 1:500 dilution of the antibody in PBS was added and the cells were incubated overnight in the fridge. The next day, the solution was replaced by 1:5000 Hoechst 33342 (Promega) in PBS. After 5 min of incubation, the cells were washed with PBS and imaged using a TCS SPE microscope (LEICA) microscope. The FITC-fluorescence was detected at 525 nm after irradiation at 470 nm, the Hoechst dye was irradiated at 361 nm and its emission was detected at 497 nm. The results were processed and visualized with LEICA Application Suite X 3.5.7.23225 from Leica Microsystems CMS GmbH.

## 5.4 Synthesis and Characterization of Plinabulin Derivatives

### 5.4.1 Precursor Synthesis

*Ethyl 5-(tert-butyl)oxazole-4-carboxylate*
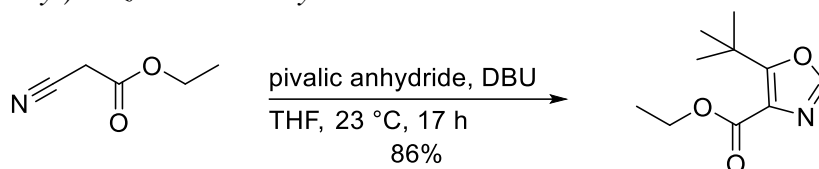


Ethylisocyanoacetate (**3**) (10.0 g, 88.4 mmol, 1.00 equiv.) was dissolved in THF (80 mL), and pivalic anhydride (19.7 mL, 18.1 g, 97.3 mmol, 1.10 equiv.) and DBU (14.8 g, 97.3 mmol, 1.10 equiv.) were added. The reaction mixture was stirred overnight at 23 °C. Subsequently, the solvent was removed *in vacuo* and the residue was dissolved in ethyl acetate (150 mL). Brine (110 mL) and saturated aq. $Na_2CO_3$ solution (55 mL) were added and the phases were separated, and the aqueous phase was extracted three more times with ethyl acetate. After washing the organic phase with saturated aq. $Na_2CO_3$ solution (75 mL), citric acid (75 mL, 0.1 M) and drying over $Na_2SO_4$, the solvent was removed *in vacuo*. The residual oil was purified by flash column chromatography (cyclohexane:ethyl acetate, 20:1 → 9:1 → 6:1) to yield 15.0 g (76.1 mmol, 86%) of ethyl 5-(*tert*-butyl)oxazole-4-carboxylate as a yellow oil.[100]

**¹H NMR (400 MHz, CDCl₃):** $\delta$ = 7.69 (s, 1H, C*H*), 4.38 (q, $J$ = 7.1 Hz, 2H, C*H₂*), 1.45 (s, 9H, C(C*H₃*)₃), 1.40 (t, $J$ = 7.1 Hz, 3H, C*H₃*) ppm.

**¹³C NMR (101 MHz, CDCl₃):** $\delta$ = 166.1 (*C*-C(CH₃)₃), 162.2 (*C*OOEt), 147.3 (*C*H), 126.1 (*C*-COOEt), 61.3 (*C*H₂), 33.4 (*C*(CH₃)₃), 28.2 (C(*C*H₃)₃), 14.4 (*C*H₃) ppm.

**TLC:** $R_f$ = 0.34 (cyclohexane:ethyl acetate, 4:1).

**IR (ATR):** $v$ = 3118 (vw), 2975 (w), 2962 (w), 2938 (w), 2908 (w), 2874 (vw), 1718 (m), 1572 (m), 1527 (m), 1504 (w), 1482 (w), 1463 (w), 1448 (w), 1397 (w), 1368 (m), 1333 (m), 1302 (m), 1254 (m), 1221 (w), 1204 (w), 1180 (m), 1160 (m), 1129 (m), 1098 (m), 1052 (s), 1023 (m), 1006 (m), 942 (w), 864 (w), 844 (m), 820 (w), 793 (m), 773 (w), 708 (w), 649 (m), 606 (w), 541 (w), 401 (w) cm⁻¹.

**HRMS (EI):** $m/z$ calcd. for $C_{10}H_{15}NO_3$ [M], 197.1051; found, 197.1052.

*Ethyl 5-(tert-butyl)-1H-imidazole-4-carboxylate*
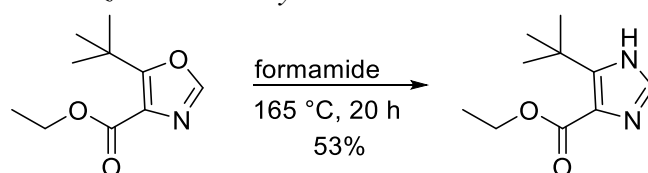
Ethyl 5-(*tert*-butyl)oxazole-4-carboxylate (15.0 g, 76.0 mmol, 1.00 equiv.) was dissolved in formamide (90.0 mL, 102 g, 2.27 mol, 29.8 equiv.) and the mixture reacted at 165 °C overnight. After cooling down, ethyl acetate (180 mL) and brine (90 mL) were added and the aqueous phase was extracted with ethyl acetate (2×90 mL). Subsequently, the organic layer was washed with saturated aq. $Na_2CO_3$ solution (3×75 mL) and brine (3×75 mL), dried over $Na_2SO_4$ and concentrated *in vacuo*. The residual oil was purified by flash column chromatography (10% MeOH in toluene) to yield 7.98 g (40.7 mmol, 53%) of ethyl 5-(*tert*-butyl)-1*H*-imidazole-4-carboxylate as a yellow solid.[100]

**¹H NMR (400 MHz, CDCl₃):** $\delta$ = 9.76 (s, 1H, N*H*), 7.47 (d, *J* = 1.7 Hz, 1H, C*H*), 4.44 – 4.09 (m, 2H, C*H₂*), 1.44 (s, 9H, C(C*H₃*)₃), 1.32 – 1.22 (m, 3H, C*H₃*) ppm.

**¹³C NMR (101 MHz, CDCl₃):** $\delta$ = 162.4 (*C*OOEt), 150.8 (*C*-C(CH₃)₃), 133.4 (*C*H), 123.5 (*C*-COOEt), 60.5 (*C*H₂), 32.6 (*C*(CH₃)₃), 29.2 (C(*C*H₃)₃), 14.3 (*C*H₃) ppm.

**TLC:** $R_f$ = 0.15 (10% MeOH in toluene).

**IR (ATR):** $v$ = 3119 (vw), 3033 (vw), 2955 (w), 2907 (w), 2871 (w), 2840 (w), 2747 (vw), 2630 (vw), 1700 (w), 1560 (vw), 1499 (vw), 1434 (w), 1394 (vw), 1366 (vw), 1296 (m), 1271 (w), 1224 (vw), 1198 (w), 1171 (w), 1147 (w), 1096 (vw), 1058 (m), 1024 (w), 952 (w), 935 (w), 864 (w), 847 (w), 793 (w), 711 (vw), 663 (w), 605 (vw), 564 (vw), 483 (vw), 401 (vw) cm$^{-1}$.

**HRMS (EI):** *m/z* calcd. for $C_{10}H_{16}N_2O_2$ [M], 196.1212; found, 196.1212.


*(5-(tert-Butyl)-1H-imidazol-4-yl)methanol*
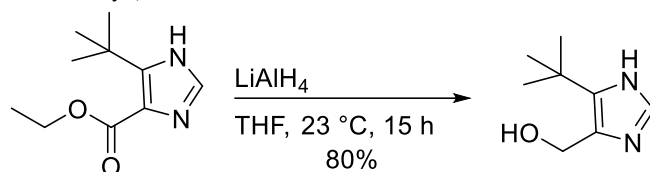


Ethyl 5-(*tert*-butyl)-1*H*-imidazole-4-carboxylate (4.40 g, 22.4 mmol, 1.00 equiv.) was dissolved in THF (140 mL). LiAlH₄ (1.70 g, 44.8 mmol, 2.00 equiv.) was added in small portions over 45 min, while cooling the mixture in an ice water bath to 0 °C. The reaction mixture was stirred overnight at 23 °C and subsequently ethyl acetate (100 mL) and water (50 mL) were added at 0 °C. After another 1 hour of stirring, the precipitate was filtered off, the filtrate was dried over $Na_2SO_4$ and the solvent was removed *in vacuo*. The residual solid was purified by flash column chromatography (20% MeOH in CH₂Cl₂) to yield 2.78 g (18.0 mmol, 80%) of (5-(*tert*-butyl)-1*H*-imidazol-4-yl)methanol as a pale yellow solid.[106]

**¹H NMR (400 MHz, DMSO-*d₆*):** $\delta$ = 7.35 (s, 1H, C*H*), 4.46 (s, 2H, C*H₂*), 1.28 (s, 9H, C(C*H₃*)₃) ppm.

**¹³C NMR (101 MHz, DMSO-$d_6$):** $\delta = 139.7$ ($C$-C(CH₃)₃), 131.8 ($C$H), 129.1 ($C$-CH₂), 56.0 ($C$H₂), 31.9 ($C$(CH₃)₃), 30.7 (C($C$H₃)₃) ppm.

**TLC:** R$_f$ = 0.25 (20% MeOH in CH₂Cl₂, stained with KMnO₄).

**IR (ATR):** $v$ = 3159 (vw), 3119 (w), 3106 (w), 3067 (w), 3019 (w), 2959 (w), 2901 (w), 2894 (w), 2884 (w), 2840 (w), 2730 (w), 2694 (w), 2670 (w), 2630 (w), 1578 (w), 1492 (w), 1469 (w), 1390 (vw), 1356 (w), 1332 (vw), 1298 (w), 1262 (w), 1230 (vw), 1204 (vw), 1187 (w), 1163 (w), 1094 (w), 1026 (w), 1013 (m), 953 (w), 901 (w), 858 (w), 823 (w), 765 (w), 715 (w), 649 (w), 595 (w), 520 (w), 473 (w), 405 (vw), 399 (vw), 380 (w) cm⁻¹.

**HRMS (EI):** $m/z$ calcd. for C₈H₁₄N₂O [M], 154.1106; found, 154.1104.

*5-(tert-Butyl)-1H-imidazole-4-carbaldehyde (4)*
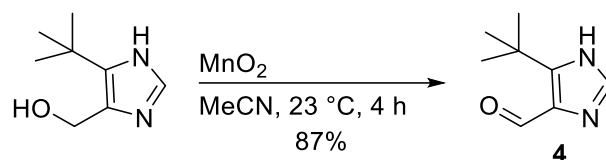


(5-(*tert*-Butyl)-1*H*-imidazol-4-yl)methanol (751 mg, 4.87 mmol, 1.00 equiv.) was dissolved in acetonitrile (50 mL). Subsequently, activated MnO₂ (4.23 g, 48.7 mmol, 10.0 eq, c.a. 85%, <10 μm) was added and the mixture was stirred at room temperature for 4 hours. Subsequently, the mixture was filtered through celite® and the solvent was removed *in vacuo* to yield 644 mg (4.23 mmol, 87%) of 5-(*tert*-butyl)-1*H*-imidazole-4-carbaldehyde (**4**) as a yellow solid.[106]

**¹H NMR (400 MHz, CDCl₃):** $\delta$ = 10.06 (s, 1H, C$H$O), 7.74 (s, 1H, C$H$), 1.48 (s, 9H, C(C$H_3$)₃) ppm.

**¹³C NMR (101 MHz, CDCl₃):** $\delta$ = 181.9 ($C$HO), 137.5 ($C$H), 34.1 ($C$(CH₃)₃), 31.3 (C($C$H₃)₃) ppm.

**IR (ATR):** $v$ = 3121 (vw), 3053 (vw), 2963 (w), 2902 (vw), 2864 (vw), 1670 (w), 1558 (vw), 1507 (w), 1465 (vw), 1435 (w), 1398 (vw), 1377 (w), 1370 (w), 1349 (vw), 1336 (vw), 1295 (w), 1271 (w), 1204 (vw), 1186 (vw), 1057 (vw), 1023 (vw), 950 (w), 933 (vw), 864 (w), 837 (w), 786 (w), 666 (w), 582 (vw), 445 (vw) cm⁻¹.

**HRMS (EI):** $m/z$ calcd. for C₈H₁₂N₂O [M], 152.0950; found, 152.0951.

*Piperazine-2,5-dione*
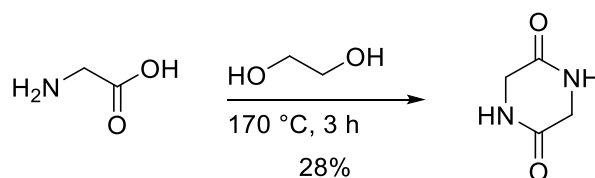
Glycine (**1**) (100 g, 1.33 mol, 1.00 equiv.) was dissolved in ethylene glycol (500 mL, 557 g, 8.97 mmol, 6.73 equiv.) and stirred at 170 ºC for 3 hours. Afterwards, the solution was cooled at 5 ºC for 20 hours and the precipitate was filtered off and washed with methanol (500 mL). Subsequently, the crude product was recrystallized from water and the solution was cooled overnight. The residual solid was filtered off and washed with methanol to yield 42.2 g (370 mmol, 28%) of piperazine-2,5-dione as a beige solid.[104]

**$^1$H NMR (400 MHz, DMSO-$d_6$):** $\delta$ = 8.01 (s, 2H, CON*H*), 3.70 (d, J = 1.9 Hz, 4H, C*H$_2$*) ppm.

**$^{13}$C NMR (101 MHz, DMSO-$d_6$):** $\delta$ = 166.1 (*C*ONH), 44.3 (*C*H$_2$) ppm.

**IR (ATR):** $v$ = 3173 (vw), 3041 (vw), 2980 (vw), 2912 (vw), 2874 (vw), 1662 (w), 1591 (w), 1519 (w), 1468 (w), 1411 (w), 1333 (w), 1251 (w), 1132 (w), 1116 (w), 1072 (w), 1038 (w), 996 (vw), 914 (w), 892 (w), 829 (w), 805 (w), 701 (w), 605 (w), 518 (w), 479 (w), 445 (w), 408 (w), 397 (w) cm$^{-1}$.

**HRMS (EI):** $m/z$ calcd. for C$_4$H$_6$N$_2$O$_2$ [M], 114.0429; found, 114.0428

*1,4-Diacetylpiperazine-2,5-dione (**2**)*
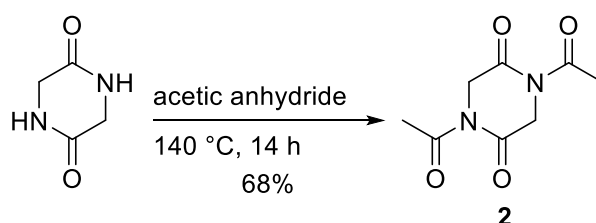


Piperazine-2,5-dione (5.00 g, 43.8 mmol, 1.00 equiv.) was dissolved in acetic anhydride (1.50 L, 15.9 mol, 352 equiv.) and stirred with a reflux condenser at 140 °C for 14 hours. Subsequently, the solvent was removed *in vacuo*, and the product was washed with diethyl ether and filtered off to yield 5.94 g (30.0 mmol, 68%) of 1,4-diacetylpiperazine-2,5-dione (**2**) as a brown solid.[104]

**$^1$H NMR (400 MHz, CDCl$_3$):** $\delta$ = 4.59 (s, 4H, C*H$_2$*), 2.58 (s, 6H, C*H$_3$*) ppm.

**$^{13}$C NMR (101 MHz, CDCl$_3$):** $\delta$ = 172.7 (*C*OCH$_3$), 166.0 (*C*OCH$_2$), 47.3 (*C*H$_2$), 26.9 (*C*H$_3$) ppm.

**TLC:** R$_f$ = 0.25 (0.5% MeOH in CH$_2$Cl$_2$).

**IR (ATR):** $v$ = 3349 (vw), 3336 (vw), 3271 (w), 3085 (vw), 3053 (vw), 2944 (vw), 2929 (vw), 1701 (w), 1642 (w), 1554 (w), 1469 (vw), 1453 (vw), 1418 (w), 1358 (w), 1306 (w), 1259 (w), 1224 (w), 1180 (w), 1129 (w), 1078 (w), 1030 (w), 996 (vw), 975 (w), 946 (w), 924 (vw), 902 (vw), 813 (vw), 690 (w), 622 (w), 596 (w), 565 (w), 550 (w) cm$^{-1}$.

**HRMS (EI):** $m/z$ calcd. for C$_8$H$_{10}$N$_2$O$_4$ [M], 198.0641; found, 198.0642.

*(Z)-1-Acetyl-3-((5-(tert-butyl)-1H-imidazol-4-yl)methylene)piperazine-2,5-dione (5)*
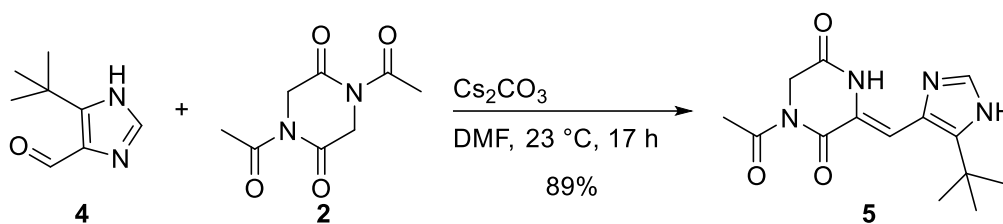


(5-(*tert*-Butyl)-1*H*-imidazol-4-carbaldehyde (**4**) (1.50 g, 9.86 mmol, 1.00 equiv.) was dissolved in dry DMF (17 mL) under argon atmosphere. 1,4-Diacetyl-piperazine-2,5-dione (**2**) (3.91 g, 19.7 mmol, 2.00 equiv.) was dissolved in the mixture and Cs$_2$CO$_3$ (4.82 g, 14.8 mmol, 1.50 equiv.) was added. Subsequently, the mixture was stirred for 17 hours under argon atmosphere at room temperature. The reaction mixture was poured on an ice water/brine mix (30 mL) and the precipitate was filtered off and dried to yield 2.54 g (8.73 mmol, 89%) of (*Z*)-1-acetyl-3-((5-(*tert*-butyl)-1*H*-imidazol-4-yl)methylene)piperazine-2,5-dione (**5**) as a beige solid.[106]

**$^1$H NMR (400 MHz, CDCl$_3$):** $\delta$ = 12.36 (s, 1H, N*H*, imidazole), 12.01 (s, 1H, CON*H*), 7.85 (s, 1H, C*H*), 7.04 (s, 1H, C*H*), 4.30 (s, 2H, C*H*$_2$), 2.49 (s, 3H, C*H*$_3$), 1.39 (s, 9H, C(C*H*$_3$)$_3$) ppm.

**$^{13}$C NMR (101 MHz, CDCl$_3$):** $\delta$ = 172.2 (1C, *C*OCH$_3$), 162.2 (1C, *C*ONH), 160.1 (1C, *C*ON-COCH$_3$), 141.0 (1C, *C*-C(CH$_3$)$_3$), 134.5 (1C, *C*H, imidazole), 130.6 (1C, NH-*C*-CH), 123.7 (*C*-CH, imidazole), 107.3 (1C, *C*H, double bond), 46.3 (1C, *C*H$_2$), 31.9 (1C, *C*(CH$_3$)$_3$), 30.6 (3C, C(*C*H$_3$)$_3$), 27.0 (1C, CO*C*H$_3$) ppm.

**IR (ATR):** $\nu$ = 3145 (vw), 3080 (w), 3023 (w), 3010 (w), 2978 (w), 2961 (w), 2901 (w), 2877 (w), 2850 (w), 2791 (w), 2765 (w), 2727 (w), 2684 (vw), 1706 (m), 1649 (m), 1612 (w), 1567 (w), 1509 (w), 1485 (w), 1436 (m), 1417 (w), 1397 (w), 1373 (w), 1364 (w), 1346 (w), 1258 (w), 1225 (m), 1200 (m), 1186 (m), 1162 (w), 1105 (w), 1048 (w), 1030 (w), 999 (w), 980 (w), 943 (w), 897 (vw), 871 (w), 829 (w), 778 (w), 741 (w), 730 (w), 688 (w), 664 (w), 586 (w), 578 (w), 533 (vw), 518 (w), 475 (w), 439 (w) cm$^{-1}$.

**HRMS (FAB):** *m/z* calcd. for C$_{14}$H$_{19}$N$_4$O$_3$ [M+H], 291.1457; found, 291.1458.

**UV/Vis (MeCN):** $\lambda_{max}$ = 343 nm.

### 5.4.2  Synthesis of Aldehydes

*2,6-Bis(methylthio)benzaldehyde and 2-chloro-6-(methylthio)benzaldehyde*
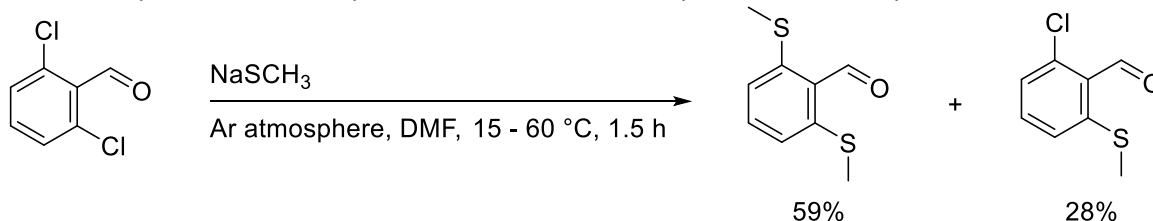
2,6-Dichlorobenzaldehyde (300 mg, 1.71 mmol, 1.00 equiv.) was dissolved in dry DMF (2 mL) under argon atmosphere. Sodium methanethiolate (252 mg, 3.60 mmol, 2.10 equiv.) was added at 15 °C portionwise to the mixture. After 20 min of stirring, the solution was heated to 60 °C and stirred for an additional 60 min. Subsequently, the mixture was cooled to room temperature, diluted with ethyl acetate (6 mL) and washed with water (3×3 mL). The solution was dried over $Na_2SO_4$ and the solvent was removed *in vacuo*. The crude residue was purified by flash column chromatography (cyclohexane:$CH_2Cl_2$, 1:1) to yield 200 mg (1.01 mmol, 59%) of 2,6-bis(methylthio)benzaldehyde as a yellow solid and 89.0 mg (0.477 mmol, 28%) of 2-chloro-6-(methylthio)benzaldehyde as a yellow solid.[146]

*2,6-Bis(methylthio)benzaldehyde*

**$^1$H NMR (400 MHz, CDCl$_3$):** $\delta$ = 10.71 (s, 1H, C*H*O), 7.42 (t, $J$ = 8.0 Hz, 1H, $H_{arom}$), 7.11 (d, $J$ = 7.9 Hz, 2H, $H_{arom}$), 2.48 (s, 6H, C$H_3$) ppm.

**$^{13}$C NMR (101 MHz, CDCl$_3$):** $\delta$ = 190.2 (*C*HO), 145.9 (*C*-SCH$_3$), 133.1 ($C_{arom}$), 129.3 (*C*-CHO), 122.0 ($C_{arom}$), 16.3 (*C*H$_3$) ppm.

**IR (ATR):** $v$ = 2989 (w), 2975 (w), 2912 (w), 2860 (w), 2840 (w), 2758 (w), 1663 (m), 1560 (w), 1547 (w), 1509 (w), 1502 (w), 1442 (w), 1432 (w), 1412 (w), 1390 (w), 1324 (w), 1310 (w), 1281 (w), 1203 (m), 1193 (w), 1174 (w), 1102 (w), 1086 (w), 972 (w), 960 (w), 846 (w), 776 (w), 758 (m), 720 (w), 704 (w), 669 (w), 475 (w), 415 (w) cm$^{-1}$.

**HRMS (EI):** $m/z$ calcd. for $C_9H_{10}OS_2$ [M], 198.0173; found, 198.0172.

*2-Chloro-6-(methylthio)benzaldehyde*

**$^1$H NMR (400 MHz, CDCl$_3$):** $\delta$ = 10.64 (s, 1H, C*H*O), 7.42 (t, $J$ = 8.0 Hz, 1H, $H_{arom}$), 7.24 – 7.16 (m, 2H, $H_{arom}$), 2.46 (s, 3H, C$H_3$) ppm.

**$^{13}$C NMR (101 MHz, CDCl$_3$):** $\delta$ = 190.7 (*C*HO), 147.0 ($C_{arom}$-SCH$_3$), 140.5 ($C_{arom}$-Cl), 133.7 ($C_{arom}$), 128.3 ($C_{arom}$-CHO), 125.7 ($C_{arom}$), 123.1 ($C_{arom}$), 15.7 (*C*H$_3$) ppm.

**IR (ATR):** $v$ = 1666 (w), 1571 (w), 1557 (w), 1543 (w), 1490 (vw), 1434 (w), 1409 (w), 1395 (w), 1326 (vw), 1317 (w), 1283 (vw), 1194 (m), 1162 (w), 1092 (w), 1079 (w), 990 (vw), 972 (vw), 962 (w), 945 (w), 894 (vw), 877 (vw), 837 (w), 775 (m), 704 (w), 663 (w), 545 (vw), 523 (vw), 428 (w), 412 (w) cm$^{-1}$.

**HRMS (EI):** $m/z$ calcd. for $C_8H_7ClOS$ [M], 185.9906; found, 185.9905.

*[3-(Dibromomethyl)phenyl]-phenylmethanone*
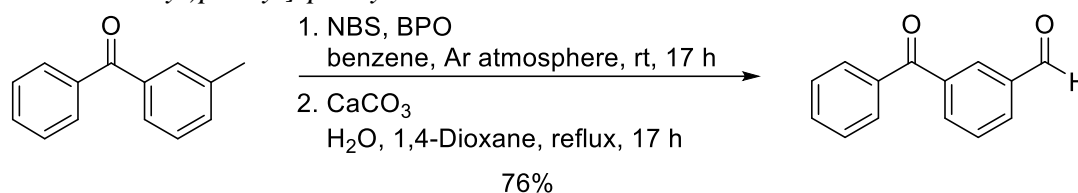


3-Methylbenzophenone (2.00 g, 1.83 mL, 10.2 mmol, 1.00 equiv.), *N*-bromosuccinimide (4.53 g, 25.5 mmol, 2.50 equiv.) and benzoyl peroxide (39.5 mg, 163 μmol, 0.0160 equiv.) in benzene (20.0 mL) were refluxed under argon atmosphere for 17 h. The mixture was allowed to cool down to room temperature, washed twice with 50 mL of distilled $H_2O$ and dried over anhydrous $Na_2SO_4$. The solvent was then removed *in vacuo* to yield 4.28 g of crude [3-(dibromomethyl)phenyl]-phenylmethanone as a grey solid.

The crude [3-(dibromomethyl)phenyl]-phenylmethanone (4.28 g, 12.1 mmol, 1.00 equiv.) was combined with $CaCO_3$ (5.00 g, 50.0 mmol, 4.13 equiv.) in 60 mL $H_2O$/dioxane (1:1) and refluxed overnight for 17 h. After the reaction mixture has been cooled down, the solvent was removed *in vacuo*. Subsequently, 40 mL of $CH_2Cl_2$ and 80 mL of 1 mol/L HCl were added under continued stirring to dissolve the solid. The organic phase was isolated and the aqueous phase extracted twice with 20 mL of $CH_2Cl_2$. The organic fractions were combined, washed twice with 40 mL sat. aq. $NaHCO_3$ and dried over anhydrous $Na_2SO_4$. The crude residue was purified by flash column chromatography (diethyl ether:cyclohexane, 1:1) to yield 1.63 g (7.77 mmol, 76%) of 3-benzoylbenzaldehyde as colorless oil.[147]

**TLC:** $R_f$ = 0.45 (cyclohexane:diethyl ether 1:1)

**$^1$H NMR (400 MHz, CDCl$_3$):** $\delta$ = 10.06 (s, 1H, C*H*O), 8.25 (t, $J$ = 1.8 Hz, 1H, $H_{arom}$), 8.09 (dt, $J$ = 7.6, 1.5 Hz, 1H, $H_{arom}$), 8.05 (dt, $J$ = 7.7, 1.5 Hz, 1H, $H_{arom}$), 7.81 – 7.76 (m, 2H, $H_{arom}$), 7.66 (t, $J$ = 7.7 Hz, 1H, $H_{arom}$), 7.63 – 7.58 (m, 1H, $H_{arom}$), 7.53 – 7.41 (m, 2H, $H_{arom}$) ppm.

*tert-Butyl 3-formylpyrrole-1-carboxylate*
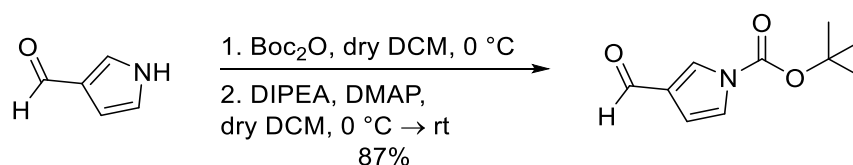


Boc$_2$O (1.24 g, 5.68 mmol, 1.08 equiv.) dissolved in dry $CH_2Cl_2$ (7.5 mL) was added dropwise to a solution of 1*H*-pyrrole-3-carbaldehyde (500 mg, 5.26 mmol, 1.00 equiv.) in dry $CH_2Cl_2$ (7.5 mL) at 0 °C. After 15 min a solution of DIPEA (734 mg, 5.68 mmol, 1.08 equiv.) and DMAP (19.3 mg, 158 μmol, 0.0300 equiv.) in dry $CH_2Cl_2$ (7.5 mL) was added dropwise over 30 min. The reaction was stirred for 1 h at 0 °C and then allowed to warm to room temperature over the course of 1.5 h.

The mixture was washed with a sat. aq. solution of $NH_4Cl$ (30 mL), extracted with $CH_2Cl_2$ (30 mL) and purified by flash chromatography (cyclohexane/ethyl acetate 9:1). The reaction yielded 896 mg of *tert*-butyl 3-formylpyrrole-1-carboxylate as a colorless oil (4.59 mmol, 87%).[148]

**$^1$H NMR (400 MHz, CDCl$_3$):** $\delta = 9.83$ (s, 1H), 7.83 (t, $J = 1.9$ Hz, 1H), 7.25 – 7.27 (m, 1H), 6.64 (dd, $J = 3.4$, 1.7 Hz, 1H), 1.62 (s, 9H) ppm.

**$^{13}$C NMR (101 MHz, CDCl$_3$):** $\delta = 185.8$, 148.1, 129.0, 128.4, 122.3, 109.5, 85.7, 28.0 ppm.

### 5.4.3 Synthesis of Plinabulin Derivatives

The following compounds were synthesized under my supervision by students working on their bachelor thesis: **7**, **11**, **12** and **13** by Angelika Seliwjorstow; **9**, **19**-**22** by Jonas Springer; **23**, **25**, **26** and **28** by Sven Schenk.

**6**: 65%   **7**: 81%   **8**: 45%   **9**: 23%   **10**: 58%   **11**: 24%

**12**: 24%   **13**: 32%   **14**: 49%   **15**: 40%   **16**: 23%   **17**: 30%

**18**: 30%   **19**: 45%   **20**: 39%   **21**: 25%   **22**: 28%

**23**: 27%   **24**: 54%   **25**: 41%   **26**: 28%   **27**: 98%   **28**: 27%
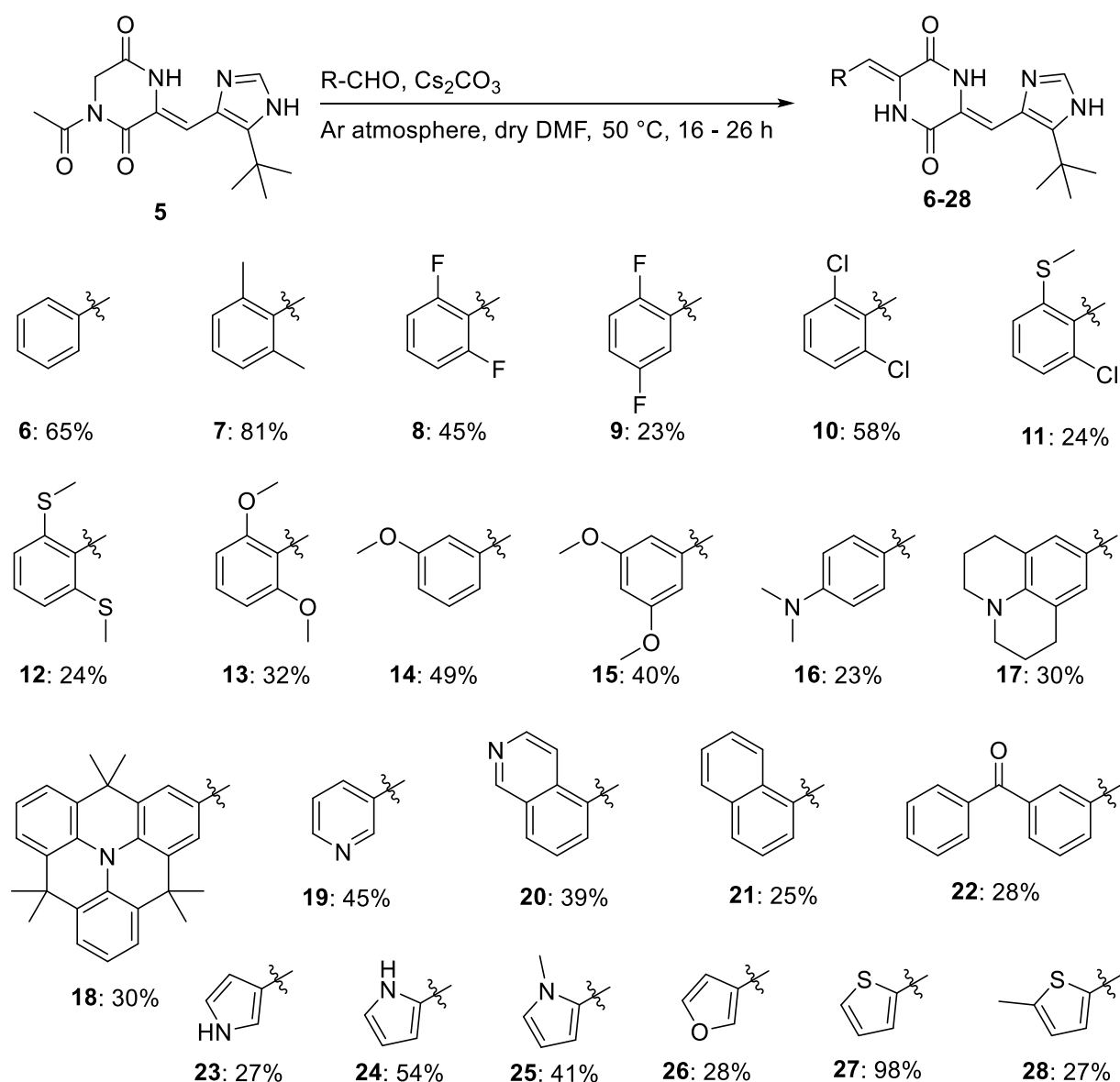
(*Z*)-1-Acetyl-3-((5-(*tert*-butyl)-1*H*-imidazol-4-yl)methylene)piperazine-2,5-dione (**5**) (100 mg, 344 µmol, 1.00 equiv.) was dissolved in 1.0 mL of dry DMF under an argon atmosphere. The respective aldehyde (517 µmol, 1.50 equiv.) was dissolved in the mixture and $Cs_2CO_3$ (168 mg, 517 µmol, 1.50 equiv.) was added. The mixture was stirred for 17-23 h under an argon atmosphere at 50 °C. The reaction mixture was subsequently poured on ice water (20 mL) and the precipitate was filtered off. The crude product was purified *via* HPLC (gradient of 20-80% MeCN in $H_2O$ within 40 min, 0.1% TFA (v/v) in the solvents) and washed with sat. aq. solution of $NaHCO_3$.

For selected compounds the respective *E*-isomers were isolated. This was achieved by irradiating a solution of the respective compound in DMSO with 407 nm for 1 hour followed by the seperation of the two photoisomers *via* HPLC and washing with sat. aq. solution of $NaHCO_3$.

In case of compounds **7**, **11**, **12** and **13** the neutralization step after the purification was omitted.

For the synthesis of compound **23** a Boc-protected aldehyde was used and an additional deprotection step was included before the purification as described in the respective subchapter. The aldehyde applied for the synthesis of compound **18** was synthesized and provided by the group of Prof. Dr. Milan Kivala from Heidelberg University.

*Plinabulin (**6**)*
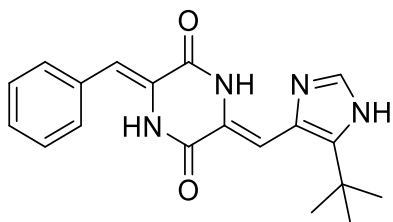


**Z-isomer**

**$^1$H NMR (400 MHz, DMSO-$d_6$):** $\delta$ = 12.11 (bs, 1H, N*H*), 11.33 (bs, 2H, N*H*), 7.79 (s, 1H, C*H*), 7.64 (d, *J* = 7.6 Hz, 2H, *H*$_{arom}$), 7.38 (t, *J* = 7.6 Hz, 2H, *H*$_{arom}$), 7.26 (t, *J* = 7.4 Hz, 1H, *H*$_{arom}$), 6.80 (s, 1H, C*H*, double bond), 6.65 (s, 1H, C*H*, double bond), 1.38 (s, 9H, C(C*H*$_3$)$_3$) ppm.

**$^{13}$C NMR (101 MHz, DMSO-$d_6$):** $\delta$ = 158.0 (1C, *C*ONH), 156.7 (1C, *C*ONH), 140.2 (1C, *C*-C(CH$_3$)$_3$), 134.3 (1C, *C*H, imidazole), 133.8 (1C, *C*$_{arom}$-CH), 130.9 (1C, *C*-CH), 129.3 (2C, *C*$_{arom}$), 128.6 (2C, *C*$_{arom}$), 128.0 (1C, *C*$_{arom}$), 127.6 (1C, *C*-CH), 124.2 (1C, *C*-CH), 113.3 (1C, *C*H, double bond), 104.5 (1C, *C*H, double bond), 31.9 (1C, *C*(CH$_3$)$_3$), 30.7 (3C, C(*C*H$_3$)$_3$) ppm.

**TLC:** R$_f$= 0.22 (developed in 7.5% MeOH in CH$_2$Cl$_2$:toluene; 1:1).

**HRMS (FAB):** *m/z* calcd. for C$_{19}$H$_{20}$N$_4$O$_2$ [M], 337.1665; found: 337.1665.

**IR (ATR):** $v$ = 2977 (vw), 1684 (w), 1644 (w), 1400 (w), 1353 (w), 1186 (w), 1144 (w), 953 (vw), 801 (w), 765 (w), 719 (w), 689 (w), 645 (vw), 520 (vw), 459 (vw), 442 (vw) cm$^{-1}$.

**UV/Vis (MeCN):** $\lambda_{max}$ = 362 nm.

**Fluorescence (MeCN):** $\lambda_{em}$= 512 nm (excited with $\lambda$ = 370 nm).

**$\Phi_F$ (MeCN):** 0.045.


**E-isomer**

**$^1$H NMR (400 MHz, DMSO-$d_6$):** $\delta$ = 12.26 (bs, 1H, N*H*), 12.07 (s, 1H, N*H*), 10.75 (bs, 1H, N*H*), 7.82 (s, 1H, C*H*), 7.54 (dd, J = 7.7, 1.6 Hz, 2H, *H*$_{arom}$), 7.28 (t, J = 7.3 Hz, 2H, *H*$_{arom}$), 7.22 (t, J = 7.3 Hz, 1H, *H*$_{arom}$), 6.79 (s, 1H, C*H*, double bond), 6.51 (s, 1H, C*H*, double bond), 1.38 (s, 9H, C(C*H*$_3$)$_3$) ppm.

**$^{13}$C NMR (101 MHz, DMSO-$d_6$):** $\delta$ = 157.9 (1C, *C*ONH), 155.9 (1C, *C*ONH), 140.6 (1C, *C*-C(CH$_3$)$_3$), 134.8 (1C, *C*H, imidazole), 131.2 (1C, *C*$_{arom}$-CH), 130.8 (2C, *C*$_{arom}$), 127.9 (2C, *C*$_{arom}$),

127.8 (1C, $C_{arom}$), 127.7 (1C, $C$-CH), 124.2 (1C, $C$-CH), 120.2 (1C, $CH$, double bond), 104.5 (1C, $CH$, double bond), 32.4(1C, $C(CH_3)_3$), 31.1 (3C, C($CH_3)_3$) ppm.

**UV/Vis (MeCN):** $\lambda_{max}$ = 360 nm.

**Fluorescence (MeCN):** $\lambda_{em}$= 533 nm (excited with $\lambda$ = 400 nm).

**$\Phi_F$ (MeCN):** 0.020.

*(Z)-3-((5-(tert-Butyl)-1H-imidazol-4-yl)methylene)-6-((Z)-2,6-dimethylbenzylidene)piperazine-2,5-dione (7)*
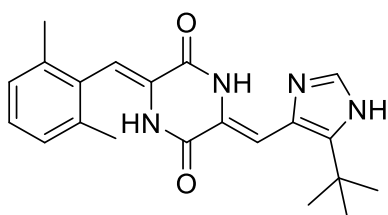


**¹H NMR (400 MHz, DMSO-$d_6$):** $\delta$ = 12.70 (s, 1H, N$H$), 11.94 (s, 1H, N$H$), 9.69 (s, 1H, C$H$), 8.13 (s, 1H, N$H$), 7.14 (dd, $J$ = 8.5, 6.5 Hz, 1H, $H_{arom}$), 7.07 (d, $J$ = 7.4 Hz, 2H, $H_{arom}$), 6.77 (s, 1H, C$H$), 6.73 (s, 1H, C$H$), 2.16 (s, 6H, C$H_3$), 1.36 (s, 9H, C(C$H_3)_3$) ppm.

**¹³C NMR (101 MHz, DMSO-$d_6$):** $\delta$ = 157.1 ($C$ONH), 156.2 ($C$ONH), 140.0 ($C$-C(CH_3)_3), 136.2 ($C_{arom}$-CH_3), 134.3 ($C$H), 131.7 ($C_{arom}$-CH), 128.2 ($C$-CH), 127.6 ($C_{arom}$), 127.4 ($C_{arom}$), 114.1 ($C$H), 104.2 ($C$H), 99.6 ($C$-CH), 31.9 ($C$(CH_3)_3), 30.4 (C($C$H_3)_3), 20.1 ($C$H_3) ppm.

**IR (ATR):** $v$ = 3165 (vw), 3111 (vw), 3024 (vw), 2969 (vw), 2871 (vw), 1690 (w), 1664 (w), 1655 (w), 1646 (w), 1630 (w), 1605 (w), 1536 (vw), 1496 (vw), 1466 (vw), 1439 (vw), 1400 (w), 1343 (w), 1323 (vw), 1177 (w), 1140 (w), 1133 (w), 1031 (vw), 949 (vw), 922 (vw), 858 (vw), 837 (w), 816 (w), 798 (w), 778 (w), 768 (w), 745 (w), 717 (w), 686 (vw), 640 (w), 596 (vw), 554 (vw), 520 (vw), 494 (vw), 486 (w), 467 (w), 455 (w), 441 (w), 412 (vw), 399 (vw) cm$^{-1}$.

**HRMS (FAB):** $m/z$ calcd. for $C_{21}H_{25}N_4O_2$ [M+H], 365.1978; found, 365.1977.

**UV/Vis (MeCN):** $\lambda_{max}$ = 351 nm.

*(Z)-3-((5-(tert-Butyl)-1H-imidazol-4-yl)methylene)-6-((Z)-2,6-difluorobenzylidene)piperazine-2,5-dione (8)*
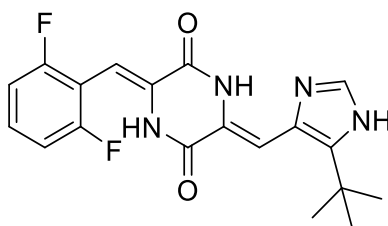


**Z-isomer**

**¹H NMR (400 MHz, DMSO-$d_6$):** $\delta$ = 12.36 (s, 2H, N$H$), 10.42 (s, 1H, N$H$), 7.87 (s, 1H, C$H$), 7.43 (tt, $J$ = 8.3, 6.5 Hz, 1H, $H_{arom}$), 7.13 (t, $J$ = 8.2 Hz, 2H, $H_{arom}$), 6.90 (s, 1H, C$H$, double bond), 6.49 (s, 1H, C$H$, double bond), 1.39 (s, 9H, C(C$H_3$)$_3$) ppm.

**¹³C NMR (101 MHz, DMSO-$d_6$):** $\delta$ = 161.4 (d, $J$ = 8.2 Hz, 1C, $C_{arom}$-F), 158.9 (d, $J$ = 7.7 Hz, 1C, $C_{arom}$-F), 157.3 (1C, $C$ONH), 155.4 (1C, $C$ONH), 140.7 (1C, $C$-C(CH$_3$)$_3$), 134.5 (1C, $C$H, imidazole), 130.5 (d, $J$ = 15.7 Hz, 1C, $C_{arom}$), 123.5 (2C, $C$-CH), 111.7 (d, $J$ = 24.3 Hz, 2C, $C_{arom}$), 110.6 (d, $J$ = 19.9, 1C, $C_{arom}$-CH), 105.8 (1C, $C$H, double bond), 99.7 (1C, $C$H, double bond), 31.9 (1C, $C$(CH$_3$)$_3$), 30.6 (3C, C($C$H$_3$)$_3$) ppm.

**¹⁹F NMR (376 MHz, DMSO-$d_6$):** $\delta$ = -108.5 ppm.

**IR (ATR):** $\nu$ = 3109 (w), 3050 (w), 2973 (w), 2876 (w), 1693 (vs), 1647 (vs), 1601 (m), 1469 (s), 1402 (vs), 1349 (m), 1273 (w), 1238 (w), 1204 (s), 1184 (vs), 1142 (vs), 1001 (vs), 952 (w), 904 (w), 837 (m), 813 (s), 803 (s), 783 (vs), 768 (vs), 717 (vs), 697 (w), 662 (w), 643 (w), 581 (w), 517 (w), 486 (m), 460 (s), 442 (m), 411 (w) cm$^{-1}$.

**HRMS (FAB):** $m/z$ calcd. for C$_{19}$H$_{18}$O$_2$N$_4$F$_2$ [M+H], 373.1476; found: 373.1477.

**UV/Vis (MeCN):** $\lambda_{max}$ = 362 nm.

**Fluorescence (MeCN):** $\lambda_{em}$=525 nm (excited with $\lambda$ = 370 nm).

**$\Phi_F$ (MeCN):** 0.055.


***E*-isomer**

**¹H NMR (400 MHz, DMSO-$d_6$):** $\delta$ = 12.34 (bs, 1H, N$H$), 12.11 (s, 1H, N$H$), 11.05 (s, 1H, N$H$), 7.83 (s, 1H, C$H$), 7.33 (tt, J = 8.3, 6.6 Hz, 1H, $H_{arom}$), 7.02 (t, J = 7.8 Hz, 2H, $H_{arom}$), 6.83 (s, 1H, C$H$, double bond), 6.13 (s, 1H, C$H$, double bond), 1.38 (s, 9H, C(C$H_3$)$_3$) ppm.

**¹³C NMR (101 MHz, DMSO-$d_6$):** $\delta$ = 161.1 (d, $J$ = 7.0 Hz, 1C, $C_{arom}$-F), 158.6 (d, $J$ = 7.2 Hz, 1C, $C_{arom}$-F), 157.2 (1C, $C$ONH), 154.6 (1C, $C$ONH), 140.4 (1C, $C$-C(CH$_3$)$_3$), 134.4 (1C, $C$H, imidazole), 131.1 (1C, $C$-CH), 130.5 (1C, m, $C_{arom}$-CH), 129.1 (t, $J$ = 10.8 Hz, 1C, $C_{arom}$-H), 123.5 (1C, $C$-CH), 113.30 – 112.67 (1C, $C_{arom}$-CH), 110.9 (d, $J$ = 25.5 Hz, 2C, $C_{arom}$-H), 105.0 (1C, $C$H, double bond), 102.3 (1C, $C$H, double bond), 31.9 (1C, $C$(CH$_3$)$_3$), 30.6 (3C, C($C$H$_3$)$_3$) ppm.

**¹⁹F NMR (376 MHz, DMSO-$d_6$):** $\delta$ = -110.0 ppm.

**UV/Vis (MeCN):** $\lambda_{max}$ = 363 nm.

**Fluorescence (MeCN):** $\lambda_{em}$= 532 nm (excited with $\lambda$ = 400 nm).

**$\Phi_F$ (MeCN):** 0.025.


*(3Z,6Z)-3-[(5-tert-Butyl-1H-imidazol-4-yl)methylidene]-6-[(2,5-difluorophenyl)methylidene]-piperazine-2,5-dione (**9**)*
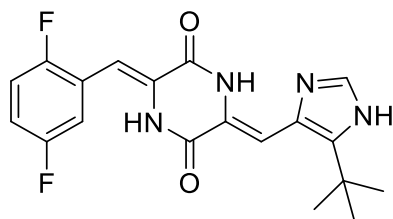
**Z-isomer**

**¹H NMR (400 MHz, DMSO-$d_6$):** $\delta$ = 12.33 (s, 2H), 10.44 (s, 1H), 7.86 (s, 1H), 7.45 – 7.36 (m, 1H), 7.29 (td, $J$ = 9.3, 4.7 Hz, 1H), 7.24 – 7.16 (m, 1H), 6.88 (s, 1H), 6.61 (s, 1H), 1.39 (s, 9H) ppm.

**¹³C NMR (101 MHz, DMSO-$d_6$):** $\delta$ = 159.1, 157.6, 157.2, 156.7, 155.7, 154.8, 140.6, 134.4, 130.6, 129.4, 123.6, 122.7, 122.5, 117.1, 117.1, 117.0, 116.9, 116.8, 116.8, 116.4, 116.3, 116.2, 116.2, 116.1, 116.0, 105.6, 104.8, 31.9, 30.6 ppm.

**IR (ATR):** $v$ = 3264 (w), 3257 (w), 3245 (w), 3217 (w), 3189 (w), 3159 (w), 3070 (w), 3044 (w), 3026 (w), 2970 (w), 2935 (w), 2912 (w), 2874 (w), 1669 (vs), 1629 (vs), 1551 (w), 1492 (s), 1469 (m), 1448 (m), 1409 (vs), 1368 (vs), 1343 (vs), 1315 (vs), 1276 (vs), 1262 (s), 1247 (m), 1201 (s), 1181 (m), 1145 (s), 1091 (w), 1045 (m), 1023 (w), 970 (w), 958 (s), 885 (w), 840 (s), 833 (s), 805 (vs), 796 (vs), 766 (vs), 751 (vs), 742 (vs), 728 (s), 717 (s), 701 (m), 662 (s), 602 (w), 582 (w), 561 (m), 551 (m), 528 (m), 504 (m), 492 (w), 459 (m), 441 (vs), 435 (vs) cm⁻¹.

**HRMS (FAB):** $m/z$ calcd. for $C_{19}H_{19}F_2N_4O_2$ [M+H], 373.1471; found, 373.1469.

**UV/Vis (DMSO):** $\lambda_{max}$ = 371 nm.

**Fluorescence (DMSO):** $\lambda_{em}$= 544 nm (excited with $\lambda$ = 400 nm).

**$\Phi_F$ (DMSO):** 0.031.


**E-isomer**

**¹H NMR (400 MHz, DMSO-$d_6$):** $\delta$ = 12.33 (s, 1H), 12.14 (s, 1H), 10.96 (s, 1H), 7.83 (s, 1H), 7.52 – 7.43 (m, 1H), 7.20 – 7.10 (ddp, $J$ = 12.9, 8.8, 4.4 Hz, 2H), 6.82 (s, 1H), 6.36 (s, 1H), 1.38 (s, 9H) ppm.


*(Z)-3-((5-(tert-Butyl)-1H-imidazol-4-yl)methylene)-6-((Z)-2,6-dichlorobenzylidene)piperazine-2,5-dione (**10**)*
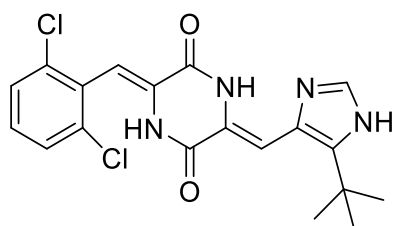
**Z-isomer**

**$^1$H NMR (400 MHz, DMSO-$d_6$):** $\delta$ = 12.37 (s, 2H, N*H*), 10.42 (s, 1H, N*H*), 7.87 (s, 1H, C*H*, imidazole), 7.50 (d, *J* = 8.1 Hz, 2H, $H_{arom}$), 7.37 (t, *J* = 8.1 Hz, 1H, $H_{arom}$), 6.89 (s, 1H, C*H*, double bond), 6.55 (s, 1H, C*H*, double bond), 1.38 (s, 9H, C(C*H$_3$*)$_3$) ppm.

**$^{13}$C NMR (101 MHz, DMSO-$d_6$):** $\delta$ = 157.8 (1C, *C*ONH), 155.8 (1C, *C*ONH), 141.2 (1C, *C*-C(CH$_3$)$_3$), 135.0 (1C, *C*H, imidazole), 134.9 (1C, *C*-CH), 131.6 (1C, *C*-CH, imidazole), 131.1 (1C, $C_{arom}$-H), 130.7 (1C, $C_{arom}$-CH), 128.7 (2C, $C_{arom}$-H), 124.0 (1C, *C*-CH), 108.6 (1C, *C*H, double bond), 106.4 (1C, *C*H, double bond), 32.4 (1C, *C*(CH$_3$)$_3$), 31.1 (3C, C(*C*H$_3$)$_3$) ppm.

**IR (ATR):** $\nu$ = 3111 (w), 3046 (w), 2978 (w), 2911 (w), 2873 (w), 1691 (s), 1645 (vs), 1599 (m), 1555 (w), 1490 (w), 1473 (w), 1405 (vs), 1347 (w), 1205 (s), 1183 (vs), 1143 (vs), 1096 (w), 953 (w), 904 (w), 817 (s), 802 (vs), 778 (vs), 765 (vs), 717 (vs), 700 (w), 656 (w), 642 (w), 601 (w), 558 (w), 537 (w), 518 (w), 469 (w), 446 (m), 426 (w), 402 (w) cm$^{-1}$.

**HRMS (FAB):** *m/z* calcd. for $C_{19}H_{18}Cl_2N_4O_2$ [M+H], 405.0885; found: 405.0886.

**UV/Vis (MeCN):** $\lambda_{max}$ = 358 nm.

**Fluorescence (MeCN):** $\lambda_{em}$= 527 nm (excited with $\lambda$ = 400 nm).

**$\Phi_F$ (MeCN):** 0.056.


**E-isomer**

**$^1$H NMR (400 MHz, DMSO-$d_6$):** $\delta$ = 12.32 (bs, 1H, N*H*), 12.10 (s, 1H, N*H*), 11.05 (s, 1H, N*H*), 7.82 (s, 1H, C*H*, imidazole), 7.42 (d, J = 8.0 Hz, 2H, $H_{arom}$), 7.27 (t, J = 8.1 Hz, 1H, $H_{arom}$), 6.84 (s, 1H, C*H*, double bond), 6.23 (s, 1H, C*H*, double bond), 1.37 (s, 9H, C(C*H$_3$*)$_3$ ppm.

**$^{13}$C NMR (126 MHz, DMSO-$d_6$):** $\delta$ = 157.2 (1C, *C*ONH), 154.6 (1C, *C*ONH), 140.5 (1C, *C*-C(CH$_3$)$_3$), 134.4 (1C, *C*-CH), 134.0 (1C, *C*-CH, imidazole), 133.9 (1C, *C*H, imidazole), 130.5 (1C, *C*-CH), 129.0 (1C, $C_{arom}$-H), 127.5 (2C, $C_{arom}$-H), 123.4 (1C, *C*-CH), 111.0 (1C, *C*H, double bond), 105.1 (1C, *C*H, double bond), 31.9 (1C, *C*(CH$_3$)$_3$), 30.6 (3C, C(*C*H$_3$)$_3$) ppm.

**UV/Vis (MeCN):** $\lambda_{max}$ = 356 nm.

**Fluorescence (MeCN):** $\lambda_{em}$= 534 nm (excited with $\lambda$ = 400 nm).

**$\Phi_F$ (MeCN):** 0.027.


*(Z)-3-((5-(tert-Butyl)-1H-imidazol-4-yl)methylene)-6-((Z)-2-chloro-6-(methylthio)benzylidene)-piperazine-2,5-dione (11)*
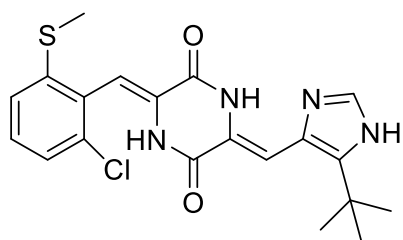
**¹H NMR (400 MHz, DMSO-$d_6$):** $\delta$ = 12.59 (s, 1H, N*H*), 12.14 (s, 1H, N*H*), 10.27 (s, 1H, C*H*), 8.04 (s, 1H, N*H*), 7.35 (t, *J* = 7.9 Hz, 1H, $H_{arom}$), 7.25 (ddd, *J* = 18.5, 8.0, 1.1 Hz, 2H, $H_{arom}$), 6.82 (s, 1H, C*H*), 6.52 (s, 1H, C*H*), 2.45 (s, 3H, SC*H*$_3$), 1.37 (s, 9H, C(C*H*$_3$)$_3$) ppm.

**¹³C NMR (101 MHz, DMSO-$d_6$):** $\delta$ = 157.0 (*C*ONH), 156.3, 155.6 (*C*ONH), 141.1 ($C_{arom}$-SCH$_3$), 140.4 (*C*-C(CH$_3$)$_3$), 134.4, 133.2 ($C_{arom}$-CH), 130.1 (*C*-CH), 129.6 ($C_{arom}$), 129.0, 125.3 ($C_{arom}$), 122.9 ($C_{arom}$), 109.0 (*C*H), 105.1 (*C*H), 31.9 (*C*(CH$_3$)$_3$), 30.5 (C(*C*H$_3$)$_3$), 14.9 (S*C*H$_3$) ppm.

**IR (ATR):** $\nu$ = 3174 (vw), 3116 (vw), 3067 (vw), 3036 (vw), 2973 (vw), 2871 (vw), 1687 (w), 1645 (m), 1599 (w), 1574 (vw), 1553 (vw), 1493 (vw), 1465 (vw), 1432 (w), 1398 (m), 1344 (w), 1323 (vw), 1265 (vw), 1205 (w), 1186 (w), 1145 (w), 1098 (vw), 950 (vw), 899 (vw), 836 (w), 820 (w), 813 (w), 802 (w), 785 (w), 773 (w), 739 (vw), 717 (w), 700 (vw), 656 (vw), 642 (vw), 601 (vw), 554 (vw), 541 (vw), 518 (vw), 470 (vw), 459 (vw), 443 (w), 429 (vw), 419 (vw), 407 (vw), 397 (vw) cm$^{-1}$.

**HRMS (FAB):** *m/z* calcd. for $C_{20}H_{22}ClN_4O_2S$ [M+H], 417.1152; found, 417.1151.

**UV/Vis (MeCN):** $\lambda_{max}$ = 358 nm.

*(Z)-3-((Z)-2,6-Bis(methylthio)benzylidene)-6-((5-(tert-butyl)-1H-imidazol-4-yl)methylene)-piperazine-2,5-dione (**12**)*
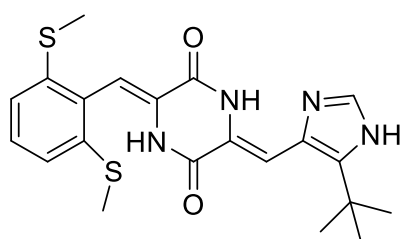


**¹H NMR (400 MHz, DMSO-$d_6$):** $\delta$ = 12.63 (s, 1H, N*H*), 12.08 (s, 1H, N*H*), 9.93 (s, 1H, C*H*), 8.08 (s, 1H, N*H*), 7.34 (t, *J* = 8.0 Hz, 1H, $H_{arom}$), 7.06 (d, *J* = 8.0 Hz, 2H, $H_{arom}$), 6.80 (s, 1H, C*H*), 6.51 (s, 1H, C*H*), 2.42 (s, 6H, SC*H*$_3$), 1.37 (s, 9H, C(C*H*$_3$)$_3$) ppm.

**¹³C NMR (101 MHz, DMSO-$d_6$):** $\delta$ = 156.9 (*C*ONH), 155.6 (*C*ONH), 140.3 (*C*-C(CH$_3$)$_3$), 138.8 ($C_{arom}$-SCH$_3$), 134.3 (*C*-CH), 129.9 (*C*-CH), 128.9 ($C_{arom}$), 127.6 ($C_{arom}$-CH), 120.6 ($C_{arom}$), 110.3 (*C*H), 31.9 (*C*(CH$_3$)$_3$), 30.4 (C(*C*H$_3$)$_3$), 14.7 (S*C*H$_3$) ppm.

**IR (ATR):** $v$ = 1687 (w), 1645 (w), 1598 (vw), 1555 (vw), 1493 (vw), 1469 (vw), 1432 (vw), 1394 (w), 1346 (vw), 1322 (vw), 1205 (vw), 1186 (w), 1146 (w), 949 (vw), 836 (vw), 813 (vw), 803 (vw), 764 (w), 717 (vw), 698 (vw), 640 (vw) cm$^{-1}$.

**HRMS (FAB):** $m/z$ calcd. for $C_{21}H_{25}N_4O_2S_2$ [M+H], 429.1419; found, 429.1421.

**UV/Vis (MeCN):** $\lambda_{max}$ = 359 nm.

*(Z)-3-((5-(tert-Butyl)-1H-imidazol-4-yl)methylene)-6-((Z)-2,6-dimethoxybenzylidene)piperazine-2,5-dione (**13**)*
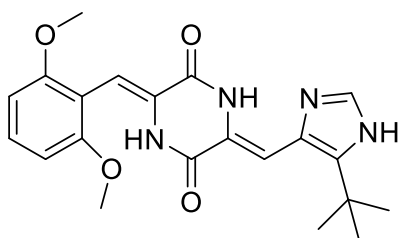


**¹H NMR (400 MHz, DMSO-$d_6$):** $\delta$ = 12.60 (s, 1H, N*H*), 11.95 (s, 1H, N*H*), 9.25 (s, 1H, C*H*), 8.07 (s, 1H, N*H*), 7.33 (t, $J$ = 8.4 Hz, 1H, $H_{arom}$), 6.78 (s, 1H, C*H*), 6.75 (s, 1H, C*H*), 6.71 (d, $J$ = 8.4 Hz, 2H, $H_{arom}$), 3.83 (s, 6H, OC*H*$_3$), 1.37 (s, 9H, C(C*H*$_3$)$_3$) ppm.

**¹³C NMR (101 MHz, DMSO-$d_6$):** $\delta$ = 157.6 ($C_{arom}$-OCH$_3$), 156.5 (*C*ONH), 156.3 (*C*ONH), 140.0 (*C*-C(CH$_3$)$_3$), 134.3 (*C*H), 130.3 ($C_{arom}$), 126.6 (*C*-CH), 110.1 ($C_{arom}$-CH), 107.3 (*C*H), 104.2 ($C_{arom}$), 99.6 (*C*-CH), 55.8 (O*C*H$_3$), 31.9 (*C*(CH$_3$)$_3$), 30.5 (C(*C*H$_3$)$_3$) ppm.

**IR (ATR):** $v$ = 3189 (vw), 3179 (vw), 3166 (vw), 3091 (vw), 3082 (vw), 3071 (vw), 3041 (vw), 2970 (w), 2945 (vw), 2919 (vw), 2908 (vw), 2874 (vw), 2840 (vw), 1687 (m), 1649 (m), 1625 (m), 1594 (w), 1473 (w), 1428 (w), 1400 (m), 1347 (w), 1306 (w), 1283 (vw), 1255 (w), 1204 (w), 1184 (m), 1136 (m), 1106 (m), 1030 (w), 948 (w), 909 (w), 890 (w), 836 (w), 813 (w), 799 (w), 776 (m), 721 (m), 669 (w), 640 (w), 630 (w), 602 (w), 572 (w), 545 (w), 510 (w), 484 (w), 463 (w), 441 (w), 414 (w), 388 (w) cm$^{-1}$.

**HRMS (FAB):** $m/z$ calcd. for $C_{21}H_{25}N_4O_4$ [M+H], 397.1876; found, 397.1875.

**UV/Vis (MeCN):** $\lambda_{max}$ = 366 nm.

*(Z)-3-((5-(tert-Butyl)-1H-imidazol-4-yl)methylene)-6-((Z)-3-methoxybenzylidene)piperazine-2,5-dione (**14**)*
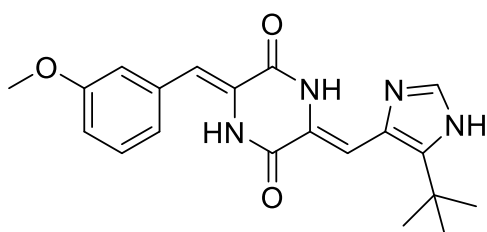
**Z-isomer**

**$^1$H NMR (400 MHz, DMSO-$d_6$):** $\delta$ = 12.34 (bs, 1H, N*H*), 12.25 (s, 1H, N*H*), 10.04 (s, 1H, N*H*), 7.85 (s, 1H, C*H*, imidazole), 7.33 (t, *J* = 7.9 Hz, 1H, $H_{arom}$), 7.12 – 7.04 (m, 2H, $H_{arom}$), 6.93 – 6.87 (m, 1H, $H_{arom}$), 6.86 (s, 1H, C*H*, double bond), 6.72 (s, 1H, C*H*, double bond), 3.79 (s, 3H, O-C*H*$_3$), 1.38 (s, 9H, C(C*H*$_3$)$_3$) ppm.

**$^{13}$C NMR (101 MHz, DMSO-$d_6$):** $\delta$ = 159.3 (1C, $C_{arom}$-OCH$_3$), 157.5 (1C, *C*ONH), 156.3 (1C, *C*ONH), 140.4 (1C, *C*-C(CH$_3$)$_3$), 134.5 (1C, *C*H, imidazole), 134.4 (1C, C-*C*H, imidazole), 130.7 (1C, $C_{arom}$-CH), 129.8 (1C, $C_{arom}$-H), 126.8 (1C, *C*-CH), 123.8 (1C, *C*-CH), 121.5 (1C, $C_{arom}$-H), 114.5 (1C, $C_{arom}$-H), 113.9 (1C, $C_{arom}$-H), 113.8 (1C, *C*H, double bond), 105.1 (1C, *C*H, double bond), 55.1 (1C, O-*C*H$_3$), 31.9 (1C, *C*(CH$_3$)$_3$), 30.6 (3C, C(*C*H$_3$)$_3$) ppm.

**IR (ATR):** $\nu$ = 3159 (m), 3099 (m), 3046 (m), 2953 (m), 2921 (s), 2868 (m), 2851 (m), 1669 (vs), 1629 (vs), 1572 (s), 1507 (w), 1486 (m), 1466 (m), 1451 (m), 1412 (vs), 1375 (vs), 1343 (vs), 1316 (vs), 1293 (vs), 1279 (vs), 1262 (s), 1241 (s), 1204 (m), 1197 (m), 1184 (m), 1154 (s), 1146 (vs), 1089 (m), 1047 (vs), 1024 (m), 996 (w), 958 (vs), 898 (w), 881 (w), 871 (w), 860 (m), 840 (m), 812 (vs), 785 (vs), 775 (vs), 735 (vs), 686 (vs), 664 (vs), 615 (m), 595 (m), 582 (m), 561 (s), 551 (m), 533 (s), 500 (vs), 489 (s), 459 (s), 438 (vs), 414 (m), 394 (m), 375 (m) cm$^{-1}$.

**HRMS (FAB):** *m/z* calcd. for $C_{20}H_{23}O_3N_4$ [M+H], 367.1765; found: 367.1763.

**UV/Vis (MeCN):** $\lambda_{max}$ = 362 nm.

**Fluorescence (MeCN):** $\lambda_{em}$= 512 nm (excited with $\lambda$ = 400 nm).

**$\Phi_F$ (MeCN):** 0.045.


**E-isomer**

**$^1$H NMR (400 MHz, DMSO-$d_6$):** $\delta$ = 12.29 (bs, 1H, N*H*), 12.08 (s, 1H, N*H*), 10.73 (s, 1H, N*H*), 7.83 (s, 1H, C*H*, imidazole), 7.29 (s, 1H, $H_{arom}$), 7.19 (t, J = 7.9 Hz, 1H, $H_{arom}$), 7.03 (d, J = 7.7 Hz, 1H, $H_{arom}$), 6.81 (dd, J = 8.1, 2.6 Hz, 1H, $H_{arom}$), 6.78 (s, 1H, C*H*, double bond), 6.49 (s, 1H, C*H*, double bond), 3.74 (s, 3H, O-C*H*$_3$), 1.38 (s, 9H, C(C*H*$_3$)$_3$) ppm.

**$^{13}$C NMR (101 MHz, DMSO-$d_6$):** $\delta$ = 158.4 (1C, $C_{arom}$-OCH$_3$), 157.4 (1C, *C*ONH), 155.4 (1C, *C*ONH), 140.0 (1C, *C*-C(CH$_3$)$_3$), 135.6 (1C, C-*C*H, imidazole), 134.3 (1C, *C*H, imidazole), 130.7 (1C, $C_{arom}$-CH), 128.4 (1C, $C_{arom}$-H), 127.4 (1C, *C*-CH), 123.8 (1C, *C*-CH), 123.0 (1C, $C_{arom}$-H), 119.7 (1C, *C*H, double bond), 115.5 (1C, $C_{arom}$-H), 113.3 (1C, $C_{arom}$-H), 104.0 (1C, *C*H, double bond), 54.9 (1C, O-*C*H$_3$), 31.9 (1C, *C*(CH$_3$)$_3$), 30.6 (3C, C(*C*H$_3$)$_3$) ppm.

**UV/Vis (MeCN):** $\lambda_{max}$ = 365 nm.

**Fluorescence (MeCN):** $\lambda_{em}$= 533 nm (excited with $\lambda$ = 400 nm).

**$\Phi_F$ (MeCN):** 0.022.

*(Z)-3-((5-(tert-Butyl)-1H-imidazol-4-yl)methylene)-6-((Z)-3,5-dimethoxybenzylidene)-*

*piperazine-2,5-dione (15)*
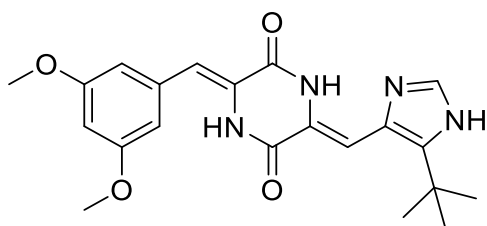


**Z-isomer**

**$^1$H NMR (400 MHz, DMSO-$d_6$):** $\delta$ = 12.34 (bs, 1H, N*H*), 12.25 (s, 1H, N*H*), 10.02 (s, 1H, N*H*), 7.85 (s, 1H, C*H*, imidazole), 6.86 (s, 1H, C*H*, double bond), 6.68 (s, 1H, C*H*, double bond), 6.65 (d, *J* = 2.3 Hz, 2H, *H*$_{arom}$), 6.46 (t, *J* = 2.3 Hz, 1H, *H*$_{arom}$), 3.77 (s, 6H, O-C*H*$_3$), 1.38 (s, 9H, C(C*H*$_3$)$_3$) ppm.

**$^{13}$C NMR (101 MHz, DMSO-$d_6$):** $\delta$ = 160.5 (2C, *C*$_{arom}$-OCH$_3$), 157.5 (1C, *C*ONH), 156.3 (1C, *C*ONH), 140.4 (1C, *C*-C(CH$_3$)$_3$), 135.0 (1C, C-*C*H, imidazole), 134.4 (1C, *C*H, imidazole), 130.7 (1C, *C*$_{arom}$-CH), 127.1 (1C, *C*-CH), 123.8 (1C, *C*-CH), 113.9 (1C, *C*H, double bond), 107.1 (2C, *C*$_{arom}$-H), 105.1 (1C, *C*H, double bond), 100.3 (1C, *C*$_{arom}$-H), 55.2 (2C, O-*C*H$_3$), 31.9 (1C, *C*(CH$_3$)$_3$), 30.6 (3C, C(*C*H$_3$)$_3$) ppm.

**IR (ATR):** $\nu$ = 3434 (w), 3193 (m), 3078 (w), 3038 (w), 3007 (w), 2983 (w), 2961 (w), 2952 (w), 2928 (w), 2873 (w), 2837 (w), 1670 (vs), 1632 (vs), 1589 (vs), 1502 (w), 1451 (s), 1441 (m), 1414 (vs), 1374 (s), 1341 (vs), 1319 (s), 1290 (s), 1275 (m), 1259 (m), 1205 (vs), 1186 (vs), 1139 (vs), 1069 (s), 1055 (vs), 1014 (m), 973 (m), 955 (s), 880 (m), 840 (s), 819 (vs), 800 (vs), 765 (vs), 752 (vs), 739 (vs), 724 (vs), 696 (s), 677 (vs), 659 (vs), 630 (s), 613 (s), 579 (s), 557 (vs), 534 (vs), 516 (vs), 499 (vs), 482 (vs), 466 (vs), 441 (vs), 394 (vs), 378 (vs) cm$^{-1}$.

**HRMS (FAB):** *m/z* calcd. for C$_{21}$H$_{25}$O$_4$N$_4$ [M+H], 397.1870; found: 397.1870.

**UV/Vis (MeCN):** $\lambda_{max}$ = 363 nm.

**Fluorescence (MeCN):** $\lambda_{em}$= 515 nm (excited with $\lambda$ = 400 nm).

**$\Phi_F$ (MeCN):** 0.045.

**E-isomer**

**$^1$H NMR (400 MHz, DMSO-$d_6$):** $\delta$ = 12.29 (bs, 1H, N*H*), 12.08 (s, 1H, N*H*), 10.72 (s, 1H, N*H*), 7.83 (s, 1H, C*H*, imidazole), 6.78 (s, 1H, C*H*, double bond), 6.76 (d, *J* = 2.3 Hz, 2H, *H*$_{arom}$), 6.44 (s, 1H, C*H*, double bond), 6.39 (t, *J* = 2.3 Hz, 1H, *H*$_{arom}$), 3.72 (s, 6H, O-C*H*$_3$), 1.38 (s, 9H, C(C*H*$_3$)$_3$) ppm.

**¹³C NMR (101 MHz, DMSO-$d_6$):** $\delta$ = 159.5 (2C, $C_{arom}$-OCH₃), 157.4 (1C, $C$ONH), 155.3 (1C, $C$ONH), 140.0 (1C, $C$-C(CH₃)₃), 136.1 (1C, C-$C$H, imidazole), 134.3 (1C, $C$H, imidazole), 130.7 (1C, $C_{arom}$-CH), 127.6 (1C, $C$H, double bond), 123.8 (1C, $C$H, double bond), 119.7 (1C, $C$H, double bond), 108.3 (2C, $C_{arom}$-H), 104.0 (1C, $C$H, double bond), 99.9 (1C, $C_{arom}$-H), 55.1 (2C, O-$C$H₃), 31.9 (1C, $C$(CH₃)₃), 30.6 (3C, C($C$H₃)₃) ppm.

**UV/Vis (MeCN):** $\lambda_{max}$ = 364 nm.

**Fluorescence (MeCN):** $\lambda_{em}$= 534 nm (excited with $\lambda$ = 400 nm).

**$\Phi_F$ (MeCN):** 0.020.

*(Z)-3-((5-(tert-Butyl)-1H-imidazol-4-yl)methylene)-6-((Z)-4-(dimethylamino)benzylidene)-piperazine-2,5-dione (**16**)*
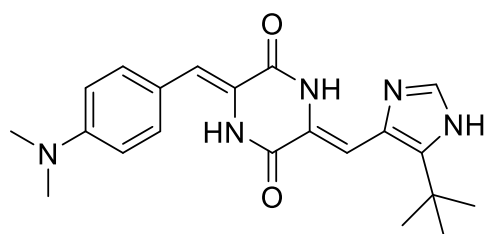


**Z-isomer**

**¹H NMR (400 MHz, DMSO-$d_6$):** $\delta$ = 12.29 (bs, 1H, N$H$), 12.11 (s, 1H, N$H$), 9.73 (s, 1H, N$H$), 7.83 (s, 1H, C$H$, imidazole), 7.42 (d, $J$ = 9.0 Hz, 2H, $H_{arom}$), 6.82 (s, 1H, C$H$, double bond), 6.75 (d, $J$ = 9.0 Hz, 2H, $H_{arom}$), 6.69 (s, 1H, C$H$, double bond), 2.96 (s, 6H, N-(C$H$₃)₂), 1.38 (s, 9H, C(C$H$₃)₃) ppm.

**¹³C NMR (101 MHz, DMSO-$d_6$):** $\delta$ = 157.4 (1C, $C$ONH), 156.9 (1C, $C$ONH), 150.0 (1C, $C_{arom}$-N(CH₃)₂), 139.9 (1C, $C$-C(CH₃)₃), 134.2 (1C, $C$H, imidazole), 130.8 (1C, $C_{arom}$-CH), 130.7 (2C, $C_{arom}$-H), 124.1 (1C, $C$-CH), 122.8 (1C, $C$-CH), 120.5 (1C, $C_{arom}$-CH), 115.6 (1C, $C$H, double bond), 112.0 (2C, $C_{arom}$-H), 104.2 (1C, $C$H, double bond), 39.4 (2C, N($C$H₃)₂), 31.9 (1C, $C$(CH₃)₃), 30.6 (3C, C($C$H₃)₃) ppm.

**IR (ATR):** $v$ = 3429 (w), 3391 (w), 3183 (m), 3119 (w), 3085 (w), 3055 (w), 3048 (w), 3012 (w), 2953 (m), 2921 (m), 2851 (m), 2802 (w), 2727 (w), 2681 (w), 2659 (w), 2640 (w), 2605 (w), 2601 (w), 2527 (w), 1672 (s), 1655 (s), 1635 (s), 1609 (vs), 1585 (vs), 1524 (s), 1502 (m), 1479 (w), 1453 (s), 1400 (vs), 1358 (vs), 1341 (vs), 1279 (vs), 1264 (vs), 1222 (s), 1183 (s), 1164 (vs), 1126 (vs), 1057 (vs), 1020 (s), 949 (vs), 935 (vs), 882 (s), 827 (vs), 802 (vs), 766 (vs), 747 (vs), 722 (vs), 656 (vs), 612 (s), 579 (s), 569 (s), 545 (s), 510 (vs), 499 (vs), 475 (vs), 449 (vs), 407 (vs), 375 (vs) cm⁻¹.

**HRMS (FAB):** $m/z$ calcd. for C₂₁H₂₅N₅O₂ [M], 379.2008; found: 379.2011.

**UV/Vis (MeCN):** $\lambda_{max}$ = 400 nm.

**Fluorescence (MeCN):** $\lambda_{em}$= 534 nm (excited with $\lambda$ = 370 nm).

$\Phi_F$ **(MeCN):** 0.027.

### *E*-isomer

**$^1$H NMR (400 MHz, DMSO-$d_6$):** $\delta$ = 12.25 (bs, 1H, N*H*), 11.98 (s, 1H, N*H*), 10.51 (s, 1H, N*H*), 7.82 (s, 1H, C*H*, imidazole), 7.68 (d, J = 9.0 Hz, 2H, $H_{arom}$), 6.71 (s, 1H, C*H*, double bond), 6.64 (d, J = 9.0 Hz, 2H, $H_{arom}$), 6.44 (s, 1H, C*H*, double bond), 2.94 (s, 6H, N-(C*H*$_3$)$_2$), 1.37 (s, 9H, C(C*H*$_3$)$_3$) ppm.

**$^{13}$C NMR (126 MHz, DMSO-$d_6$):** $\delta$ = 157.1 (1C, *C*ONH), 156.1 (1C, *C*ONH), 149.9 (1C, $C_{arom}$-N(CH$_3$)$_2$), 139.4 (1C, *C*-C(CH$_3$)$_3$), 134.1 (1C, *C*H, imidazole), 132.6 (2C, $C_{arom}$-H), 130.9 (1C, $C_{arom}$-CH), 124.3 (1C, *C*-CH), 123.1 (1C, *C*-CH), 122.5 (1C, *C*H, double bond), 121.2 (1C, $C_{arom}$-CH), 111.0 (2C, $C_{arom}$-H), 102.7 (1C, *C*H, double bond), 39.4 (2C, N(*C*H$_3$)$_2$), 31.8 (1C, *C*(CH$_3$)$_3$), 30.6 (3C, C(*C*H$_3$)$_3$) ppm.

**UV/Vis (MeCN):** $\lambda_{max}$ = 416 nm.

**Fluorescence (MeCN):** $\lambda_{em}$= 544 nm (excited with $\lambda$ = 400 nm).

$\Phi_F$ **(MeCN):** 0.008.

*(3Z,6Z)-3-((5-(tert-Butyl)-1H-imidazol-4-yl)methylene)-6-((2,3,6,7-tetrahydro-1H,5H-pyrido[3,2,1-ij]quinolin-9-yl)methylene)piperazine-2,5-dione (**17**)*
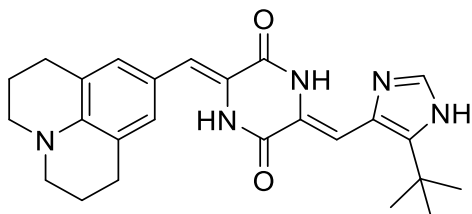


**$^1$H NMR (400 MHz, DMSO-$d_6$):** $\delta$ = 12.09 (s, 1H), 11.02 (s, 2H), 7.78 (s, 1H), 6.97 (s, 2H), 6.79 (s, 1H), 6.55 (s, 1H), 3.17 (t, J = 5.7 Hz, 4H), 2.69 (t, J = 6.4 Hz, 4H), 1.86 (p, J = 6.5 Hz, 4H), 1.38 (s, 9H) ppm.

**$^{13}$C NMR (101 MHz, DMSO-$d_6$):** $\delta$ = 157.6, 157.1, 142.8, 140.3, 134.5, 130.9, 128.4, 124.1, 122.5, 120.6, 119.7, 115.9, 103.9, 49.2, 31.9, 30.7, 27.1, 21.3 ppm.

**IR (ATR):** $\nu$ = 3393 (w), 3211 (m), 3116 (w), 3094 (w), 2932 (w), 2902 (w), 2861 (w), 2837 (w), 2800 (w), 1670 (s), 1633 (s), 1613 (m), 1595 (m), 1519 (m), 1506 (m), 1466 (w), 1429 (m), 1395 (vs), 1371 (vs), 1346 (vs), 1329 (s), 1307 (vs), 1282 (vs), 1262 (s), 1207 (s), 1183 (m), 1162 (vs), 1147 (s), 1077 (w), 1050 (m), 1023 (m), 987 (w), 952 (s), 939 (s), 907 (w), 892 (m), 857 (w), 840 (m), 824 (w), 809 (m), 778 (m), 759 (s), 737 (s), 718 (s), 656 (s), 640 (m), 622 (m), 608 (m), 592 (m), 565 (w), 554 (w), 530 (m), 501 (m), 490 (m), 433 (vs), 394 (w) cm$^{-1}$.

**HRMS (FAB):** *m/z* calcd. for $C_{25}H_{29}N_5O_2$ [M], 431.2316; found: 431.2318.

**UV/Vis (MeCN):** $\lambda_{max}$ = 424 nm.

*(3Z,6Z)-3-((5-(tert-butyl)-1H-imidazol-4-yl)methylene)-6-((4,4,8,8,12,12-hexamethyl-8,12-dihydro-4H-benzo[9,1]quinolizino[3,4,5,6,7-defg]acridin-2-yl)methylene)piperazine-2,5-dione (18)*
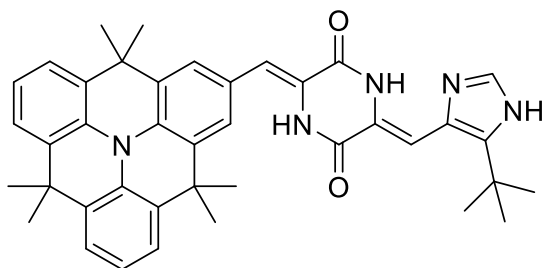


**¹H NMR (400 MHz, DMSO-*d₆*):** $\delta$ = 12.38 (br, 1H), 12.20 (br, 1H), 10.08 (br, 1H), 7.84 (s, 1H), 7.61 (s, 2H), 7.47 (d, *J* = 7.8 Hz, 4H), 7.17 (t, *J* = 7.7 Hz, 2H), 6.86 (s, 1H), 6.84 (s, 1H), 1.59 (s, 18H), 1.39 (s, 9H) ppm.

**¹³C NMR (101 MHz, DMSO-*d₆*):** $\delta$ = 158.2, 157.9, 157.6, 156.8, 140.2, 134.3, 131.4, 130.8, 130.6, 129.7, 129.6, 129.3, 128.0, 125.0, 124.7, 124.0, 123.7, 123.5, 114.9, 104.8, 35.2, 35.0, 33.4, 32.5, 31.9, 30.6 ppm.

**IR (ATR):** $v$ = 3398 (w), 2963 (w), 2922 (vw), 2864 (vw), 1676 (vs), 1426 (m), 1395 (m), 1370 (w), 1341 (w), 1316 (w), 1292 (w), 1197 (vs), 1133 (vs), 1051 (w), 1020 (w), 953 (w), 939 (w), 897 (w), 844 (m), 803 (s), 773 (w), 762 (w), 742 (m), 725 (vs), 656 (w), 615 (m), 599 (m), 582 (m), 572 (w), 560 (m), 554 (m), 517 (m), 496 (m), 486 (m), 480 (m), 453 (m), 445 (m), 433 (m), 419 (m), 412 (m), 405 (m), 398 (m), 382 (m), 375 (m) cm⁻¹.

**HRMS (FAB):** *m/z* calcd. for $C_{40}H_{41}N_5O_2$ [M], 623.3255; found, 623.3254.

**UV/Vis (MeCN):** $\lambda_{max}$ = 413 nm.

**Fluorescence (MeCN):** $\lambda_{em}$= 554 nm (excited with $\lambda$ = 420 nm).

**$\Phi_F$ (MeCN):** 0.236.

**$\Phi_F$ (DMSO):** 0.275.

*(3Z,6Z)-3-[(5-tert-Butyl-1H-imidazol-4-yl)methylidene]-6-(pyridin-3-ylmethylidene)piperazine-2,5-dione (19)*
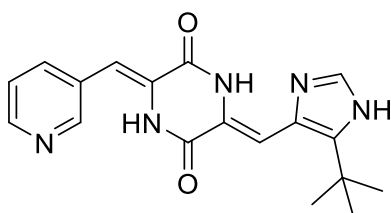
**¹H NMR (400 MHz, DMSO-*d₆*):** $\delta$ = 12.30 (br, 2H), 10.48 (br, 1H), 8.67 (d, *J* = 2.3 Hz, 1H), 8.47 (dd, *J* = 4.8, 1.6 Hz, 1H), 7.91 (dt, *J* = 8.1, 2.0 Hz, 1H), 7.86 (s, 1H), 7.41 (dd, *J* = 7.8, 4.8 Hz, 1H), 6.87 (s, 1H), 6.72 (s, 1H), 1.39 (s, 9H) ppm.

**¹³C NMR (101 MHz, DMSO-*d₆*):** $\delta$ = 157.7, 156.0, 150.1, 148.3, 140.5, 136.2, 134.4, 130.7, 129.5, 128.4, 123.8, 123.5, 110.2, 105.3, 31.9, 30.6 ppm.

**IR (ATR):** $\nu$ = 3493 (w), 3418 (w), 3135 (w), 3071 (m), 2969 (m), 2902 (m), 2815 (w), 1672 (s), 1628 (s), 1604 (vs), 1572 (s), 1507 (m), 1466 (m), 1408 (vs), 1398 (vs), 1371 (vs), 1357 (s), 1334 (vs), 1279 (vs), 1262 (s), 1220 (s), 1179 (s), 1149 (s), 1054 (m), 1021 (m), 948 (vs), 860 (m), 840 (s), 807 (vs), 793 (s), 762 (s), 754 (vs), 725 (s), 696 (vs), 654 (vs), 626 (s), 611 (s), 598 (s), 579 (s), 555 (s), 518 (vs), 504 (vs), 484 (vs), 443 (vs), 419 (s), 409 (s), 392 (s), 375 (s) cm⁻¹.

**HRMS (FAB):** *m/z* calcd. for $C_{18}H_{20}N_5O_2$ [M+H], 338.1612; found, 338.1611.

**UV/Vis (DMSO):** $\lambda_{max}$ = 369 nm.

**Fluorescence (DMSO):** $\lambda_{em}$ = 540 nm (excited with $\lambda$ = 400 nm).

**$\Phi_F$ (DMSO):** 0.032.


*(3Z,6Z)-3-[(5-tert-Butyl-1H-imidazol-4-yl)methylidene]-6-(isoquinolin-5-ylmethylidene)-piperazine-2,5-dione (**20**)*
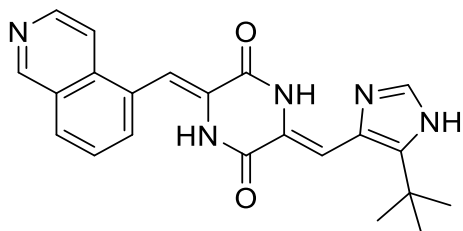


**¹H NMR (400 MHz, DMSO-*d₆*):** $\delta$ = 12.35 (br, 2H), 10.20 (br, 1H), 9.35 (s, 1H), 8.53 (d, *J* = 5.9 Hz, 1H), 8.10 (d, *J* = 7.5 Hz, 1H), 7.88 (s, 1H), 7.86 (dt, *J* = 7.3, 1.2 Hz, 1H), 7.77 (dt, *J* = 6.0, 1.1 Hz, 1H), 7.72 (t, *J* = 7.7 Hz, 1H), 7.12 (s, 1H), 6.87 (s, 1H), 1.39 (s, 9H) ppm.

**¹³C NMR (101 MHz, DMSO-*d₆*):** $\delta$ = 157.5, 155.9, 152.8, 143.4, 140.4, 134.4, 133.7, 131.3, 130.7, 129.6, 129.4, 128.6, 127.7, 127.3, 123.9, 117.4, 109.7, 105.2, 31.9, 30.6 ppm.

**IR (ATR):** $\nu$ = 3485 (m), 3303 (w), 3138 (m), 3072 (m), 3050 (m), 3004 (m), 2955 (s), 2902 (m), 2868 (m), 2823 (m), 1672 (vs), 1629 (vs), 1611 (vs), 1587 (s), 1502 (m), 1472 (m), 1459 (w), 1417 (vs), 1397 (vs), 1368 (vs), 1344 (vs), 1316 (vs), 1262 (vs), 1220 (m), 1190 (m), 1150 (s), 1096 (w), 1043 (m), 1020 (m), 977 (vw), 955 (vs), 877 (w), 827 (vs), 816 (vs), 802 (vs), 782 (vs), 762 (vs), 749 (s), 735 (s), 724 (m), 664 (m), 657 (m), 608 (s), 582 (s), 560 (s), 544 (s), 531 (s), 513 (s), 496 (vs), 480 (vs), 467 (s), 445 (vs), 412 (s), 397 (s) cm⁻¹.

**HRMS (FAB):** *m/z* calcd. for $C_{22}H_{22}N_5O_2$ [M+H], 388.1768; found, 388.1769.

**UV/Vis (DMSO):** $\lambda_{max}$ = 370 nm.

**Fluorescence (DMSO):** $\lambda_{em}$= 557 nm (excited with $\lambda$ = 400 nm).

$\Phi_F$ **(DMSO):** 0.021.

*(3Z,6Z)-3-[(5-tert-Butyl-1H-imidazol-4-yl)methylidene]-6-(naphthalen-1-ylmethylidene)-piperazine-2,5-dione (21)*
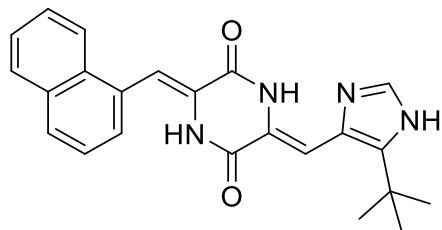


**¹H NMR (400 MHz, DMSO-$d_6$):** $\delta$ = 12.33 (s, 2H), 10.00 (s, 1H), 8.04 – 7.96 (m, 1H), 7.95 – 7.83 (m, 3H), 7.67 – 7.61 (m, 1H), 7.60 – 7.48 (m, 3H), 7.20 (s, 1H), 6.86 (s, 1H), 1.39 (s, 9H) ppm.

**¹³C NMR (101 MHz, DMSO-$d_6$):** $\delta$ = 157.4, 156.1, 140.3, 134.4, 133.4, 131.2, 130.7, 130.1, 128.5, 128.3, 127.1, 126.5, 126.1, 125.8, 124.3, 123.9, 111.4, 105.1, 31.9, 30.6 ppm.

**IR (ATR):** $v$ = 3371 (w), 3308 (w), 3292 (w), 3271 (w), 3235 (w), 3200 (w), 3123 (w), 3060 (w), 2963 (w), 2905 (w), 2873 (w), 1666 (vs), 1639 (vs), 1611 (vs), 1554 (w), 1506 (m), 1456 (m), 1445 (w), 1415 (vs), 1373 (vs), 1340 (vs), 1310 (s), 1275 (m), 1259 (s), 1215 (w), 1180 (w), 1147 (s), 1085 (w), 1050 (w), 1020 (m), 959 (s), 949 (m), 884 (w), 840 (s), 816 (m), 793 (vs), 771 (vs), 752 (vs), 731 (vs), 653 (s), 628 (m), 602 (m), 582 (m), 560 (s), 527 (s), 511 (m), 492 (s), 472 (s), 443 (vs), 415 (s), 402 (s), 378 (m) cm⁻¹.

**HRMS (FAB):** *m/z* calcd. for $C_{23}H_{23}N_4O_2$ [M+H], 387.1816; found, 387.1818.

**UV/Vis (DMSO):** $\lambda_{max}$ = 373 nm.

**Fluorescence (DMSO):** $\lambda_{em}$= 544 nm (excited with $\lambda$ = 400 nm).

$\Phi_F$ **(DMSO):** 0.028.

*(3Z,6Z)-3-[(3-Benzoylphenyl)methylidene]-6-[(5-tert-butyl-1H-imid¬azol-4-yl)methylidene]-piperazine-2,5-dione (22)*
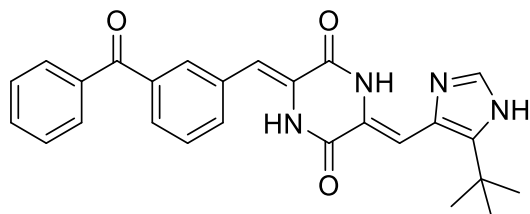
**¹H NMR (400 MHz, DMSO-$d_6$):** $\delta$ = 12.33 (s, 1H), 12.28 (s, 1H), 10.35 (s, 1H), 7.87 – 7.79 (m, 4H), 7.75 (dt, $J$ = 7.8, 1.7 Hz, 1H), 7.72 – 7.67 (m, 1H), 7.66 – 7.62 (m, 1H), 7.58 (t, $J$ = 7.6 Hz, 3H), 6.85 (s, 1H), 6.80 (s, 1H), 1.38 (s, 9H) ppm.

**¹³C NMR (101 MHz, DMSO-$d_6$):** $\delta$ = 195.5, 157.7, 156.1, 140.4, 137.4, 136.8, 134.4, 133.6, 133.3, 132.8, 130.7, 130.1, 129.8, 128.8, 128.6, 127.7, 123.8, 112.7, 105.2, 31.9, 30.6 ppm.

**IR (ATR):** $\nu$ = 3492 (w), 3446 (w), 3191 (w), 3082 (w), 3068 (w), 3037 (w), 2968 (w), 2953 (w), 2904 (w), 2873 (w), 1683 (m), 1650 (vs), 1598 (s), 1577 (w), 1548 (w), 1504 (w), 1446 (m), 1411 (vs), 1381 (vs), 1346 (vs), 1322 (s), 1313 (s), 1290 (vs), 1276 (vs), 1211 (m), 1177 (w), 1152 (m), 1095 (w), 1078 (w), 1048 (w), 1023 (w), 993 (w), 973 (w), 953 (s), 904 (m), 881 (w), 839 (m), 819 (s), 783 (s), 765 (vs), 741 (m), 724 (vs), 714 (vs), 696 (s), 688 (s), 653 (vs), 598 (s), 581 (m), 572 (m), 557 (m), 537 (m), 526 (s), 493 (s), 466 (m), 448 (vs), 439 (vs), 401 (w) cm$^{-1}$.

**HRMS (FAB):** $m/z$ calcd. for $C_{26}H_{25}N_4O_3$ [M+H], 441.1782; found, 441.1780.

**UV/Vis (DMSO):** $\lambda_{max}$ = 371 nm.

**Fluorescence (DMSO):** $\lambda_{em}$= 535 nm (excited with $\lambda$ = 400 nm).

**$\Phi_F$ (DMSO):** 0.029.

*(3Z,6Z)-3-((1H-Pyrrol-3-yl)methylene)-6-((5-(tert-butyl)-1H-imidazol-4-yl)methylene)-piperazine-2,5-dione (23)*
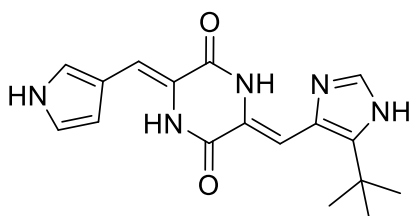


(3Z-1-Acetyl-3-[(5-*tert*-butyl-1*H*-imidazol-4-yl)methylene]piperazine-2,5-dione (**5**) and *tert*-butyl-3-formylpyrrole-1-carboxylate (161 mg, 827 μmol, 1.20 equiv.) were reacted according to the general procedure. The crude product **23** (200 mg, 470 μmol, 1.00 equiv; impure) was dissolved in 21.7 mL of a 20% (v/v) TFA (7.24 g, 4.86 mL, 63.5 mmol, 135 equiv.) and 80% (v/v) $CH_2Cl_2$ (17.6 mL), containing 1% (v/v) TIPS (189 mg, 245 μL, 1.19 mmol, 2.54 equiv.) at 0 °C (ice bath). Subsequently, the ice bath was removed and the solution was allowed to warm to ambient temperature. The reaction was monitored *via* TLC. After 2.5 hours toluene (100 mL) was added and the mixture was concentrated *in vacuo*. The obtained solid was dissolved in MeOH and purified *via* HPLC according to the general procedure.

**¹H NMR (400 MHz, DMSO-$d_6$):** $\delta$ = 12.30 (s, 1H), 12.05 (s, 1H), 11.29 (s, 1H), 9.08 (s, 1H), 7.82 (s, 1H), 7.35 (s, 1H), 6.87 (q, $J$ = 2.4 Hz, 1H), 6.81 (s, 1H), 6.76 (s, 1H), 6.47 (d, $J$ = 2.4 Hz, 1H), 1.38 (s, 9H) ppm.

**$^{13}$C NMR (101 MHz, DMSO-$d_6$):** $\delta$ = 157.2, 157.0, 139.7, 134.1, 130.9, 124.2, 121.3, 121.0, 119.6, 116.1, 111.4, 108.5, 103.9, 31.9, 30.6 ppm.

**IR (ATR):** $v$ = 3378 (m), 3264 (m), 3211 (s), 3109 (m), 3087 (m), 3048 (m), 2989 (m), 2955 (m), 2922 (m), 2870 (m), 2853 (m), 1659 (vs), 1623 (vs), 1554 (m), 1502 (m), 1452 (m), 1445 (m), 1404 (vs), 1371 (vs), 1361 (vs), 1340 (vs), 1316 (vs), 1276 (s), 1261 (s), 1241 (s), 1201 (vs), 1181 (vs), 1133 (vs), 1096 (vs), 1082 (s), 1067 (s), 1051 (s), 1017 (s), 977 (m), 952 (vs), 939 (vs), 880 (s), 841 (vs), 803 (s), 783 (vs), 754 (vs), 744 (vs), 720 (vs), 653 (vs), 625 (vs), 599 (vs), 579 (vs), 560 (vs), 534 (vs), 506 (vs), 486 (vs), 448 (vs), 414 (vs), 397 (vs), 377 (vs) cm$^{-1}$.

**HRMS (FAB):** $m/z$ calcd. for C$_{17}$H$_{20}$N$_5$O$_2$ [M+H], 326.1612; found, 326.1613.

**UV/Vis (DMSO):** $\lambda_{max}$ = 374 nm.

*(3Z,6Z)-3-((1H-Pyrrol-2-yl)methylene)-6-((5-(tert-butyl)-1H-imidazol-4-yl)methylene)-*
*piperazine-2,5-dione (24)*
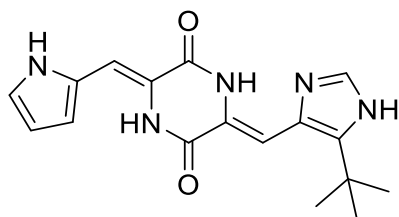


**$^1$H NMR (400 MHz, DMSO-$d_6$):** $\delta$ = 12.38 (br, 1H), 12.02 (br, 1H), 11.38 (s, 1H), 9.38 (s, 1H), 7.91 (br, 1H), 7.00 (s, 1H), 6.81 (s, 1H), 6.78 (s, 1H), 6.76 (s, 1H), 6.22 (d, $J$ = 3.4 Hz, 1H), 1.38 (s, 9H) ppm.

**IR (ATR):** $v$ = 3244 (w), 3234 (w), 3224 (w), 3217 (w), 3211 (w), 3203 (w), 3128 (w), 2968 (w), 2910 (w), 2873 (w), 1670 (vs), 1640 (vs), 1492 (w), 1428 (m), 1401 (vs), 1373 (vs), 1343 (vs), 1281 (w), 1203 (vs), 1184 (vs), 1129 (vs), 1055 (m), 1021 (w), 955 (m), 936 (w), 926 (w), 884 (m), 839 (s), 795 (vs), 754 (vs), 724 (vs), 657 (s), 639 (s), 598 (s), 561 (s), 541 (s), 517 (s), 486 (s), 446 (s), 441 (s), 409 (m), 387 (m), 380 (m) cm$^{-1}$.

**HRMS (FAB):** $m/z$ calcd. for C$_{17}$H$_{20}$N$_5$O$_2$ [M+H], 326.1612; found, 326.1610.

**UV/Vis (MeCN):** $\lambda_{max}$ = 389 nm.

**Fluorescence (DMSO):** $\lambda_{em}$= 510 nm (excited with $\lambda$ = 400 nm).

*(3Z,6Z)-3-[(5-tert-Butyl-1H-imidazol-4-yl)methylene]-6-[(1-methylpyrrol-2-yl)methylene]-*
*piperazine-2,5-dione (25)*
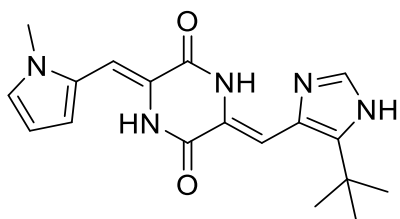
**¹H NMR (400 MHz, DMSO-*d₆*):** $\delta$ = 12.30 (s, 1H), 12.16 (s, 1H), 9.18 (s, 1H), 7.84 (s, 1H), 6.98 (dd, $J$ = 2.6, 1.4 Hz, 1H), 6.84 (s, 1H), 6.77 (dd, $J$ = 4.0, 0.9 Hz, 1H), 6.73 (s, 1H), 6.21 – 6.14 (m, 1H), 3.66 (s, 3H), 1.39 (s, 9H) ppm.

**¹³C NMR (101 MHz, DMSO-*d₆*):** $\delta$ = 157.2, 156.5, 140.1, 134.3, 130.8, 125.8, 123.9, 122.1, 111.7, 108.8, 104.6, 103.4, 33.8, 31.9, 30.6 ppm.

**IR (ATR):** $\nu$ = 3167 (w), 3152 (w), 3136 (w), 3109 (w), 3084 (w), 3072 (w), 3058 (w), 2955 (m), 2921 (m), 2870 (w), 2854 (w), 1666 (s), 1632 (vs), 1626 (vs), 1557 (w), 1497 (w), 1489 (w), 1456 (m), 1442 (m), 1408 (vs), 1370 (vs), 1337 (vs), 1299 (s), 1273 (s), 1256 (s), 1217 (s), 1190 (s), 1160 (s), 1102 (m), 1092 (m), 1067 (s), 1051 (s), 1020 (m), 952 (vs), 902 (m), 853 (m), 841 (s), 817 (vs), 802 (vs), 778 (s), 752 (vs), 717 (vs), 657 (vs), 633 (vs), 599 (vs), 582 (s), 524 (vs), 504 (vs), 493 (vs), 452 (vs), 414 (s), 391 (m), 380 (s) cm⁻¹.

**HRMS (FAB):** $m/z$ calcd. for $C_{18}H_{21}O_2N_5$ [M], 339.1690; found, 339.1692; calc. for $C_{18}H_{22}O_2N_5$ [M+H], 340.1768; found, 340.1767.

**UV/Vis (DMSO):** $\lambda_{max}$ = 399 nm.

*(3Z,6Z)-3-[(5-tert-Butyl-1H-imidazol-4-yl)methylene]-6-(3-furylmethylene)piperazine-2,5-dione (26)*
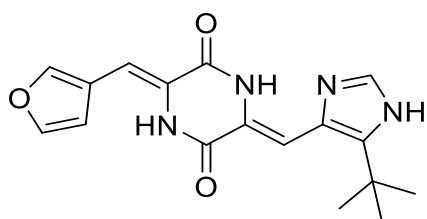


**¹H NMR (400 MHz, DMSO-*d₆*):** $\delta$ = 12.32 (s, 1H), 12.21 (s, 1H), 9.59 (s, 1H), 8.24 (dt, $J$ = 1.8, 0.9 Hz, 1H), 7.84 (d, $J$ = 1.0 Hz, 1H), 7.75 (t, $J$ = 1.8 Hz, 1H), 6.92 (d, $J$ = 1.5 Hz, 1H), 6.86 (s, 1H), 6.65 (s, 1H), 1.38 (s, 9H) ppm.

**¹³C NMR (101 MHz, DMSO-*d₆*):** $\delta$ = 157.5, 156.3, 143.9, 143.9, 140.2, 134.3, 130.7, 125.4, 123.8, 118.5, 110.7, 105.4, 105.0, 31.9, 30.6 ppm.

**IR (ATR):** $\nu$ = 3213 (s), 3109 (m), 3075 (m), 3019 (m), 2989 (m), 2953 (s), 2922 (m), 2894 (m), 2861 (m), 1677 (s), 1667 (s), 1626 (vs), 1604 (vs), 1544 (m), 1500 (s), 1482 (w), 1455 (vs), 1445 (s), 1415 (vs), 1373 (vs), 1360 (vs), 1341 (vs), 1316 (vs), 1278 (vs), 1259 (s), 1222 (s), 1204 (m), 1184 (s), 1162 (m), 1137 (vs), 1098 (m), 1084 (w), 1071 (s), 1052 (s), 1030 (s), 1017 (s), 992 (m),

952 (vs), 941 (vs), 905 (w), 875 (s), 853 (m), 843 (m), 816 (vs), 781 (vs), 739 (s), 730 (vs), 713 (vs), 653 (vs), 635 (s), 606 (s), 589 (vs), 562 (m), 538 (s), 514 (s), 486 (s), 452 (vs), 415 (w), 395 (w), 384 (m) cm$^{-1}$.

**HRMS (FAB):** *m/z* calcd. for C$_{17}$H$_{19}$O$_3$N$_4$ [M+H], 327.1452; found, 327.1481.

**UV/Vis (DMSO):** $\lambda_{max}$ = 368 nm.


*(3Z,6Z)-3-((5-(tert-Butyl)-1H-imidazol-4-yl)methylene)-6-(thiophen-2-ylmethylene)piperazine-2,5-dione (27)*
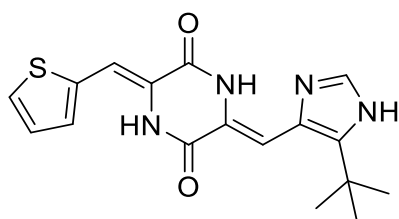


**$^1$H NMR (400 MHz, DMSO-*d$_6$*):** $\delta$ = 12.40 (br, 1H), 12.25 (s, 1H), 9.52 (s, 1H), 7.85 (s, 1H), 7.72 (dd, *J* = 5.1, 1.1 Hz, 1H), 7.55 (dt, *J* = 3.8, 1.1 Hz, 1H), 7.19 (dd, *J* = 5.1, 3.6 Hz, 1H), 6.91 (s, 1H), 6.88 (s, 1H), 1.39 (s, 9H) ppm.

**$^{13}$C NMR (101 MHz, DMSO-*d$_6$*):** $\delta$ = 157.4, 156.1, 140.6, 135.7, 134.4, 130.7, 129.6, 128.4, 128.0, 124.8, 123.6, 107.1, 105.4, 48.6, 31.9, 30.6 ppm.

**IR (ATR):** $v$ = 3378 (w), 3199 (m), 3119 (w), 3084 (w), 2962 (w), 2929 (w), 2871 (w), 1664 (vs), 1630 (vs), 1598 (s), 1502 (w), 1453 (s), 1438 (m), 1402 (vs), 1364 (vs), 1341 (vs), 1330 (vs), 1276 (s), 1262 (s), 1207 (vs), 1184 (vs), 1132 (vs), 1051 (s), 1018 (s), 953 (vs), 941 (s), 901 (w), 881 (m), 871 (m), 840 (vs), 819 (vs), 805 (vs), 781 (vs), 748 (vs), 724 (vs), 708 (s), 688 (vs), 656 (vs), 595 (s), 586 (s), 572 (s), 558 (s), 537 (m), 507 (vs), 482 (vs), 465 (m), 446 (vs), 418 (s), 390 (s), 377 (s) cm$^{-1}$.

**HRMS (FAB):** *m/z* calcd. for C$_{17}$H$_{19}$O$_2$N$_4$S [M+H], 343.1223; found, 343.1224.

**UV/Vis (MeCN):** $\lambda_{max}$ = 271, 377 nm.

**UV/Vis (DMSO):** $\lambda_{max}$ = 387 nm.

**Fluorescence (DMSO):** $\lambda_{em}$= 532 nm (excited with $\lambda$ = 400 nm).

**$\Phi_F$ (MeCN):** 0.033.

**$\Phi_F$ (DMSO):** 0.031.


*(3Z,6Z)-3-[(5-tert-Butyl-1H-imidazol-4-yl)methylene]-6-[(5-methyl-2-thienyl)methylene]-piperazine-2,5-dione (28)*
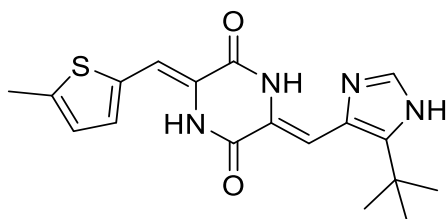
**¹H NMR (400 MHz, DMSO-*d₆*):** $\delta$ = 12.02 (s, 1H), 11.32 (br, 2H), 7.77 (s, 1H), 7.14 (d, *J* = 3.6 Hz, 1H), 6.77 (d, *J* = 2.5 Hz, 1H), 6.73 (s, 1H), 6.71 (s, 1H), 2.45 (s, 2H), 1.38 (s, 9H) ppm.

**¹³C NMR (101 MHz, DMSO-*d₆*):** $\delta$ = 158.9, 157.6, 140.8, 138.9, 136.0, 133.8, 131.4, 127.7, 127.4, 125.8, 125.7, 106.8, 31.8, 30.7, 15.1 ppm.

**IR (ATR):** $v$ = 3492 (w), 3391 (w), 3241 (m), 3128 (w), 3088 (w), 3071 (w), 2972 (m), 2952 (m), 2911 (w), 2863 (w), 1663 (m), 1595 (s), 1502 (m), 1451 (s), 1404 (vs), 1367 (vs), 1337 (vs), 1286 (s), 1261 (s), 1220 (m), 1201 (m), 1181 (m), 1152 (vs), 1125 (m), 1055 (m), 1017 (m), 948 (m), 935 (s), 878 (m), 840 (m), 824 (m), 796 (vs), 749 (vs), 721 (s), 679 (m), 670 (s), 652 (vs), 622 (s), 601 (s), 582 (s), 564 (s), 541 (m), 510 (vs), 497 (vs), 477 (vs), 443 (vs), 424 (s), 407 (s), 397 (m), 382 (s) cm⁻¹.

**HRMS (EI):** *m/z* calcd. for $C_{18}H_{21}O_2N_4S$ [M], 357.1380; found, 357.1382.

**UV/Vis (DMSO):** $\lambda_{max}$ = 387 nm.

### 5.4.4 NMR Spectra



**Figure 64:** $^1$H NMR spectrum (400 MHz, DMSO-$d_6$) of compound Z-**5**.



**Figure 65:** $^{13}$C NMR spectrum (101 MHz, DMSO-$d_6$) of compound Z-**5**.
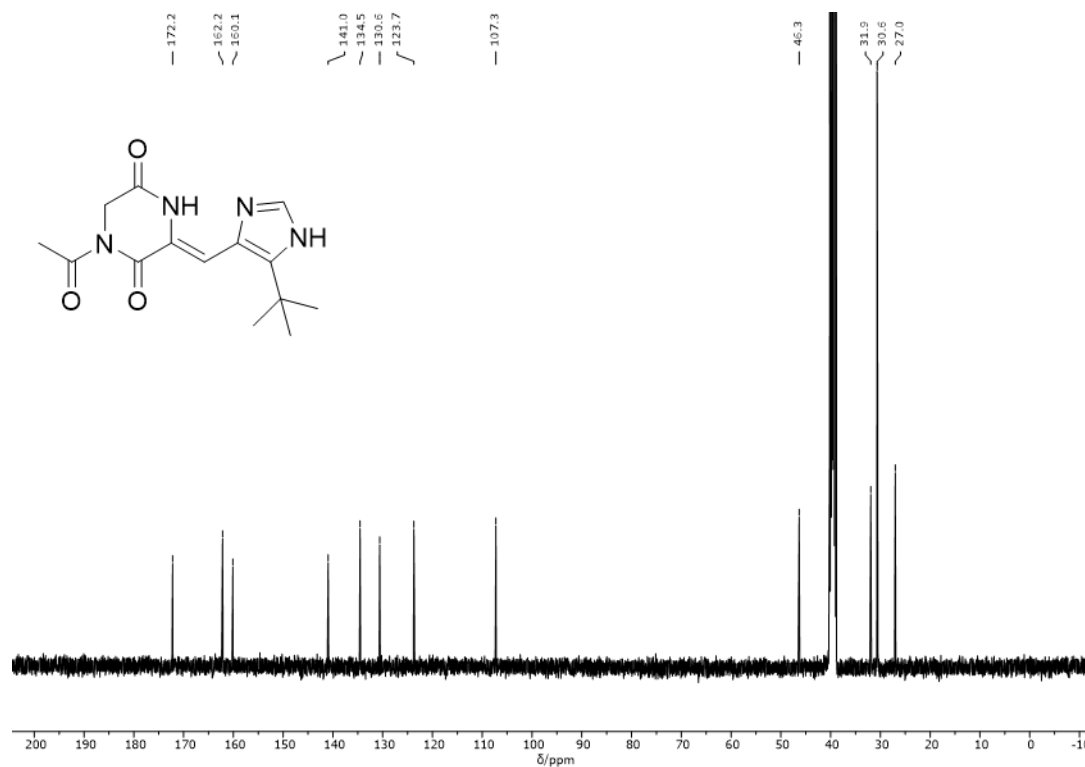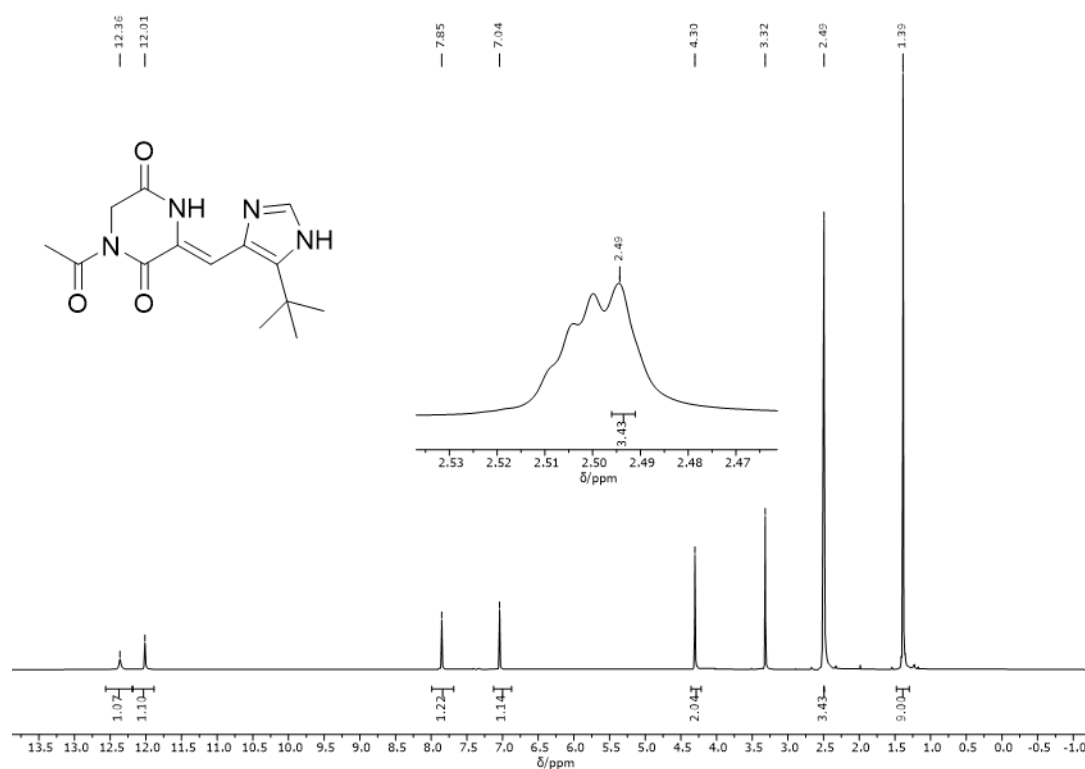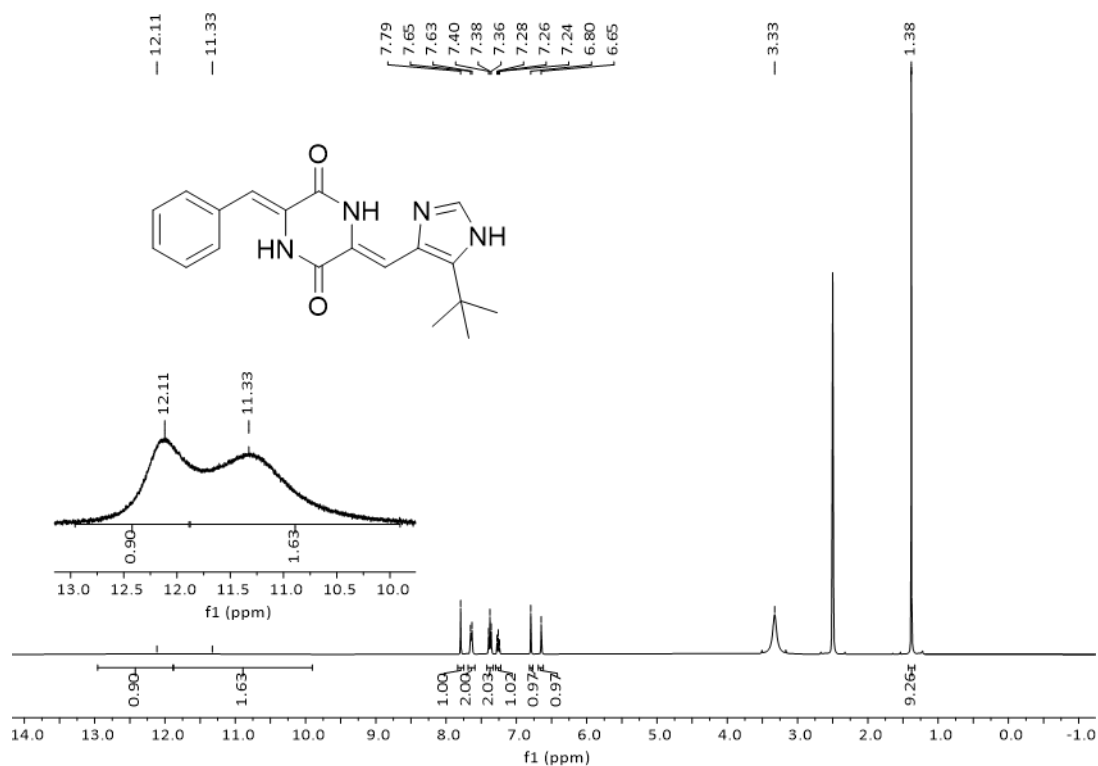
**Figure 66:** $^1$H NMR spectrum (400 MHz, DMSO-$d_6$) of compound *Z*-**6**.
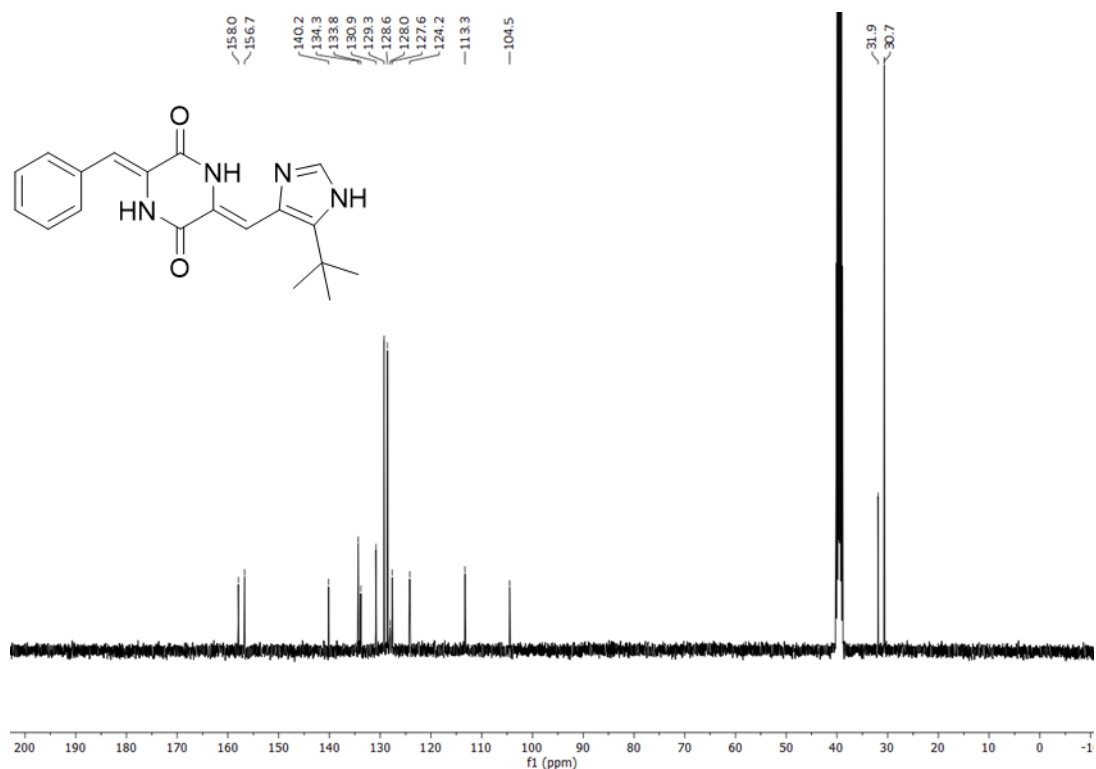


**Figure 67:** $^{13}$C NMR spectrum (101 MHz, DMSO-$d_6$) of compound *Z*-**6**.
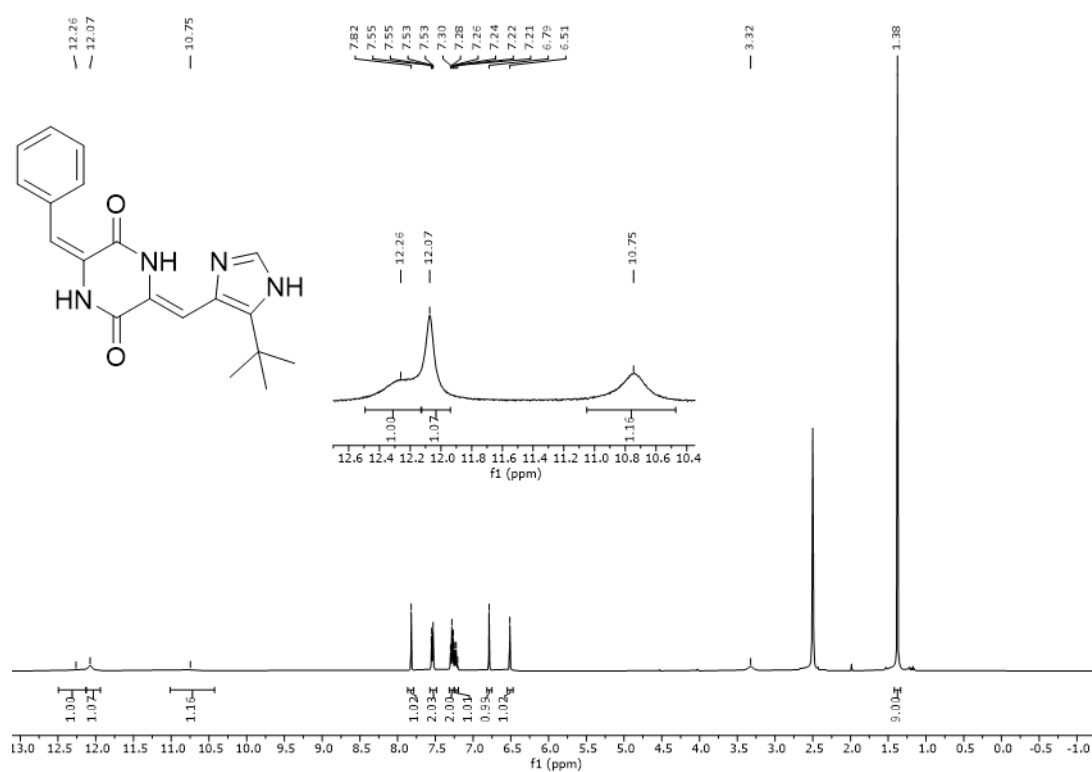
**Figure 68:** $^1$H NMR spectrum (400 MHz, DMSO-$d_6$) of compound *E*-**6**.
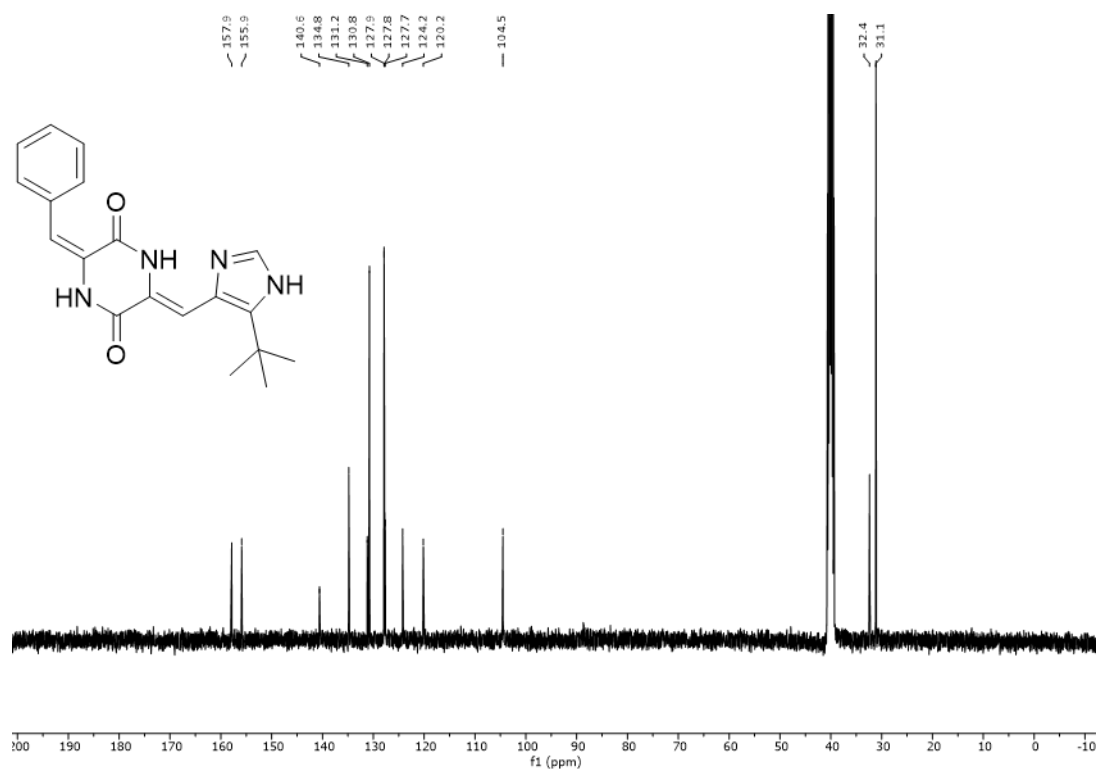


**Figure 69:** $^{13}$C NMR spectrum (101 MHz, DMSO-$d_6$) of compound *E*-**6**.
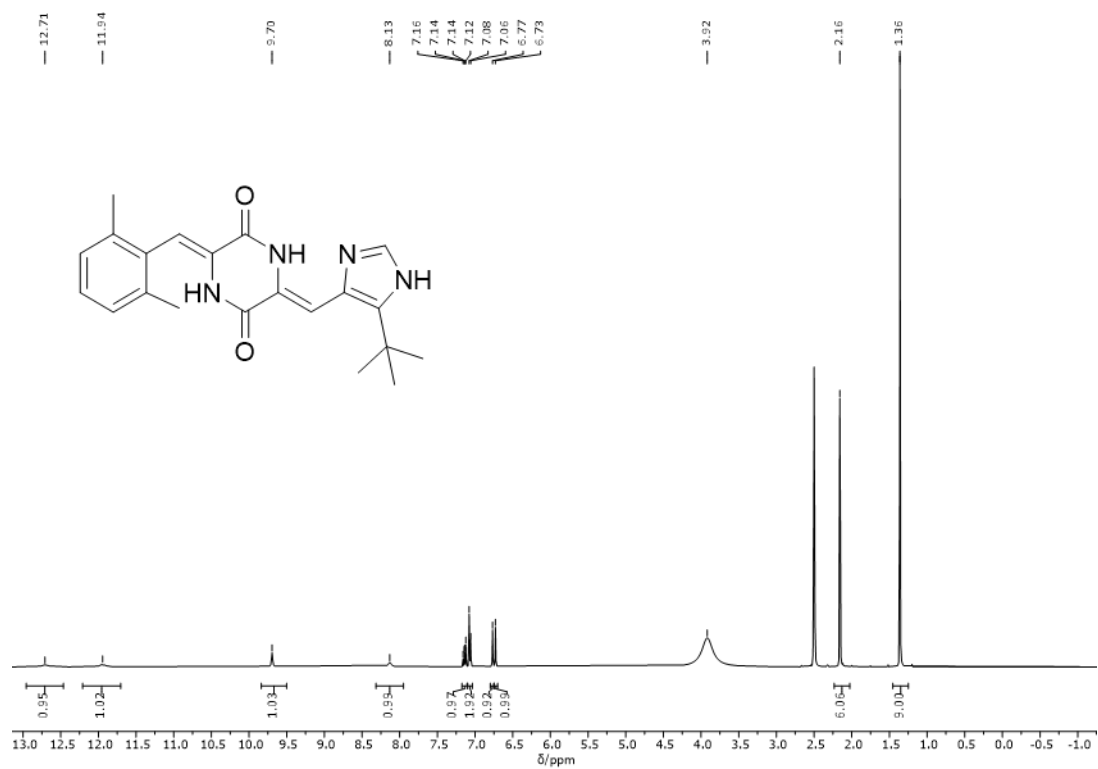
**Figure 70:** $^1$H NMR spectrum (400 MHz, DMSO-$d_6$) of compound *Z*-**7**.
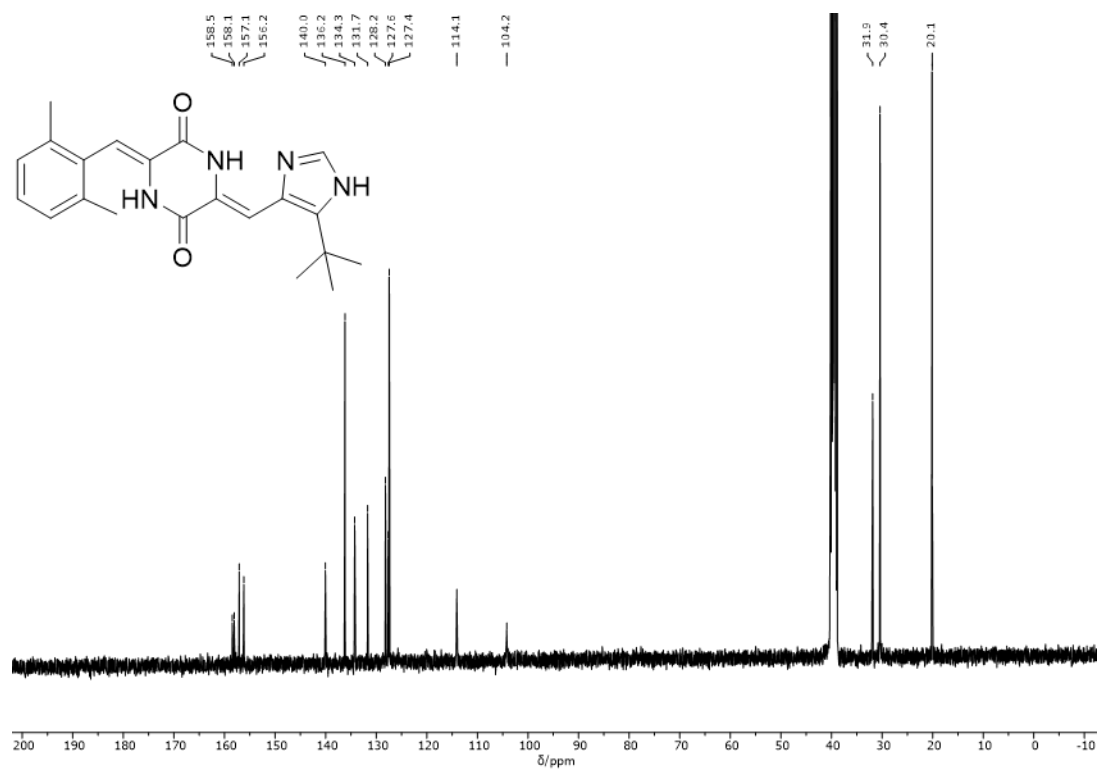


**Figure 71:** $^{13}$C NMR spectrum (101 MHz, DMSO-$d_6$) of compound *Z*-**7**.
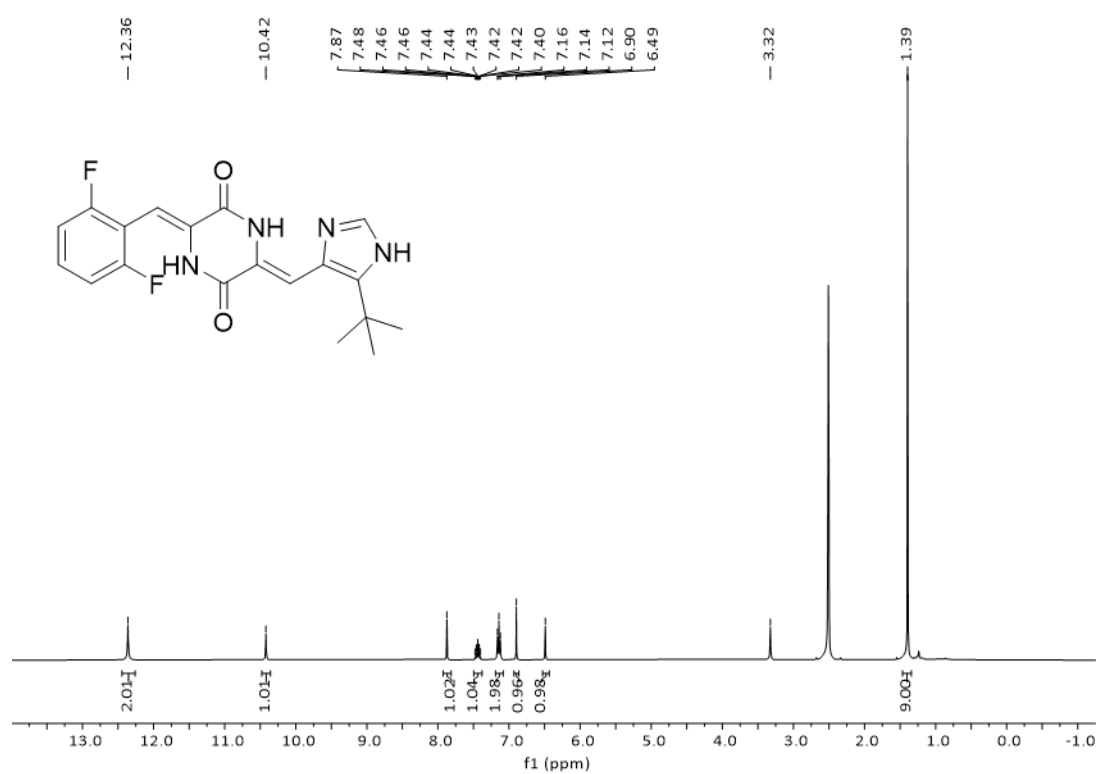
**Figure 72:** $^1$H NMR spectrum (400 MHz, DMSO-$d_6$) of compound Z-**8**.
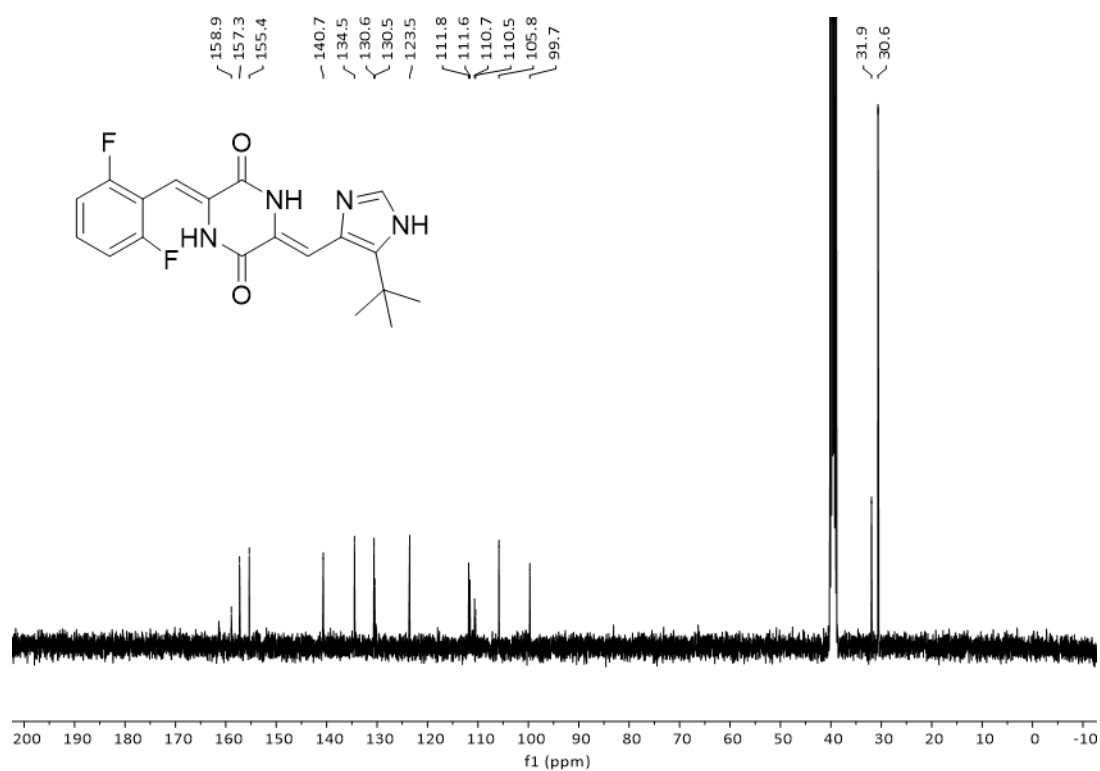


**Figure 73:** $^{13}$C NMR spectrum (101 MHz, DMSO-$d_6$) of compound Z-**8**.
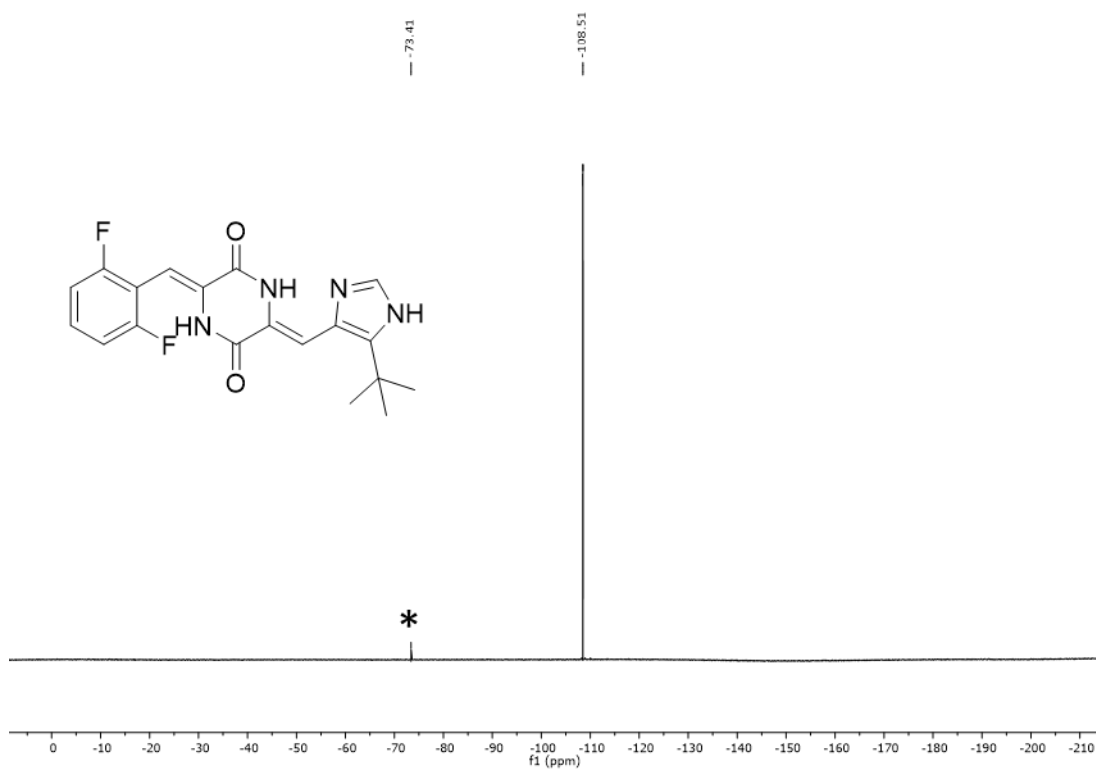
**Figure 74:** $^{19}$F NMR spectrum (376 MHz, DMSO-$d_6$) of compound *Z*-**8**. *TFA.
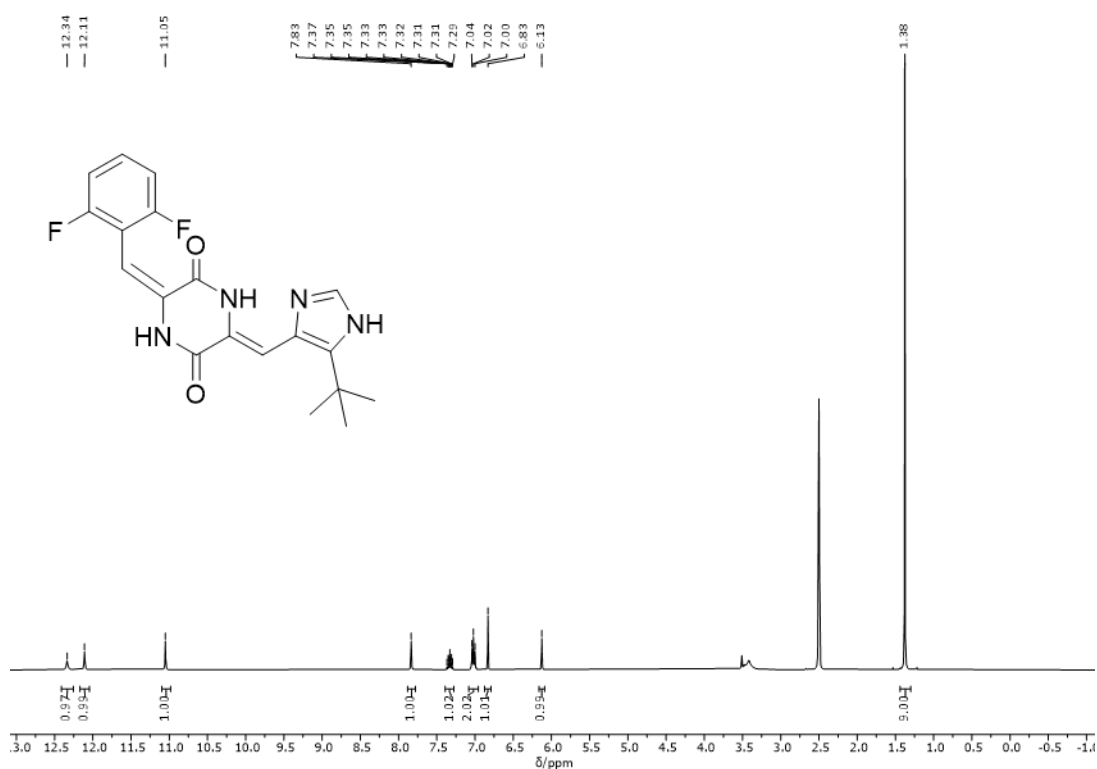


**Figure 75:** $^1$H NMR spectrum (400 MHz, DMSO-$d_6$) of compound *E*-**8**.
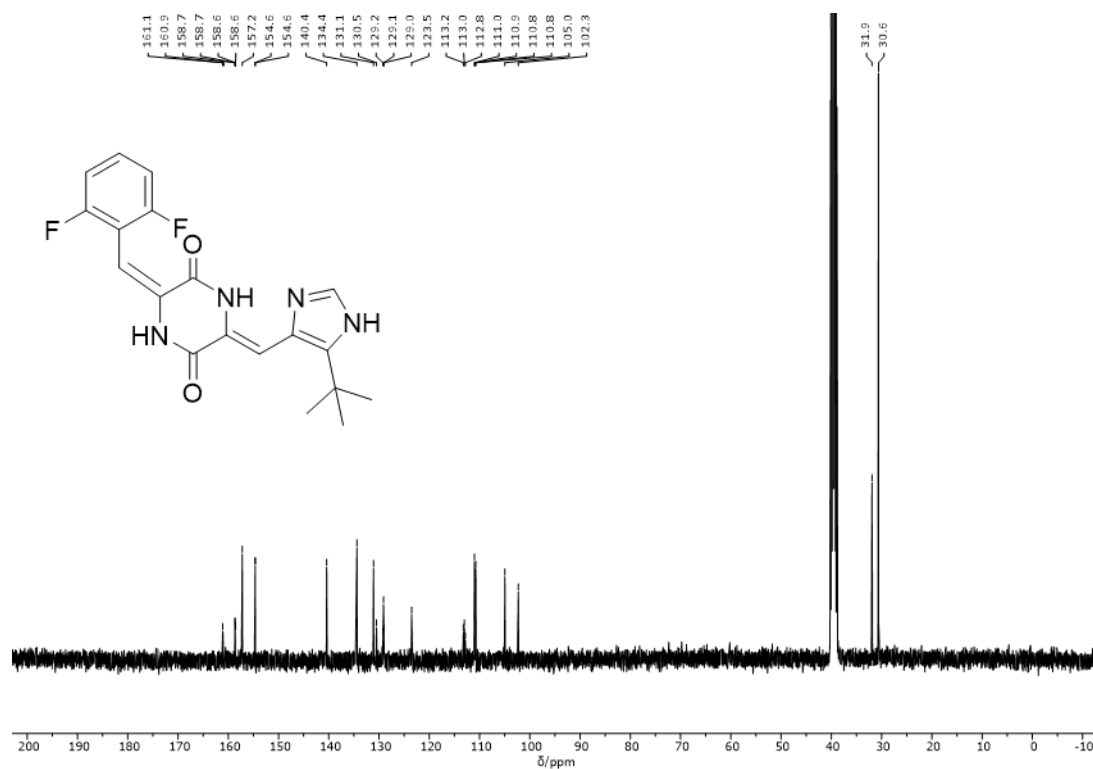
**Figure 76:** $^{13}$C NMR spectrum (101 MHz, DMSO-$d_6$) of compound *E*-**8**.
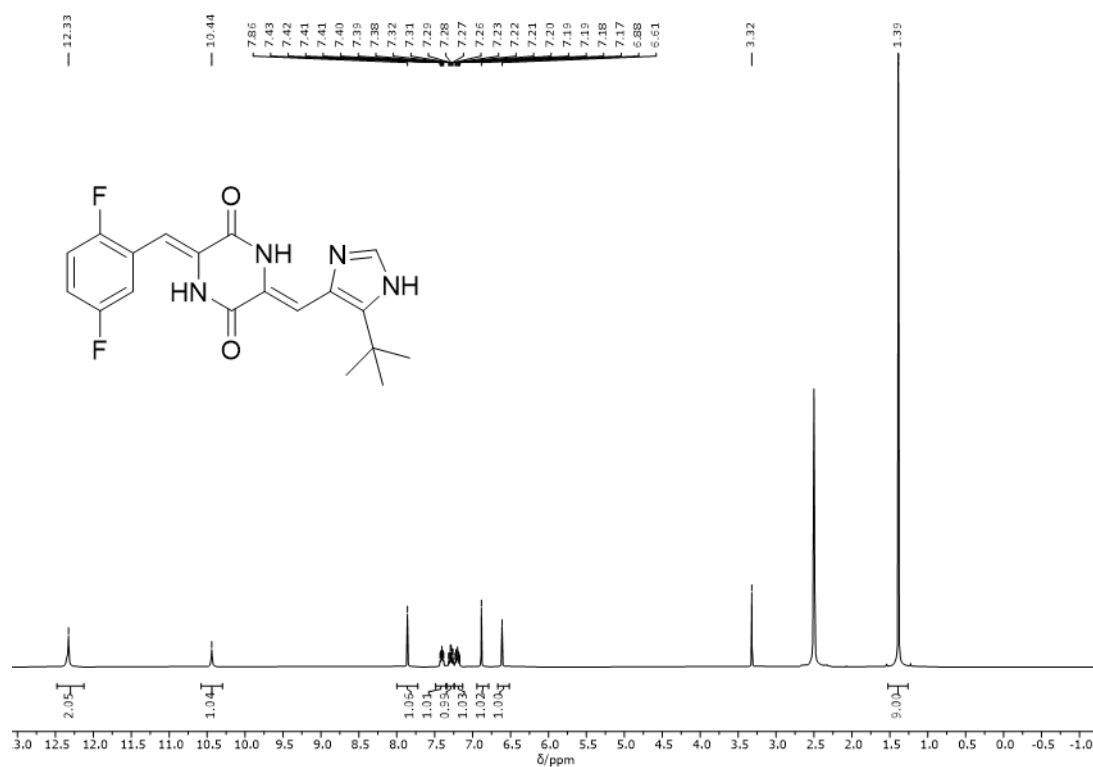


**Figure 77:** $^1$H NMR spectrum (400 MHz, DMSO-$d_6$) of compound *Z*-**9**.
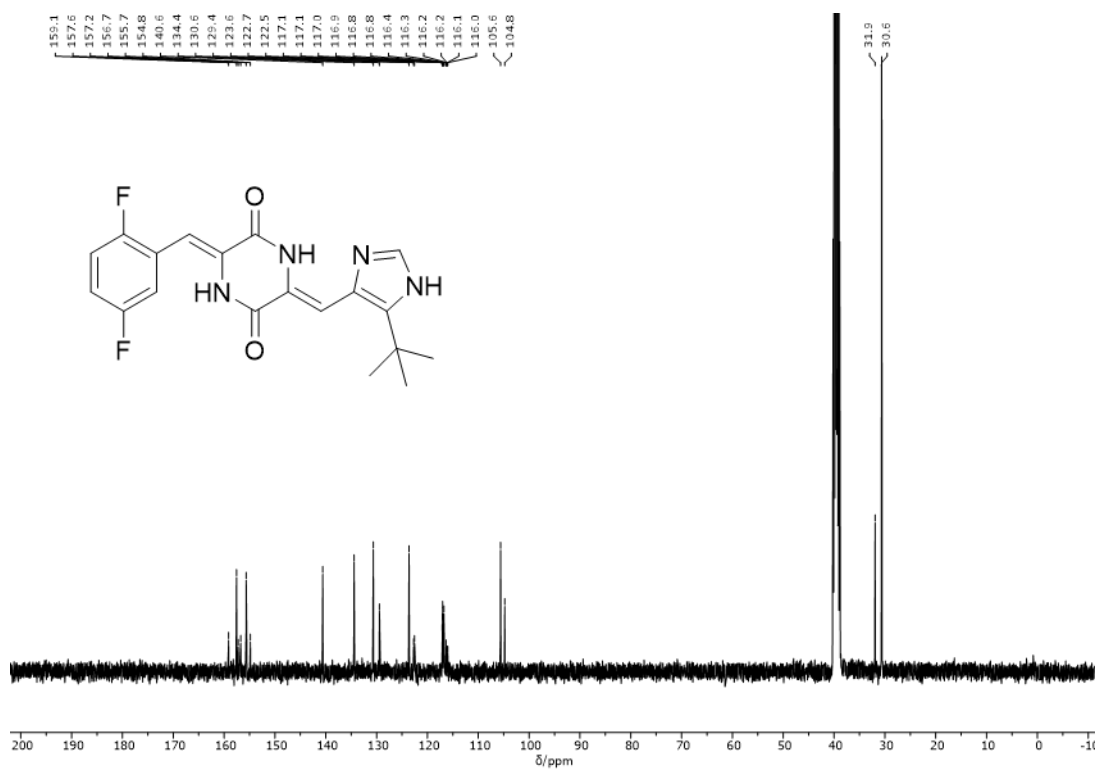
**Figure 78:** $^{13}$C NMR spectrum (101 MHz, DMSO-$d_6$) of compound *Z*-**9**.
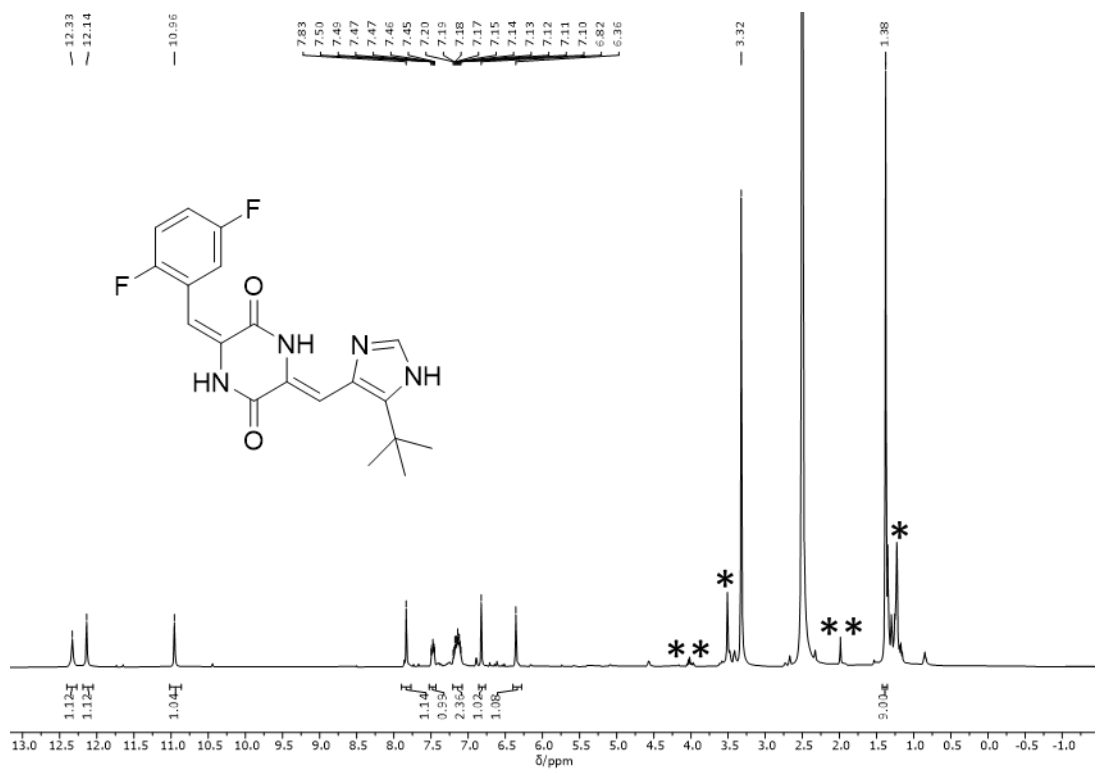


**Figure 79:** $^1$H NMR spectrum (400 MHz, DMSO-$d_6$) of compound *E*-**9**. * unknown impurity, ** ethyl acetate.
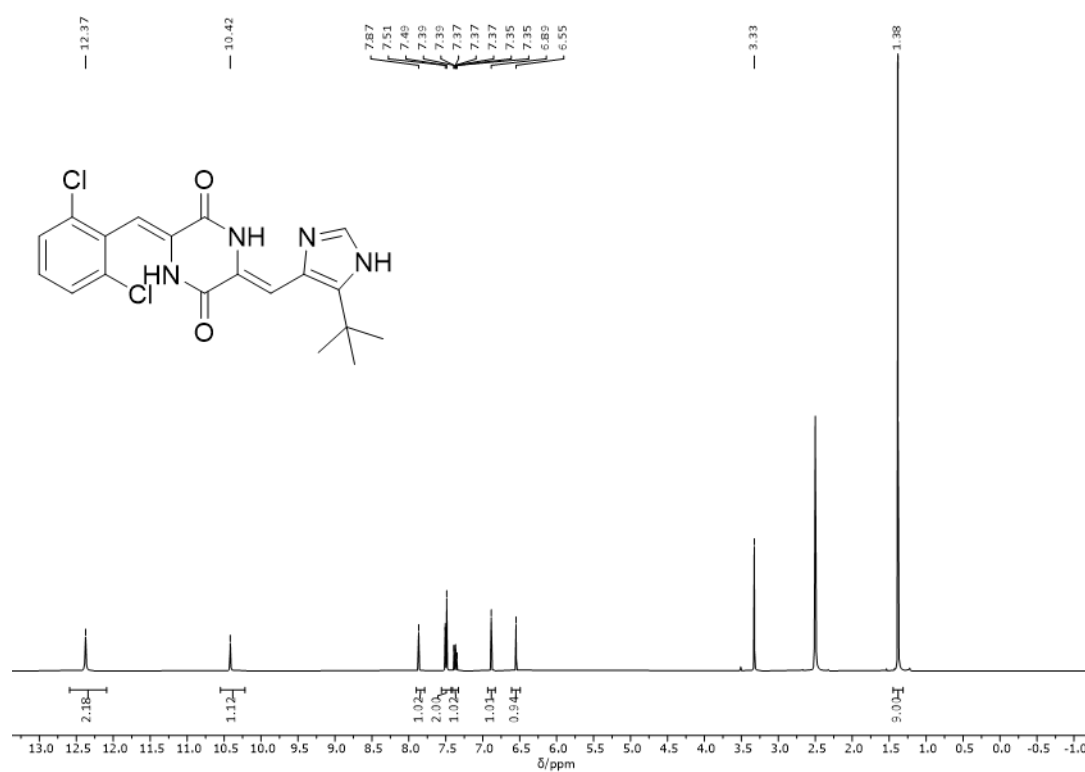
**Figure 80:** $^1$H NMR spectrum (400 MHz, DMSO-$d_6$) of compound Z-**10**.
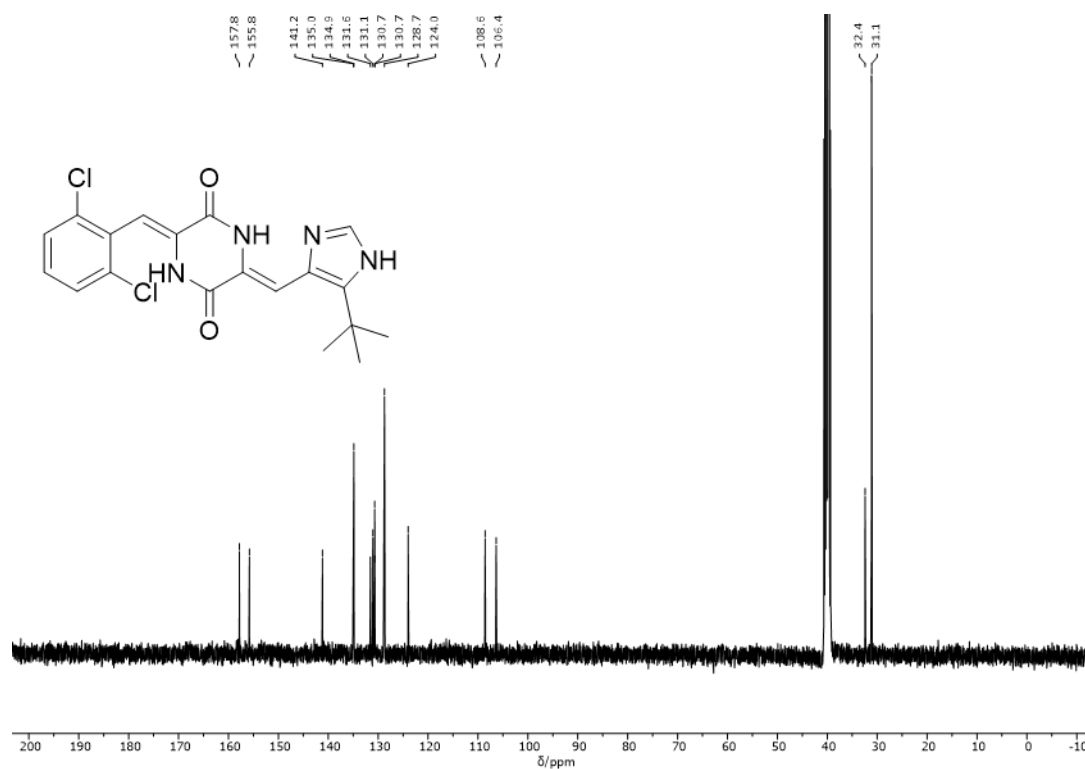


**Figure 81:** $^{13}$C NMR spectrum (101 MHz, DMSO-$d_6$) of compound Z-**10**.

**Figure 82:** $^1$H NMR spectrum (400 MHz, DMSO-$d_6$) of compound *E*-**10**.



**Figure 83:** $^{13}$C NMR spectrum (101 MHz, DMSO-$d_6$) of compound *E*-**10**.
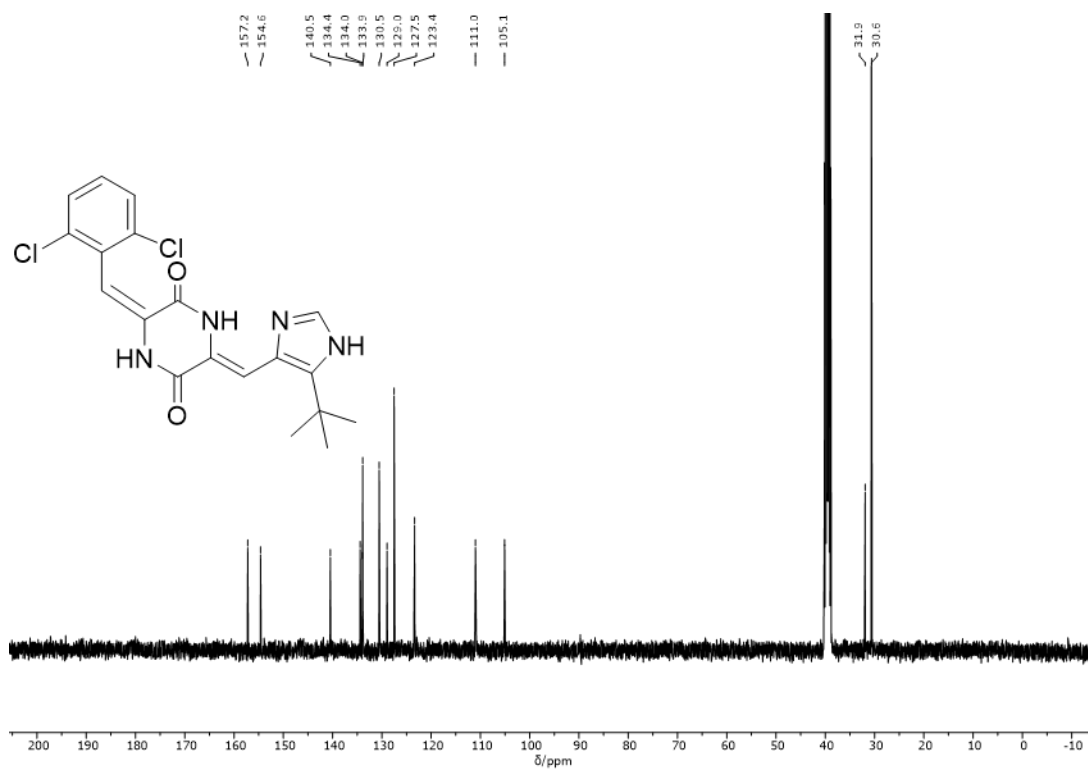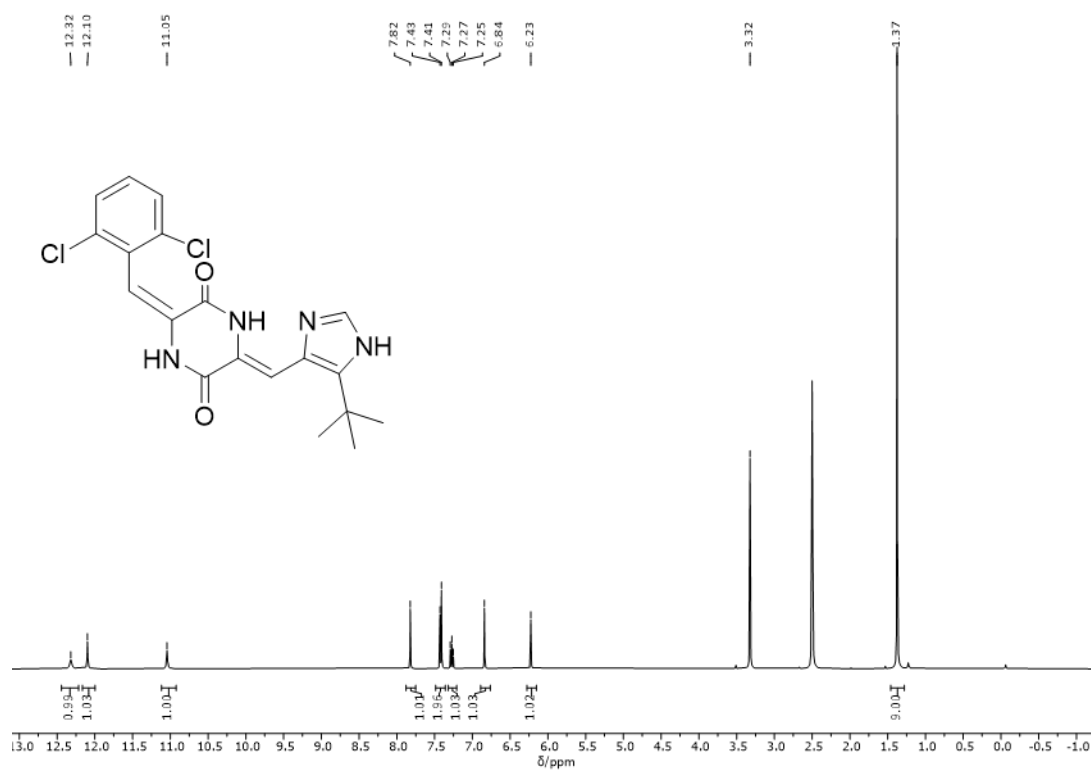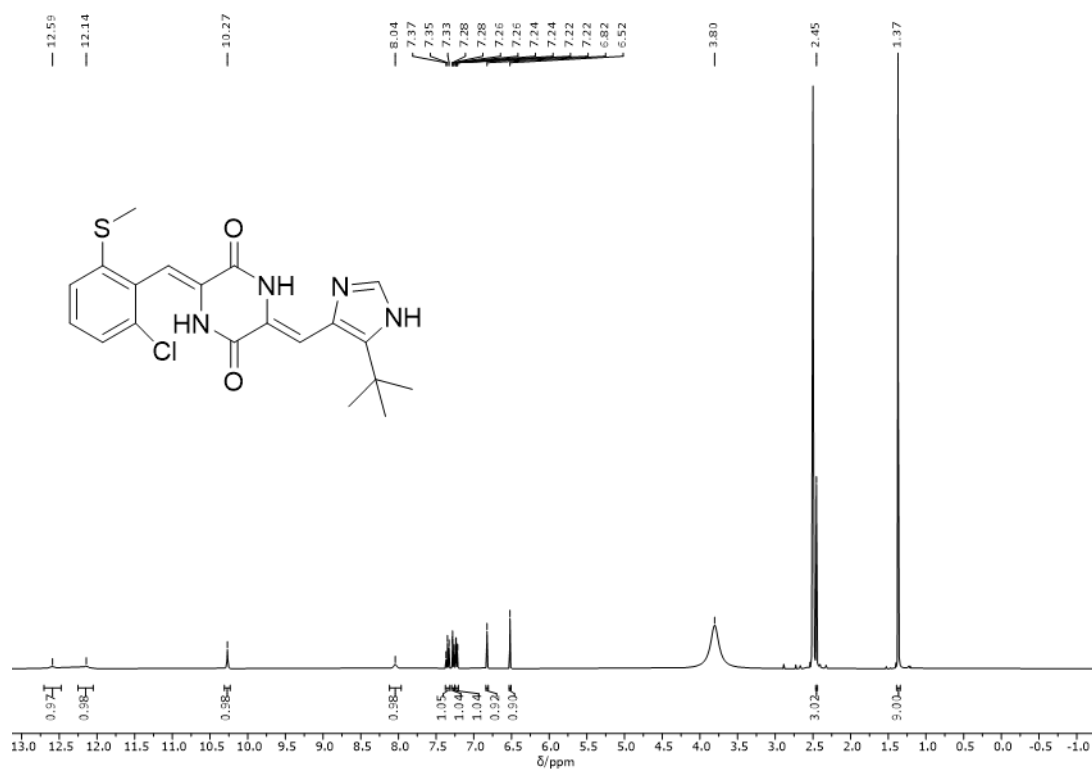
**Figure 84:** $^1$H NMR spectrum (400 MHz, DMSO-$d_6$) of compound Z-**11**.
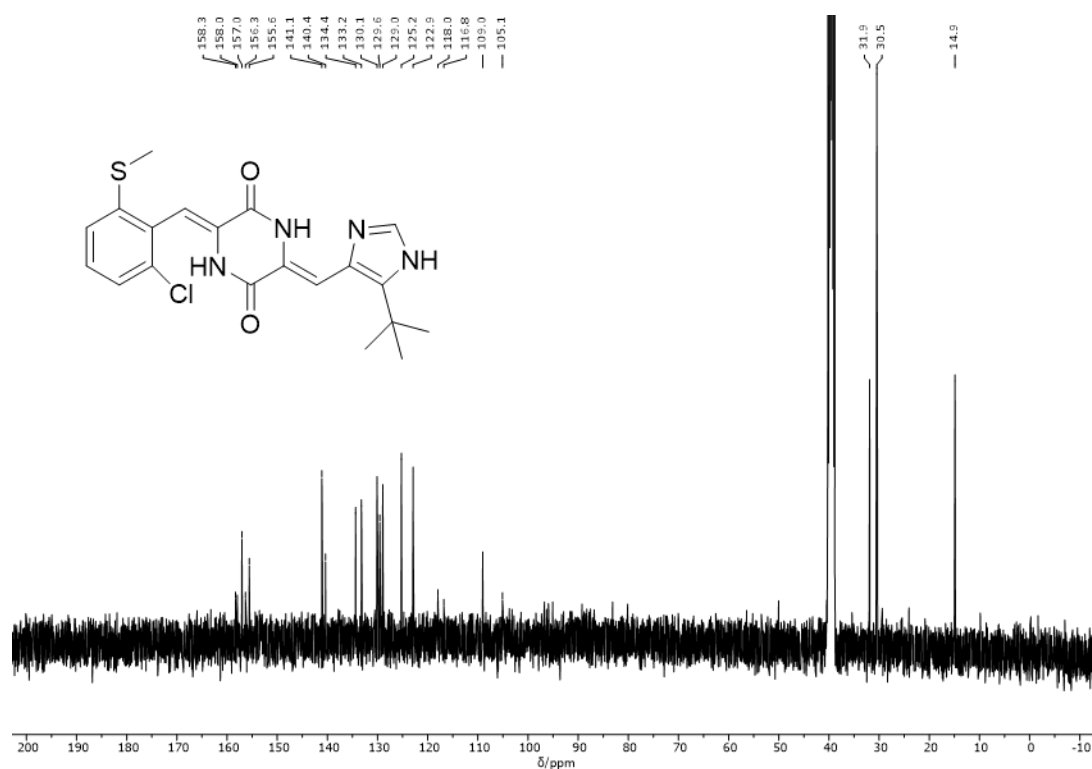


**Figure 85:** $^{13}$C NMR spectrum (101 MHz, DMSO-$d_6$) of compound Z-**11**.
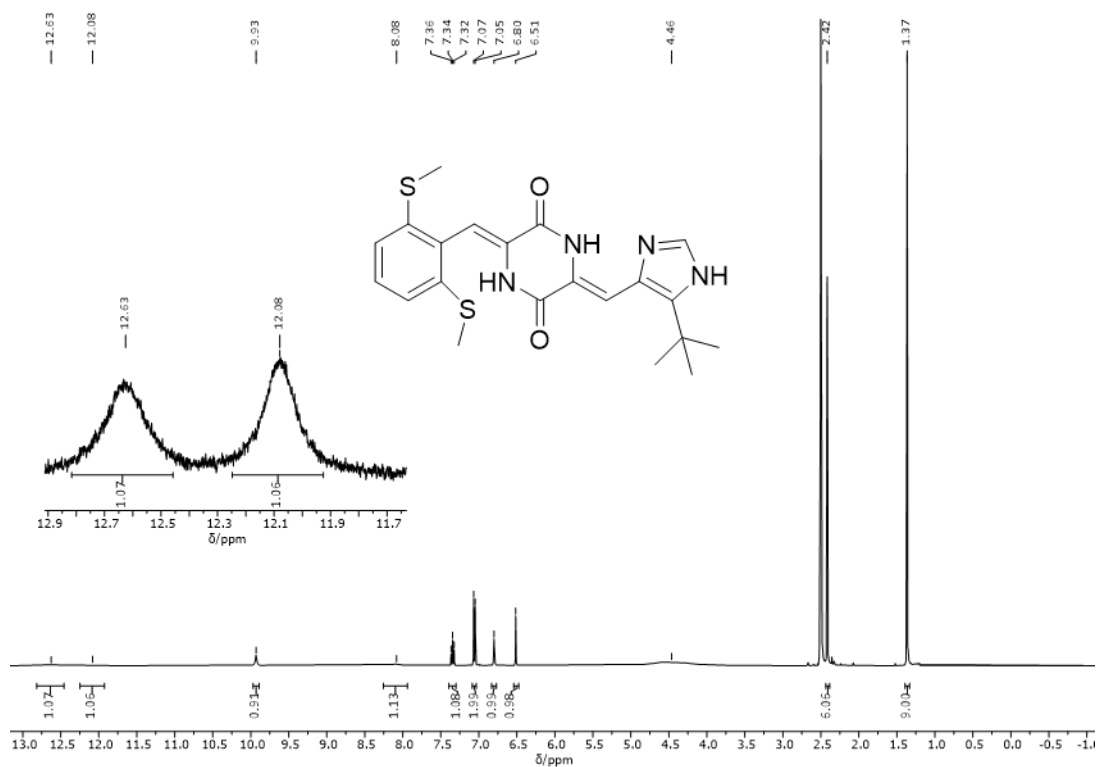
**Figure 86:** $^1$H NMR spectrum (400 MHz, DMSO-$d_6$) of compound *Z*-**12**.
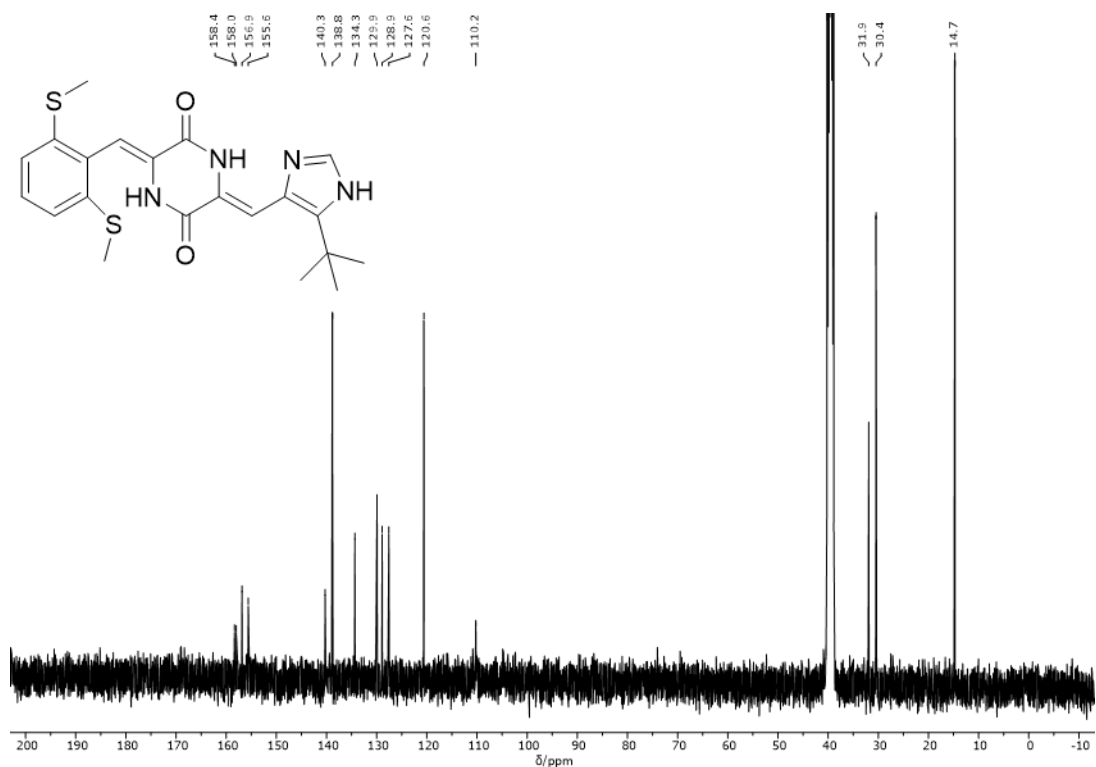


**Figure 87:** $^{13}$C NMR spectrum (101 MHz, DMSO-$d_6$) of compound *Z*-**12**.
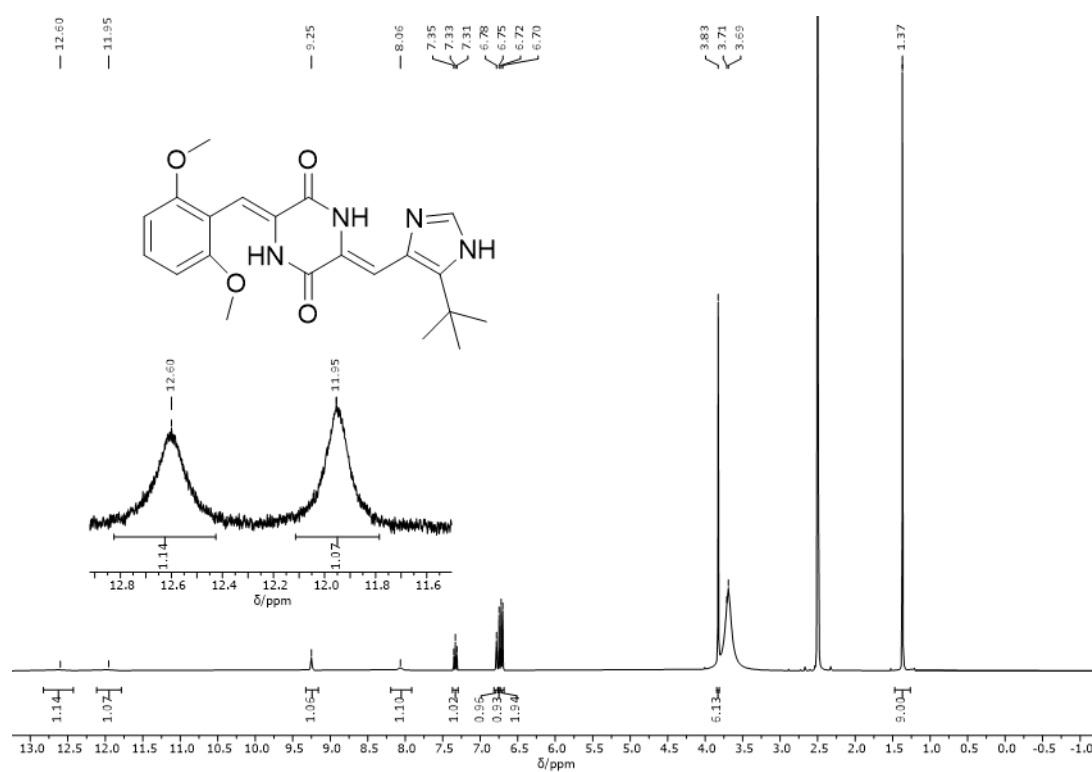
**Figure 88:** $^1$H NMR spectrum (400 MHz, DMSO-$d_6$) of compound Z-**13**.
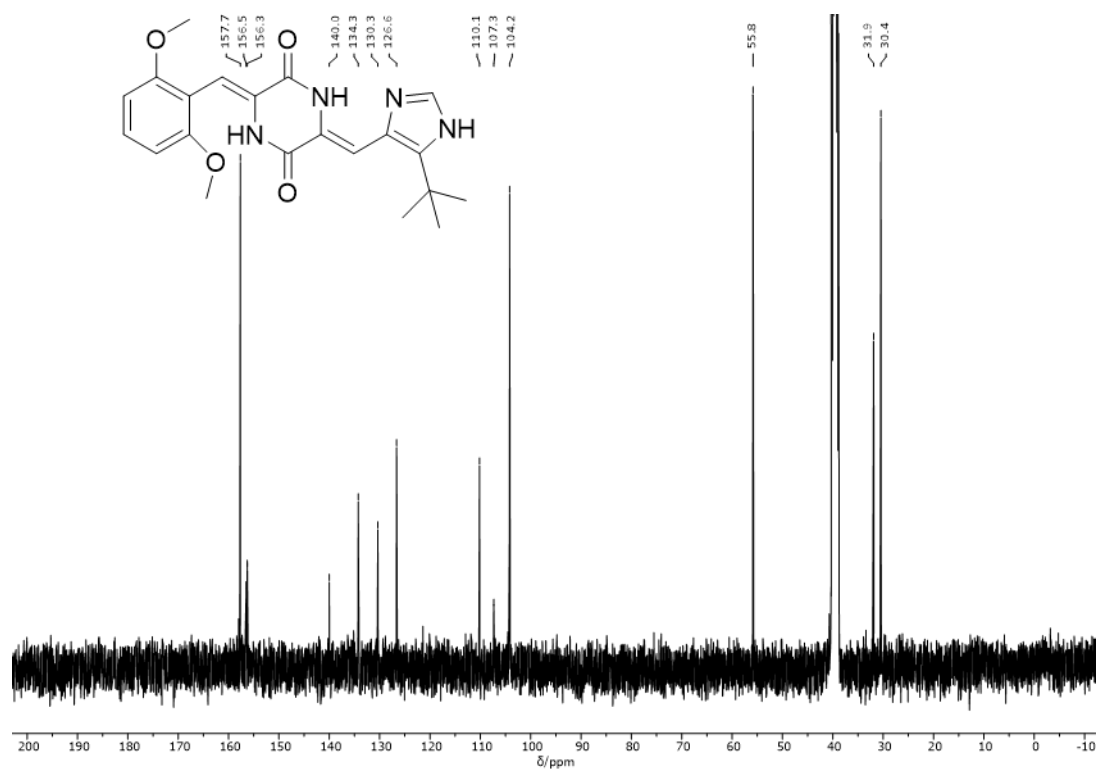


**Figure 89:** $^{13}$C NMR spectrum (101 MHz, DMSO-$d_6$) of compound Z-**13**.
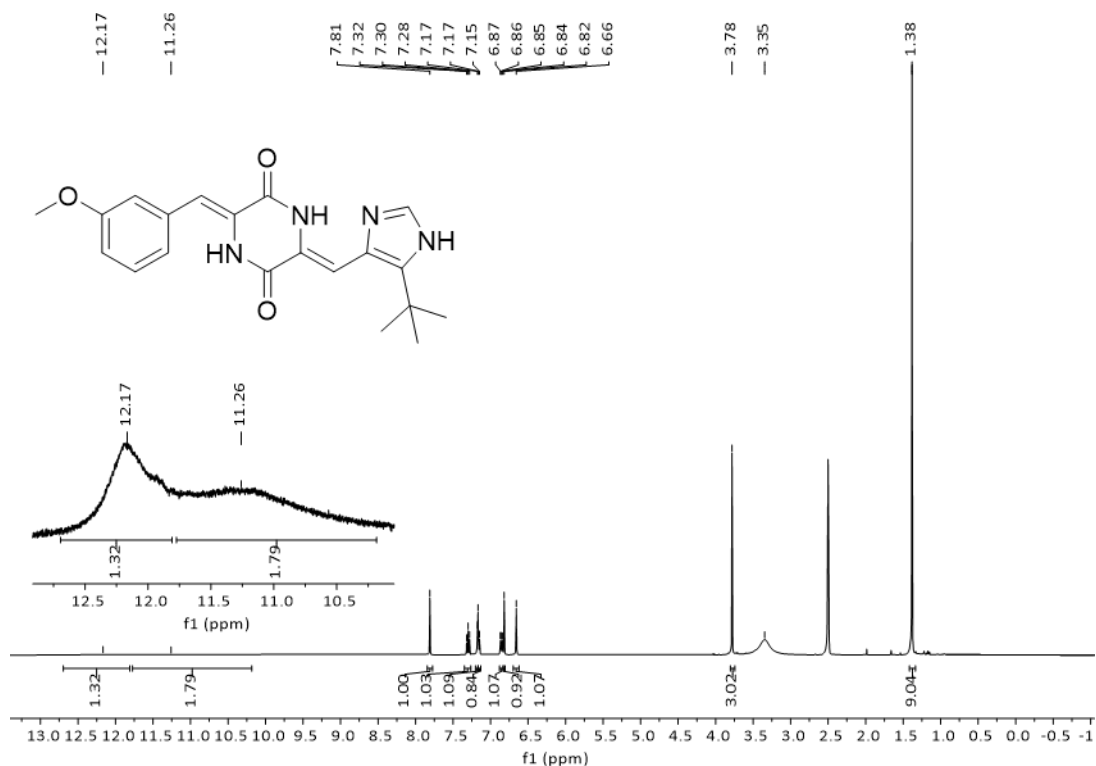
**Figure 90:** $^1$H NMR spectrum (400 MHz, DMSO-$d_6$) of compound *Z*-**14**.
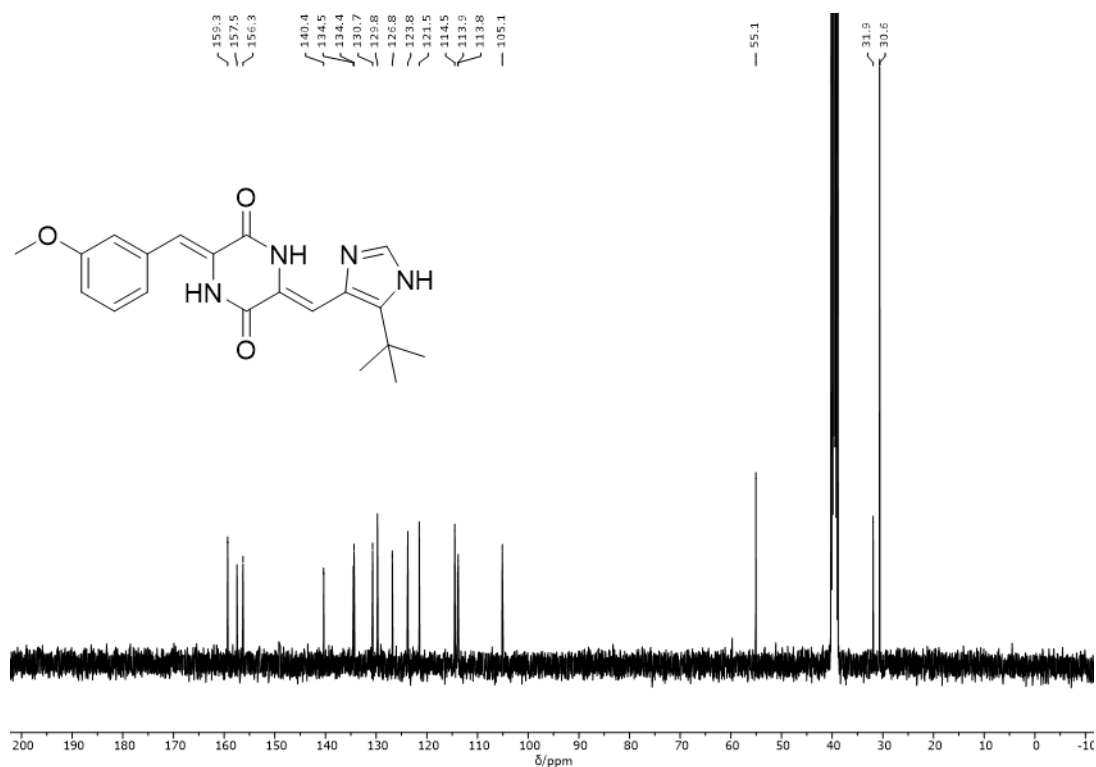


**Figure 91:** $^{13}$C NMR spectrum (101 MHz, DMSO-$d_6$) of compound *Z*-**14**.
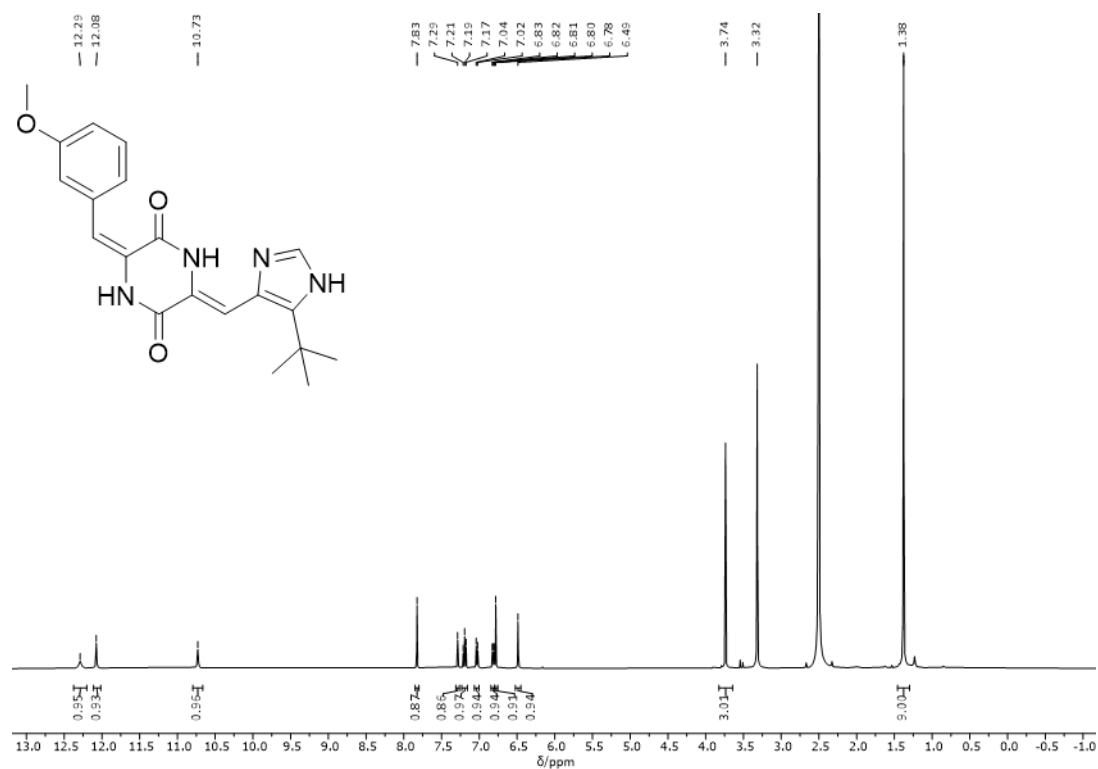
**Figure 92:** $^1$H NMR spectrum (400 MHz, DMSO-$d_6$) of compound *E*-**14**.
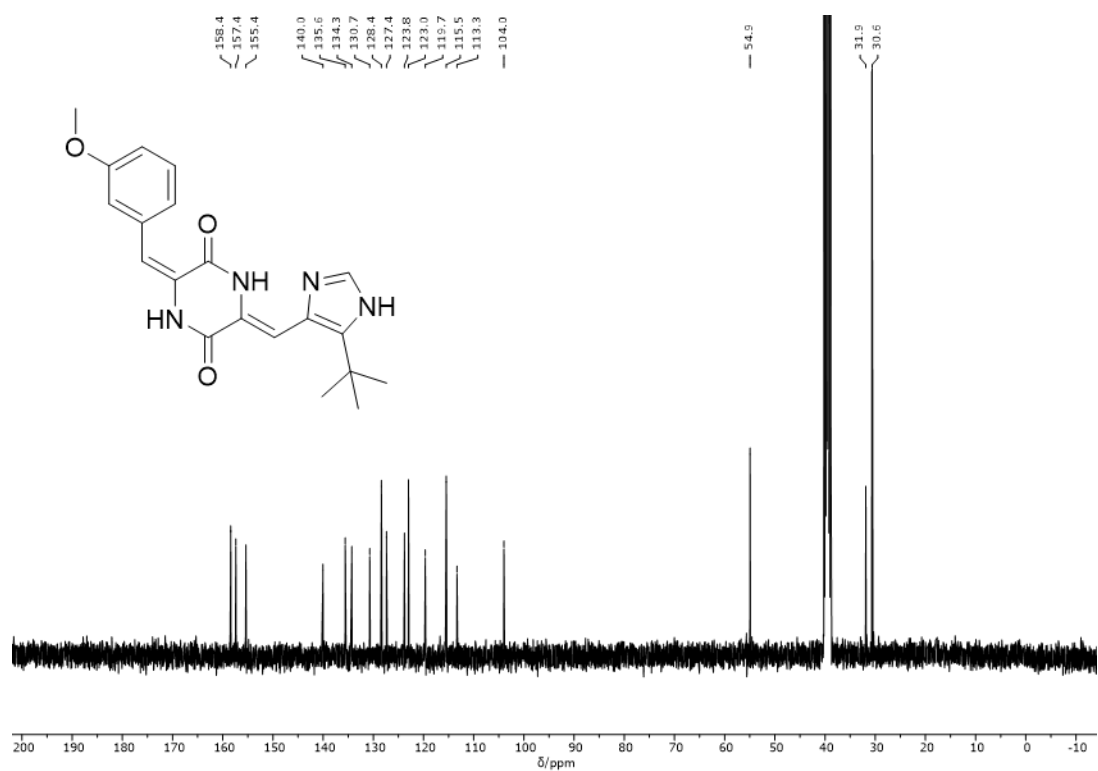


**Figure 93:** $^{13}$C NMR spectrum (101 MHz, DMSO-$d_6$) of compound *E*-**14**.
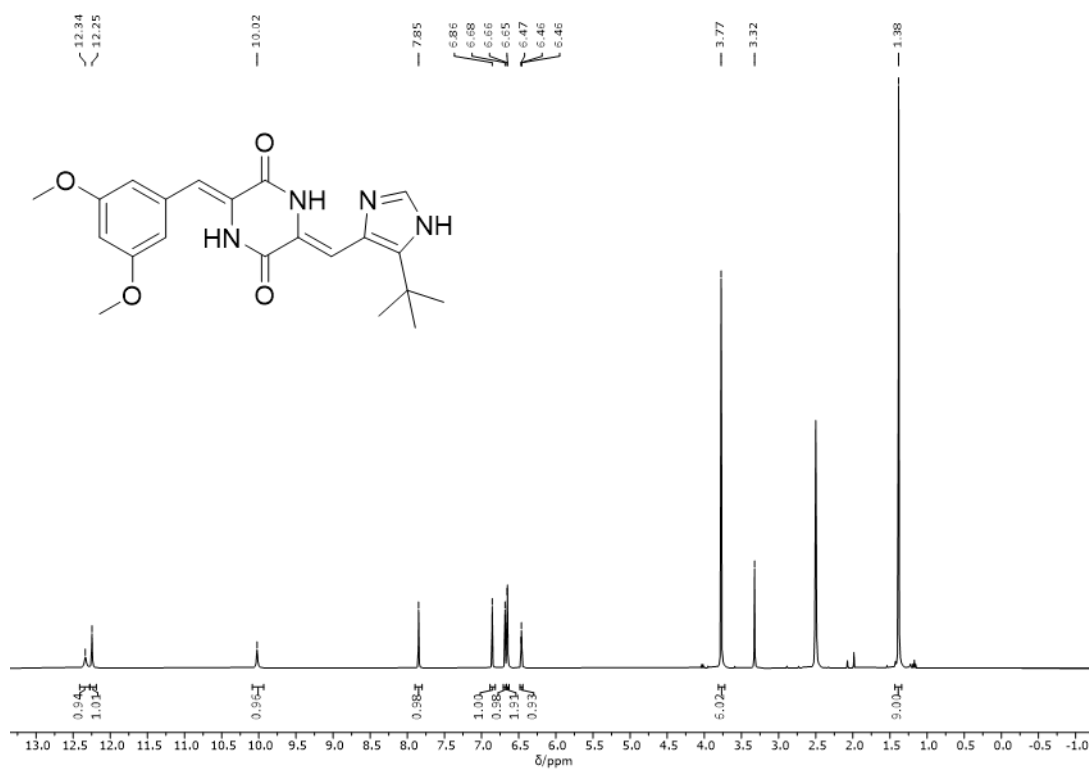
**Figure 94:** ¹H NMR spectrum (400 MHz, DMSO-$d_6$) of compound *Z*-**15**.
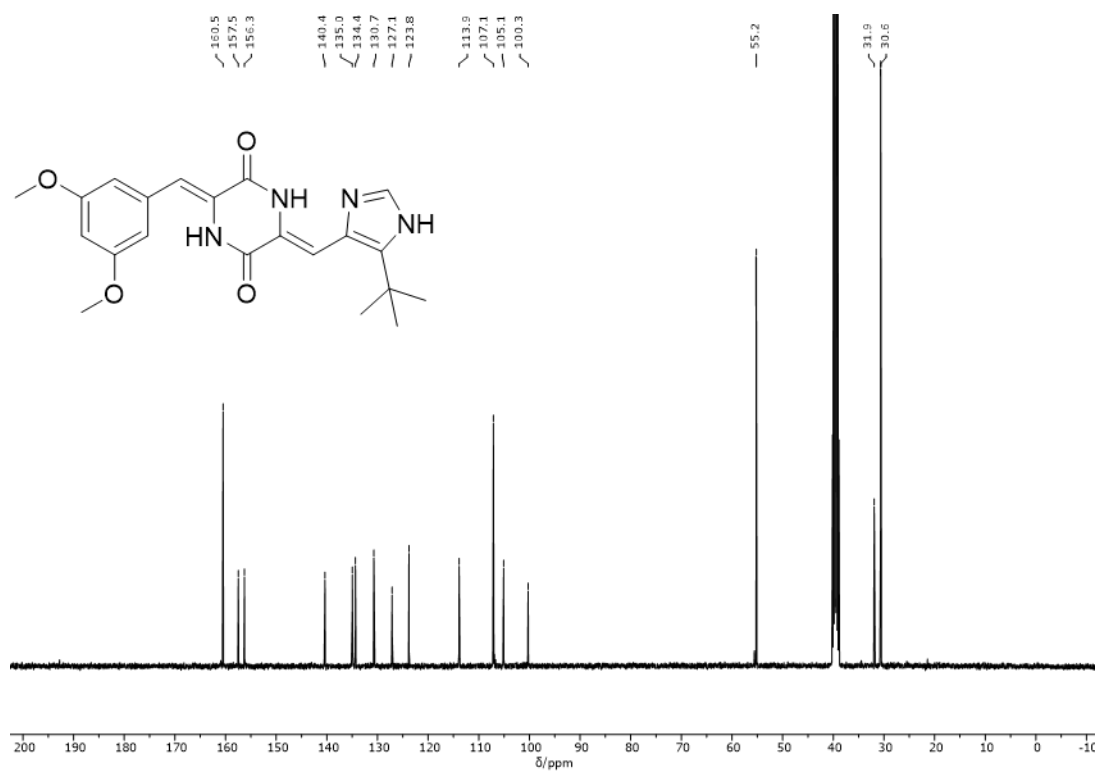


**Figure 95:** ¹³C NMR spectrum (101 MHz, DMSO-$d_6$) of compound *Z*-**15**.

**Figure 96:** $^1$H NMR spectrum (400 MHz, DMSO-$d_6$) of compound *E*-**15**.



**Figure 97:** $^{13}$C NMR spectrum (101 MHz, DMSO-$d_6$) of compound *E*-**15**.
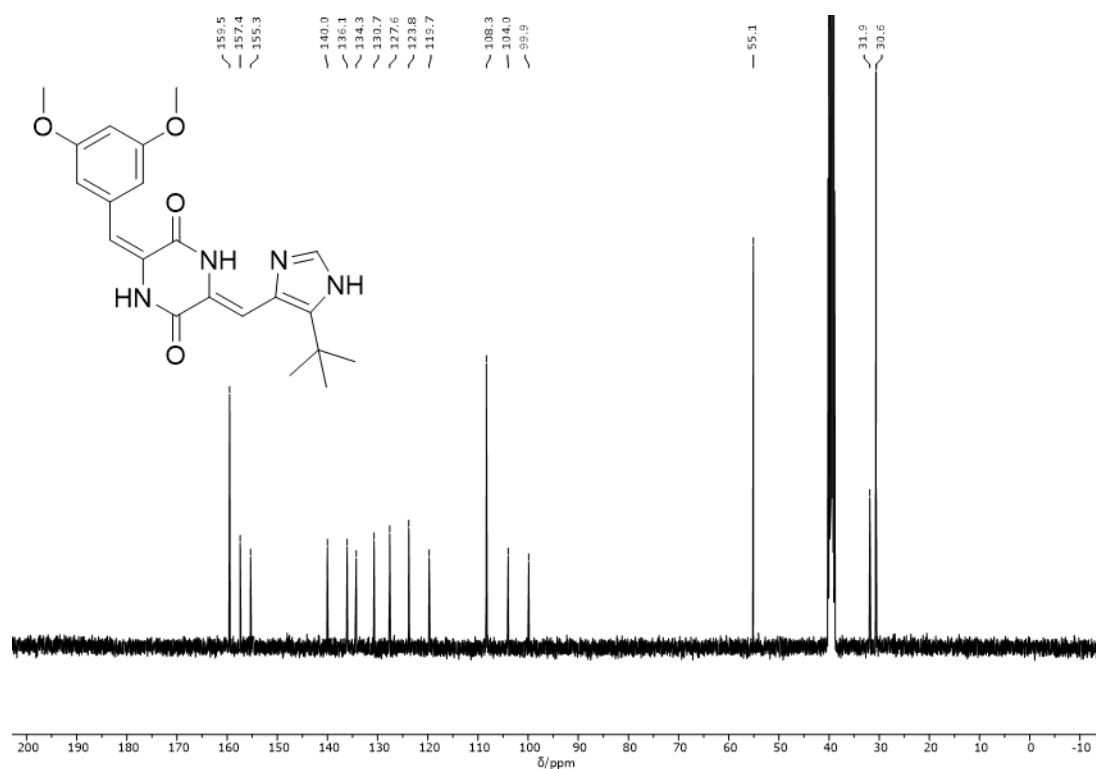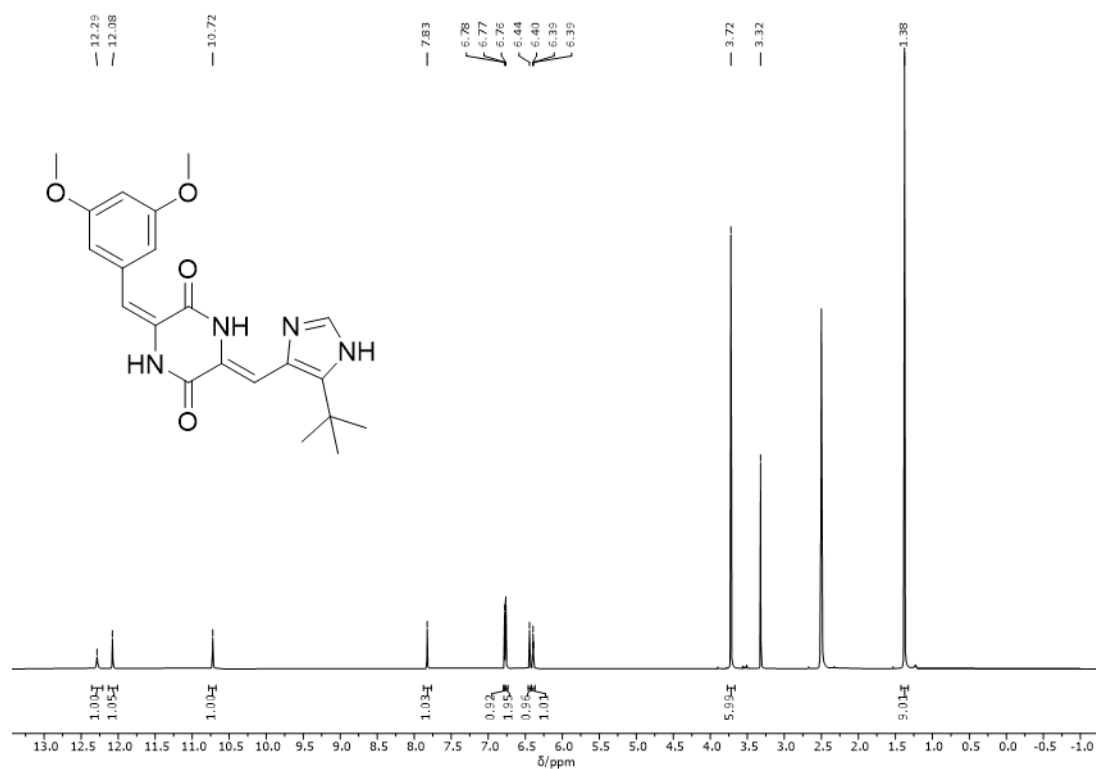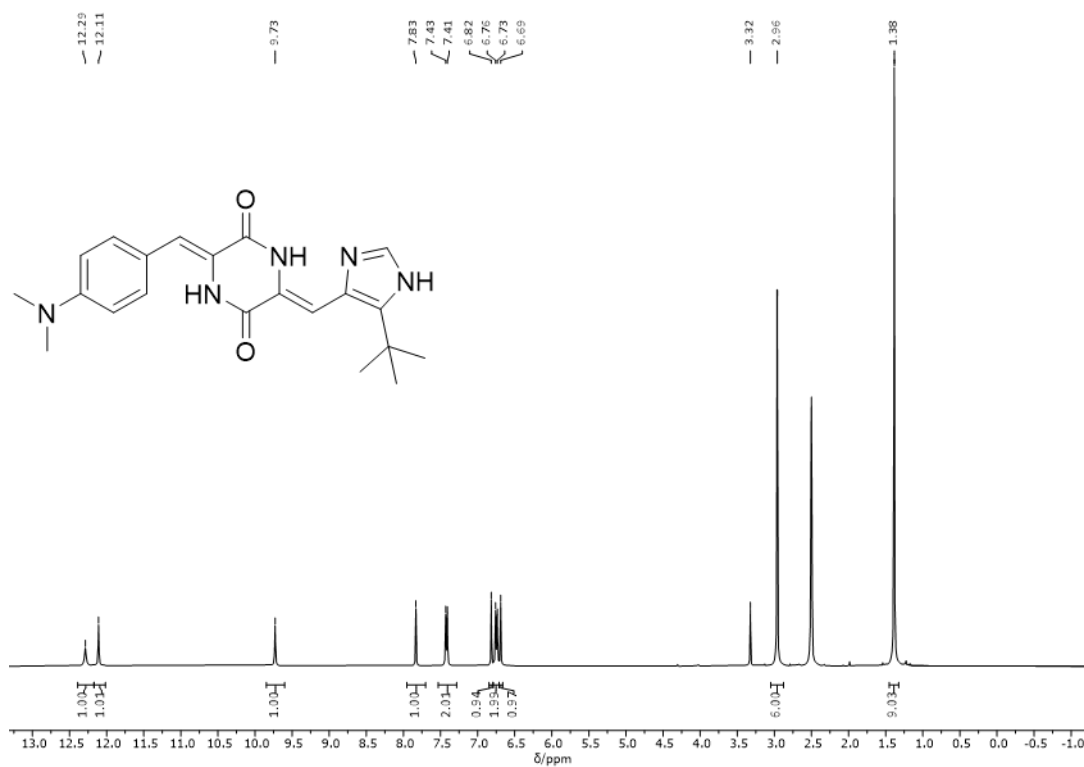
**Figure 98:** $^1$H NMR spectrum (400 MHz, DMSO-$d_6$) of compound Z-**16**.
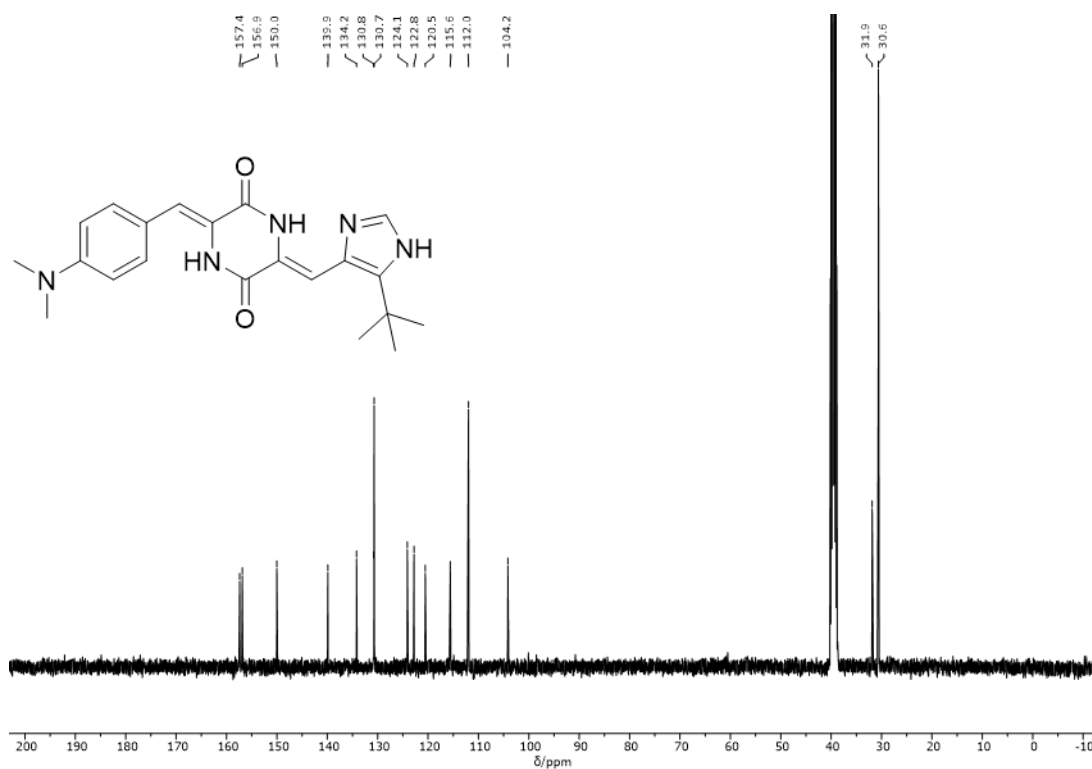


**Figure 99:** $^{13}$C NMR spectrum (101 MHz, DMSO-$d_6$) of compound Z-**16**.
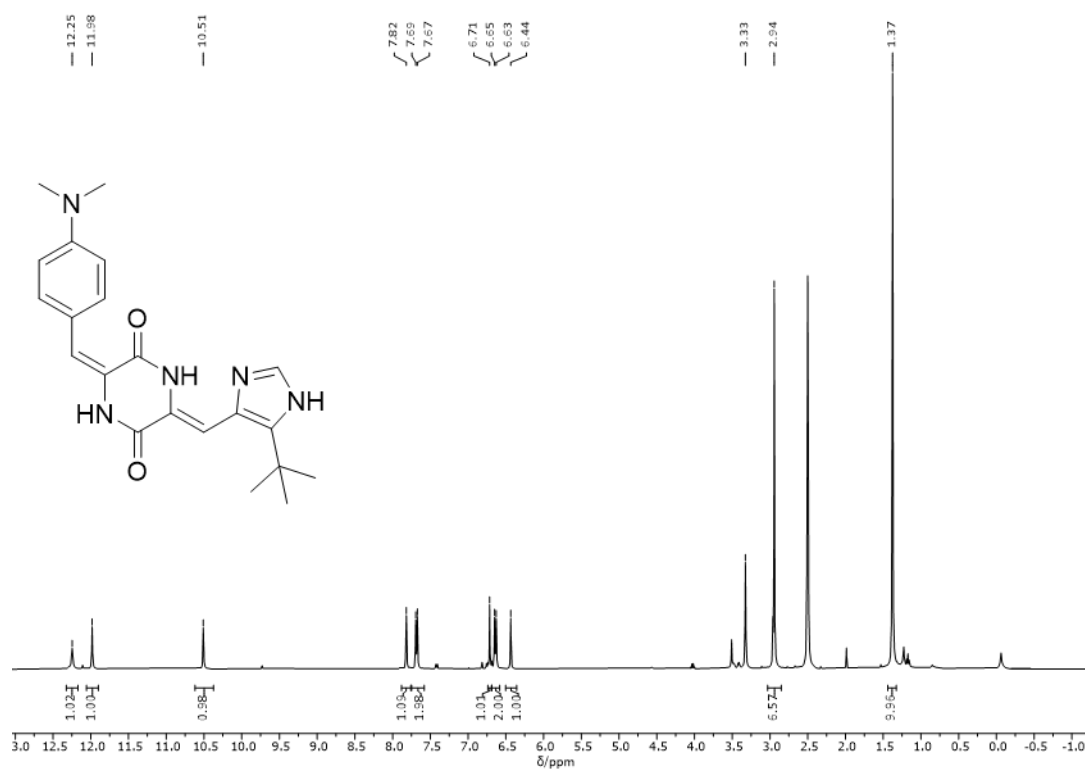
**Figure 100:** $^1$H NMR spectrum (400 MHz, DMSO-$d_6$) of compound *E*-**16**.
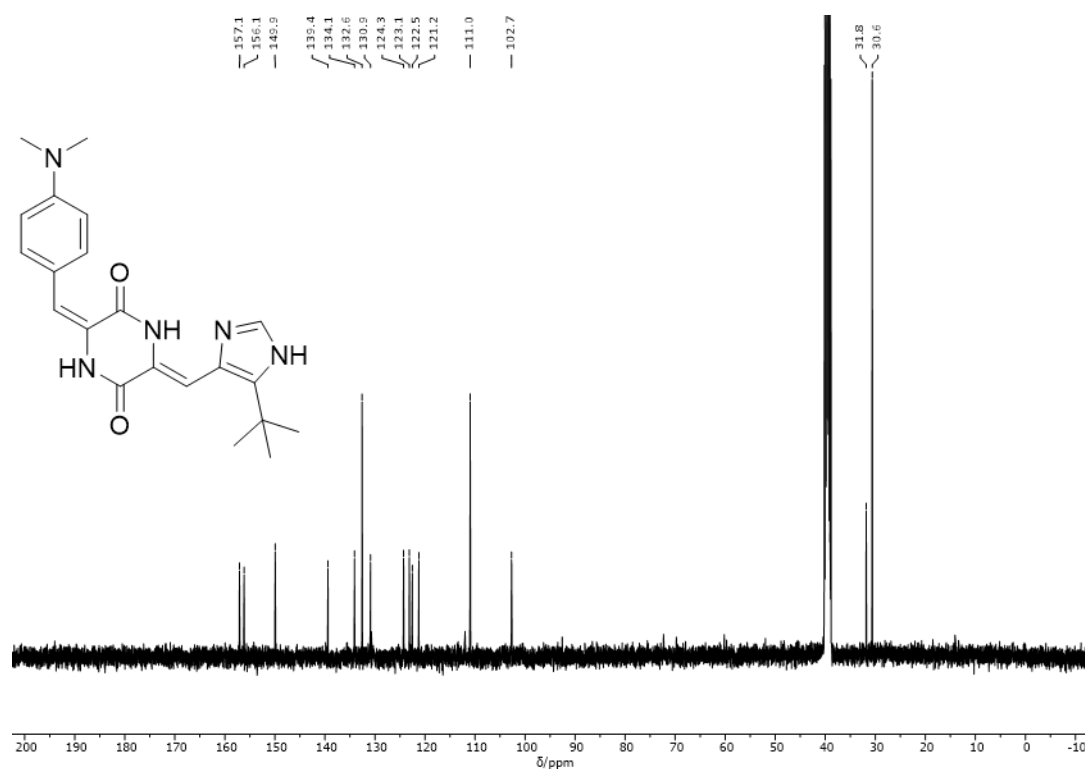


**Figure 101:** $^{13}$C NMR spectrum (101 MHz, DMSO-$d_6$) of compound *E*-**16**.
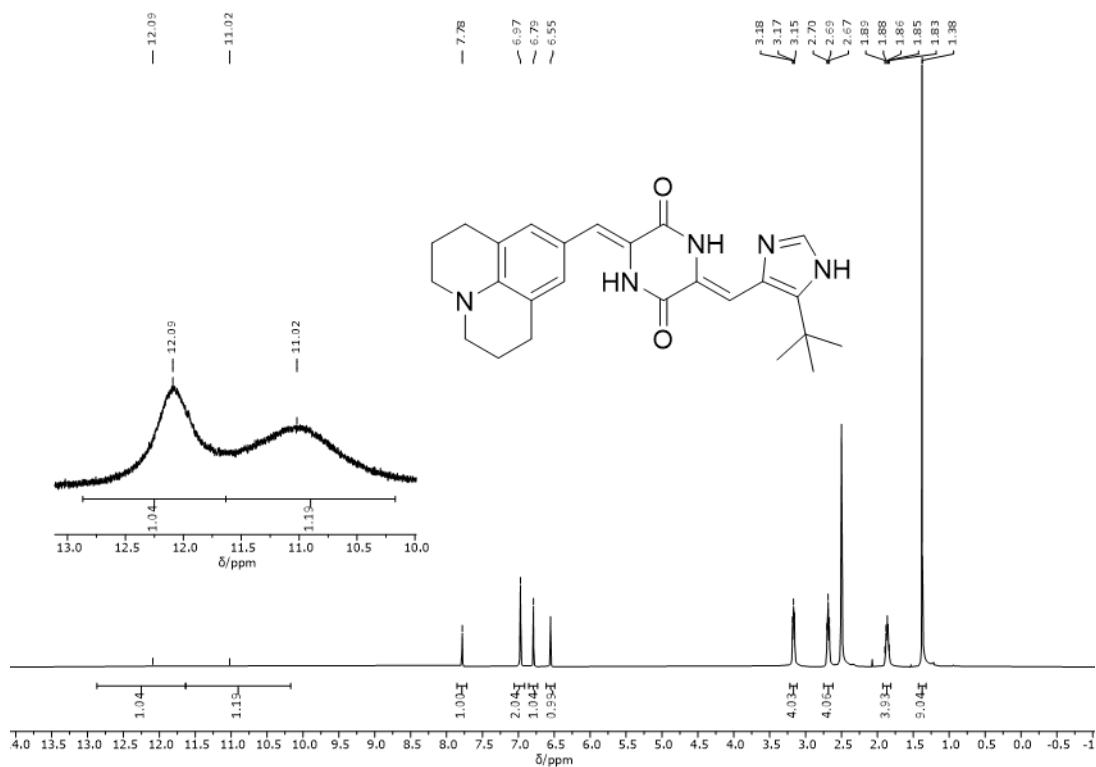
**Figure 102:** $^1$H NMR spectrum (400 MHz, DMSO-$d_6$) of compound Z-**17**.
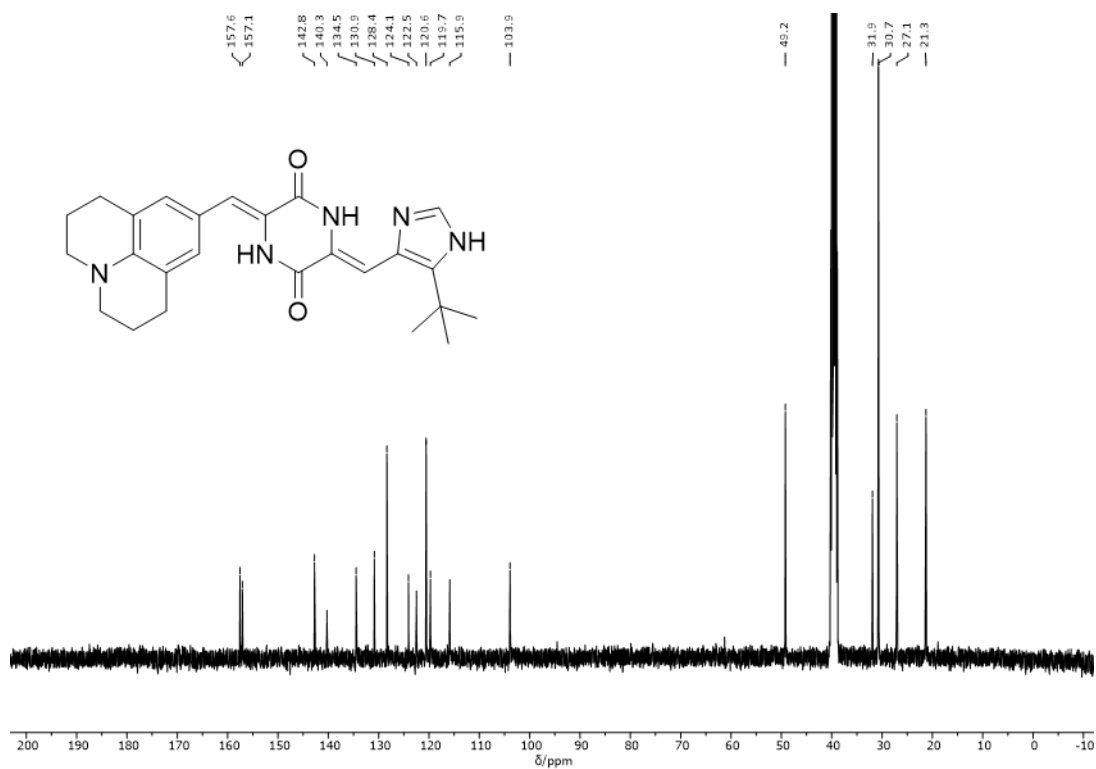


**Figure 103:** $^{13}$C NMR spectrum (101 MHz, DMSO-$d_6$) of compound Z-**17**.
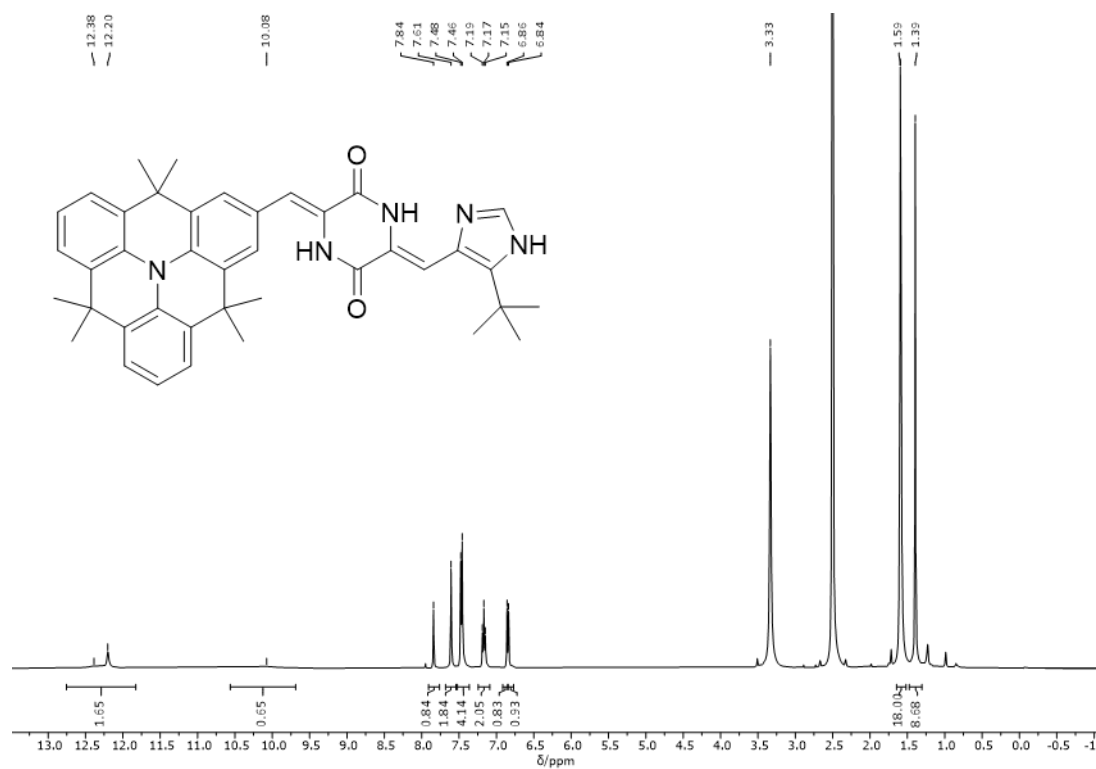
**Figure 104:** $^1$H NMR spectrum (400 MHz, DMSO-$d_6$) of compound Z-**18**.
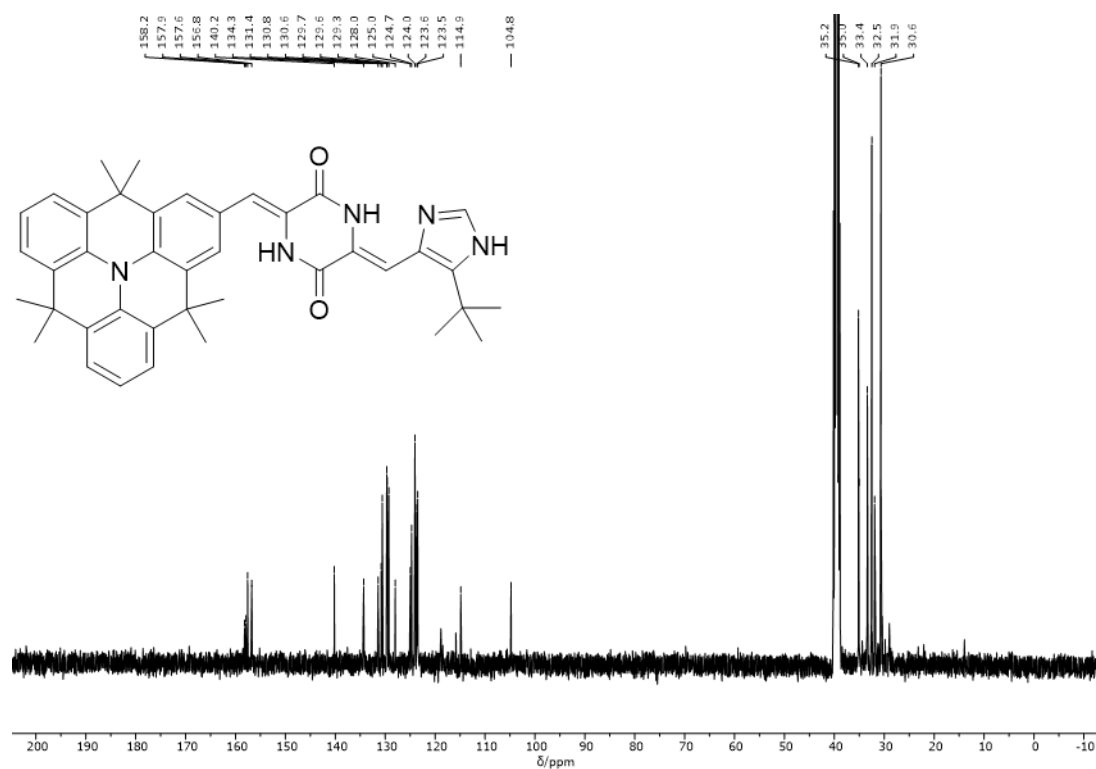


**Figure 105:** $^{13}$C NMR spectrum (101 MHz, DMSO-$d_6$) of compound Z-**18**.
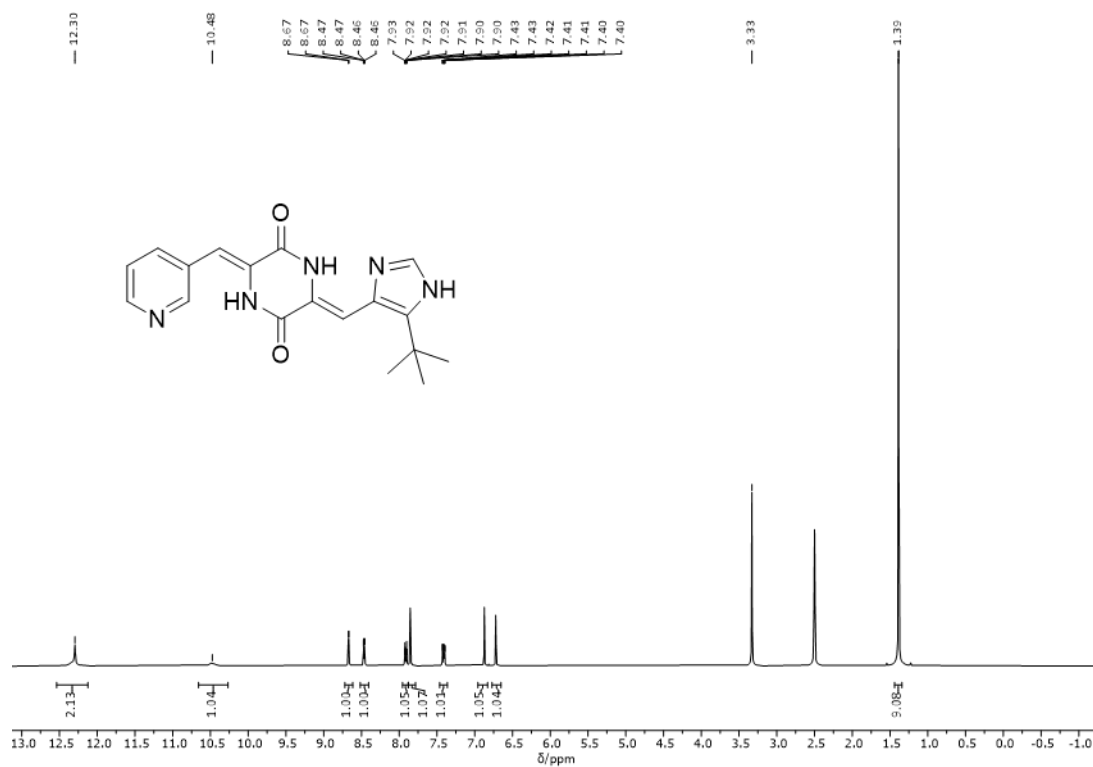
**Figure 106:** $^1$H NMR spectrum (400 MHz, DMSO-$d_6$) of compound Z-**19**.
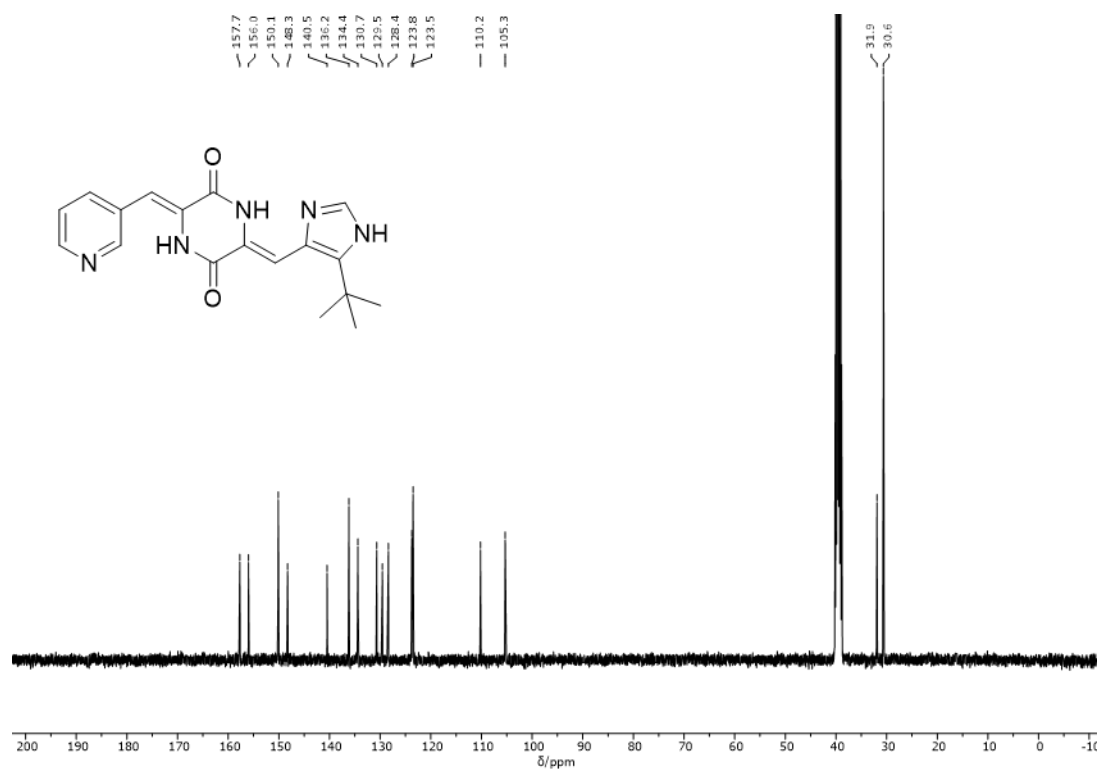


**Figure 107:** $^{13}$C NMR spectrum (101 MHz, DMSO-$d_6$) of compound Z-**19**.
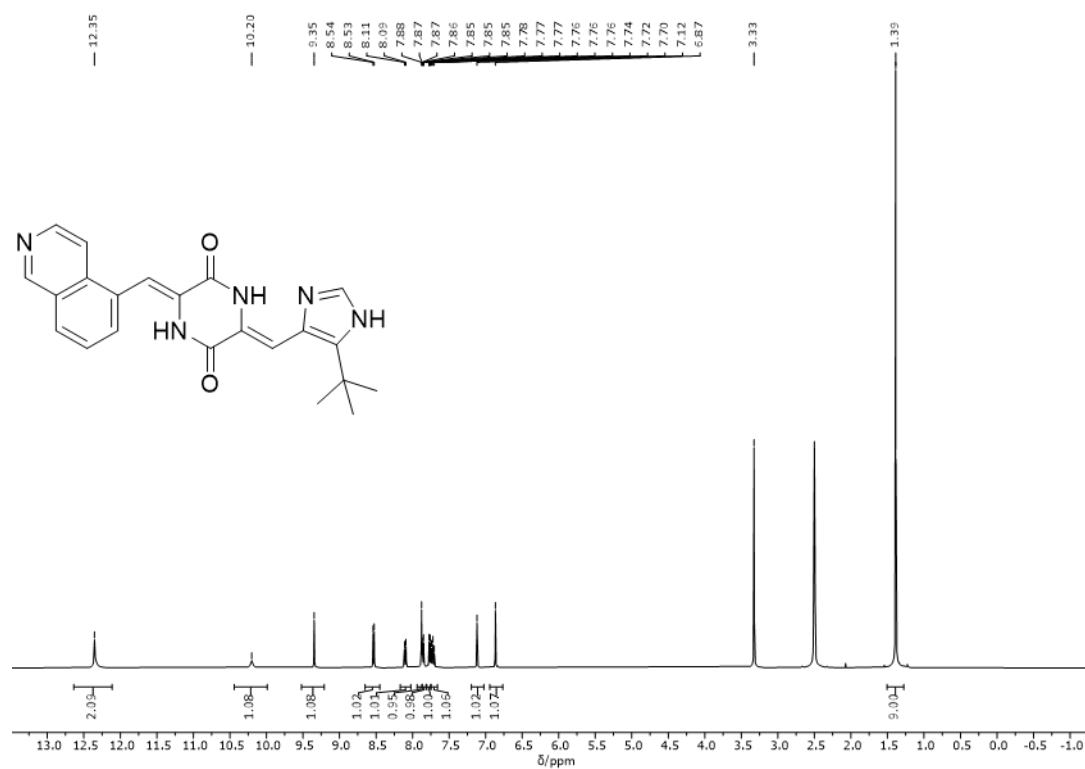
**Figure 108:** $^1$H NMR spectrum (400 MHz, DMSO-$d_6$) of compound Z-**20**.
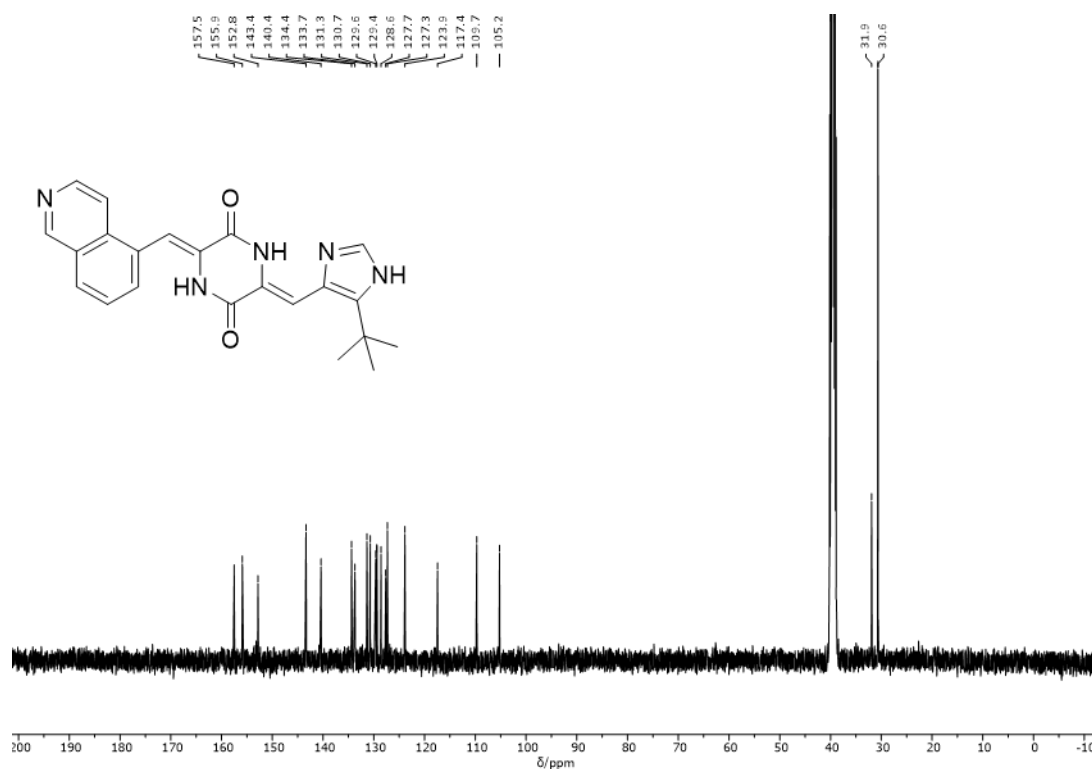


**Figure 109:** $^{13}$C NMR spectrum (101 MHz, DMSO-$d_6$) of compound Z-**20**.
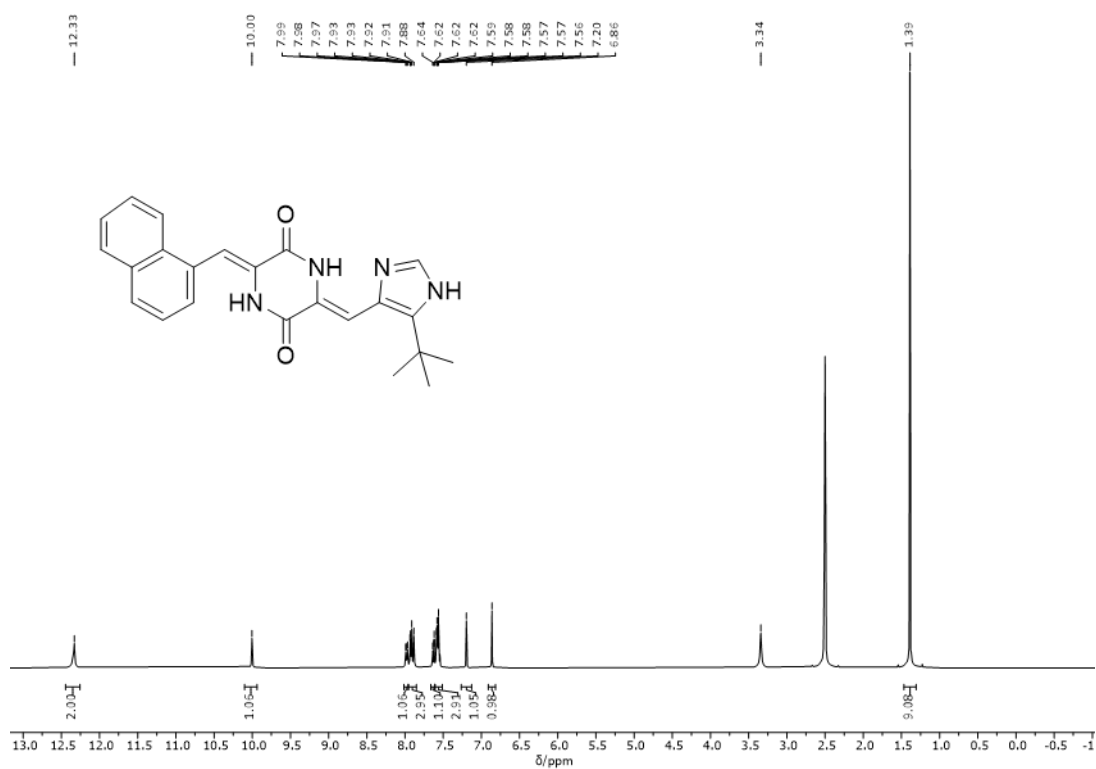
**Figure 110:** ¹H NMR spectrum (400 MHz, DMSO-$d_6$) of compound Z-**21**.
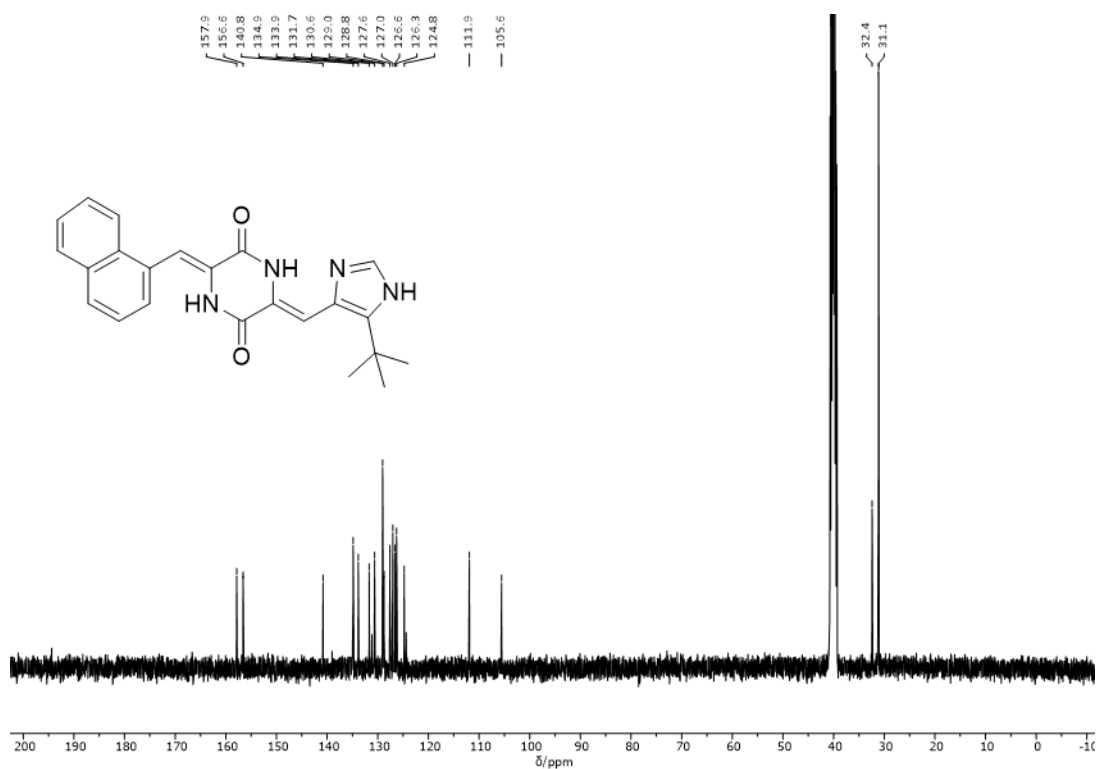


**Figure 111:** ¹³C NMR spectrum (101 MHz, DMSO-$d_6$) of compound Z-**21**.
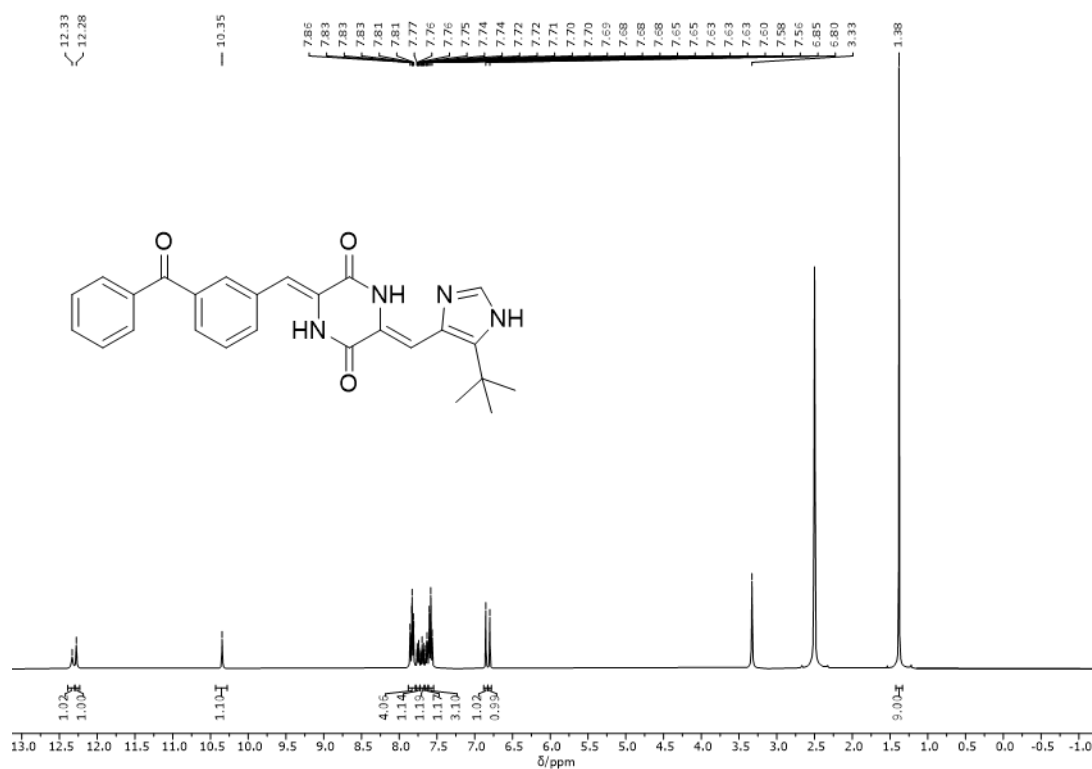
**Figure 112:** $^1$H NMR spectrum (400 MHz, DMSO-$d_6$) of compound Z-**22**.
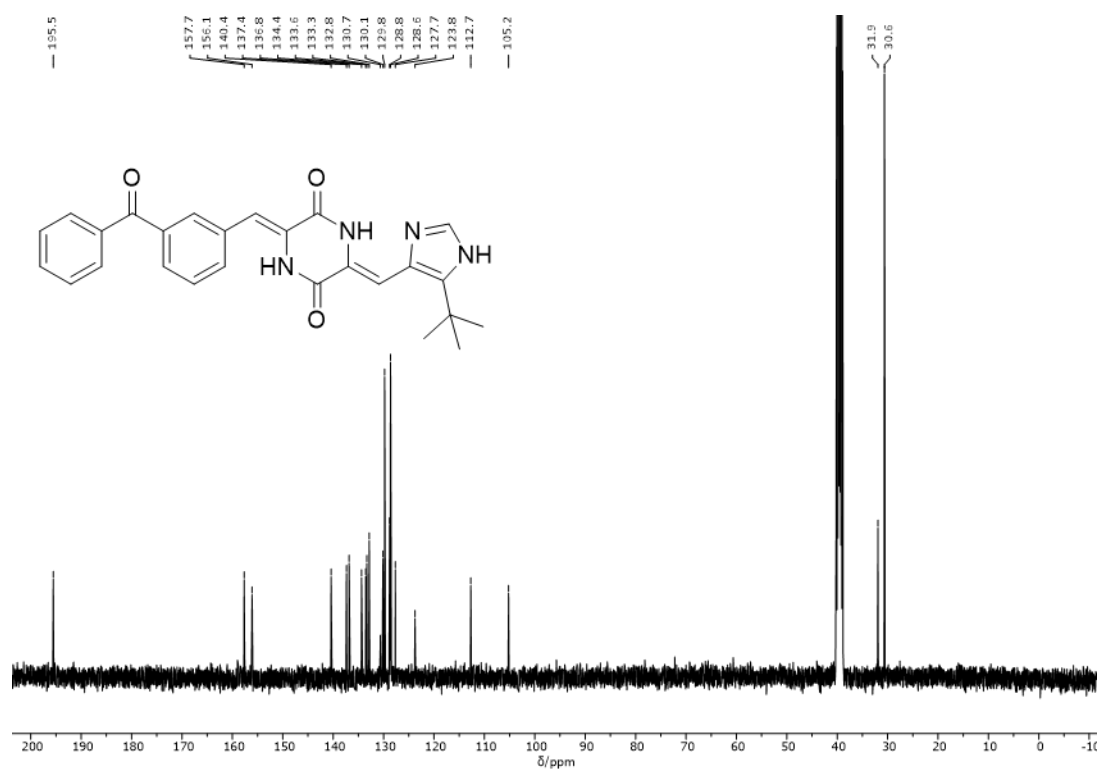


**Figure 113:** $^{13}$C NMR spectrum (101 MHz, DMSO-$d_6$) of compound Z-**22**.
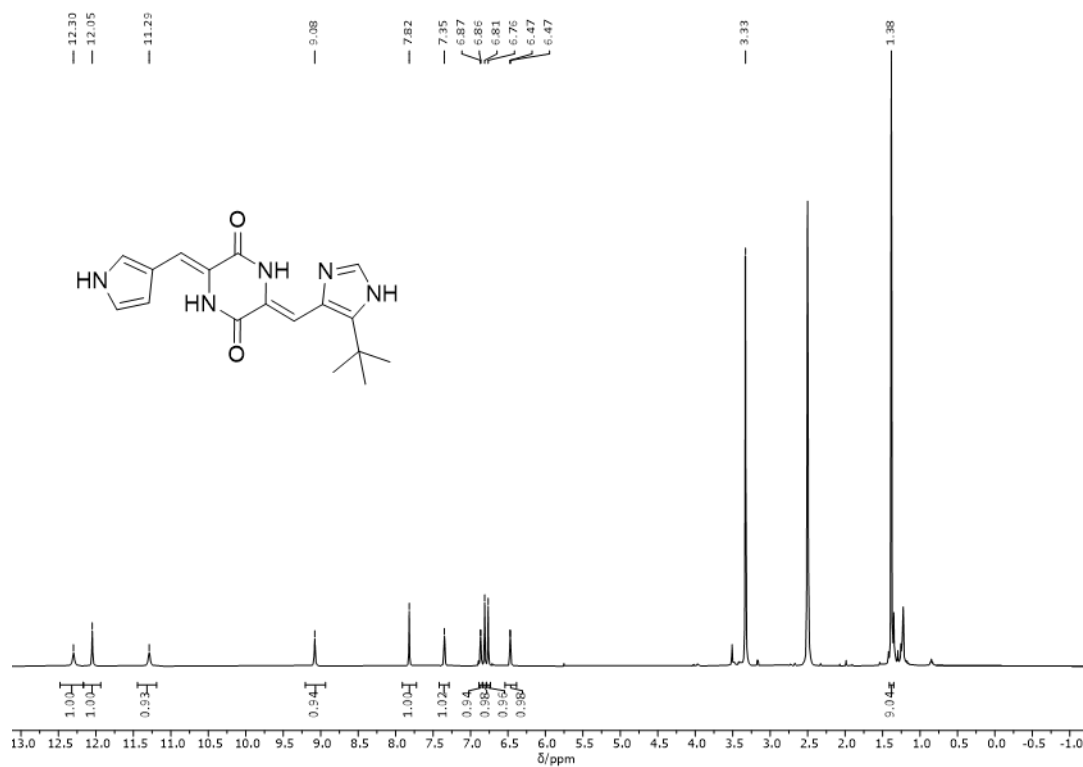
**Figure 114:** $^{1}$H NMR spectrum (400 MHz, DMSO-$d_6$) of compound Z-**23**.
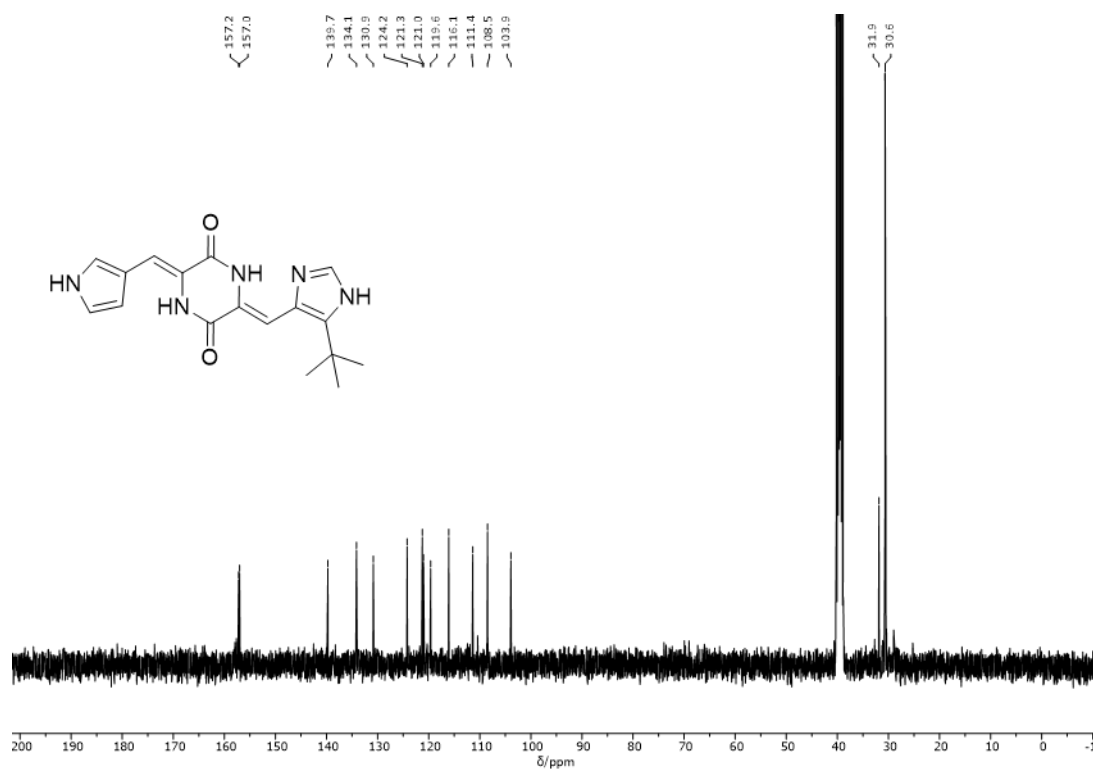


**Figure 115:** $^{13}$C NMR spectrum (101 MHz, DMSO-$d_6$) of compound Z-**23**.
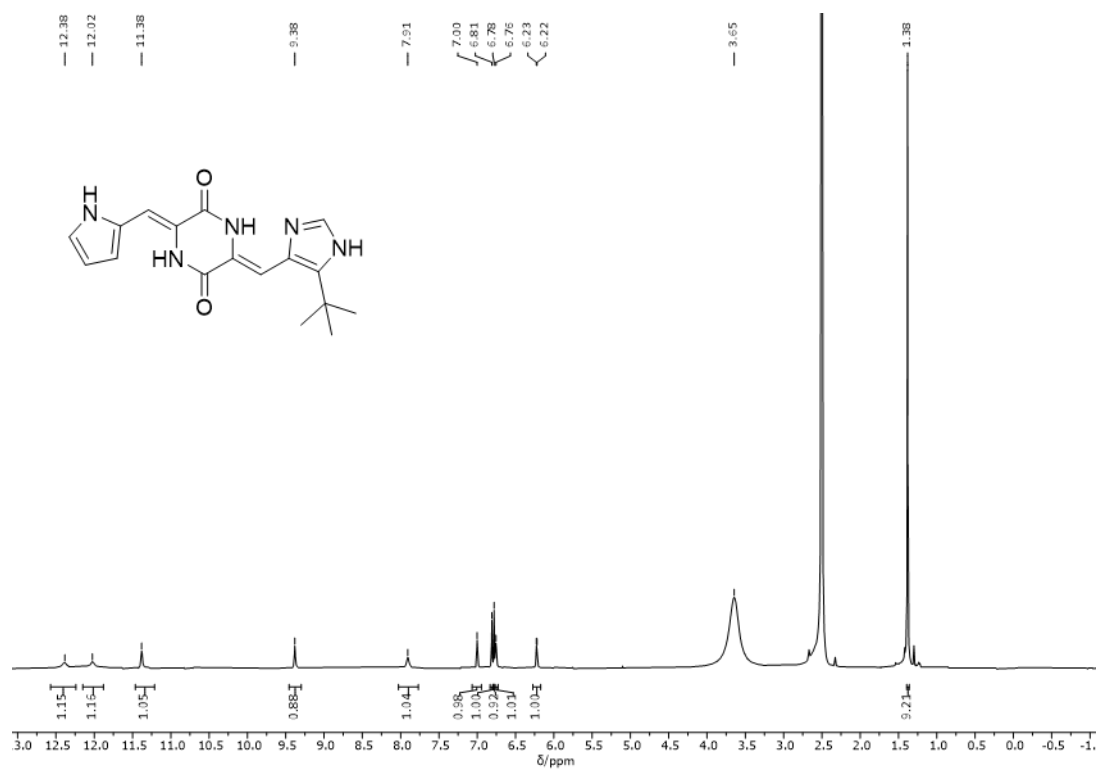
**Figure 116:** $^1$H NMR spectrum (400 MHz, DMSO-$d_6$) of compound Z-**24**.
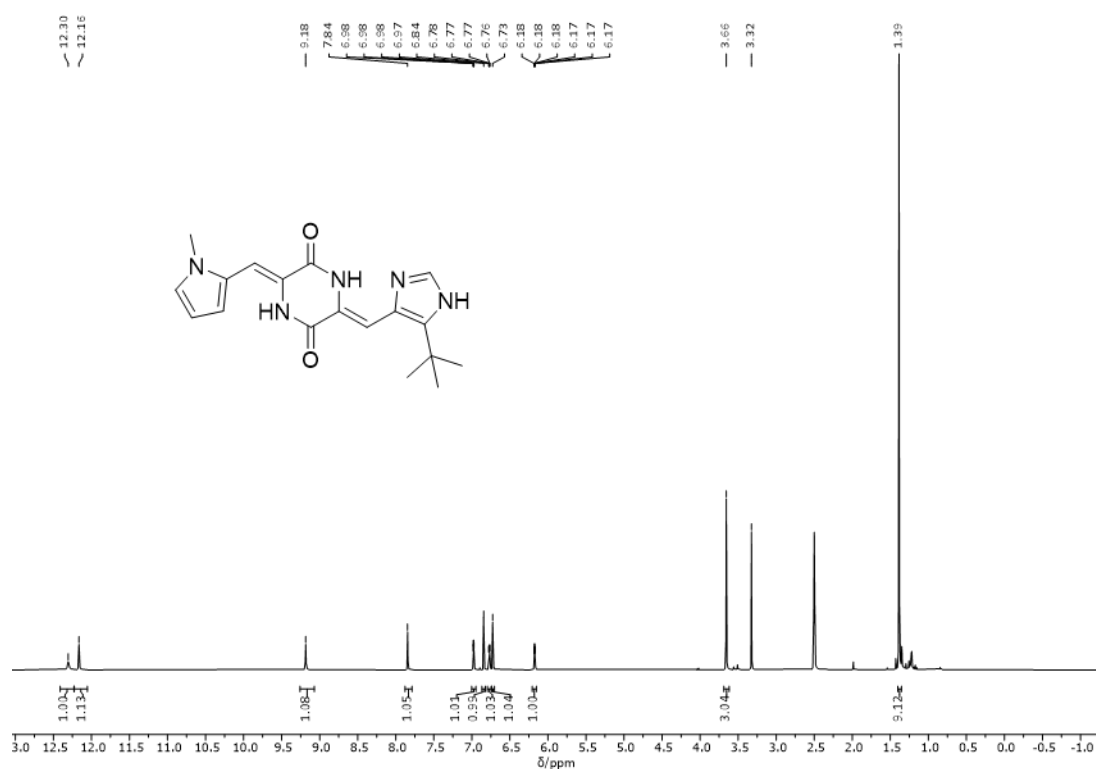


**Figure 117:** $^1$H NMR spectrum (400 MHz, DMSO-$d_6$) of compound Z-**25**.
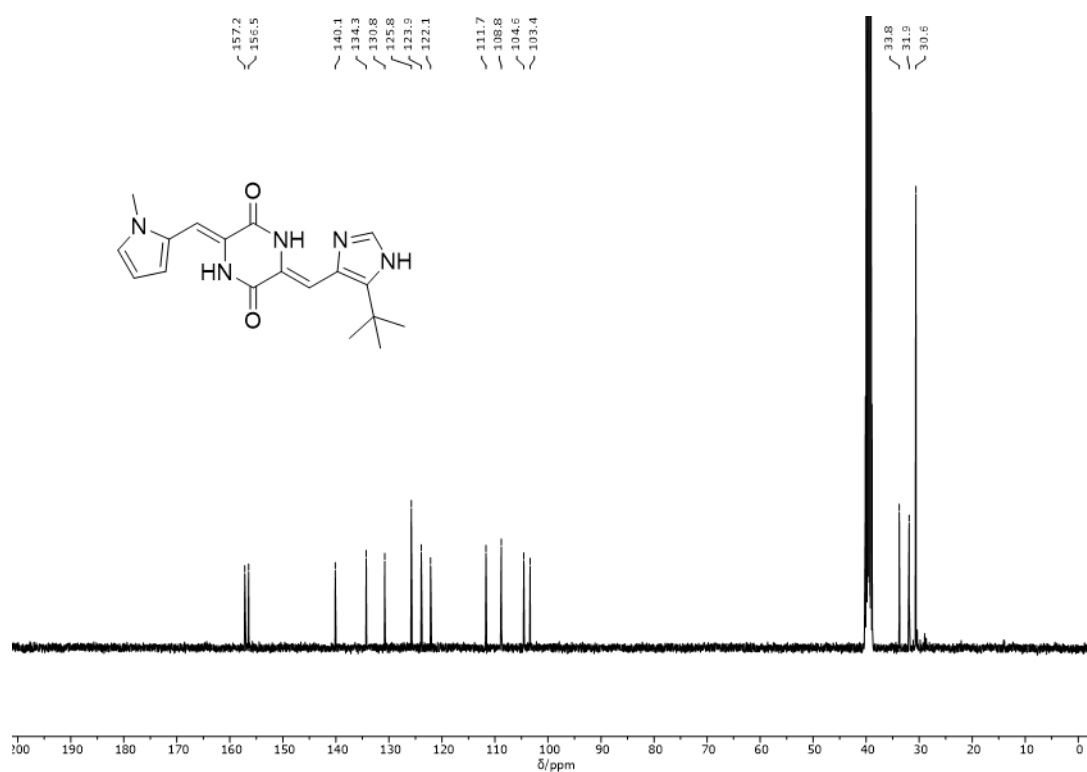
**Figure 118:** $^{13}$C NMR spectrum (101 MHz, DMSO-$d_6$) of compound *Z*-**25**.
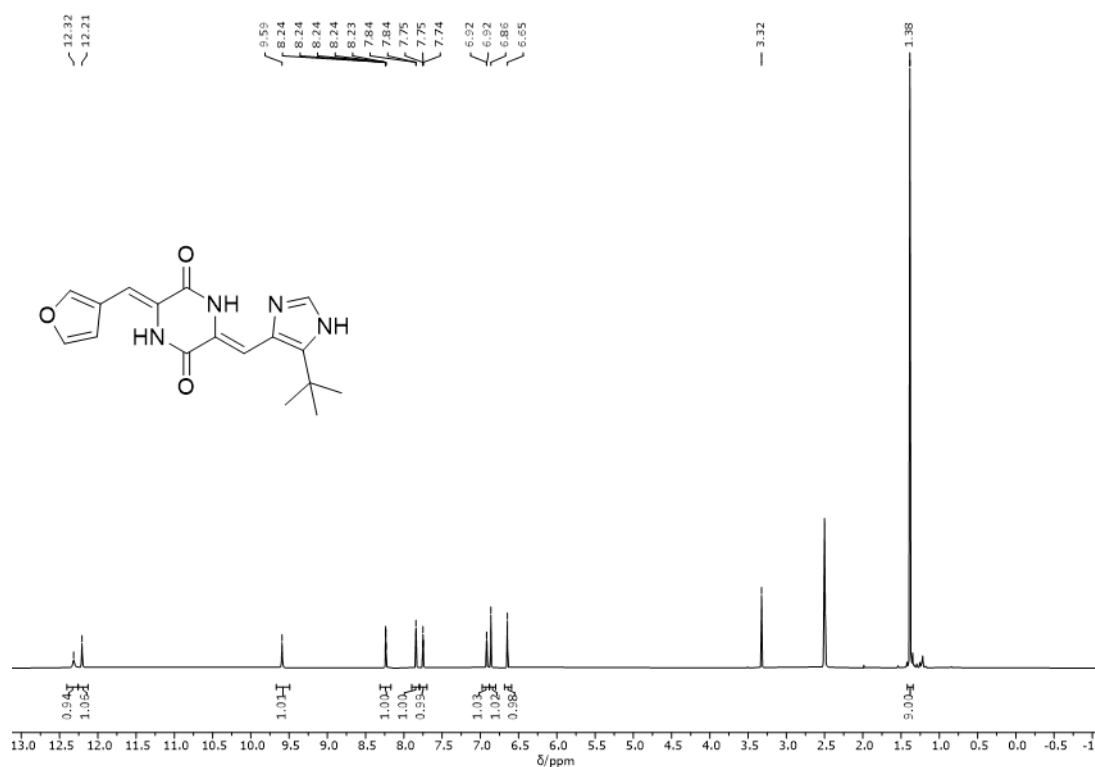


**Figure 119:** $^1$H NMR spectrum (400 MHz, DMSO-$d_6$) of compound *Z*-**26**.
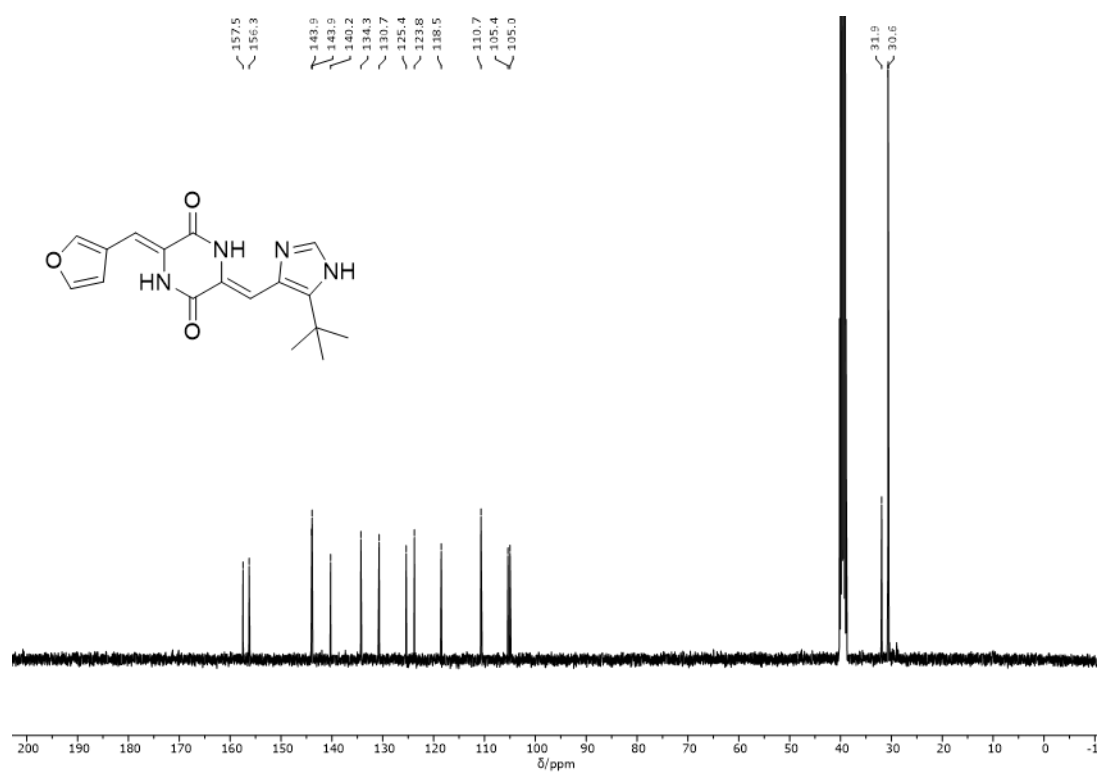
**Figure 120:** $^{13}$C NMR spectrum (101 MHz, DMSO-$d_6$) of compound Z-**26**.
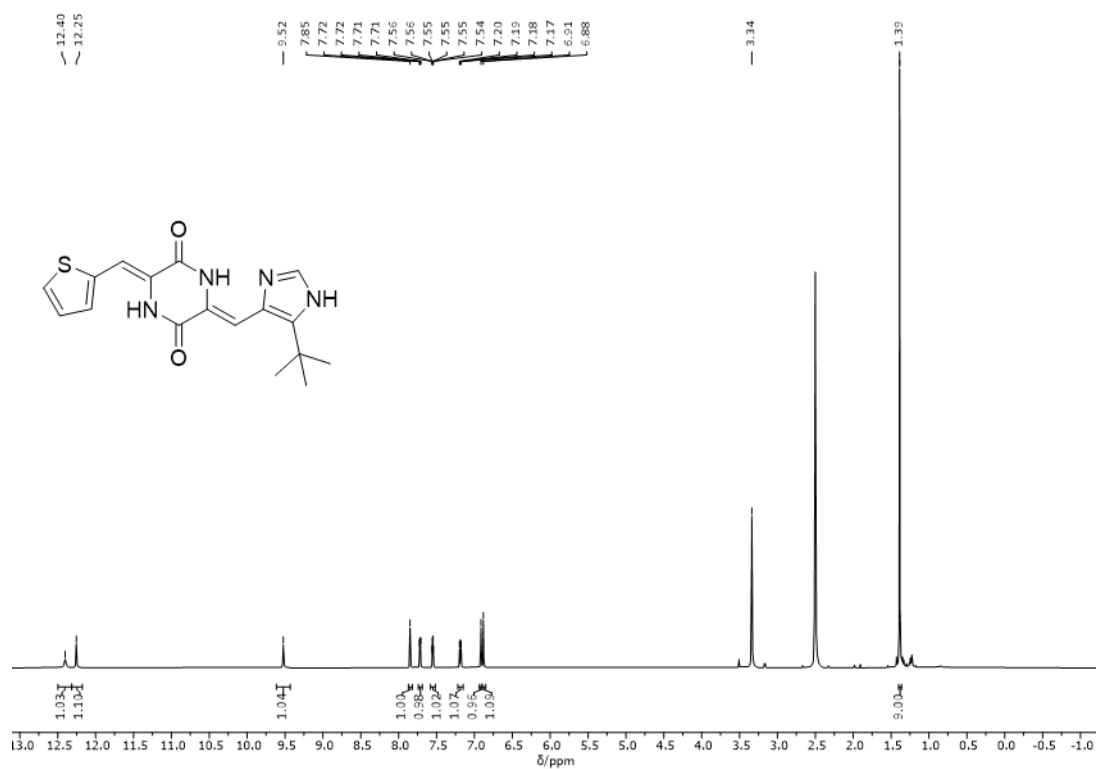


**Figure 121:** $^1$H NMR spectrum (400 MHz, DMSO-$d_6$) of compound Z-**27**.
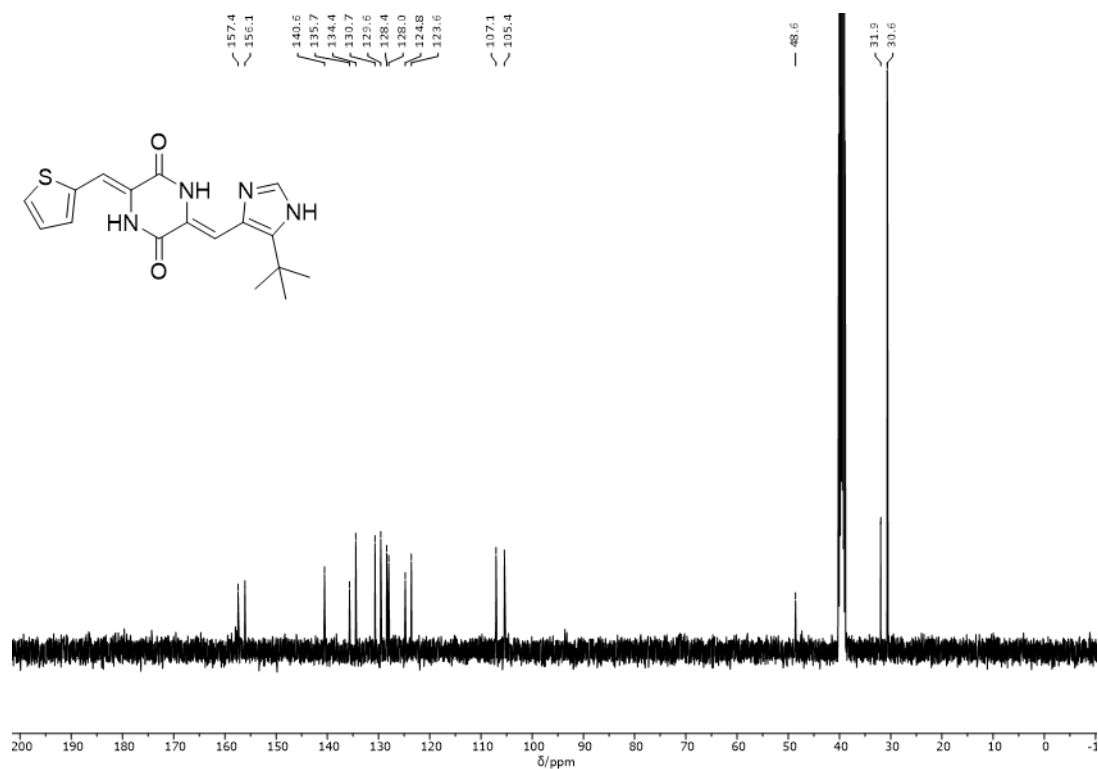
**Figure 122:** $^{13}C$ NMR spectrum (101 MHz, DMSO-$d_6$) of compound *Z*-**27**.
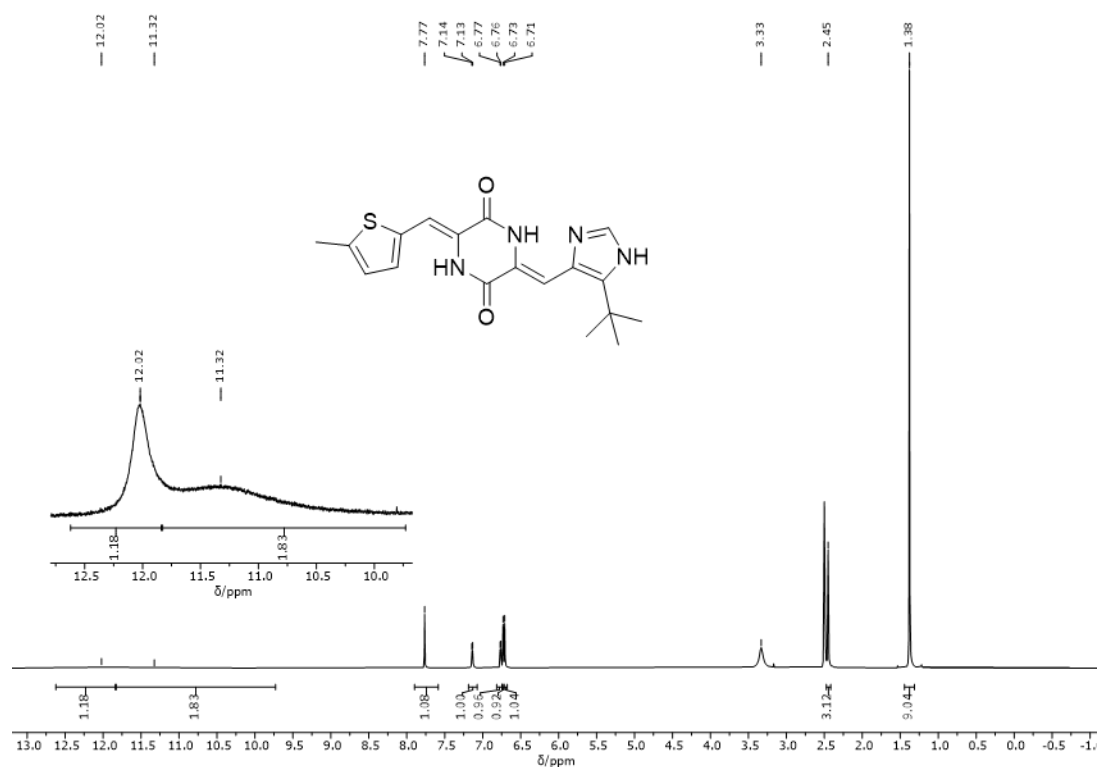


**Figure 123:** $^1H$ NMR spectrum (400 MHz, DMSO-$d_6$) of compound *Z*-**28**.
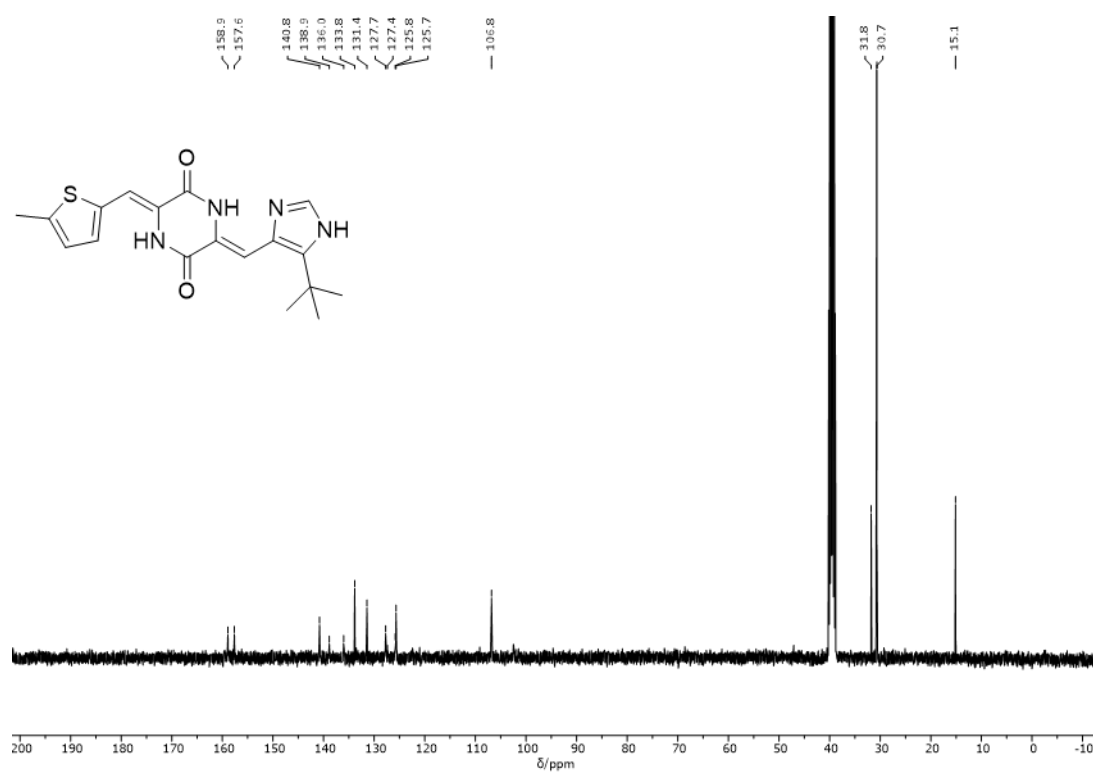
**Figure 124:** $^{13}$C NMR spectrum (101 MHz, DMSO-$d_6$) of compound *Z*-**28**.

### 5.4.5   Absorption Spectra of Non-Irradiated Samples
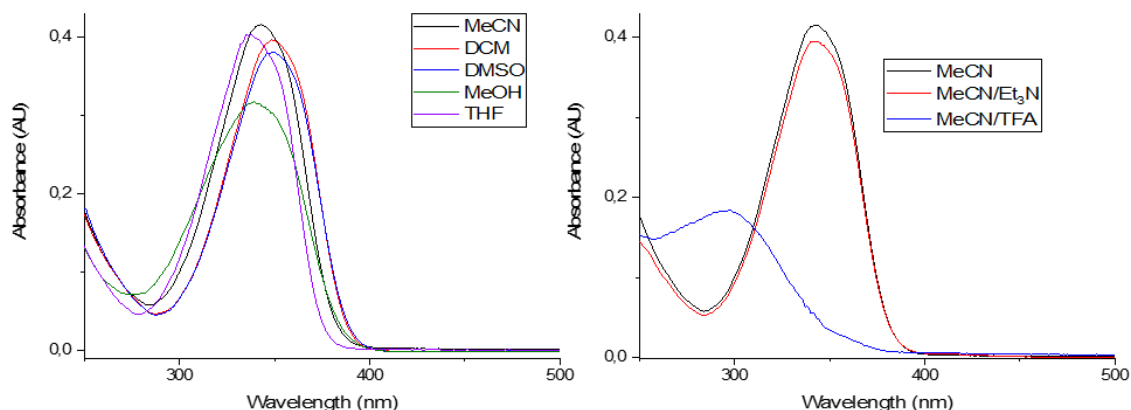


**Figure 125:** Compound *Z*-**5** was dissolved in different solvents (80 µM) and in mixtures of 1% (v/v) TFA in MeCN and 1% (v/v) Et₃N in MeCN, respectively. Absorption spectra were measured in the dark (d = 2 mm). The spectra are assigned to the respective solvents *via* color code.
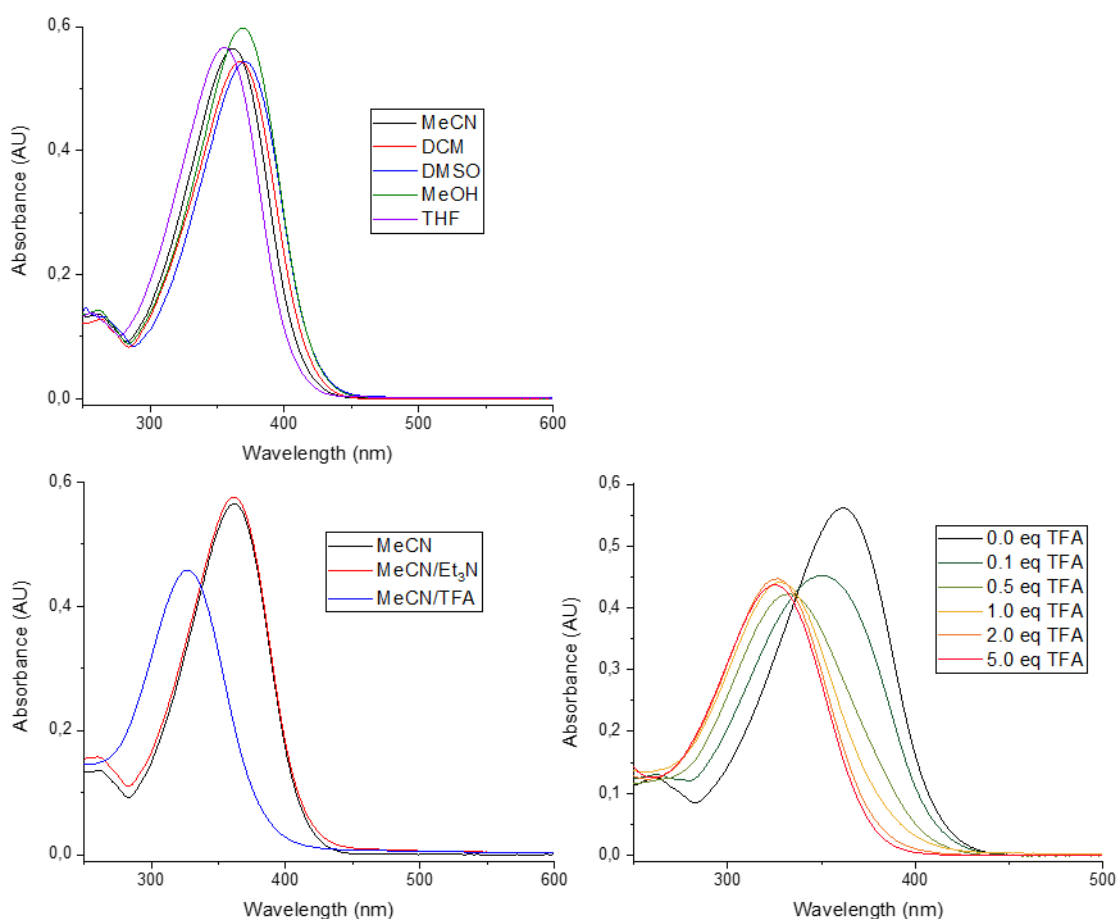


**Figure 126:** Compound *Z*-**6** was dissolved in different solvents (80 µM) and in mixtures of 1% (v/v) TFA in MeCN and 1% (v/v) Et₃N in MeCN, respectively. Absorption spectra were measured in the dark (d = 2 mm). The spectra are assigned to the respective solvents *via* color code. Additionally, absorption spectra of 80 µM solutions (d=2 mm) of **6** in MeCN with different amounts of TFA were measured.
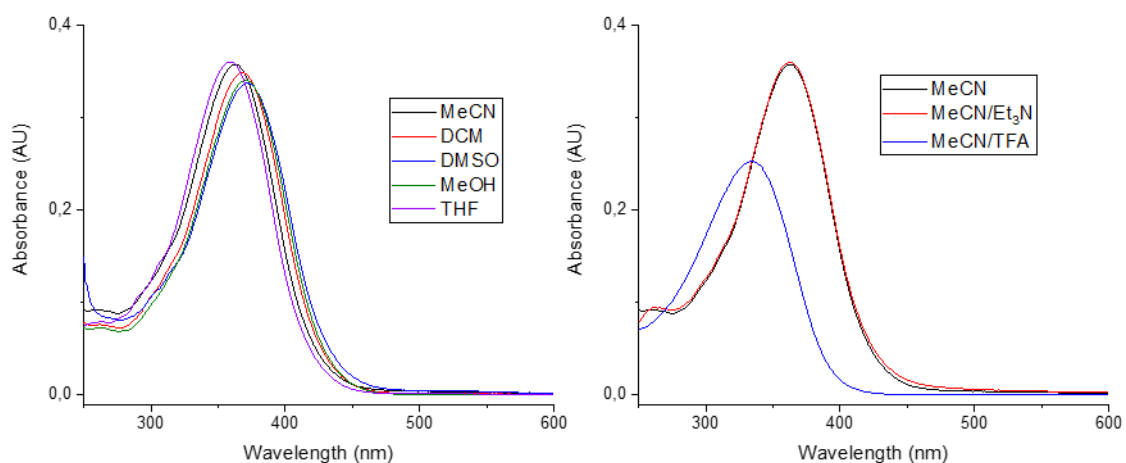
**Figure 127:** Compound *E*-**6** was dissolved in different solvents (80 µM) and in mixtures of 1% (v/v) TFA in MeCN and 1% (v/v) Et₃N in MeCN, respectively. Absorption spectra were measured in the dark (d = 2 mm). The spectra are assigned to the respective solvents *via* color code.
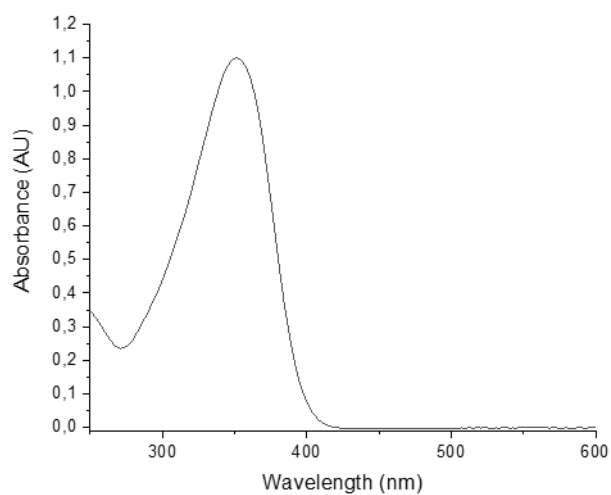


**Figure 128:** Absorption spectrum of compound *Z*-**7** (52 µM) MeCN (d = 10 mm).
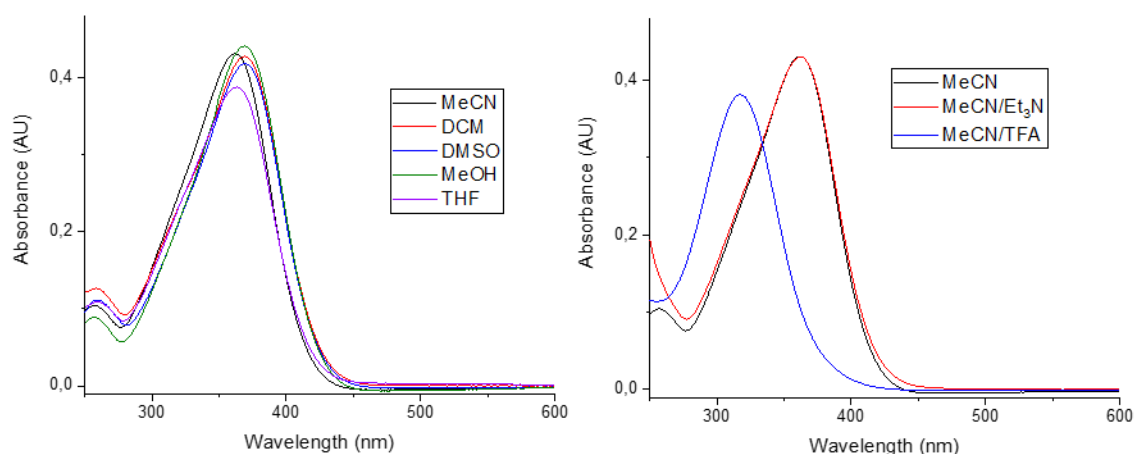
**Figure 129:** Compound *Z*-**8** was dissolved in different solvents (80 µM) and in mixtures of 1% (v/v) TFA in MeCN and 1% (v/v) Et₃N in MeCN, respectively. Absorption spectra were measured in the dark (d = 2 mm). The spectra are assigned to the respective solvents *via* color code.
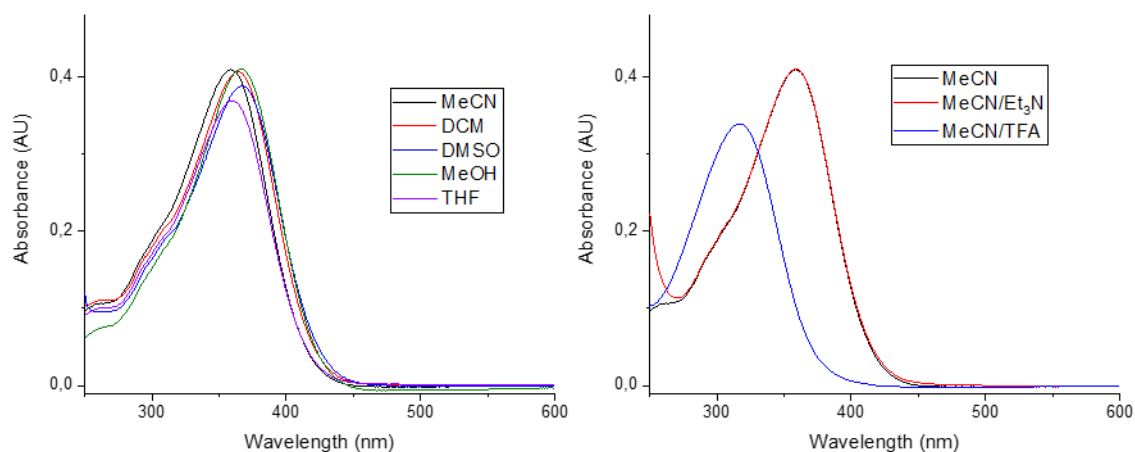


**Figure 130:** Compound *E*-**8** was dissolved in different solvents (80 µM) and in mixtures of 1% (v/v) TFA in MeCN and 1% (v/v) Et₃N in MeCN, respectively. Absorption spectra were measured in the dark (d = 2 mm). The spectra are assigned to the respective solvents *via* color code.
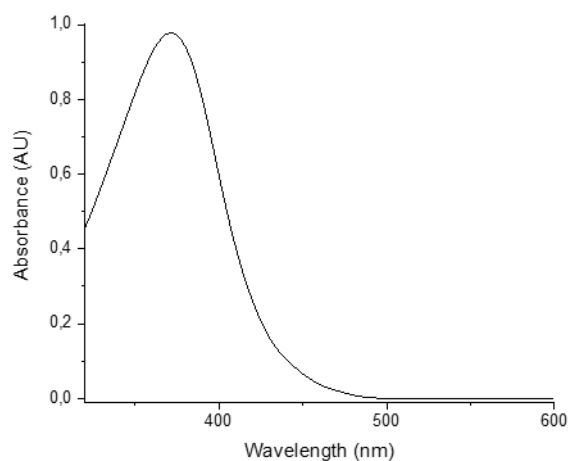


**Figure 131:** Absorption spectrum of compound *Z*-**9** (160 µM) DMSO (d = 2 mm).
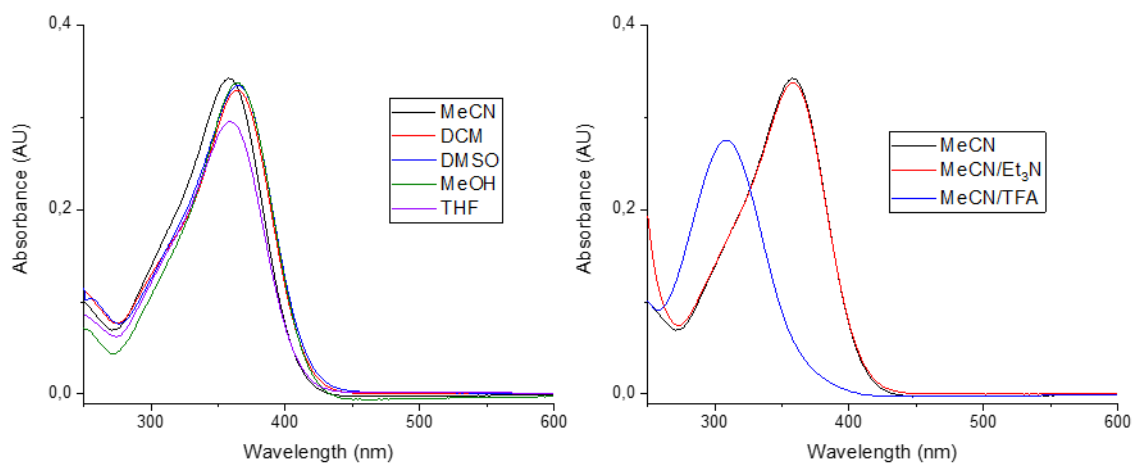
**Figure 132:** Compound *Z*-**10** was dissolved in different solvents (80 µM) and in mixtures of 1% (v/v) TFA in MeCN and 1% (v/v) Et₃N in MeCN, respectively. Absorption spectra were measured in the dark (d = 2 mm). The spectra are assigned to the respective solvents *via* color code.
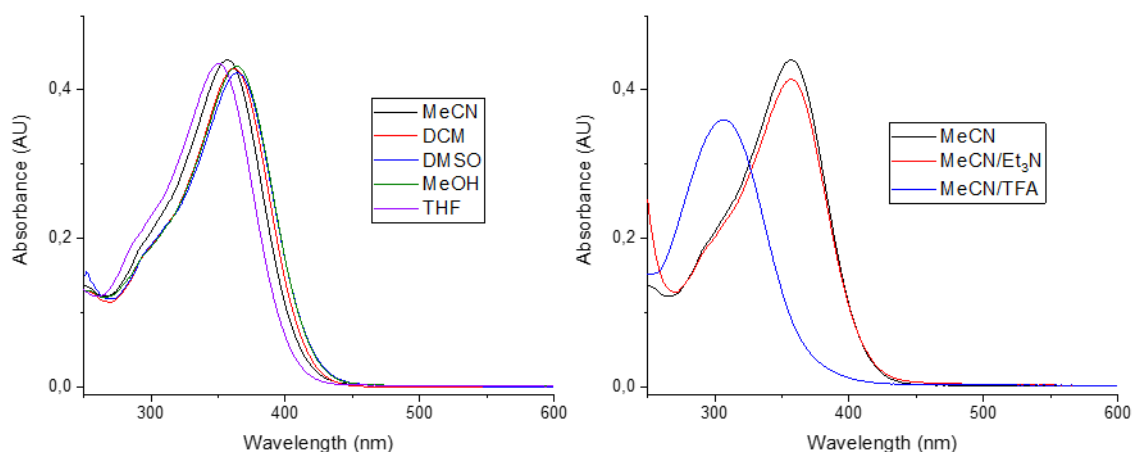


**Figure 133:** Compound *E*-**10** was dissolved in different solvents (80 µM) and in mixtures of 1% (v/v) TFA in MeCN and 1% (v/v) Et₃N in MeCN, respectively. Absorption spectra were measured in the dark (d = 2 mm). The spectra are assigned to the respective solvents *via* color code.
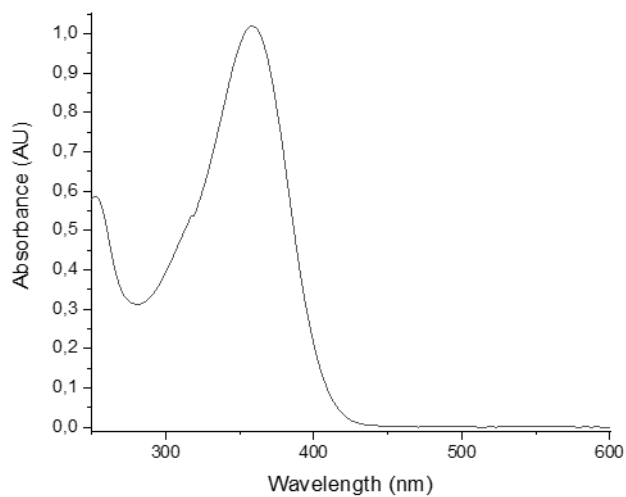
**Figure 134:** Absorption spectrum of compound *Z*-**11** (42 µM) MeCN (d = 10 mm).
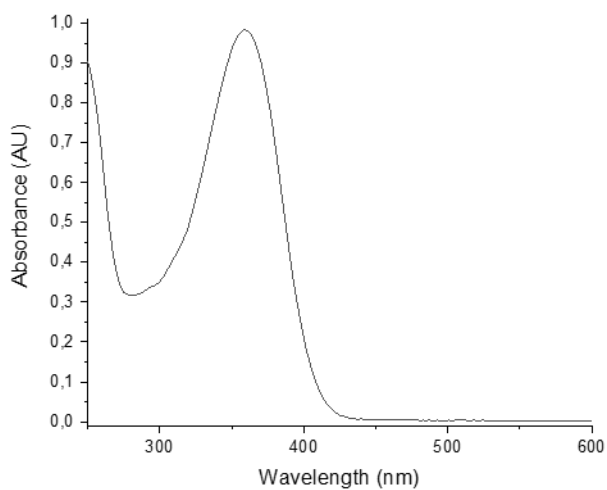


**Figure 135:** Absorption spectrum of compound *Z*-**12** (41 µM) MeCN (d = 10 mm).
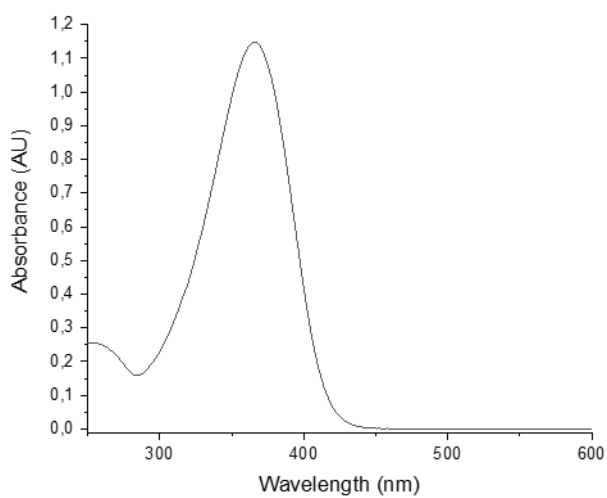


**Figure 136:** Absorption spectrum of compound *Z*-**13** (45 µM) MeCN (d = 10 mm).
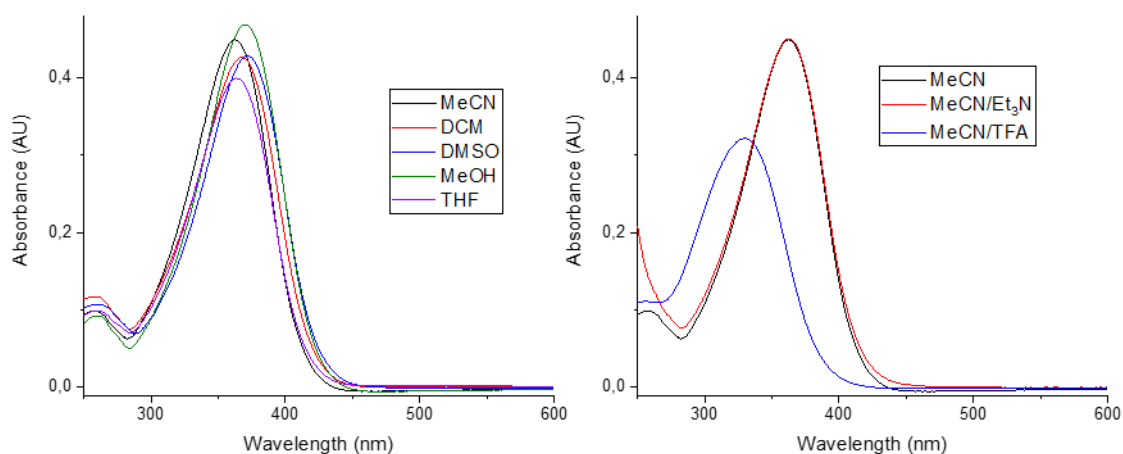
**Figure 137:** Compound *Z*-**14** was dissolved in different solvents (80 µM) and in mixtures of 1% (v/v) TFA in MeCN and 1% (v/v) Et$_3$N in MeCN, respectively. Absorption spectra were measured in the dark (d = 2 mm). The spectra are assigned to the respective solvents *via* color code.
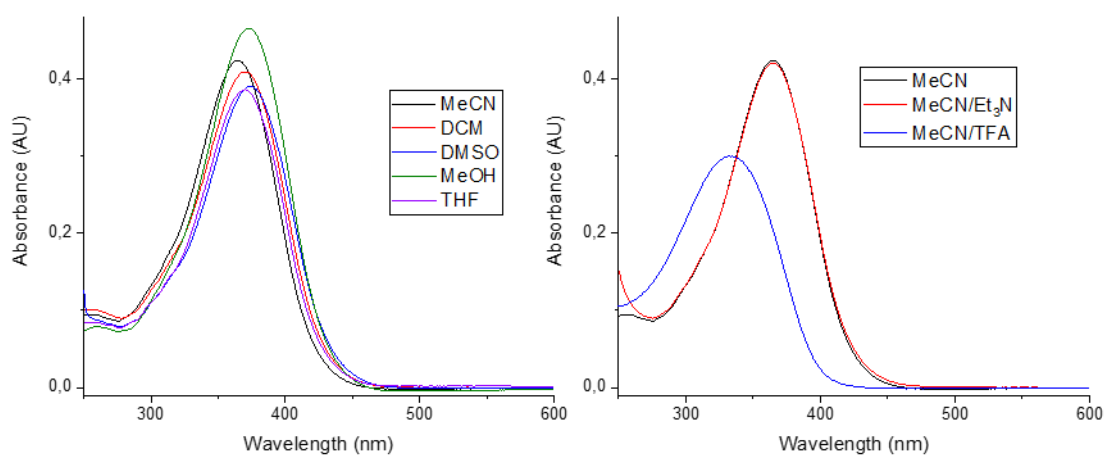


**Figure 138:** Compound *E*-**14** was dissolved in different solvents (80 µM) and in mixtures of 1% (v/v) TFA in MeCN and 1% (v/v) Et$_3$N in MeCN, respectively. Absorption spectra were measured in the dark (d = 2 mm). The spectra are assigned to the respective solvents *via* color code.
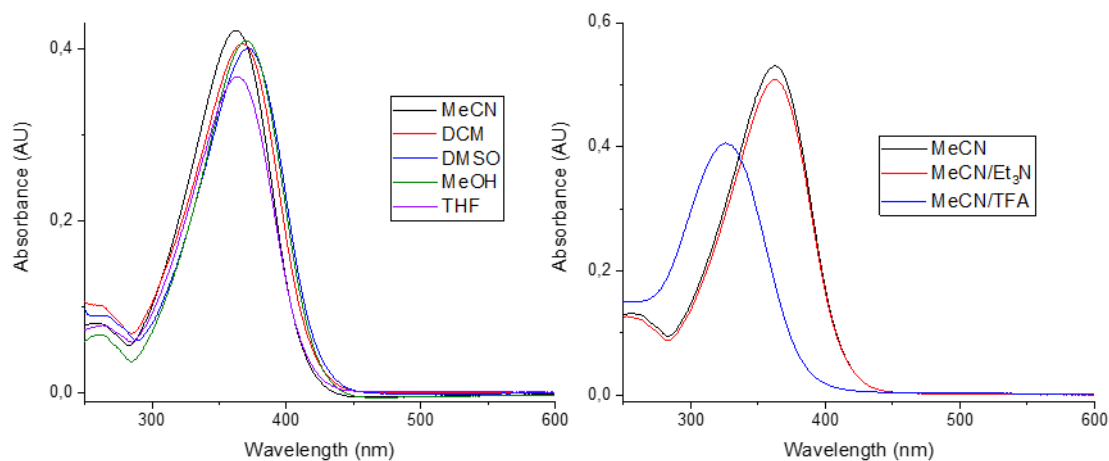
**Figure 139:** Compound *Z*-**15** was dissolved in different solvents (80 µM) and in mixtures of 1% (v/v) TFA in MeCN and 1% (v/v) Et₃N in MeCN, respectively. Absorption spectra were measured in the dark (d = 2 mm). The spectra are assigned to the respective solvents *via* color code.
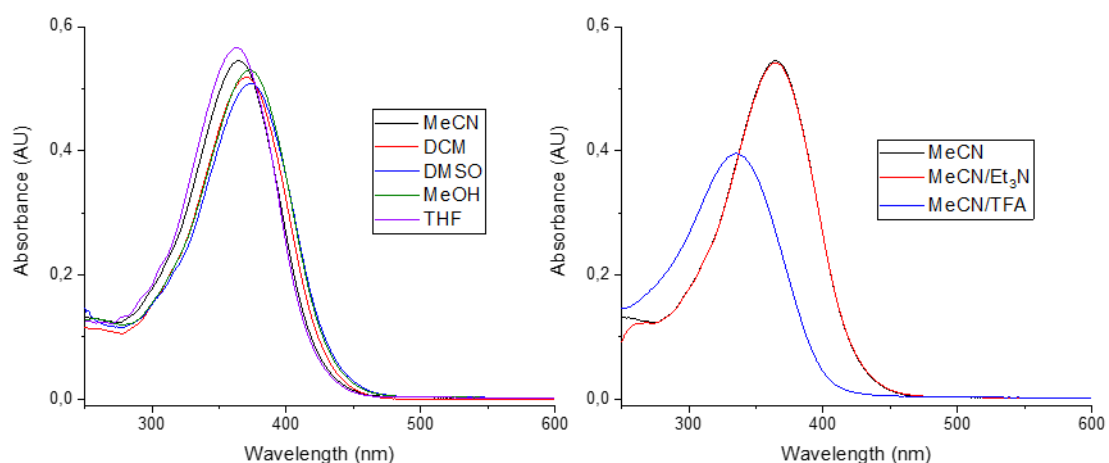


**Figure 140:** Compound *E*-**15** was dissolved in different solvents (80 µM) and in mixtures of 1% (v/v) TFA in MeCN and 1% (v/v) Et₃N in MeCN, respectively. Absorption spectra were measured in the dark (d = 2 mm). The spectra are assigned to the respective solvents *via* color code.
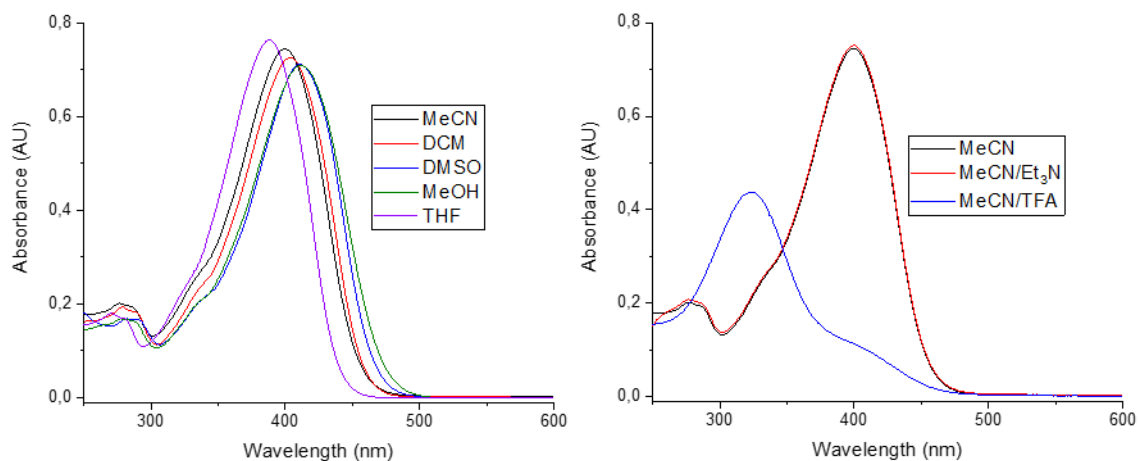
**Figure 141:** Compound *Z*-**16** was dissolved in different solvents (80 µM) and in mixtures of 1% (v/v) TFA in MeCN and 1% (v/v) Et₃N in MeCN, respectively. Absorption spectra were measured in the dark (d = 2 mm). The spectra are assigned to the respective solvents *via* color code.
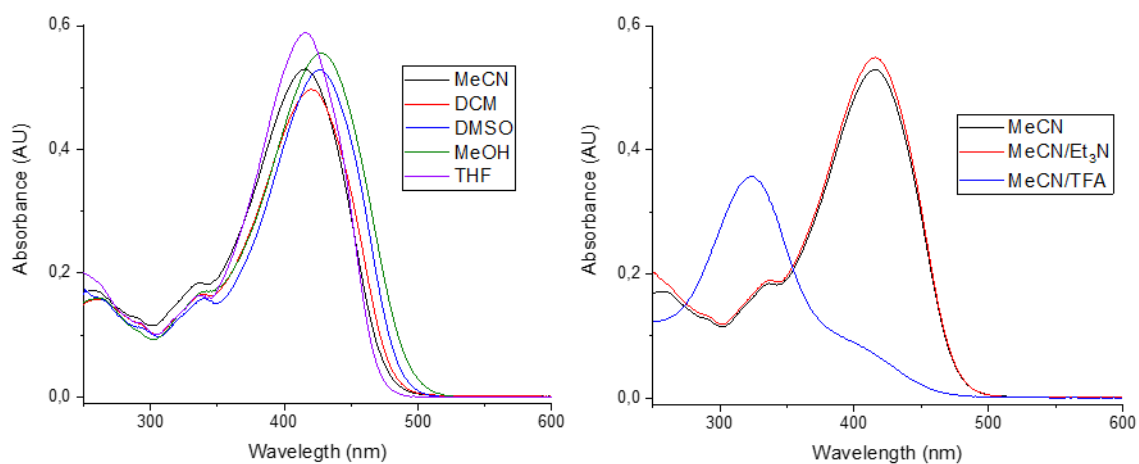


**Figure 142:** Compound *E*-**16** was dissolved in different solvents (80 µM) and in mixtures of 1% (v/v) TFA in MeCN and 1% (v/v) Et₃N in MeCN, respectively. Absorption spectra were measured in the dark (d = 2 mm). The spectra are assigned to the respective solvents *via* color code.
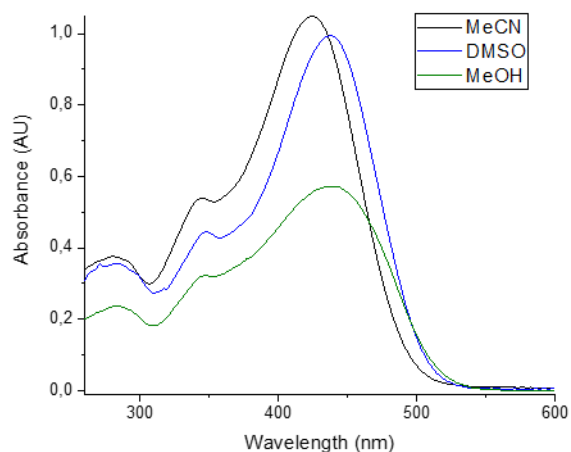
**Figure 143:** Compound *Z*-**17** was dissolved in different solvents (80 µM), respectively. Absorption spectra were measured in the dark (d = 10 mm). The spectra are assigned to the respective solvents *via* color code.
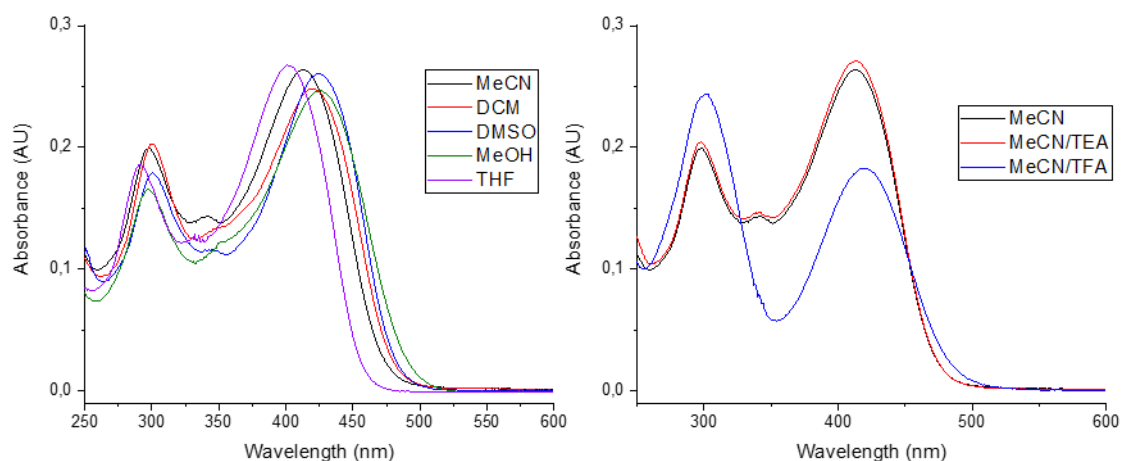


**Figure 144:** Compound *Z*-**18** was dissolved in different solvents (80 µM) and in mixtures of 1% (v/v) TFA in MeCN and 1% (v/v) Et₃N in MeCN, respectively. Absorption spectra were measured in the dark (d = 2 mm). The spectra are assigned to the respective solvents *via* color code.
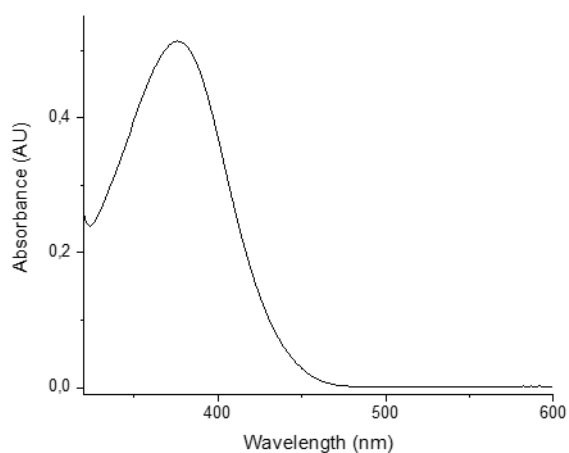
**Figure 145:** Absorption spectrum of compound *Z*-**19** (160 μM) in a saturated solution of sodium ascorbate in DMSO (d = 2 mm).
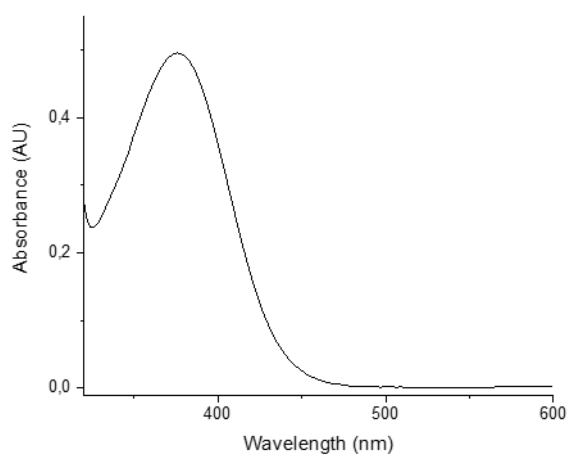


**Figure 146:** Absorption spectrum of compound *Z*-**20** (160 μM) in a saturated solution of sodium ascorbate in DMSO (d = 2 mm).
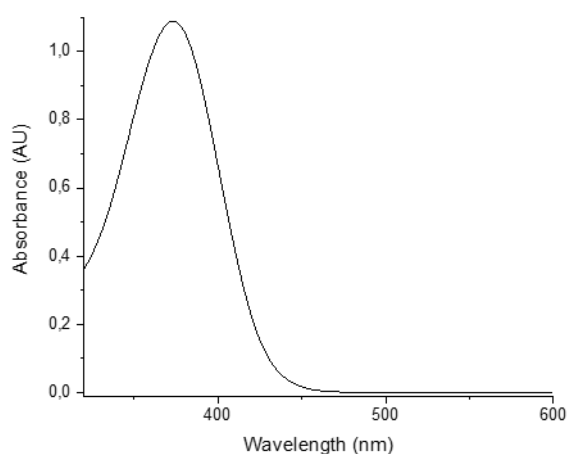


**Figure 147:** Absorption spectrum of compound *Z*-**21** (160 μM) in a saturated solution of sodium ascorbate in DMSO (d = 2 mm).
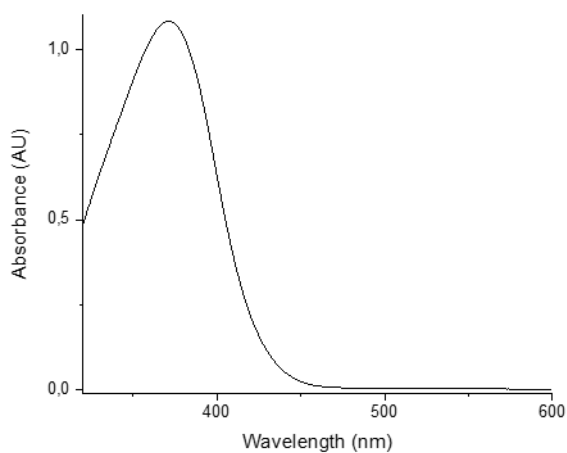
**Figure 148:** Absorption spectrum of compound *Z*-**22** (160 µM) in a saturated solution of sodium ascorbate in DMSO (d = 2 mm).
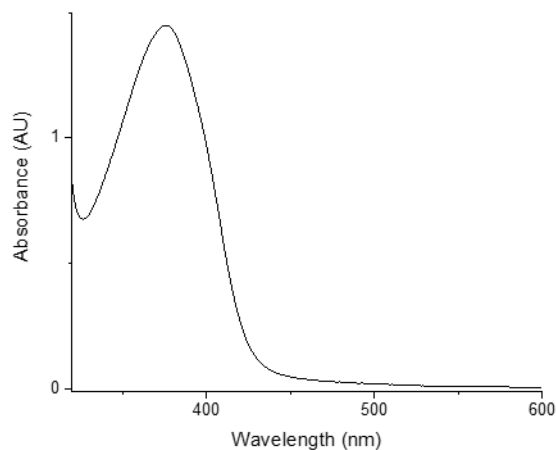


**Figure 149:** Absorption spectrum of compound *Z*-**23** (48 µM) in a saturated solution of sodium ascorbate in DMSO (d = 10 mm).
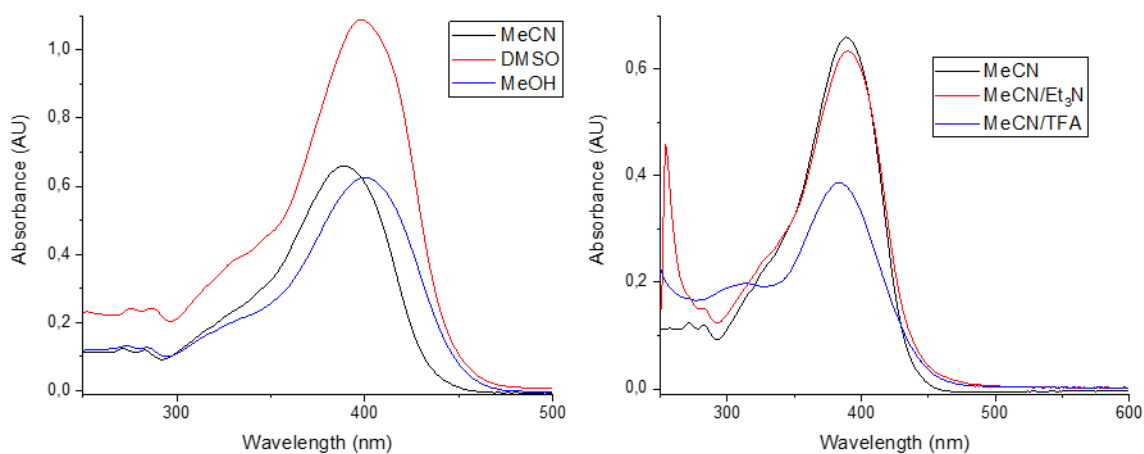


**Figure 150:** Compound *Z*-**24** was dissolved in different solvents (160 µM) and in mixtures of 1% (v/v) TFA in MeCN and 1% (v/v) Et₃N in MeCN, respectively. Absorption spectra were measured in the dark (d = 2 mm). The spectra are assigned to the respective solvents *via* color code.
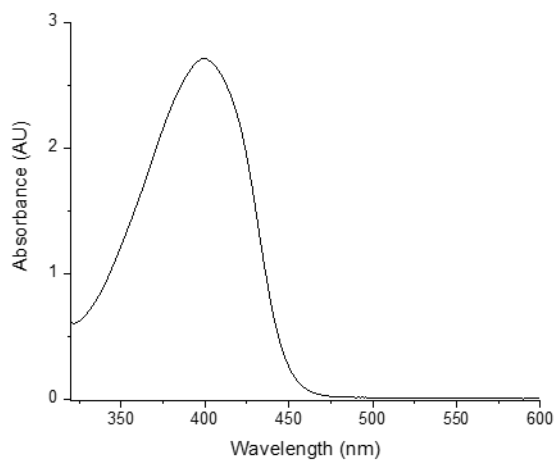
**Figure 151:** Absorption spectrum of compound *Z*-**25** (81 μM) in a saturated solution of sodium ascorbate in DMSO (d = 10 mm).
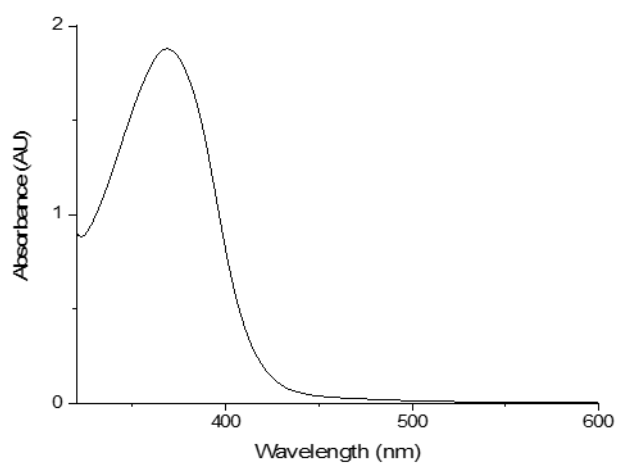


**Figure 152:** Absorption spectrum of compound *Z*-**26** (48 μM) in a saturated solution of sodium ascorbate in DMSO (d = 10 mm).
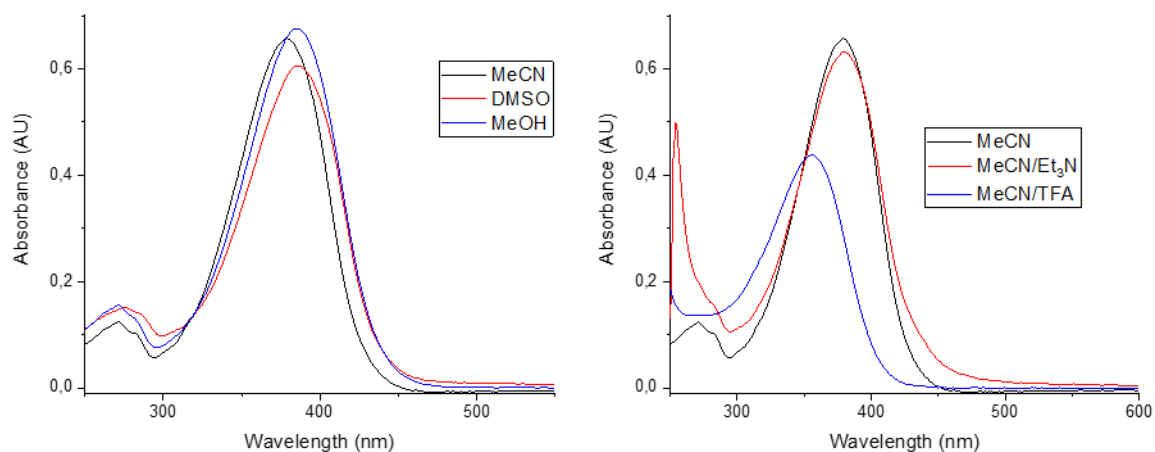
**Figure 153:** Compound *Z*-**27** was dissolved in different solvents (160 μM) and in mixtures of 1% (v/v) TFA in MeCN and 1% (v/v) Et₃N in MeCN, respectively. Absorption spectra were measured in the dark (d = 2 mm). The spectra are assigned to the respective solvents *via* color code.
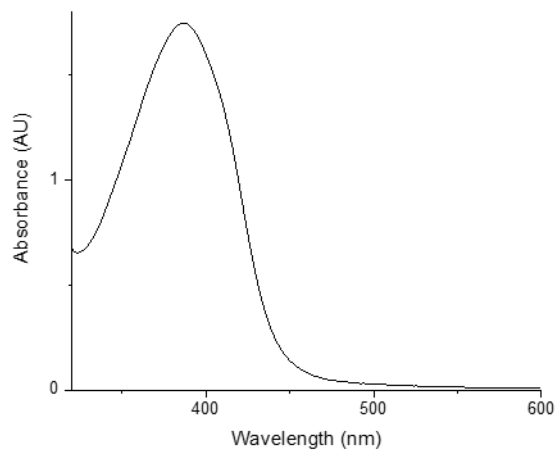


**Figure 154:** Absorption spectrum of compound *Z*-**28** (48 μM) in a saturated solution of sodium ascorbate in DMSO (d = 10 mm).

### 5.4.6 Absorption Spectra of Irradiated Samples
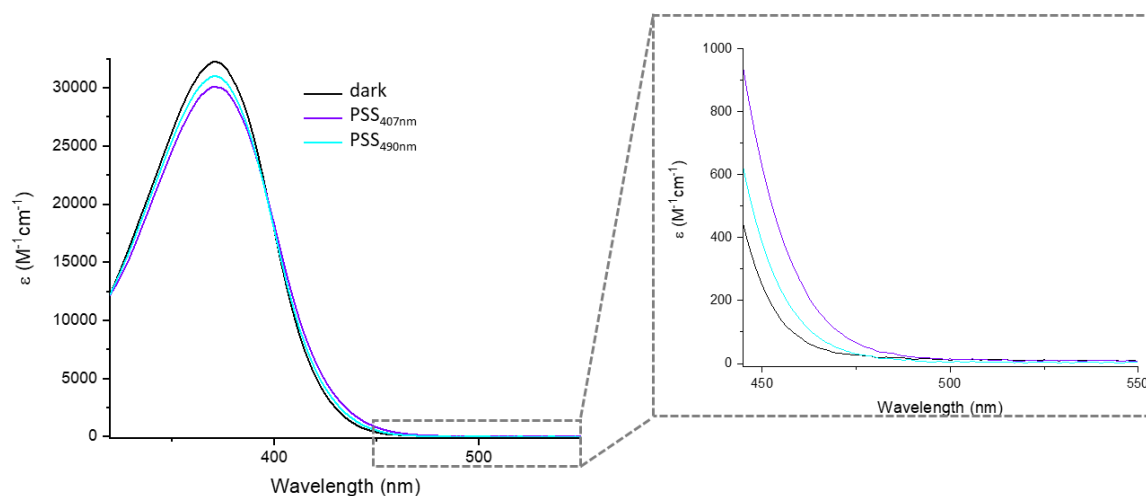


**Figure 155:** Compound **6** was dissolved in a saturated solution of sodium ascorbate in DMSO (80 µM). Absorption spectra (d = 2 mm) were first measured in the dark. The samples were then first irradiated with 407 nm (2 min), then with 490 nm (15 min) and an absorption spectrum was measured after each irradiation step.
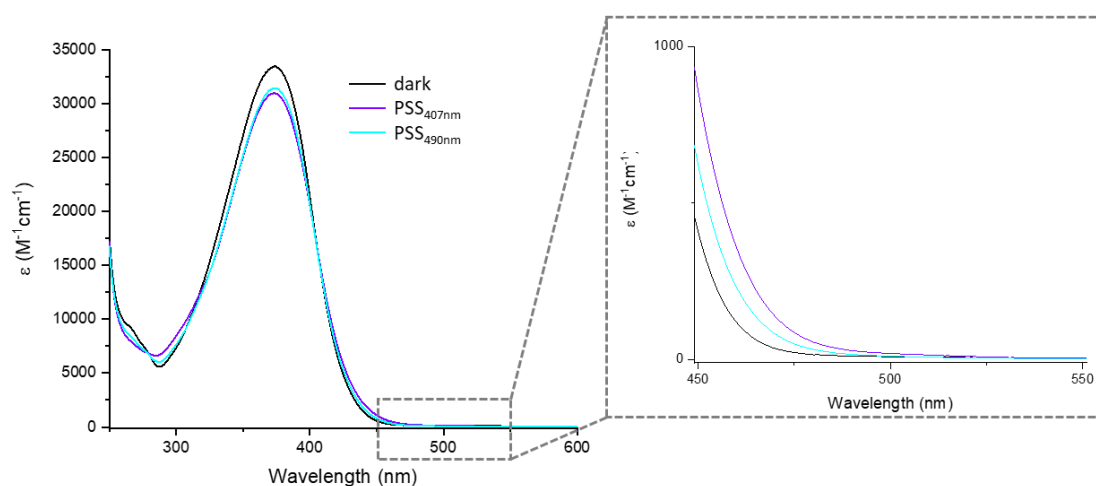


**Figure 156: A**bsorption spectra (d=2 mm) of a solution of 2.0 mM (cutout) and 400 µM (full spectrum) compound **6** with 10 mM glutathione and 5.0 mM tris(2-carboxyethyl)phosphine in 25% PBS in DMSO (v/v) were first measured in the dark. The samples were then first irradiated with 407 nm (2 min), then with 490 nm (15 min) and an absorption spectrum was measured after each irradiation step.
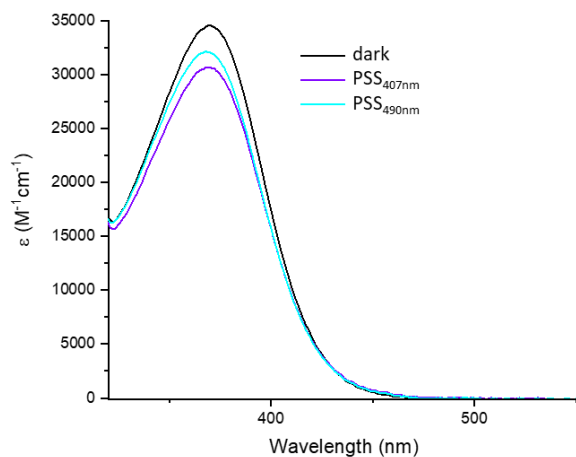
**Figure 157:** Compound **8** was dissolved in a saturated solution of sodium ascorbate in DMSO (80 µM). An absorption spectrum (d = 2 mm) was first measured in the dark. The sample was then first irradiated with 407 nm (2 min), then with 490 nm (15 min) and an absorption spectrum was measured after each irradiation step.
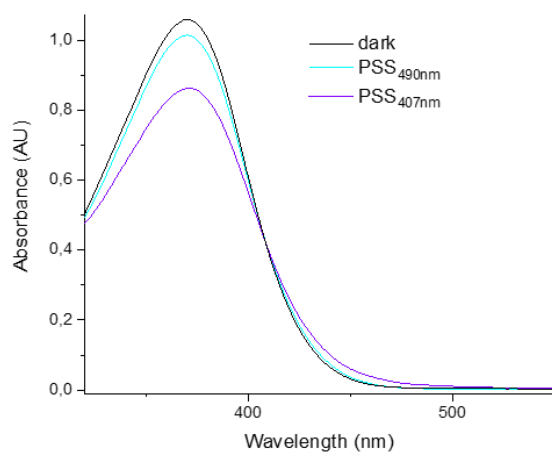


**Figure 158:** Compound **9** was dissolved in a saturated solution of sodium ascorbate in DMSO (160 µM). An absorption spectrum (d = 2 mm) was first measured in the dark. The sample was then first irradiated with 490 nm (15 min), then with 407 nm (1 min) and an absorption spectrum was measured after each irradiation step.
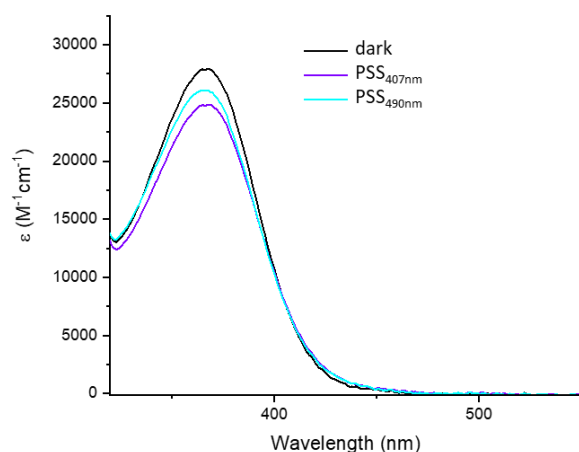
**Figure 159:** Compound **10** was dissolved in a saturated solution of sodium ascorbate in DMSO (80 µM). An absorption spectrum (d = 2 mm) was first measured in the dark. The sample was then first irradiated with 407 nm (2 min), then with 490 nm (15 min) and an absorption spectrum was measured after each irradiation step.
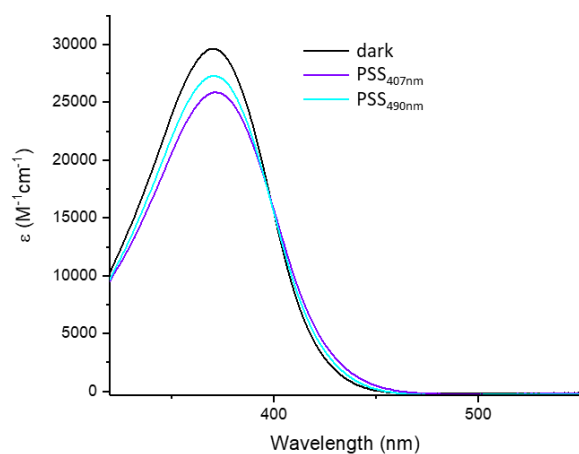


**Figure 160:** Compound **14** was dissolved in a saturated solution of sodium ascorbate in DMSO (80 µM). An absorption spectrum (d = 2 mm) was first measured in the dark. The sample was then first irradiated with 407 nm (2 min), then with 490 nm (15 min) and an absorption spectrum was measured after each irradiation step.
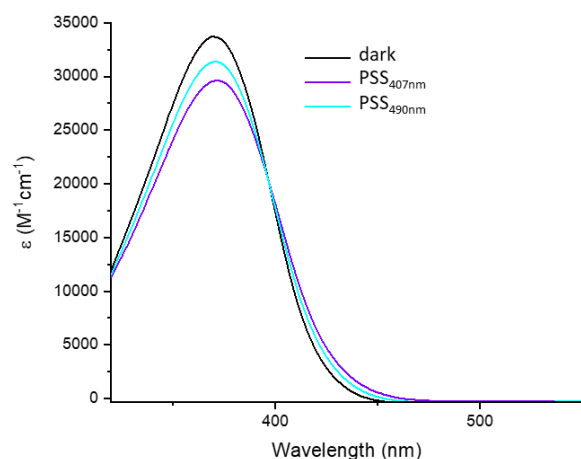
**Figure 161:** Compound **15** was dissolved in a saturated solution of sodium ascorbate in DMSO (80 µM). An absorption spectrum (d = 2 mm) was first measured in the dark. The sample was then first irradiated with 407 nm (2 min), then with 490 nm (15 min) and an absorption spectrum was measured after each irradiation step.
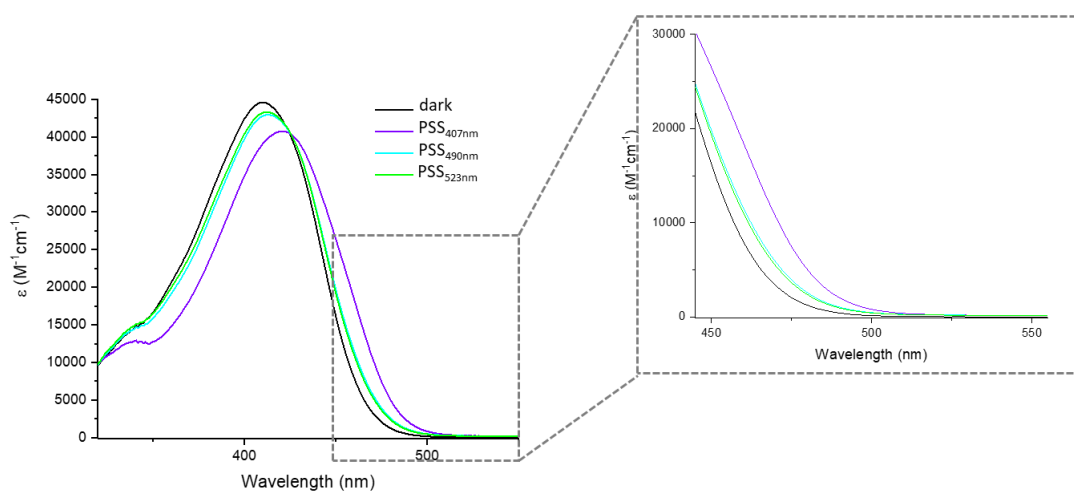


**Figure 162:** Compound **16** was dissolved in a saturated solution of sodium ascorbate in DMSO (80 µM). An absorption spectrum (d = 2 mm) was first measured in the dark. The sample was then first irradiated with 407 nm (2 min), then with 490 nm (15 min) and with 523 nm (5 min) and an absorption spectrum was measured after each irradiation step.
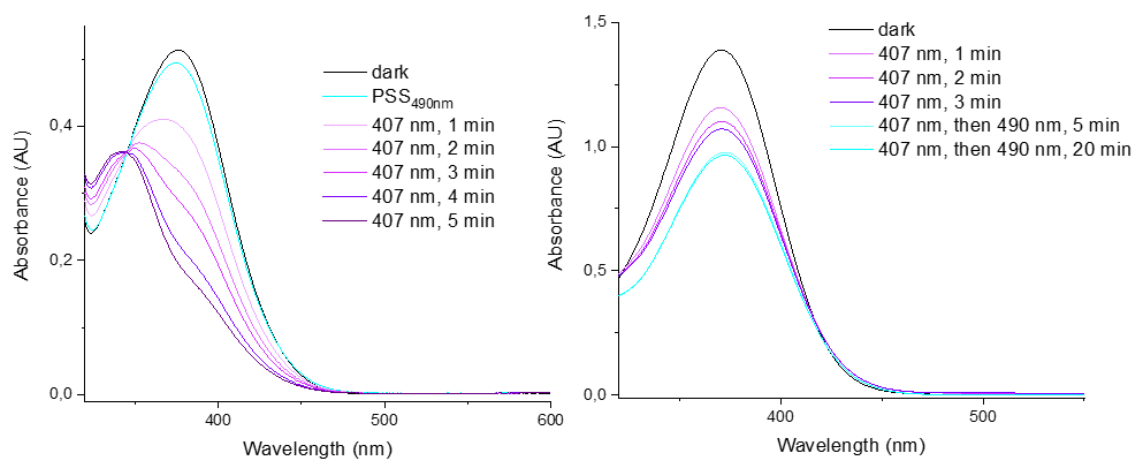
**Figure 163:** Left: Compound **19** was dissolved in 25% PBS in a saturated solution of sodium ascorbate in DMSO (80 µM). An absorption spectrum (d = 2 mm) was first measured in the dark. The sample was then first irradiated with 490 nm (5 min), then with 407 nm and an absorption spectrum was measured after each irradiation step. Right: Compound **19** was dissolved in a saturated solution of sodium ascorbate in DMSO (160 µM). An absorption spectrum (d = 2 mm) was first measured in the dark. The sample was then first irradiated with 407 nm, then with 490 nm (15 min) and an absorption spectrum was measured after each irradiation step.
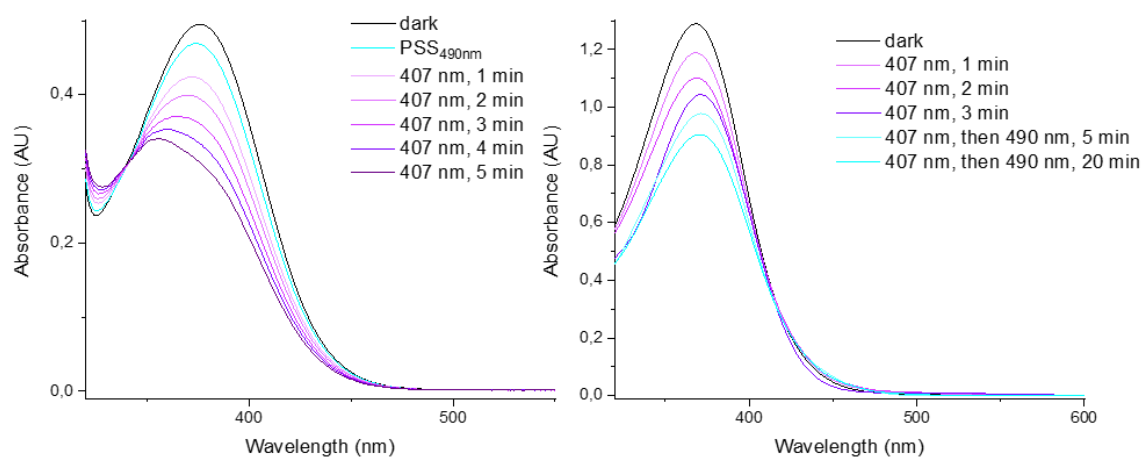


**Figure 164:** Left: Compound **20** was dissolved in 25% PBS in a saturated solution of sodium ascorbate in DMSO (80 µM). An absorption spectrum (d = 2 mm) was first measured in the dark. The sample was then first irradiated with 490 nm (5 min), then with 407 nm and an absorption spectrum was measured after each irradiation step. Right: Compound **20** was dissolved in a saturated solution of sodium ascorbate in DMSO (160 µM). An absorption spectrum (d = 2 mm) was first measured in the dark. The sample was then first irradiated with 407 nm, then with 490 nm (15 min) and an absorption spectrum was measured after each irradiation step.
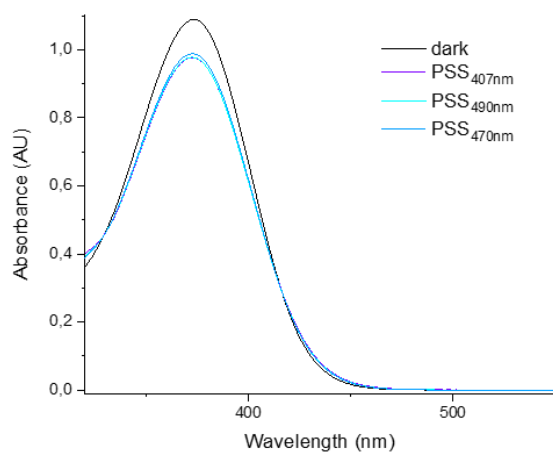
**Figure 165:** Compound **21** was dissolved in a saturated solution of sodium ascorbate in DMSO (160 µM). An absorption spectrum (d = 2 mm) was first measured in the dark. The sample was then first irradiated with 407 nm (1 min), then with 490 nm (15 min) and 470 nm (5 min) and an absorption spectrum was measured after each irradiation step.
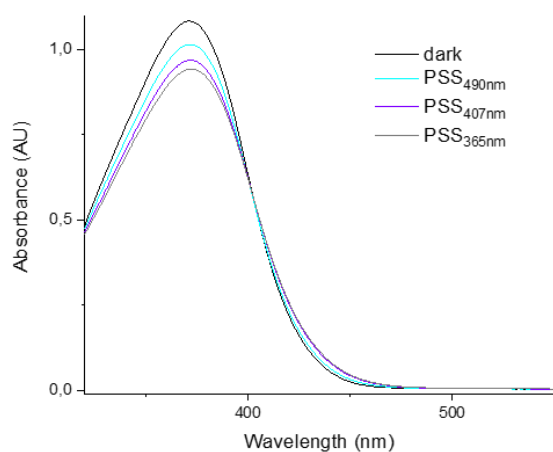


**Figure 166:** Compound **22** was dissolved in a saturated solution of sodium ascorbate in DMSO (160 µM). An absorption spectrum (d = 2 mm) was first measured in the dark. The sample was then first irradiated with 407 nm (1 min), then with 490 nm (13 min) and 365 nm (1 min) and an absorption spectrum was measured after each irradiation step.
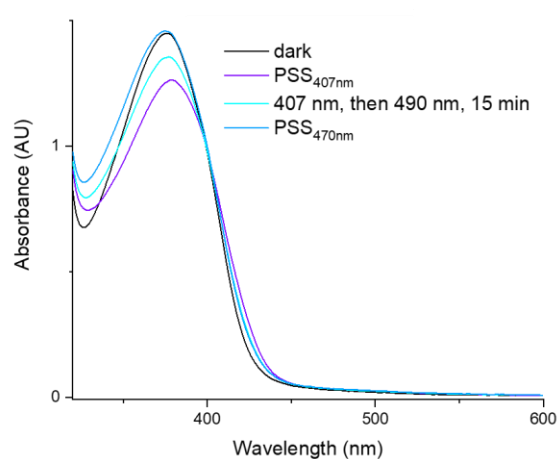
**Figure 167:** Compound **23** was dissolved in a saturated solution of sodium ascorbate in DMSO (48 µM) and purged with argon. An absorption spectrum (d = 10 mm) was first measured in the dark. The sample was then first irradiated with 407 nm (1 min), then with 490 nm (15 min) and 470 nm (20 min) and an absorption spectrum was measured after each irradiation step.
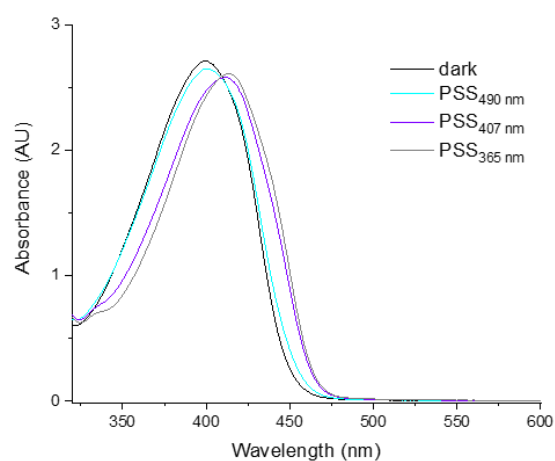


**Figure 168:** Compound **25** was dissolved in a saturated solution of sodium ascorbate in DMSO (81 µM) and purged with argon. An absorption spectrum (d = 10 mm) was first measured in the dark. The sample was then first irradiated with 490 nm (15 min), then with 407 nm (2 min) and 365 nm (2 min) and an absorption spectrum was measured after each irradiation step.
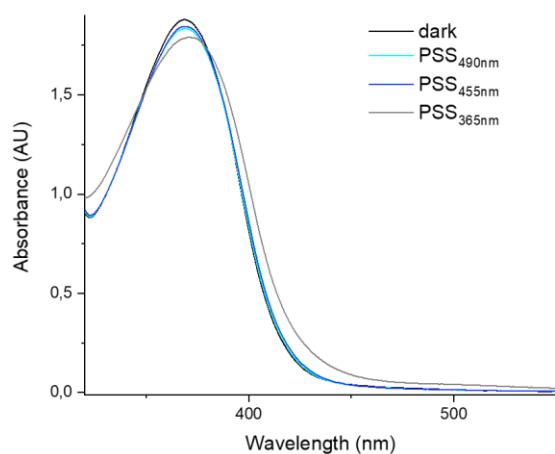
**Figure 169:** Compound **26** was dissolved in a saturated solution of sodium ascorbate in DMSO (48 µM) and purged with argon. An absorption spectrum (d = 10 mm) was first measured in the dark. The sample was then first irradiated with 490 nm (15 min), then with 455 nm (15 min) and 365 nm (2 min) and an absorption spectrum was measured after each irradiation step.
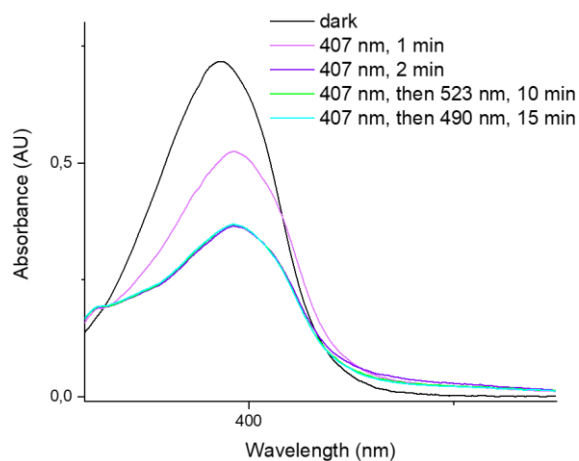


**Figure 170:** Compound **27** was dissolved in a saturated solution of sodium ascorbate in DMSO (160 µM). An absorption spectrum (d = 2 mm) was first measured in the dark. The sample was then first irradiated with 407 nm (2 min), then with 523 nm and an absorption spectrum was measured after each irradiation step.
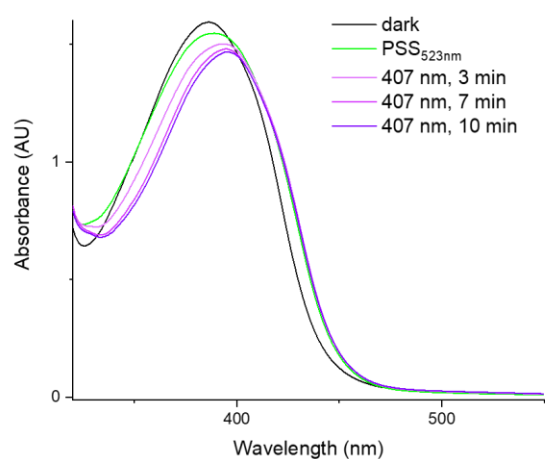
**Figure 171:** Compound **28** was dissolved in a saturated solution of sodium ascorbate in DMSO (48 µM) and purged with argon. An absorption spectrum (d = 10 mm) was first measured in the dark. The sample was then first irradiated with 523 nm (20 min), then with 407 nm and an absorption spectrum was measured after each irradiation step.

## 5.4.7 Emission Spectra
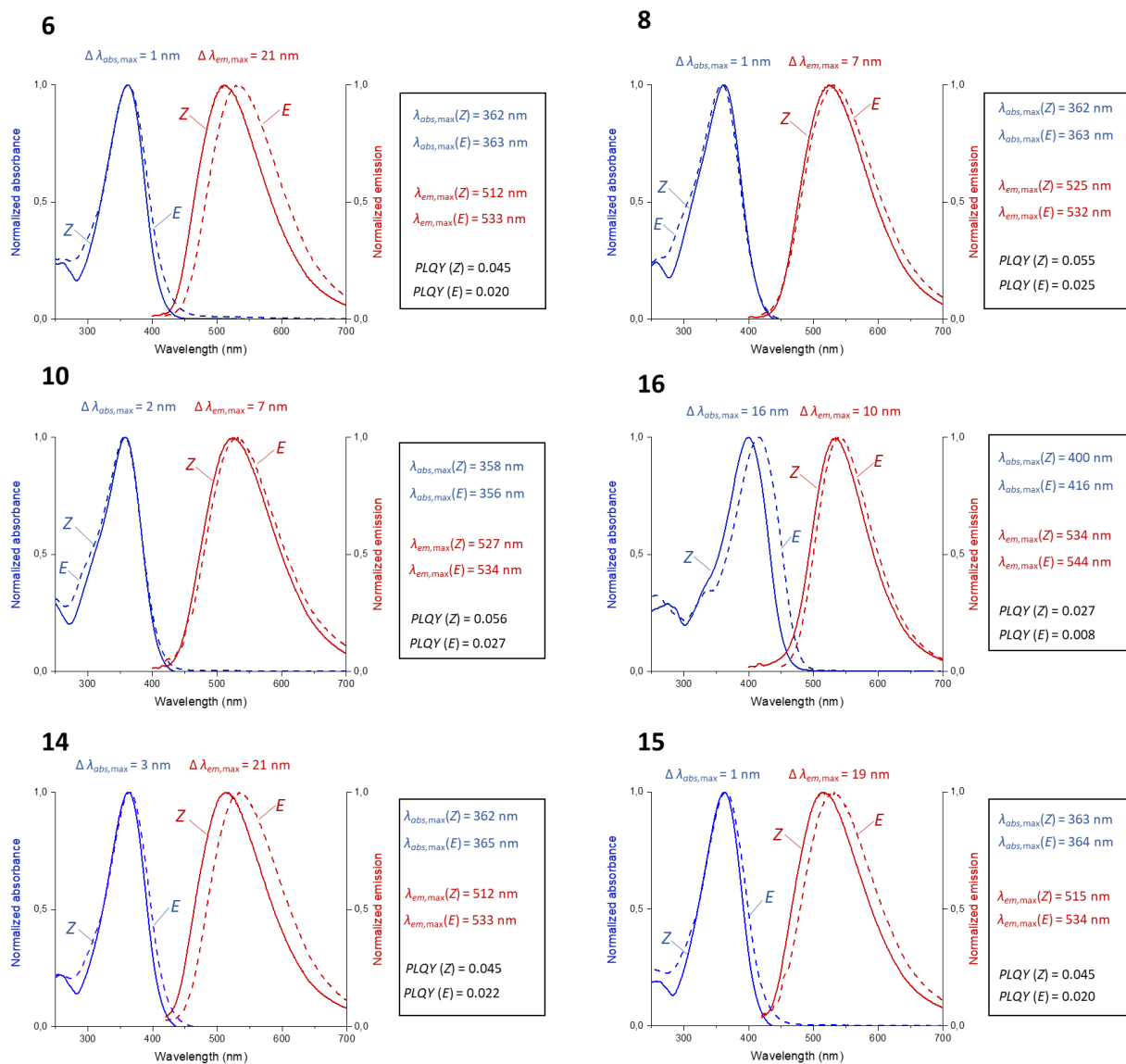


**Figure 172:** Normalized absorption (blue) and emission (red) spectra of 80 µM solutions of the respective Z-isomers (solid line) and E-isomers (dashed line) of **6**, **8**, and **14**-**16** in MeCN.
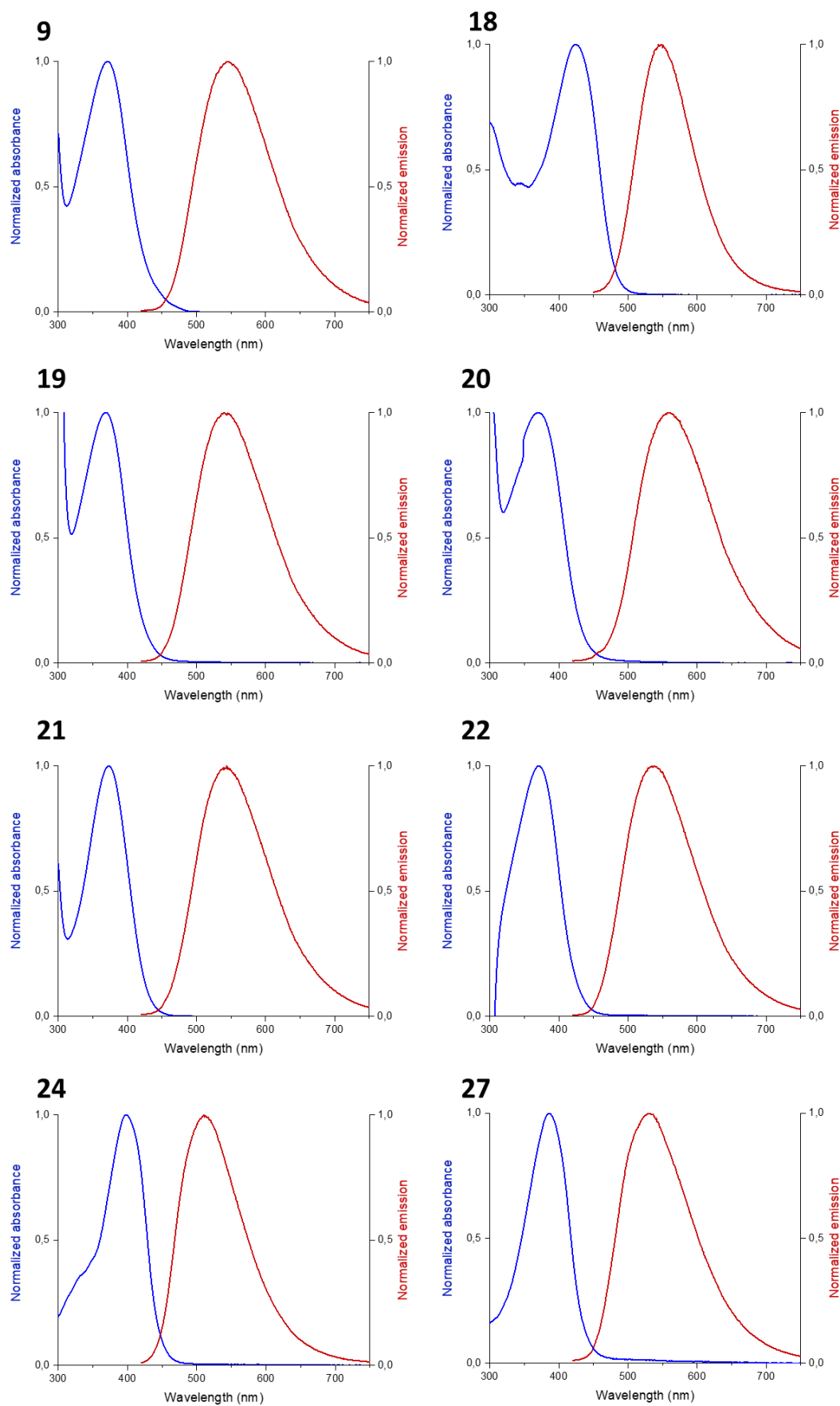
**Figure 173:** Normalized absorption (blue) and fluorescence (red) spectra of solutions of the respective Z-isomers of **9**, **18**-**22**, **24** and **27** in DMSO.
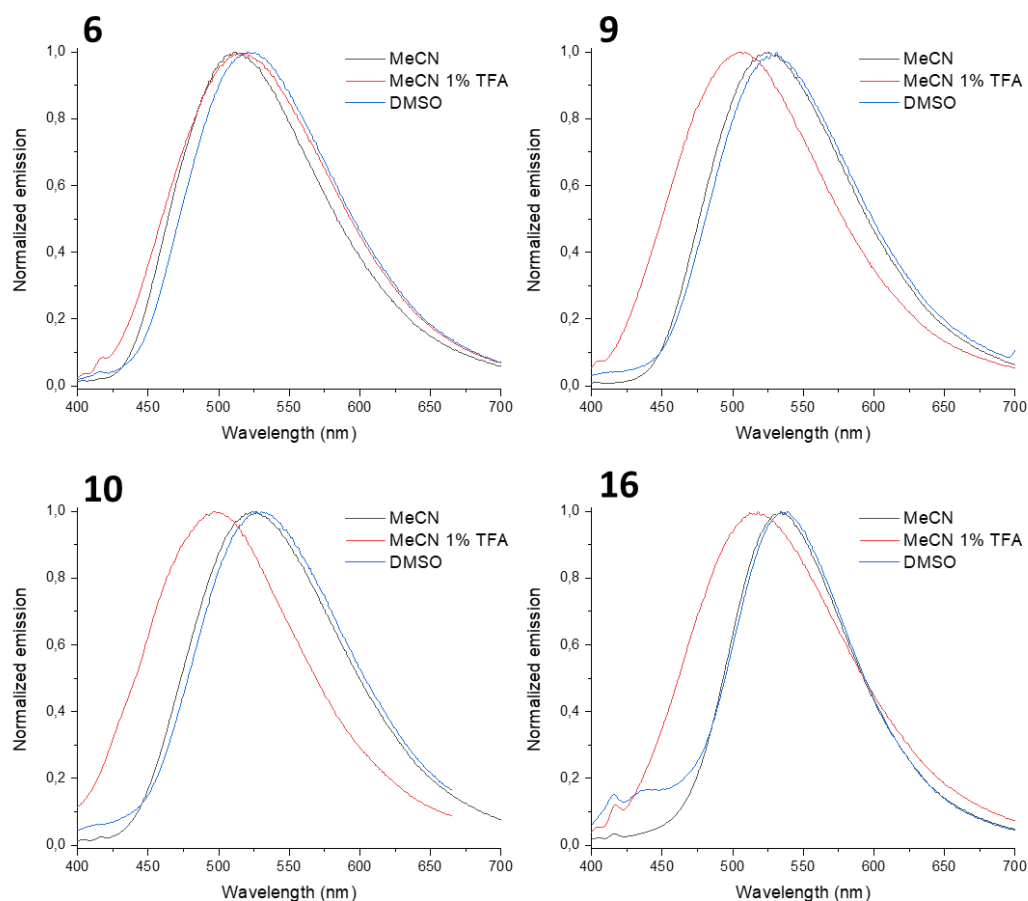
**Figure 174:** Normalized fluorescence spectra of compounds *Z*-**6**, *Z*-**9**, *Z*-**10** and *Z*-**16** in different solvents (80 μM) and in mixtures of 1% (v/v) TFA in MeCN, respectively. The spectra are assigned to the respective solvents *via* color code.
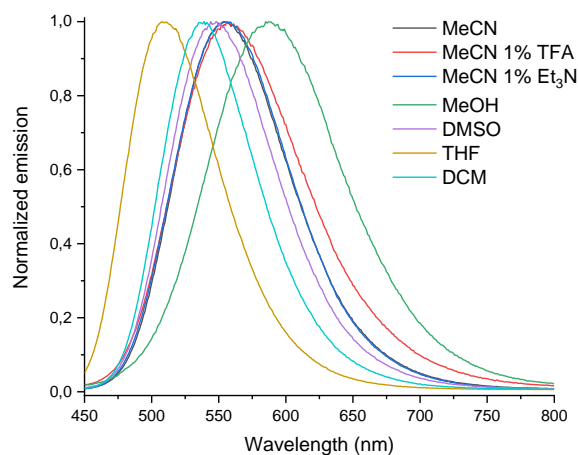


**Figure 175:** Normalized fluorescence spectra of compound *Z*-**18** in different solvents (80 μM) and in mixtures of 1% (v/v) TFA in MeCN and 1% (v/v) Et₃N in MeCN, respectively. The spectra are assigned to the respective solvents *via* color code.

### 5.4.8   Composition of Photostationary States (PSSs)

The PSS composition was determined by measuring $^1$H NMR spectra of the respective compounds after irradiation. The PSS values in the NMR tubes (0.5 mL of the 30-60 mM solutions in DMSO-$d_6$) have been achieved within 1 h (365, 407, 523 nm), 2 h (430, 450, 470 nm) or 4 h (380, 490 nm). Signal pairs were determined for each compound: two signals assigned to the same proton for the respective photoisomers were integrated and the % of $E$-isomer = $I_E/(I_E+I_Z)*100\%$ was determined. The final $E/Z$ ratios result from the average value determined from three signal pairs.

**Table 6:** PSS composition in DMSO-$d_6$ determined by measuring $^1$H NMR spectra of the respective compounds after irradiation. *It was not verified that the PSS had already been reached.

| Compound | 365 nm (% of $E$-isomer) | 380 nm (% of $E$-isomer) | 407 nm (% of $E$-isomer) | 430 nm (% of $E$-isomer) | 450 nm (% of $E$-isomer) | 470 nm (% of $E$-isomer) | 490 nm (% of $E$-isomer) | 523 nm (% of $E$-isomer) |
|---|---|---|---|---|---|---|---|---|
| **5** | 67 | 56 | <5 | - | - | - | - | - |
| **6** | 62 | 58 | 56 | 42 | 38 | 19 | 13 | - |
| **8** | 59 | 64 | 64 | 62 | 61 | 58 | 56 | - |
| **10** | 48 | 51 | 44 | 41 | 39 | 34 | 29 | - |
| **14** | 63 | 56 | 54 | 42 | 24 | 19 | 16 | - |
| **15** | 63 | 62 | 52 | 39 | 31 | 17 | 11 | - |
| **16** | 61 | 59 | 55 | 46 | 19 | 17 | 12 | 10 |
| **18** | - | - | - | - | - | 27 | 18 | 14 |
| **23** | - | - | - | - | 15 | - | 14 | - |
| **24** | - | - | 66 | - | - | - | - | - |
| **25** | - | - | 41* | - | 14 | - | <5 | - |

| 26 | - | - | - | - | 14 | - | 12 | - |
|----|---|---|---|---|----|---|----|---|
| 27 | - | - | 47 | - | - | - | - | - |



**Figure 176:** Sections of $^1$H NMR spectra (400 MHz, DMSO-$d_6$) of compound **5** in the dark (top) and after reaching the PSS upon irradiation with 365 nm and 407 nm.

**Figure 177:** Sections of ¹H NMR spectra (400 MHz, DMSO-$d_6$) of compound **6** in the dark (top) and after reaching the PSS upon irradiation with 365 nm, 407 nm and 490 nm.
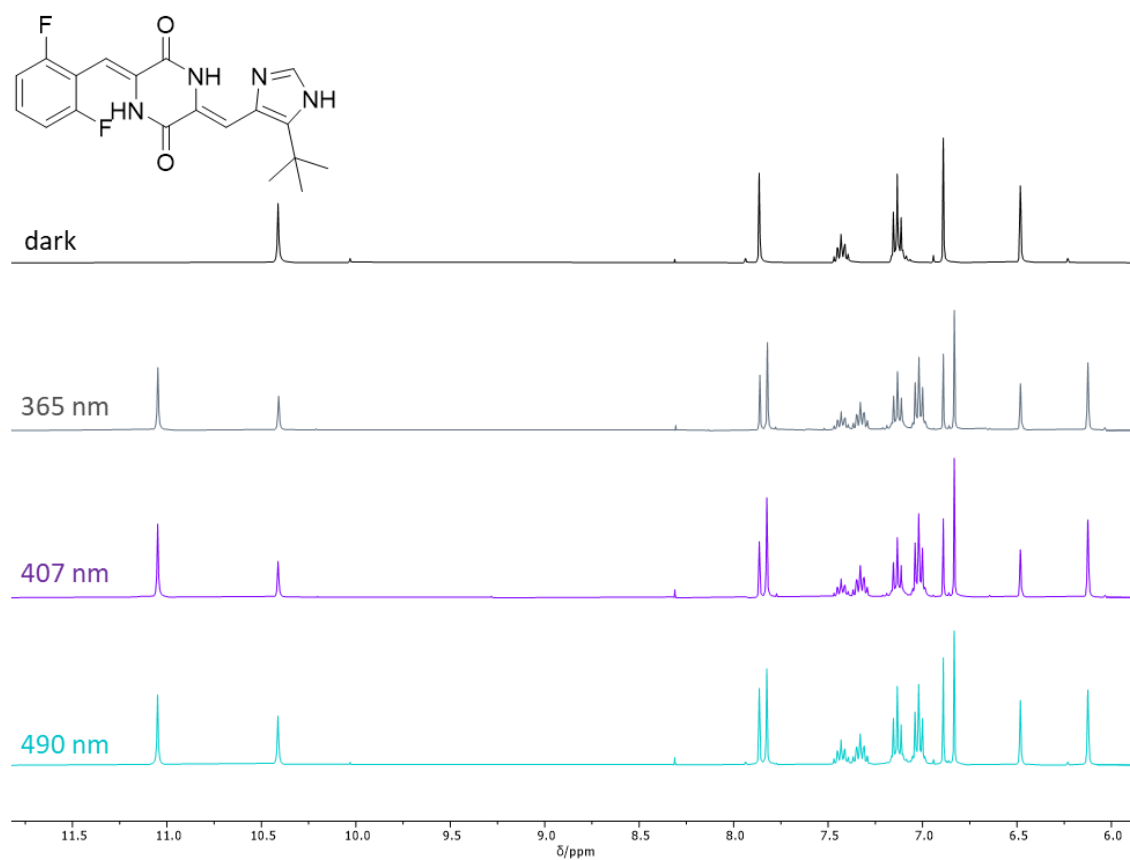


**Figure 178:** Sections of ¹H NMR spectra (400 MHz, DMSO-$d_6$) of compound **8** in the dark (top) and after reaching the PSS upon irradiation with 365 nm, 407 nm and 490 nm.
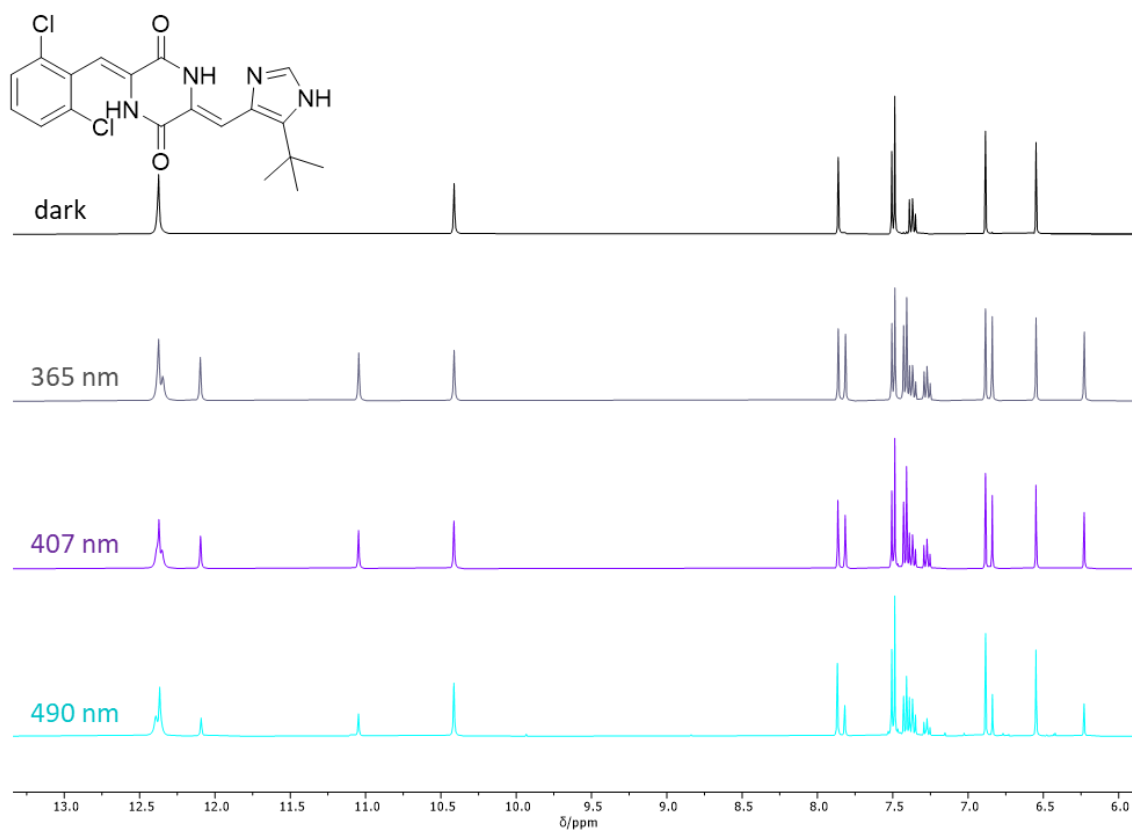
**Figure 179:** Sections of ${}^1$H NMR spectra (400 MHz, DMSO-$d_6$) of compound **10** in the dark (top) and after reaching the PSS upon irradiation with 365 nm, 407 nm and 490 nm.
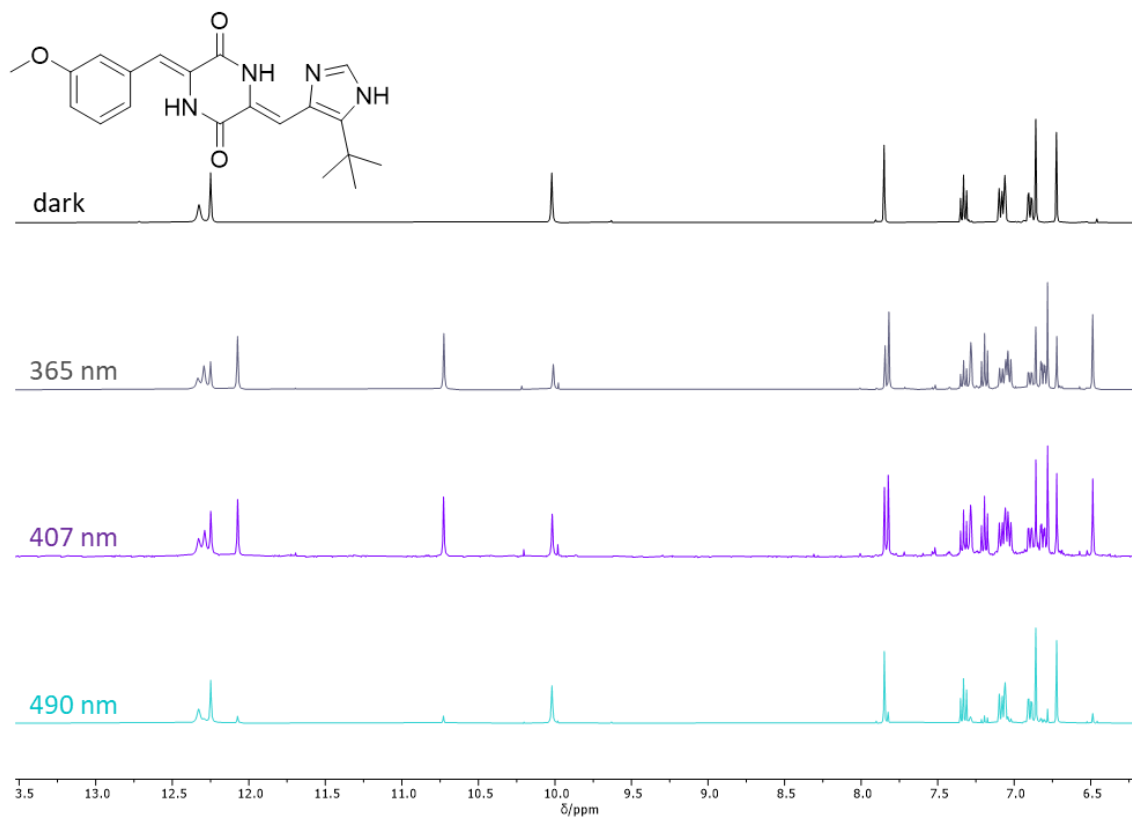


**Figure 180:** Sections of ${}^1$H NMR spectra (400 MHz, DMSO-$d_6$) of compound **14** in the dark (top) and after reaching the PSS upon irradiation with 365 nm, 407 nm and 490 nm.
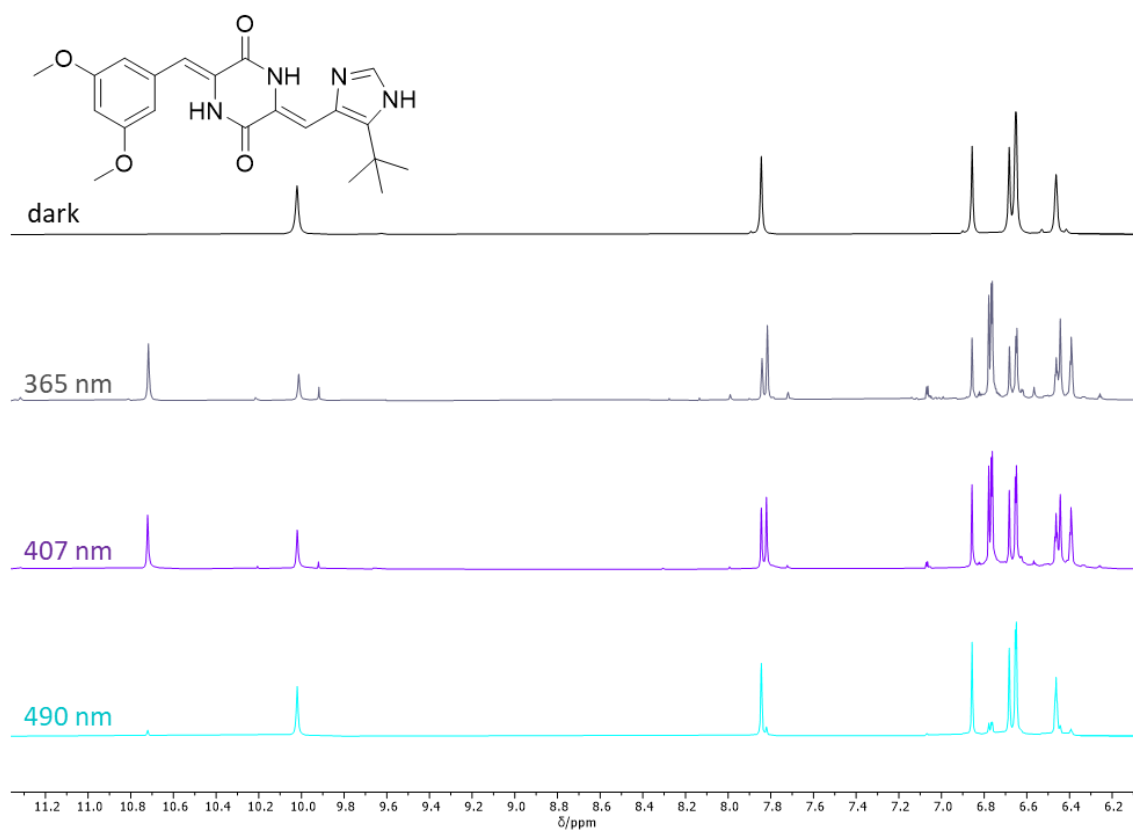
**Figure 181:** Sections of $^1$H NMR spectra (400 MHz, DMSO-$d_6$) of compound **15** in the dark (top) and after reaching the PSS upon irradiation with 365 nm, 407 nm and 490 nm.
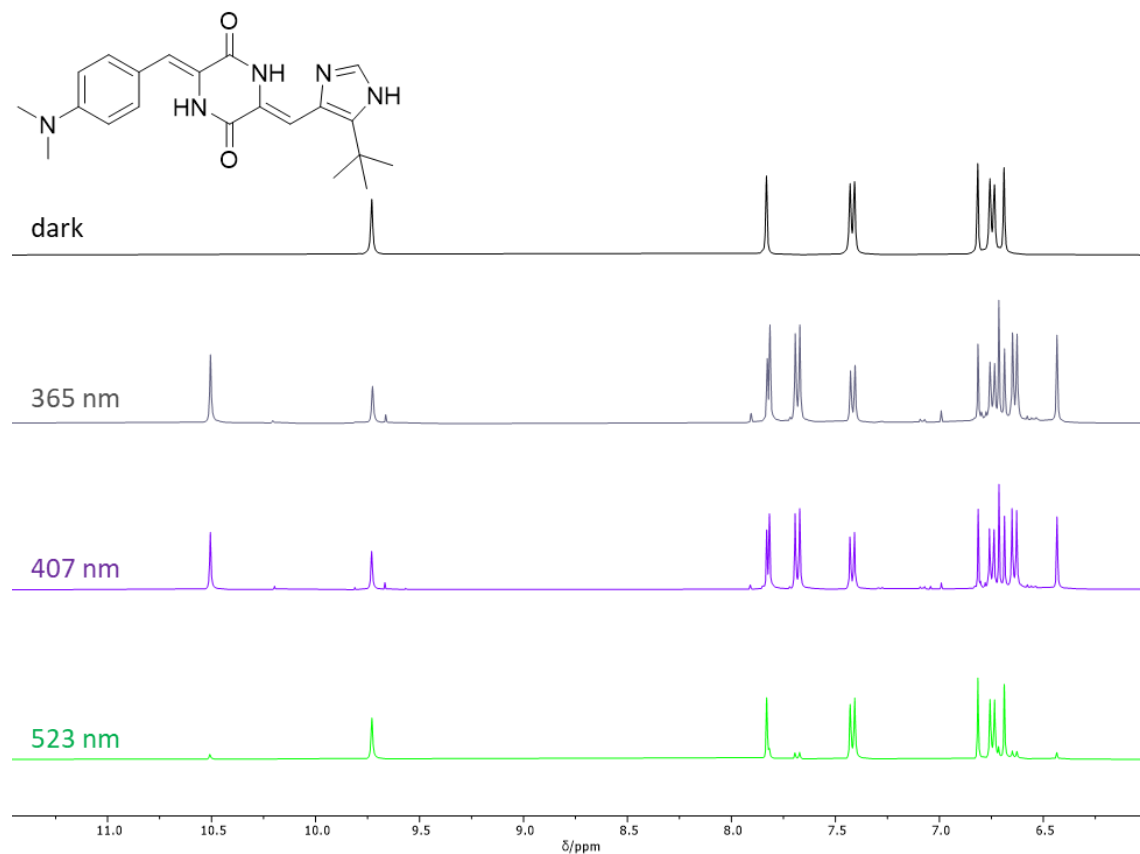


**Figure 182:** Sections of $^1$H NMR spectra (400 MHz, DMSO-$d_6$) of compound **16** in the dark (top) and after reaching the PSS upon irradiation with 365 nm, 407 nm and 523 nm.
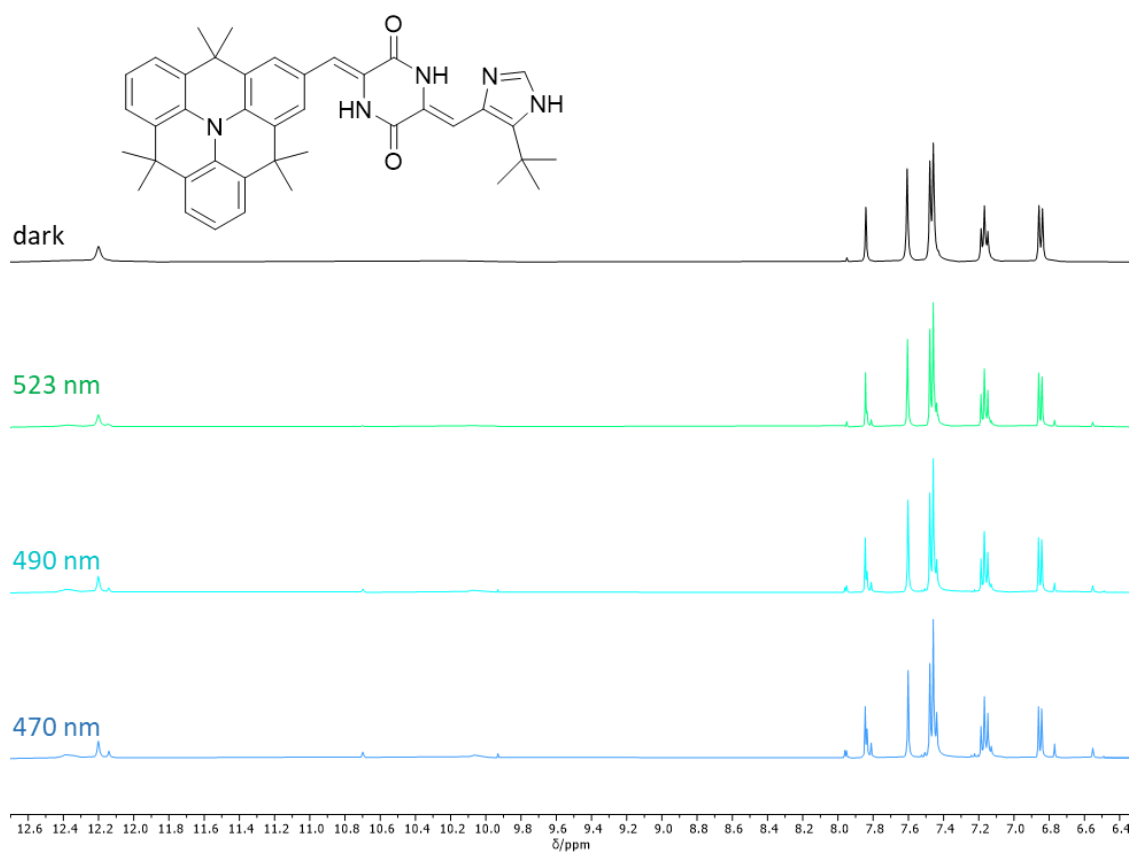
**Figure 183:** Sections of $^{1}$H NMR spectra (400 MHz, DMSO-$d_6$) of compound **18** in the dark (top) and after reaching the PSS upon irradiation with 470 nm, 490 nm and 523 nm.
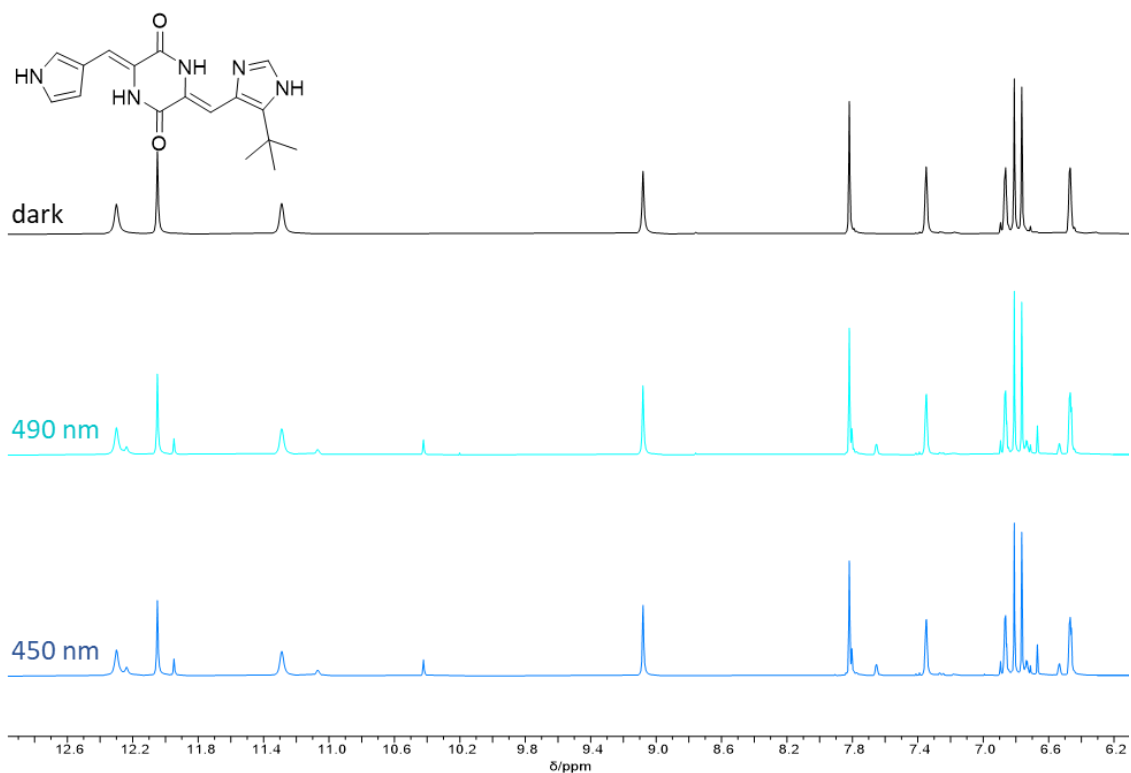


**Figure 184:** Sections of $^{1}$H NMR spectra (400 MHz, DMSO-$d_6$) of compound **23** in the dark (top) and after reaching the PSS upon irradiation with 450 nm and 490 nm.
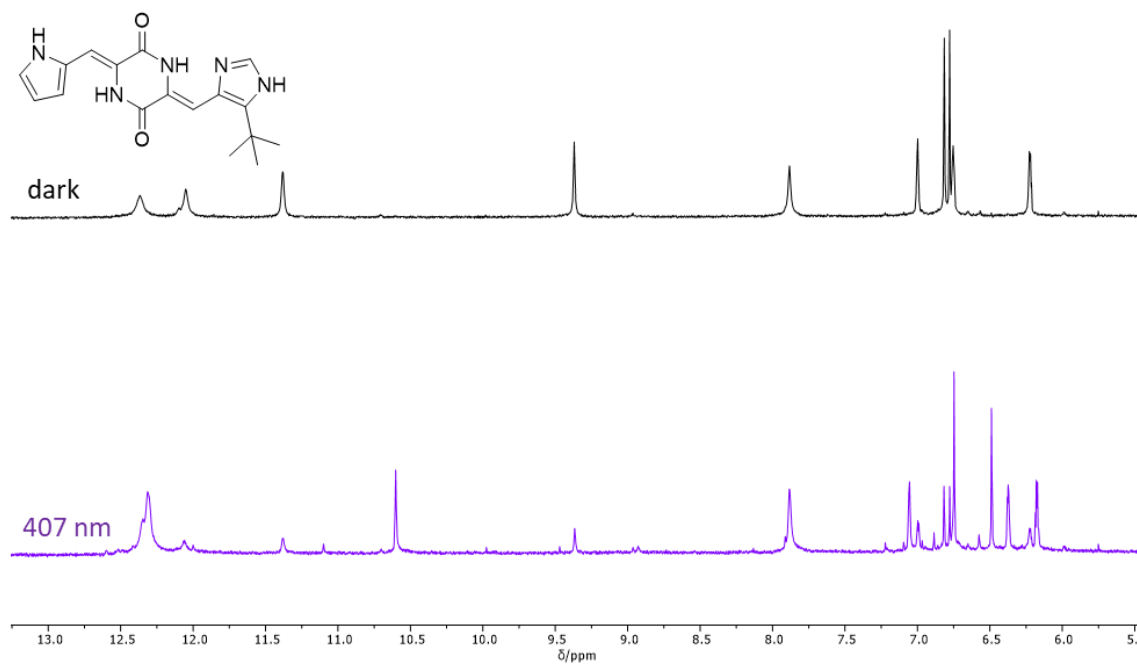
**Figure 185:** Sections of $^1$H NMR spectra (400 MHz, DMSO-$d_6$) of compound **24** in the dark (top) and after reaching the PSS upon irradiation with 407 nm.
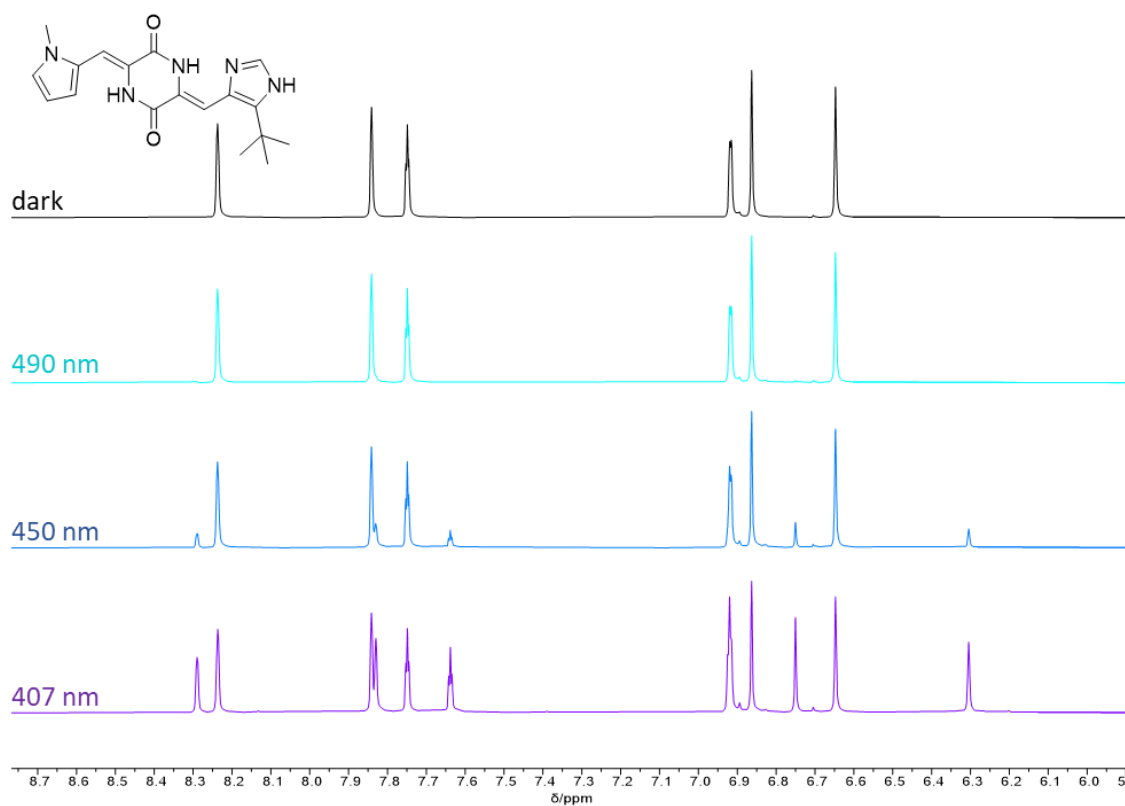


**Figure 186:** Sections of $^1$H NMR spectra (400 MHz, DMSO-$d_6$) of compound **25** in the dark (top) and after reaching the PSS upon irradiation 450 nm and 490 nm. For the sample irradiated with 407 nm the PSS was not reached.
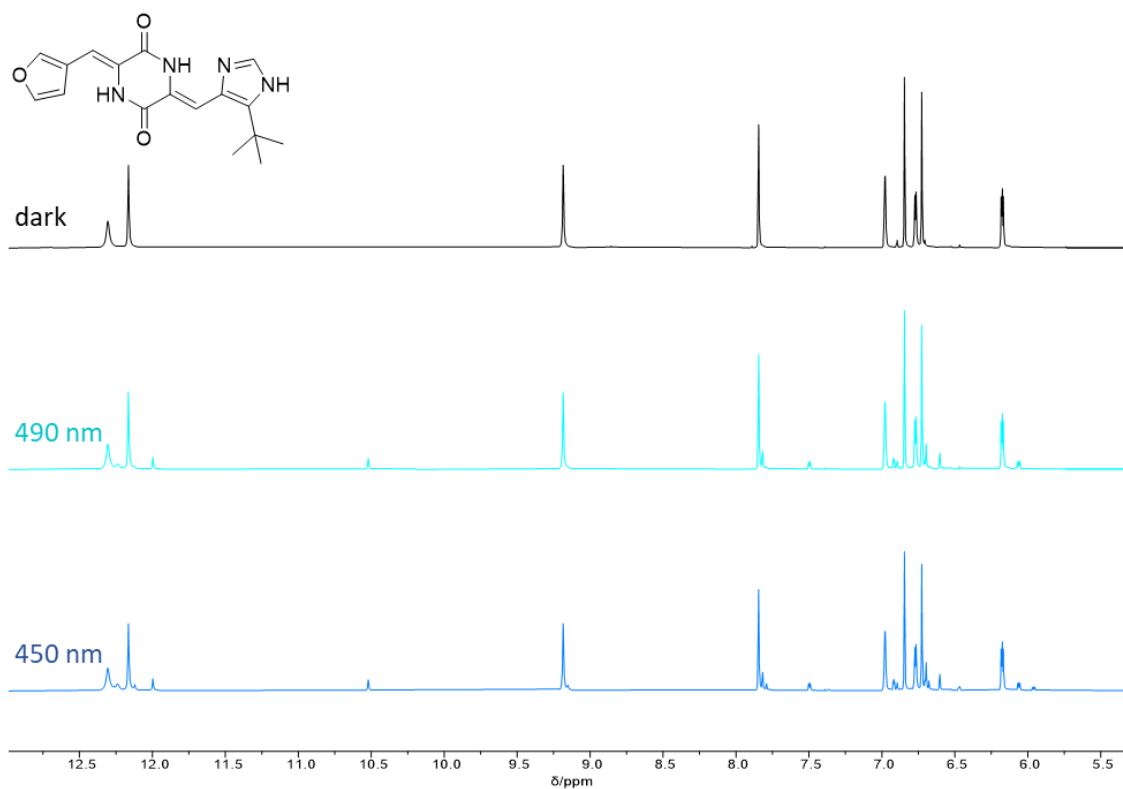
**Figure 187:** Sections of ${}^1$H NMR spectra (400 MHz, DMSO-$d_6$) of compound **26** in the dark (top) and after reaching the PSS upon irradiation with 450 nm and 490 nm.
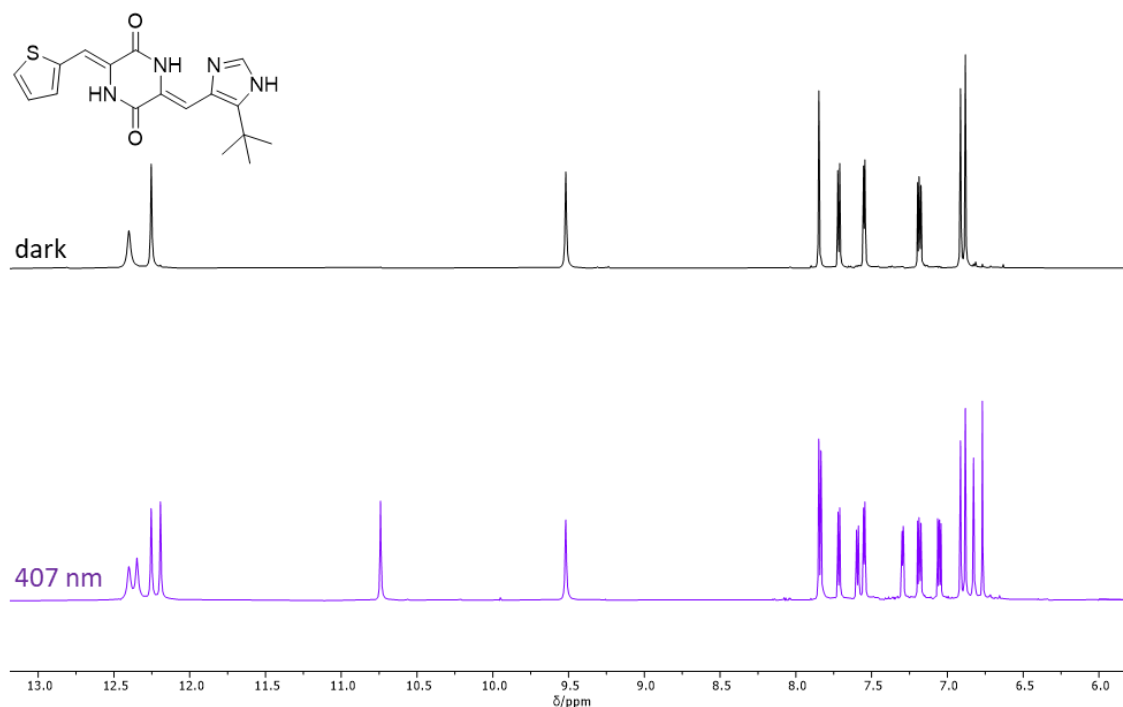


**Figure 188:** Sections of ${}^1$H NMR spectra (400 MHz, DMSO-$d_6$) of compound **27** in the dark (top) and after reaching the PSS upon irradiation with 407 nm.

### 5.4.9   Thermal Relaxation of *E*-Isomers

**a)**



**b)**



**c)**
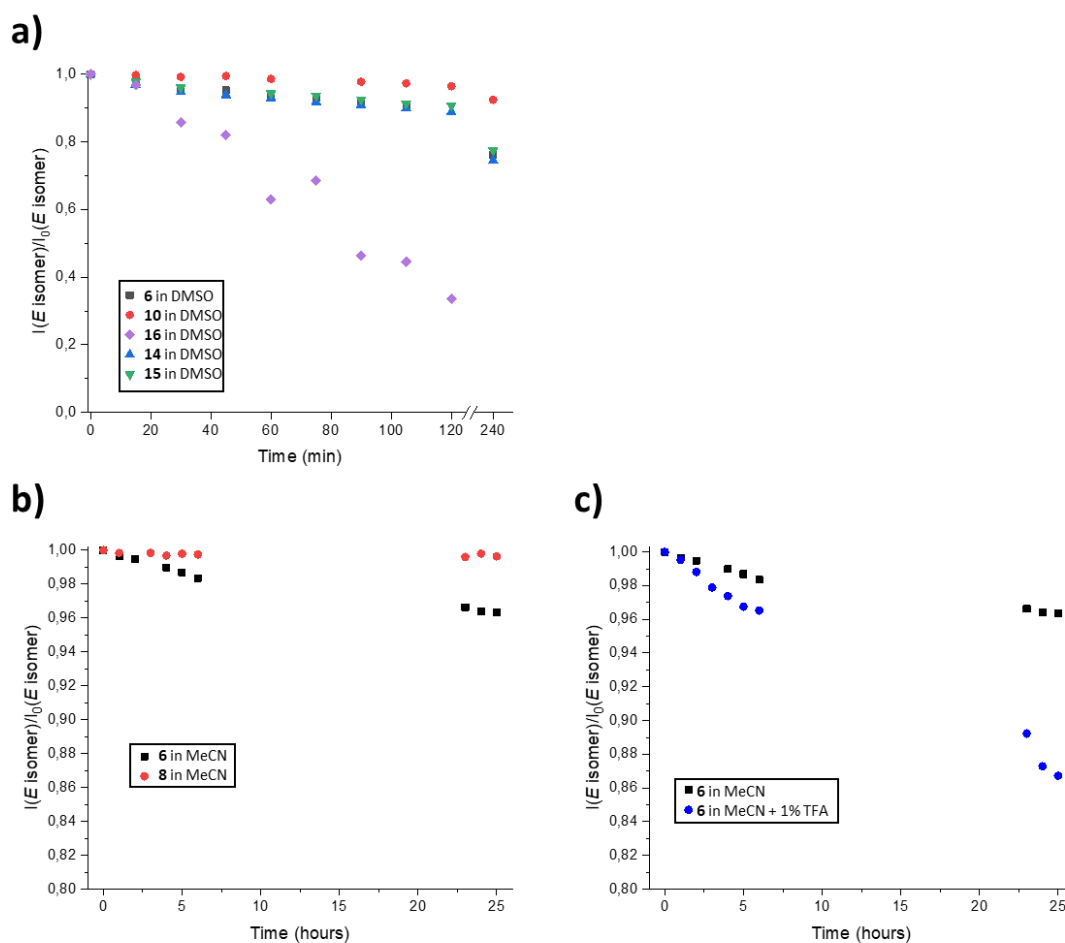


**Figure 189:** The thermal relaxation of the respective *E*-isomers of **6**, **8**, **10**, and **14**-**16** was monitored *via* analytical HPLC. The integrals of the signals assigned to the respective *E*-isomer were determined at 330 nm: $I_0$ = initial integral, I = integral at given time point. (a) Thermal relaxation in DMSO at 150 °C. (b) Thermal relaxation in MeCN at 60 °C. (c) Thermal relaxation in MeCN at 60 °C in absence and presence of TFA.
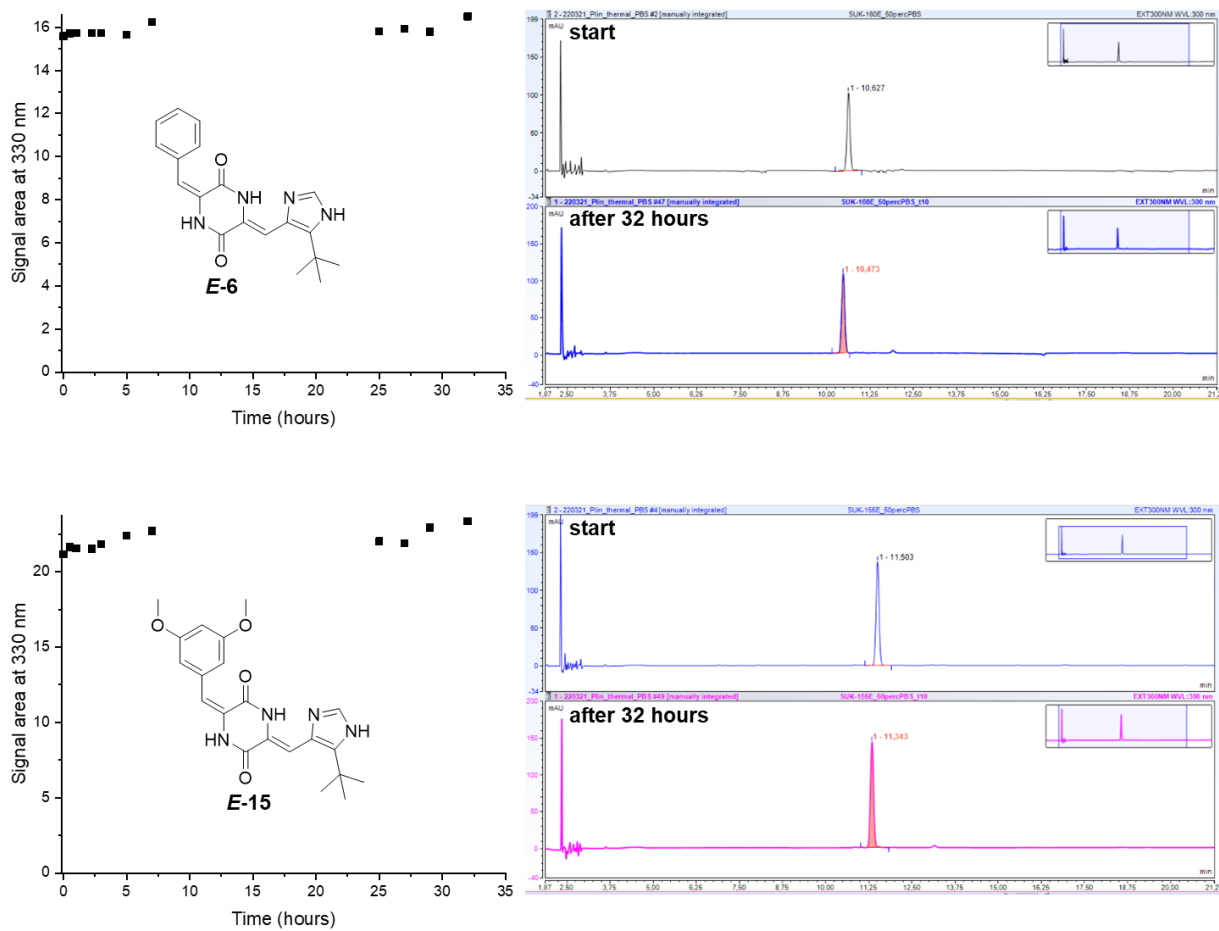
**Figure 190:** Solutions of compounds *E*-**6** (top) and *E*-**15** (bottom) in PBS/DMSO (1:1) with a concentration of 33 µM were incubated at 37 °C for 32 hours. Samples were taken after certain time intervals and analyzed *via* analytical HPLC at 330 nm.

## 5.4.10 Switching Stability
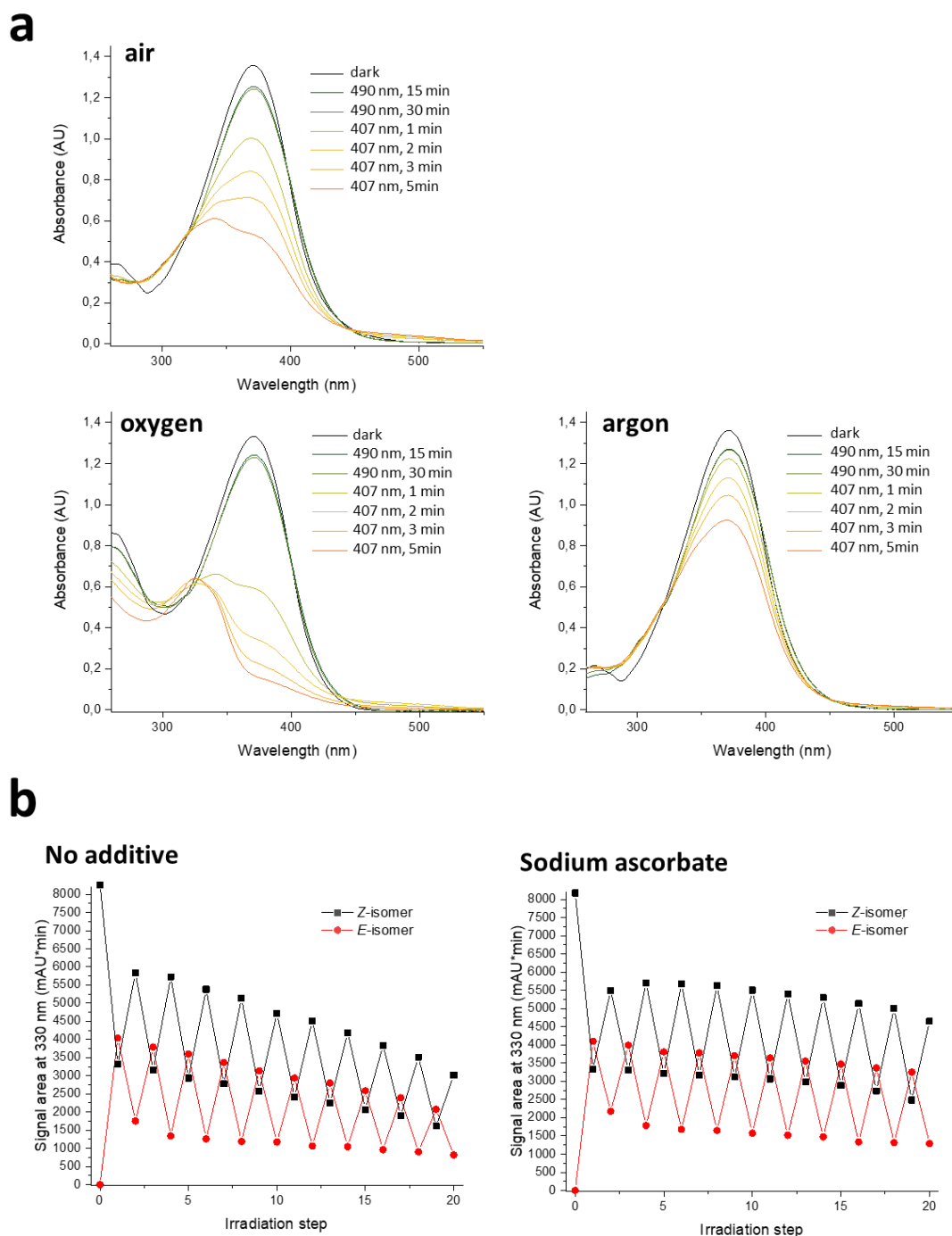


**Figure 191:** (a) A 40 µM solution of **6** in DMSO was prepared and split up into three samples. One sample was kept under ambient atmosphere (top), the other samples were purged for 5 min with oxygen (bottom left) or argon (bottom right), respectively. Absorption spectra were first recorded in the dark and then after each irradiation step. Afterwards, the samples were first irradiated twice for 15 min with 490 nm and subsequently five times for 1 min with 407 nm. (b) Solutions of pure *Z*-**6** (1.0 mM) in DMSO (left) and in a saturated solution of sodium ascorbate in DMSO (right) were analyzed *via* analytical HPLC. The samples were irradiated with 407 nm for 2 min and with 490 nm for 35 min, respectively. The irradiation cycles were repeated ten times and after every irradiation step the solutions were analyzed *via* analytical HPLC.

## 5.4.11 Stability in Presence of Glutathione
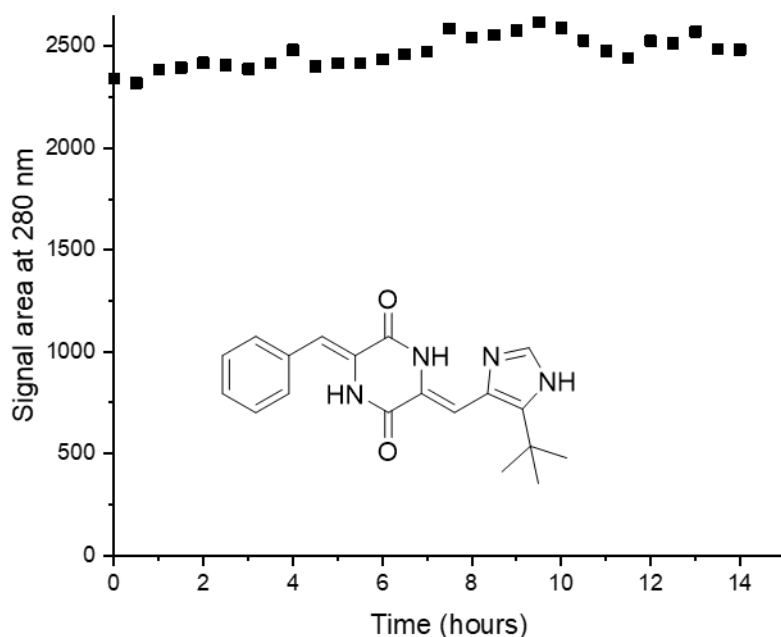


**Figure 192:** A 1.0 mM solution of **6** with 10.0 mM glutathione and 5.0 mM tris(2-carboxyethyl)phosphine in 25% PBS in DMSO (v/v) was monitored for 14 hours *via* analytical HPLC. The area of the signal assigned to **6** at 280 nm was determined after each HPLC run.

## 5.4.12 Viability Assays

*Isolated Photoisomers*

**Table 7:** The IC$_{50}$ values were determined *via* viability assays with HT-29 cells after treatment with the respective photoisomers of **6-17**, and **19-22** for 48 hours. Data were processed using GraphPad Prism.

| Compound | IC$_{50}$: *Z*-isomer (nM) [95% profile likelihood] | IC$_{50}$: *E*-isomer (nM) [95% profile likelihood] | IC$_{50}$ ratio |
|---|---|---|---|
| **6** | 0.30 [0.26 to 0.35] | 92 [80 to 100] | 306 |
| **7** | 5420 [n.d.] | 6250 [n.d.] | 1.15 |
| **8** | 0.27 [0.18 to 0.40] | 420 [347 to 510] | 1555 |
| **9** | 5.47 [3.83 to 7.83] | 75.4 [55.6 to 102] | 13.8 |
| **10** | 38 [31 to 46] | 1046 [650 to 1548] | 27.5 |

| | | | |
|---|---|---|---|
| **11** | 273<br>[253 to 301] | 1720<br>[1648 to 1786] | 6.30 |
| **12** | 14400<br>[n.d.] | 8600<br>[n.d.] | 6.14 |
| **13** | 4130000<br>[106800 to 4216000000] | 129100<br>[35220 to 3576000] | 32.0 |
| **14** | 0.09<br>[0.05 to 0.15] | 471<br>[352 to 636] | 5233 |
| **15** | 0.21<br>[0.16 to 0.28] | 618<br>[487 to 788] | 2942 |
| **16** | 8614<br>[8073 to 9189] | - | - |
| **17** | 5730<br>[n.d.] | n.d. | > 17 |
| **19** | 80.3<br>[48.8 to 132] | - | - |
| **20** | 26.7<br>[19.0 to 37.4] | 808<br>[592 to 1099] | 30.3 |
| **21** | 4.96<br>[3.46 to 7.11] | 70.4<br>[51.8 to 95.5] | 14.2 |
| **22** | 0.68<br>[0.47 to 1.01] | 73.4<br>[54.6 to 98.7] | 108 |
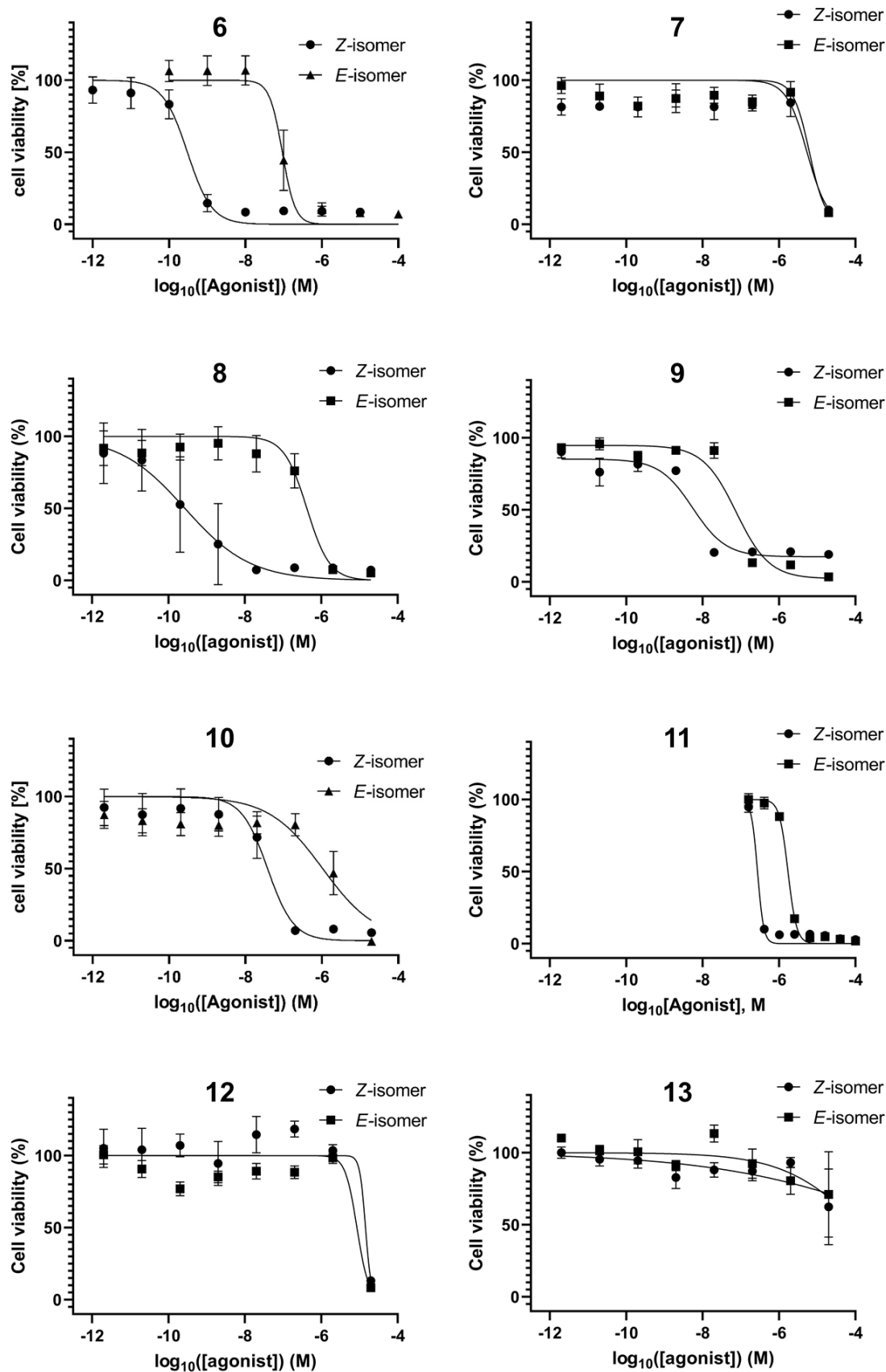
**Figure 193:** Viability of HT-29 cells after treatment with the HPLC-purified *Z*- and *E*-isomers of **6**-**13** for 48 hours. Data were plotted against the log of agonist concentration (log10([agonist]) (M)) with mean and SD values in GraphPad Prism.
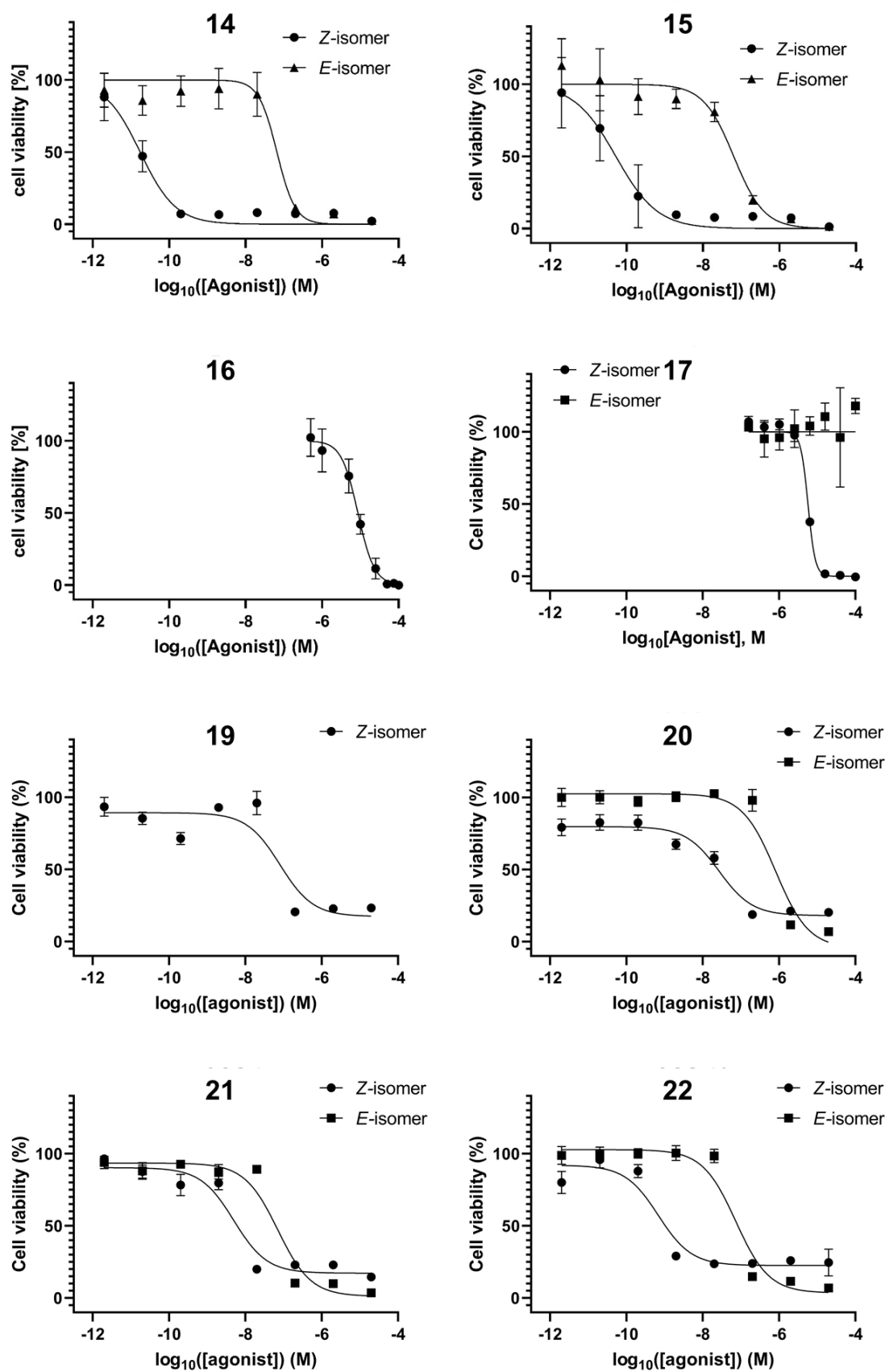
**Figure 194:** Viability of HT-29 cells after treatment with the HPLC-purified *Z*- and *E*-isomers of **14-17** and **19-22** for 48 hours. For compounds **16** and **19** the *E*-isomers were not tested. Data were plotted against the log of agonist concentration (log10([agonist]) (M)) with mean and SD values in GraphPad Prism.
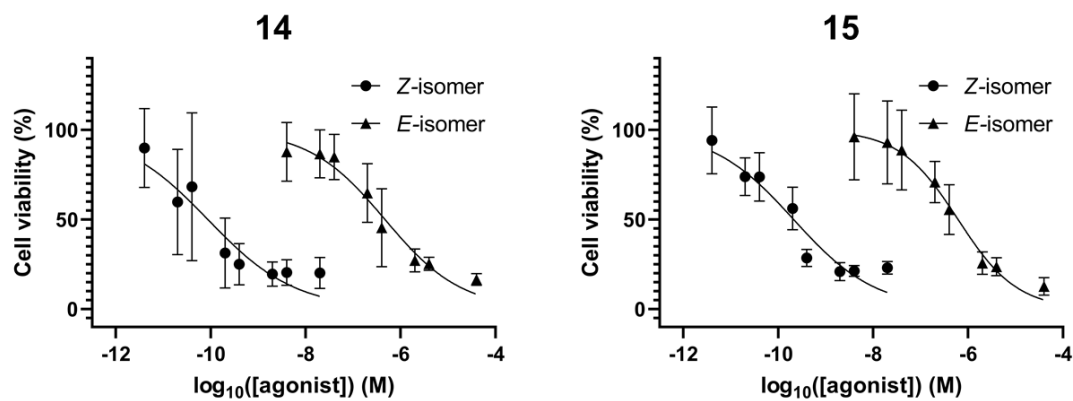
**Figure 195:** Viability of HT-29 cells after treatment with the respective photoisomers of **14** and **15** with concentrations in close range of the respective $IC_{50}$ values.

*Irradiated Samples*

**Table 8:** The IC$_{50}$ values were determined *via* viability assays with HT-29 cells after treatment with the respective mixtures of photoisomers of 1-6 for 48 hours. Before the addition to the cells DMSO solutions were irradiated with 490 nm irradiation (cyan light), 407 nm (violet light) or 365 nm (UV-light), respectively. Data were processed using GraphPad Prism.

| Compound | IC$_{50}$: PSS 490 nm (nM) [95% profile likelihood] | IC$_{50}$: PSS 407 nm (nM) [95% profile likelihood] | IC$_{50}$: PSS 365 nm (nM) [95% profile likelihood] |
|---|---|---|---|
| 6 | 4.45 [2.71 to 7.0] | 12.2 [8.79 to 16.9] | 44.9 [25.5 to 73.3] |
| 8 | 29 [22 to 40] | - | - |
| 15 | 0.34 [0.24 to 0.49] | 39.5 [29.9 to 52.1] | - |
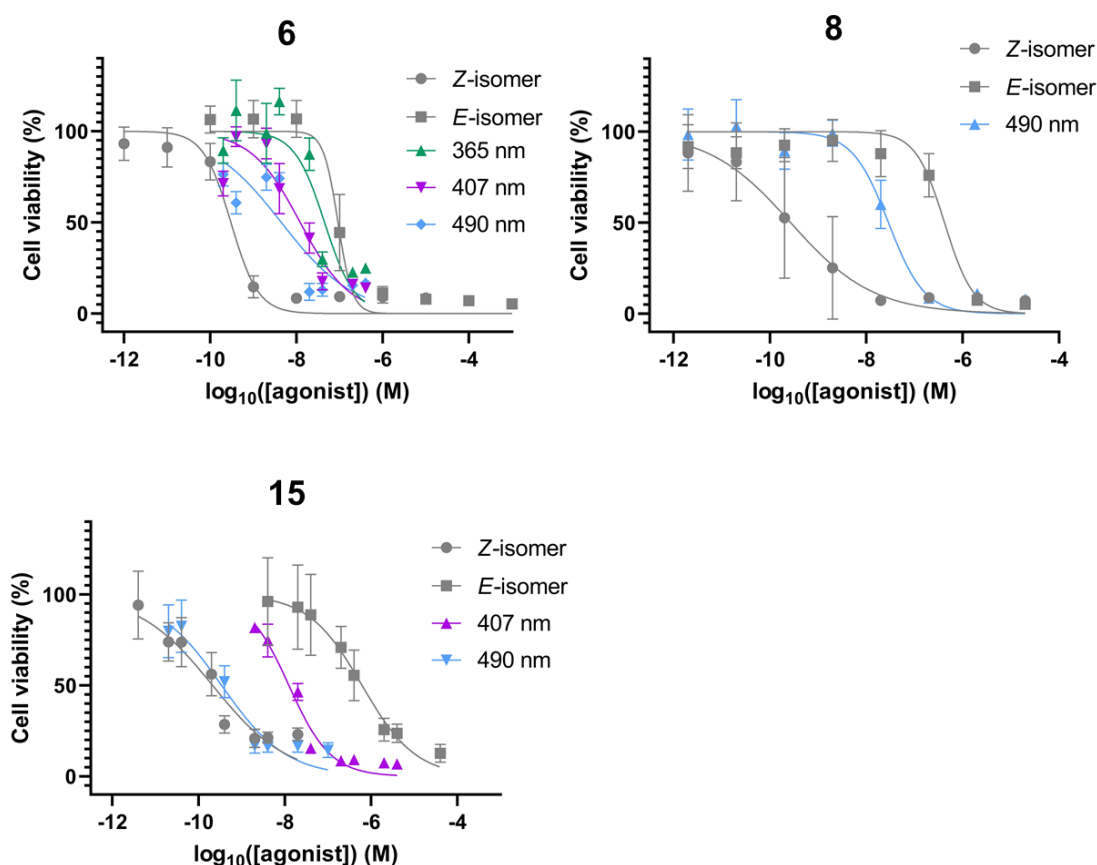


**Figure 196:** Viability of HT-29 cells after treatment with the mixture of the *E*- and *Z*-isomers generated upon equilibration under 490 nm irradiation (cyan light), 407 nm (violet light) or 365 nm (UV-light), respectively. Data were plotted against the log of agonist concentration (log$_{10}$([agonist]) (M)) with mean and SD values in GraphPad Prism. Number of independent experiments (six technical replicates per test): Non-irradiated N ≥ 2. Irradiated N = 1.

*Samples Exposed to Daylight*

**Table 9:** The $IC_{50}$ values determined *via* viability assays with HT-29 cells after treatment with the isolated photoisomers of **6**, **14** and **15** for 48 hours, as well as the results of the same procedure for samples of HPLC-purified *Z*-isomers exhibited on daylight for one day before the assay (where the content of *E*-isomer has been determined by analytical HPLC). However, incubation for further two days at daylight almost doubled the amount of *E*-isomer ($IC_{50}$ values were not determined for these samples). These data are compared with the values reported in literature (with the unknown final *Z*/*E*-isomer ratio).[100] Data were processed using GraphPad Prism.

| Compound | $IC_{50}$: *Z*-isomer (nM) [95% profile likelihood] | $IC_{50}$: *E*-isomer (nM) [95% profile likelihood] | $IC_{50}$: 1 day daylight (nM) [95% profile likelihood] | $IC_{50}$: 3 days daylight (nM) [95% profile likelihood] | $IC_{50}$: literature report [100] (nM) |
|---|---|---|---|---|---|
| **6** | 0.30 [0.26 to 0.35] | 92 [80 to 100] | 1.08 [0.66 to 1.8] (15% *E*-**6**) | n.d. (32% *E*-**6**) | 14.9 ± 3.8 |
| **14** | 0.09 [0.05 to 0.15] | 471 [352 to 636] | 1.46 [0.96 to 2.26] (21% *E*-**14**) | n.d. (34% *E*-**14**) | 26.1 ± 8.5 |
| **15** | 0.21 [0.16 to 0.28] | 618 [487 to 788] | 0.63 [0.43 to 0.94] (16% *E*-**15**) | n.d. (30% *E*-**15**) | 45.4 ± 12 |

**6**

**ambient light (14.7% *E*)**



**14**

**ambient light (20.9% *E*)**



**15**
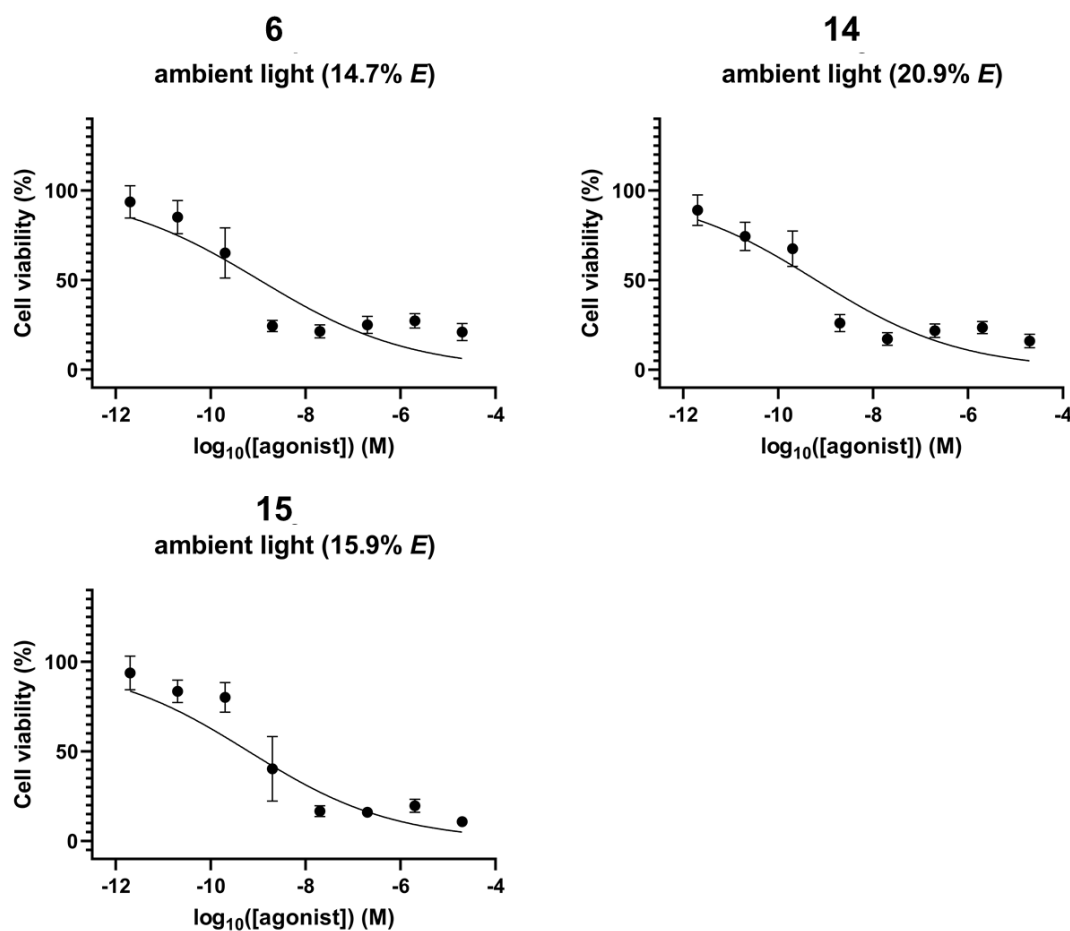
**ambient light (15.9% *E*)**



**Figure 197:** Viability of HT-29 cells after treatment with the mixtures of the respective photoisomers of **6**, **14** and **15** for 48 hours. The mixtures were obtained after incubation of DMSO solutions under ambient light for 24 hours. Data were plotted against the log of agonist concentration ($\log_{10}$([agonist]) (M)) with mean and SD values in GraphPad Prism. Number of independent experiments (six technical replicates per test): $N \geq 2$.

### 5.4.13  Immunofluorescence Assays
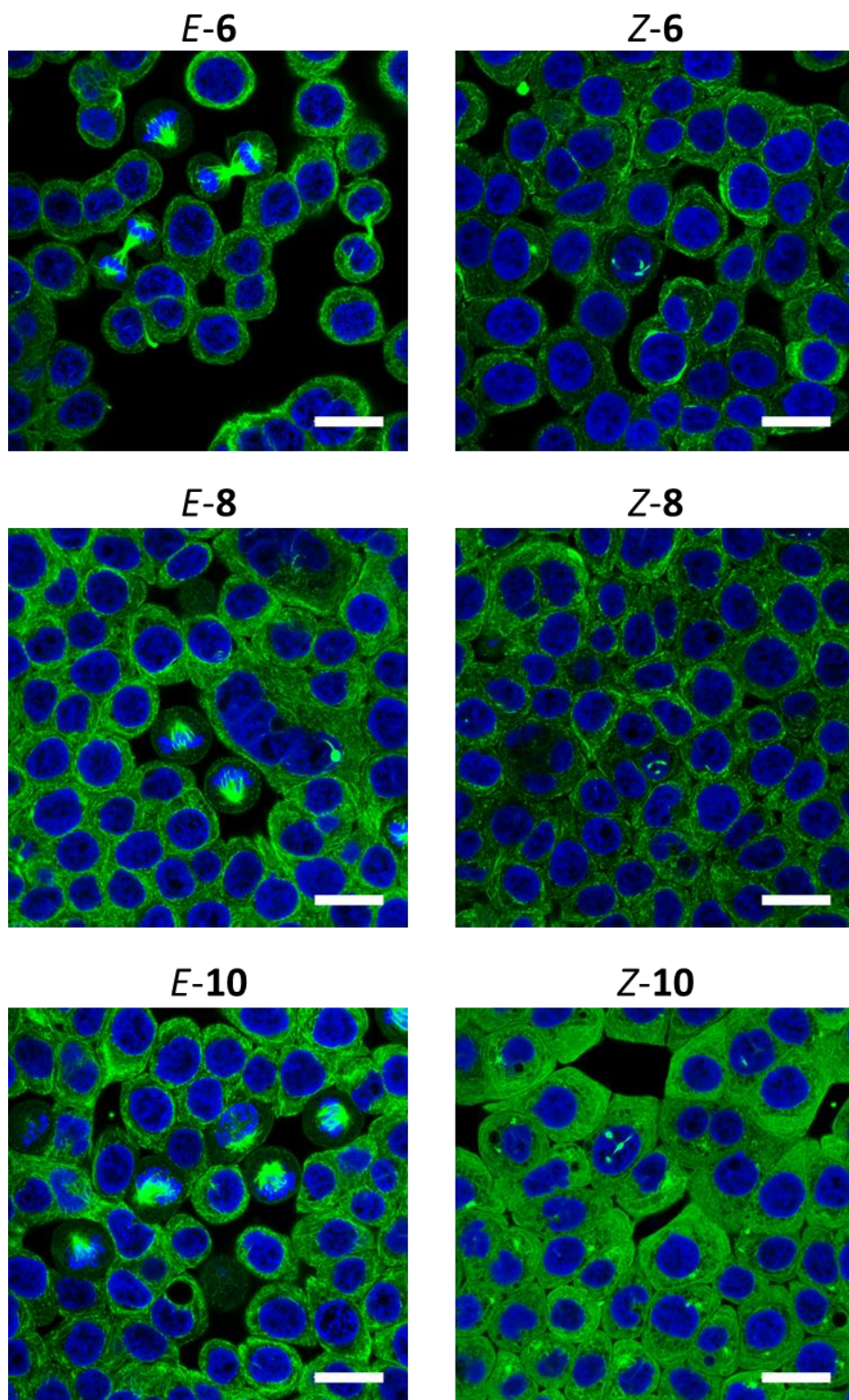


**Figure 198:** Immunofluorescence imaging of microtubule network structure with compounds **6**, **8** and **10**. Confocal microscopy assessment of cellular microtubule networks after treatment with the respective photoisomers of **6** (2 nM), **8** (20 nM) and **10** (200 nM). (HT-29 cells, 6 h treatment, green: α-tubulin stain for microtubule polymer network, blue: DAPI nuclear counterstain, all scale bars 20 µm). The results were processed and visualized with Leica Application Suite X 3.5.7.23225 from Leica Microsystems CMS GmbH.

### 5.4.14  Crystal Structure Determinations

Crystal structures in this section were measured and solved by Dr. Martin Nieger at the University of Helsinki (Finland).

The crystals of *Z*-**14** and *Z*-**15** were provided by my colleague Anna-Lena Leistner and *Z*-**12** and *Z*-**13** by Angelika Seliwjorstow while working on her bachelor thesis under my supervision.

The absolute of *Z*-**10** (SB1192_HY) was determined by refinement of Parsons' x-parameter [149]. For *Z*-**16** (SB1373_HY) and *Z*-**15** (SB1336_HY) an extinction correction was applied. In *Z*-**14** (SB1342_HY), the 3-methoxybenzylidene moiety is disordered.

**Table 10:** Overview of the numbering and sample code of crystal structures solved by Dr. Martin Nieger.

| Entry | Compound Number | Code Assigned by Dr. Martin Nieger | CCDC Number |
|:-----:|:---------------:|:----------------------------------:|:-----------:|
| 1 | *Z*-**8** | SB1177_HY | 2076713 |
| 2 | *Z*-**10** | SB1192_HY | 2076714 |
| 3 | *E*-**10** | SB1354_HY | 2076715 |
| 4 | *Z*-**12** | SB1270_HY | - |
| 5 | *Z*-**13** | SB1271_HY | - |
| 6 | *Z*-**14** | SB1342_HY | 2076717 |
| 7 | *Z*-**15** | SB1336_HY | 2076718 |
| 8 | *Z*-**16** | SB1373_HY | 2076716 |
| 9 | *Z*-**17** | SB1275_HY | - |
| 10 | *Z*-**27** | SB1492_HY | - |
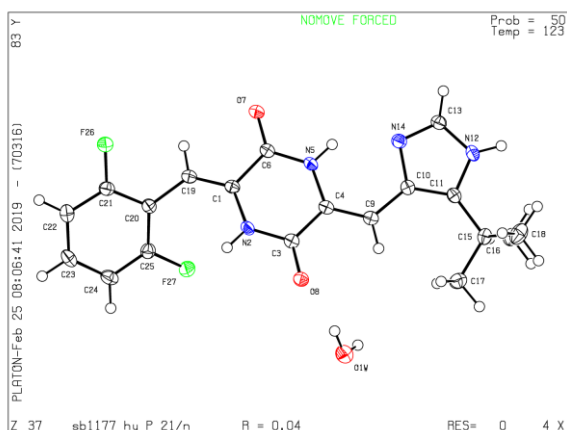
# (*Z*)-3-((5-(*tert*-butyl)-1*H*-imidazol-4-yl)methylene)-6-((*Z*)-2,6-difluorobenzylidene)-piperazine-2,5-dione hydrate – SB1177_HY

*Crystal data*

| | |
|---|---|
| $C_{19}H_{18}F_2N_4O_2 \cdot H_2O$ | $F(000) = 816$ |
| $M_r = 390.39$ | $D_x = 1.458$ Mg m$^{-3}$ |
| Monoclinic, $P2_1/n$ (*no.14*) | Cu $K\alpha$ radiation, $\lambda = 1.54178$ Å |
| $a = 7.0552$ (2) Å | Cell parameters from 8981 reflections |
| $b = 9.6541$ (3) Å | $\theta = 3.3–72.2°$ |
| $c = 26.1751$ (8) Å | $\mu = 0.97$ mm$^{-1}$ |
| $\beta = 94.157$ (2)° | $T = 123$ K |
| $V = 1778.14$ (9) Å$^3$ | Plates, yellow |
| $Z = 4$ | $0.18 \times 0.14 \times 0.02$ mm |

*Data collection*

| | |
|---|---|
| Bruker D8 VENTURE diffractometer with PhotonII CPAD detector | 3133 reflections with $I > 2\sigma(I)$ |
| Radiation source: INCOATEC microfocus sealed tube | $R_{int} = 0.037$ |
| rotation in $\phi$ and $\omega$, 1°, shutterless scans | $\theta_{max} = 72.2°$, $\theta_{min} = 3.4°$ |
| Absorption correction: multi-scan *SADABS* (Sheldrick, 2014) | $h = -8 \rightarrow 8$ |
| $T_{min} = 0.782$, $T_{max} = 0.971$ | $k = -11 \rightarrow 11$ |
| 15347 measured reflections | $l = -32 \rightarrow 32$ |
| 3502 independent reflections | |

*Refinement*

| | |
|---|---|
| Refinement on $F^2$ | Primary atom site location: dual |
| Least-squares matrix: full | Secondary atom site location: difference Fourier map |
| $R[F^2 > 2\sigma(F^2)] = 0.041$ | Hydrogen site location: difference Fourier map |
| $wR(F^2) = 0.102$ | H atoms treated by a mixture of independent and constrained refinement |
| $S = 1.09$ | $w = 1/[\sigma^2(F_o^2) + (0.0449P)^2 + 0.8261P]$ where $P = (F_o^2 + 2F_c^2)/3$ |
| 3502 reflections | $(\Delta/\sigma)_{max} = 0.001$ |
| 268 parameters | $\Delta\rangle_{max} = 0.32$ e Å$^{-3}$ |
| 6 restraints | $\Delta\rangle_{min} = -0.20$ e Å$^{-3}$ |
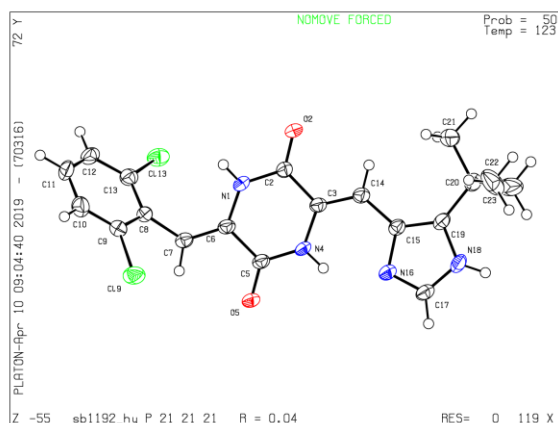
*absolute structure*
*determined crystallographically*

## (Z)-3-((5-(*tert*-butyl)-1*H*-imidazol-4-yl)methylene)-6-((Z)-2,6-dichlorobenzylidene)-piperazine-2,5-dione SB1192_HY

### Crystal data

| | |
|---|---|
| $C_{19}H_{18}Cl_2N_4O_2$ | $D_x = 1.422$ Mg m$^{-3}$ |
| $M_r = 405.27$ | Cu $K\alpha$ radiation, $\lambda = 1.54178$ Å |
| Orthorhombic, $P2_12_12_1$ (no.19) | Cell parameters from 5481 reflections |
| $a = 7.7969$ (3) Å | $\theta = 4.0–71.9°$ |
| $b = 14.3794$ (6) Å | $\mu = 3.28$ mm$^{-1}$ |
| $c = 16.8804$ (7) Å | $T = 123$ K |
| $V = 1892.54$ (13) Å$^3$ | Rods, yellow |
| $Z = 4$ | $0.16 \times 0.06 \times 0.02$ mm |
| $F(000) = 840$ | |

### Data collection

| | |
|---|---|
| Bruker D8 VENTURE diffractometer with PhotonII CPAD detector | 3264 reflections with $I > 2\sigma(I)$ |
| Radiation source: INCOATEC microfocus sealed tube | $R_{int} = 0.066$ |
| rotation in $\phi$ and $\omega$, 1°, shutterless scans | $\theta_{max} = 72.2°$, $\theta_{min} = 4.0°$ |
| Absorption correction: multi-scan *SADABS* (Sheldrick, 2014) | $h = -9 \rightarrow 9$ |
| $T_{min} = 0.684$, $T_{max} = 0.841$ | $k = -17 \rightarrow 17$ |
| 15438 measured reflections | $l = -20 \rightarrow 19$ |
| 3736 independent reflections | |

### Refinement

| | |
|---|---|
| Refinement on $F^2$ | Secondary atom site location: difference Fourier map |
| Least-squares matrix: full | Hydrogen site location: difference Fourier map |
| $R[F^2 > 2\sigma(F^2)] = 0.044$ | H atoms treated by a mixture of independent and constrained refinement |
| $wR(F^2) = 0.102$ | $w = 1/[\sigma^2(F_o^2) + (0.0551P)^2]$ where $P = (F_o^2 + 2F_c^2)/3$ |
| $S = 1.06$ | $(\Delta/\sigma)_{max} < 0.001$ |
| 3736 reflections | $\Delta\rangle_{max} = 0.27$ e Å$^{-3}$ |
| 253 parameters | $\Delta\rangle_{min} = -0.20$ e Å$^{-3}$ |
| 3 restraints | Absolute structure: Flack x determined using 1190 quotients [(I+)-(I-)]/[(I+)+(I-)] (Parsons, Flack and Wagner, Acta Cryst. B69 (2013) 249-259). |
| Primary atom site location: dual | Absolute structure parameter: 0.013 (13) |
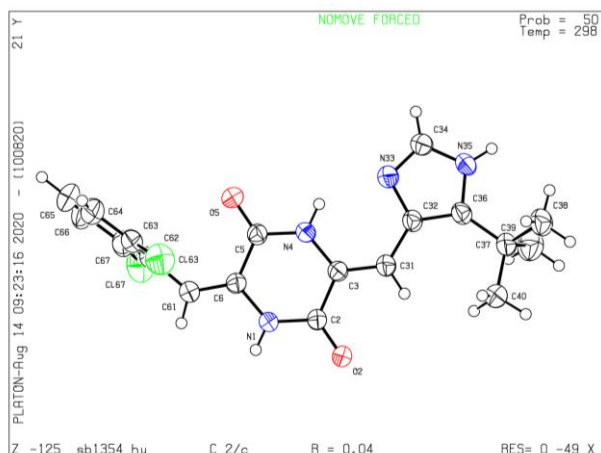
# SB1354_HY

## SUK-158 switched



## (Z)-3-((5-(*tert*-butyl)-1*H*-imidazol-4-yl)methylene)-6-((*E*)-2,6-dichlorobenzylidene)-piperazine-2,5-dione – SB1354_HY

### *Crystal data*

| | |
|---|---|
| $C_{19}H_{18}Cl_2N_4O_2$ | $F(000) = 1680$ |
| $M_r = 405.27$ | $D_x = 1.436$ Mg m$^{-3}$ |
| Monoclinic, $C2/c$ (*no.15*) | Cu $K\alpha$ radiation, $\lambda = 1.54178$ Å |
| $a = 27.8992$ (10) Å | Cell parameters from 8711 reflections |
| $b = 10.2709$ (4) Å | $\theta = 3.5–71.6°$ |
| $c = 14.6321$ (5) Å | $\mu = 3.31$ mm$^{-1}$ |
| $\beta = 116.603$ (2)° | $T = 298$ K |
| $V = 3748.9$ (2)  Å$^3$ | Plates, yellow |
| $Z = 8$ | $0.15 \times 0.05 \times 0.03$ mm |

### *Data collection*

| | |
|---|---|
| Bruker D8 VENTURE diffractometer with PhotonII CPAD detector | 3057 reflections with $I > 2\sigma(I)$ |
| Radiation source: INCOATEC microfocus sealed tube | $R_{int} = 0.039$ |
| rotation in $\phi$ and $\omega$, 1°, shutterless scans | $\theta_{max} = 72.4°$, $\theta_{min} = 3.5°$ |
| Absorption correction: multi-scan *SADABS* (Sheldrick, 2014) | $h = -34 \rightarrow 34$ |
| $T_{min} = 0.730$, $T_{max} = 0.915$ | $k = -12 \rightarrow 12$ |
| 21109 measured reflections | $l = -16 \rightarrow 18$ |
| 3705 independent reflections | |

### *Refinement*

| | |
|---|---|
| Refinement on $F^2$ | Primary atom site location: dual |
| Least-squares matrix: full | Secondary atom site location: difference Fourier map |
| $R[F^2 > 2\sigma(F^2)] = 0.041$ | Hydrogen site location: difference Fourier map |
| $wR(F^2) = 0.103$ | H atoms treated by a mixture of independent and constrained refinement |
| $S = 1.03$ | $w = 1/[\sigma^2(F_o^2) + (0.0417P)^2 + 3.5483P]$ where $P = (F_o^2 + 2F_c^2)/3$ |
| 3705 reflections | $(\Delta/\sigma)_{max} < 0.001$ |
| 253 parameters | $\Delta\rangle_{max} = 0.28$ e Å$^{-3}$ |
| 219 restraints | $\Delta\rangle_{min} = -0.39$ e Å$^{-3}$ |
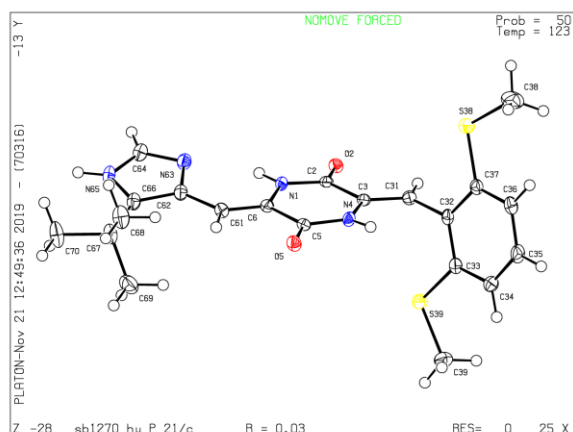
## SB1270_HY

### ANS-18

## (Z)-3-((Z)-2,6-bis(methylthio)benzylidene)-6-((5-(*tert*-butyl)-1*H*-imidazol-4-yl)methylene)-piperazine-2,5-dione – SB1270_HY

### *Crystal data*

| | |
|---|---|
| $C_{21}H_{24}N_4O_2S_2$ | $F(000) = 904$ |
| $M_r = 428.56$ | $D_x = 1.331$ Mg m$^{-3}$ |
| Monoclinic, $P2_1/c$ (*no.14*) | Cu $K\alpha$ radiation, $\lambda = 1.54178$ Å |
| $a = 15.5291$ (4) Å | Cell parameters from 9908 reflections |
| $b = 14.8828$ (4) Å | $\theta = 2.8–72.2°$ |
| $c = 9.3549$ (3) Å | $\mu = 2.46$ mm$^{-1}$ |
| $\beta = 98.333$ (1)° | $T = 123$ K |
| $V = 2139.25$ (11) Å$^3$ | Plates, colourless |
| $Z = 4$ | $0.16 \times 0.06 \times 0.02$ mm |

### *Data collection*

| | |
|---|---|
| Bruker D8 VENTURE diffractometer with PhotonII CPAD detector | 3917 reflections with $I > 2\sigma(I)$ |
| Radiation source: INCOATEC microfocus sealed tube | $R_{int} = 0.025$ |
| rotation in $\phi$ and $\omega$, 1°, shutterless scans | $\theta_{max} = 72.2°$, $\theta_{min} = 2.9°$ |
| Absorption correction: multi-scan *SADABS* (Sheldrick, 2014) | $h = -19 \rightarrow 19$ |
| $T_{min} = 0.813$, $T_{max} = 0.929$ | $k = -18 \rightarrow 18$ |
| 23307 measured reflections | $l = -11 \rightarrow 11$ |
| 4223 independent reflections | |

### *Refinement*

| | |
|---|---|
| Refinement on $F^2$ | Primary atom site location: dual |
| Least-squares matrix: full | Secondary atom site location: difference Fourier map |
| $R[F^2 > 2\sigma(F^2)] = 0.030$ | Hydrogen site location: difference Fourier map |
| $wR(F^2) = 0.081$ | H atoms treated by a mixture of independent and constrained refinement |
| $S = 1.06$ | $w = 1/[\sigma^2(F_o^2) + (0.0447P)^2 + 0.8133P]$ where $P = (F_o^2 + 2F_c^2)/3$ |
| 4223 reflections | $(\Delta/\sigma)_{max} = 0.001$ |
| 273 parameters | $\Delta\rangle_{max} = 0.30$ e Å$^{-3}$ |
| 3 restraints | $\Delta\rangle_{min} = -0.21$ e Å$^{-3}$ |

**SB1271_HY**

**ANS-09**

*with 0.5 water/molecule*
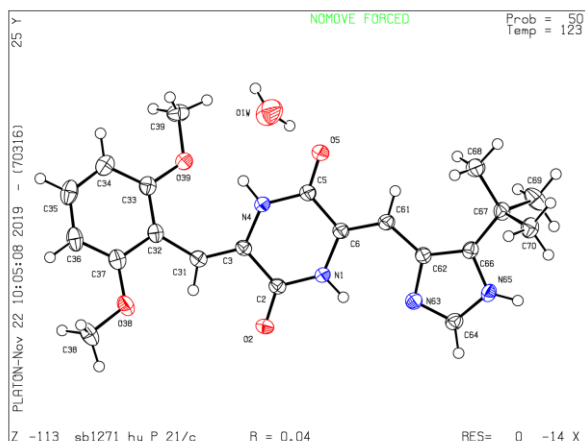
# (Z)-3-((5-(*tert*-butyl)-1*H*-imidazol-4-yl)methylene)-6-((Z)-2,6-dimethoxybenzylidene)-piperazine-2,5-dione – SB1271_HY

***Crystal data***

| | |
|---|---|
| $C_{21}H_{24}N_4O_4 \cdot 0.5(H_2O)$ | $F(000) = 860$ |
| $M_r = 405.45$ | $D_x = 1.324$ Mg m$^{-3}$ |
| Monoclinic, $P2_1/c$ *(no.14)* | Cu $K\alpha$ radiation, $\lambda = 1.54178$ Å |
| $a = 11.7919$ (3) Å | Cell parameters from 9886 reflections |
| $b = 15.6508$ (4) Å | $\theta = 4.2–72.2°$ |
| $c = 12.4266$ (3) Å | $\mu = 0.78$ mm$^{-1}$ |
| $\beta = 117.473$ (1)° | $T = 123$ K |
| $V = 2034.73$ (9)  Å$^3$ | Plates, yellow |
| $Z = 4$ | $0.18 \times 0.14 \times 0.04$ mm |

***Data collection***

| | |
|---|---|
| Bruker D8 VENTURE diffractometer with PhotonII CPAD detector | 3487 reflections with $I > 2\sigma(I)$ |
| Radiation source: INCOATEC microfocus sealed tube | $R_{int} = 0.039$ |
| rotation in $\phi$ and $\omega$, 1°, shutterless scans | $\theta_{max} = 72.3°$, $\theta_{min} = 4.2°$ |
| Absorption correction: multi-scan *SADABS* (Sheldrick, 2014) | $h = -14 \rightarrow 13$ |
| $T_{min} = 0.830$, $T_{max} = 0.971$ | $k = -19 \rightarrow 19$ |
| 22602 measured reflections | $l = -15 \rightarrow 15$ |
| 4030 independent reflections | |

***Refinement***

| | |
|---|---|
| Refinement on $F^2$ | Primary atom site location: dual |
| Least-squares matrix: full | Secondary atom site location: difference Fourier map |
| $R[F^2 > 2\sigma(F^2)] = 0.038$ | Hydrogen site location: difference Fourier map |
| $wR(F^2) = 0.099$ | H atoms treated by a mixture of independent and constrained refinement |
| $S = 1.03$ | $w = 1/[\sigma^2(F_o^2) + (0.0452P)^2 + 0.8125P]$ where $P = (F_o^2 + 2F_c^2)/3$ |
| 4030 reflections | $(\Delta/\sigma)_{max} = 0.001$ |
| 288 parameters | $\Delta\rangle_{max} = 0.27$ e Å$^{-3}$ |
| 5 restraints | $\Delta\rangle_{min} = -0.22$ e Å$^{-3}$ |
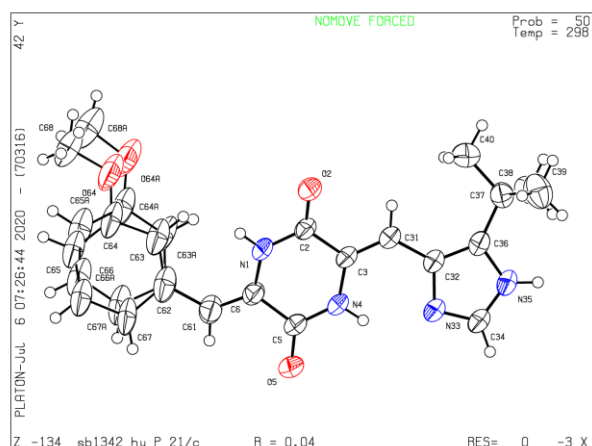
## ALL-52

### *3-methoxybenzylidene moiety disordered*

## (Z)-3-((5-(*tert*-butyl)-1*H*-imidazol-4-yl)methylene)-6-((Z)-3-methoxybenzylidene)-piperazine-2,5-dione – SB1342_HY

### *Crystal data*

| | |
|---|---|
| $C_{20}H_{22}N_4O_3$ | $F(000) = 776$ |
| $M_r = 366.41$ | $D_x = 1.248$ Mg m$^{-3}$ |
| Monoclinic, $P2_1/c$ (no.14) | Cu $K\alpha$ radiation, $\lambda = 1.54178$ Å |
| $a = 11.5196$ (2) Å | Cell parameters from 9090 reflections |
| $b = 14.6170$ (2) Å | $\theta = 4.9–72.1°$ |
| $c = 11.8196$ (2) Å | $\mu = 0.70$ mm$^{-1}$ |
| $\beta = 101.496$ (1)° | $T = 298$ K |
| $V = 1950.28$ (5) Å$^3$ | Blocks, yellow |
| $Z = 4$ | $0.36 \times 0.24 \times 0.12$ mm |

### *Data collection*

| | |
|---|---|
| Bruker D8 VENTURE diffractometer with PhotonII CPAD detector | 3513 reflections with $I > 2\sigma(I)$ |
| Radiation source: INCOATEC microfocus sealed tube | $R_{int} = 0.024$ |
| rotation in $\phi$ and $\omega$, 1°, shutterless scans | $\theta_{max} = 72.2°$, $\theta_{min} = 3.9°$ |
| Absorption correction: multi-scan | $h = -14 \rightarrow 14$ |
| $T_{min} = 0.786$, $T_{max} = 0.915$ | $k = -18 \rightarrow 17$ |
| 25765 measured reflections | $l = -14 \rightarrow 13$ |
| 3836 independent reflections | |

### *Refinement*

| | |
|---|---|
| Refinement on $F^2$ | Primary atom site location: dual |
| Least-squares matrix: full | Secondary atom site location: difference Fourier map |
| $R[F^2 > 2\sigma(F^2)] = 0.044$ | Hydrogen site location: mixed |
| $wR(F^2) = 0.130$ | H atoms treated by a mixture of independent and constrained refinement |
| $S = 1.03$ | $w = 1/[\sigma^2(F_o^2) + (0.0744P)^2 + 0.3731P]$ where $P = (F_o^2 + 2F_c^2)/3$ |
| 3836 reflections | $(\Delta/\sigma)_{max} < 0.001$ |
| 318 parameters | $\Delta\rangle_{max} = 0.21$ e Å$^{-3}$ |
| 646 restraints | $\Delta\rangle_{min} = -0.18$ e Å$^{-3}$ |
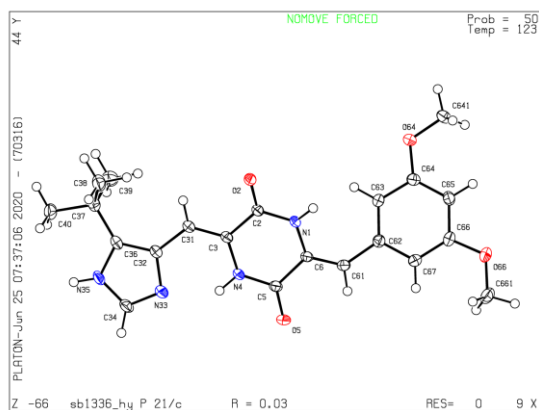
**(*Z*)-3-((5-(*tert*-butyl)-1*H*-imidazol-4-yl)methylene)-6-((*Z*)-3,5-dimethoxybenzylidene)-piperazine-2,5-dione – SB1336_HY**

*Crystal data*

| | |
|---|---|
| $C_{21}H_{24}N_4O_4$ | $F(000) = 840$ |
| $M_r = 396.44$ | $D_x = 1.325$ Mg m$^{-3}$ |
| Monoclinic, $P2_1/c$ *(no.14)* | Cu $K\alpha$ radiation, $\lambda = 1.54178$ Å |
| $a = 11.2851$ (4) Å | Cell parameters from 9792 reflections |
| $b = 15.2971$ (5) Å | $\theta = 4.9$–$72.1°$ |
| $c = 11.6703$ (4) Å | $\mu = 0.77$ mm$^{-1}$ |
| $\beta = 99.474$ (1)° | $T = 123$ K |
| $V = 1987.16$ (12)  Å$^3$ | Blocks, yellow |
| $Z = 4$ | $0.14 \times 0.10 \times 0.06$ mm |

*Data collection*

| | |
|---|---|
| Bruker D8 VENTURE diffractometer with PhotonII CPAD detector | 3736 reflections with $I > 2\sigma(I)$ |
| Radiation source: INCOATEC microfocus sealed tube | $R_{int} = 0.027$ |
| rotation in $\phi$ and $\omega$, 1°, shutterless scans | $\theta_{max} = 72.3°$, $\theta_{min} = 4.0°$ |
| Absorption correction: multi-scan *SADABS* (Sheldrick, 2014) | $h = -13 \rightarrow 13$ |
| $T_{min} = 0.879$, $T_{max} = 0.958$ | $k = -18 \rightarrow 17$ |
| 29490 measured reflections | $l = -13 \rightarrow 14$ |
| 3924 independent reflections | |

*Refinement*

| | |
|---|---|
| Refinement on $F^2$ | Secondary atom site location: difference Fourier map |
| Least-squares matrix: full | Hydrogen site location: difference Fourier map |
| $R[F^2 > 2\sigma(F^2)] = 0.032$ | H atoms treated by a mixture of independent and constrained refinement |
| $wR(F^2) = 0.085$ | $w = 1/[\sigma^2(F_o^2) + (0.041P)^2 + 0.7398P]$ where $P = (F_o^2 + 2F_c^2)/3$ |
| $S = 1.03$ | $(\Delta/\sigma)_{max} = 0.001$ |
| 3924 reflections | $\Delta\rangle_{max} = 0.30$ e Å$^{-3}$ |
| 274 parameters | $\Delta\rangle_{min} = -0.18$ e Å$^{-3}$ |
| 3 restraints | Extinction correction: *SHELXL2014*/7 (Sheldrick 2014), Fc$^*$=kFc[1+0.001xFc$^2\lambda^3$/sin(2$\theta$)]$^{-1/4}$ |
| Primary atom site location: dual | Extinction coefficient: 0.0010 (2) |
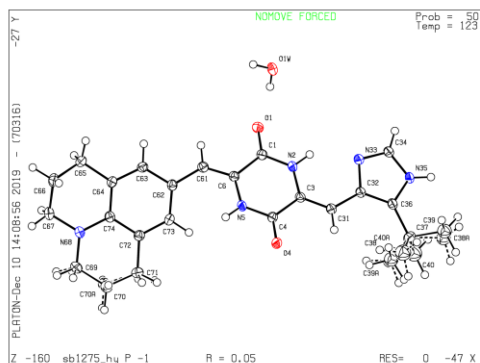
# (3Z,6Z)-3-((5-(*tert*-butyl)-1*H*-imidazol-4-yl)methylene)-6-((2,3,6,7-tetrahydro-1*H*,5*H*-pyrido[3,2,1-ij]quinolin-9-yl)methylene)piperazine-2,5-dione SB1275_HY

*Crystal data*

| | |
|---|---|
| $C_{25}H_{29}N_5O_2 \cdot H_2O$ | $Z = 2$ |
| $M_r = 449.55$ | $F(000) = 480$ |
| Triclinic, $P$-1 (no.2) | $D_x = 1.304$ Mg m$^{-3}$ |
| $a = 10.9039$ (4) Å | Cu $K\alpha$ radiation, $\lambda = 1.54178$ Å |
| $b = 11.3091$ (4) Å | Cell parameters from 9906 reflections |
| $c = 11.9916$ (4) Å | $\theta = 4.2–72.1°$ |
| $\alpha = 116.003$ (1)° | $\mu = 0.71$ mm$^{-1}$ |
| $\beta = 91.840$ (1)° | $T = 123$ K |
| $\gamma = 116.213$ (1)° | Plates, orange |
| $V = 1144.66$ (7)  Å$^3$ | $0.18 \times 0.08 \times 0.04$ mm |

*Data collection*

| | |
|---|---|
| Bruker D8 VENTURE diffractometer with PhotonII CPAD detector | 4239 reflections with $I > 2\sigma(I)$ |
| Radiation source: INCOATEC microfocus sealed tube | $R_{int} = 0.022$ |
| rotation in $\phi$ and $\omega$, 1°, shutterless scans | $\theta_{max} = 72.3°$, $\theta_{min} = 4.3°$ |
| Absorption correction: multi-scan *SADABS* (Sheldrick, 2014) | $h = -13 \rightarrow 13$ |
| $T_{min} = 0.865$, $T_{max} = 0.971$ | $k = -13 \rightarrow 13$ |
| 18554 measured reflections | $l = -14 \rightarrow 14$ |
| 4488 independent reflections | |

*Refinement*

| | |
|---|---|
| Refinement on $F^2$ | Secondary atom site location: difference Fourier map |
| Least-squares matrix: full | Hydrogen site location: mixed |
| $R[F^2 > 2\sigma(F^2)] = 0.050$ | H atoms treated by a mixture of independent and constrained refinement |
| $wR(F^2) = 0.118$ | $w = 1/[\sigma^2(F_o^2) + (0.042P)^2 + 1.1534P]$ where $P = (F_o^2 + 2F_c^2)/3$ |
| $S = 1.02$ | $(\Delta/\sigma)_{max} < 0.001$ |
| 4488 reflections | $\Delta\rangle_{max} = 0.67$ e Å$^{-3}$ |
| 308 parameters | $\Delta\rangle_{min} = -0.61$ e Å$^{-3}$ |
| 59 restraints | Extinction correction: *SHELXL2014*/7 (Sheldrick 2014), Fc$^*$=kFc[1+0.001xFc$^2\lambda^3$/sin(2$\theta$)]$^{-1/4}$ |
| Primary atom site location: dual | Extinction coefficient: 0.0026 (5) |
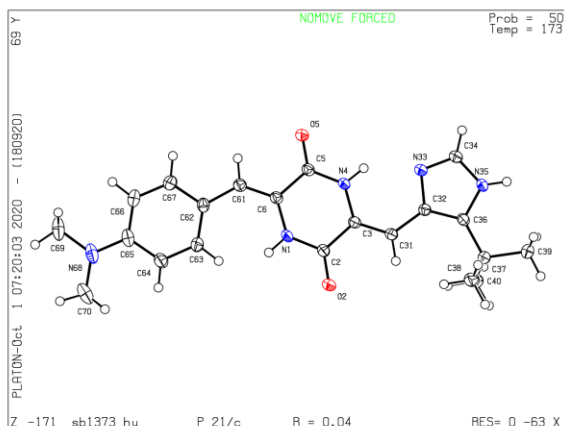
## (*Z*)-3-((5-(*tert*-butyl)-1*H*-imidazol-4-yl)methylene)-6-((*Z*)-4-(dimethylamino)benzylidene) piperazine-2,5-dione – SB1373_HY

### *Crystal data*

| | |
|---|---|
| $C_{21}H_{25}N_5O_2$ | $F(000) = 808$ |
| $M_r = 379.46$ | $D_x = 1.329$ Mg m$^{-3}$ |
| Monoclinic, $P2_1/c$ (*no.14*) | Cu $K\alpha$ radiation, $\lambda = 1.54178$ Å |
| $a = 7.2824$ (2) Å | Cell parameters from 9933 reflections |
| $b = 14.1512$ (4) Å | $\theta = 3.9–72.1°$ |
| $c = 18.4592$ (5) Å | $\mu = 0.71$ mm$^{-1}$ |
| $\beta = 94.740$ (1)° | $T = 173$ K |
| $V = 1895.80$ (9) Å$^3$ | Plates, orange |
| $Z = 4$ | $0.15 \times 0.09 \times 0.03$ mm |

### *Data collection*

| | |
|---|---|
| Bruker D8 VENTURE diffractometer with PhotonII CPAD detector | 3420 reflections with $I > 2\sigma(I)$ |
| Radiation source: INCOATEC microfocus sealed tube | $R_{int} = 0.026$ |
| rotation in $\phi$ and $\omega$, 1°, shutterless scans | $\theta_{max} = 72.1°$, $\theta_{min} = 3.9°$ |
| Absorption correction: multi-scan *SADABS* (Sheldrick, 2014) | $h = -8 \rightarrow 8$ |
| $T_{min} = 0.876$, $T_{max} = 0.971$ | $k = -17 \rightarrow 16$ |
| 22924 measured reflections | $l = -22 \rightarrow 22$ |
| 3722 independent reflections | |

### *Refinement*

| | |
|---|---|
| Refinement on $F^2$ | Secondary atom site location: difference Fourier map |
| Least-squares matrix: full | Hydrogen site location: difference Fourier map |
| $R[F^2 > 2\sigma(F^2)] = 0.036$ | H atoms treated by a mixture of independent and constrained refinement |
| $wR(F^2) = 0.093$ | $w = 1/[\sigma^2(F_o^2) + (0.0443P)^2 + 0.7553P]$ where $P = (F_o^2 + 2F_c^2)/3$ |
| $S = 1.03$ | $(\Delta/\sigma)_{max} = 0.001$ |
| 3722 reflections | $\Delta\rangle_{max} = 0.25$ e Å$^{-3}$ |
| 265 parameters | $\Delta\rangle_{min} = -0.17$ e Å$^{-3}$ |
| 3 restraints | Extinction correction: *SHELXL2014*/7 (Sheldrick 2014), Fc$^*$=kFc[1+0.001xFc$^2\lambda^3$/sin(2$\theta$)]$^{-1/4}$ |
| Primary atom site location: dual | Extinction coefficient: 0.00082 (16) |
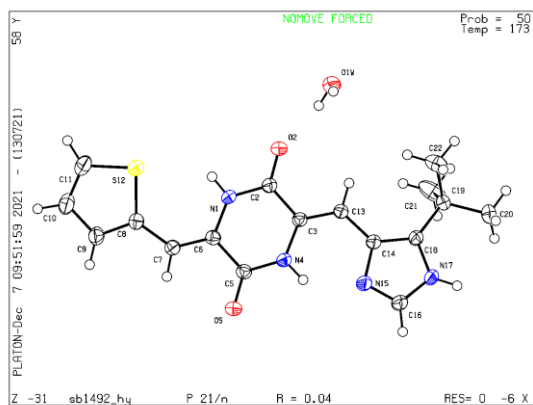
**(3Z,6Z)-3-((5-(*tert*-butyl)-1*H*-imidazol-4-yl)methylene)-6-(thiophen-2-yl-methylene)piperazine-2,5-dione water solvate – SB1492_HY**

### *Crystal data*

| | |
|---|---|
| $C_{17}H_{18}N_4O_2S \cdot H_2O$ | $F(000) = 760$ |
| $M_r = 360.43$ | $D_x = 1.396$ Mg m$^{-3}$ |
| Monoclinic, $P2_1/n$ *(no.14)* | Cu $K\alpha$ radiation, $\lambda = 1.54178$ Å |
| $a = 8.1914$ (4) Å | Cell parameters from 9904 reflections |
| $b = 9.5544$ (5) Å | $\theta = 5.0$–72.2° |
| $c = 22.1266$ (11) Å | $\mu = 1.89$ mm$^{-1}$ |
| $\beta = 98.071$ (2)° | $T = 173$ K |
| $V = 1714.56$ (15) Å$^3$ | Plates, orange |
| $Z = 4$ | $0.16 \times 0.12 \times 0.04$ mm |

### *Data collection*

| | |
|---|---|
| Bruker D8 VENTURE diffractometer with PhotonII CPAD detector | 3148 reflections with $I > 2\sigma(I)$ |
| Radiation source: INCOATEC microfocus sealed tube | $R_{int} = 0.060$ |
| rotation in $\phi$ and $\omega$, 1°, shutterless scans | $\theta_{max} = 72.4°$, $\theta_{min} = 4.0°$ |
| Absorption correction: multi-scan *SADABS* (Sheldrick, 2014) | $h = -10 \rightarrow 10$ |
| $T_{min} = 0.703$, $T_{max} = 0.942$ | $k = -11 \rightarrow 11$ |
| 22718 measured reflections | $l = -27 \rightarrow 27$ |
| 3369 independent reflections | |

### *Refinement*

| | |
|---|---|
| Refinement on $F^2$ | Secondary atom site location: difference Fourier map |
| Least-squares matrix: full | Hydrogen site location: difference Fourier map |
| $R[F^2 > 2\sigma(F^2)] = 0.045$ | H atoms treated by a mixture of independent and constrained refinement |
| $wR(F^2) = 0.119$ | $w = 1/[\sigma^2(F_o^2) + (0.0564P)^2 + 1.129P]$ where $P = (F_o^2 + 2F_c^2)/3$ |
| $S = 1.03$ | $(\Delta/\sigma)_{max} = 0.001$ |
| 3369 reflections | $\Delta\rangle_{max} = 0.30$ e Å$^{-3}$ |
| 242 parameters | $\Delta\rangle_{min} = -0.41$ e Å$^{-3}$ |
| 6 restraints | Extinction correction: *SHELXL2014*/7 (Sheldrick 2014), Fc$^*$=kFc[1+0.001xFc$^2\lambda^3$/sin(2$\theta$)]$^{-1/4}$ |
| Primary atom site location: dual | Extinction coefficient: 0.0021 (4) |

## 5.5   Synthesis and Characterization of Hemiperazines

### 5.5.1   Synthesis of Hemipierazines

Compound **33** was also synthesized by my colleague Peter Gödtel, who provided me with some of the corresponding NMR, IR and mass spectra. Usually, 200 – 500 mg of the starting material 1,4-diacetylpiperazine-2,5-dione **2** were applied.

General procedure A

The aldehyde (1.00 equiv.) was dissolved in dry DMF (2.0 mL/1 mmol aldehyde) under argon atmosphere. 1,4-Diacetylpiperazine-2,5-dione (1.50 equiv.) and $Cs_2CO_3$ (1.50 equiv.) were added and the reaction mixture was stirred at room temperature until the complete consumption of the aldehyde was detected. The reaction mixture was then poured on ice water and the precipitate was filtered off and dried under reduced pressure.

General procedure B

The aldehyde (1.00 equiv.) and 1,4-diacetylpiperazine-2,5-dione (1.50 equiv.) were dissolved in dry THF (6.0 mL/1 mmol aldehyde) under argon atmosphere and cooled down to 0 °C. KO$^t$Bu (1.10 equiv.) was added carefully and subsequently the reaction mixture was allowed to warm up to room temperature and stirred until the complete consumption of the aldehyde was detected. The reaction was quenched by the slow addition of ice water, THF was removed under reduced pressure and the precipitate was filtered off and dried under reduced pressure. The aqueous phase was additionally extracted with ethyl acetate. The organic phase was concentrated *in vacuo* and before purification combined with the precipitate collected before.

*(Z)-1-Acetyl-3-benzylidenepiperazine-2,5-dione (**29**)*
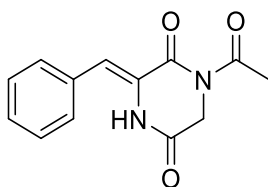


General procedure A.

The crude residue was purified *via* column chromatography (CH$_2$Cl$_2$:ethyl acetate; 10:1). (*Z*)-1-Acetyl-3-benzylidenepiperazine-2,5-dione (**29**) was isolated as a colorless solid in 57% yield (210 mg, 860 µmol).

To isolate the *E*-isomer, a solution of compound **29** in ethyl acetate was irradiated at 365 nm for 1 hour. The two photoisomers were then separated *via* column chromatography (CH$_2$Cl$_2$:ethyl acetate; 9:1).

**Z-isomer**

**$^1$H NMR (400 MHz, CDCl$_3$):** $\delta$ = 7.96 (s, 1H, N*H*), 7.51 – 7.42 (m, 2H, H$_{arom}$), 7.39 (ddt, *J* = 6.1, 3.0, 1.9 Hz, 3H, H$_{arom}$), 7.18 (s, 1H, Ph-C*H*), 4.51 (s, 2H, C*H$_2$*), 2.66 (s, 3H, C*H$_3$*) ppm.

**$^{13}$C NMR (101 MHz, CDCl$_3$):** $\delta$ = 172.6 (1C, *C*OCH$_3$), 162.8 (1C, *C*ONH), 160.1 (1C, *C*ONCOCH$_3$), 132.7 (1C, *C*$_{arom}$-CH$_2$), 129.7 (2C, *C*$_{arom}$-H), 129.6 (2C, *C*$_{arom}$-H), 128.7 (1C, *C*$_{arom}$-H), 125.8 (1C, CO-*C*), 120.1 (1C, Ph-*C*H), 46.3 (1C, *C*H$_2$), 27.4 (1C, CO*C*H$_3$) ppm.

**IR (ATR):** $v$ = 3269 (w), 3125 (w), 3044 (w), 3006 (w), 2939 (w), 1698 (vs), 1677 (vs), 1629 (vs), 1494 (w), 1455 (m), 1428 (m), 1404 (m), 1360 (vs), 1262 (vs), 1222 (vs), 1203 (vs), 1098 (vs), 1077 (s), 1034 (s), 1006 (s), 999 (s), 979 (vs), 960 (s), 933 (s), 873 (m), 860 (m), 853 (m), 837 (s), 790 (m), 768 (vs), 735 (s), 715 (vs), 701 (s), 680 (vs), 653 (vs), 618 (s), 596 (s), 584 (s), 555 (vs), 534 (vs), 476 (vs), 428 (vs), 401 (s) cm$^{-1}$.

**HRMS (FAB):** *m/z* calcd. for C$_{13}$H$_{13}$N$_2$O$_3$ [M+H], 245.0921; found, 245.0923.

**EA (C$_{13}$H$_{12}$N$_2$O$_3$):** calcd. C 63.93; H 4.95; N 11.47; O 19.65; found C 63.95; H 4.98; N 11.28.

**UV/Vis (MeCN):** $\lambda_{max}$ = 316 nm.

**E-isomer**

**$^1$H NMR (400 MHz, CDCl$_3$):** $\delta$ = 9.50 (s, 1H, N*H*), 7.50 – 7.49 (m, 2H, H$_{arom}$), 7.39 – 7.99 (m, 3H, H$_{arom}$), 6.66 (s, 1H, Ph-C*H*), 4.50 (s, 2H, C*H$_2$*), 2.57 (s, 3H, C*H$_3$*) ppm.

**$^{13}$C NMR (101 MHz, CDCl$_3$):** $\delta$ = 172.5 (1C, *C*OCH$_3$), 165.6 (1C, *C*ONH), 159.8 (1C, *C*ONCOCH$_3$), 133.1 (1C, *C*$_{arom}$-CH$_2$), 130.0 (2C, *C*$_{arom}$-H), 129.0 (1C, *C*$_{arom}$-H), 128.2 (2C, *C*$_{arom}$-H), 127.5 (1C, Ph-*C*H), 125.3 (1C, CO-*C*), 45.8 (1C, *C*H$_2$), 27.4 (1C, CO*C*H$_3$) ppm.

*(Z)-1-Acetyl-3-(4-methoxybenzylidene)piperazine-2,5-dione (**30**)*
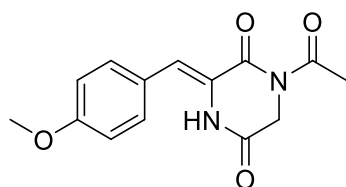


General procedure A.

The crude residue was purified *via* column chromatography (cyclohexane:ethyl acetate; 2:1 -> 3:2). The target compound was isolated as a pale-yellow solid in 55% yield.

To isolate the *E*-isomer a solution of compound **30** in ethyl acetate was irradiated at 365 nm for 1 hour. The two photoisomers were then separated *via* column chromatography (cyclohexane:ethyl acetate; 2:1 -> 3:2).

*Z*-isomer

**$^1$H NMR (400 MHz, DMSO-$d_6$):** $\delta$ = 10.28 (s, 1H), 7.58 (d, *J* = 8.8 Hz, 2H), 7.01 (d, *J* = 8.8 Hz, 2H), 6.95 (s, 1H), 4.37 (s, 2H), 3.81 (s, 3H), 2.50 (s, 3H) ppm.

**$^{13}$C NMR (101 MHz, DMSO-$d_6$):** $\delta$ = 171.8, 164.2, 162.1, 159.7, 131.5, 125.4, 124.9, 119.7, 114.2, 55.3, 45.5, 26.6 ppm.

**IR (ATR):** $v$ = 387 (w), 402 (w), 419 (m), 453 (s), 470 (m), 504 (s), 538 (vs), 550 (s), 574 (m), 603 (m), 626 (m), 652 (m), 721 (s), 745 (vs), 754 (s), 779 (s), 810 (vs), 820 (vs), 882 (m), 894 (m), 933 (m), 948 (m), 982 (s), 1000 (s), 1021 (vs), 1040 (m), 1101 (s), 1119 (m), 1181 (vs), 1205 (vs), 1222 (s), 1261 (vs), 1302 (w), 1356 (vs), 1370 (vs), 1407 (vs), 1445 (m), 1455 (w), 1513 (s), 1570 (w), 1601 (vs), 1622 (vs), 1679 (vs), 1696 (s), 2840 (w), 2904 (w), 2929 (w), 2969 (w), 3000 (w), 3014 (w), 3038 (w), 3065 (w), 3075 (w), 3091 (w), 3099 (w), 3122 (w), 3173 (w), 3206 (w), 3223 (w), 3231 (w) cm$^{-1}$.

**HRMS (FAB):** *m*/*z* calcd. for $C_{14}H_{14}N_2O_4$ [M+H], 274.0948; found, 274.0947.

**EA ($C_{13}H_{12}N_2O_3$):** calcd. C 61.31; H 5.15; N 10.21; O 23.33. Found C 61.41; H 5.18; N 10.17.

**UV/Vis (MeCN):** $\lambda_{max}$ = 333 nm.

*E*-isomer

**$^1$H NMR (400 MHz, DMSO-$d_6$):** $\delta$ = 10.51 (s, 1H), 7.51 (d, *J* = 8.8 Hz, 2H), 6.89 (d, *J* = 8.8 Hz, 2H), 6.54 (s, 1H), 4.29 (s, 2H), 3.77 (s, 3H), 2.42 (s, 3H) ppm.

**$^{13}$C NMR (101 MHz, DMSO-$d_6$):** $\delta$ = 171.9, 164.1, 160.5, 159.1, 131.8, 126.1, 125.5, 124.0, 113.2, 55.1, 45.7, 26.9 ppm.

**UV/Vis (MeCN):** $\lambda_{max}$ = 343 nm.

*(Z)-1-Acetyl-3-(3-methoxybenzylidene)piperazine-2,5-dione (**31**)*
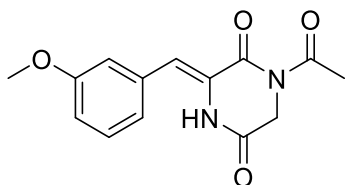


General procedure A.

The crude residue was purified *via* column chromatography (CH$_2$Cl$_2$:ethyl acetate; 9:1) followed by recrystallization from toluene. The target compound was isolated as a colorless solid in 18% yield.

**¹H NMR (400 MHz, DMSO-$d_6$):** $\delta$ = 10.37 (s, 1H), 7.36 (t, $J$ = 8.2 Hz, 1H), 7.18-7.16 (brm, 1.3 Hz, 2H), 6.99 – 6.92 (brm, 2H), 4.38 (s, 2H), 3.81 (s, 3H), 2.51 (s, 3H) ppm.

**¹³C NMR (101 MHz, DMSO-$d_6$):** $\delta$ = 171.8, 164.1, 161.6, 159.2, 134.2, 129.7, 127.0, 122.1, 118.8, 114.8, 114.5, 55.1, 45.6, 26.7 ppm.

**IR (ATR):** $v$ = 3184 (w), 3160 (w), 3098 (w), 3074 (w), 3030 (w), 3014 (w), 2968 (w), 2919 (w), 2873 (w), 2851 (w), 2842 (w), 1700 (vs), 1677 (vs), 1628 (vs), 1602 (m), 1572 (s), 1487 (w), 1456 (w), 1432 (m), 1408 (s), 1378 (vs), 1366 (vs), 1315 (m), 1300 (m), 1278 (m), 1251 (vs), 1227 (vs), 1197 (vs), 1180 (s), 1162 (vs), 1105 (m), 1047 (vs), 1003 (m), 994 (m), 984 (m), 970 (w), 938 (m), 914 (w), 890 (w), 880 (w), 851 (m), 823 (m), 789 (vs), 775 (s), 747 (vs), 720 (m), 691 (vs), 657 (s), 615 (w), 605 (m), 562 (m), 551 (s), 516 (w), 477 (w), 462 (w), 442 (s), 414 (w) cm⁻¹.

**HRMS (FAB):** $m/z$ calcd. for $C_{14}H_{14}N_2O_4$ [M+H], 274.2022; found, 274.2023.

**UV/Vis (MeCN):** $\lambda_{max}$ = 317 nm.

*(Z)-1-Acetyl-3-(2-methoxybenzylidene)piperazine-2,5-dione (**32**)*
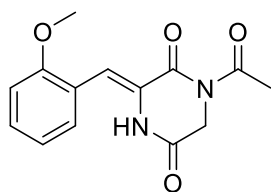


General procedure A.

The crude residue was purified *via* column chromatography (toluene:ethyl acetate; 1:0 -> 4:1) followed by recrystallization from toluene. The target compound was isolated as a colorless solid in 58% yield.

**¹H NMR (400 MHz, DMSO-$d_6$):** $\delta$ = 10.10 (s, 1H), 7.54 (dd, $J$ = 7.8, 1.9 Hz, 1H), 7.36 (ddd, $J$ = 8.8, 7.4, 1.8 Hz, 1H), 7.08 (s, 1H), 7.08 (d, $J$ = 8.5 Hz, 1H), 7.02 (t, $J$ = 7.5 Hz, 1H), 4.35 (s, 2H), 3.85 (s, 3H), 2.50 (s, 3H) ppm.

**¹³C NMR (101 MHz, DMSO-$d_6$):** $\delta$ = 171.9, 163.7, 161.4, 157.2, 130.4, 129.7, 126.6, 121.6, 120.5, 114.3, 111.4, 55.6, 45.7, 26.7 ppm.

**IR (ATR):** $v$ = 3189 (w), 3094 (vw), 3019 (vw), 2978 (vw), 2934 (w), 2836 (vw), 1697 (vs), 1676 (vs), 1630 (s), 1594 (w), 1574 (w), 1486 (w), 1459 (m), 1401 (m), 1373 (vs), 1361 (vs), 1306 (w), 1289 (m), 1259 (s), 1245 (vs), 1221 (vs), 1191 (s), 1157 (s), 1105 (m), 1047 (w), 1017 (m), 1001 (m), 983 (w), 884 (w), 861 (w), 834 (w), 807 (w), 758 (vs), 744 (m), 731 (m), 720 (m), 659 (w), 605 (w), 579 (w), 545 (s), 527 (w), 470 (w), 432 (w) cm⁻¹.

**HRMS (FAB):** $m/z$ calcd. for $C_{14}H_{14}N_2O_4$ [M+H],; 274.2093; found, 274.2094.

**UV/Vis (MeCN):** $\lambda_{max}$ = 328 nm.

*(Z)-1-Acetyl-3-(3,4,5-trimethoxybenzylidene)piperazine-2,5-dione (**33**)*
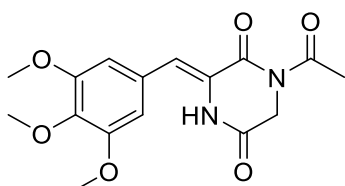


General procedure A.

The crude residue was purified *via* column chromatography (CH$_2$Cl$_2$:ethyl acetate; 10:1 -> 4:1). The target compound was isolated as a pale-yellow solid in 52% yield.

**$^1$H NMR (400 MHz, DMSO-$d_6$):** $\delta$ = 10.40 (s, 1H), 6.92 (s, 1H), 6.90 (s, 2H), 4.36 (s, 2H), 3.81 (s, 6H), 3.70 (s, 3H), 2.50 (s, 3H) ppm.

**$^{13}$C NMR (101 MHz, DMSO-$d_6$):** $\delta$ = 171.8, 164.1, 161.8, 152.8, 138.1, 128.3, 126.2, 119.4, 107.4, 60.0, 55.9, 45.6, 26.7 ppm.

**IR (ATR):** $v$ = 3196 (w), 3104 (w), 2999 (w), 2962 (w), 2944 (w), 2844 (w), 1687 (vs), 1623 (s), 1579 (s), 1507 (m), 1468 (w), 1459 (m), 1438 (s), 1408 (s), 1380 (vs), 1361 (vs), 1334 (s), 1305 (w), 1273 (w), 1227 (vs), 1187 (s), 1156 (m), 1125 (vs), 1101 (vs), 1050 (w), 1034 (m), 1003 (vs), 966 (m), 882 (w), 854 (m), 834 (m), 816 (m), 773 (s), 756 (m), 738 (vs), 667 (w), 649 (s), 629 (w), 609 (m), 598 (s), 562 (vs), 530 (w), 526 (w), 494 (m), 456 (s), 443 (m), 419 (w), 408 (w), 399 (w), 377 (w) cm$^{-1}$.

**HRMS (FAB):** *m/z* calcd. for C$_{16}$H$_{18}$N$_2$O$_6$ [M], 334.1159; found, 334.1160.

**UV/Vis (DMSO):** $\lambda_{max}$ = 341 nm.

*(Z)-1-Acetyl-3-(4-(trifluoromethyl)benzylidene)piperazine-2,5-dione (**34**)*
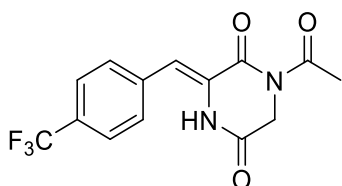


General procedure A.

The crude residue was purified *via* column chromatography (cyclohexane:ethyl acetate; 3:1 -> 5:2). The target compound was isolated as a pale-yellow solid in 36% yield.

**$^1$H NMR (400 MHz, DMSO-$d_6$):** $\delta$ = 10.49 (s, 1H), 7.70 (d, *J* = 8.4 Hz, 2H), 7.43 (d, *J* = 7.9 Hz, 1H), 4.37 (s, 2H), 2.51 (s, 3H) ppm.

**$^{13}$C NMR (101 MHz, DMSO-$d_6$):** $\delta$ = 171.8, 164.1, 161.4, 147.9, 132.5, 131.5, 127.7, 121.1, 118.8, 117.1, 45.7, 26.7 ppm.

**IR (ATR):** $v$ = 3196 (w), 3189 (w), 3088 (w), 3081 (w), 1720 (m), 1683 (vs), 1629 (s), 1606 (m), 1587 (w), 1507 (w), 1458 (w), 1442 (m), 1422 (m), 1415 (m), 1384 (m), 1370 (w), 1353 (w), 1266

(vs), 1232 (vs), 1203 (vs), 1150 (vs), 1096 (vs), 1040 (s), 1017 (s), 997 (m), 980 (m), 970 (s), 953 (m), 921 (m), 890 (s), 877 (m), 863 (m), 850 (m), 833 (s), 810 (vs), 778 (s), 754 (s), 735 (s), 703 (m), 671 (s), 656 (m), 636 (m), 611 (s), 595 (m), 568 (m), 552 (s), 540 (m), 518 (m), 504 (w), 494 (w), 476 (m), 450 (s), 408 (w), 392 (w) cm$^{-1}$.

**HRMS (FAB):** $m/z$ calcd. for $C_{14}H_{12}N_2O_4F_3$ [M+H], 329.0744; found, 329.0743.

**UV/Vis (DMSO):** $\lambda_{max}$ = 325 nm.

*(Z)-4-((4-Acetyl-3,6-dioxopiperazin-2-ylidene)methyl)benzonitrile (**35**)*
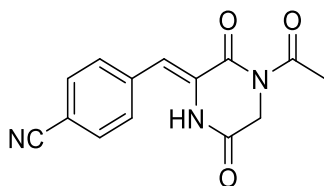


General procedure A.

The crude residue was purified *via* column chromatography (cyclohexane:ethyl acetate; 4:1 -> 1:1). The target compound was isolated as a pale-yellow solid in 52% yield.

**$^1$H NMR (400 MHz, DMSO-$d_6$):** $\delta$ = 10.61 (s, 1H), 7.88 (d, $J$ = 8.4 Hz, 2H), 7.73 (d, $J$ = 8.1 Hz, 2H), 6.96 (s, 1H), 4.37 (s, 2H), 2.50 (s, 3H) ppm.

**$^{13}$C NMR (101 MHz, DMSO-$d_6$):** $\delta$ = 171.8, 164.2, 161.1, 138.1, 132.4, 130.3, 129.2, 118.8, 116.2, 110.3, 45.8, 26.8 ppm.

**IR (ATR):** $v$ = 3279 (w), 3268 (w), 3223 (w), 3114 (w), 3104 (w), 3072 (w), 3050 (w), 3041 (w), 3036 (w), 3013 (w), 2997 (w), 2942 (w), 2227 (w), 1686 (vs), 1621 (vs), 1604 (s), 1506 (w), 1436 (m), 1421 (w), 1397 (m), 1358 (vs), 1285 (m), 1256 (vs), 1222 (vs), 1201 (vs), 1098 (s), 1043 (s), 1021 (m), 997 (s), 976 (s), 962 (m), 891 (s), 885 (s), 839 (s), 827 (s), 813 (s), 800 (s), 764 (s), 748 (vs), 718 (s), 696 (s), 654 (m), 632 (s), 599 (m), 561 (vs), 544 (vs), 487 (s), 462 (s), 449 (vs), 429 (vs), 404 (s), 387 (m) cm$^{-1}$.

**HRMS (FAB):** $m/z$ calcd. for $C_{14}H_{12}N_3O_3$ [M+H], 270.0873; found, 270.0870.

**UV/Vis (MeCN):** $\lambda_{max}$ = 325 nm.

*(Z)-1-Acetyl-3-(4-(dimethylamino)benzylidene)piperazine-2,5-dione (**36**)*
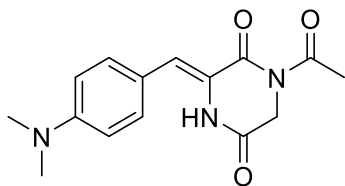


General procedure B.

The crude residue was purified *via* column chromatography (CH$_2$Cl$_2$:ethyl acetate; 9:1). The target compound was isolated as a yellow solid in 57% yield.

To isolate the *E*-isomer a solution of compound **36** in ethyl acetate was irradiated at 365 nm for 1 hour. The two photoisomers were then separated *via* column chromatography (CH$_2$Cl$_2$:ethyl acetate; 9:1 -> 9:2).

**Z-isomer**

**$^1$H NMR (400 MHz, DMSO-$d_6$):** $\delta$ = 10.12 (s, 1H), 7.49 (d, $J$ = 8.9 Hz, 2H), 6.91 (s, 1H), 6.75 (d, $J$ = 9.0 Hz, 2H), 4.35 (s, 2H), 2.98 (s, 6H), 2.48 (s, 3H) ppm.

**$^{13}$C NMR (101 MHz, DMSO-$d_6$):** $\delta$ = 171.7, 164.1, 162.6, 150.6, 131.5, 122.3, 121.8, 120.2, 111.7, 45.3, 39.7, 26.4 ppm.

**IR (ATR):** $v$ = 3169 (w), 3084 (w), 3077 (w), 3067 (w), 3014 (w), 3002 (w), 2959 (w), 2891 (w), 2860 (w), 2803 (w), 1679 (vs), 1615 (m), 1589 (vs), 1550 (m), 1523 (s), 1485 (w), 1458 (m), 1441 (m), 1411 (s), 1351 (vs), 1329 (s), 1313 (s), 1262 (vs), 1224 (vs), 1198 (s), 1181 (vs), 1166 (vs), 1098 (s), 1067 (s), 1037 (s), 1003 (s), 982 (s), 963 (s), 942 (s), 899 (s), 882 (s), 854 (s), 812 (vs), 793 (vs), 752 (s), 741 (vs), 718 (s), 694 (s), 657 (s), 628 (s), 599 (vs), 578 (s), 551 (vs), 524 (vs), 506 (vs), 482 (vs), 456 (vs), 428 (s), 419 (s), 404 (s), 390 (s), 378 (s) cm$^{-1}$.

**HRMS (FAB):** $m/z$ calcd. for C$_{15}$H$_{17}$N$_3$O$_3$ [M+H], 287.1264; found, 287.1264.

**EA (C$_{15}$H$_{17}$N$_3$O$_3$):** calcd. C 62.71; H 5.96; N 14.63; O 16.71. Found C 62.64; H 5.98; N 14.28.

**UV/Vis (MeCN):** $\lambda_{max}$ = 386 nm.

**Fluorescence (DMSO):** $\lambda_{em}$= 516 nm (excited with $\lambda$ = 400 nm).

**$\Phi_F$ (DMSO):** 0.004.


**E-isomer**

**$^1$H NMR (400 MHz, DMSO-$d_6$):** $\delta$ = 10.35 (s, 1H), 7.56 (d, $J$ = 9.0 Hz, 2H), 6.66 (d, $J$ = 9.0 Hz, 2H), 6.50 (s, 1H), 4.28 (s, 2H), 2.95 (s, 6H), 2.45 (s, 3H) ppm.

**$^{13}$C NMR (101 MHz, DMSO-$d_6$):** $\delta$ = 171.8, 164.1, 161.0, 150.3, 132.3, 126.5, 122.7, 120.6, 111.0, 45.5, 39.5, 26.8 ppm.


*(Z)-1-Acetyl-3-(4-(diphenylamino)benzylidene)piperazine-2,5-dione (**37**)*
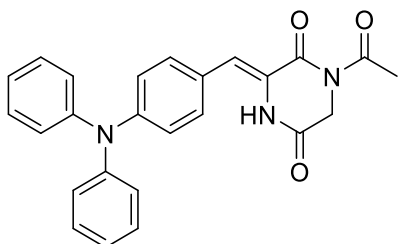
General procedure A.

The crude residue was purified *via* column chromatography (CH₂Cl₂:ethyl acetate; 1:0 -> 9:1). The target compound was isolated as a yellow solid in 65% yield.

**¹H NMR (400 MHz, DMSO-*d₆*):** $\delta$ = 10.27 (s, 1H), 7.50 (d, $J$ = 8.9 Hz, 2H), 7.35 (dd, $J$ = 8.5, 7.4 Hz, 4H), 7.12 (tt, $J$ = 7.3, 1.3 Hz, 2H), 7.08 (d, $J$ = 7.4 Hz, 4H), 6.93 (d, $J$ = 8.9 Hz, 2H), 6.91 (s, 1H), 4.35 (s, 2H), 2.45 (d, $J$ = 15.3 Hz, 3H) ppm.

**¹³C NMR (101 MHz, DMSO-*d₆*):** $\delta$ = 171.8, 164.1, 162.0, 147.7, 146.5, 131.1, 129.7, 126.3, 125.1, 124.8, 124.0, 121.3, 119.5, 45.5, 26.6 ppm.

**¹H NMR (400 MHz, CDCl₃):** $\delta$ = 7.89 (s, 1H), 7.39 – 7.27 (m, 4H), 7.25 (d, $J$ = 8.0 Hz, 3H), 7.16 – 7.09 (m, 7H), 7.06 (d, $J$ = 8.8 Hz, 2H), 4.51 (s, 2H), 2.64 (s, 3H) ppm.

**¹³C NMR (101 MHz, CDCl₃):** $\delta$ = 172.7, 162.9, 160.5, 149.2, 146.8, 130.0, 129.7, 125.6, 125.1, 124.4, 123.9, 122.1, 120.6, 46.2, 27.3 ppm.

**IR (ATR):** $v$ = 3234 (w), 3196 (w), 3101 (w), 3057 (w), 3038 (w), 1687 (vs), 1677 (vs), 1618 (m), 1602 (m), 1585 (vs), 1509 (m), 1485 (vs), 1455 (w), 1442 (m), 1432 (m), 1409 (s), 1374 (s), 1366 (s), 1356 (m), 1333 (s), 1302 (m), 1288 (m), 1265 (vs), 1207 (s), 1196 (s), 1176 (s), 1150 (s), 1130 (m), 1099 (m), 1079 (s), 1044 (m), 1038 (m), 1031 (s), 1000 (m), 984 (s), 970 (m), 952 (m), 929 (m), 921 (m), 904 (m), 894 (s), 841 (s), 827 (vs), 793 (s), 778 (s), 751 (vs), 734 (vs), 722 (vs), 694 (vs), 654 (s), 630 (vs), 622 (vs), 603 (s), 595 (s), 569 (m), 560 (s), 543 (vs), 517 (s), 500 (vs), 455 (vs), 428 (vs), 415 (s), 407 (vs), 392 (m), 377 (m) cm⁻¹.

**HRMS (FAB):** *m*/*z* calcd. for C₂₅H₂₁N₃O₃ [M+H], 411.1577; found, 411.1579.

**UV/Vis (MeCN):** $\lambda_{max}$ = 389 nm.

**Fluorescence (MeCN):** $\lambda_{em}$= 569 nm (excited with $\lambda$ = 400 nm).

**Fluorescence (DMSO):** $\lambda_{em}$= 565 nm (excited with $\lambda$ = 400 nm).

**$\Phi_F$ (DMSO):** 0.030.

*(Z)-4-((4-Acetyl-3,6-dioxopiperazin-2-ylidene)methyl)benzonitrile (**56**)*
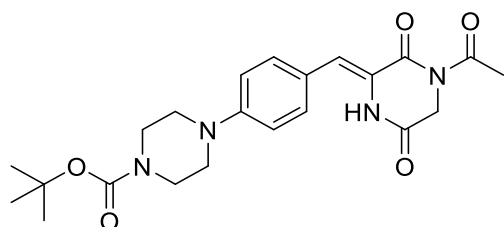


General procedure B.

The crude residue was purified *via* column chromatography (CH₂Cl₂:ethyl acetate; 4:1 -> 7:3). The target compound was isolated as a yellow solid in 47% yield.

**¹H NMR (400 MHz, DMSO-*d₆*):** $\delta$ = 10.20 (s, 1H), 7.51 (d, *J* = 9.0 Hz, 2H), 6.99 (d, *J* = 9.0 Hz, 2H), 6.91 (s, 1H), 4.35 (s, 2H), 3.49 – 3.42 (m, 4H), 3.30 – 3.20 (m, 4H), 2.48 (s, 3H), 1.42 (s, 9H) ppm.

**¹³C NMR (101 MHz, DMSO-*d₆*):** $\delta$ = 171.7, 164.1, 162.4, 153.8, 150.8, 131.3, 123.7, 123.0, 120.7, 114.7, 79.0, 47.1, 45.4, 28.0, 26.5 ppm.

**IR (ATR):** $\nu$ = 3201 (w), 3190 (w), 2972 (w), 2946 (w), 2931 (w), 2918 (w), 2868 (w), 2847 (w), 2837 (w), 1679 (vs), 1622 (s), 1604 (vs), 1513 (m), 1466 (m), 1453 (w), 1441 (m), 1408 (vs), 1364 (vs), 1354 (vs), 1340 (s), 1268 (vs), 1252 (s), 1241 (vs), 1218 (vs), 1196 (vs), 1169 (vs), 1153 (vs), 1140 (vs), 1099 (s), 1065 (s), 1041 (vs), 1014 (m), 997 (s), 979 (s), 960 (m), 945 (m), 935 (m), 908 (s), 897 (s), 884 (m), 864 (s), 834 (s), 817 (s), 798 (s), 771 (s), 759 (s), 748 (s), 741 (s), 720 (s), 705 (m), 656 (m), 640 (w), 628 (m), 599 (s), 577 (m), 557 (s), 543 (s), 516 (m), 492 (m), 459 (s), 435 (w), 419 (w), 409 (w), 392 (m) cm$^{-1}$.

**HRMS (FAB):** *m/z* calcd. for $C_{22}H_{28}N_4O_5$ [M], 428.2054; found, 428.2053.

*(Z)-4-((4-Acetyl-3,6-dioxopiperazin-2-ylidene)methyl)benzonitrile (**38**)*
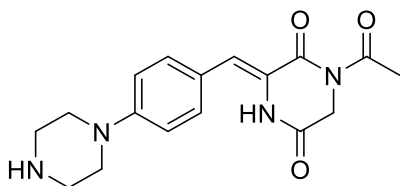


(Z)-4-((4-Acetyl-3,6-dioxopiperazin-2-ylidene)methyl)benzonitrile (**56**) (200 mg, 467 μmol, 1.00 equiv) was dissolved in 26 mL of a solution of 20% (v/v) TFA (7.70 g, 5.20 mL, 67.5 mmol, 145 equiv) and 80% dry $CH_2Cl_2$ (20.8 mL) containing 1% (v/v) TIPS (201 mg, 260 μL, 1.27 mmol, 2.72 equiv) at 0 °C (ice bath). Subsequently, the ice bath was removed and the solution was allowed to warm to ambient temperature. The reaction was monitored *via* TLC. After 2 hours the starting material had been consumed and toluene (30 mL) was added and the mixture was concentrated *in vacuo*. The crude product was purified *via* HPLC (gradient of 10-25% MeCN in $H_2O$ within 40 min, 0.1% TFA (v/v) in the solvents). The TFA salt of the target compound was isolated as a yellow solid in 74% yield.

**¹H NMR (400 MHz, D₂O):** $\delta$ = 7.48 (d, *J* = 9.0 Hz, 2H), 7.07 (d, *J* = 8.9 Hz, 2H), 6.97 (s, 1H), 4.24 (s, 2H), 3.54 (d, *J* = 5.5 Hz, 4H), 3.42 (d, *J* = 4.3 Hz, 4H), 2.52 (s, 3H) ppm.

**¹³C NMR (101 MHz, D₂O):** $\delta$ = 174.9, 165.9, 161.8, 150.1, 131.1, 124.4, 123.0, 122.3, 116.2, 45.7, 45.2, 42.9, 26.6 ppm.

**IR (ATR):** $\nu$ = 3007 (w), 2997 (w), 2844 (w), 2836 (w), 2745 (w), 2495 (w), 1672 (vs), 1625 (s), 1595 (vs), 1519 (m), 1441 (w), 1418 (s), 1364 (vs), 1302 (w), 1258 (s), 1186 (vs), 1129 (vs), 1102

(vs), 1040 (m), 1001 (m), 982 (w), 926 (m), 830 (s), 798 (s), 754 (w), 738 (m), 721 (vs), 657 (w), 629 (w), 595 (m), 574 (m), 547 (m), 517 (vs), 470 (m), 442 (m), 407 (m), 378 (w) cm$^{-1}$.

**HRMS (FAB):** $m/z$ calcd. for $C_{17}H_{21}N_4O_3$ [M+H], 329.1608; found, 329.1606.

### 5.5.2 NMR Spectra
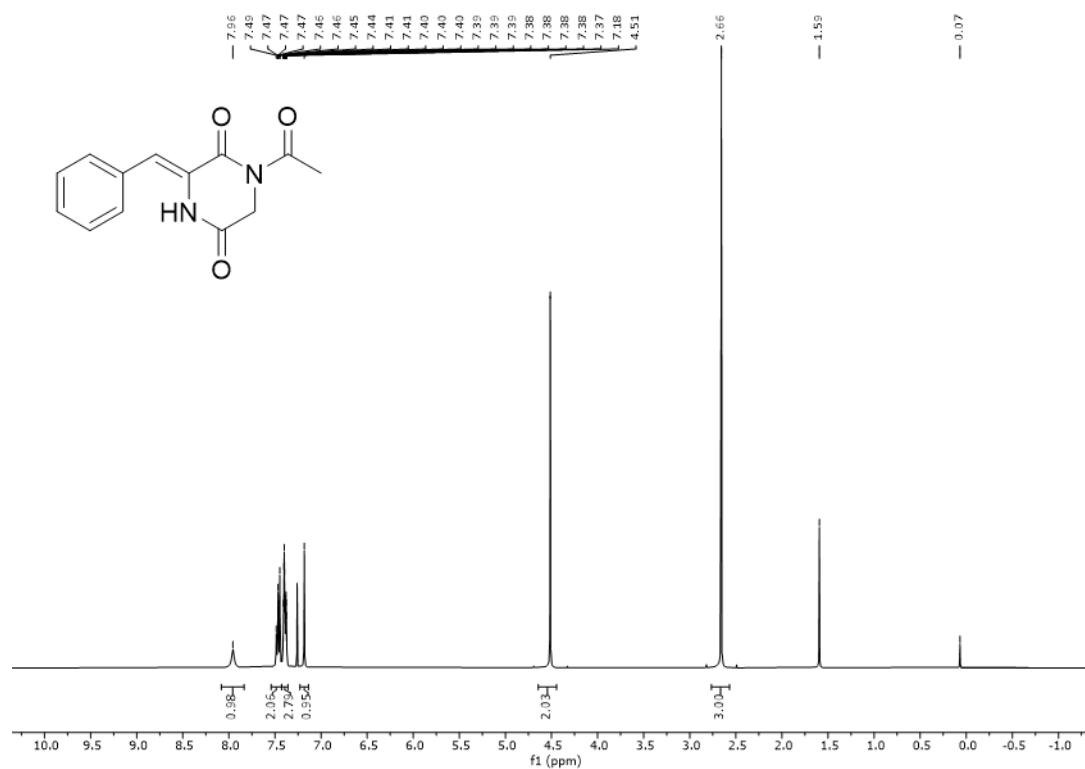


**Figure 199:** $^1$H NMR spectrum (400 MHz, CDCl$_3$) of compound Z-**29**.
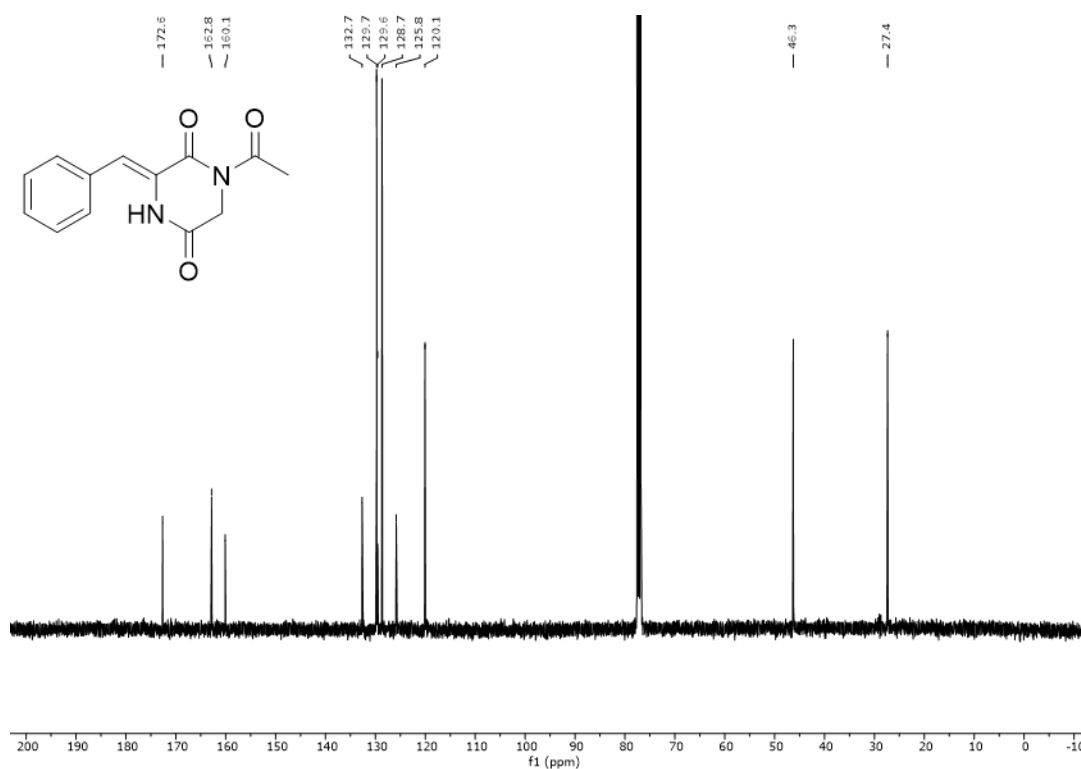
**Figure 200:** $^{13}$C NMR spectrum (101 MHz, CDCl$_3$) of compound Z-**29**.
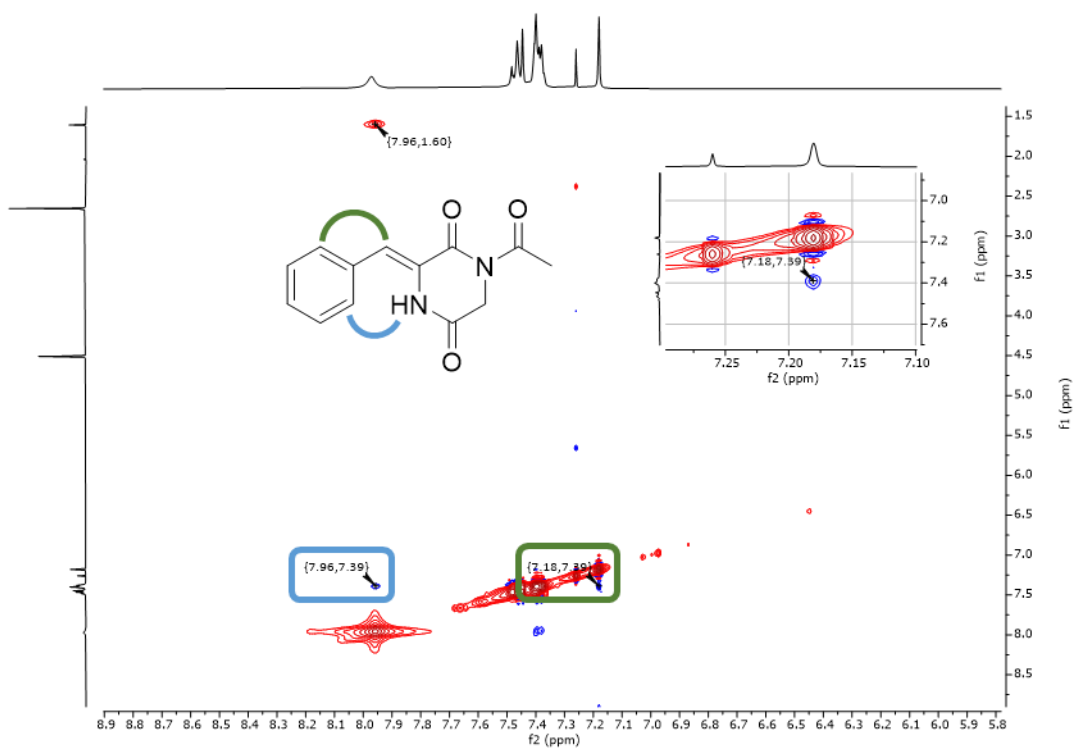


**Figure 201:** Extract of NOESY NMR spectrum (400 MHz, CDCl$_3$) of compound Z-**29**. Several relevant signals were assigned to the corresponding protons *via* color code.
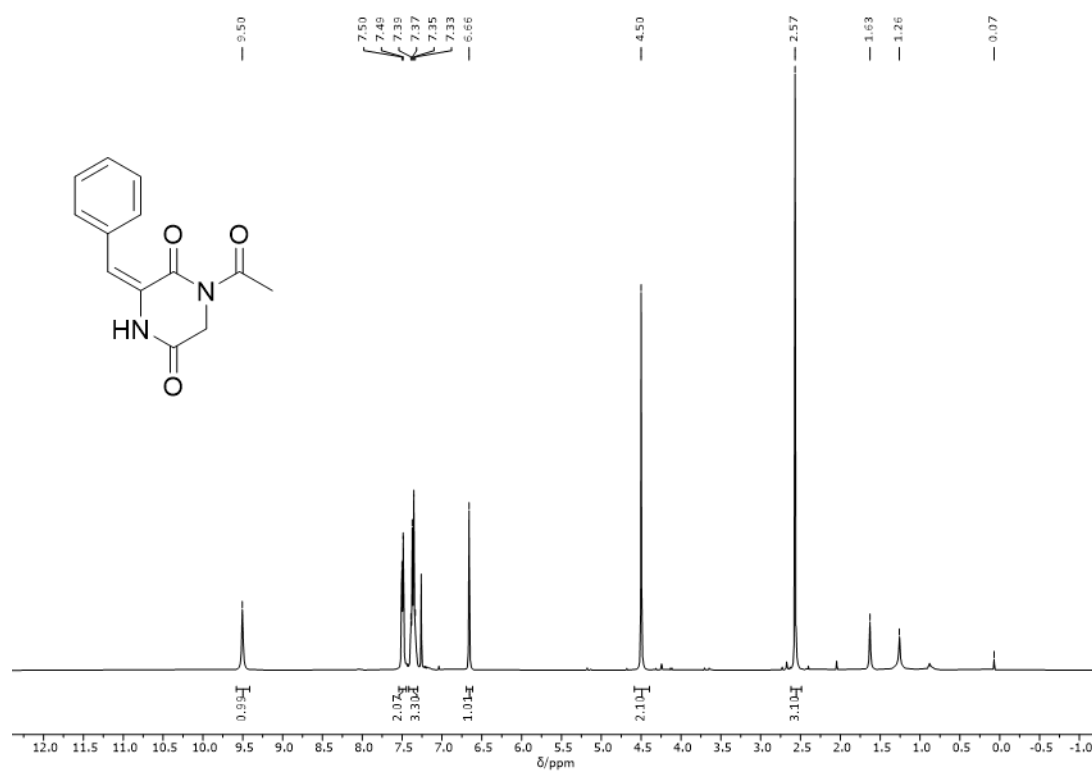
**Figure 202:** $^1$H NMR spectrum (400 MHz, CDCl$_3$) of compound *E*-**29**.
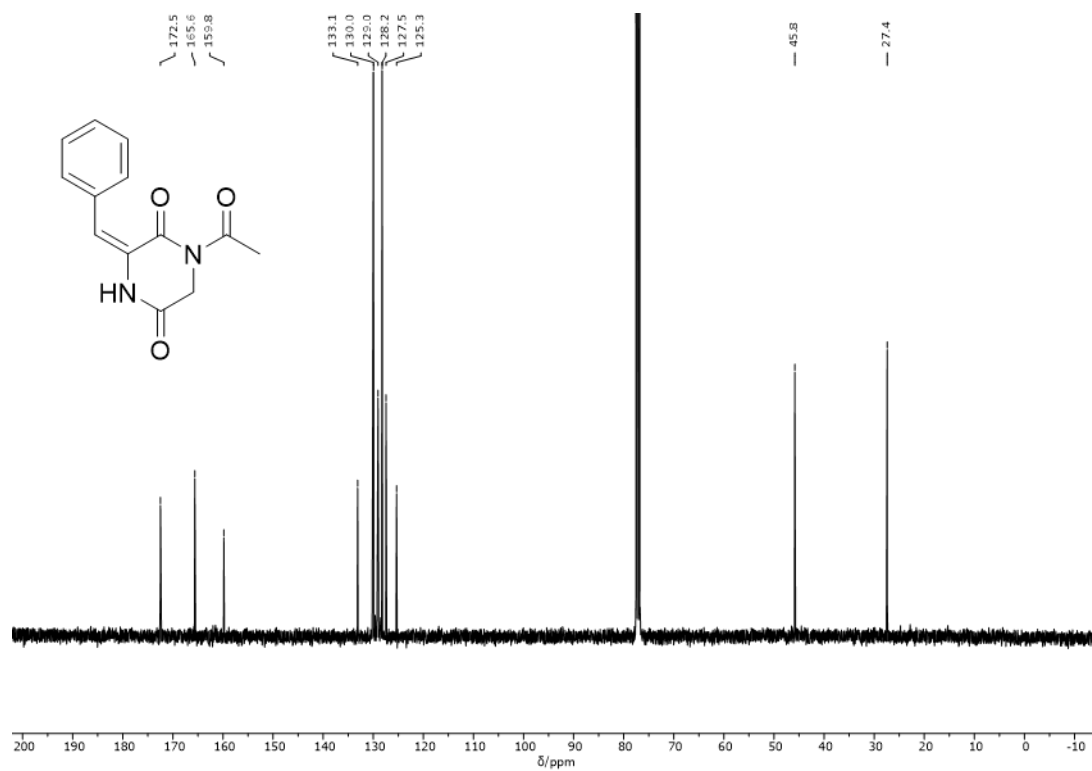


**Figure 203:** $^{13}$C NMR spectrum (101 MHz, CDCl$_3$) of compound *E*-**29**.
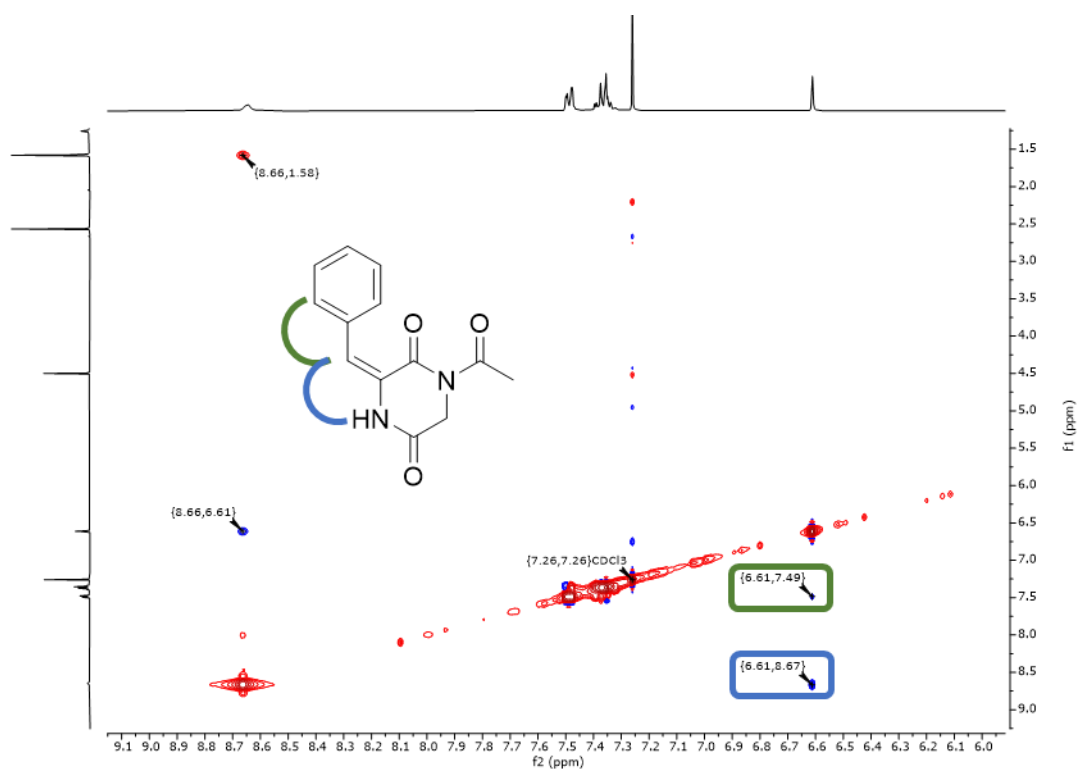
**Figure 204:** Extract of NOESY NMR spectrum (400 MHz, CDCl$_3$) of compound *E*-**29**. Several relevant signals were assigned to the corresponding protons *via* color code.
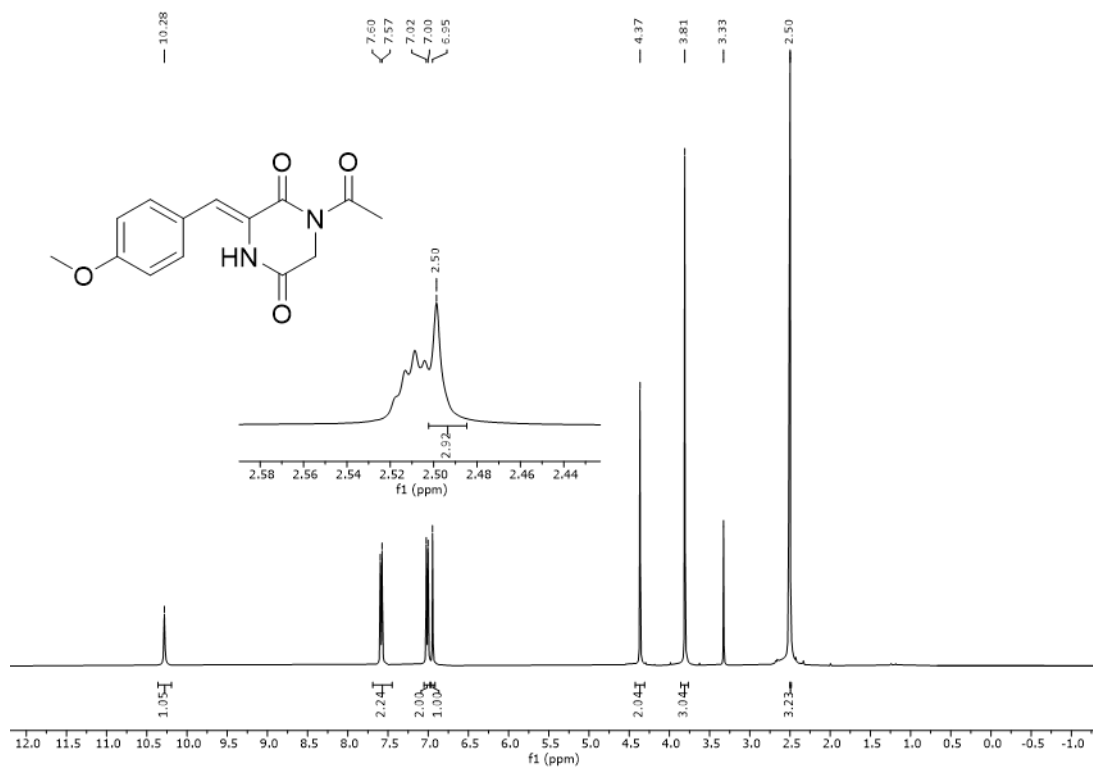


**Figure 205:** $^1$H NMR spectrum (400 MHz, DMSO-*d*$_6$) of compound *Z*-**30**.
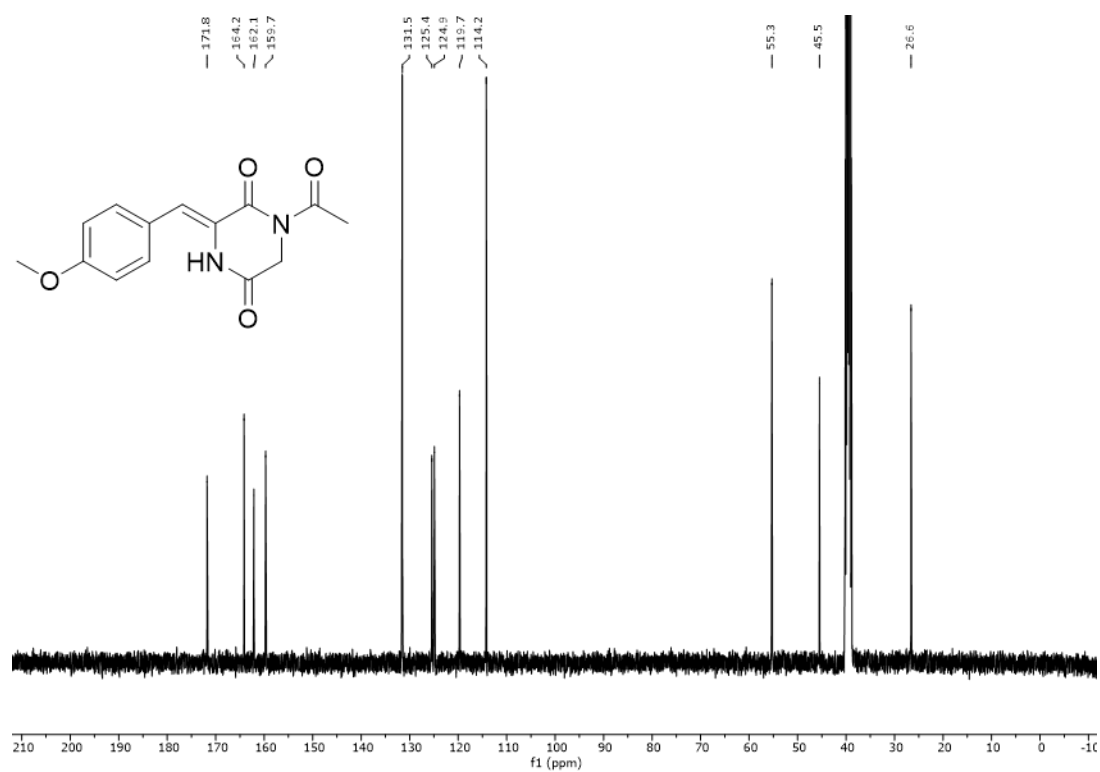
**Figure 206:** $^{13}$C NMR spectrum (101 MHz, DMSO-$d_6$) of compound Z-**30**.
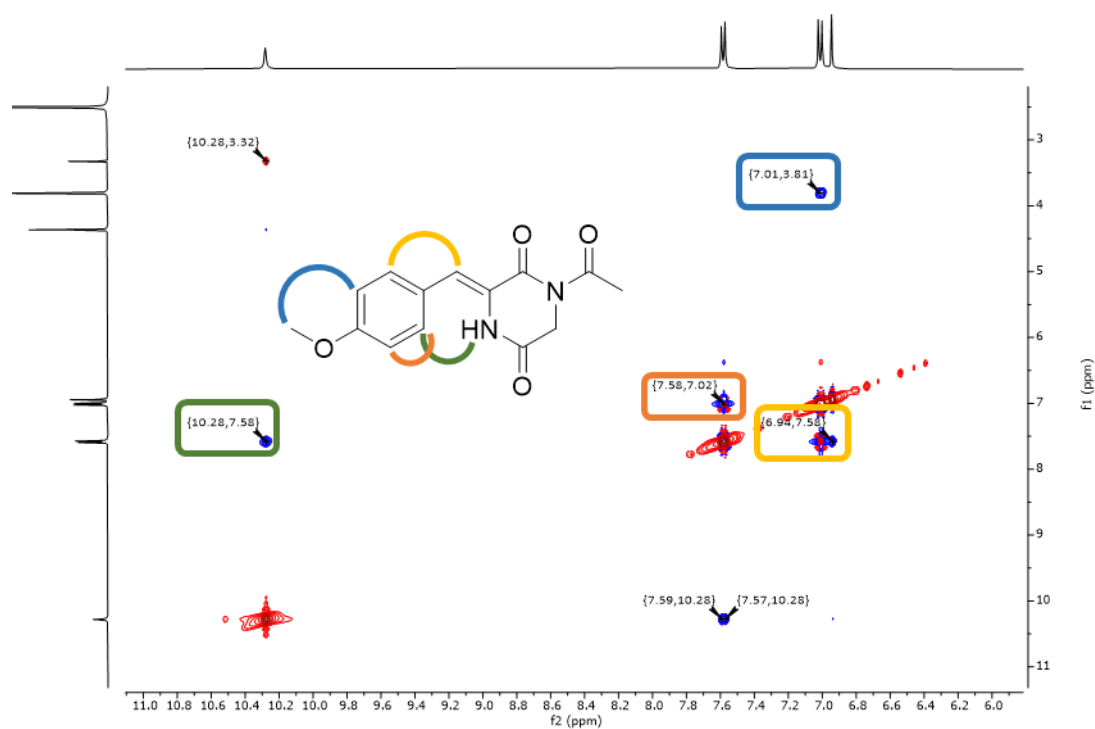


**Figure 207:** Extract of NOESY NMR spectrum (400 MHz, DMSO-$d_6$) of compound Z-**30**. Several relevant signals were assigned to the corresponding protons *via* color code.
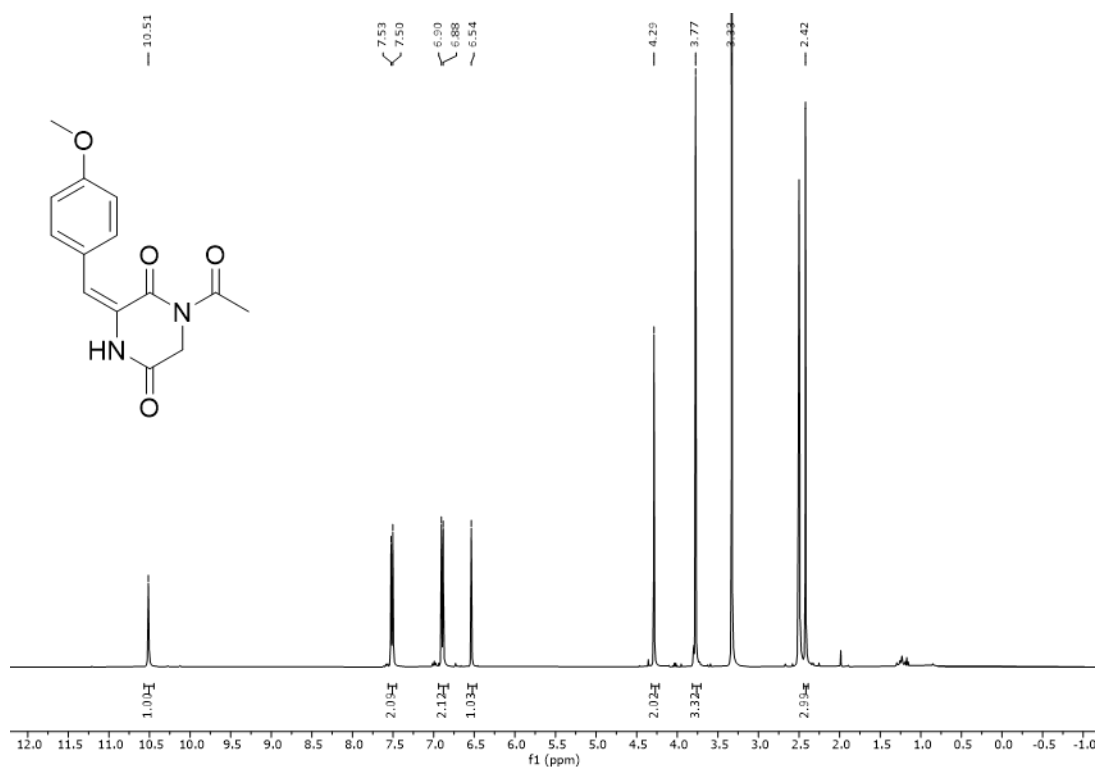
**Figure 208:** $^1$H NMR spectrum (400 MHz, DMSO-$d_6$) of compound *E*-**30**.
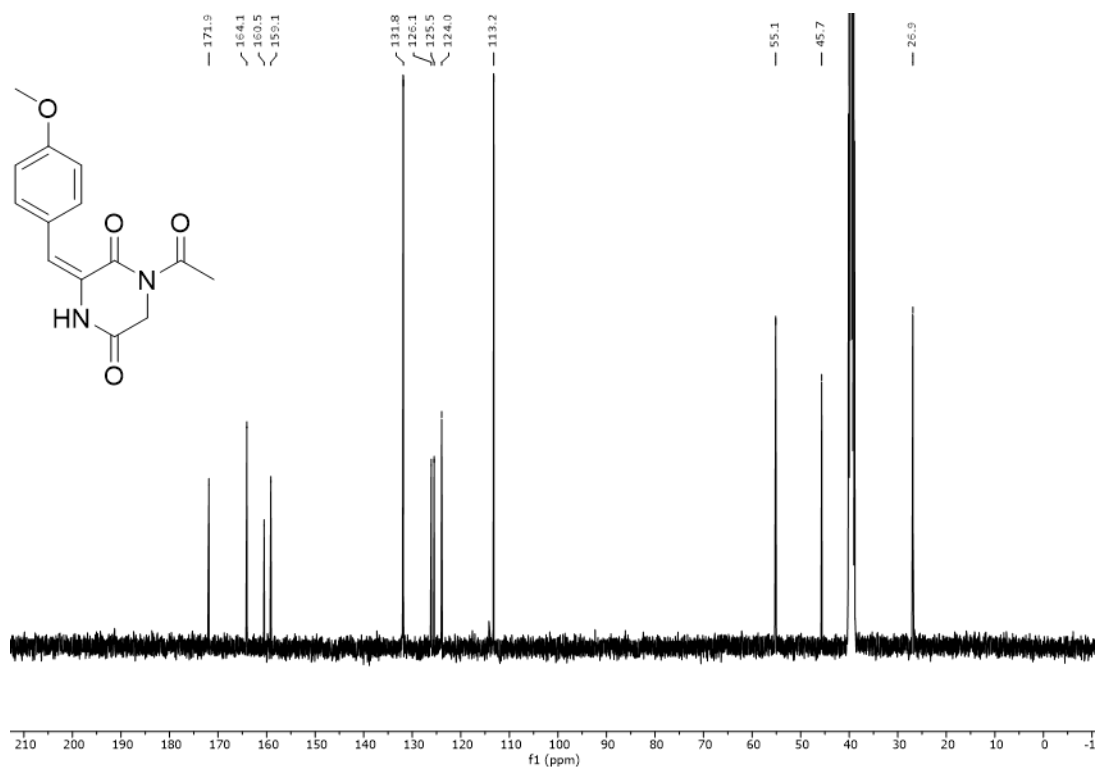


**Figure 209:** $^{13}$C NMR spectrum (101 MHz, DMSO-$d_6$) of compound *E*-**30**.
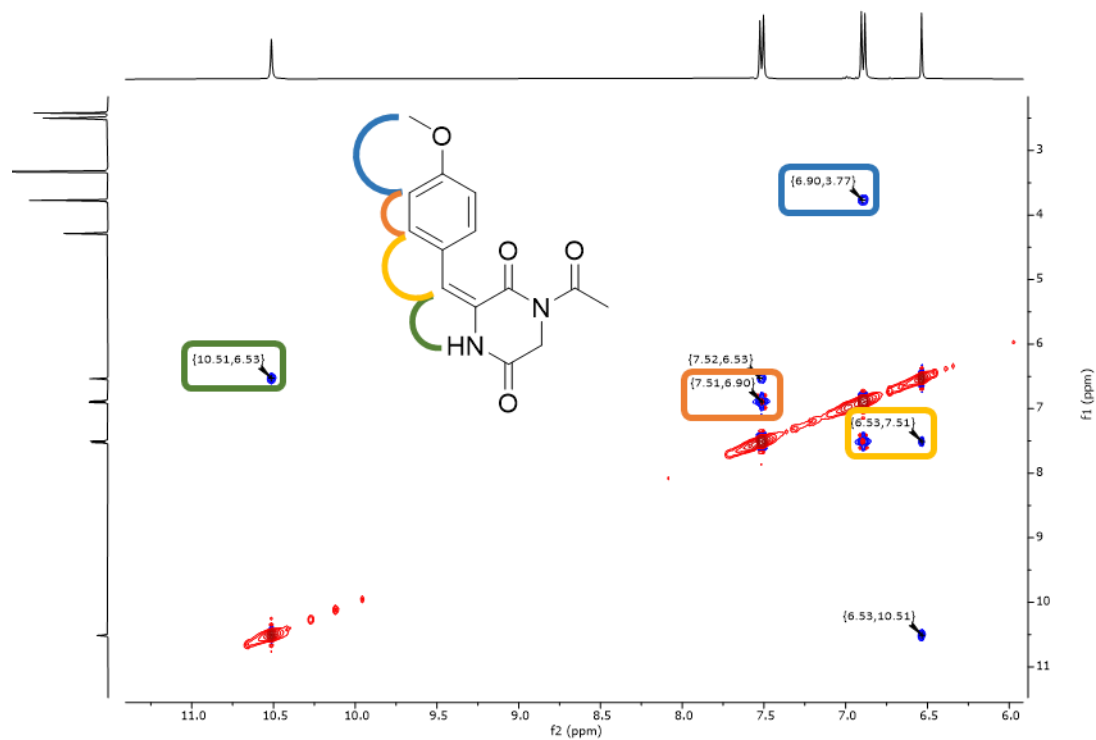
**Figure 210:** Extract of NOESY NMR spectrum (400 MHz, DMSO-$d_6$) of compound *E*-**30**. Several relevant signals were assigned to the corresponding protons *via* color code.
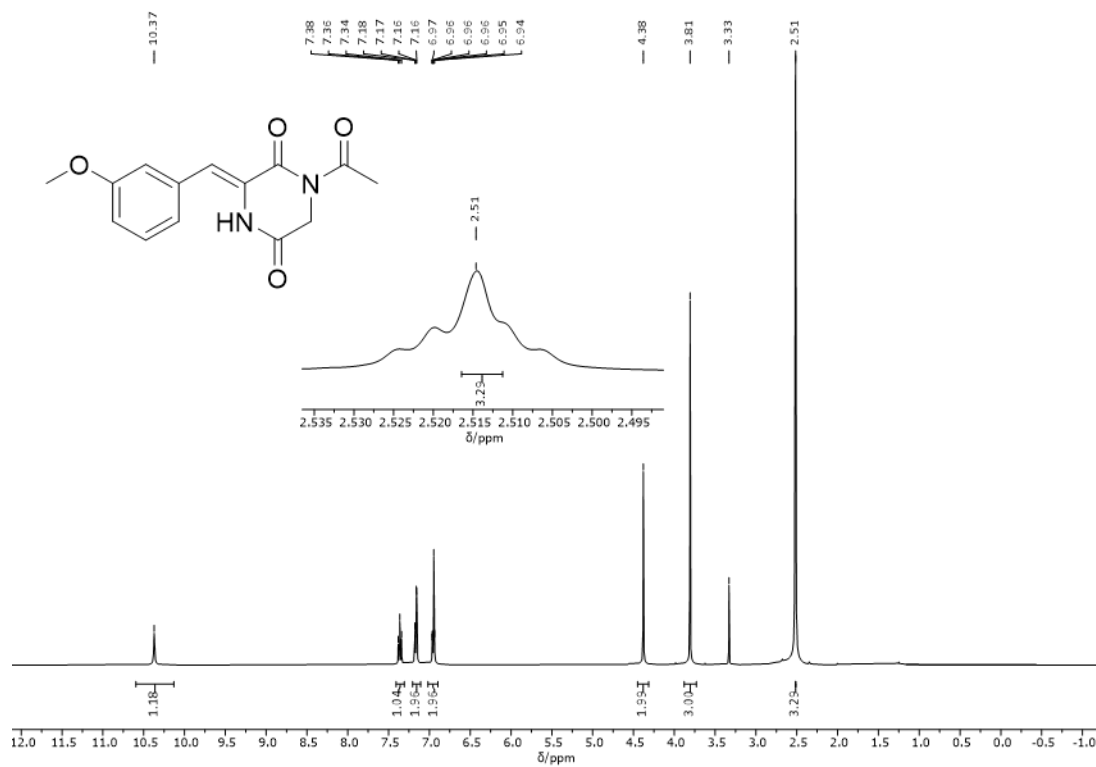


**Figure 211:** $^1$H NMR spectrum (400 MHz, DMSO-$d_6$) of compound *Z*-**31**.
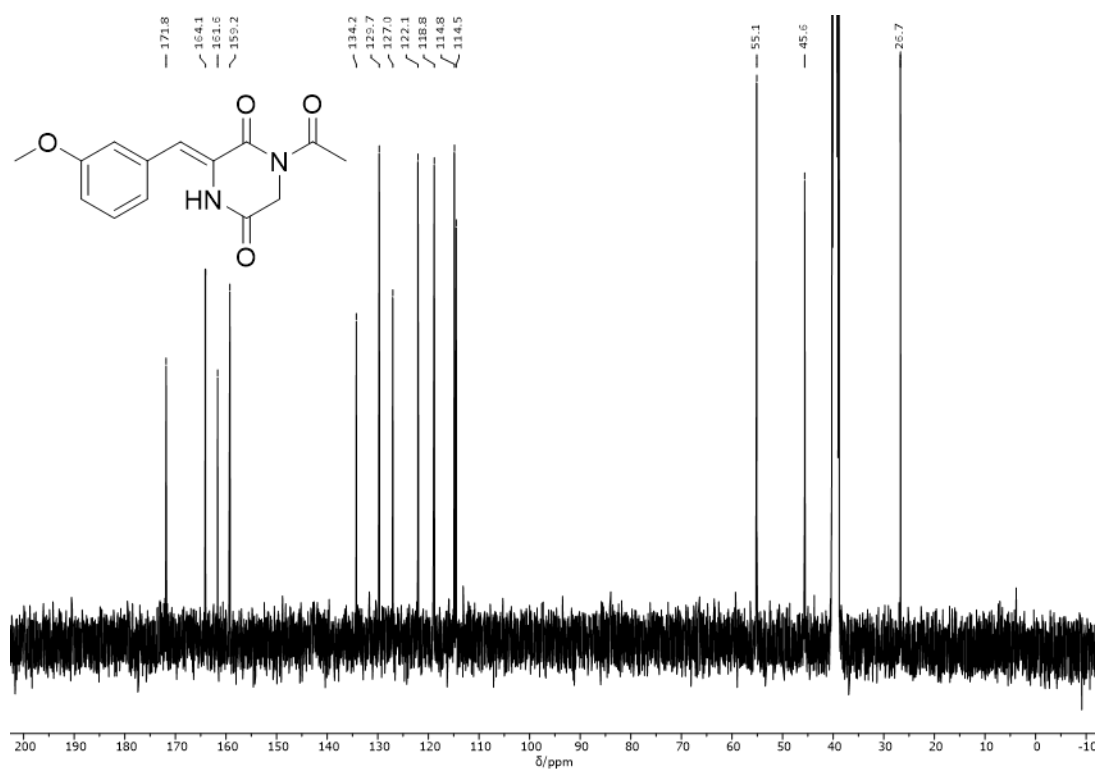
**Figure 212:** $^{13}$C NMR spectrum (101 MHz, DMSO-$d_6$) of compound Z-**31**.
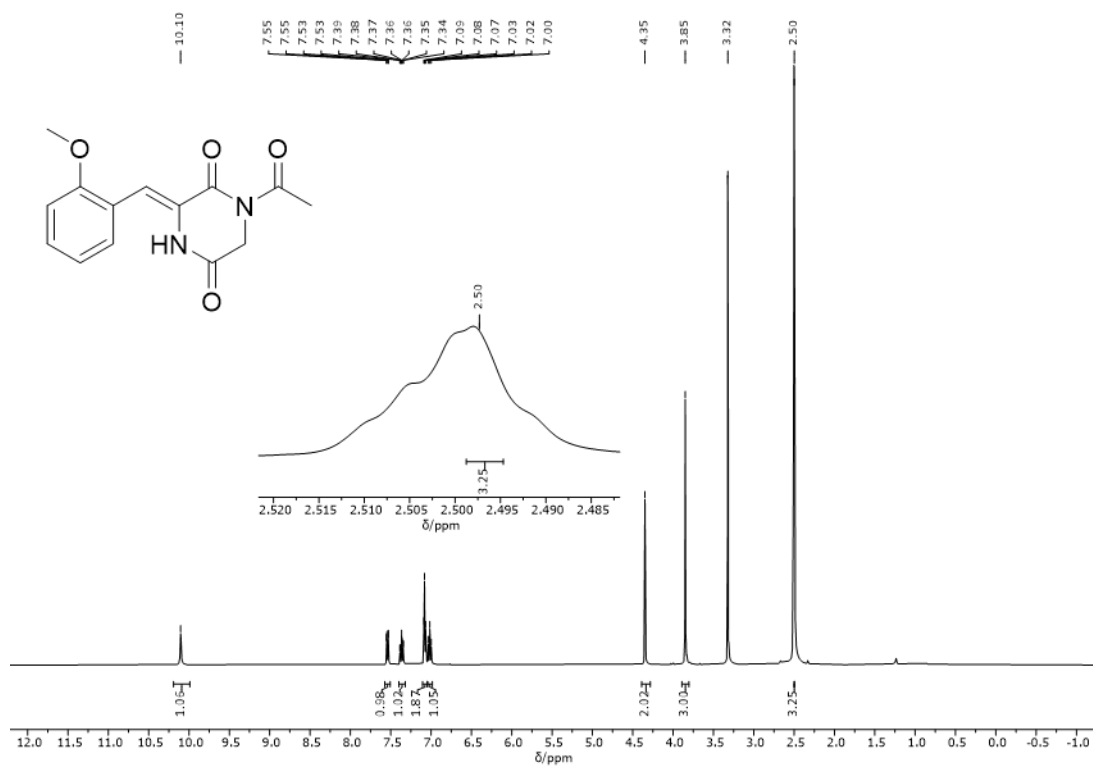


**Figure 213:** $^1$H NMR spectrum (400 MHz, DMSO-$d_6$) of compound Z-**32**.
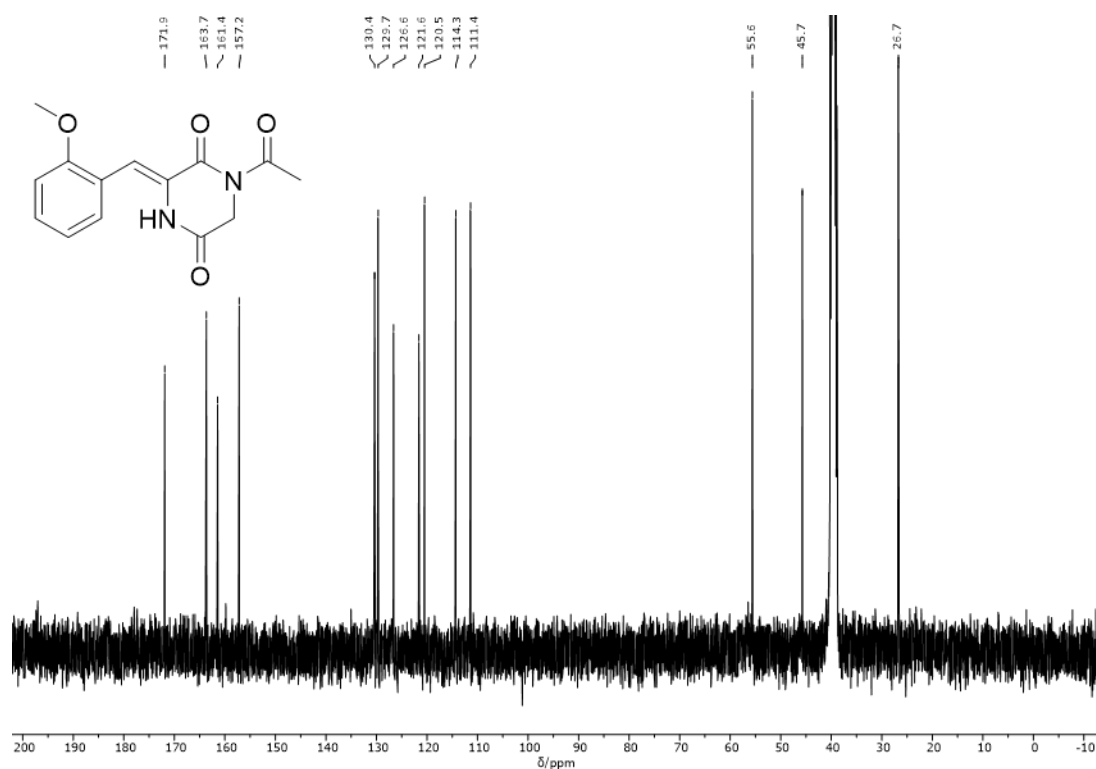
**Figure 214:** $^{13}$C NMR spectrum (101 MHz, DMSO-$d_6$) of compound *Z*-**32**.
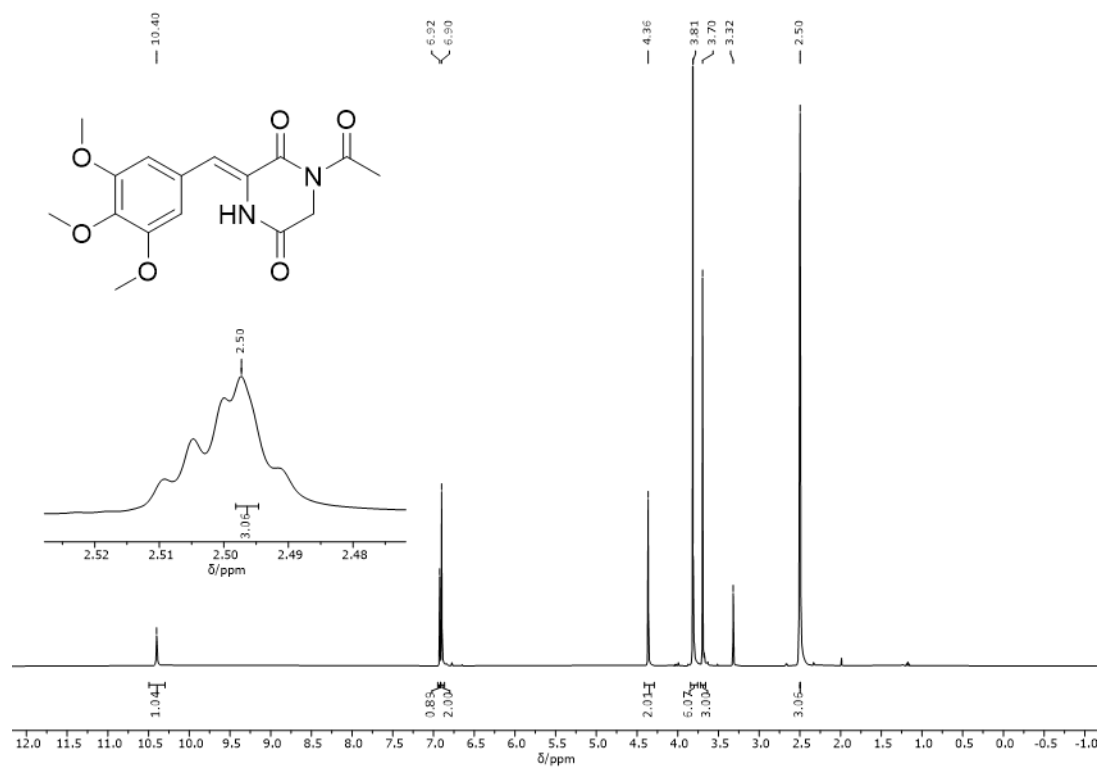


**Figure 215:** $^1$H NMR spectrum (400 MHz, DMSO-$d_6$) of compound *Z*-**33**.
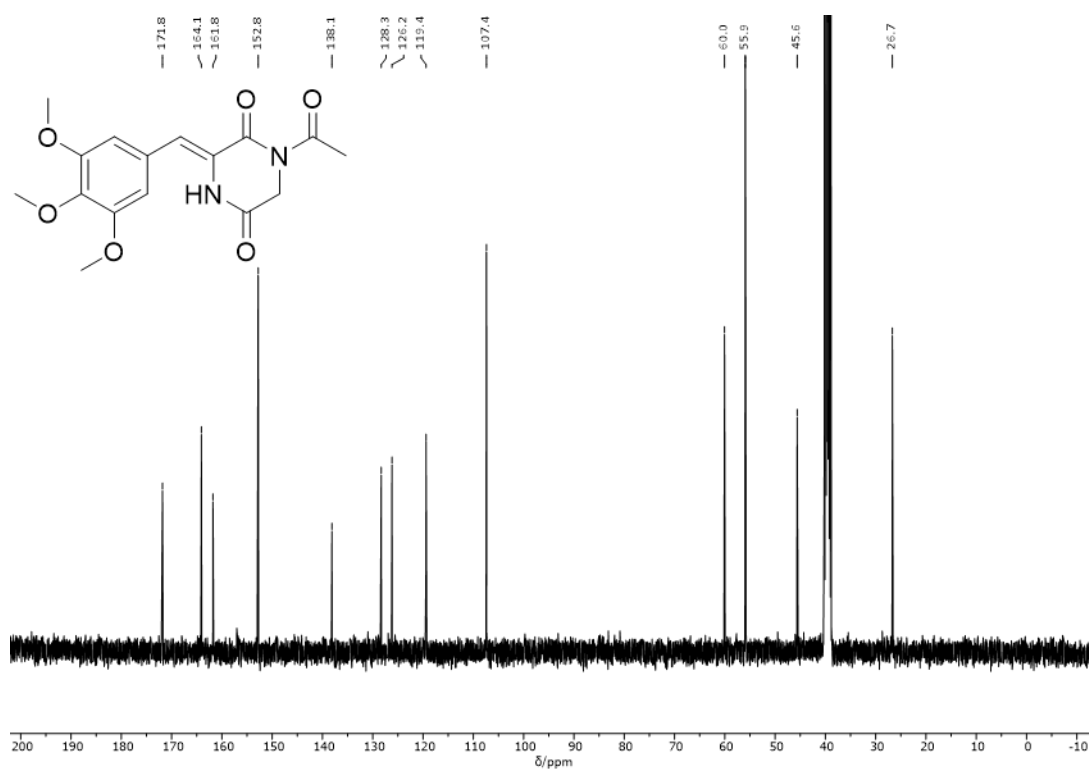
**Figure 216:** $^{13}$C NMR spectrum (101 MHz, DMSO-$d_6$) of compound Z-**33**.
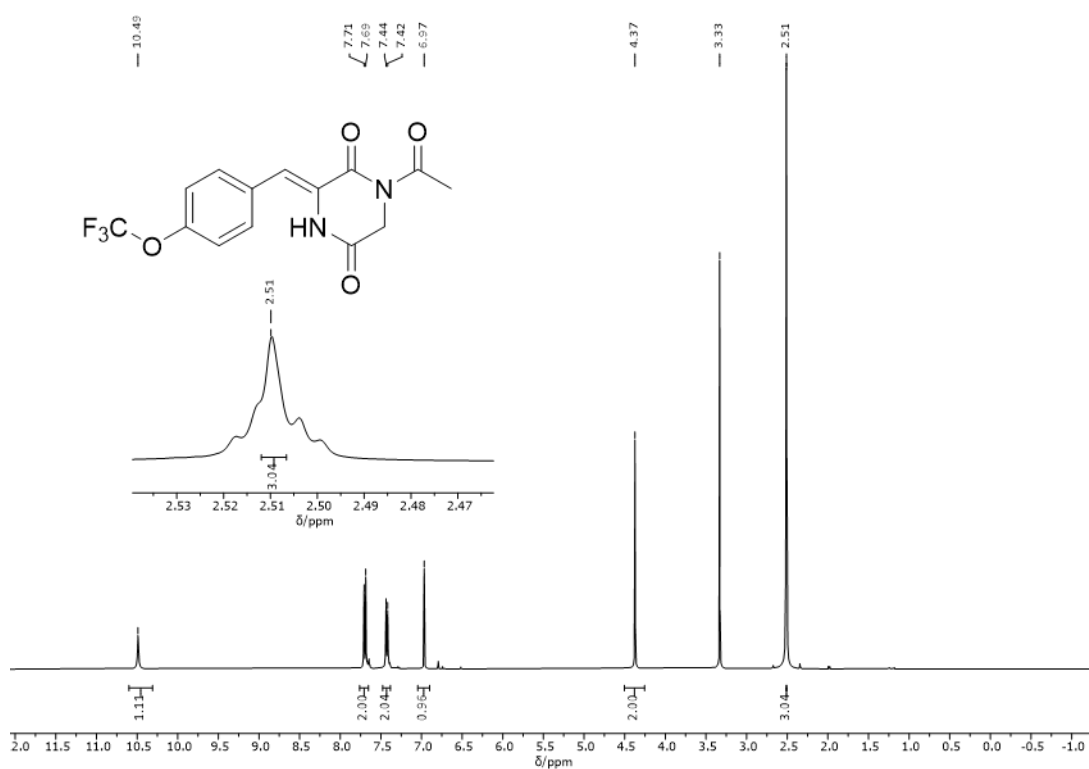


**Figure 217:** $^1$H NMR spectrum (400 MHz, DMSO-$d_6$) of compound Z-**34**.
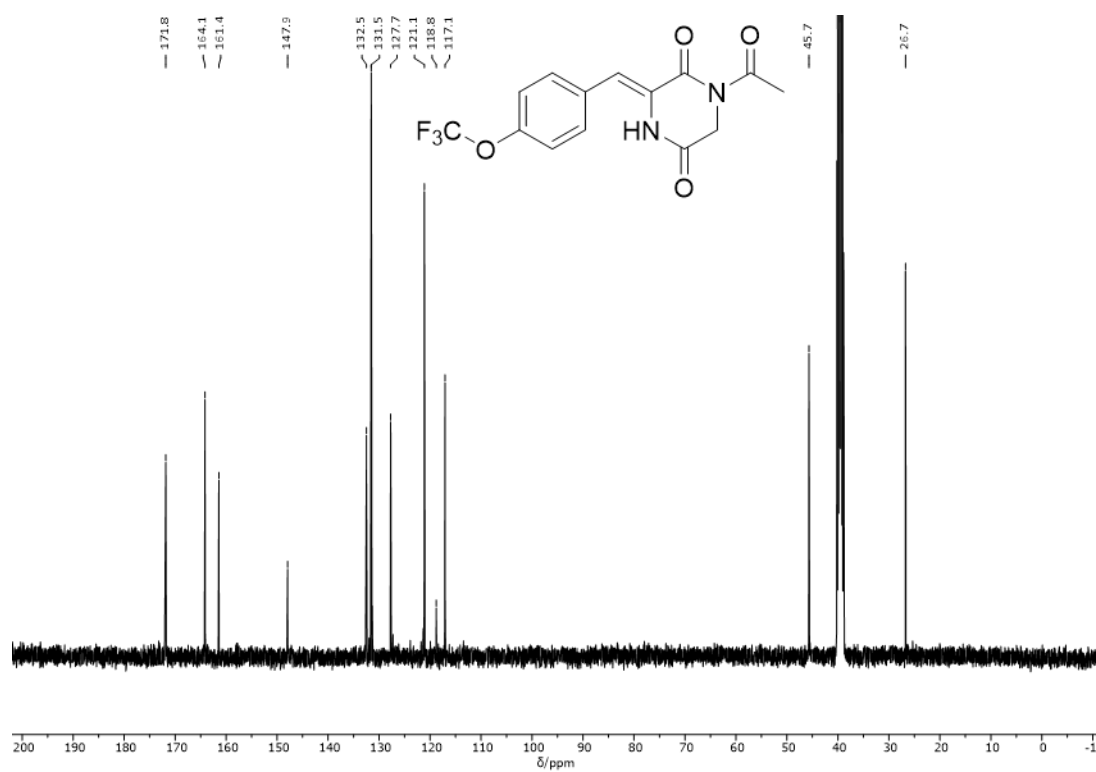
**Figure 218:** $^{13}$C NMR spectrum (101 MHz, DMSO-$d_6$) of compound Z-**34**.
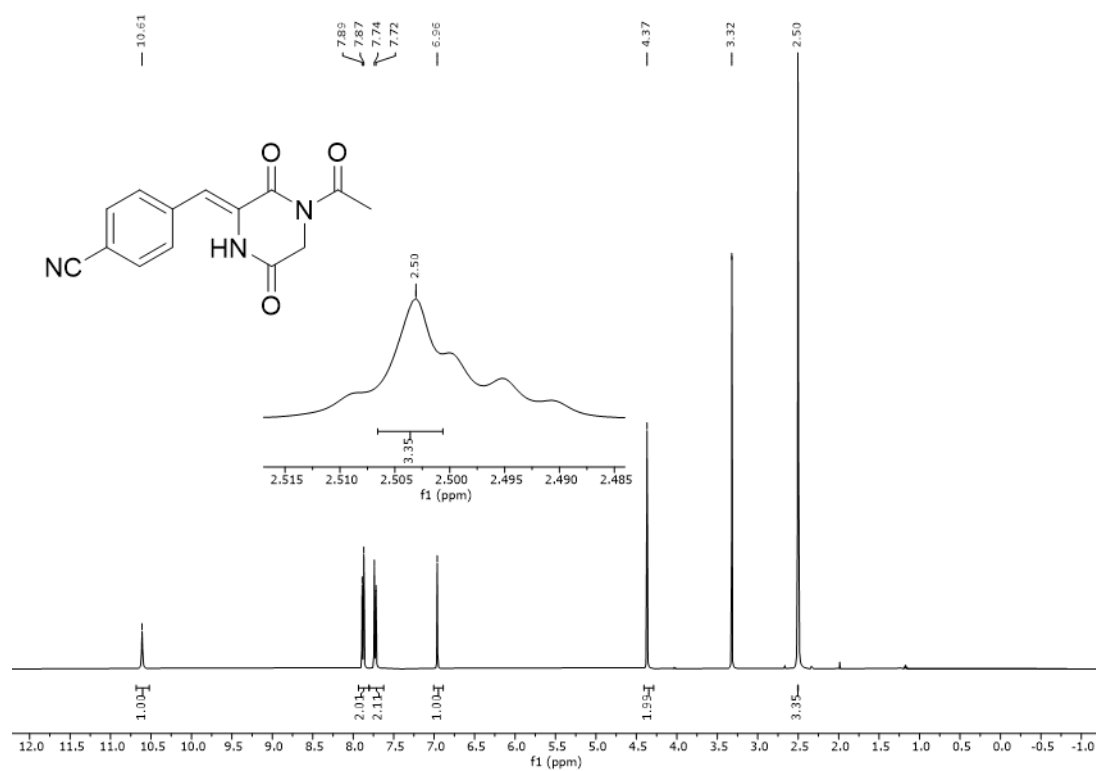


**Figure 219:** $^1$H NMR spectrum (400 MHz, DMSO-$d_6$) of compound Z-**35**.
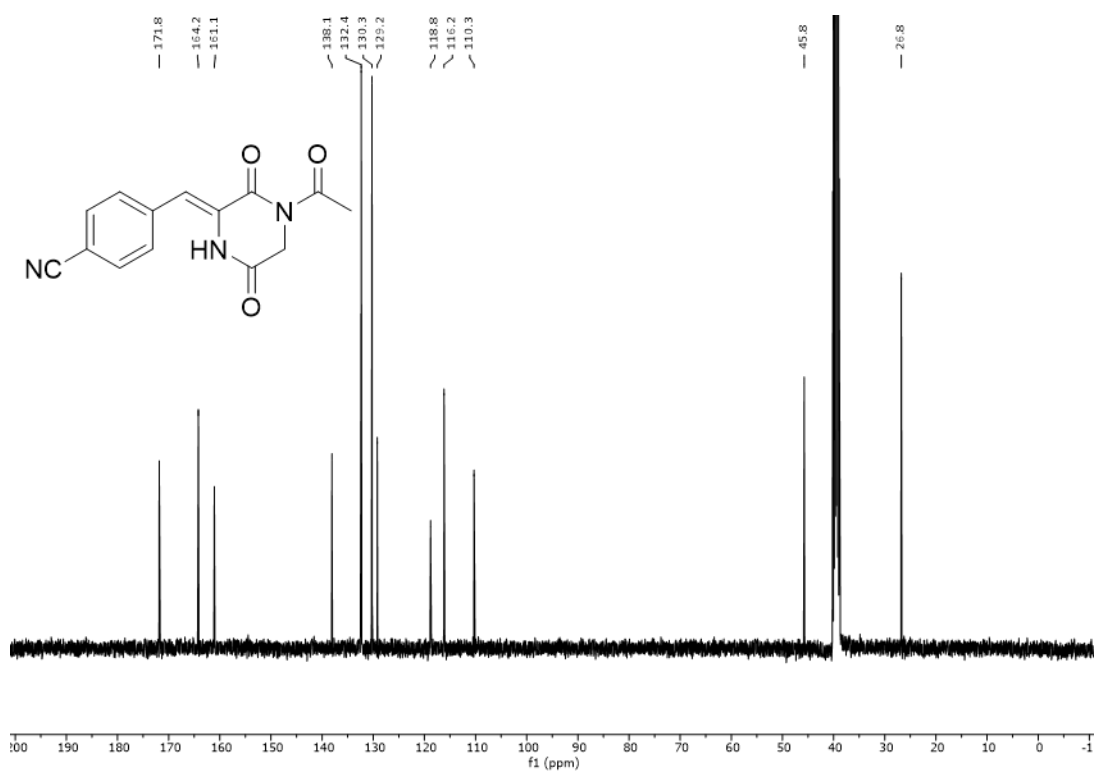
**Figure 220:** $^{13}C$ NMR spectrum (101 MHz, DMSO-$d_6$) of compound Z-**35**.
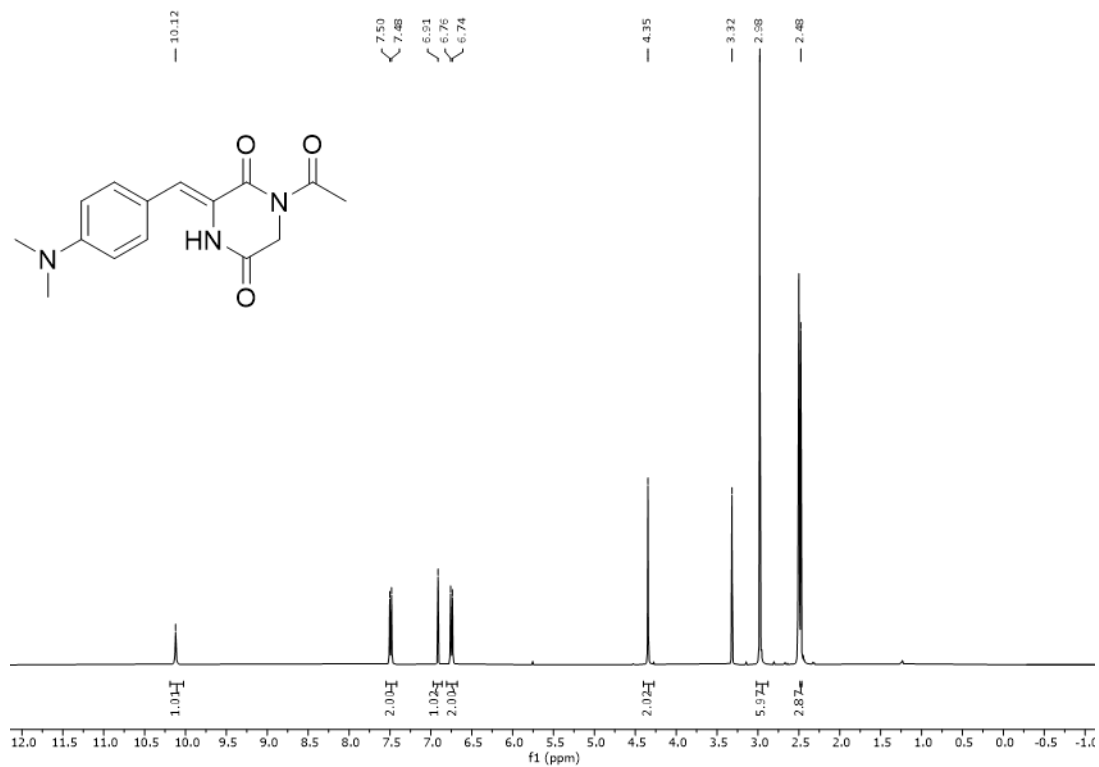


**Figure 221:** $^{1}H$ NMR spectrum (400 MHz, DMSO-$d_6$) of compound Z-**36**.
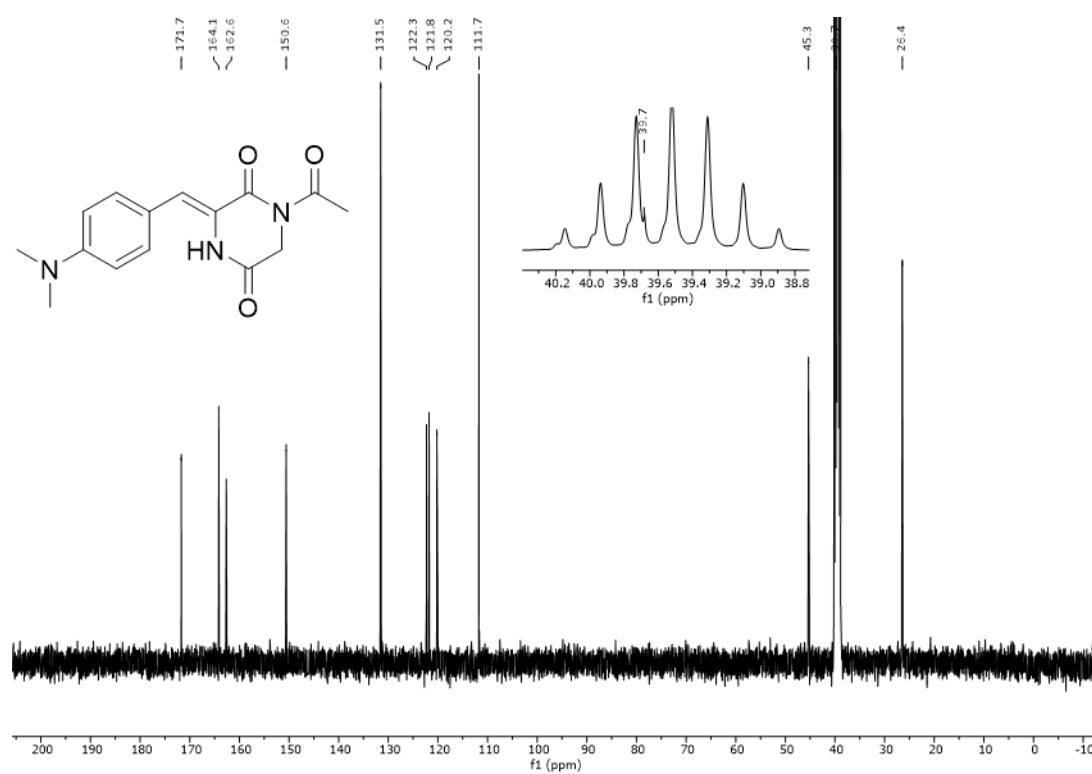
**Figure 222:** $^{13}$C NMR spectrum (101 MHz, DMSO-$d_6$) of compound Z-**36**.
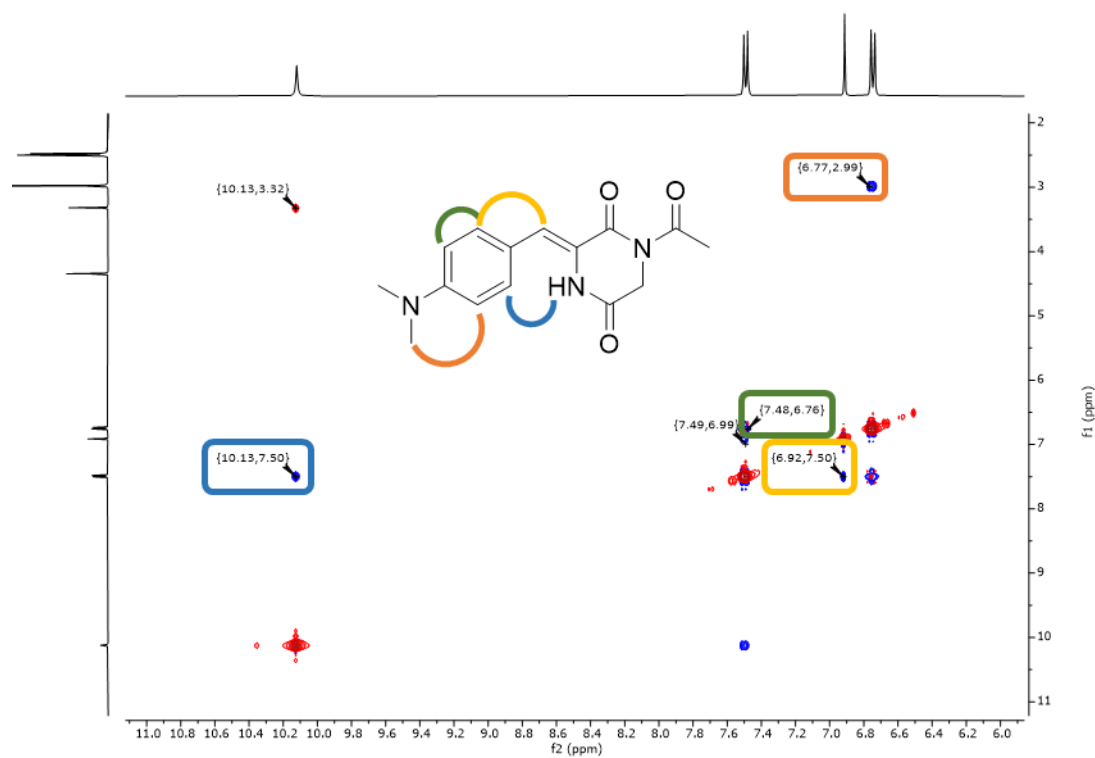


**Figure 223:** Extract of NOESY NMR spectrum (400 MHz, DMSO-$d_6$) of compound Z-**36**. Several relevant signals were assigned to the corresponding protons *via* color code.
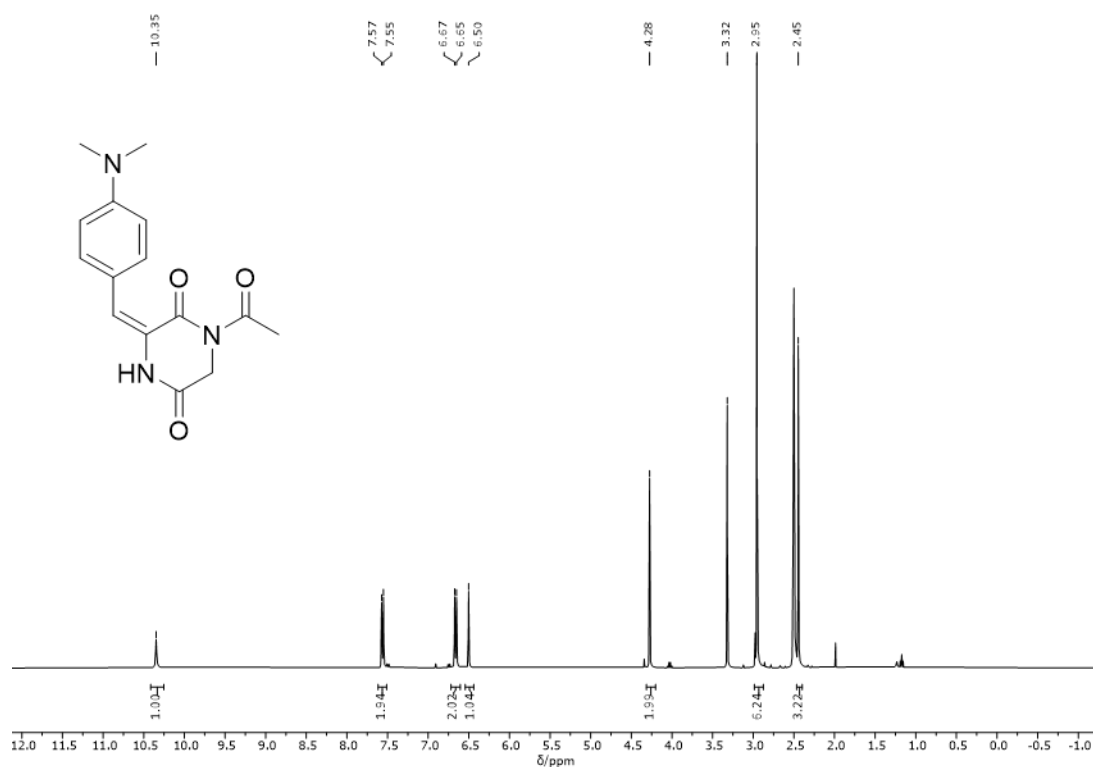
**Figure 224:** $^1$H NMR spectrum (400 MHz, DMSO-$d_6$) of compound *E*-**36**.
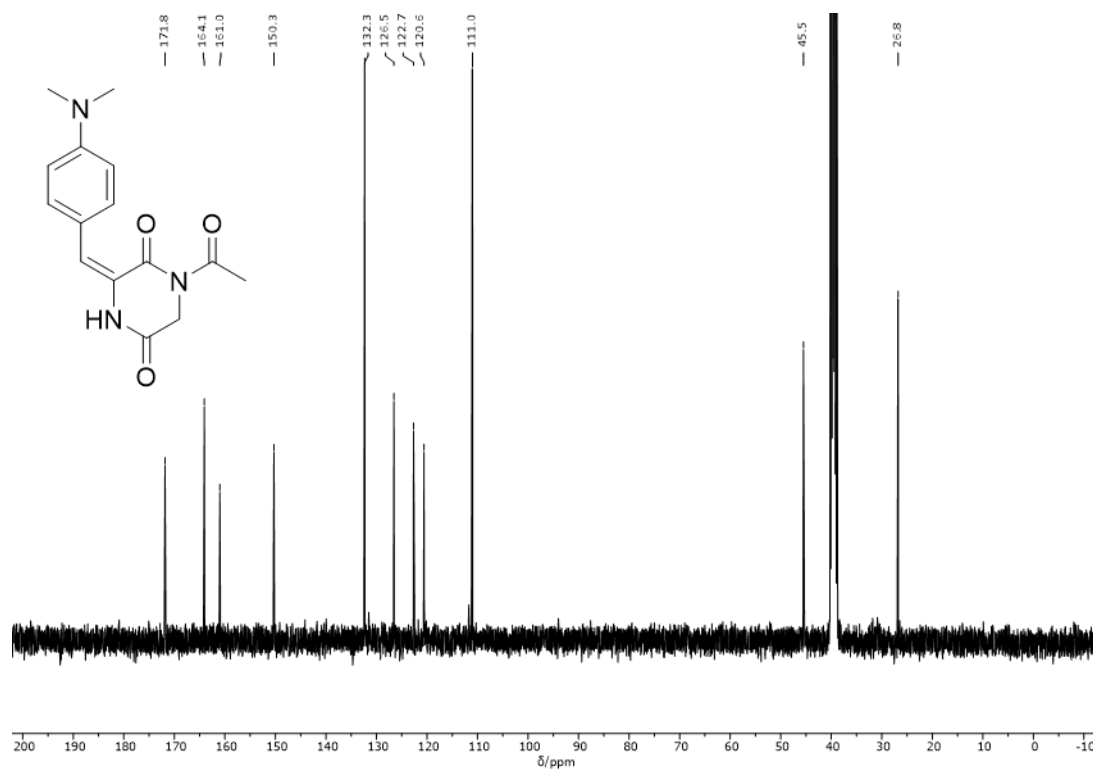


**Figure 225:** $^{13}$C NMR spectrum (101 MHz, DMSO-$d_6$) of compound *E*-**36**. One signal with a chemical shift of $\delta = 39.5$ overlaps with the solvent signal and was detected *via* $^1$H-$^{13}$C HSQC NMR spectroscopy.
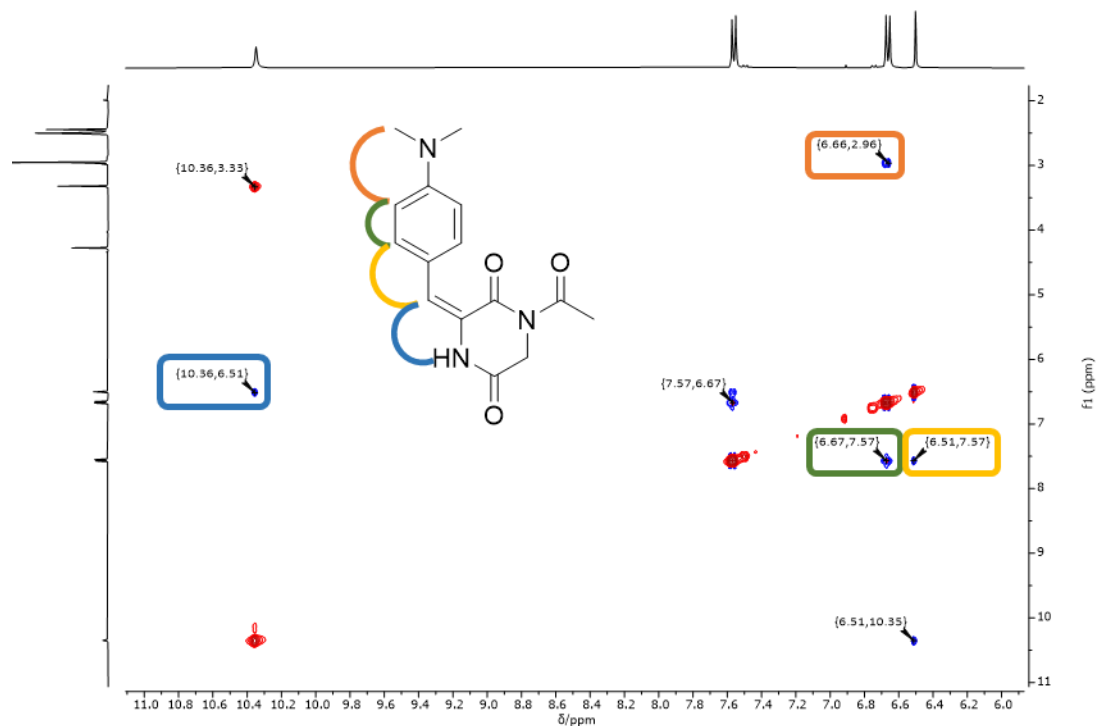
**Figure 226:** Extract of NOESY NMR spectrum (400 MHz, DMSO-$d_6$) of compound *E*-**36**. Several relevant signals were assigned to the corresponding protons *via* color code.



**Figure 227:** $^1$H NMR spectrum (400 MHz, CDCl$_3$) of compound *Z*-**37**.
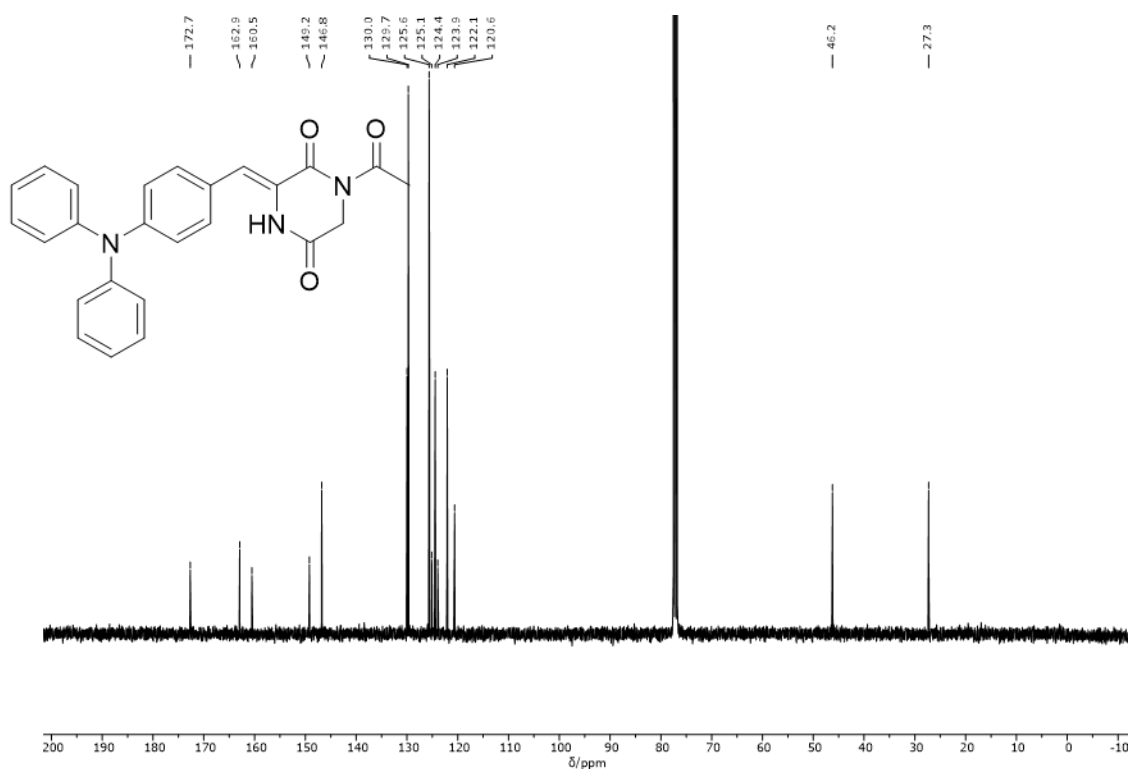
**Figure 228:** $^{13}$C NMR spectrum (101 MHz, CDCl$_3$) of compound Z-**37**.
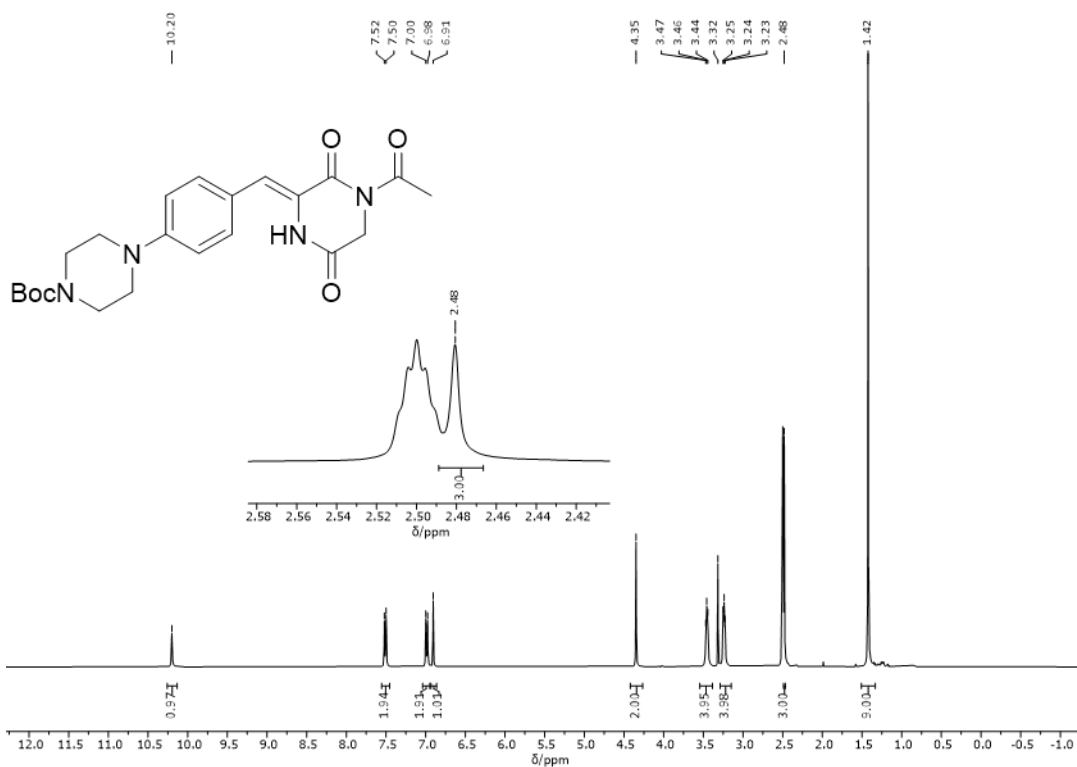


**Figure 229:** $^1$H NMR spectrum (400 MHz, DMSO-$d_6$) of compound Z-**56**.
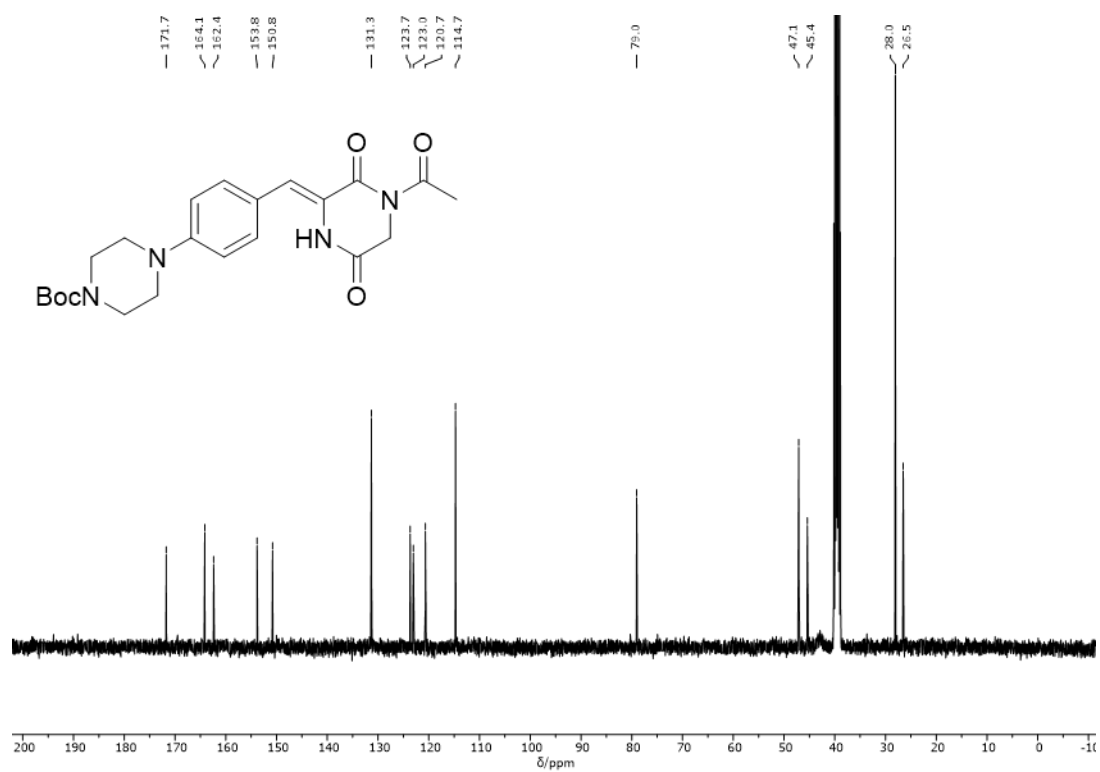
**Figure 230:** $^{13}$C NMR spectrum (101 MHz, DMSO-$d_6$) of compound Z-**56**.
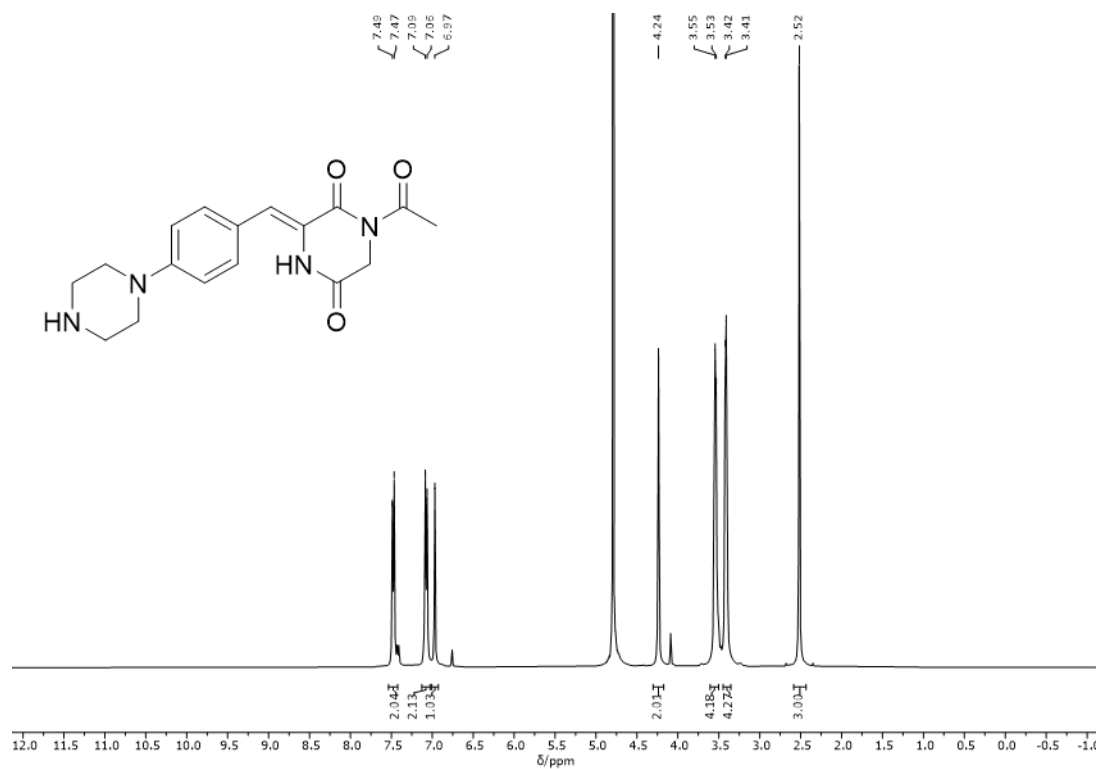


**Figure 231:** $^1$H NMR spectrum (400 MHz, D$_2$O) of compound Z-**38**.
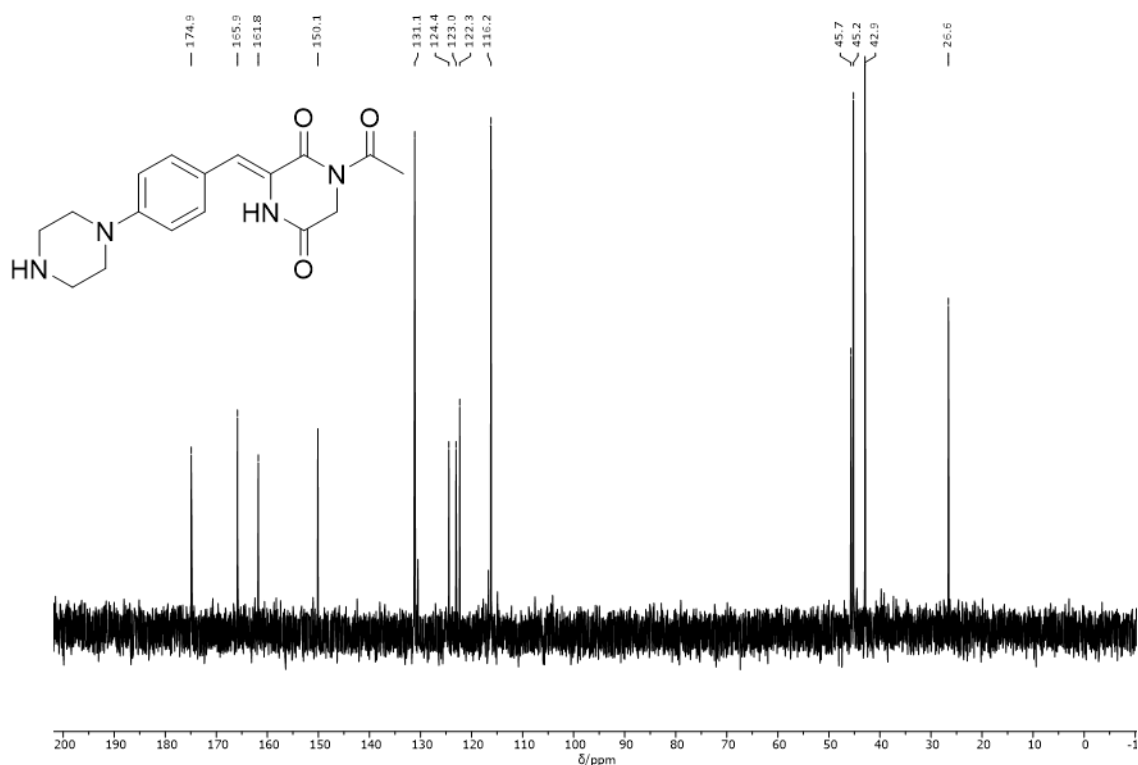
**Figure 232:** $^{13}C$ NMR spectrum (101 MHz, $D_2O$) of compound *Z*-**38**.

### 5.5.3 Absorption Spectra of Non-Irradiated Samples
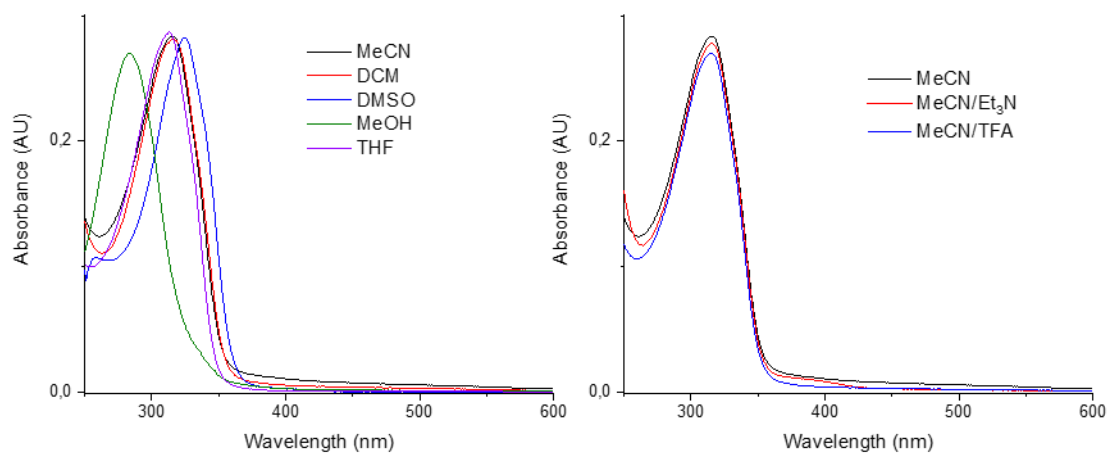


**Figure 233:** Compound *Z*-**29** was dissolved in different solvents (80 µM) and in mixtures of 1% (v/v) TFA in MeCN and 1% (v/v) Et₃N in MeCN, respectively. Absorption spectra were measured in the dark (d = 2 mm). The spectra are assigned to the respective solvents *via* color code.
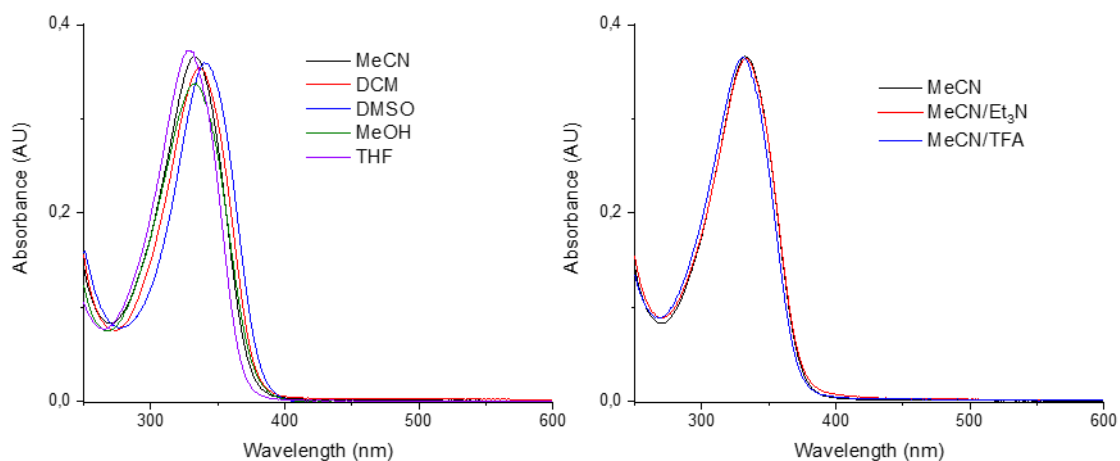
**Figure 234:** Compound *Z*-**30** was dissolved in different solvents (80 µM) and in mixtures of 1% (v/v) TFA in MeCN and 1% (v/v) Et₃N in MeCN, respectively. Absorption spectra were measured in the dark (d = 2 mm). The spectra are assigned to the respective solvents *via* color code.
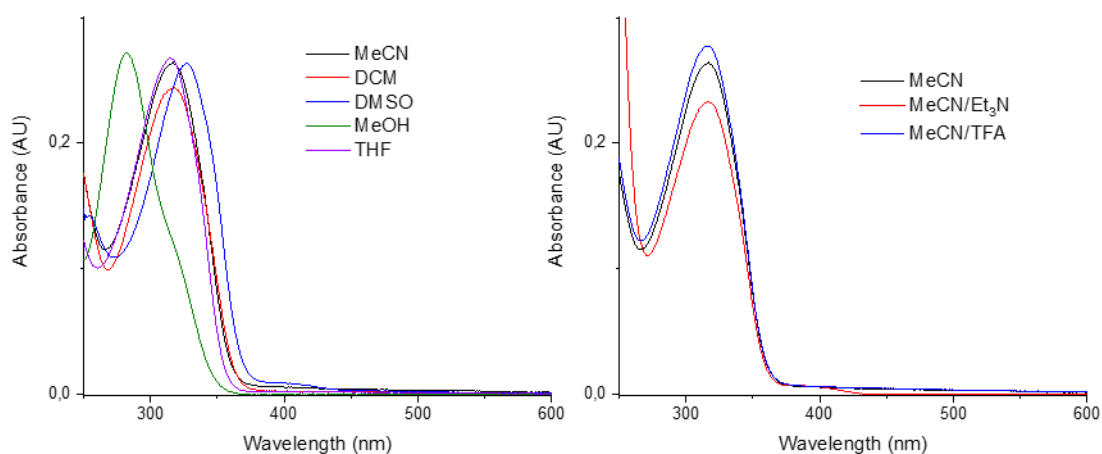


**Figure 235:** Compound *Z*-**31** was dissolved in different solvents (80 µM) and in mixtures of 1% (v/v) TFA in MeCN and 1% (v/v) Et₃N in MeCN, respectively. Absorption spectra were measured in the dark (d = 2 mm). The spectra are assigned to the respective solvents *via* color code.
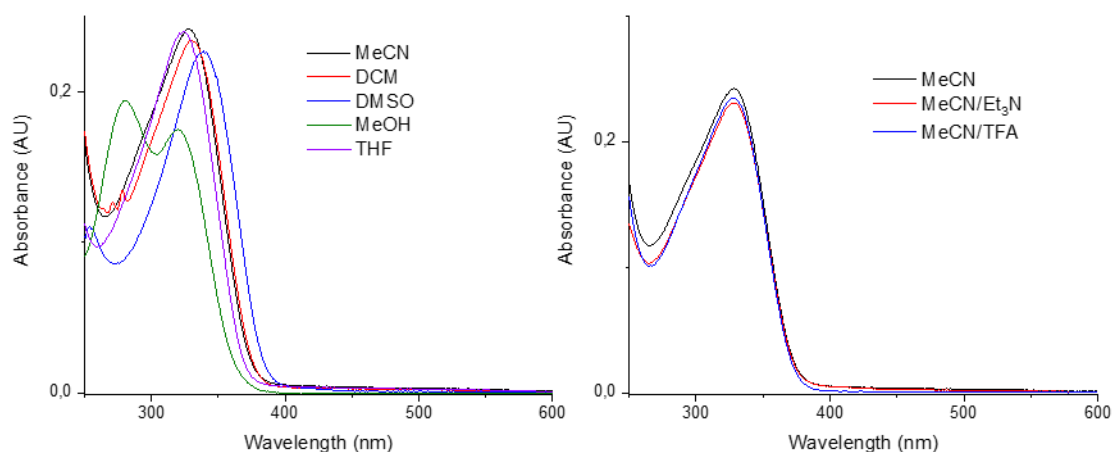
**Figure 236:** Compound *Z*-**32** was dissolved in different solvents (80 µM) and in mixtures of 1% (v/v) TFA in MeCN and 1% (v/v) Et₃N in MeCN, respectively. Absorption spectra were measured in the dark (d = 2 mm). The spectra are assigned to the respective solvents *via* color code.
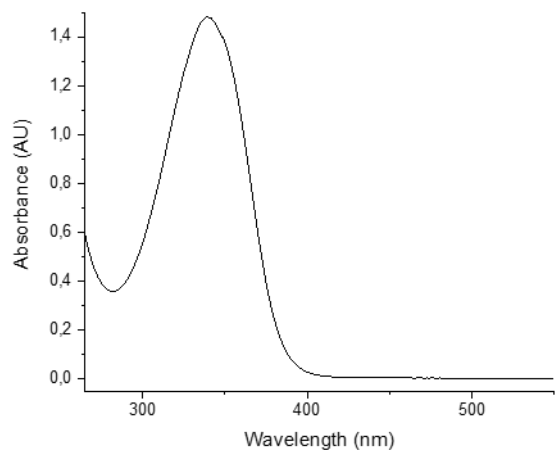


**Figure 237:** Absorption spectrum of compound *Z*-**33** (80 μM) in DMSO (d = 10 mm).
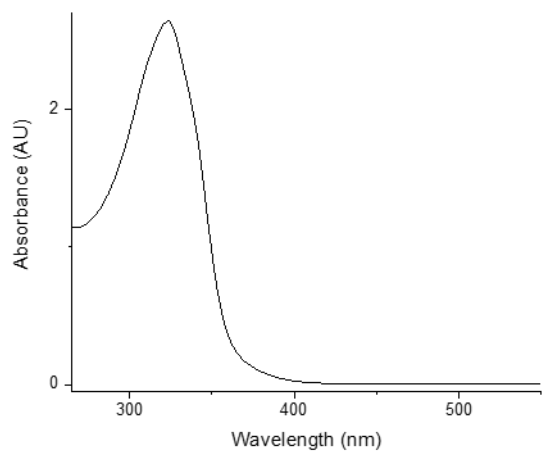


**Figure 238:** Absorption spectrum of compound *Z*-**34** (160 μM) in DMSO (d = 10 mm).
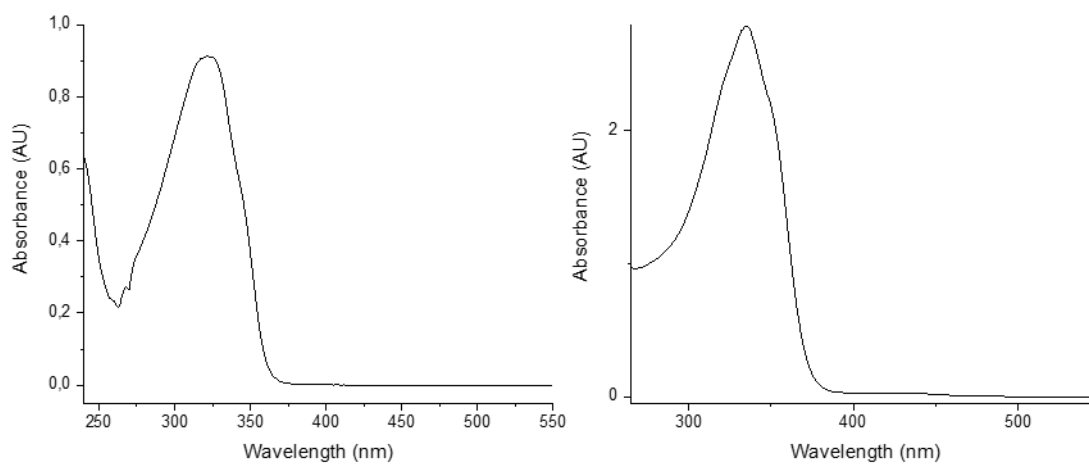
**Figure 239:** Absorption spectrum of compound *Z*-**35** (d = 10 mm). Left: 80 μM in CH$_2$Cl$_2$; right: 160 μM in DMSO.
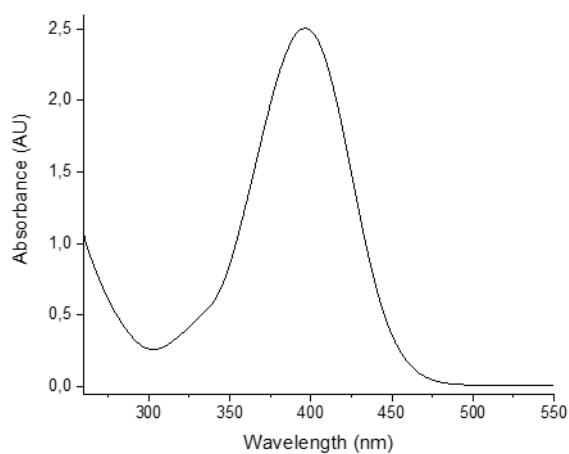


**Figure 240:** Absorption spectrum of compound *Z*-**36** (80 μM) in DMSO (d = 10 mm).
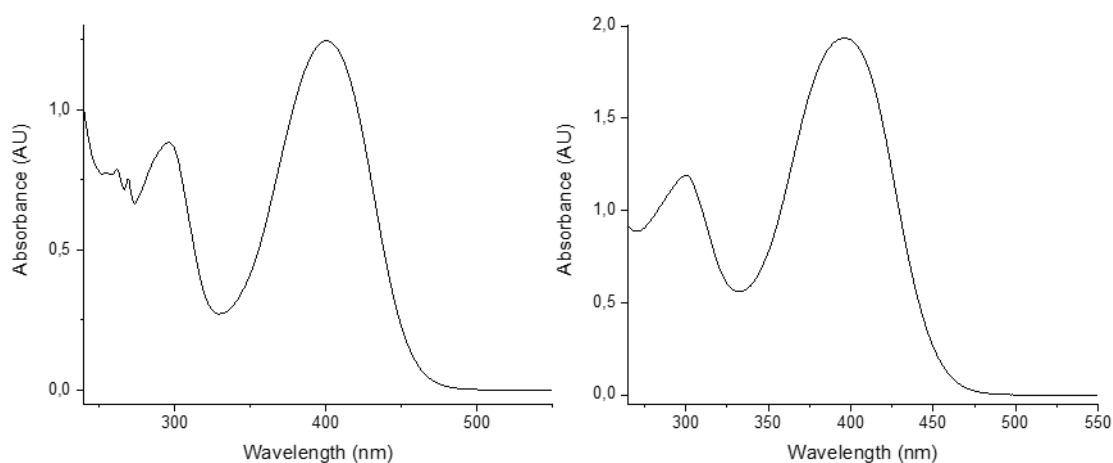


**Figure 241:** Absorption spectrum of compound *Z*-**37** (d = 10 mm). Left: 80 μM in CH$_2$Cl$_2$; right: 80 μM in DMSO.

### 5.5.4 Absorption Spectra of Irradiated Samples
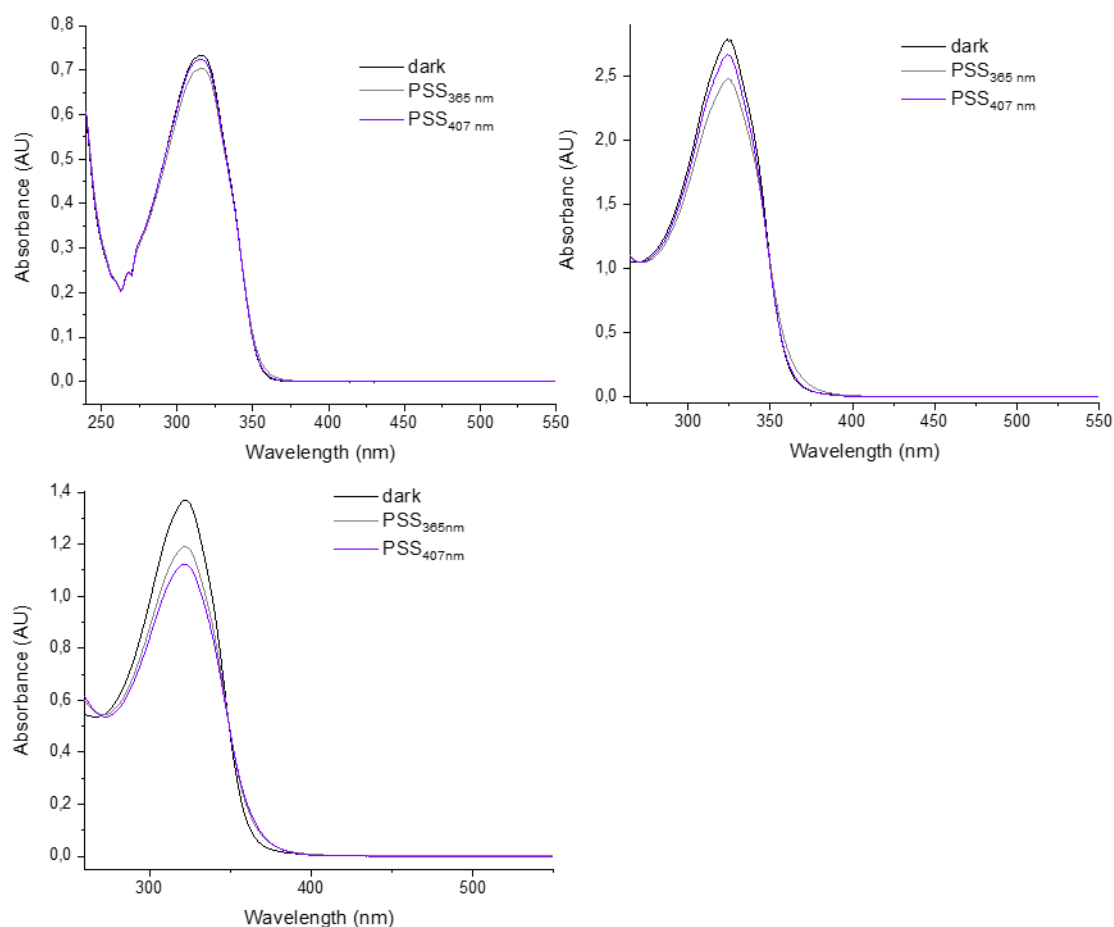


**Figure 242:** Compound **29** was dissolved in CH$_2$Cl$_2$ (80 µM, top left), DMSO (160 µM, top right) and 25% PBS in DMSO (v/v) (80 µM, bottom left), respectively. Absorption spectra (d=10 mm) were first measured in the dark. The samples were then irradiated with 365 nm and with 407 nm. An absorption spectrum was measured after each irradiation step until the PSS was reached, respectively.
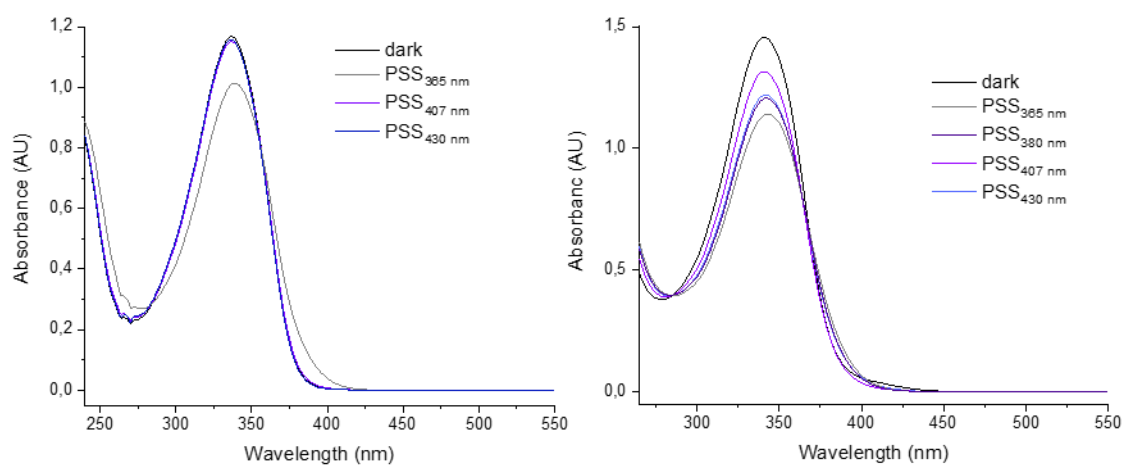


**Figure 243:** Compound **30** was dissolved in CH$_2$Cl$_2$ (80 µM, left) and DMSO (80 µM, right), respectively. Absorption spectra (d=10 mm) were first measured in the dark. The samples were then

irradiated with 365 nm, 407 nm and 430 nm. An absorption spectrum was measured after each irradiation step until the PSS was reached, respectively.
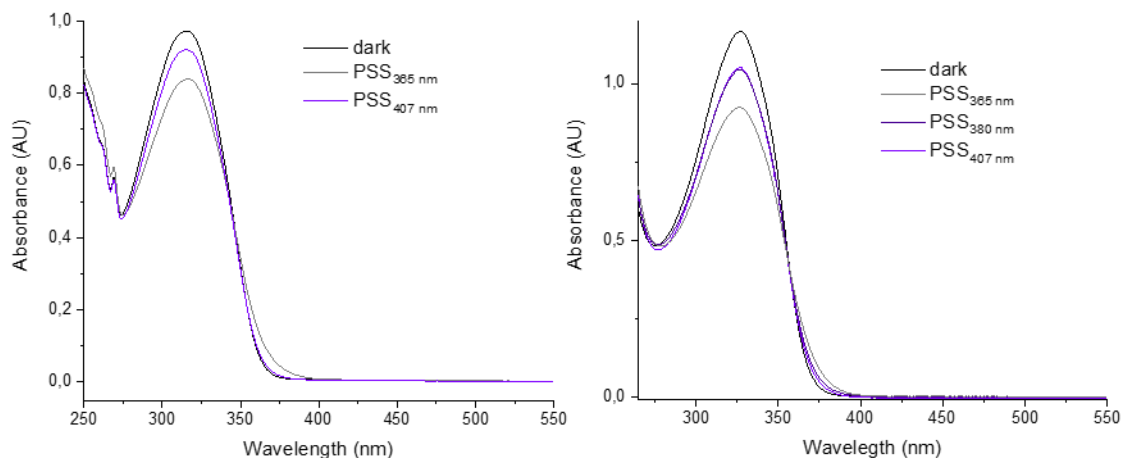


**Figure 244:** Compound **31** was dissolved in $CH_2Cl_2$ (80 µM, left) and DMSO (80 µM, right), respectively. Absorption spectra (d=10 mm) were first measured in the dark. The samples were then irradiated with 365 nm, 380 nm and 407 nm. An absorption spectrum was measured after each irradiation step until the PSS was reached, respectively.
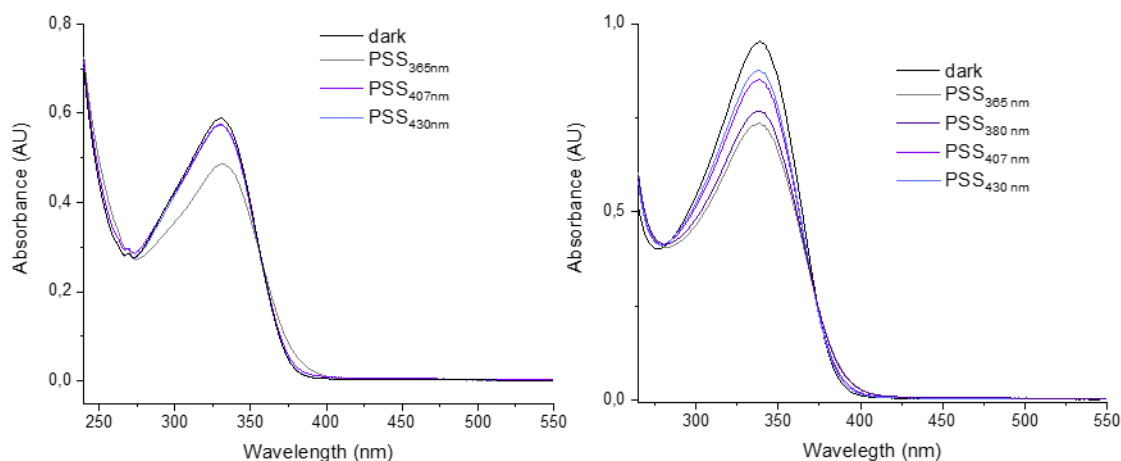


**Figure 245:** Compound **32** was dissolved in $CH_2Cl_2$ (80 µM, left) and DMSO (80 µM, right), respectively. Absorption spectra (d=10 mm) were first measured in the dark. The samples were then irradiated with 365 nm, 380 nm, 407 nm and 430 nm. An absorption spectrum was measured after each irradiation step until the PSS was reached, respectively.
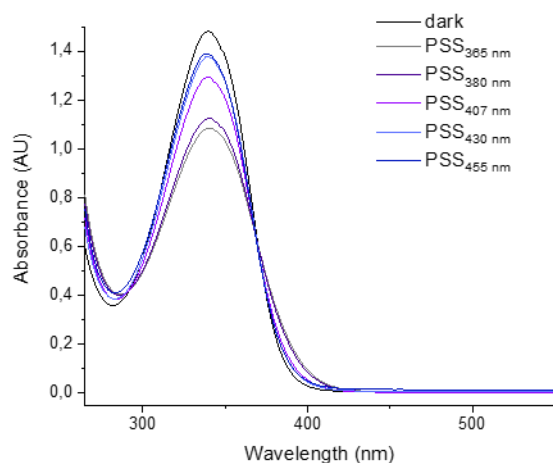
**Figure 246:** Compound **33** was dissolved in DMSO (80 µM) and an absorption spectrum (d=10 mm) was first measured in the dark. The sample was then irradiated with 365 nm, 380 nm, 407 nm, 430 nm and 455 nm. An absorption spectrum was measured after each irradiation step until the PSS was reached, respectively.
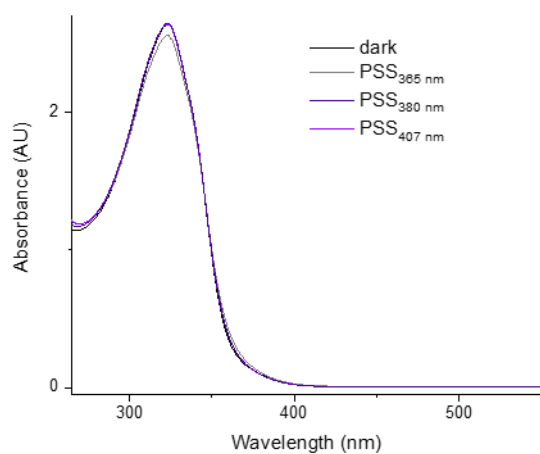


**Figure 247:** Compound **34** was dissolved in DMSO (80 µM) and an absorption spectrum (d=10 mm) was first measured in the dark. The sample was then irradiated with 365 nm, 380 nm and 407 nm. An absorption spectrum was measured after each irradiation step until the PSS was reached, respectively.
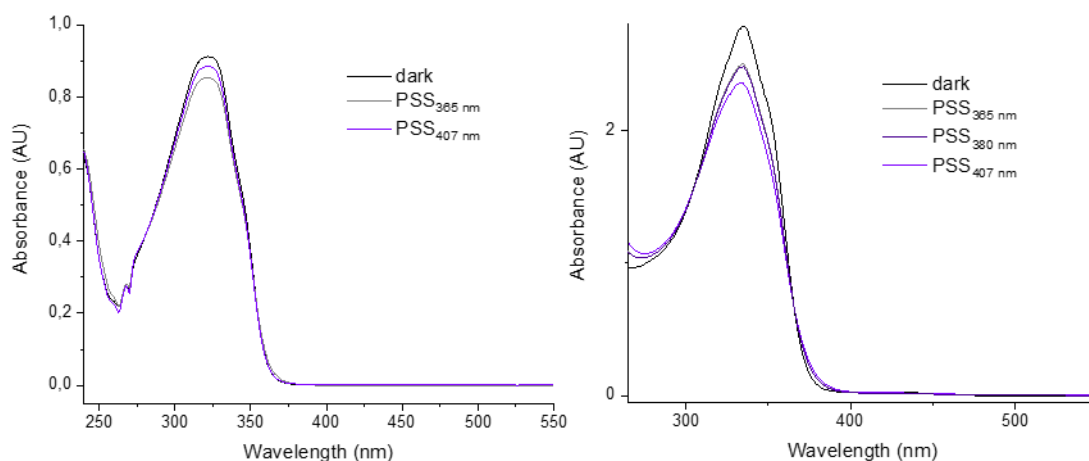
**Figure 248:** Compound **35** was dissolved in CH₂Cl₂ (80 µM, left) and DMSO (160 µM, right), respectively. Absorption spectra (d=10 mm) were first measured in the dark. The samples were then irradiated with 365 nm, 380 nm and 407 nm. An absorption spectrum was measured after each irradiation step until the PSS was reached, respectively.
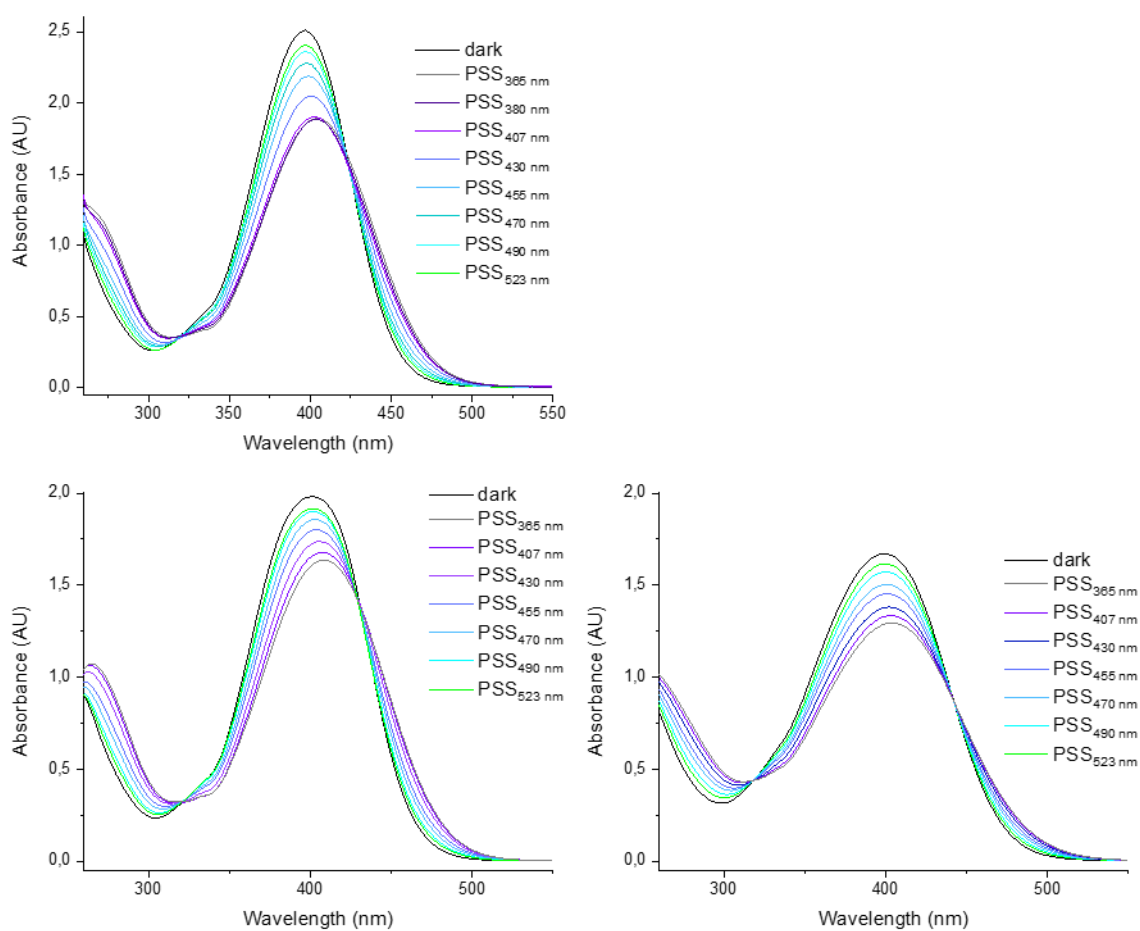


**Figure 249:** Compound **36** was dissolved in DMSO (80 µM, top left), 25% PBS in DMSO (v/v) (80 µM, bottom left) and 75% PBS in DMSO (v/v) (80 µM, bottom right), respectively. Absorption spectra (d=10 mm) were first measured in the dark. The samples were then irradiated with 365 nm,

380 nm, 407 nm, 430 nm, 455 nm, 470 nm, 490 nm and with 523 nm. An absorption spectrum was measured after each irradiation step until the PSS was reached, respectively.
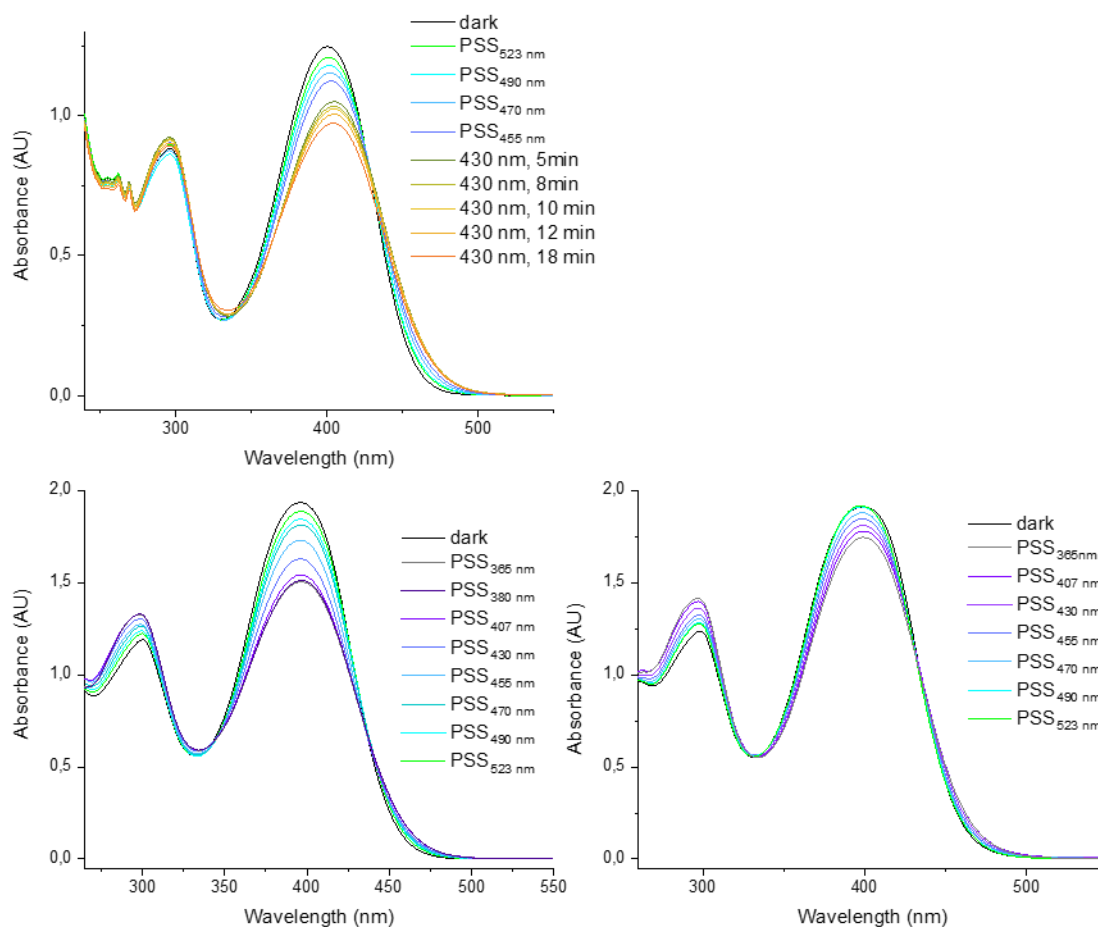


**Figure 250:** Compound **37** was dissolved in $CH_2Cl_2$ (80 µM, top left), DMSO (80 µM, bottom left) and 25% PBS in DMSO (v/v) (80 µM, bottom right), respectively. Absorption spectra (d=10 mm) were first measured in the dark. The samples were then irradiated with 365 nm, 380 nm, 407 nm, 430 nm, 455 nm, 470 nm, 490 nm and with 523 nm. An absorption spectrum was measured after each irradiation step until the PSS was reached, respectively. In case of the sample in $CH_2Cl_2$ degradation was observed upon irradiation with wavelengths < 455 nm.

### 5.5.5 Emission Spectra



| $\lambda_{abs,max}(Z) = 397$ nm |
| $\lambda_{em,max}(Z) = 516$ nm |
| PLQY $(Z) = 0.004$ |

| $\lambda_{abs,max}(Z) = 397$ nm |
| $\lambda_{em,max}(Z) = 565$ nm |
| PLQY $(Z) = 0.030$ |
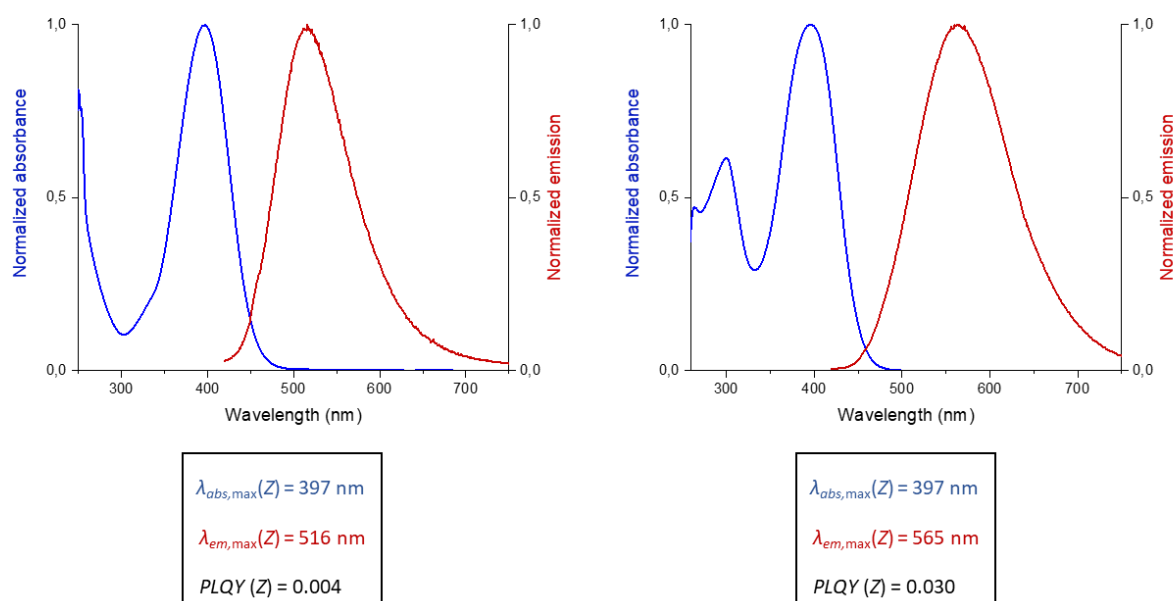
**Figure 251:** Normalized absorption (blue) and emission (red) spectra of 80 μM solutions of the respective Z-isomers of **36** (left) and **37** (right) in DMSO.

### 5.5.6 Composition of the Photostationary States (PSSs)

The PSS composition was determined by measuring $^1$H NMR spectra of the respective compounds after irradiation. The PSS values in the NMR tubes (0.5 mL of the 30-60 mM solutions in DMSO-$d_6$ or CD$_2$Cl$_2$) have been achieved within 1 h (365, 407, 523 nm) or 2 h (430 nm). Signal pairs were determined for each compound: two signals assigned to the same proton for the respective photoisomers were integrated and the % of E-isomer = $I_E/(I_E+I_Z)*100$% was determined. The final E/Z ratios result from the average value determined from three signal pairs.

**Table 11:** PSS composition in DMSO-$d_6$ or CD$_2$Cl$_2$ determined by measuring $^1$H NMR spectra of the respective compounds after irradiation.

| Compound | 365 nm (% of E-isomer) | 407 nm (% of E-isomer) | 430 nm (% of E-isomer) | 450 nm (% of E-isomer) | 470 nm (% of E-isomer) | 490 nm (% of E-isomer) | 523 nm (% of E-isomer) |
|---|---|---|---|---|---|---|---|
| **29** (DMSO-$d_6$) | 19 | 6 | - | - | - | - | - |
| **29** (CD$_2$Cl$_2$) | 10 | 2 | - | - | - | - | - |
| **30** (CD$_2$Cl$_2$) | 29 | 3 | <1 | - | - | - | - |

| | | | | | | | |
|---|---|---|---|---|---|---|---|
| **31** (CD$_2$Cl$_2$) | 31 | 6 | - | - | - | - | - |
| **32** (CD$_2$Cl$_2$) | 34 | 5 | <1 | - | - | - | - |
| **35** (CD$_2$Cl$_2$) | 12 | 4 | - | - | - | - | - |
| **36** (DMSO-$d_6$) | 71 | 62 | 53 | 20 | 13 | 7 | 3 |
| **37** (DMSO-$d_6$) | 58 | 54 | 47 | 26 | 19 | 15 | 14 |
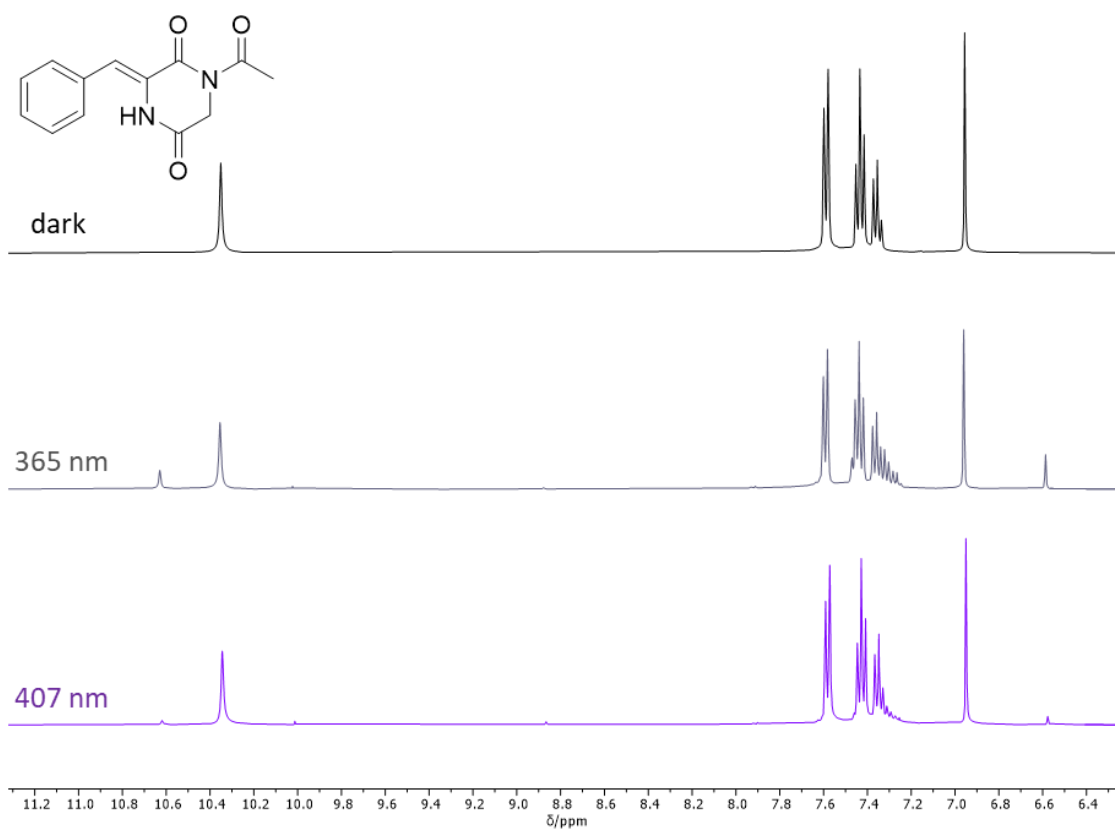


**Figure 252:** Sections of $^1$H NMR spectra (400 MHz, DMSO-$d_6$) of compound **29** in the dark (top) and after reaching the PSS upon irradiation with 365 nm (middle) and 407 nm (bottom).
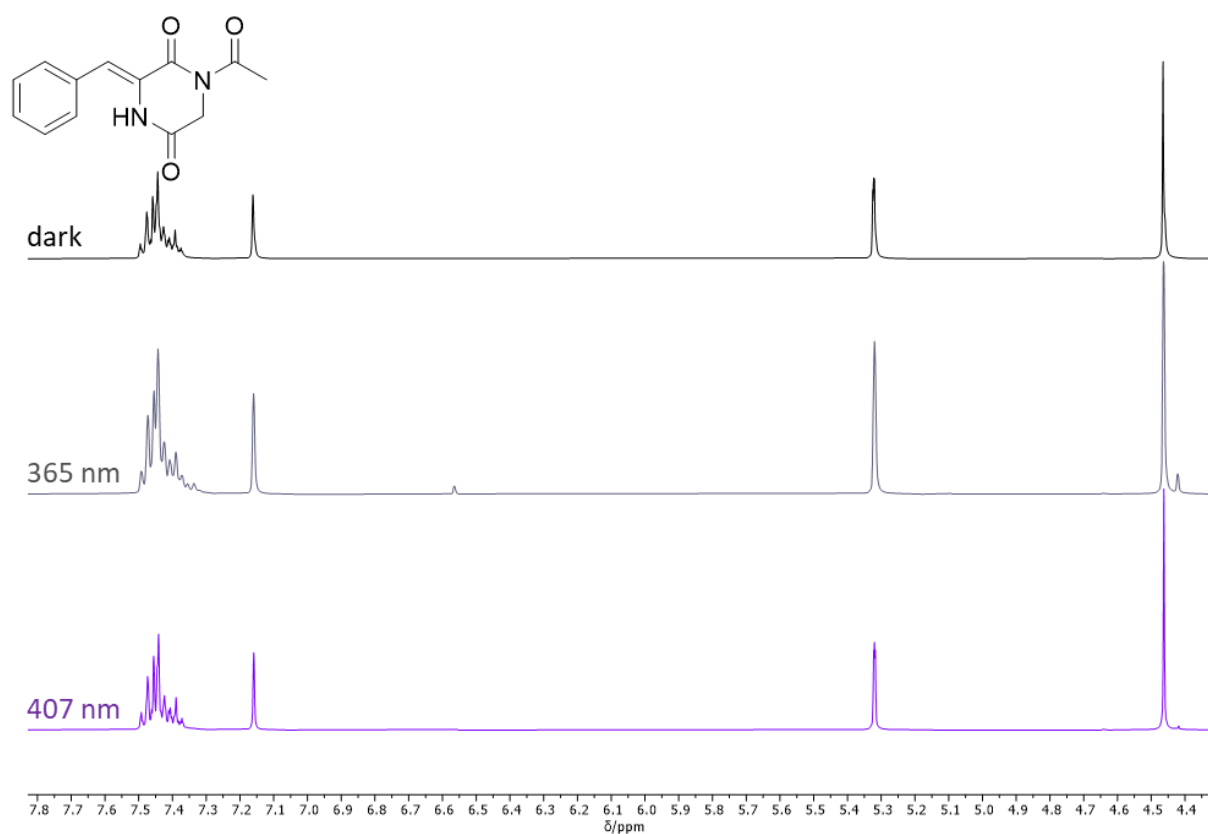
**Figure 253:** Sections of $^1$H NMR spectra (400 MHz, CD$_2$Cl$_2$) of compound **29** in the dark (top) and after reaching the PSS upon irradiation with 365 nm (middle) and 407 nm (bottom).
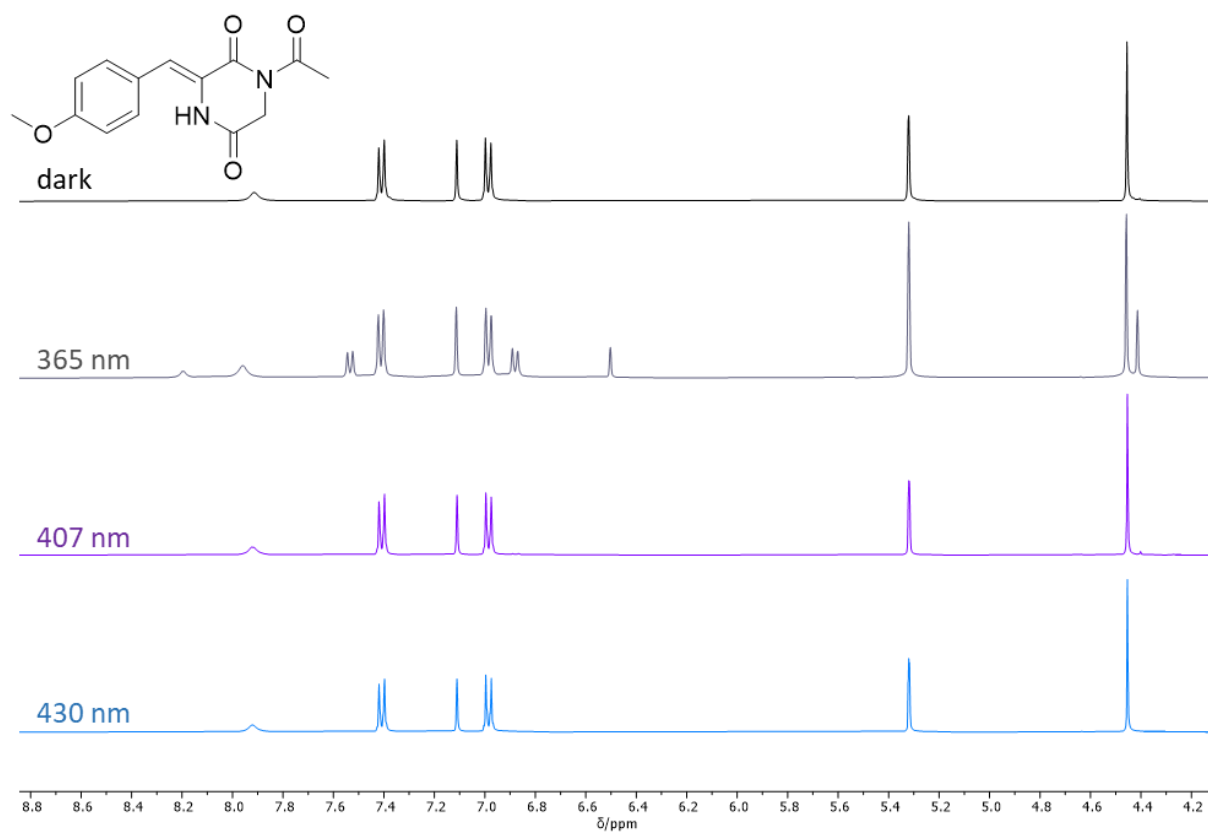


**Figure 254:** Sections of $^1$H NMR spectra (400 MHz, CD$_2$Cl$_2$) of compound **30** in the dark (top) and after reaching the PSS upon irradiation with 365 nm, 407 nm and 430 nm.
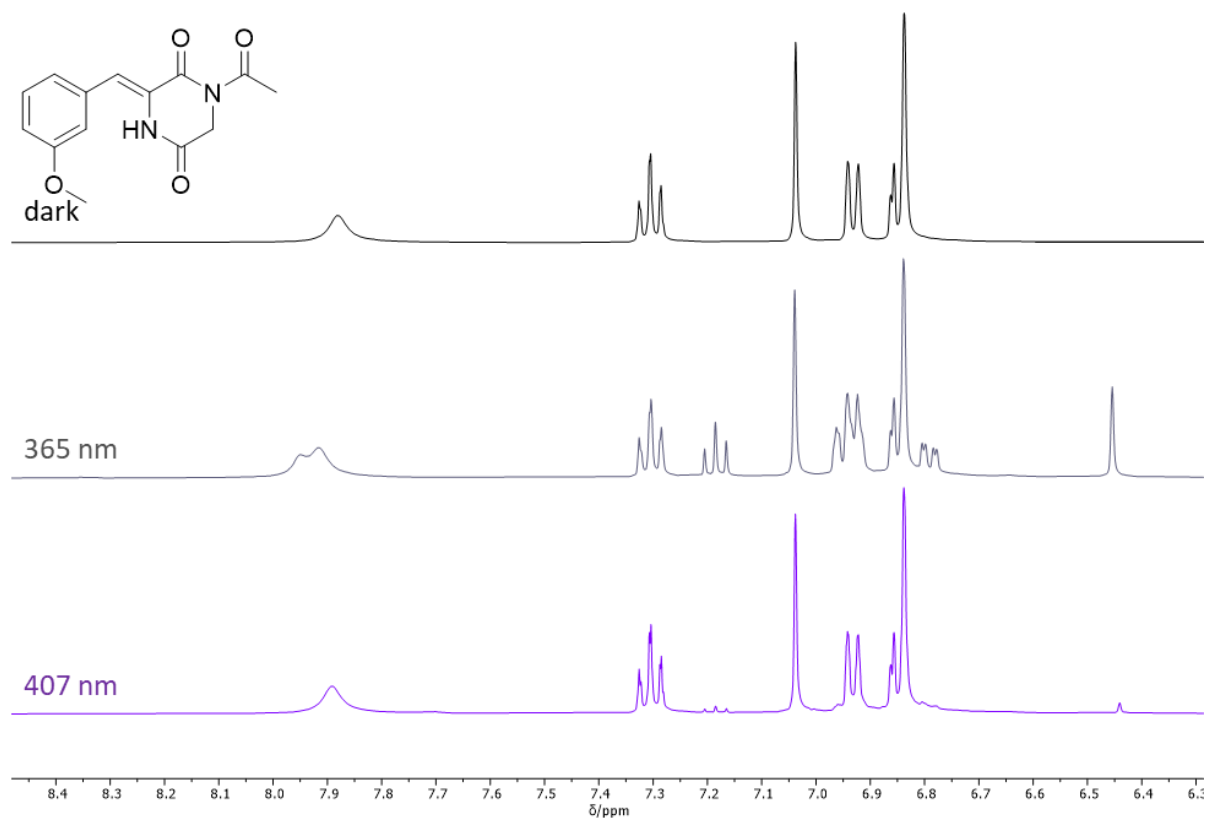
**Figure 255:** Sections of $^1$H NMR spectra (400 MHz, CD$_2$Cl$_2$) of compound **31** in the dark (top) and after reaching the PSS upon irradiation with 365 nm and 407 nm.
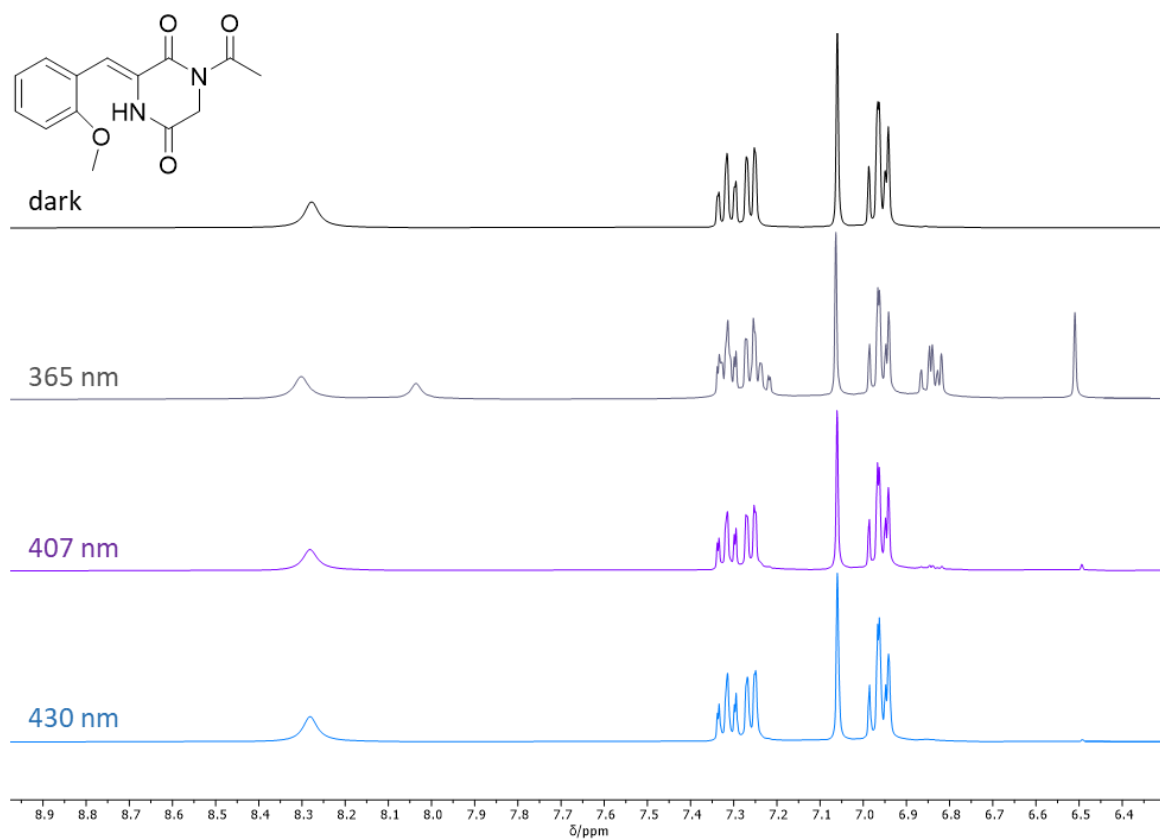


**Figure 256:** Sections of $^1$H NMR spectra (400 MHz, CD$_2$Cl$_2$) of compound **32** in the dark (top) and after reaching the PSS upon irradiation with 365 nm, 407 nm and 430 nm.
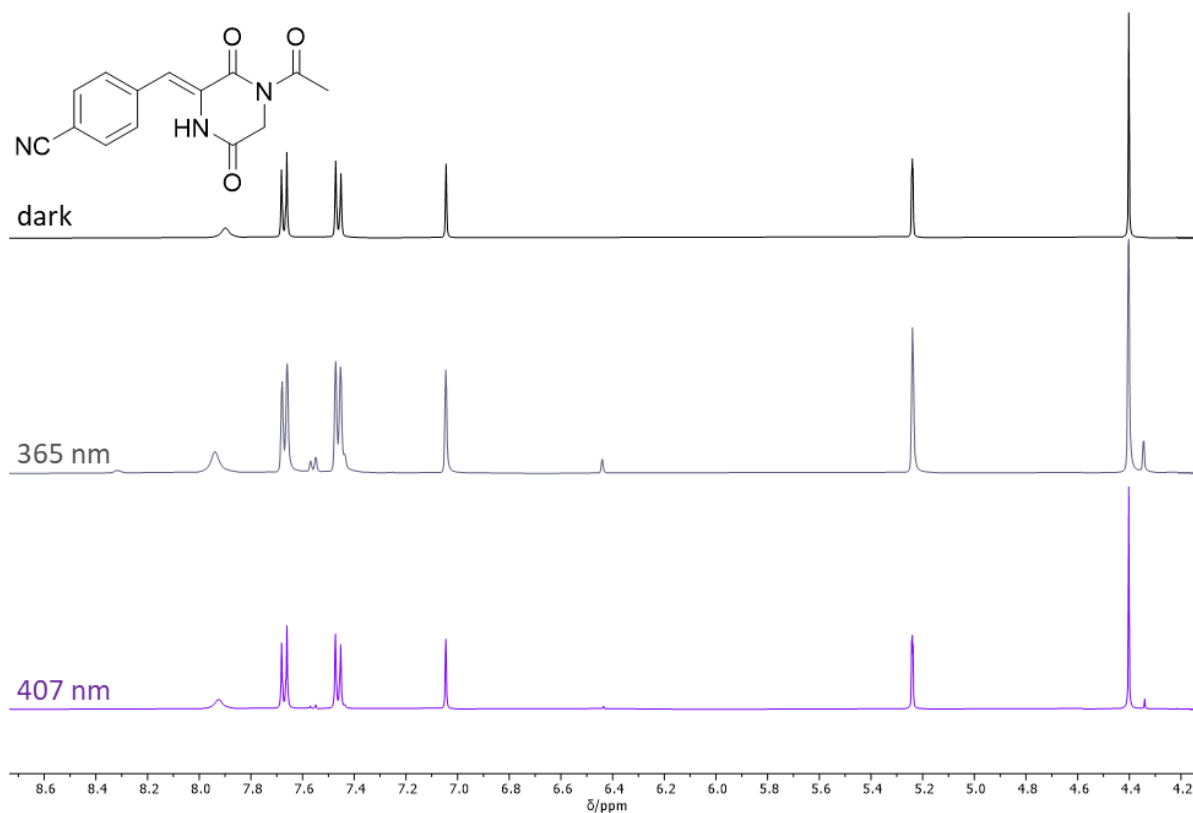
**Figure 257:** Sections of $^1$H NMR spectra (400 MHz, CD$_2$Cl$_2$) of compound **35** in the dark (top) and after reaching the PSS upon irradiation with 365 nm and 407 nm.
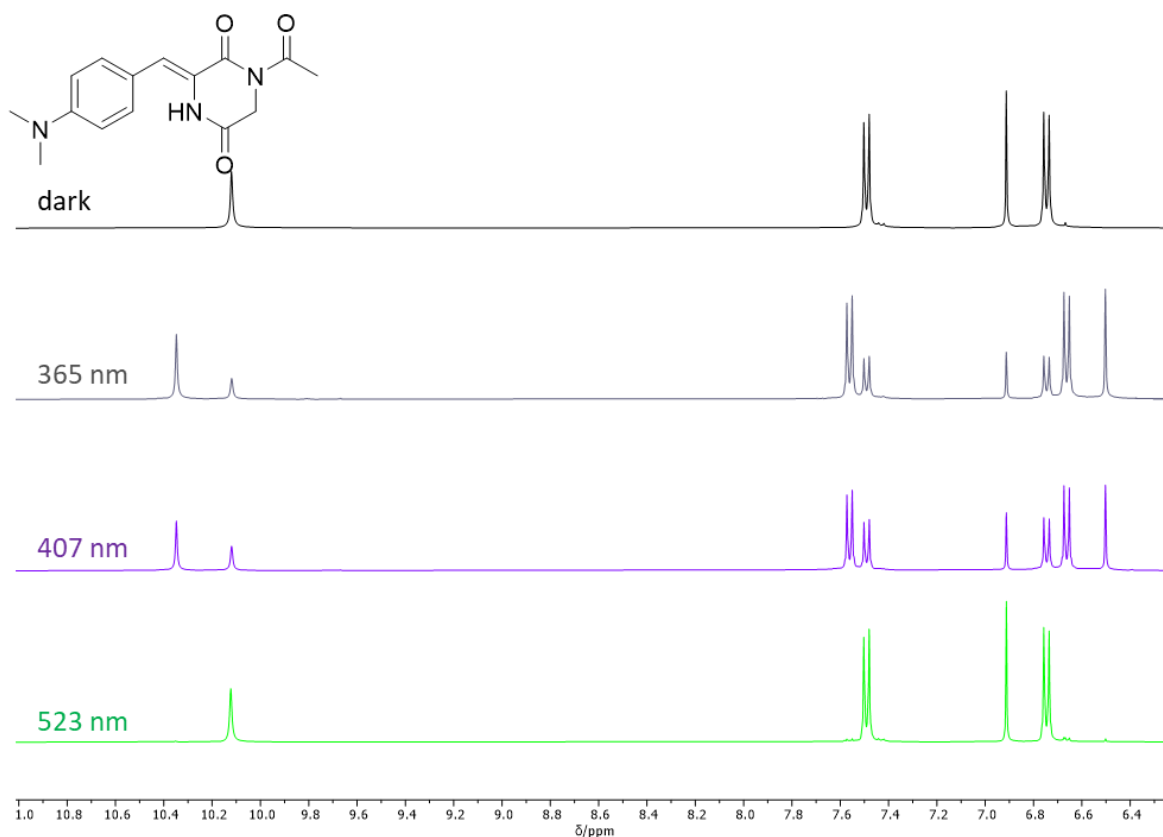


**Figure 258:** Sections of $^1$H NMR spectra (400 MHz, DMSO-$d_6$) of compound **36** in the dark (top) and after reaching the PSS upon irradiation with 365 nm, 407 nm and 523 nm.
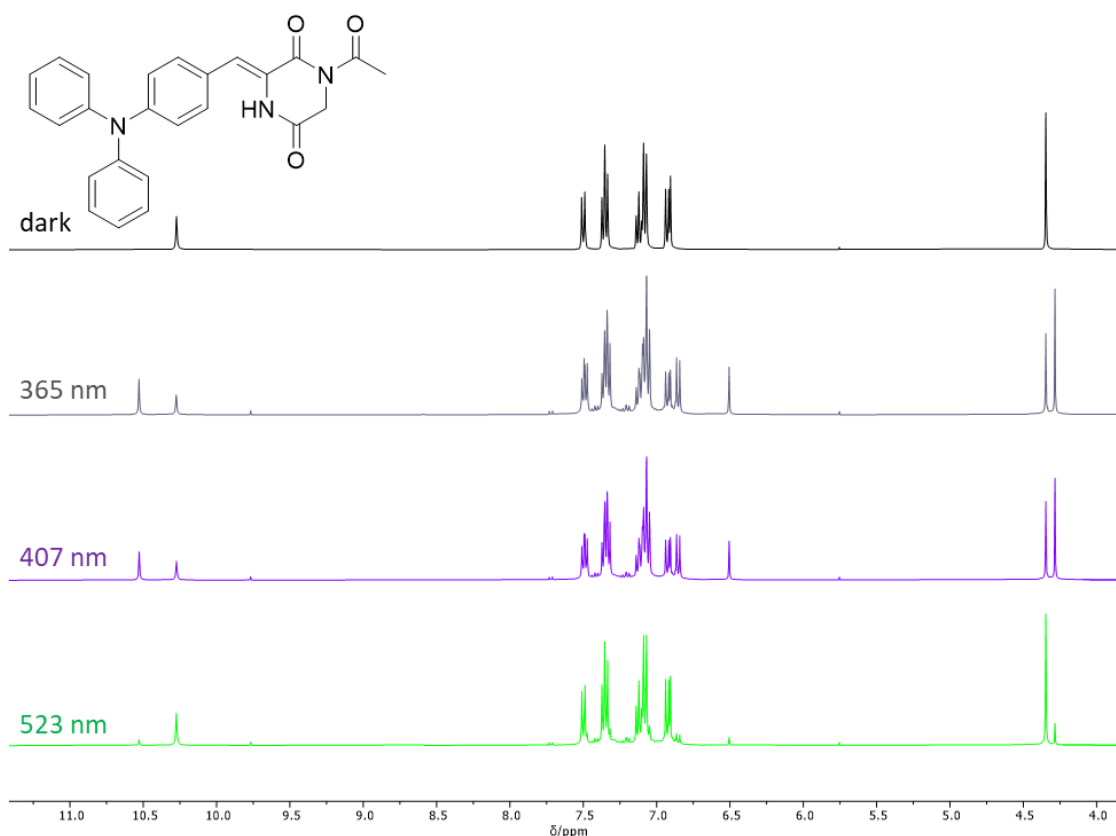
**Figure 259:** Sections of $^1$H NMR spectra (400 MHz, DMSO-$d_6$) of compound **37** in the dark (top) and after reaching the PSS upon irradiation with 365 nm, 407 nm and 523 nm.

### 5.5.7 Photoisomerization Quantum Yield

The measurements to determine the photoisomerization quantum yields were performed by Peter Gödtel.

A 2.5 mM solution of **37** in DMSO was irradiated with 398 nm (Edison Opto, EDEV-SLC1-03) and 520 nm (OSRAM Opto Semiconductors Inc., LTCP7P-KXKZ) in succession. Several samples were taken from the solution during irradiation and the isomer-ratio was analyzed *via* HPLC. After reaching the PSS at 398 nm (55.9% *E*-isomer), the same solution was irradiated with 520 nm for a maximum of 115 min. The LEDs were driven at 4.0 V and 100 mA (398 nm) as well as 3.7 V and 59 mA (520 nm), to ensure the same irradiation intensity at the sample of 3.095 mW/cm$^2$ for both wavelengths of light.

Since continuous irradiation well after the PSS is reached will eventually lead to a measured reaction quantum yield of $\Phi_{t\to\infty} = 0$, only samples were taken into account, which still lie in the linear regime of the reaction progress.[150] This ensures that $F_{max}$ can be determined accurately, which more closely represents the switching efficiency of each individual molecule, rather than the efficiency of reaching the PSS of the whole mixture.

$$\Phi_{Z \to E} = 0.16 \pm 0.01 \qquad\qquad \Phi_{E \to Z} = 0.15 \pm 0.01$$
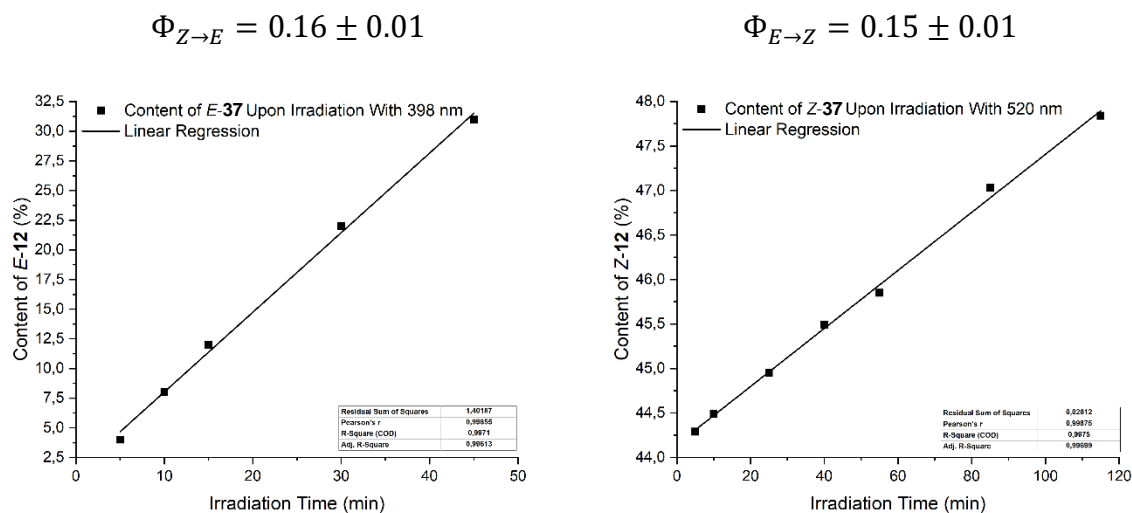


**Figure 260:** Content of *E*-**37** upon irradiation with 398 nm over time (left) and content of *Z*-**37** upon irradiation with 520 nm over time (right) in the isomer mixture, determined *via* HPLC.

### 5.5.8   Thermal Relaxation of *E*-Isomers

**Table 12**: The thermal relaxation of the respective *E*-isomers of **29**-**32**, **35**, and **37** in MeCN at 60 °C after one week was monitored *via* analytical HPLC.

| Compound | 29 | 30 | 31 | 32 | 35 | 37 |
|---|---|---|---|---|---|---|
| Decrease of *E*-isomer after 7 days | 4.0% | 0.8% | 2.2% | 1.3% | 0.8% | 12.1% |
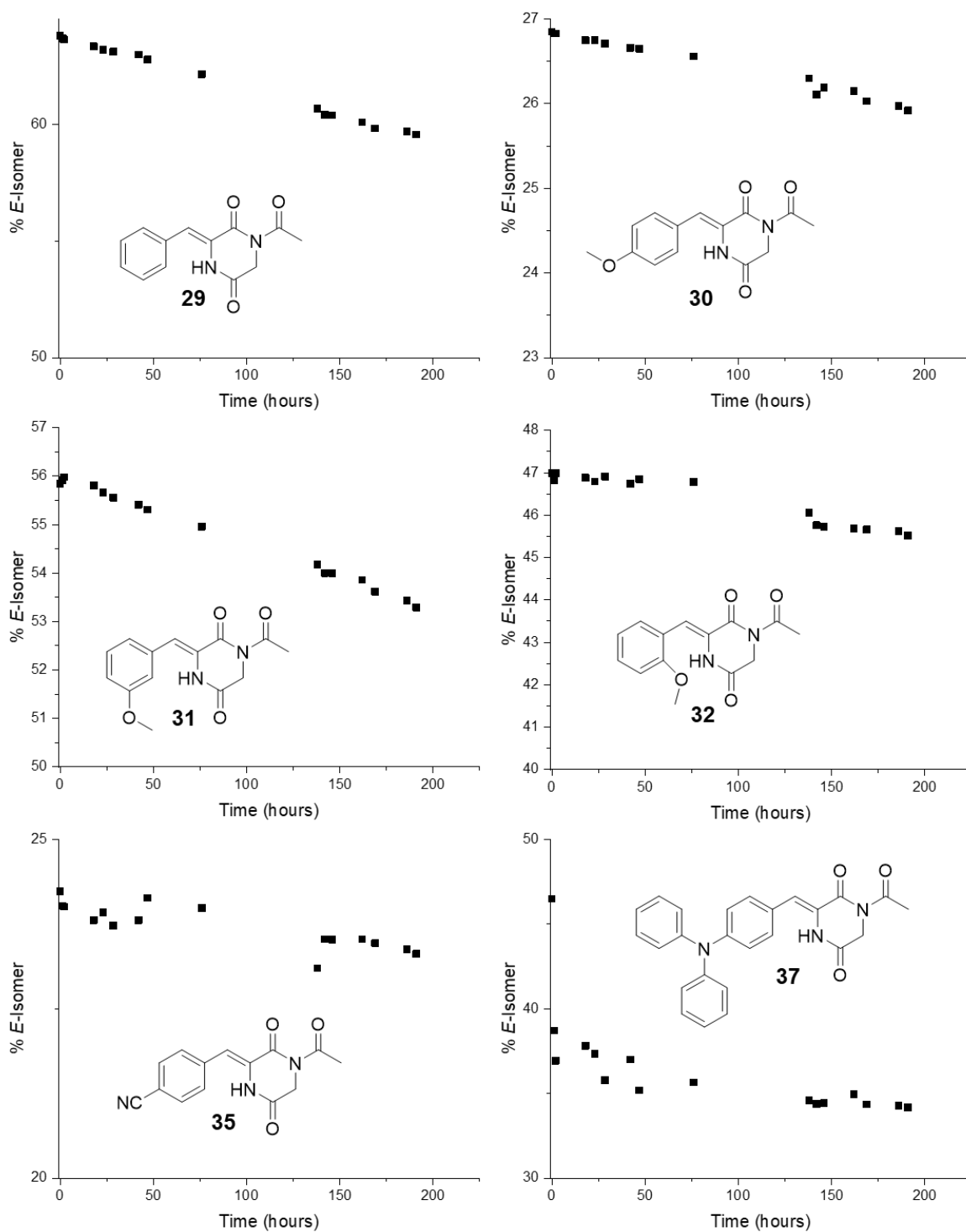
**Figure 261:** Thermal relaxation of the *E*-isomers in MeCN at 60 °C was monitored *via* analytical HPLC. The percentage of *E*-isomer was determined with the integrals of the signals assigned to the respective isomer.

## 5.5.9   Switching Stability
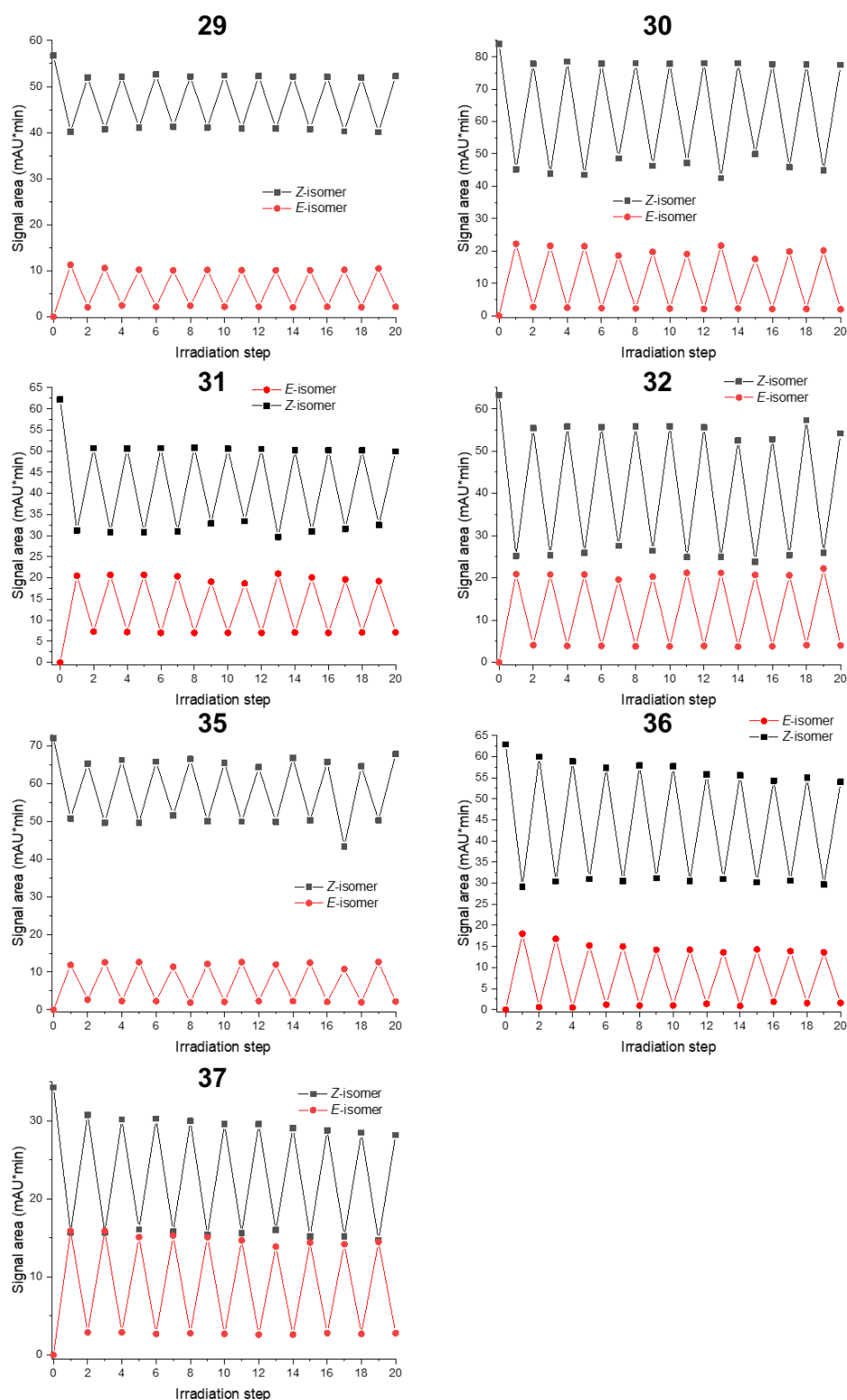


**Figure 262:** Solutions of pure *Z*-isomers in DMSO (1.0 mM) were alternately irradiated with two wavelengths and after every irradiation step the solutions were analyzed *via* analytical HPLC. **29**: 365 nm for 2 min and with 407 nm for 10 min; **30**: 365 nm for 2 min and with 430 nm for 20 min; **31**: 365 nm for 2 min and with 407 nm for 5 min; **32**, **35**: 365 nm for 4 min and with 430 nm for 45 min; **36**: 407 nm for 4 min and with 523 nm for 10 min; **37**: 407 nm for 5 min and with 523 nm for 35 min.

### 5.5.10  DFT Calculations

*Cartesian Coordinates of the Optimized Structures*

The presented data were obtained and visualized with Avogadro 1.2.0.

**Z-Ph-DKP-Ac (29)**

| | | | |
|---|---|---|---|
| C | 0.01014 | -0.25951 | 0.03984 |
| N | 0.04214 | 108.230 | -0.36206 |
| C | 111.005 | 191.026 | -0.21019 |
| C | 230.061 | 126.510 | 0.47215 |
| N | 245.572 | -0.15556 | 0.11808 |
| C | 131.778 | -0.97876 | 0.17524 |
| O | 136.902 | -218.065 | 0.32721 |
| O | 110.948 | 307.763 | -0.55863 |
| C | -112.539 | -0.96717 | 0.20852 |
| C | 374.057 | -0.70190 | -0.13105 |
| O | 387.757 | -179.366 | -0.63218 |
| C | 492.389 | 0.16076 | 0.24686 |
| C | -251.118 | -0.51741 | 0.12356 |
| C | -349.068 | -145.816 | -0.24290 |
| C | -482.790 | -109.607 | -0.34504 |
| C | -522.222 | 0.21127 | -0.06154 |
| C | -426.879 | 114.834 | 0.33416 |
| C | -292.775 | 0.79250 | 0.42568 |
| H | -0.77902 | 147.865 | -0.80240 |
| H | 317.274 | 182.410 | 0.15783 |
| H | 218.960 | 138.410 | 155.537 |
| H | -0.97102 | -202.537 | 0.38099 |
| H | 482.198 | 0.58722 | 124.602 |
| H | 581.010 | -0.46798 | 0.20277 |
| H | 504.976 | 0.98273 | -0.46277 |
| H | -318.857 | -247.722 | -0.45578 |
| H | -556.419 | -183.437 | -0.63954 |
| H | -626.528 | 0.49428 | -0.13631 |
| H | -457.092 | 215.921 | 0.58058 |
| H | -221.367 | 152.540 | 0.77807 |



**E-Ph-DKP-Ac (29)**

| | | | |
|---|---|---|---|
| C | -0.08584 | 0.81837 | -0.31780 |
| N | -0.96407 | 191.055 | -0.54488 |
| C | -220.371 | 201.006 | -0.00111 |
| C | -260.200 | 0.77604 | 0.78569 |
| N | -211.491 | -0.45296 | 0.14039 |

| | | | |
|---|---|---|---|
| C | -0.75711 | -0.51221 | -0.22479 |
| O | -0.18519 | -155.758 | -0.45101 |
| O | -292.054 | 299.015 | -0.10953 |
| C | 124.055 | 109.532 | -0.25838 |
| C | -297.551 | -156.766 | -0.03643 |
| O | -268.951 | -248.271 | -0.77260 |
| C | -427.559 | -154.349 | 0.73748 |
| C | 248.645 | 0.35497 | -0.08142 |
| C | 363.185 | 115.486 | 0.12747 |
| C | 488.323 | 0.59212 | 0.33511 |
| C | 503.141 | -0.79406 | 0.33117 |
| C | 391.543 | -160.061 | 0.11375 |
| C | 265.888 | -104.242 | -0.09269 |
| H | -0.60659 | 272.923 | -102.070 |
| H | -220.599 | 0.86147 | 180.317 |
| H | -368.230 | 0.76930 | 0.83961 |
| H | 143.150 | 216.387 | -0.32562 |
| H | -498.275 | -0.84000 | 0.28993 |
| H | -470.343 | -254.159 | 0.67876 |
| H | -413.139 | -126.361 | 178.207 |
| H | 352.715 | 223.397 | 0.13198 |
| H | 574.151 | 123.334 | 0.49675 |
| H | 600.632 | -123.994 | 0.48886 |
| H | 402.390 | -267.895 | 0.09849 |
| H | 180.849 | -167.685 | -0.27512 |



**Z-*p*-OMe-Ph-DKP-Ac (30)**

| | | | |
|---|---|---|---|
| C | 347.744 | 112.595 | -0.35417 |
| C | 443.380 | 0.14264 | -0.05949 |
| C | 401.735 | -117.443 | 0.16566 |
| C | 266.485 | -148.395 | 0.10624 |
| C | 168.685 | -0.50918 | -0.15231 |
| C | 213.358 | 0.80782 | -0.39700 |
| C | 0.29615 | -0.92808 | -0.19591 |
| C | -0.83204 | -0.20395 | -0.02619 |
| N | -0.84634 | 114.625 | 0.35772 |
| C | -190.689 | 198.475 | 0.20493 |
| C | -309.632 | 135.233 | -0.48312 |
| N | -326.384 | -0.06832 | -0.13640 |
| C | -214.229 | -0.90554 | -0.14441 |
| O | -221.858 | -211.755 | -0.23681 |
| O | -189.359 | 315.160 | 0.55789 |

| C | -459.521 | -0.51703 | 0.02389 |
|---|----------|----------|---------|
| C | -484.529 | -192.381 | 0.49704 |
| O | -550.683 | 0.25911 | -0.18762 |
| O | 572.179 | 0.55878 | -0.02924 |
| C | 674.093 | -0.40229 | 0.25907 |
| H | 381.734 | 213.415 | -0.55537 |
| H | 473.149 | -195.698 | 0.37839 |
| H | 235.409 | -250.890 | 0.27360 |
| H | 143.178 | 158.410 | -0.67096 |
| H | 0.12208 | -198.668 | -0.34729 |
| H | -0.03212 | 152.760 | 0.82237 |
| H | -399.315 | 188.220 | -0.18358 |
| H | -298.112 | 146.675 | -156.631 |
| H | -418.856 | -220.103 | 132.067 |
| H | -588.883 | -197.656 | 0.80228 |
| H | -465.869 | -263.015 | -0.31197 |
| H | 767.862 | 0.14776 | 0.23660 |
| H | 659.733 | -0.84218 | 124.974 |
| H | 676.129 | -119.239 | -0.49653 |
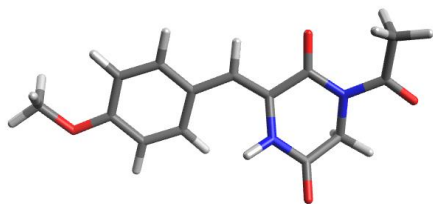


**E-p-OMe-Ph-DKP-Ac (30)**

| C | -315.280 | -120.594 | 0.38847 |
|---|----------|----------|---------|
| C | -426.358 | -0.37969 | 0.15743 |
| C | -405.788 | 0.95758 | -0.19667 |
| C | -276.064 | 143.792 | -0.31178 |
| C | -162.952 | 0.62466 | -0.10201 |
| C | -186.705 | -0.72019 | 0.25854 |
| C | -0.34269 | 128.996 | -0.22511 |
| C | 0.96589 | 0.92760 | -0.21713 |
| N | 192.806 | 195.754 | -0.39419 |
| C | 318.296 | 193.025 | 0.12161 |
| C | 350.445 | 0.63417 | 0.83325 |
| N | 287.879 | -0.52057 | 0.17213 |
| C | 152.134 | -0.45018 | -0.16523 |
| O | 0.86015 | -143.844 | -0.42828 |
| O | 396.896 | 286.090 | 0.04500 |
| C | 368.571 | -167.370 | 0.02298 |
| C | 316.316 | -284.571 | -0.76358 |
| O | 480.065 | -167.756 | 0.50772 |
| O | -547.739 | -0.96063 | 0.30280 |
| C | -664.370 | -0.16566 | 0.07218 |
| H | -332.886 | -223.771 | 0.66728 |
| H | -488.887 | 162.488 | -0.37499 |

H   -261.745   248.043   -0.57281
H   -103.576   -138.436   0.42423
H   -0.46719   236.460   -0.33998
H   163.216   282.415   -0.82537
H   457.760   0.48430   0.83422
H   316.581   0.70574   187.231
H   269.373   -253.565   -169.623
H   401.041   -350.090   -0.95798
H   240.623   -337.799   -0.18740
H   -748.942   -0.82893   0.23711
H   -669.279   0.67230   0.77285
H   -666.641   0.20974   -0.95452
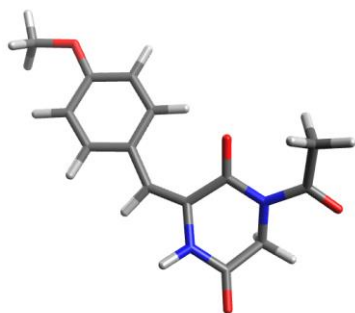


**Z-*m*-OMe-Ph-DKP-Ac (31)**

C   335.422   203.008   -0.46303
C   444.179   122.304   -0.16475
C   425.265   -0.14982   0.04806
C   297.206   -0.69260   -0.03521
C   186.275   0.13033   -0.30955
C   206.699   150.032   -0.53487
C   0.55362   -0.51246   -0.38123
C   -0.66077   0.01183   -0.11709
N   -0.86178   130.191   0.38679
C   -204.937   196.725   0.37880
C   -318.460   121.565   -0.27797
N   -309.158   -0.24403   -0.11095
C   -185.588   -0.87696   -0.26040
O   -173.921   -206.791   -0.48100
O   -218.396   309.322   0.82468
C   -432.544   -0.92644   0.02924
C   -432.360   -240.097   0.32843
O   -535.715   -0.29061   -0.05783
O   537.374   -0.86697   0.32245
C   524.123   -227.239   0.54097
H   350.935   308.608   -0.64887
H   544.501   162.576   -0.10286
H   280.721   -174.960   0.11913
H   124.448   214.305   -0.81729
H   0.54373   -156.669   -0.62927
H   -0.07380   178.818   0.79710
H   -411.774   154.861   0.16218

| H | -320.546 | 147.430 | -134.218 |
|---|----------|---------|----------|
| H | -359.471 | -266.180 | 109.469 |
| H | -533.042 | -266.160 | 0.64982 |
| H | -406.170 | -296.504 | -0.56685 |
| H | 624.651 | -263.617 | 0.74065 |
| H | 459.965 | -247.926 | 140.248 |
| H | 484.014 | -277.400 | -0.34451 |
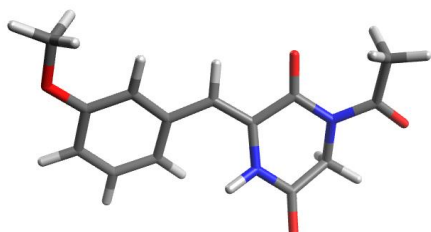


**_E_-_m_-OMe-Ph-DKP-Ac (31)**

| C | -292.573 | -227.214 | -0.13940 |
|---|----------|----------|----------|
| C | -413.474 | -163.935 | 0.10903 |
| C | -418.423 | -0.24022 | 0.15935 |
| C | -302.054 | 0.49644 | -0.03770 |
| C | -178.131 | -0.14522 | -0.27110 |
| C | -175.123 | -154.676 | -0.33030 |
| C | -0.65322 | 0.76692 | -0.44558 |
| C | 0.70048 | 0.68791 | -0.42393 |
| N | 142.337 | 187.694 | -0.69890 |
| C | 260.945 | 220.139 | -0.11904 |
| C | 314.859 | 111.174 | 0.78088 |
| N | 284.613 | -0.22895 | 0.25861 |
| C | 154.661 | -0.51398 | -0.17443 |
| O | 115.203 | -165.147 | -0.34920 |
| O | 317.158 | 327.087 | -0.28146 |
| C | 389.511 | -117.979 | 0.33160 |
| C | 371.863 | -252.987 | -0.30915 |
| O | 493.105 | -0.86660 | 0.88409 |
| O | -540.877 | 0.30386 | 0.39917 |
| C | -551.741 | 172.622 | 0.45223 |
| H | -289.486 | -335.428 | -0.19063 |
| H | -504.951 | -219.980 | 0.25724 |
| H | -304.730 | 157.653 | -0.00609 |
| H | -0.82373 | -205.235 | -0.53302 |
| H | -0.99406 | 178.921 | -0.59167 |
| H | 0.97216 | 259.904 | -124.593 |
| H | 422.483 | 121.184 | 0.85631 |
| H | 272.160 | 123.520 | 178.170 |
| H | 329.313 | -245.469 | -130.908 |
| H | 470.206 | -299.523 | -0.34316 |
| H | 303.768 | -314.220 | 0.28208 |
| H | -656.626 | 193.557 | 0.65015 |
| H | -490.431 | 214.060 | 125.814 |
| H | -522.780 | 218.156 | -0.49955 |

**Z-*o*-OMe-Ph-DKP-Ac (32)**

| | | | |
|---|---|---|---|
| C | 422.552 | 0.33703 | 0.07527 |
| C | 491.771 | -0.72522 | -0.49908 |
| C | 424.774 | -189.706 | -0.83982 |
| C | 288.215 | -198.630 | -0.61235 |
| C | 213.858 | -0.92114 | -0.07140 |
| C | 285.142 | 0.24392 | 0.30092 |
| C | 0.70424 | -114.989 | 0.08360 |
| C | -0.36613 | -0.32960 | -0.00165 |
| N | -0.30600 | 104.970 | -0.21176 |
| C | -132.496 | 180.826 | -0.68695 |
| C | -258.354 | 104.293 | -102.716 |
| N | -279.865 | -0.13273 | -0.16817 |
| C | -171.708 | -0.95479 | 0.15860 |
| O | -185.130 | -209.828 | 0.55483 |
| O | -123.145 | 301.179 | -0.87173 |
| C | -414.825 | -0.43585 | 0.13202 |
| C | -445.948 | -153.639 | 111.025 |
| O | -502.539 | 0.23164 | -0.38061 |
| O | 214.104 | 123.443 | 0.91734 |
| C | 283.496 | 237.711 | 143.512 |
| H | 476.392 | 123.036 | 0.35642 |
| H | 598.430 | -0.63419 | -0.66512 |
| H | 478.321 | -273.302 | -127.183 |
| H | 235.286 | -289.642 | -0.86993 |
| H | 0.43152 | -218.908 | 0.22362 |
| H | 0.56710 | 151.123 | 0.03374 |
| H | -343.301 | 170.691 | -0.91323 |
| H | -253.557 | 0.73955 | -207.868 |
| H | -381.309 | -150.084 | 198.618 |
| H | -550.341 | -142.114 | 139.660 |
| H | -430.863 | -250.870 | 0.64111 |
| H | 207.241 | 298.425 | 191.682 |
| H | 358.300 | 207.052 | 216.907 |
| H | 330.734 | 294.715 | 0.63197 |



**E-*o*-OMe-Ph-DKP-Ac (32)**

| C | -338.453 | -105.045 | 0.53777 |
| C | -451.880 | -0.52195 | -0.07812 |
| C | -447.790 | 0.73419 | -0.67352 |
| C | -328.627 | 145.302 | -0.65912 |
| C | -212.010 | 0.93470 | -0.08566 |
| C | -218.998 | -0.32950 | 0.54751 |
| C | -0.90571 | 175.548 | -0.07981 |
| C | 0.36579 | 136.089 | -0.25012 |
| N | 144.358 | 226.799 | -0.15394 |
| C | 263.960 | 190.339 | 0.38401 |
| C | 269.432 | 0.43860 | 0.77927 |
| N | 199.706 | -0.43635 | -0.17802 |
| C | 0.76457 | -0.02111 | -0.68264 |
| O | 0.08796 | -0.66743 | -145.370 |
| O | 356.200 | 267.567 | 0.57884 |
| C | 261.462 | -168.178 | -0.45155 |
| C | 197.546 | -262.170 | -143.568 |
| O | 365.101 | -195.932 | 0.11949 |
| O | -106.057 | -0.76087 | 116.754 |
| C | -103.274 | -207.781 | 171.534 |
| H | -344.194 | -201.889 | 101.402 |
| H | -543.660 | -109.802 | -0.07816 |
| H | -536.093 | 115.243 | -114.032 |
| H | -324.263 | 243.487 | -111.724 |
| H | -106.319 | 281.619 | 0.09853 |
| H | 128.470 | 325.412 | -0.31978 |
| H | 373.013 | 0.12585 | 0.83120 |
| H | 225.144 | 0.33359 | 177.566 |
| H | 182.655 | -214.173 | -240.238 |
| H | 263.544 | -348.185 | -153.052 |
| H | 0.99119 | -293.432 | -108.671 |
| H | -0.02209 | -221.588 | 209.329 |
| H | -174.745 | -218.190 | 253.638 |
| H | -124.223 | -282.625 | 0.94637 |
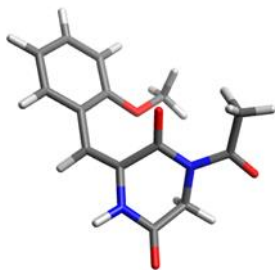


**Z-*m*,*m*,*p*-(OMe)₃-Ph-DKP-Ac (33)**

| C | -273.188 | 105.762 | -0.40660 |
| C | -368.597 | 0.04977 | -0.19424 |
| C | -326.993 | -128.322 | -0.05056 |
| C | -191.563 | -160.531 | -0.14439 |
| C | -0.96086 | -0.59649 | -0.34142 |
| C | -137.631 | 0.73781 | -0.48486 |

| C | 0.43903 | -0.99824 | -0.41910 |
|---|---|---|---|
| C | 154.039 | -0.28589 | -0.10098 |
| N | 150.308 | 0.98733 | 0.48206 |
| C | 254.732 | 185.870 | 0.52152 |
| C | 380.050 | 136.146 | -0.16257 |
| N | 397.445 | -0.09726 | -0.06596 |
| C | 287.492 | -0.93514 | -0.27203 |
| O | 297.945 | -211.283 | -0.56105 |
| O | 247.326 | 296.422 | 102.948 |
| C | 530.891 | -0.55153 | 0.06836 |
| C | 556.944 | -201.528 | 0.30069 |
| O | 621.050 | 0.26255 | 0.03222 |
| O | -426.191 | -218.142 | 0.17314 |
| C | -390.074 | -355.464 | 0.33032 |
| O | -501.887 | 0.35648 | -0.15803 |
| C | -548.353 | 0.77848 | 113.542 |
| O | -323.153 | 231.349 | -0.52997 |
| C | -230.854 | 338.945 | -0.70856 |
| H | -158.385 | -262.851 | -0.04453 |
| H | -0.65782 | 150.769 | -0.71672 |
| H | 0.63497 | -201.879 | -0.72381 |
| H | 0.64069 | 129.342 | 0.91576 |
| H | 377.222 | 167.090 | -121.300 |
| H | 465.800 | 183.653 | 0.30034 |
| H | 542.638 | -257.346 | -0.62462 |
| H | 660.211 | -210.588 | 0.63279 |
| H | 488.920 | -243.951 | 103.821 |
| H | -483.402 | -408.555 | 0.50294 |
| H | -342.090 | -394.259 | -0.57258 |
| H | -323.670 | -369.268 | 118.836 |
| H | -654.693 | 0.98679 | 102.687 |
| H | -533.821 | -0.01576 | 187.288 |
| H | -496.206 | 168.439 | 145.454 |
| H | -291.391 | 429.194 | -0.74753 |
| H | -160.862 | 345.293 | 0.12976 |
| H | -175.314 | 328.236 | -164.458 |
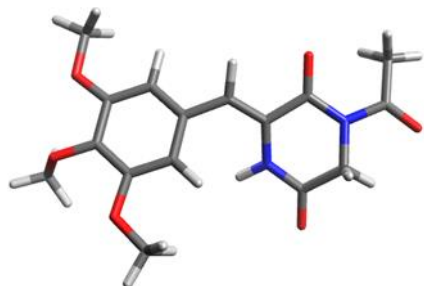


**E-m,m,p-(OMe)-Phe-DKP-Ac (33)**

| C | -246.206 | -118.932 | 0.13028 |
|---|---|---|---|
| C | -355.329 | -0.31852 | 0.27870 |
| C | -334.603 | 106.653 | 0.18659 |

| | | | |
|---|---|---|---|
| C | -206.092 | 156.355 | -0.01570 |
| C | -0.96042 | 0.69065 | -0.14400 |
| C | -117.685 | -0.69465 | -0.07736 |
| C | 0.32345 | 135.606 | -0.32797 |
| C | 163.606 | 100.864 | -0.34738 |
| N | 257.189 | 204.290 | -0.61347 |
| C | 381.786 | 210.394 | -0.07527 |
| C | 416.122 | 0.89242 | 0.76306 |
| N | 358.186 | -0.33834 | 0.20487 |
| C | 223.567 | -0.34342 | -0.17531 |
| O | 161.942 | -137.583 | -0.37003 |
| O | 457.649 | 304.659 | -0.22748 |
| C | 442.486 | -147.779 | 0.19221 |
| C | 396.196 | -273.591 | -0.49154 |
| O | 552.243 | -139.938 | 0.70778 |
| O | -446.104 | 183.392 | 0.30739 |
| C | -431.106 | 325.112 | 0.22218 |
| O | -480.804 | -0.80490 | 0.52295 |
| C | -550.645 | -124.430 | -0.65482 |
| O | -276.371 | -251.335 | 0.20337 |
| C | -169.587 | -345.000 | 0.05177 |
| H | -189.552 | 262.918 | -0.07814 |
| H | -0.34458 | -136.079 | -0.20785 |
| H | 0.19132 | 242.823 | -0.45125 |
| H | 225.642 | 285.761 | -112.435 |
| H | 523.784 | 0.77550 | 0.79741 |
| H | 379.990 | 105.292 | 178.428 |
| H | 351.640 | -253.224 | -146.434 |
| H | 483.383 | -337.946 | -0.59421 |
| H | 320.140 | -323.392 | 0.10995 |
| H | -531.196 | 366.011 | 0.34010 |
| H | -366.559 | 362.948 | 102.015 |
| H | -390.662 | 354.940 | -0.74953 |
| H | -648.065 | -159.705 | -0.31952 |
| H | -563.767 | -0.41380 | -135.416 |
| H | -496.645 | -206.036 | -114.059 |
| H | -215.106 | -443.292 | 0.14970 |
| H | -122.659 | -335.864 | -0.93191 |
| H | -0.93964 | -331.562 | 0.83008 |



**Z-*p*-OCF₃-Ph-DKP-Ac (34)**

| | | | |
|---|---|---|---|
| C | 255.720 | 0.58591 | -0.98389 |

C    342.227    -0.42684    -0.59595
C    295.707    -165.873    -0.15749
C    158.678    -186.929    -0.09108
C    0.67600    -0.85629    -0.44006
C    118.748    0.36928     -0.90415
C    -0.75085   -115.114    -0.35045
C    -177.505   -0.30280    -0.12889
N    -161.793   105.466     0.16994
C    -260.470   199.077     0.08209
C    -392.274   146.057     -0.43382
N    -418.825   0.07106     -0.02618
C    -316.107   -0.87094    -0.08951
O    -335.345   -207.184    -0.10338
O    -243.177   316.479     0.35480
C    -554.305   -0.24148    0.25215
C    -588.960   -160.280    0.79027
O    -638.599   0.61650     0.08269
O    481.000    -0.22585    -0.73018
F    500.836    146.694     0.73025
C    546.693    0.26028     0.34203
F    675.235    0.38610     0.01142
F    538.307    -0.55040    141.608
H    295.386    152.189     -135.388
H    365.844    -243.559    0.11586
H    121.066    -282.894    0.24186
H    0.51951    114.714     -124.833
H    -103.501   -219.346    -0.42360
H    -0.71716   138.063     0.49798
H    -472.044   208.526     -0.04852
H    -392.930   154.229     -152.599
H    -520.397   -191.833    157.569
H    -690.867   -154.584    116.844
H    -582.912   -234.661    -0.00445



### *E*-*p*-OCF₃-Ph-DKP-Ac (34)

C    -220.122   0.02293     -117.358
C    -319.004   -0.66334    -0.48043
C    -288.912   -170.726    0.37972
C    -155.604   -205.999    0.55648
C    -0.52610   -136.249    -0.09444
C    -0.87355   -0.32865    -0.97763
C    0.84857    -182.527    0.11355
C    201.946    -115.800    0.15884
N    321.170    -187.885    0.37513

| C | 444.040 | -146.381 | -0.03571 |
|---|---------|----------|----------|
| C | 443.854 | -0.09615 | -0.68151 |
| N | 344.220 | 0.81019 | -0.08982 |
| C | 215.595 | 0.33660 | 0.17050 |
| O | 121.846 | 106.005 | 0.43849 |
| O | 544.754 | -214.218 | 0.06668 |
| C | 384.984 | 216.096 | 0.07013 |
| C | 294.257 | 312.963 | 0.77736 |
| O | 494.154 | 249.223 | -0.34628 |
| O | -454.211 | -0.34392 | -0.72389 |
| F | -509.804 | 0.24937 | 136.865 |
| C | -510.300 | 0.59297 | 0.06467 |
| F | -637.020 | 0.74852 | -0.32196 |
| F | -448.463 | 178.820 | -0.02289 |
| H | -247.469 | 0.81192 | -186.149 |
| H | -368.305 | -223.785 | 0.88804 |
| H | -130.848 | -288.320 | 121.595 |
| H | -0.10521 | 0.19665 | -152.518 |
| H | 0.92954 | -289.930 | 0.26208 |
| H | 314.745 | -282.692 | 0.72555 |
| H | 541.803 | 0.35112 | -0.55895 |
| H | 425.284 | -0.21667 | -175.408 |
| H | 255.873 | 271.767 | 171.001 |
| H | 352.364 | 403.085 | 0.96402 |
| H | 207.881 | 336.338 | 0.15480 |



### Z-*p*-CN-Ph-DKP-Ac (35)

| C | -367.659 | 0.89600 | 0.43456 |
|---|----------|---------|---------|
| C | -458.178 | -0.08957 | 0.01634 |
| C | -411.610 | -136.868 | -0.32247 |
| C | -276.191 | -164.543 | -0.25301 |
| C | -183.463 | -0.65930 | 0.13166 |
| C | -232.201 | 0.61168 | 0.48985 |
| C | -0.42385 | -102.424 | 0.18356 |
| C | 0.65820 | -0.23603 | 0.01865 |
| N | 0.60266 | 110.778 | -0.35418 |
| C | 163.283 | 199.487 | -0.23385 |
| C | 287.713 | 143.055 | 0.41075 |
| N | 309.200 | 0.00342 | 0.12073 |
| C | 201.150 | -0.87582 | 0.13533 |
| O | 212.908 | -208.262 | 0.22532 |
| O | 154.435 | 315.910 | -0.57631 |

C   444.866   -0.40062   0.00989
C   476.741   -181.036   -0.40580
O   531.755   0.42127   0.21893
C   -597.664   0.20427   -0.05030
N   -710.618   0.44247   -0.10511
H   -403.912   187.433   0.72144
H   -481.608   -213.354   -0.63210
H   -240.598   -263.607   -0.50790
H   -164.771   137.350   0.85644
H   -0.20092   -207.406   0.32623
H   -0.24853   146.648   -0.76917
H   373.407   198.430   0.04418
H   281.271   159.153   149.212
H   415.546   -213.587   -124.614
H   582.388   -183.402   -0.66661
H   457.173   -249.818   0.41697



### E-p-CN-Ph-DKP-Ac (35)

C   338.361   0.78489   -0.73559
C   432.383   0.13072   0.07348
C   396.562   -104.309   0.75124
C   268.119   -154.265   0.61777
C   171.422   -0.87552   -0.15673
C   209.545   0.28702   -0.84558
C   0.39902   -151.216   -0.26725
C   -0.86239   -102.671   -0.29426
N   -191.754   -192.631   -0.53446
C   -319.391   -177.517   -0.08443
C   -343.697   -0.49210   0.67409
N   -259.395   0.61966   0.21064
C   -124.315   0.40257   -0.07060
O   -0.43080   130.403   -0.12981
O   -406.024   -261.612   -0.24369
C   -320.268   190.193   0.23294
C   -247.612   307.811   -0.36055
O   -432.030   200.624   0.69639
C   564.734   0.65055   0.19427
N   671.904   107.225   0.29229
H   366.858   167.783   -127.660
H   469.269   -155.720   136.597
H   241.251   -245.861   113.005
H   138.049   0.79700   -147.009
H   0.45617   -259.743   -0.30698

| H | -170.129 | -280.993 | -0.97900 |
|---|---|---|---|
| H | -447.541 | -0.20615 | 0.55069 |
| H | -326.593 | -0.68119 | 173.934 |
| H | -201.072 | 283.289 | -131.442 |
| H | -320.868 | 387.384 | -0.48329 |
| H | -168.104 | 340.612 | 0.30913 |
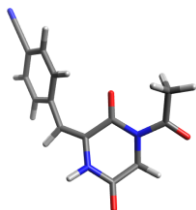


**Z-*p*-NMe₂-Ph-DKP-Ac (36)**

| C | 318.890 | 0.91175 | -0.22947 |
|---|---|---|---|
| C | 413.052 | -0.12524 | -0.00407 |
| C | 361.983 | -144.212 | 0.12525 |
| C | 226.301 | -168.402 | 0.06240 |
| C | 131.733 | -0.65186 | -0.11444 |
| C | 183.348 | 0.65251 | -0.27468 |
| C | -0.08138 | -100.835 | -0.16758 |
| C | -119.265 | -0.24672 | -0.01468 |
| N | -116.366 | 110.687 | 0.37071 |
| C | -218.638 | 198.383 | 0.19440 |
| C | -337.714 | 139.103 | -0.52742 |
| N | -360.969 | -0.01445 | -0.15858 |
| C | -251.768 | -0.89774 | -0.15343 |
| O | -264.696 | -210.636 | -0.25681 |
| O | -214.425 | 314.867 | 0.55637 |
| C | -495.417 | -0.40402 | 0.01178 |
| C | -525.908 | -179.424 | 0.50376 |
| O | -583.784 | 0.40416 | -0.20547 |
| N | 546.882 | 0.13226 | 0.07321 |
| C | 641.818 | -0.96121 | 0.22724 |
| C | 597.128 | 148.152 | -0.14600 |
| H | 352.571 | 192.689 | -0.38056 |
| H | 429.219 | -227.544 | 0.26780 |
| H | 190.924 | -270.471 | 0.15963 |
| H | 117.181 | 148.038 | -0.49221 |
| H | -0.29439 | -206.031 | -0.31962 |
| H | -0.35448 | 144.977 | 0.87210 |
| H | -426.236 | 196.014 | -0.26832 |
| H | -321.975 | 147.835 | -160.797 |
| H | -460.624 | -209.100 | 132.363 |
| H | -630.068 | -179.960 | 0.82008 |
| H | -511.121 | -251.607 | -0.29948 |
| H | 621.586 | -153.652 | 113.560 |
| H | 639.322 | -164.791 | -0.62693 |
| H | 742.138 | -0.54972 | 0.30578 |

H   575.838   183.742   -116.080
H   553.230   218.825   0.56446
H   704.882   148.490   -0.00168
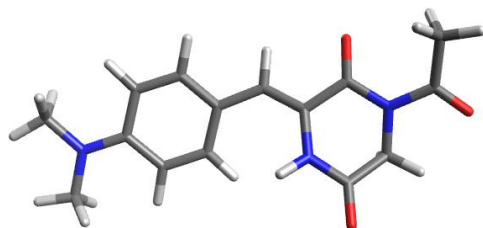


**E-p-NMe₂-Ph-DKP-Ac (36)**

C   295.169   0.96995   0.07510

C   401.740   0.03310   0.05455

C   366.697   -133.410   -0.08527

C   234.633   -171.425   -0.18600

C   127.550   -0.78751   -0.15910

C   163.444   0.57319   -0.02937

C   -0.04832   -135.565   -0.24752

C   -134.306   -0.92246   -0.22652

N   -234.855   -191.682   -0.40809

C   -359.603   -186.023   0.11690

C   -386.827   -0.56672   0.85357

N   -320.392   0.57116   0.20387

C   -183.553   0.46217   -0.10792

O   -113.640   144.876   -0.27464

O   -441.681   -276.100   0.02349

C   -396.781   174.534   0.04719

C   -339.916   289.686   -0.74034

O   -508.926   179.190   0.51871

N   531.772   0.42899   0.15965

C   639.224   -0.55223   0.09415

C   564.947   184.185   0.28535

H   316.418   202.550   0.16629

H   443.320   -209.508   -0.11295

H   212.075   -277.065   -0.28609

H   0.85891   132.069   -0.02517

H   0.00360   -243.860   -0.34257

H   -209.230   -277.621   -0.87667

H   -493.532   -0.37758   0.86295

| H | -352.603 | -0.66616 | 188.939 |
|---|----------|----------|---------|
| H | -289.540 | 256.686  | -164.777 |
| H | -422.984 | 355.833  | -0.98043 |
| H | -266.216 | 343.193  | -0.14144 |
| H | 639.189  | -108.785 | -0.86140 |
| H | 734.579  | -0.04052 | 0.19695 |
| H | 631.167  | -128.873 | 0.90017 |
| H | 518.463  | 228.382  | 117.226 |
| H | 672.735  | 194.478  | 0.38143 |
| H | 532.687  | 241.313  | -0.59201 |



**Z-*p*-NPh₂-Ph-DKP-Ac (37)**

| C | -330.268 | -0.34333 | 0.02277 |
|---|----------|----------|---------|
| N | -323.581 | 105.856  | 0.06087 |
| C | -424.467 | 189.458  | -0.30411 |
| C | -547.215 | 118.442  | -0.83025 |
| N | -572.164 | -0.09717 | -0.15074 |
| C | -465.071 | -0.97516 | 0.05833 |
| O | -480.035 | -216.777 | 0.25823 |
| O | -416.043 | 310.980  | -0.24710 |
| C | -221.781 | -115.101 | 0.05920 |
| C | -0.80752 | -0.81622 | 0.02329 |
| C | 0.11579  | -175.717 | 0.52107 |
| C | 147.615  | -151.142 | 0.53104 |
| C | 198.780  | -0.31051 | 0.00858 |
| C | 108.135  | 0.61926  | -0.53135 |
| C | -0.27971 | 0.37486  | -0.51657 |
| C | 385.133  | 128.376  | 0.08834 |
| N | 336.303  | -0.05051 | 0.01192 |
| C | 430.609  | -111.417 | -0.05772 |
| C | 415.923  | -213.063 | -100.696 |

C   508.873    -316.371    -107.013
C   618.132    -318.420    -0.20369
C   633.361    -216.344    0.73385
C   539.882    -113.608    0.81425
C   487.818    170.102     -0.76414
C   537.217    299.878     -0.67690
C   483.958    389.610     0.24790
C   381.253    348.035     109.480
C   332.518    217.935     102.517
O   -794.174   0.33433     -0.31028
C   -707.606   -0.41644    0.09686
C   -740.757   -164.741    0.89733
H   -239.773   149.459     0.42431
H   -633.483   182.255     -0.67738
H   -535.505   102.586     -190.776
H   -245.555   -220.189    0.17334
H   -0.25400   -269.064    0.92990
H   215.278    -224.718    0.94403
H   145.531    153.182     -0.97550
H   -0.93081   109.704     -0.99054
H   331.868    -210.606    -168.905
H   496.592    -394.682    -180.902
H   690.742    -398.607    -0.26019
H   717.724    -217.141    141.396
H   551.061    -0.34686    154.712
H   528.468    100.553     -148.763
H   616.822    331.209     -134.213
H   522.198    490.771     0.30966
H   339.785    416.645     182.395
H   253.825    185.197     169.287
H   -845.070   -156.157    119.655
H   -726.886   -253.972    0.28679
H   -676.416   -175.409    176.975
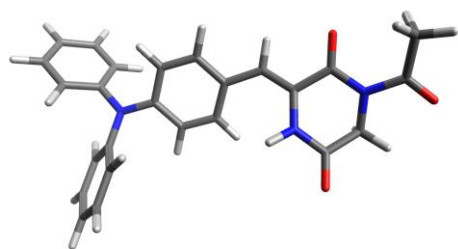
**_E-p_-NPh₂-Ph-DKP-Ac (37)**

| | | | |
|---|---|---|---|
| C | 344.645 | -0.84883 | -0.54797 |
| N | 450.989 | -165.887 | -103.529 |
| C | 573.672 | -174.580 | -0.46610 |
| C | 591.324 | -0.79554 | 0.70240 |
| N | 522.414 | 0.47906 | 0.45803 |
| C | 385.779 | 0.42129 | 0.09595 |
| O | 309.819 | 134.495 | 0.30872 |
| O | 661.054 | -251.223 | -0.83932 |
| C | 218.298 | -131.015 | -0.76727 |
| C | 0.82118 | -0.86449 | -0.54905 |
| C | -0.18547 | -181.151 | -0.85313 |
| C | -152.917 | -154.180 | -0.68895 |
| C | -194.800 | -0.28880 | -0.20666 |
| C | -0.96092 | 0.66738 | 0.09215 |
| C | 0.38334 | 0.39104 | -0.07636 |
| C | -378.829 | 133.394 | -0.15240 |
| N | -330.529 | -0.00039 | -0.03620 |
| C | -424.137 | -103.279 | 0.25337 |
| C | -397.079 | -197.628 | 124.965 |
| C | -489.558 | -297.682 | 153.032 |
| C | -610.406 | -303.607 | 0.83678 |
| C | -637.806 | -208.748 | -0.14766 |
| C | -545.077 | -109.388 | -0.44551 |
| C | -466.115 | 184.581 | 0.81219 |
| C | -515.267 | 314.163 | 0.68902 |
| C | -476.906 | 394.231 | -0.38605 |
| C | -389.525 | 343.188 | -134.566 |
| C | -341.284 | 213.158 | -123.790 |
| O | 540.864 | 275.607 | 0.23903 |
| C | 587.816 | 171.737 | 0.64710 |
| C | 720.765 | 167.706 | 136.978 |
| H | 431.646 | -230.109 | -179.304 |
| H | 553.037 | -127.265 | 161.094 |
| H | 697.587 | -0.63487 | 0.82546 |
| H | 219.460 | -229.704 | -122.521 |
| H | 0.10494 | -278.299 | -123.750 |
| H | -226.415 | -229.376 | -0.94198 |
| H | -125.854 | 163.869 | 0.46412 |
| H | 111.346 | 114.572 | 0.16096 |
| H | -303.907 | -192.039 | 179.834 |
| H | -467.671 | -370.317 | 230.418 |

H   -682.540   -381.190   106.301
H   -731.269   -212.600   -0.69477
H   -565.815   -0.36090   -121.503
H   -495.116   122.469    165.040
H   -582.872   352.960    144.186
H   -514.864   495.284    -0.47654
H   -359.825   404.246    -219.023
H   -274.567   172.927    -198.978
H   798.816    125.767    0.72946
H   747.560    270.361    160.867
H   716.322    108.502    228.529



**Z-*p*-Pip-Ph-DKP-Ac (38)**

C   -220.600   -0.26496   -0.02083
N   -212.821   109.921    0.31142
C   -312.570   200.189    0.11656
C   -434.848   142.326    -0.56122
N   -461.873   0.03757    -0.14518
C   -355.636   -0.87786   -0.11697
O   -372.175   -208.471   -0.16735
O   -303.762   317.797    0.42885
C   -112.516   -106.921   -0.15874
C   0.28666    -0.75265   -0.13322
C   120.247    -179.462   0.10243
C   256.841    -158.145   0.15171
C   311.563    -0.29702   -0.06727
C   219.922    0.74712    -0.33872
C   0.83701    0.52601    -0.36829
C   499.601    121.007    0.44954
N   448.205    -0.06739   -0.06633
C   539.607    -118.878   0.15998
C   639.908    148.572    -0.07320
N   727.351    0.37123    0.28746
C   679.462    -0.85406   -0.34818
O   -683.295   0.52368    -0.19705
C   -597.529   -0.30533   0.04220
C   -632.170   -166.967   0.57633
H   -129.574   143.826    0.77632
H   -520.978   202.839    -0.30312
H   -421.097   147.281    -164.686

| | | | |
|---|---|---|---|
| H | -137.309 | -211.849 | -0.26884 |
| H | 0.82384 | -279.582 | 0.27650 |
| H | 321.020 | -241.983 | 0.37715 |
| H | 255.977 | 173.975 | -0.56727 |
| H | 0.19819 | 135.636 | -0.63794 |
| H | 434.023 | 202.297 | 0.15197 |
| H | 501.891 | 117.742 | 154.893 |
| H | 503.437 | -205.909 | -0.38539 |
| H | 544.214 | -144.538 | 122.916 |
| H | 634.492 | 164.239 | -116.400 |
| H | 677.299 | 240.435 | 0.38410 |
| H | 822.151 | 0.56600 | -0.01593 |
| H | 746.543 | -167.926 | -0.09969 |
| H | 675.305 | -0.76671 | -144.733 |
| H | -736.247 | -163.343 | 0.89330 |
| H | -619.739 | -241.964 | -0.20494 |
| H | -567.680 | -196.156 | 140.413 |



### E-p-Pip-Ph-DKP-Ac (38)

| | | | |
|---|---|---|---|
| C | -235.490 | -0.91093 | -0.23330 |
| N | -341.830 | -184.525 | -0.39859 |
| C | -464.417 | -172.321 | 0.16298 |
| C | -482.259 | -0.41181 | 0.90446 |
| N | -413.810 | 0.68582 | 0.20771 |
| C | -276.652 | 0.50281 | -0.09732 |
| O | -200.857 | 144.374 | -0.22972 |
| O | -551.813 | -257.395 | 0.09358 |
| C | -108.967 | -141.858 | -0.28224 |
| C | 0.26857 | -0.92739 | -0.22052 |
| C | 0.71098 | 0.40822 | -0.09595 |
| C | 205.224 | 0.72391 | -0.02138 |
| C | 306.348 | -0.26746 | -0.05937 |
| C | 262.607 | -160.509 | -0.20536 |
| C | 128.160 | -191.100 | -0.27644 |
| C | 541.094 | -100.400 | 0.01022 |
| N | 440.132 | 0.05607 | 0.06703 |
| C | 489.077 | 135.339 | -0.42006 |
| C | 670.958 | -0.55436 | 0.67134 |
| N | 718.230 | 0.67993 | 0.04943 |
| C | 619.773 | 173.916 | 0.25953 |
| O | -432.524 | 271.334 | -0.84859 |
| C | -479.763 | 189.769 | -0.08780 |
| C | -613.800 | 212.096 | 0.58042 |
| H | -322.170 | -271.749 | -0.87244 |

H   -588.552   -0.22012   0.96443
H   -443.502   -0.52168   192.301
H   -110.157   -250.197   -0.38469
H   -0.01745   120.074    -0.06397
H   231.629    176.554    0.08945
H   333.806    -241.264   -0.28312
H   0.99717    -295.166   -0.38972
H   504.363    -187.691   0.54631
H   560.710    -129.556   -103.223
H   415.417    212.672    -0.22574
H   504.876    129.922    -150.709
H   652.579    -0.43396   175.269
H   745.821    -133.874   0.54114
H   807.053    0.95055    0.45760
H   656.278    266.922    -0.18146
H   599.859    192.174    132.934
H   -610.513   191.777    165.202
H   -641.279   315.963    0.41195
H   -690.797   148.473    0.13612
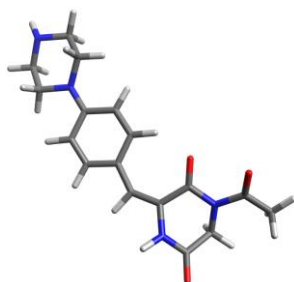


*Molecular Orbitals*

The orbital energies and the 3D representations (left: HOMO, right: LUMO) of the electron probability distributions were extracted with Avogadro 1.2.0.

**Table 13:** HOMO-1 (H-1), HOMO (H), LUMO (L) and LUMO+1 Kohn-Sham orbital energies (in eV) of the *E*-isomers and *Z*-isomers of the compounds **29**-**38** calculated on the TD-B3LYP-GD3BJ/6-311G(d,p) level of theory.

| Compound | | $\varepsilon_{H-1}$ | $\varepsilon_H$ | $\varepsilon_L$ | $\varepsilon_{L+1}$ |
|---|---|---|---|---|---|
| **29** | *Z* | -7.218 | -6.335 | -2.281 | -0.803 |
| | *E* | -7.207 | -6.287 | -2.331 | -0.829 |
| **30** | *Z* | -7.318 | -5.959 | -2.197 | -0.707 |
| | *E* | -7.288 | -5.896 | -2.269 | -0.691 |
| **31** | *Z* | -6.709 | -6.213 | -2.296 | -0.786 |
| | *E* | -6.628 | -6.159 | -2.338 | -0.806 |

| | | | | | |
|---|---|---|---|---|---|
| **32** | *Z* | -6.848 | -6.134 | -2.192 | -0.714 |
| | *E* | -6.703 | -6.085 | -1.962 | -0.752 |
| **33** | *Z* | -6.450 | -6.011 | -2.273 | -0.747 |
| | *E* | -6.341 | -5.952 | -2.339 | -0.786 |
| **34** | *Z* | -7.542 | -6.463 | -2.391 | -0.961 |
| | *E* | -7.468 | -6.439 | -2.366 | -0.870 |
| **35** | *Z* | -7.604 | -6.531 | -2.669 | -1.263 |
| | *E* | -7.539 | -6.545 | -2.597 | -1.314 |
| **36** | *Z* | -6.844 | -5.358 | -2.088 | -0.607 |
| | *E* | -6.838 | -5.327 | -2.153 | -0.582 |
| **37** | *Z* | -6.573 | -5.372 | -2.252 | -0.970 |
| | *E* | -6.543 | -5.356 | -2.312 | -0.911 |
| **38** | *Z* | -6.457 | -5.477 | -2.145 | -0.644 |
| | *E* | -6.462 | -5.423 | -2.197 | -0.627 |

*Z-Ph-DKP-Ac (29)*
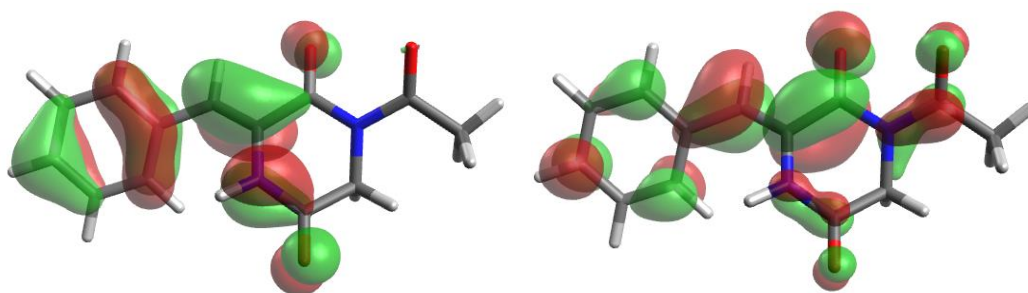


*E-Ph-DKP-Ac (29)*
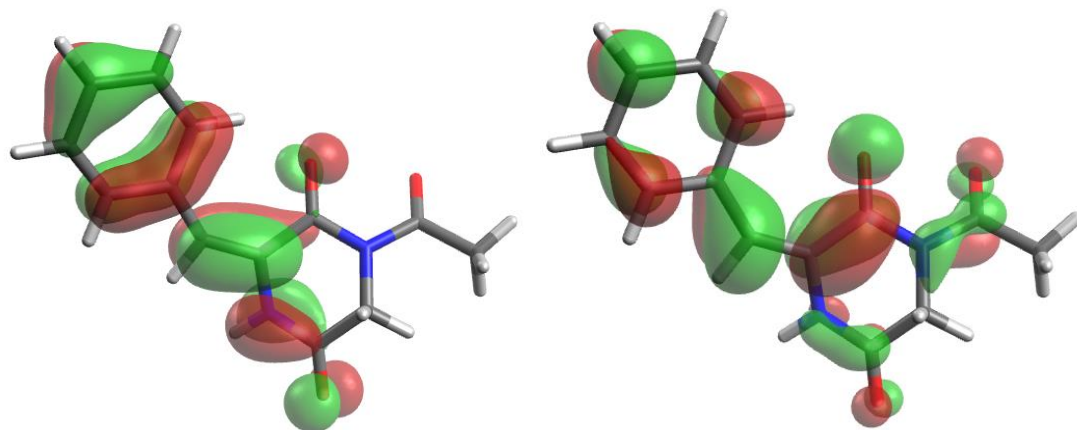
*Z-p-OMe-Ph-DKP-Ac (30)*
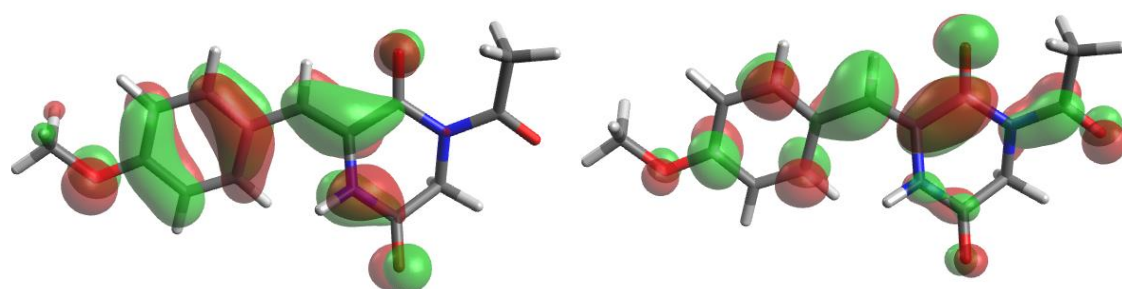


*E-p-OMe-Ph-DKP-Ac (30)*
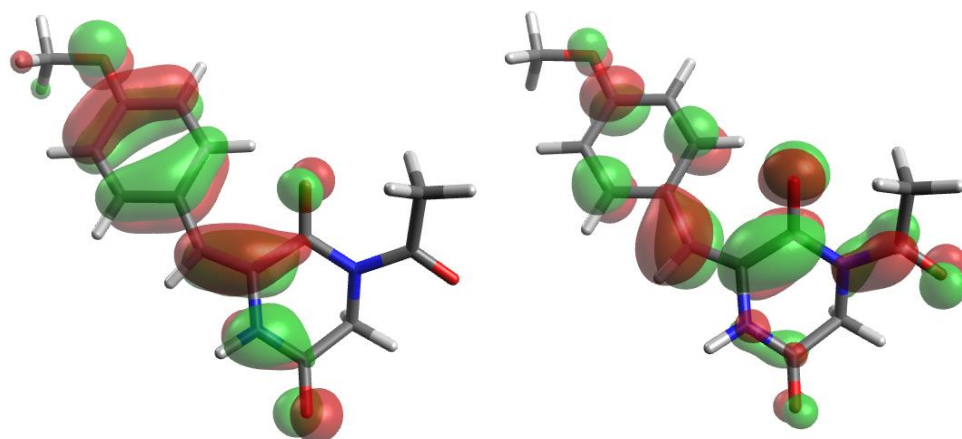


*Z-m-OMe-Ph-DKP-Ac (31)*
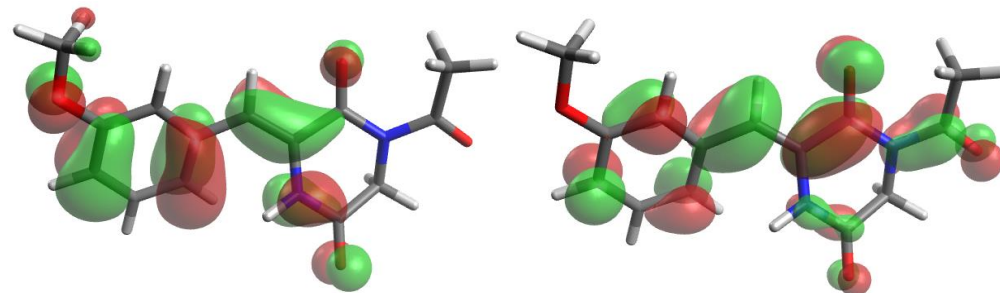


*E-m-OMe-Ph-DKP-Ac (31)*
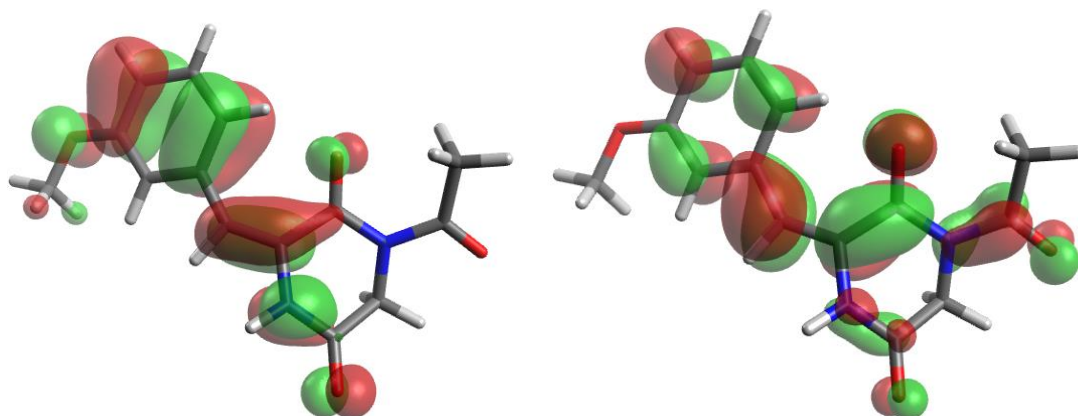
*Z-o-OMe-Ph-DKP-Ac (32)*
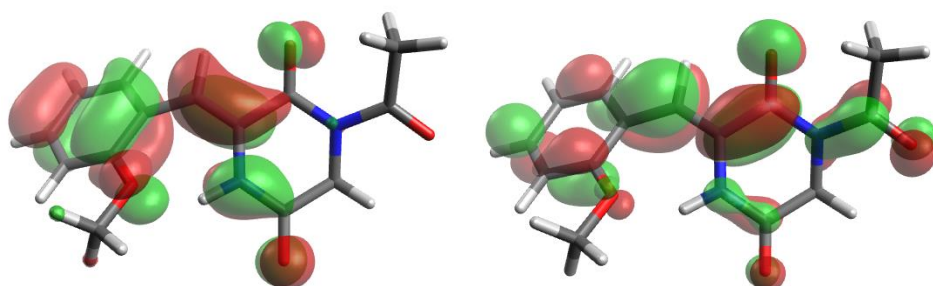


*E-o-OMe-Ph-DKP-Ac (32)*
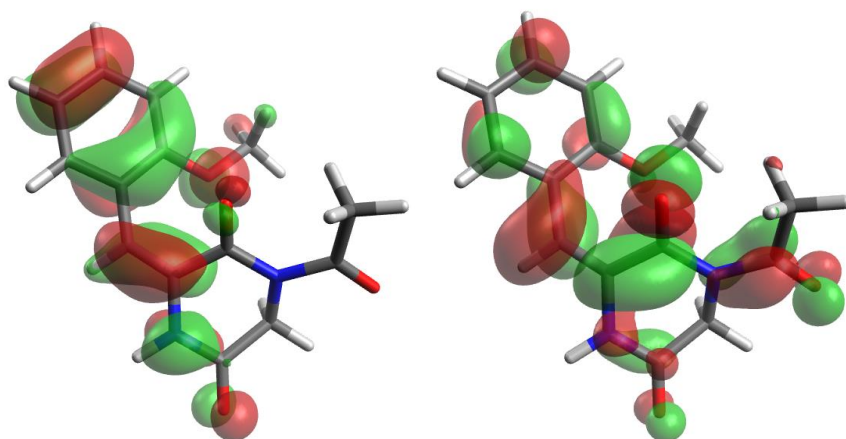


*Z-m,m,p-(OMe)₃-Ph-DKP-Ac (33)*
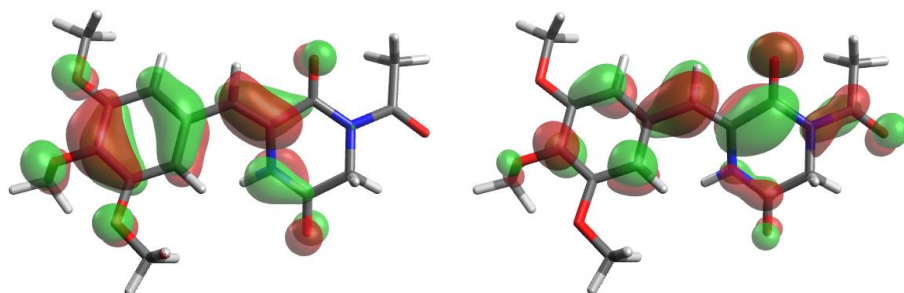


*E-m,m,p-(OMe)₃-Ph-DKP-Ac (33)*
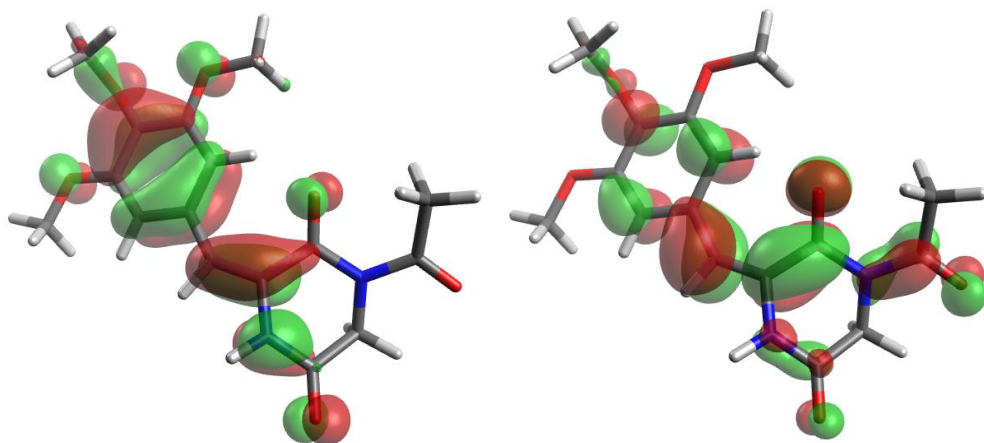
*Z-p-OCF₃-Ph-DKP-Ac (34)*
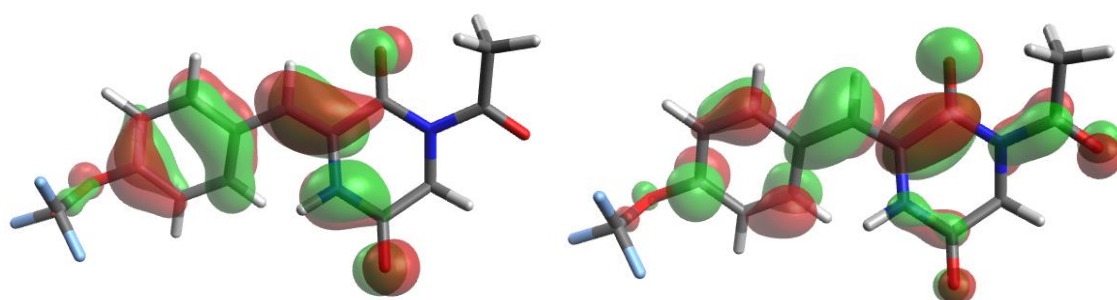


*E-p-OCF₃-Ph-DKP-Ac (34)*
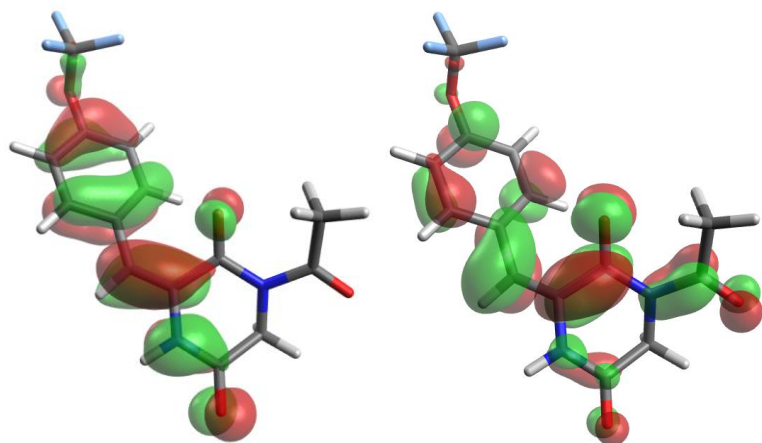


*Z-p-CN-Ph-DKP-Ac (35)*
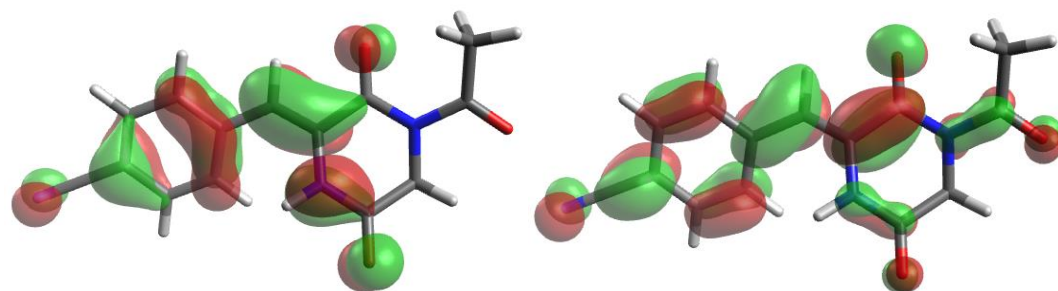


*E-p-CN-Ph-DKP-Ac (35)*
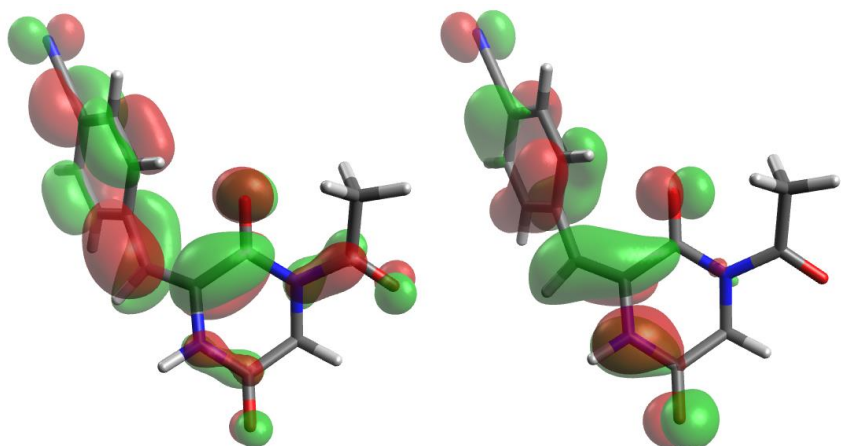
*Z-p-NMe₂-Ph-DKP-Ac (36)*
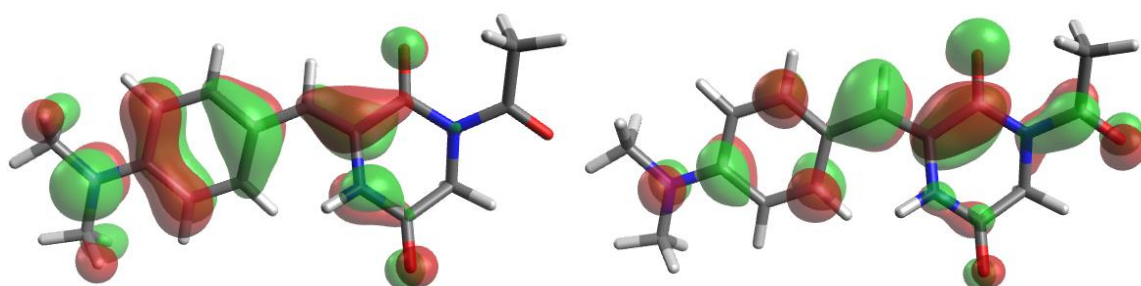


*E-p-NMe₂-Ph-DKP-Ac (36)*
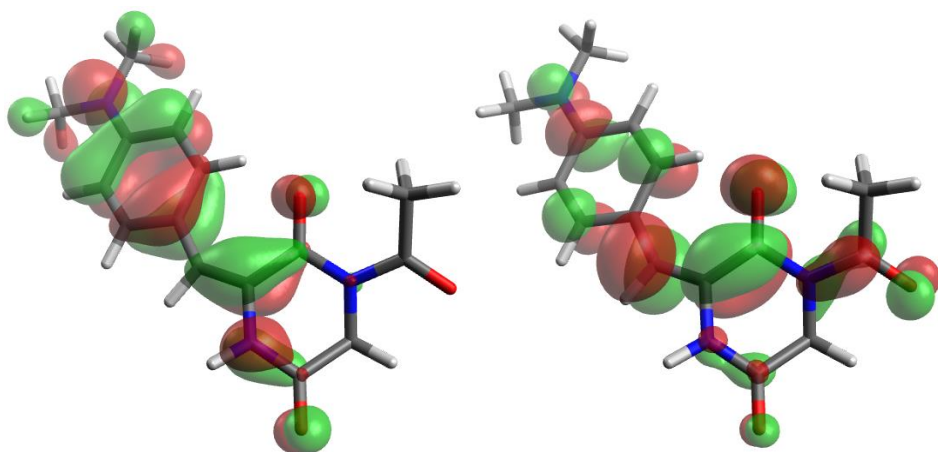


*Z-p-NPh₂-Ph-DKP-Ac (37)*
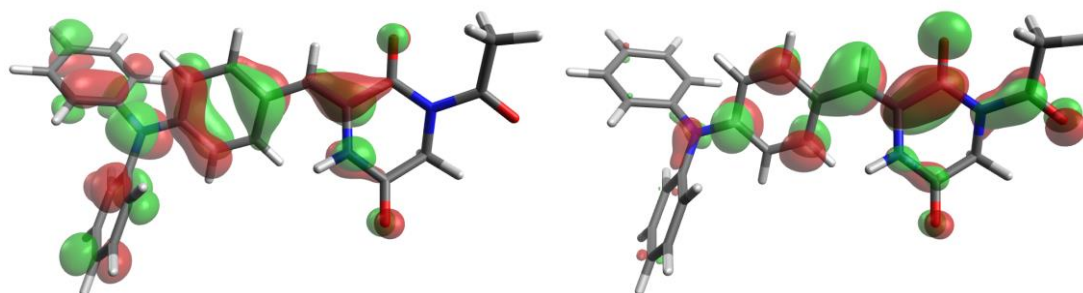


*E-p-NPh₂-Ph-DKP-Ac (37)*
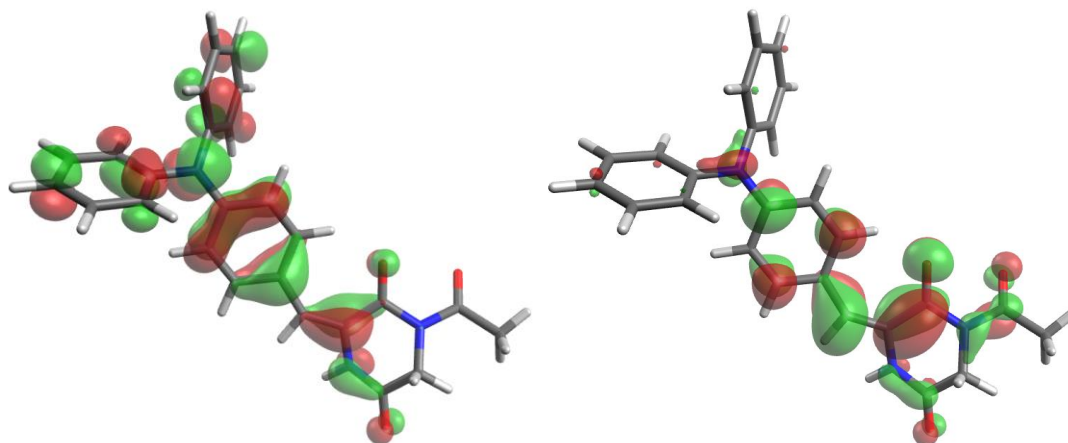
***Z-p-Pip-Ph-DKP-Ac (38)***
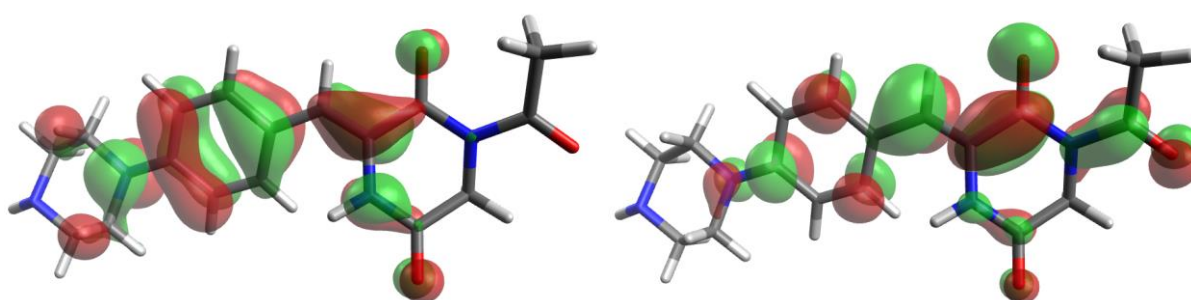


***E-p-Pip-Ph-DKP-Ac (38)***
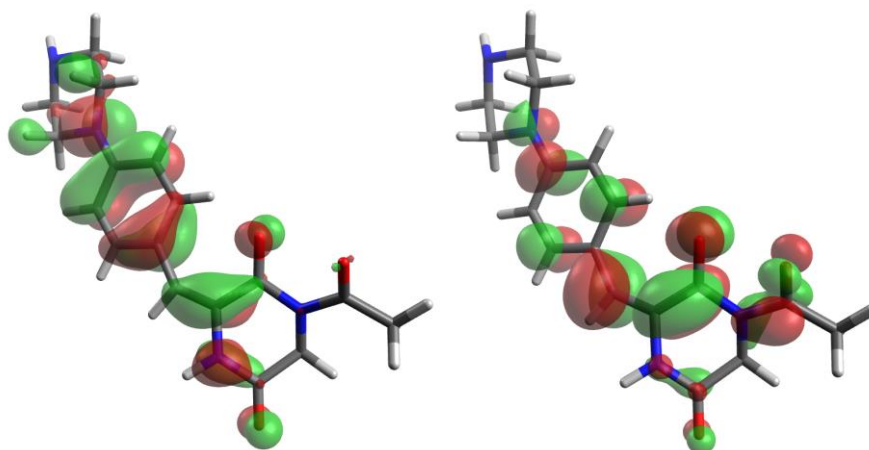


*Excitation Energies*

The five lowest transitions computed in the TD calculations (10 states in total) are reported. For each excited state the energy (in eV), the associated wavelength (in nm) and the oscillator strength of the transition is given. The numbers of the orbitals involved in the transition (with general formula occupied $\rightarrow$ unoccupied) and the associated (largest) coefficient in the CI expansion is presented.

**Z-Ph-DKP-Ac (29)**

Excited State 1: 3.6659 eV  338.21 nm  f=0.5614

    63 -> 65       0.13464

    64 -> 65       0.68835

Excited State  2: 3.8710 eV  320.29 nm  f=0.0553

    61 -> 65       0.16695

    62 -> 65     -0.12144

    63 -> 65       0.62555

    63 -> 66       0.14669

    64 -> 65     -0.14257

Excited State  3: 4.3807 eV  283.02 nm  f=0.0048

    61 -> 65     -0.17565

    62 -> 65       0.60897

    63 -> 65       0.17388

    64 -> 67     -0.23825

Excited State  4: 4.4377 eV  279.39 nm  f=0.0353

    61 -> 65       0.63143

    62 -> 65       0.19905

    63 -> 65     -0.15136

Excited State  5: 4.8883 eV  253.64 nm  f=0.0500

    58 -> 65       0.34338

    58 -> 66       0.10534

    59 -> 65       0.22563

    60 -> 65       0.28207

    63 -> 66     -0.23256

    63 -> 69     -0.11949

    64 -> 66       0.37336

*E*-**Ph-DKP-Ac (29)**

Excited State  1: 3.5756 eV  346.75 nm  f=0.5345

    63 -> 65       0.18410

    64 -> 65       0.67042

Excited State  2: 3.8216 eV  324.43 nm  f=0.0931

    61 -> 65       0.15493

    62 -> 65       0.19230

    63 -> 65       0.59700

   63 -> 66        0.14135

   64 -> 65       -0.20573

Excited State   3: 4.2219 eV  293.67 nm  f=0.0095

   62 -> 65        0.64429

   63 -> 65       -0.20771

   64 -> 67        0.18412

Excited State   4: 4.3346 eV  286.03 nm  f=0.0439

   61 -> 65        0.66557

   63 -> 65       -0.16952

Excited State   5: 4.8421 eV  256.05 nm  f=0.1842

   58 -> 65        0.19942

   59 -> 65       -0.29870

   63 -> 66       -0.13519

   64 -> 66        0.56144

**Z-*p*-OMe-Ph-DKP-Ac (30)**

Excited State   1: 3.4188 eV  362.66 nm  f=0.7882

   72 -> 73        0.70342

Excited State   2: 4.2986 eV  288.43 nm  f=0.0233

   67 -> 73       -0.32573

   68 -> 73       -0.32261

   71 -> 73        0.49482

Excited State   3: 4.3997 eV  281.80 nm  f=0.0131

   69 -> 73        0.24852

   70 -> 73       -0.43173

   72 -> 74        0.44380

   72 -> 75       -0.18940

Excited State   4: 4.5054 eV  275.19 nm  f=0.0025

   68 -> 73       -0.14421

   69 -> 73        0.46407

   70 -> 73        0.42017

   71 -> 73       -0.21480

   72 -> 74        0.12723

Excited State   5: 4.7342 eV  261.89 nm  f=0.1474

   68 -> 73        0.10544

72 -> 74      0.21583

72 -> 75      0.64538

**E-*p*-OMe-Ph-DKP-Ac (30)**

Excited State   1: 3.2811 eV 377.87 nm f=0.7129

   72 -> 73      0.70320

Excited State   2: 4.1795 eV 296.65 nm f=0.0019

   67 -> 73      -0.30644

   68 -> 73      0.28669

   69 -> 73      -0.15157

   70 -> 73      0.31176

   71 -> 73      0.42080

   72 -> 75      0.10506

Excited State   3: 4.3188 eV 287.08 nm f=0.0032

   67 -> 73      0.12218

   68 -> 73      -0.13517

   70 -> 73      0.53737

   71 -> 73      -0.29196

   72 -> 75      0.28718

Excited State   4: 4.4033 eV 281.57 nm f=0.0107

   67 -> 73      0.13740

   68 -> 73      -0.26550

   69 -> 73      0.47813

   71 -> 73      0.37451

   72 -> 75      0.10067

Excited State   5: 4.6794 eV 264.96 nm f=0.2732

   67 -> 73      -0.17381

   69 -> 73      0.13680

   72 -> 74      0.64568

   72 -> 75      -0.10003

**Z-*m*-OMe-Ph-DKP-Ac (31)**

Excited State   1: 3.4943 eV 354.82 nm f=0.3787

   71 -> 73      0.11538

   72 -> 73      0.69350

Excited State   2: 3.8829 eV 319.31 nm f=0.2400

    71 -> 73        0.68326

    72 -> 73        -0.11481

Excited State   3: 4.3248 eV  286.68 nm  f=0.0468

    66 -> 73        0.11215

    67 -> 73        0.34337

    68 -> 73        0.12955

    69 -> 73        0.55509

    70 -> 73        0.12009

Excited State   4: 4.4718 eV  277.26 nm  f=0.0166

    69 -> 73        -0.13567

    70 -> 73        0.67050

Excited State   5: 4.7584 eV  260.56 nm  f=0.0012

    67 -> 73        -0.36847

    68 -> 73        0.53035

    68 -> 74        0.13439

    70 -> 73        0.10096

    70 -> 74        -0.11132

### *E-m*-OMe-Ph-DKP-Ac (31)

Excited State   1: 3.3839 eV  366.40 nm  f=0.3224

    71 -> 73        0.15348

    72 -> 73        0.68376

Excited State   2: 3.7655 eV  329.27 nm  f=0.2875

    71 -> 73        0.67619

    72 -> 73        -0.14705

Excited State   3: 4.2930 eV  288.80 nm  f=0.0939

    67 -> 73        -0.33967

    69 -> 73        0.42826

    70 -> 73        0.41285

Excited State   4: 4.3876 eV  282.58 nm  f=0.0024

    67 -> 73        0.16081

    69 -> 73        -0.37488

    70 -> 73        0.55112

Excited State   5: 4.7268 eV  262.30 nm  f=0.0179

    67 -> 73        0.47210

|          |          |
|----------|----------|
| 67 -> 74 | 0.10954  |
| 68 -> 73 | 0.33188  |
| 68 -> 74 | 0.10713  |
| 69 -> 73 | 0.26210  |
| 69 -> 74 | 0.12074  |
| 72 -> 74 | -0.18479 |

**Z-*o*-OMe-Ph-DKP-Ac (32)**

Excited State   1: 3.4915 eV  355.11 nm  f=0.4938

    72 -> 73     0.69329

Excited State   2: 4.0665 eV  304.89 nm  f=0.0870

    71 -> 73     0.67839

    72 -> 75     -0.10584

Excited State   3: 4.4285 eV  279.97 nm  f=0.0809

    66 -> 73     0.13494

    67 -> 73     0.37524

    69 -> 73     0.53208

    69 -> 74     0.11567

    70 -> 73     0.12988

Excited State   4: 4.4625 eV  277.83 nm  f=0.0080

    69 -> 73     -0.13758

    70 -> 73     0.67490

Excited State   5: 4.7785 eV  259.46 nm  f=0.0254

    66 -> 73     0.10871

    67 -> 73     0.47992

    67 -> 74     0.10644

    68 -> 73     -0.12994

    69 -> 73     -0.34232

    69 -> 74     -0.13846

    72 -> 74     0.23275

**E-*o*-OMe-Ph-DKP-Ac (32)**

Excited State   1: 3.4567 eV  358.68 nm  f=0.1699

    71 -> 73     -0.11610

    72 -> 73     0.69294

Excited State   2: 4.1009 eV  302.33 nm  f=0.1563

67 -> 73      -0.10843

70 -> 73       0.10628

71 -> 73       0.65908

72 -> 73       0.11095

Excited State   3: 4.3919 eV  282.30 nm  f=0.0066

67 -> 73      -0.22448

69 -> 73      -0.29037

70 -> 73       0.53223

71 -> 73      -0.15027

72 -> 74      -0.11635

72 -> 75      -0.10587

Excited State   4: 4.6849 eV  264.65 nm  f=0.0445

69 -> 73       0.49962

70 -> 73       0.23901

72 -> 74      -0.39127

Excited State   5: 4.7441 eV  261.34 nm  f=0.2603

67 -> 73      -0.10228

69 -> 73       0.32182

70 -> 73       0.23959

72 -> 74       0.54917

**Z-*m,m,p*-(OMe)₃-Ph-DKP-Ac (33)**

Excited State   1: 3.3717 eV  367.72 nm  f=0.5980

88 -> 89       0.70271

Excited State  2: 3.5939 eV  344.99 nm  f=0.0285

87 -> 89       0.69657

Excited State  3: 4.2054 eV  294.82 nm  f=0.0113

82 -> 89       0.24723

83 -> 89      -0.29434

86 -> 89       0.56978

Excited State  4: 4.4769 eV  276.94 nm  f=0.0004

83 -> 89       0.27113

83 -> 90       0.11140

85 -> 89       0.60030

86 -> 89       0.17553

Excited State   5: 4.5268 eV  273.89 nm  f=0.0869

    81 -> 89        0.11161

    82 -> 89       -0.26940

    83 -> 89        0.40009

    85 -> 89       -0.32494

    86 -> 89        0.35192

### *E-m,m,p*-(OMe)₃-Phe-DKP-Ac (33)

Excited State   1: 3.2666 eV  379.55 nm  f=0.6036

    88 -> 89        0.69958

Excited State   2: 3.4008 eV  364.58 nm  f=0.0278

    87 -> 89        0.69737

Excited State   3: 4.1452 eV  299.10 nm  f=0.0022

    82 -> 89        0.25259

    83 -> 89       -0.19539

    84 -> 89        0.22492

    86 -> 89        0.56668

Excited State   4: 4.3749 eV  283.40 nm  f=0.0020

    82 -> 89        0.16898

    83 -> 89       -0.24504

    84 -> 89        0.23474

    85 -> 89        0.54954

    86 -> 89       -0.16861

Excited State   5: 4.4649 eV  277.69 nm  f=0.1020

    82 -> 89       -0.22261

    83 -> 89        0.21219

    84 -> 89       -0.29490

    85 -> 89        0.40712

    86 -> 89        0.36654

### *Z-p*-OCF₃-Phe-DKP-Ac (34)

Excited State   1: 3.6780 eV  337.10 nm  f=0.6140

    84 -> 85        0.69942

Excited State   2: 4.3078 eV  287.81 nm  f=0.0688

    79 -> 85        0.27311

    80 -> 85        0.17398

81 -> 85        0.56006

81 -> 87        0.11911

82 -> 85        0.18180

Excited State   3: 4.4120 eV  281.02 nm  f=0.0140

83 -> 85        0.67935

Excited State   4: 4.5110 eV  274.85 nm  f=0.0008

81 -> 85        -0.18336

82 -> 85        0.52733

84 -> 86        -0.41609

Excited State   5: 4.7245 eV  262.43 nm  f=0.0024

79 -> 85        0.23533

80 -> 85        0.55082

80 -> 87        0.12414

81 -> 85        -0.25499

81 -> 87        -0.12045

83 -> 87        0.10361

### *E-p*-OCF₃-Phe-DKP-Ac (34)

Excited State   1: 3.6151 eV  342.96 nm  f=0.4699

84 -> 85        0.70044

Excited State   2: 4.1059 eV  301.96 nm  f=0.0062

78 -> 85        -0.22462

79 -> 85        0.10892

81 -> 85        -0.33374

83 -> 85        0.54672

Excited State   3: 4.3962 eV  282.03 nm  f=0.0431

82 -> 85        0.68351

Excited State   4: 4.4622 eV  277.85 nm  f=0.0023

81 -> 85        0.53357

83 -> 85        0.36144

84 -> 86        0.11318

84 -> 87        -0.20896

Excited State   5: 4.7107 eV  263.20 nm  f=0.0023

78 -> 85        -0.19061

80 -> 85        0.62143

80 -> 86        0.15114

**Z-*p*-CN-Ph-DKP-Ac (35)**

Excited State   1: 3.5225 eV  351.98 nm  f=0.7568

70 -> 71        0.70090

Excited State   2: 4.2033 eV  294.97 nm  f=0.0934

64 -> 71        0.10523

65 -> 71        0.27297

66 -> 71        -0.15079

67 -> 71        0.48409

67 -> 72        0.13969

68 -> 71        0.32219

Excited State   3: 4.2488 eV  291.81 nm  f=0.0111

69 -> 71        0.68655

Excited State   4: 4.3963 eV  282.02 nm  f=0.0081

67 -> 71        -0.32060

68 -> 71        0.50371

70 -> 72        -0.11198

70 -> 73        -0.34074

Excited State   5: 4.5957 eV  269.78 nm  f=0.0039

65 -> 71        -0.26720

66 -> 71        0.53586

66 -> 72        0.13442

67 -> 71        0.25797

**E-*p*-CN-Ph-DKP-Ac (35)**

Excited State   1: 3.4883 eV  355.42 nm  f=0.5765

70 -> 71        0.68501

Excited State   2: 4.1753 eV  296.95 nm  f=0.1761

64 -> 71        -0.10829

65 -> 71        0.22582

67 -> 71        -0.23517

68 -> 71        0.53756

69 -> 71        0.13260

70 -> 71        0.15266

70 -> 72        0.10768

70 -> 73        0.10297

Excited State   3: 4.2472 eV  291.92 nm  f=0.0319

  68 -> 71        -0.10236

  69 -> 71        0.67620

Excited State   4: 4.4147 eV  280.84 nm  f=0.0523

  65 -> 71        -0.18713

  66 -> 71        -0.12554

  67 -> 71        0.47755

  68 -> 71        0.35689

  70 -> 72        -0.10895

  70 -> 73        0.20666

Excited State   5: 4.5552 eV  272.18 nm  f=0.0307

  65 -> 71        0.15644

  66 -> 71        0.35106

  67 -> 71        0.33220

  70 -> 72        0.44764

### Z-p-NMe₂-Ph-DKP-Ac (36)

Excited State   1: 3.0013 eV  413.11 nm  f=0.9372

  76 -> 77        0.70538

Excited State   2: 4.1325 eV  300.02 nm  f=0.0165

  74 -> 77        -0.23561

  75 -> 77        -0.10829

  76 -> 78        -0.31753

  76 -> 79        0.56259

Excited State   3: 4.2123 eV  294.34 nm  f=0.0115

  71 -> 77        -0.21055

  72 -> 77        -0.29105

  75 -> 77        0.57360

Excited State   4: 4.3014 eV  288.24 nm  f=0.1362

  76 -> 78        0.61727

  76 -> 79        0.31658

Excited State   5: 4.5330 eV  273.51 nm  f=0.0023

  72 -> 77        -0.26501

  73 -> 77        0.51935

74 -> 77       -0.33592

75 -> 77       -0.12175

**E-*p*-NMe₂-Ph-DKP-Ac (36)**

Excited State   1: 2.9135 eV  425.55 nm  f=0.8714

   76 -> 77       0.70512

Excited State   2: 4.1381 eV  299.62 nm  f=0.0051

   71 -> 77       0.20759

   72 -> 77       -0.26265

   73 -> 77       0.13476

   74 -> 77       0.21015

   75 -> 77       0.51400

   76 -> 78       0.14576

   76 -> 79       -0.16012

Excited State   3: 4.1915 eV  295.80 nm  f=0.0291

   71 -> 77       0.10028

   72 -> 77       -0.13473

   73 -> 77       0.13454

   74 -> 77       -0.36792

   75 -> 77       0.20765

   76 -> 78       -0.25145

   76 -> 79       0.44811

Excited State   4: 4.2953 eV  288.65 nm  f=0.2551

   72 -> 77       0.12387

   74 -> 77       -0.20697

   76 -> 78       0.61586

   76 -> 79       0.19529

Excited State   5: 4.4170 eV  280.70 nm  f=0.0101

   71 -> 77       -0.23912

   72 -> 77       0.39560

   73 -> 77       -0.19842

   74 -> 77       -0.12830

   75 -> 77       0.40340

   76 -> 78       -0.14252

   76 -> 79       -0.13923

**Z-*p*-NPh₂-Ph-DKP-Ac (37)**

Excited State   1: 2.7577 eV  449.60 nm  f=0.8975

   108 ->109       0.70398

 Excited State   2: 3.7043 eV  334.70 nm  f=0.0178

   108 ->110       0.69127

Excited State   3: 3.9060 eV  317.42 nm  f=0.1705

   107 ->109       0.67985

Excited State   4: 3.9695 eV  312.34 nm  f=0.1889

   108 ->112       0.69138

Excited State   5: 4.0934 eV  302.89 nm  f=0.0741

   108 ->111       0.68039

**E-*p*-NPh₂-Ph-DKP-Ac (37)**

Excited State   1: 2.6959 eV  459.89 nm  f=0.8950

   108 ->109       0.70404

Excited State   2: 3.7501 eV  330.62 nm  f=0.0432

   103 ->109       0.19029

   104 ->109       -0.35147

   105 ->109       -0.12455

   106 ->109       -0.31698

   107 ->109       0.41356

   108 ->110       -0.11484

Excited State   3: 3.7564 eV  330.06 nm  f=0.0242

   104 ->109       -0.12971

   108 ->110       0.67063

Excited State   4: 3.8920 eV  318.56 nm  f=0.1522

   103 ->109       -0.10679

   104 ->109       0.31339

   106 ->109       0.22729

   107 ->109       0.54829

Excited State   5: 3.9657 eV  312.64 nm  f=0.1728

   108 ->112       0.68797

**Z-*p*-Pip-Ph-DKP-Ac (38)**

Excited State   1: 3.0366 eV  408.30 nm  f=0.9535

   87 -> 88       0.70518

Excited State 2: 3.9287 eV 315.58 nm f=0.0069

   86 -> 88     0.70421

Excited State 3: 4.1457 eV 299.07 nm f=0.0164

   84 -> 88    -0.28083

   87 -> 90     0.63203

Excited State 4: 4.1975 eV 295.37 nm f=0.0097

   81 -> 88    -0.20787

   82 -> 88    -0.28532

   85 -> 88     0.58568

Excited State 5: 4.3648 eV 284.05 nm f=0.1326

   87 -> 89     0.69309

**_E-p_-Pip-Ph-DKP-Ac (38)**

Excited State 1: 2.9501 eV 420.28 nm f=0.9165

   87 -> 88     0.70478

Excited State 2: 3.8267 eV 324.00 nm f=0.0003

   82 -> 88     0.21411

   84 -> 88     0.59748

   84 -> 89     0.12941

   85 -> 88     0.18757

Excited State 3: 3.8691 eV 320.45 nm f=0.0053

   86 -> 88     0.69910

Excited State 4: 4.1752 eV 296.96 nm f=0.0078

   83 -> 88     0.49130

   87 -> 89     0.16383

   87 -> 90    -0.46091

Excited State 5: 4.2149 eV 294.16 nm f=0.0135

   82 -> 88     0.23971

   84 -> 88    -0.26627

   85 -> 88     0.57333

   87 -> 89     0.13954

*Calculated Absorption Spectra*

The absorption spectra were simulated based on TD calculations (10 states in total) with Gaussview assuming a gaussian band shape (characterized by a standard deviation s = 0.2 eV) and the extracted data was plotted using OriginPro 2020 9.7.188 with the peaks, furnished by the calculation.
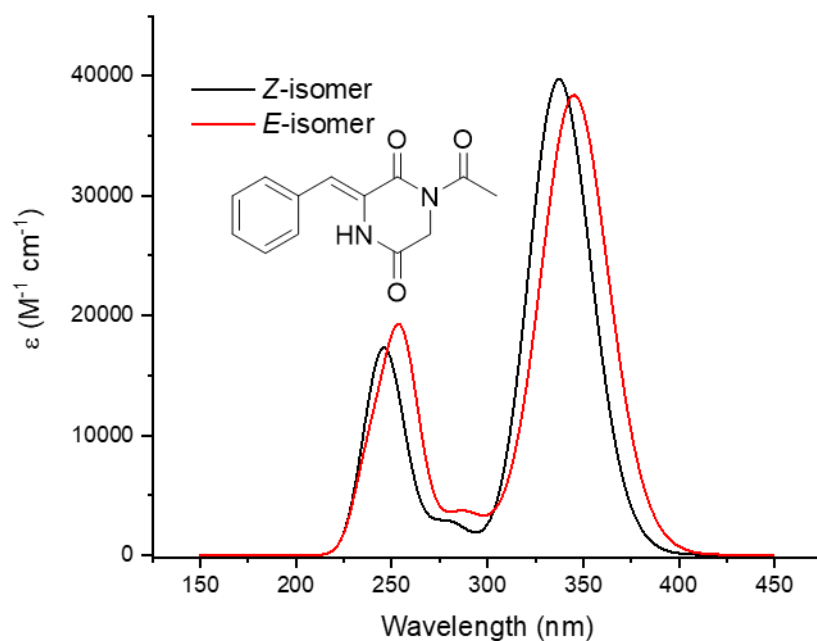


**Figure 263:** Simulated absorption spectrum of *E*-**29** and *Z*-**29** based on TD calculations (10 states in total)**.**
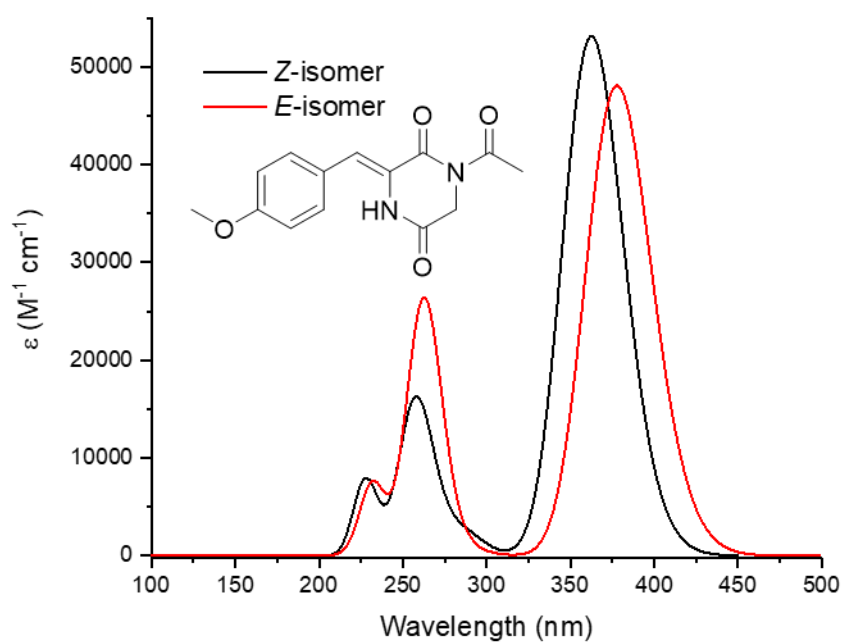
**Figure 264:** Simulated absorption spectrum of *E*-**30** and *Z*-**30** based on TD calculations (10 states in total).
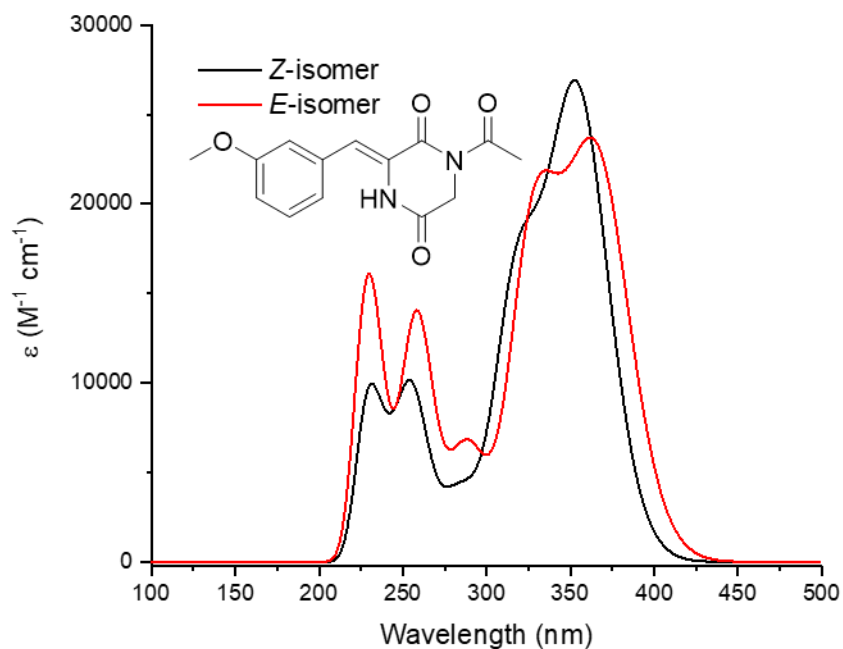


**Figure 265:** Simulated absorption spectrum of *E*-**31** and *Z*-**31** based on TD calculations (10 states in total).
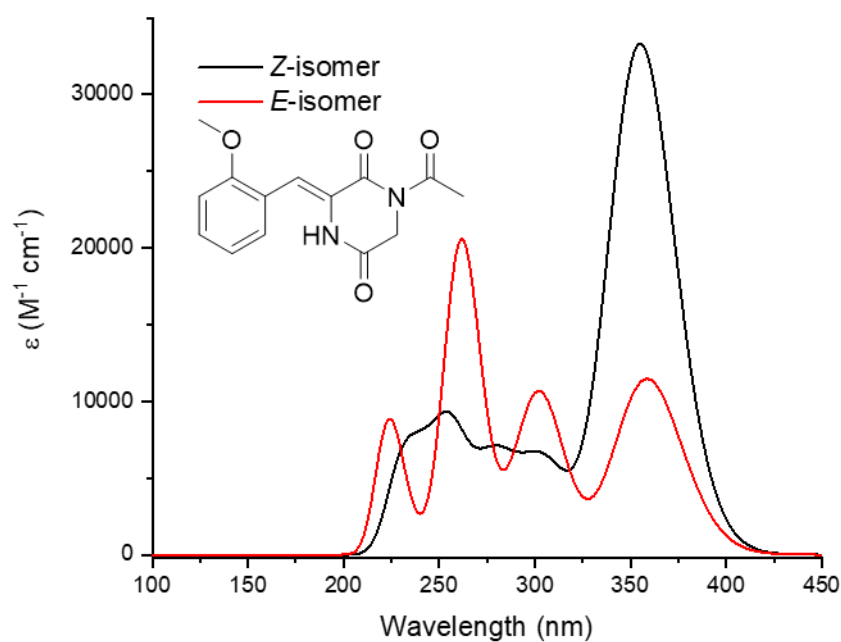
**Figure 266:** Simulated absorption spectrum of *E*-**32** and *Z*-**32** based on TD calculations (10 states in total).
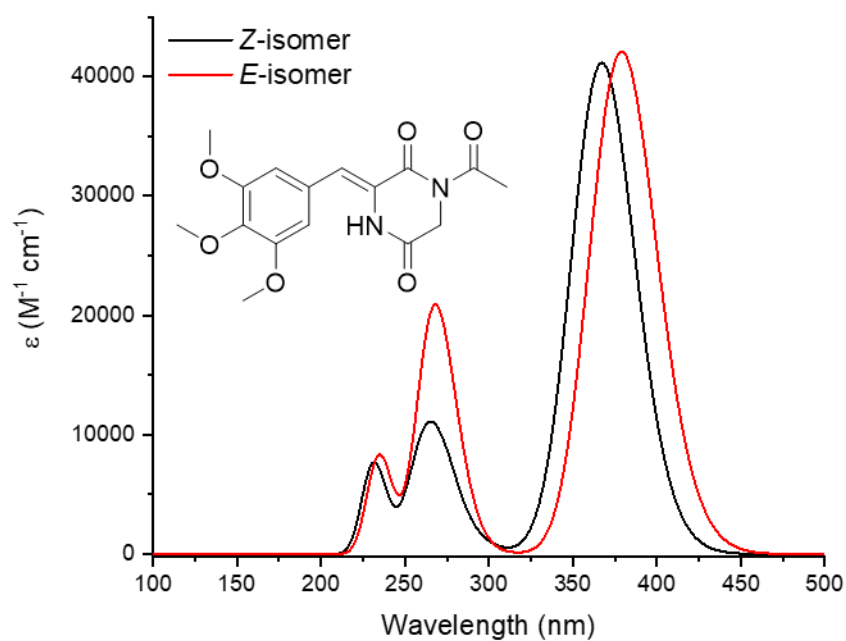


**Figure 267:** Simulated absorption spectrum of *E*-**33** and *Z*-**33** based on TD calculations (10 states in total).
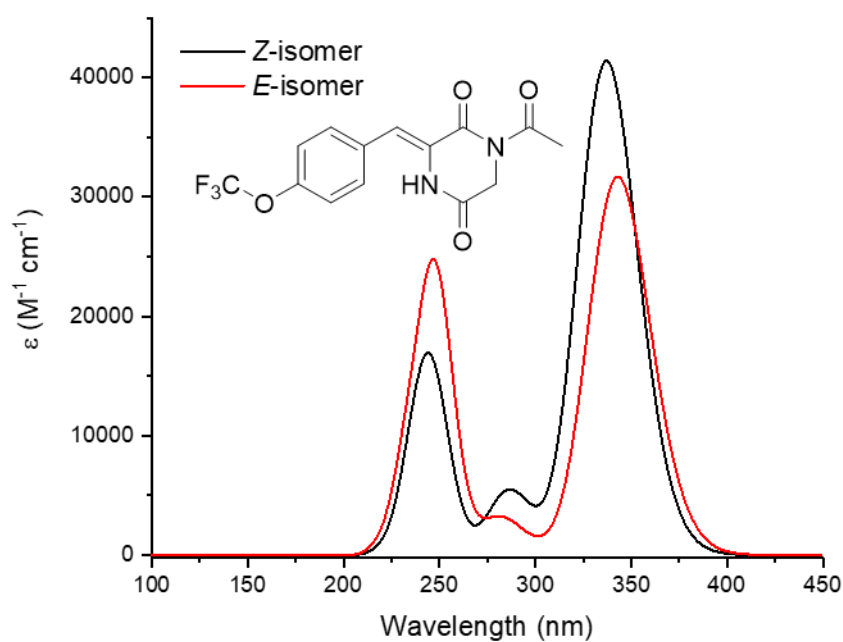
**Figure 268:** Simulated absorption spectrum of *E*-**34** and *Z*-**34** based on TD calculations (10 states in total).
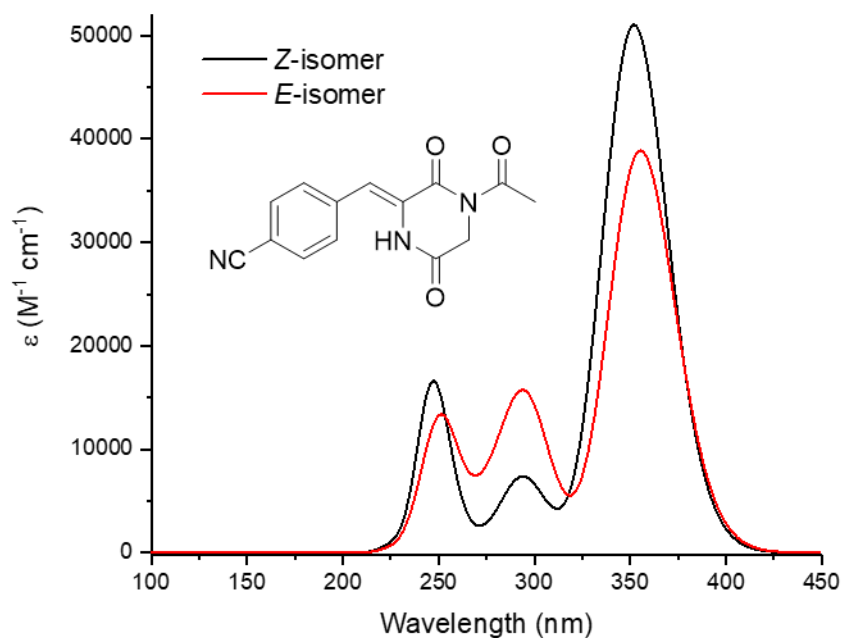


**Figure 269:** Simulated absorption spectrum of *E*-**35** and *Z*-**35** based on TD calculations (10 states in total).
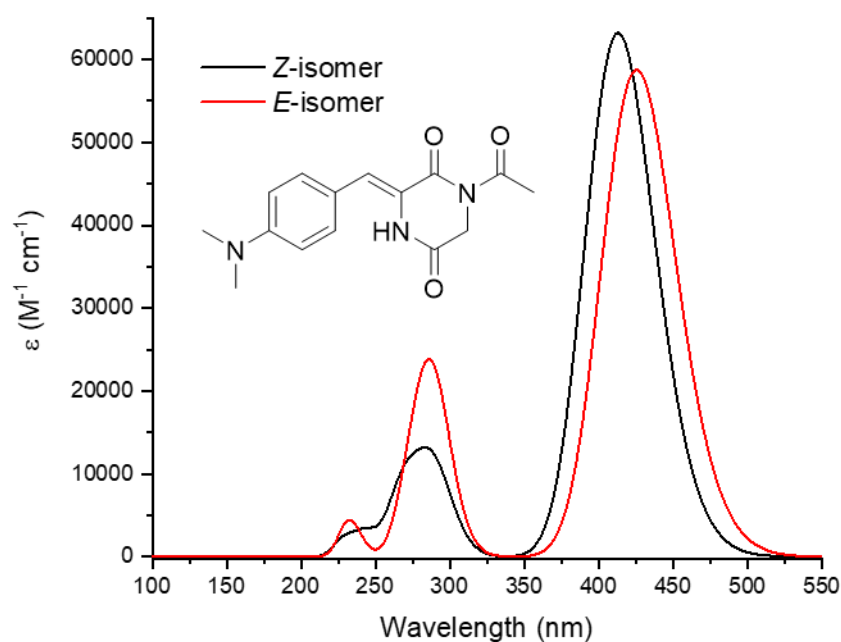
**Figure 270:** Simulated absorption spectrum of *E*-**36** and *Z*-**36** based on TD calculations (10 states in total).
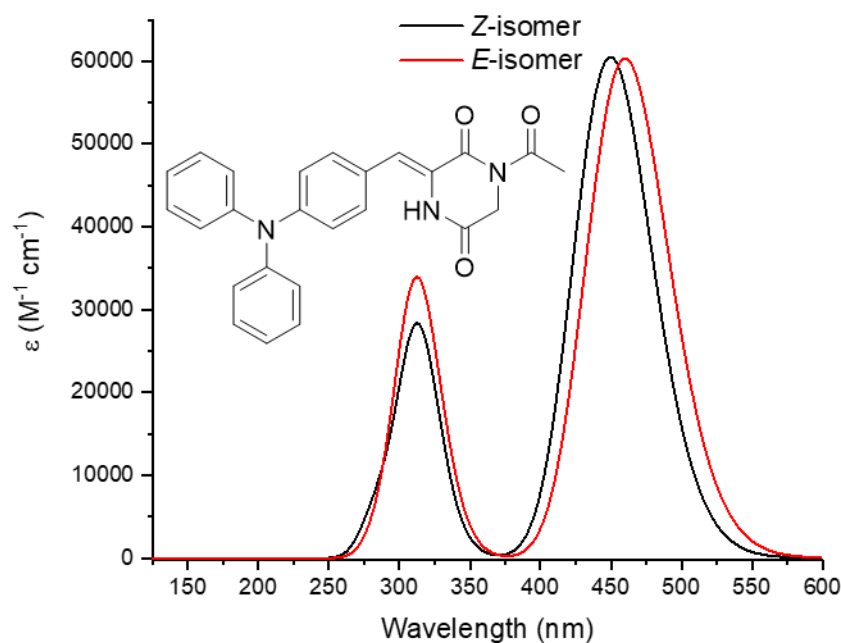


**Figure 271:** Simulated absorption spectrum of *E*-**37** and *Z*-**37** based on TD calculations (10 states in total).
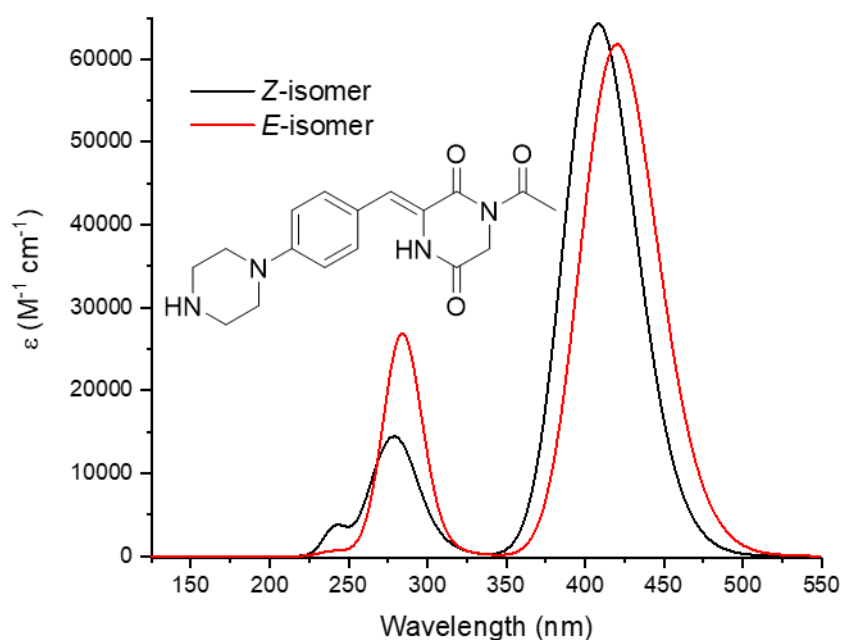
**Figure 272:** Simulated absorption spectrum of *E*-**38** and *Z*-**38** based on TD calculations (10 states in total).

### 5.5.11  Crystal Structure Determinations

Crystal structures in this section were measured and solved by Dr. Martin Nieger at the University of Helsinki (Finland).

**Table 14:** Overview of the numbering and sample code of crystal structures solved by Dr. Martin Nieger.

| Entry | Compound Number | Code Assigned by Dr. Martin Nieger | CCDC Number |
|-------|-----------------|------------------------------------|-------------|
| 1 | 29 | SB1440_HY_SUK170 | |
| 2 | 30 | SB1440_HY | |
| 3 | 33 | SB1465_HY | |
| 4 | 35 | SB1440_HY_SUK130 | |
| 5 | 36 | SB1393_HY | |
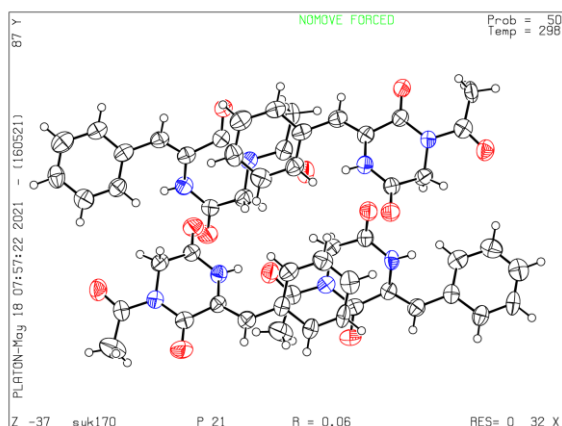
**SUK170**

**SB1440_HY_SUK170**

*pseudo-merohedral twin with 4 crystallographic independent molecules in the asymmetric unit*

*additional refinement as inversion twin failed*

## (*Z*)-1-Acetyl-3-benzylidenepiperazine-2,5-dione – SB1440_HY_SUK170

*Crystal data*

| | |
|---|---|
| $C_{13}H_{12}N_2O_3$ | $F(000) = 1024$ |
| $M_r = 244.25$ | $D_x = 1.416$ Mg m$^{-3}$ |
| Monoclinic, $P2_1$ (no.4) | Cu $K\alpha$ radiation, $\lambda = 1.54178$ Å |
| $a = 7.2931$ (5) Å | Cell parameters from 9848 reflections |
| $b = 23.1044$ (16) Å | $\theta = 3.8–72.3°$ |
| $c = 13.5985$ (9) Å | $\mu = 0.85$ mm$^{-1}$ |
| $\beta = 90.424$ (4)° | $T = 298$ K |
| $V = 2291.3$ (3)  Å$^3$ | Blocks, colourless |
| $Z = 8$ | $0.36 \times 0.18 \times 0.06$ mm |

*Data collection*

| | |
|---|---|
| Bruker D8 VENTURE diffractometer with PhotonII CPAD detector | 8174 reflections with $I > 2\sigma(I)$ |
| Radiation source: INCOATEC microfocus sealed tube | $R_{int} = 0.061$ |
| rotation in $\phi$ and $\omega$, 1°, shutterless scans | $\theta_{max} = 73.1°$, $\theta_{min} = 1.9°$ |
| Absorption correction: multi-scan *SADABS* (Sheldrick, 2014) | $h = -8 \rightarrow 9$ |
| $T_{min} = 0.614$, $T_{max} = 0.925$ | $k = -28 \rightarrow 28$ |
| 46761 measured reflections | $l = -16 \rightarrow 16$ |
| 8936 independent reflections | |

*Refinement*

| | |
|---|---|
| Refinement on $F^2$ | Secondary atom site location: difference Fourier map |
| Least-squares matrix: full | Hydrogen site location: inferred from neighbouring sites |
| $R[F^2 > 2\sigma(F^2)] = 0.060$ | H-atom parameters constrained |
| $wR(F^2) = 0.165$ | $w = 1/[\sigma^2(F_o^2) + (0.0769P)^2 + 1.2391P]$ where $P = (F_o^2 + 2F_c^2)/3$ |
| $S = 1.06$ | $(\Delta/\sigma)_{max} < 0.001$ |
| 8936 reflections | $\Delta\rangle_{max} = 0.29$ e Å$^{-3}$ |
| 654 parameters | $\Delta\rangle_{min} = -0.21$ e Å$^{-3}$ |
| 541 restraints | Absolute structure:  Flack x determined using 3539 quotients [(I+)-(I-)]/[(I+)+(I-)]  (Parsons, Flack and Wagner, Acta Cryst. B69 (2013) 249-259). |
| Primary atom site location: dual | Absolute structure parameter: 0.23 (9) |
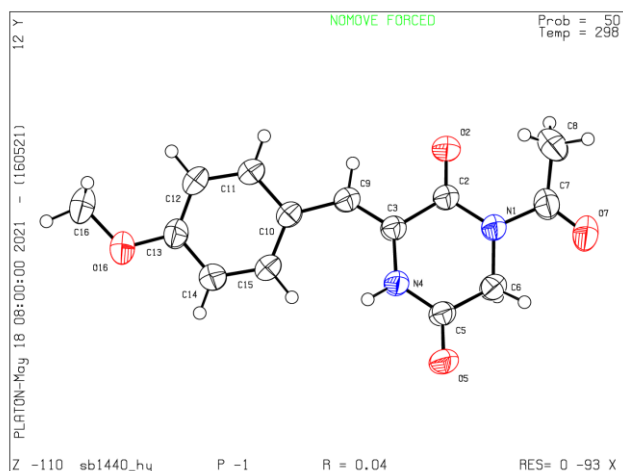
## (Z)-1-Acetyl-3-(4-methoxybenzylidene)piperazine-2,5-dione – SB1440_HY

*Crystal data*

| $C_{14}H_{14}N_2O_4$ | $Z = 2$ |
|---|---|
| $M_r = 274.27$ | $F(000) = 288$ |
| Triclinic, $P\text{-}1$ (no.2) | $D_x = 1.383$ Mg m$^{-3}$ |
| $a = 6.6984$ (2) Å | Cu $K\alpha$ radiation, $\lambda = 1.54178$ Å |
| $b = 7.3720$ (2) Å | Cell parameters from 6921 reflections |
| $c = 13.9541$ (3) Å | $\theta = 3.1$–$72.3°$ |
| $\alpha = 82.063$ (1)° | $\mu = 0.86$ mm$^{-1}$ |
| $\beta = 89.009$ (1)° | $T = 298$ K |
| $\gamma = 74.886$ (1)° | Blocks, colourless |
| $V = 658.73$ (3) Å$^3$ | $0.16 \times 0.08 \times 0.04$ mm |

*Data collection*

| Bruker D8 VENTURE diffractometer with PhotonII CPAD detector | 2336 reflections with $I > 2\sigma(I)$ |
|---|---|
| Radiation source: INCOATEC microfocus sealed tube | $R_{int} = 0.023$ |
| rotation in ω, 1°, shutterless scans | $\theta_{max} = 72.3°$, $\theta_{min} = 3.2°$ |
| Absorption correction: multi-scan *SADABS* (Sheldrick, 2014) | $h = -8 \rightarrow 7$ |
| $T_{min} = 0.888$, $T_{max} = 0.971$ | $k = -9 \rightarrow 9$ |
| 9756 measured reflections | $l = -17 \rightarrow 17$ |
| 2584 independent reflections | |

*Refinement*

| Refinement on $F^2$ | Primary atom site location: dual |
|---|---|
| Least-squares matrix: full | Secondary atom site location: difference Fourier map |
| $R[F^2 > 2\sigma(F^2)] = 0.038$ | Hydrogen site location: difference Fourier map |
| $wR(F^2) = 0.110$ | H atoms treated by a mixture of independent and constrained refinement |
| $S = 1.08$ | $w = 1/[\sigma^2(F_o^2) + (0.0573P)^2 + 0.093P]$ where $P = (F_o^2 + 2F_c^2)/3$ |
| 2584 reflections | $(\Delta/\sigma)_{max} < 0.001$ |
| 186 parameters | $\Delta\rangle_{max} = 0.16$ e Å$^{-3}$ |
| 1 restraint | $\Delta\rangle_{min} = -0.16$ e Å$^{-3}$ |
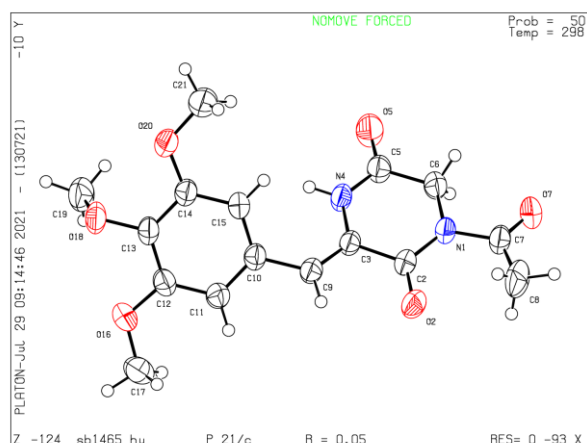
## (Z)-1-Acetyl-3-(3,4,5-trimethoxybenzylidene)piperazine-2,5-dione – SB1465_HY

### Crystal data

| | |
|---|---|
| $C_{16}H_{18}N_2O_6$ | $F(000) = 704$ |
| $M_r = 334.32$ | $D_x = 1.402$ Mg m$^{-3}$ |
| Monoclinic, $P2_1/c$ (no.14) | Cu $K\alpha$ radiation, $\lambda = 1.54178$ Å |
| $a = 9.7400$ (3) Å | Cell parameters from 9930 reflections |
| $b = 11.6320$ (4) Å | $\theta = 3.8–72.0°$ |
| $c = 14.0685$ (5) Å | $\mu = 0.91$ mm$^{-1}$ |
| $\beta = 96.509$ (2)° | $T = 298$ K |
| $V = 1583.63$ (9)  Å$^3$ | Blocks, colourless |
| $Z = 4$ | $0.20 \times 0.18 \times 0.06$ mm |

### Data collection

| | |
|---|---|
| Bruker D8 VENTURE diffractometer with PhotonII CPAD detector | 2789 reflections with $I > 2\sigma(I)$ |
| Radiation source: INCOATEC microfocus sealed tube | $R_{int} = 0.056$ |
| rotation in $\phi$ and $\omega$, 1°, shutterless scans | $\theta_{max} = 72.2°$, $\theta_{min} = 4.6°$ |
| Absorption correction: multi-scan SADABS (Sheldrick, 2014) | $h = -12 \rightarrow 12$ |
| $T_{min} = 0.671$, $T_{max} = 0.958$ | $k = -14 \rightarrow 14$ |
| 19978 measured reflections | $l = -15 \rightarrow 17$ |
| 3109 independent reflections | |

### Refinement

| | |
|---|---|
| Refinement on $F^2$ | Secondary atom site location: difference Fourier map |
| Least-squares matrix: full | Hydrogen site location: difference Fourier map |
| $R[F^2 > 2\sigma(F^2)] = 0.046$ | H atoms treated by a mixture of independent and constrained refinement |
| $wR(F^2) = 0.140$ | $w = 1/[\sigma^2(F_o^2) + (0.081P)^2 + 0.2548P]$ where $P = (F_o^2 + 2F_c^2)/3$ |
| $S = 1.07$ | $(\Delta/\sigma)_{max} < 0.001$ |
| 3109 reflections | $\Delta\rangle_{max} = 0.26$ e Å$^{-3}$ |
| 225 parameters | $\Delta\rangle_{min} = -0.27$ e Å$^{-3}$ |
| 181 restraints | Extinction correction: SHELXL2014/7 (Sheldrick 2014), Fc$^*$=kFc[1+0.001xFc$^2\lambda^3$/sin(2$\theta$)]$^{-1/4}$ |
| Primary atom site location: dual | Extinction coefficient: 0.0102 (11) |

## SUK130

### SB1440_HY_SUK130

*Due to the bad quality of the crystal, incomplete data and possible twinning only structure confirmed:*
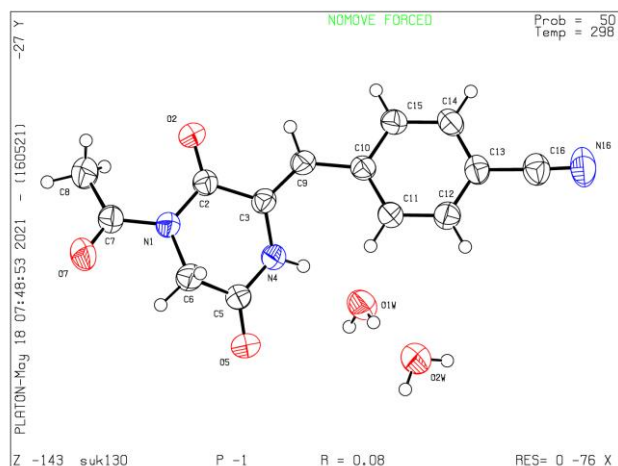
## (Z)-4-((4-Acetyl-3,6-dioxopiperazin-2-ylidene)methyl)benzonitrile – SB1440_HY_SUK130

### Crystal data

| | |
|---|---|
| $C_{14}H_{15}N_3O_5$ | $Z = 2$ |
| $M_r = 305.29$ | $F(000) = 320$ |
| Triclinic, *P*-1 (no.2) | $D_x = 1.393$ Mg m$^{-3}$ |
| $a = 7.4710$ (17) Å | Cu *K*α radiation, λ = 1.54178 Å |
| $b = 8.0460$ (17) Å | Cell parameters from 2267 reflections |
| $c = 12.747$ (3) Å | θ = 3.6–72.0° |
| α = 80.540 (15)° | μ = 0.91 mm$^{-1}$ |
| β = 74.438 (15)° | $T = 298$ K |
| γ = 86.632 (15)° | Blocks, colourless |
| $V = 728.0$ (3) Å$^3$ | $0.16 \times 0.08 \times 0.04$ mm |

### Data collection

| | |
|---|---|
| Bruker D8 VENTURE diffractometer with PhotonII CPAD detector | 2100 reflections with $I > 2\sigma(I)$ |
| Radiation source: INCOATEC microfocus sealed tube | $R_{int} = 0.047$ |
| rotation in ϕ and ω, 1°, shutterless scans | $\theta_{max} = 72.4°$, $\theta_{min} = 3.6°$ |
| Absorption correction: multi-scan *SADABS* (Sheldrick, 2014) | $h = -9 \rightarrow 9$ |
| $T_{min} = 0.723$, $T_{max} = 0.971$ | $k = -9 \rightarrow 9$ |
| 4516 measured reflections | $l = -15 \rightarrow 15$ |
| 2736 independent reflections | |

### Refinement

| | |
|---|---|
| Refinement on $F^2$ | Primary atom site location: dual |
| Least-squares matrix: full | Secondary atom site location: difference Fourier map |
| $R[F^2 > 2\sigma(F^2)] = 0.077$ | Hydrogen site location: mixed |
| $wR(F^2) = 0.221$ | H atoms treated by a mixture of independent and constrained refinement |
| $S = 1.08$ | $w = 1/[\sigma^2(F_o^2) + (0.1029P)^2 + 0.4381P]$ where $P = (F_o^2 + 2F_c^2)/3$ |
| 2736 reflections | $(\Delta/\sigma)_{max} < 0.001$ |
| 212 parameters | $\Delta\rangle_{max} = 0.28$ e Å$^{-3}$ |
| 6 restraints | $\Delta\rangle_{min} = -0.28$ e Å$^{-3}$ |
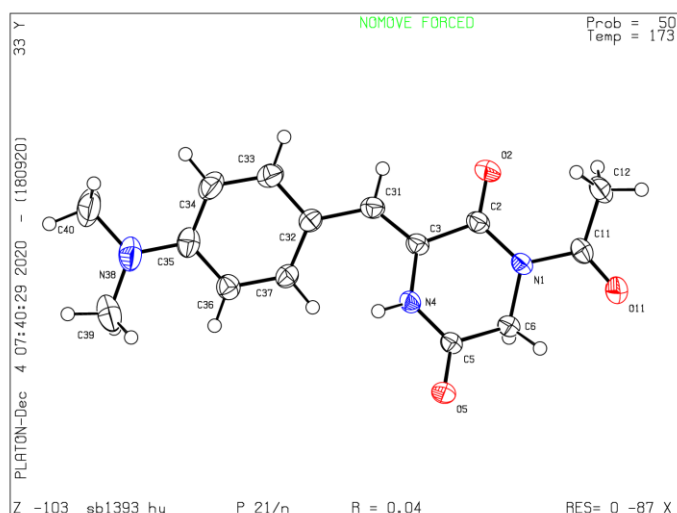
## (Z)-1-Acetyl-3-(4-(dimethylamino)benzyldene)piperazine-2,5-dione – SB1393_HY

### Crystal data

| | |
|---|---|
| $C_{15}H_{17}N_3O_3$ | $F(000) = 608$ |
| $M_r = 287.32$ | $D_x = 1.340$ Mg m$^{-3}$ |
| Monoclinic, $P2_1/n$ (no.14) | Cu $K\alpha$ radiation, $\lambda = 1.54178$ Å |
| $a = 11.9836$ (3) Å | Cell parameters from 9888 reflections |
| $b = 7.9926$ (2) Å | $\theta = 5.3$–$72.2°$ |
| $c = 15.3272$ (4) Å | $\mu = 0.78$ mm$^{-1}$ |
| $\beta = 104.010$ (1)° | $T = 173$ K |
| $V = 1424.37$ (6) Å$^3$ | Plates, yellow |
| $Z = 4$ | $0.24 \times 0.24 \times 0.06$ mm |

### Data collection

| | |
|---|---|
| Bruker D8 VENTURE diffractometer with PhotonII CPAD detector | 2644 reflections with $I > 2\sigma(I)$ |
| Radiation source: INCOATEC microfocus sealed tube | $R_{int} = 0.022$ |
| rotation in $\phi$ and $\omega$, 1°, shutterless scans | $\theta_{max} = 72.3°$, $\theta_{min} = 5.4°$ |
| Absorption correction: multi-scan *SADABS* (Sheldrick, 2014) | $h = -14 \rightarrow 14$ |
| $T_{min} = 0.790$, $T_{max} = 0.958$ | $k = -9 \rightarrow 9$ |
| 13451 measured reflections | $l = -17 \rightarrow 18$ |
| 2789 independent reflections | |

### Refinement

| | |
|---|---|
| Refinement on $F^2$ | Primary atom site location: dual |
| Least-squares matrix: full | Secondary atom site location: difference Fourier map |
| $R[F^2 > 2\sigma(F^2)] = 0.037$ | Hydrogen site location: difference Fourier map |
| $wR(F^2) = 0.102$ | H atoms treated by a mixture of independent and constrained refinement |
| $S = 1.05$ | $w = 1/[\sigma^2(F_o^2) + (0.0553P)^2 + 0.391P]$ where $P = (F_o^2 + 2F_c^2)/3$ |
| 2789 reflections | $(\Delta/\sigma)_{max} = 0.001$ |
| 196 parameters | $\Delta\rangle_{max} = 0.22$ e Å$^{-3}$ |
| 1 restraint | $\Delta\rangle_{min} = -0.23$ e Å$^{-3}$ |

## 5.6 Synthesis and Characterization of 'Locked' Plinabulin 40 and Derivatives

### 5.6.1 Precursor Synthesis

*Methyl 2-(1H-indole-2-carbonylamino)acetate (43)*
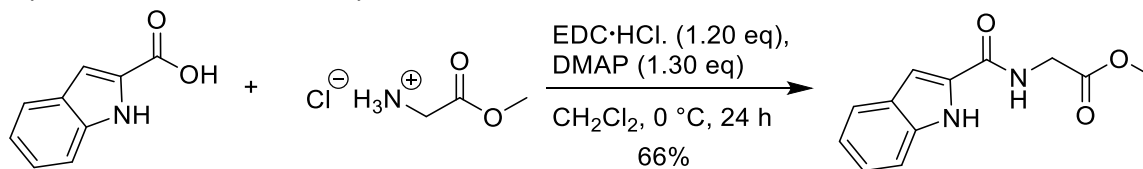


To a solution of 1*H*-indole-2-carboxylic acid (10.0 g, 62.1 mmol, 1.00 equiv.) and the methyl 2-aminoacetate hydrochloride (9.35 g, 74.5 mmol, 1.20 equiv.) in 620 mL CH$_2$Cl$_2$, EDC•HCl (14.3 g, 74.5 mmol, 1.20 equiv.) and DMAP (12.1 g, 99.3 mmol, 1.60 equiv.) were added at 0 °C. After stirring for 4 h at 0 °C, the solution was allowed to warm to ambient temperature and stirred for additional 20 h. The precipitate was filtered off and the mother liquor was washed with water (300 mL) and 10% HCl solution (300 mL) and evaporated *in vacuo*. The residual solid was combined with the precipitate from the first filtration step and purified by recrystallization from methanol to yield 9.05 g (40.9 mmol, 66% yield) of methyl 2-(1*H*-indole-2-carbonylamino)acetate (**43**) as a colorless solid.

**$^1$H NMR (400 MHz, DMSO-$d_6$):** $\delta$ = 11.62 (s, 1H), 8.95 (t, $J$ = 6.0 Hz, 1H), 7.63 (d, $J$ = 7.9, 1.1 Hz, 1H), 7.44 (d, $J$ = 8.3, 1.0 Hz, 1H), 7.19 (ddd, $J$ = 8.2, 7.0, 1.2 Hz, 1H), 7.16 (dd, $J$ = 2.2, 0.9 Hz, 1H), 7.04 (t, $J$ = 1.0 Hz, 1H), 4.06 (d, $J$ = 5.9 Hz, 2H), 3.67 (s, 3H) ppm.

**$^{13}$C NMR (101 MHz, DMSO-$d_6$):** $\delta$ = 170.5, 161.5, 136.5, 131.0, 127.0, 123.5, 121.6, 119.8, 112.3, 103.0, 51.7, 40.8 ppm.

**IR (ATR):** $v$ = 3367 (m), 3271 (vs), 3194 (w), 3153 (w), 3132 (w), 3084 (w), 3055 (w), 3043 (w), 3027 (w), 2996 (w), 2946 (w), 1737 (vs), 1639 (vs), 1621 (s), 1577 (m), 1548 (vs), 1511 (m), 1497 (w), 1449 (w), 1438 (m), 1421 (s), 1409 (s), 1370 (m), 1344 (w), 1315 (s), 1275 (s), 1215 (vs), 1184 (s), 1159 (m), 1140 (s), 1116 (m), 1077 (w), 1023 (w), 1001 (w), 983 (m), 949 (w), 932 (w), 849 (w), 822 (vs), 781 (vs), 773 (s), 747 (vs), 730 (vs), 703 (s), 628 (s), 611 (m), 585 (w), 558 (vs), 538 (s), 469 (s), 441 (vs), 375 (s) cm$^{-1}$.

**HRMS (FAB):** *m/z* calcd. for C$_{12}$H$_{12}$N$_2$O$_3$ [M+H], 232.0922; found, 232.0921.

**EA (C$_{12}$H$_{12}$N$_2$O$_3$):** calcd. C 62.06; H 5.21; N 12.06; O 20.67; found C 61.95; H 5.27; N 11.96.

*2-(1H-Indole-2-carbonylamino)acetic acid (44)*
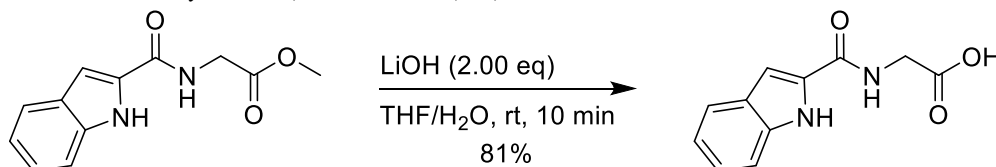
To a solution of methyl 2-(1*H*-indole-2-carbonylamino)acetate (**43**) (8.50 g, 36.6 mmol, 1.00 equiv.) in THF (170 mL) LiOH (1.75 g, 73.2 mmol, 2.00 equiv.) in water (170 mL) was added and the reaction mixture was stirred at room temperature for 10 min. The reaction was quenched by adding aq. solution of HCl (2 M, 50 mL). Subsequently, THF was removed *in vacuo* and the precipitate was filtered off and dried. 2-(1*H*-Indole-2-carbonylamino)acetic acid (6.50 g, 29.8 mmol, 81% yield) was obtained as a yellow solid and used for the next reaction step without further purification.

**$^1$H NMR (400 MHz, DMSO-$d_6$):** $\delta$ = 12.64 (s, 1H), 11.60 (s, 1H), 8.83 (t, *J* = 6.0 Hz, 1H), 7.63 (d, *J* = 8.0 Hz, 1H), 7.44 (d, *J* = 8.2 Hz, 1H), 7.19 (t, *J* = 7.6 Hz, 1H), 7.15 (d, *J* = 2.1 Hz, 1H), 7.04 (t, *J* = 7.5 Hz, 1H), 3.97 (d, *J* = 5.9 Hz, 2H) ppm.

**$^{13}$C NMR (101 MHz, DMSO-$d_6$):** $\delta$ = 171.4, 161.4, 136.5, 131.3, 127.1, 123.4, 121.6, 119.8, 112.3, 102.9, 40.8 ppm.

**IR (ATR):** $v$ = 3395 (s), 3238 (m), 3189 (w), 3152 (w), 3116 (w), 3102 (w), 3080 (w), 3058 (w), 3041 (w), 3034 (w), 3014 (w), 2982 (w), 2942 (w), 2925 (w), 2776 (w), 2755 (w), 2703 (w), 2680 (w), 2633 (w), 2626 (w), 1752 (w), 1718 (s), 1679 (w), 1615 (vs), 1578 (w), 1541 (vs), 1499 (m), 1424 (s), 1402 (m), 1370 (w), 1339 (m), 1315 (m), 1286 (m), 1256 (s), 1239 (vs), 1227 (vs), 1157 (w), 1137 (m), 1119 (w), 1078 (w), 1045 (w), 1028 (m), 1001 (w), 976 (w), 943 (w), 907 (m), 899 (m), 875 (m), 864 (w), 832 (m), 813 (s), 771 (s), 754 (vs), 742 (vs), 713 (m), 680 (s), 611 (m), 591 (m), 571 (w), 565 (m), 535 (s), 510 (vs), 492 (vs), 436 (vs), 399 (w), 395 (w), 387 (w) cm$^{-1}$.

**HRMS (EI):** *m/z* calcd. for C$_{11}$H$_{10}$N$_2$O$_3$ [M], 218.0686; found, 218.0687.

*2,3-Dihydropyrazino[1,2-a]indole-1,4-dione (**45**)*
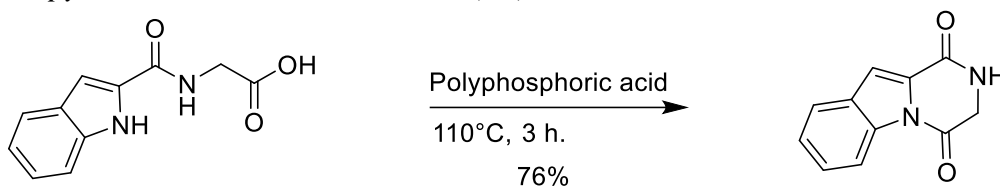


2-(1*H*-Indole-2-carbonylamino)acetic acid (**55**) (6.40 g, 29.3 mmol, 1.00 equiv.) in polyphosphoric acid (265 g, 1.49 mol, 50.8 equiv.) was stirred at 110 °C for 3 hours. The reaction was quenched carefully by adding an ice/water mixture and subsequently extracted with ethyl acetate. The combined organic layers were dried over Na$_2$SO$_4$ and concentrated *in vacuo* to yield 2,3-dihydropyrazino[1,2-a]indole-1,4-dione (**45**) (4.47 g, 22.4 mmol, 76%) as a brown solid.

**$^1$H NMR (400 MHz, DMSO-$d_6$):** $\delta$ = 8.49 (s, 1H), 8.37 (dd, *J* = 8.3, 1.0 Hz, 1H), 7.80 (d, *J* = 7.9 Hz, 1H), 7.52 (ddd, *J* = 8.5, 7.3, 1.4 Hz, 1H), 7.41 (td, *J* = 7.6, 1.2 Hz, 1H), 7.36 (s, 1H), 4.42 (d, *J* = 2.1 Hz, 2H) ppm.

**¹³C NMR (101 MHz, DMSO-*d₆*):** $\delta$ = 163.5, 156.4, 134.2, 129.9, 128.5, 127.2, 124.8, 122.5, 115.7, 111.8, 46.7 ppm.

**IR (ATR):** $\nu$ = 3390 (vw), 3367 (vw), 3350 (vw), 3322 (vw), 3308 (vw), 3291 (vw), 3284 (vw), 3275 (vw), 3267 (vw), 3254 (vw), 3245 (vw), 3170 (w), 3129 (w), 3102 (w), 3041 (w), 3034 (w), 2952 (w), 2911 (w), 2873 (w), 2825 (w), 2751 (vw), 2738 (vw), 1703 (vs), 1672 (vs), 1605 (m), 1592 (vs), 1574 (s), 1499 (w), 1477 (w), 1434 (vs), 1417 (s), 1380 (vs), 1356 (s), 1332 (vs), 1309 (m), 1298 (m), 1259 (w), 1241 (w), 1203 (m), 1187 (w), 1153 (m), 1132 (s), 1109 (m), 1079 (s), 1037 (m), 1010 (w), 986 (w), 953 (w), 919 (w), 898 (w), 867 (w), 841 (s), 823 (s), 752 (vs), 731 (vs), 693 (m), 653 (m), 623 (w), 609 (w), 595 (w), 571 (m), 538 (vs), 484 (s), 469 (vs), 433 (s), 412 (m), 398 (m) cm⁻¹.

**HRMS (EI):** *m*/*z* calcd. for $C_{11}H_8N_2O_2$ [M+H], 200.0580; found, 200.0580.

*2-Acetyl-2,3-dihydropyrazino[1,2-a]indole-1,4-dione (**39**)*
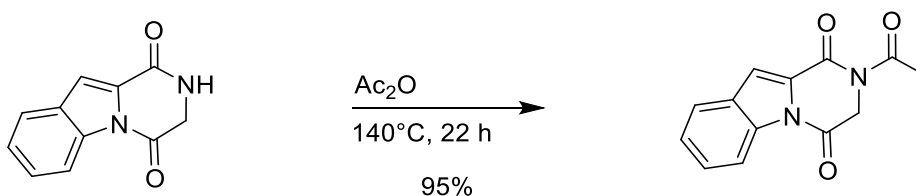


2,3-Dihydropyrazino[1,2-a]indole-1,4-dione (**45**) (2.00 g, 9.99 mmol, 1.00 equiv.) was dissolved in acetic anhydride (229 g, 212 mL, 2.24 mol, 224 equiv.) and stirred under reflux at 140 °C for 22 hours. The solvent was removed under reduced pressure and the product was washed with diethyl ether and filtered off to yield 2.30 g (9.50 mmol, 95%) of 2-acetyl-2,3-dihydropyrazino[1,2-*a*]indole-1,4-dione (**39**) as a beige solid.

**¹H NMR (400 MHz, DMSO-*d₆*):** $\delta$ = 8.35 (d, *J* = 8.3 Hz, 1H), 7.87 (dt, *J* = 7.9, 1.0 Hz, 1H), 7.70 (s, 1H), 7.60 (ddd, *J* = 8.4, 7.2, 1.3 Hz, 1H), 7.46 (td, *J* = 7.6, 7.2, 1.1 Hz, 1H), 4.69 (s, 3H), 2.58 (s, 3H) ppm.

**¹³C NMR (101 MHz, DMSO-*d₆*):** $\delta$ = 171.7, 162.1, 156.9, 134.2, 129.2, 128.7, 128.4, 125.2, 123.1, 115.7, 115.6, 48.9, 27.2 ppm.

**IR (ATR):** $\nu$ = 1720 (vs), 1696 (vs), 1679 (vs), 1606 (w), 1557 (s), 1436 (s), 1404 (vs), 1370 (s), 1360 (vs), 1336 (vs), 1266 (vs), 1234 (s), 1210 (vs), 1160 (s), 1139 (s), 1115 (m), 1099 (s), 1069 (m), 1044 (m), 1010 (m), 979 (m), 967 (s), 948 (m), 878 (m), 853 (s), 839 (m), 800 (w), 755 (vs), 739 (vs), 694 (m), 670 (m), 642 (w), 618 (m), 602 (m), 585 (m), 575 (m), 550 (m), 537 (s), 499 (w), 484 (w), 448 (w), 432 (s), 407 (w), 388 (w), 375 (m) cm⁻¹.

**HRMS (EI):** *m*/*z* calcd. for $C_{13}H_{10}N_2O_3$ [M+H], 242.0686; found, 242.0687.

**UV/Vis (MeCN):** $\lambda_{max}$ = 211, 235, 299 nm.

### 5.6.2 Synthesis of 'Locked' Derivatives



**40**: 61%  **46**: 64%  **57**: 66%  **48**: 55%  **47**: 63%  **49**: 31%  **50**: 42%

**51**: 81%  **52**: 70%  **53**: 53%  **54**: 62%  **55**: 89% from Boc deprotection
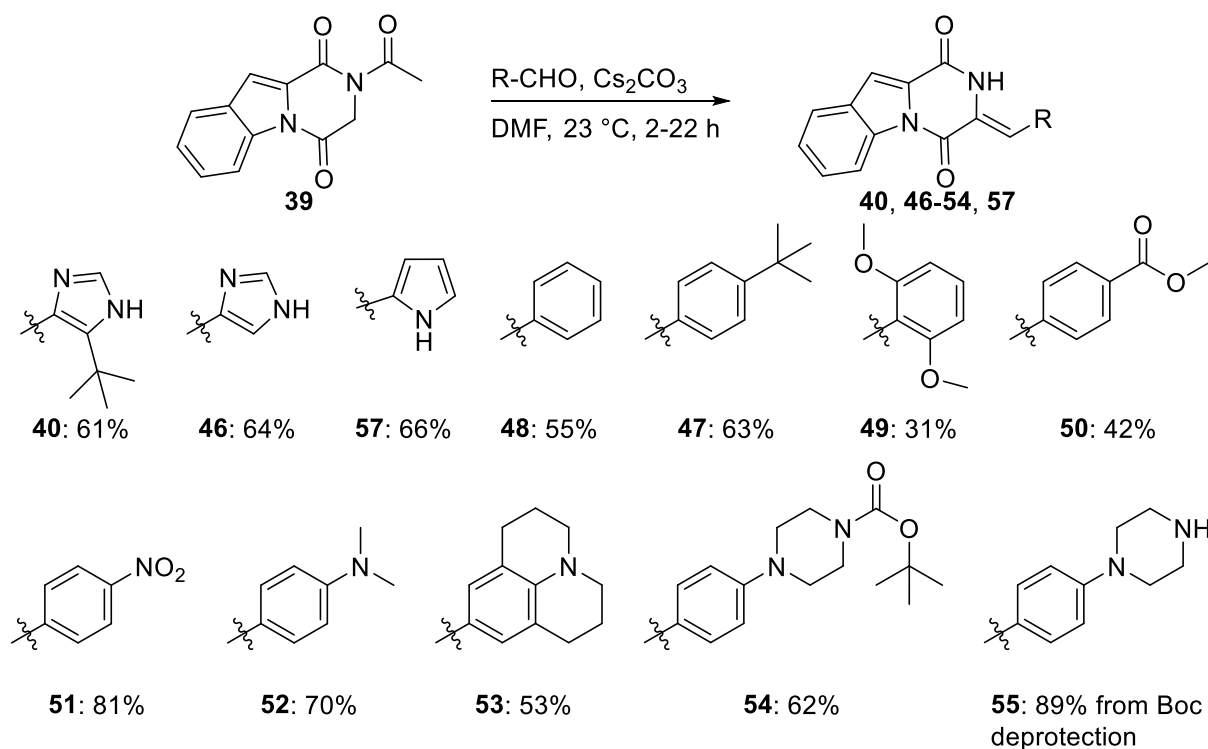
The respective aldehydes (1.00 equiv.) were dissolved in dry DMF (2.0 mL/1 mmol aldehyde) under argon atmosphere. Diketopiperazine **39** (1.00 equiv.) and $Cs_2CO_3$ (2.00 equiv.) were added and the mixture was stirred for 2-22 hours under argon atmosphere at room temperature. The reaction mixture was poured on an ice water/brine mix (30 mL) and the precipitate was filtered off and dried. Usually, 200 – 250 mg of the starting material diketopiperazine **39** were applied.

Compounds **48**, **50**-**52** were synthesized under my supervision by Rabia Elbuga-Ilica during an internship and compound **53** was synthesized by my colleague Peter Gödtel, who provided me with the corresponding NMR, IR and mass spectra.

*(Z)-3-((5-(tert-Butyl)-1H-imidazol-4-yl)methylene)-2,3-dihydropyrazino[1,2-a]indole-1,4-dione (40)*
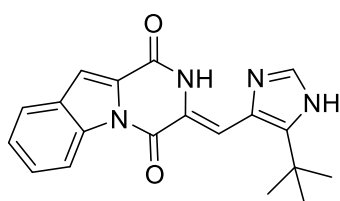


The crude product was purified *via* HPLC (gradient of 40-80% MeCN in $H_2O$ within 40 min, 0.1% TFA (v/v) in the solvents) and washed with sat. aq. solution of $NaHCO_3$. (*Z*)-3-((5-(*tert*-Butyl)-

1*H*-imidazol-4-yl)methylene)-2,3-dihydropyrazino[1,2-a]indole-1,4-dione (**40**) (210 mg, 628 µmol, 61% yield) was obtained as a yellow solid.

**¹H NMR (400 MHz, DMSO-*d*₆):** $\delta$ = 12.49 (s, 1H), 12.40 (s, 1H), 8.51 (dd, $J$ = 8.3, 0.9 Hz, 1H), 7.94 (d, $J$ = 0.8 Hz, 1H), 7.85 (dt, $J$ = 7.9, 1.1 Hz, 1H), 7.56 (ddd, $J$ = 8.4, 7.3, 1.3 Hz, 1H), 7.51 (d, $J$ = 0.9 Hz, 1H), 7.43 (ddd, $J$ = 8.1, 7.1, 1.1 Hz, 1H), 7.27 (d, $J$ = 0.8 Hz, 1H), 1.44 (s, 9H) ppm.

**¹³C NMR (101 MHz, DMSO-*d*₆):** $\delta$ = 156.3, 153.5, 142.3, 135.1, 135.0, 130.8, 128.9, 128.5, 127.4, 124.9, 124.0, 122.9, 116.2, 112.2, 109.2, 32.2, 30.7 ppm.

**IR (ATR):** $v$ = 3207 (s), 3084 (m), 3053 (m), 3029 (m), 2955 (m), 2925 (m), 2904 (m), 2868 (m), 2803 (w), 1693 (vs), 1657 (vs), 1606 (vs), 1582 (s), 1568 (s), 1502 (s), 1475 (w), 1453 (s), 1442 (vs), 1404 (vs), 1395 (vs), 1373 (vs), 1366 (vs), 1349 (vs), 1336 (vs), 1295 (s), 1245 (s), 1197 (vs), 1183 (vs), 1135 (vs), 1099 (vs), 1055 (vs), 1030 (vs), 1004 (s), 949 (vs), 933 (s), 849 (vs), 834 (vs), 829 (vs), 815 (vs), 802 (vs), 744 (vs), 732 (vs), 725 (vs), 704 (vs), 666 (s), 652 (vs), 612 (s), 589 (vs), 582 (vs), 537 (vs), 513 (vs), 477 (vs), 458 (vs), 446 (vs), 429 (vs), 405 (s), 388 (s) cm$^{-1}$.

**HRMS (EI):** $m/z$ calcd. for $C_{19}H_{18}N_4O_2$ [M], 334.1424; found, 334.1424.

**UV/Vis (MeCN):** $\lambda_{max}$ = 209, 263, 271, 389 nm.

**Fluorescence (MeCN):** $\lambda_{em}$= 470 nm (excited with $\lambda$ = 380 nm).

**$\Phi_F$ (MeCN):** 0.242.

**$\Phi_F$ (DMSO):** 0.233.

**$\Phi_F$ (DMSO/ascorbic acid):** 0.388.

*(Z)-3-((1H-Imidazol-4-yl)methylene)-2,3-dihydropyrazino[1,2-a]indole-1,4-dione (46)*
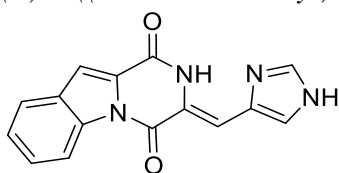


The crude product was purified *via* HPLC (gradient of 40-80% MeCN in H₂O within 40 min, 0.1% TFA (v/v) in the solvents) and washed with sat. aq. solution of NaHCO₃. The target compound was isolated as a yellow solid in 64% yield.

**¹H NMR (400 MHz, DMSO-*d*₆):** $\delta$ = 8.54 (d, $J$ = 8.3 Hz, 1H), 7.84 (d, $J$ = 7.3 Hz, 2H), 7.61 (s, 1H), 7.53 (t, $J$ = 7.1 Hz, 1H), 7.46 (s, 1H), 7.42 (t, $J$ = 7.3 Hz, 1H), 7.10 (s, 1H) ppm.

**¹³C NMR (101 MHz, DMSO-*d*₆):** $\delta$ = 156.9, 153.9, 141.5, 141.4, 136.7, 135.5, 129.8, 128.9, 127.5, 125.1, 123.2, 122.8, 116.8, 111.9, 49.1 ppm.

**HRMS (EI):** $m/z$ calcd. for $C_{15}H_{10}N_4O_2$ [M], 278.0798; found, 278.0797.

**UV/Vis (MeCN):** $\lambda_{max}$ = 378 nm.

**Fluorescence (DMSO):** $\lambda_{em}$= 473 nm (excited with $\lambda$ = 380 nm).

$\Phi_F$ **(DMSO):** 0.347.

*(Z)-3-((1H-Pyrrol-2-yl)methylene)-2,3-dihydropyrazino[1,2-a]indole-1,4-dione (**57**)*
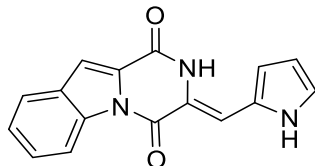


The crude product was purified *via* HPLC (gradient of 40-80% MeCN in $H_2O$ within 40 min, 0.1% TFA (v/v) in the solvents) and washed with sat. aq. solution of $NaHCO_3$. The target compound was isolated as a yellow solid in 66% yield.

**¹H NMR (400 MHz, DMSO-$d_6$):** $\delta$ = 11.49 (s, 1H), 9.98 (s, 1H), 8.52 (d, *J* = 8.3 Hz, 1H), 7.84 (d, *J* = 7.8 Hz, 1H), 7.55 (ddd, *J* = 8.5, 7.2, 1.3 Hz, 1H), 7.49 (s, 1H), 7.43 (t, *J* = 7.2 Hz, 1H), 7.20 (s, 1H), 7.13 (d, *J* = 1.6 Hz, 0H), 6.97 (d, J = 3.8 Hz, 1H), 6.30 (t, *J* = 3.0 Hz, 1H) ppm.

**¹³C NMR (101 MHz, DMSO-$d_6$):** $\delta$ = 156.9, 154.6, 135.0, 129.0, 128.5, 127.1, 126.2, 124.8, 123.1, 122.8, 120.8, 116.3, 114.4, 111.7, 111.2, 111.0 ppm.

**IR (ATR):** $v$ = 3330 (m), 3293 (m), 3142 (m), 1664 (vs), 1645 (s), 1605 (s), 1594 (vs), 1581 (s), 1565 (s), 1476 (w), 1442 (s), 1391 (vs), 1375 (vs), 1351 (vs), 1333 (vs), 1264 (s), 1227 (m), 1196 (s), 1145 (m), 1129 (vs), 1103 (s), 1069 (m), 1047 (m), 1027 (vs), 1004 (m), 967 (m), 938 (m), 901 (w), 878 (s), 858 (w), 829 (m), 816 (s), 799 (m), 734 (vs), 700 (vs), 677 (vs), 647 (s), 629 (s), 612 (m), 591 (vs), 569 (vs), 517 (m), 503 (m), 470 (m), 428 (s) $cm^{-1}$.

**HRMS (EI):** *m/z* calcd. for $C_{16}H_{11}N_3O_2$ [M], 277.0846; found, 277.0844.

**UV/Vis (MeCN):** $\lambda_{max}$ = 196, 215, 265, 273, 395, 404 nm.

*(Z)-3-Benzylidene-2,3-dihydropyrazino[1,2-a]indole-1,4-dione (**48**)*
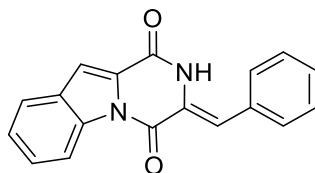


The residual solid was purified by recrystallization from toluene and the target compound was isolated as a pale-yellow solid in 55% yield.

**¹H NMR (400 MHz, DMSO-$d_6$):** $\delta$ = 10.45 (s, 1H), 8.50 (d, *J* = 8.4 Hz, 1H), 7.86 (d, *J* = 7.9 Hz, 1H), 7.66 (d, *J* = 7.6 Hz, 2H), 7.58 (t, *J* = 7.8 Hz, 1H), 7.53 (s, 1H), 7.46 (m, 3H), 7.38 (t, *J* = 7.4 Hz, 1H), 7.16 (s, 1H) ppm.

**IR (ATR):** $v$ = 3162 (w), 3123 (w), 3114 (w), 3097 (w), 3081 (w), 3051 (w), 3027 (w), 3014 (w), 1697 (w), 1673 (vs), 1612 (s), 1588 (s), 1572 (m), 1453 (w), 1445 (m), 1404 (vs), 1381 (vs), 1358 (vs), 1336 (vs), 1313 (s), 1296 (m), 1247 (m), 1221 (m), 1197 (s), 1184 (m), 1162 (w), 1145 (w), 1111 (w), 1099 (w), 1030 (s), 1006 (w), 997 (w), 925 (w), 884 (w), 854 (w), 813 (s), 762 (s), 747 (vs), 721 (s), 688 (vs), 662 (m), 616 (w), 595 (w), 579 (m), 543 (vs), 482 (s), 462 (s), 429 (m), 411 (w) cm$^{-1}$.

**HRMS (EI):** $m/z$ calcd. for $C_{18}H_{12}N_2O_2$ [M], 288.0893; found, 288.0894.

**UV/Vis (DMSO):** $\lambda_{max}$ = 271, 362 nm.

**Fluorescence (MeCN):** $\lambda_{em}$= 454 nm (excited with $\lambda$ = 350 nm).

**Fluorescence (DMSO):** $\lambda_{em}$= 460 nm (excited with $\lambda$ = 350 nm).

*(Z)-3-(4-(tert-Butyl)benzylidene)-2,3-dihydropyrazino[1,2-a]indole-1,4-dione (**47**)*
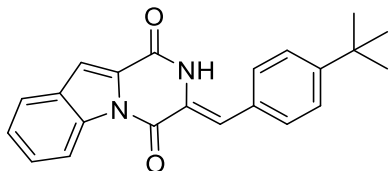


The crude residue was purified *via* column chromatography (toluene:acetone; 10:1 -> 9:1). The target compound was isolated as a pale-yellow solid in 63% yield.

**$^1$H NMR (400 MHz, DMSO-$d_6$):** $\delta$ = 9.55 (s, 1H), 7.68 (d, $J$ = 8.1 Hz, 1H), 7.05 (d, $J$ = 7.9 Hz, 1H), 6.81 – 6.74 (m, 3H), 6.73 – 6.66 (m, 3H), 6.64 (t, $J$ = 7.5 Hz, 1H), 6.33 (s, 1H), 0.50 (s, 9H) ppm.

**IR (ATR):** $v$ = 3150 (w), 3115 (w), 3050 (w), 3030 (w), 2959 (w), 2901 (w), 2868 (w), 1710 (w), 1660 (vs), 1623 (s), 1587 (m), 1570 (m), 1507 (w), 1475 (w), 1446 (w), 1400 (s), 1384 (vs), 1358 (vs), 1337 (s), 1313 (m), 1296 (m), 1269 (w), 1251 (m), 1225 (w), 1203 (m), 1160 (w), 1142 (m), 1111 (w), 1034 (m), 1018 (w), 1004 (w), 975 (w), 945 (w), 880 (w), 870 (w), 847 (w), 837 (w), 817 (s), 748 (vs), 728 (s), 696 (w), 677 (w), 654 (w), 635 (w), 611 (w), 582 (m), 560 (s), 517 (w), 493 (w), 477 (s), 432 (m), 416 (w), 407 (w), 380 (w) cm$^{-1}$.

**HRMS (EI):** $m/z$ calcd. for $C_{22}H_{21}N_2O_2$ [M+H], 345.1598; found, 345.1596.

**UV/Vis (MeCN):** $\lambda_{max}$ = 206, 268, 359, 361 nm.

**Fluorescence (DMSO):** $\lambda_{em}$= 461 nm (excited with $\lambda$ = 350 nm).

**$\Phi_F$ (DMSO):** 0.009.

*(Z)-3-(2,6-Dimethoxybenzylidene)-2,3-dihydropyrazino[1,2-a]indole-1,4-dione (**49**)*
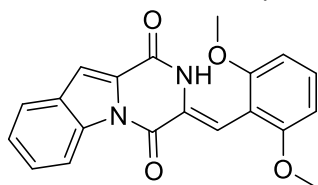


The residual solid was purified by recrystallization from acetone and the target compound was isolated as a yellow solid in 31% yield.

**¹H NMR (400 MHz, DMSO-$d_6$):** $\delta$ = 9.60 (s, 1H), 8.50 (d, $J$ = 8.3 Hz, 1H), 7.87 (d, $J$ = 7.9 Hz, 1H), 7.59 (ddd, $J$ = 8.4, 7.2, 1.4 Hz, 1H), 7.53 (s, 1H), 7.50 – 7.42 (m, 1H), 7.40 (t, $J$ = 8.4 Hz, 1H), 7.19 (s, 1H), 6.76 (d, $J$ = 8.5 Hz, 2H), 3.87 (s, 6H) ppm.

**¹³C NMR (101 MHz, DMSO-$d_6$):** $\delta$ = 158.3, 156.7, 154.1, 135.7, 131.7, 129.2, 129.1, 128.1, 127.3, 125.6, 123.5, 116.8, 113.4, 112.7, 110.5, 104.7, 56.4 ppm.

**IR (ATR):** $v$ = 3179 (w), 3099 (w), 3068 (w), 3055 (w), 3016 (w), 3002 (w), 2973 (w), 2945 (w), 2918 (w), 2836 (w), 1703 (w), 1663 (vs), 1630 (m), 1584 (s), 1570 (m), 1469 (m), 1445 (m), 1441 (m), 1426 (w), 1401 (m), 1381 (vs), 1357 (s), 1333 (s), 1315 (m), 1302 (m), 1276 (m), 1247 (vs), 1217 (s), 1194 (m), 1181 (m), 1171 (m), 1142 (m), 1103 (vs), 1098 (vs), 1030 (s), 1004 (m), 977 (m), 956 (w), 938 (w), 908 (w), 902 (w), 870 (w), 860 (w), 839 (m), 820 (m), 778 (s), 751 (vs), 742 (vs), 715 (vs), 697 (s), 659 (m), 622 (m), 606 (m), 572 (s), 543 (w), 524 (s), 507 (m), 487 (m), 459 (s), 426 (s), 409 (m), 398 (m), 390 (m), 377 (m) cm$^{-1}$.

**HRMS (EI):** $m/z$ calcd. for $C_{20}H_{17}N_2O_4$ [M+H], 349.1183; found, 349.1181.

**UV/Vis (MeCN):** $\lambda_{max}$ = 211, 269, 361, 365 nm.

**Fluorescence (MeCN):** $\lambda_{em}$= 456 nm (excited with $\lambda$ = 380 nm).

**$\Phi_F$ (MeCN):** 0.007.

**$\Phi_F$ (DMSO):** 0.006.

*Methyl (Z)-4-((1,4-dioxo-1,2-dihydropyrazino[1,2-a]indol-3(4H)-ylidene)methyl)benzoate (**50**)*
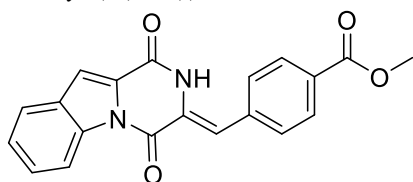


The residual solid was purified by recrystallization from toluene and the target compound was isolated as a yellow solid in 42% yield.

**¹H NMR (400 MHz, DMSO-$d_6$):** $\delta$ = 10.71 (s, 1H), 8.45 (d, $J$ = 8.6 Hz, 1H), 8.15 (d, $J$ = 8.6 Hz, 2H), 7.92 (d, $J$ = 8.3 Hz, 2H), 7.77 (d, $J$ = 8.3 Hz, 1H), 7.47 (t, $J$ = 7.8 Hz, 1H), 7.37 (t, $J$ = 7.3 Hz, 1H), 7.17 (s, 1H), 6.88 (s, 1H), 3.86 (s, 3H) ppm.

**IR (ATR):** $\nu$ = 3220 (w), 3112 (w), 3064 (w), 3034 (w), 3016 (w), 2953 (w), 2936 (w), 2844 (w), 1731 (vs), 1698 (m), 1673 (vs), 1618 (s), 1584 (m), 1568 (m), 1446 (m), 1434 (m), 1402 (vs), 1357 (s), 1339 (s), 1313 (m), 1285 (vs), 1251 (s), 1222 (m), 1188 (s), 1143 (m), 1112 (vs), 1071 (w), 1044 (m), 1021 (s), 1004 (m), 982 (w), 963 (m), 938 (w), 929 (w), 905 (w), 891 (m), 882 (m), 867 (m), 844 (m), 826 (w), 813 (m), 766 (vs), 748 (vs), 739 (vs), 708 (w), 691 (vs), 666 (m), 640 (w), 626 (w), 611 (w), 578 (w), 568 (w), 543 (m), 527 (w), 487 (m), 477 (m), 462 (m), 446 (m), 429 (m), 408 (w), 382 (w) cm$^{-1}$.

**HRMS (EI):** $m/z$ calcd. for $C_{20}H_{14}N_2O_4$ [M], 346.0948; found, 346.0947.

**UV/Vis (MeCN):** $\lambda_{max}$ = 269, 357 nm.

**UV/Vis (DMSO):** $\lambda_{max}$ = 273, 370 nm.

**Fluorescence (MeCN):** $\lambda_{em}$= 488 nm (excited with $\lambda$ = 350 nm).

**Fluorescence (DMSO):** $\lambda_{em}$= 487 nm (excited with $\lambda$ = 380 nm).

*(Z)-3-(4-Nitrobenzylidene)-2,3-dihydropyrazino[1,2-a]indole-1,4-dione (**51**)*
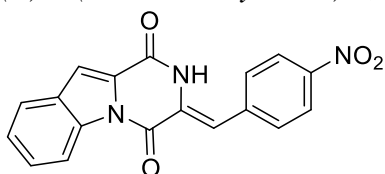


The residual solid was purified by recrystallization from acetone and the target compound was isolated as a yellow solid in 81% yield.

**$^1$H NMR (400 MHz, DMSO-$d_6$):** $\delta$ = 10.99 (s, 1H), 8.46 (d, $J$ = 8.1 Hz, 1H), 8.24 (d, $J$ = 8.9 Hz, 2H), 8.05 (d, $J$ = 8.9 Hz, 2H), 7.83 (d, $J$ = 7.9 Hz, 1H), 7.55 (t, $J$ = 7.6 Hz, 1H), 7.43 (t, $J$ = 7.4 Hz, 1H), 7.40 (s, 1H), 7.06 (s, 1H) ppm.

**IR (ATR):** $\nu$ = 3228 (w), 3101 (w), 3058 (w), 1694 (m), 1670 (vs), 1616 (s), 1595 (w), 1587 (m), 1568 (m), 1520 (vs), 1493 (w), 1448 (m), 1402 (vs), 1357 (m), 1341 (vs), 1292 (m), 1247 (s), 1222 (m), 1200 (m), 1186 (w), 1146 (w), 1106 (w), 1028 (w), 1014 (w), 1006 (w), 945 (w), 904 (vw), 891 (w), 870 (w), 844 (s), 816 (w), 764 (s), 749 (vs), 730 (m), 687 (s), 667 (w), 640 (w), 611 (w), 578 (w), 569 (w), 544 (w), 476 (w), 462 (w), 429 (w), 411 (w) cm$^{-1}$.

**HRMS (EI):** $m/z$ calcd. for $C_{18}H_{11}N_3O_4$ [M], 333.0744; found, 333.0745.

**UV/Vis (MeCN):** $\lambda_{max}$ = 268, 369 nm.

**UV/Vis (DMSO):** $\lambda_{max}$ = 277, 386 nm.

**Fluorescence (MeCN):** $\lambda_{em}$= 515 nm (excited with $\lambda$ = 380 nm).

**Fluorescence (DMSO):** $\lambda_{em}$= 525 nm (excited with $\lambda$ = 380 nm).

*(Z)-3-(4-(Dimethylamino)benzylidene)-2,3-dihydropyrazino[1,2-a]indole-1,4-dione (**52**)*
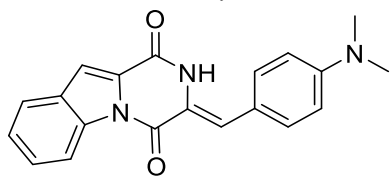


The residual solid was purified by recrystallization from toluene and the target compound was isolated as a yellow solid in 70% yield.

**$^1$H NMR (400 MHz, DMSO-$d_6$):** $\delta$ = 10.18 (s, 1H), 8.52 (dd, $J$ = 8.3, 0.9 Hz, 1H), 7.86 (d, $J$ = 7.8 Hz, 1H), 7.57 (m, 3H), 7.51 (s, 1H), 7.47 – 7.42 (m, 1H), 7.14 (s, 1H), 6.79 (d, $J$ = 9.0 Hz, 2H), 3.01 (s, 6H) ppm.

**$^1$H NMR (400 MHz, CDCl$_3$):** $\delta$ = 8.66 (dd, $J$ = 8.4, 0.9 Hz, 1H), 8.22 (s, 1H), 7.77 (d, $J$ = 8.0 Hz, 1H), 7.60 – 7.52 (m, 2H), 7.47 – 7.39 (m, 3H), 7.32 (s, 1H), 6.76 (d, $J$ = 9.0 Hz, 2H), 3.06 (s, 6H).

**$^{13}$C NMR (101 MHz, CDCl$_3$):** $\delta$ = 156.4, 154.8, 150.9, 136.0, 130.7, 128.7, 128.0, 127.8, 125.2, 123.0, 122.8, 121.6, 120.2, 117.2, 114.0, 112.5, 40.1 ppm.

**IR (ATR):** $v$ = 3225 (w), 3109 (w), 3054 (w), 2895 (w), 2854 (w), 2803 (w), 1694 (w), 1666 (vs), 1611 (m), 1584 (vs), 1524 (s), 1477 (w), 1442 (s), 1422 (w), 1401 (vs), 1363 (vs), 1334 (vs), 1261 (s), 1231 (s), 1213 (m), 1188 (vs), 1171 (vs), 1160 (s), 1143 (s), 1119 (m), 1065 (m), 1028 (vs), 1003 (m), 945 (m), 936 (m), 902 (w), 890 (m), 857 (w), 827 (m), 809 (vs), 769 (s), 756 (m), 744 (vs), 731 (vs), 705 (s), 632 (m), 609 (m), 577 (m), 544 (s), 521 (s), 507 (s), 496 (s), 477 (m), 469 (s), 428 (s), 418 (m) cm$^{-1}$.

**HRMS (EI):** $m/z$ calcd. for C$_{20}$H$_{17}$N$_3$O$_2$ [M], 331.1315; found, 331.1317.

**UV/Vis (DMSO):** $\lambda_{max}$ = 269, 275, 444 nm.

**Fluorescence (MeCN):** $\lambda_{em}$= 558 nm (excited with $\lambda$ = 410 nm).

**Fluorescence (DMSO):** $\lambda_{em}$= 568 nm (excited with $\lambda$ = 410 nm).


*(Z)-3-((2,3,6,7-Tetrahydro-1H,5H-pyrido[3,2,1-ij]quinolin-9-yl)methylene)-2,3-dihydropyrazino-[1,2-a]indole-1,4-dione (**53**)*
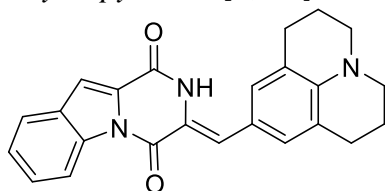


The residual solid was washed with diethyl ether and the target compound was isolated as a yellow solid in 53% yield.

**¹H NMR (400 MHz, CDCl₃):** $\delta$ = 8.66 (dd, $J$ = 8.4, 1.0 Hz, 1H), 8.25 (s, 1H), 7.76 (dt, $J$ = 7.9, 1.1 Hz, 1H), 7.59 – 7.52 (m, 1H), 7.52 (s, 1H), 7.41 (ddd, $J$ = 8.3, 7.3, 1.1 Hz, 1H), 7.23 (s, 1H), 6.97 (s, 2H), 3.26 (dd, $J$ = 6.7, 4.8 Hz, 4H), 2.77 (t, $J$ = 6.4 Hz, 4H), 2.04 – 1.93 (m, 4H) ppm.

**¹³C NMR (101 MHz, CDCl₃):** $\delta$ = 156.6, 154.9, 144.3, 136.1, 128.8, 128.5, 128.0, 127.9, 125.2, 122.8, 122.6, 122.1, 121.9, 119.4, 117.3, 113.8, 50.0, 27.9, 21.6 ppm.

**IR (ATR):** $v$ = 3116 (s), 3020 (s), 3007 (s), 2936 (s), 2928 (s), 2849 (s), 2805 (s), 2660 (w), 2514 (w), 1756 (w), 1742 (w), 1662 (m), 1588 (m), 1520 (w), 1442 (m), 1390 (vs), 1383 (vs), 1336 (vs), 1310 (vs), 1279 (s), 1242 (s), 1208 (s), 1173 (s), 1160 (s), 1145 (s), 1103 (m), 1077 (m), 1051 (w), 1028 (m), 1006 (w), 983 (w), 935 (w), 904 (w), 860 (w), 820 (w), 789 (w), 745 (m), 735 (m), 703 (w), 635 (w), 612 (w) cm$^{-1}$.

**HRMS (FAB):** $m/z$ calcd. for C₂₄H₂₁N₃O₂ [M], 383.1628; found, 383.1630.

**UV/Vis (DMSO):** $\lambda_{max}$ = 269, 481 nm.

**Fluorescence (DMSO):** $\lambda_{em}$= 599 nm (excited with $\lambda$ = 430 nm).

**$\varPhi_F$ (DMSO):** 0.011.

**$\varPhi_F$ (CH₂Cl₂):** 0.007.

*tert-Butyl (Z)-4-(4-((1,4-dioxo-1,2-dihydropyrazino[1,2-a]indol-3(4H)-ylidene)methyl)phenyl)-piperazine-1-carboxylate (54)*
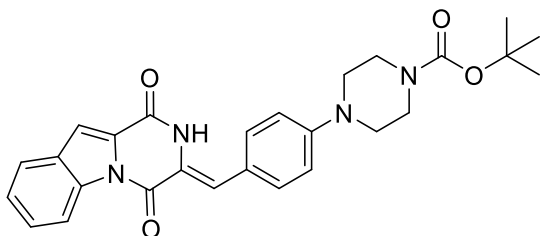


The crude residue was purified *via* column chromatography (CH₂Cl₂:ethyl acetate; 4:1 -> 3:2). The target compound was isolated as a orange solid in 62% yield.

**¹H NMR (400 MHz, CDCl₃):** $\delta$ = 8.64 (dt, $J$ = 8.4, 0.9 Hz, 1H), 8.19 (s, 1H), 7.76 (d, $J$ = 7.9 Hz, 1H), 7.61 – 7.52 (m, 2H), 7.47 – 7.38 (m, 3H), 7.30 (s, 1H), 6.96 (d, $J$ = 8.9 Hz, 2H), 3.60 (t, $J$ = 5.3 Hz, 4H), 3.28 (t, $J$ = 5.3 Hz, 4H), 1.50 (s, 9H) ppm.

**¹³C NMR (101 MHz, CDCl₃):** $\delta$ = 156.2, 154.9, 154.8, 151.5, 136.2, 130.6, 128.8, 128.3, 127.8, 125.5, 124.6, 123.5, 123.0, 120.6, 117.3, 116.0, 114.6, 80.3, 48.0, 28.6 ppm.

**IR (ATR):** $v$ = 3235 (w), 2970 (w), 2929 (w), 2905 (vw), 2868 (vw), 2851 (vw), 2829 (w), 1697 (s), 1662 (vs), 1592 (vs), 1519 (w), 1476 (w), 1462 (w), 1445 (w), 1402 (vs), 1380 (vs), 1366 (vs), 1357 (vs), 1337 (s), 1312 (w), 1290 (w), 1255 (m), 1238 (s), 1225 (vs), 1193 (vs), 1160 (vs), 1118 (s), 1082 (m), 1054 (m), 1028 (s), 1003 (m), 962 (w), 949 (w), 941 (w), 921 (m), 904 (w), 891 (w),

863 (w), 829 (m), 812 (m), 769 (s), 756 (w), 745 (vs), 731 (s), 708 (m), 662 (w), 633 (w), 609 (w), 602 (w), 568 (m), 545 (s), 509 (m), 497 (m), 469 (w), 453 (w), 428 (w), 385 (w) cm$^{-1}$.

**HRMS (EI):** $m/z$ calcd. for $C_{27}H_{28}N_4O_4$ [M], 472.2105; found, 472.2104.

**UV/Vis (MeCN):** $\lambda_{max}$ = 266, 272, 409, 411 nm.

**Fluorescence (DMSO):** $\lambda_{em}$= 561 nm (excited with $\lambda$ = 400 nm).

**$\Phi_F$ (MeCN):** 0.009.

*(Z)-3-(4-(Piperazin-1-yl)benzylidene)-2,3-dihydropyrazino[1,2-a]indole-1,4-dione (**55**)*
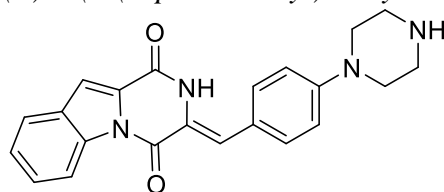


*tert*-Butyl (*Z*)-4-(4-((1,4-dioxo-1,2-dihydropyrazino[1,2-a]indol-3(4*H*)-ylidene)methyl)phenyl)-piperazine-1-carboxylate (**54**) (100 mg, 212 μmol, 1.00 equiv) was dissolved in 11 mL of a solution of 20% (v/v) TFA (3.26 g, 2.20 mL, 28.6 mmol, 135 equiv) and 80% dry dichloromethane (8.80 mL), containing 1% (v/v) TIPS (85.0 mg, 110 μL, 537 μmol, 2.54 equiv) at 0 °C (ice bath). Subsequently, the ice bath was removed and the solution was allowed to warm to ambient temperature. The reaction was monitored *via* TLC. After 2.5 hours the starting material had been consumed and toluene (50 mL) was added and the mixture was concentrated *in vacuo*. The TFA salt of the target compound was isolated as a yellow solid in 89% yield. A part of the compound was washed with sat. aq. solution of NaHCO$_3$ and extracted with ethyl acetate to obtain the neutralized compound.

**$^1$H NMR (400 MHz, DMSO-$d_6$):** $\delta$ = 8.52 (d, $J$ = 8.3 Hz, 1H), 7.86 (d, $J$ = 7.9 Hz, 1H), 7.57 (dd, $J$ = 8.4, 5.4 Hz, 3H), 7.52 (s, 1H), 7.45 (t, $J$ = 7.6 Hz, 1H), 7.12 (s, 1H), 7.00 (d, $J$ = 9.0 Hz, 2H), 3.26 – 3.17 (m, 4H), 2.89 – 2.81 (m, 4H) ppm.

**$^1$H NMR (400 MHz, acetic acid-$d_4$):** $\delta$ = 8.62 (d, $J$ = 8.4 Hz, 1H), 7.82 (d, $J$ = 7.9 Hz, 1H), 7.66 (s, 1H), 7.59 (m, 3H), 7.45 (t, $J$ = 7.6 Hz, 1H), 7.41 (s, 1H), 7.11 (d, $J$ = 8.9 Hz, 2H), 3.65 – 3.58 (m, 4H), 3.53 – 3.46 (m, 4H) ppm.

**IR (ATR):** $v$ = 3245 (w), 3054 (w), 2921 (w), 2850 (w), 1664 (vs), 1591 (vs), 1519 (s), 1469 (w), 1445 (s), 1400 (vs), 1381 (vs), 1341 (vs), 1273 (vs), 1256 (vs), 1239 (vs), 1224 (vs), 1193 (vs), 1142 (vs), 1098 (s), 1067 (m), 1048 (m), 1027 (vs), 1001 (s), 990 (s), 960 (m), 938 (m), 912 (s), 892 (m), 866 (m), 824 (s), 806 (vs), 768 (s), 745 (vs), 732 (vs), 720 (s), 710 (s), 662 (m), 649 (s), 636 (m), 623 (m), 609 (s), 602 (s), 567 (vs), 544 (vs), 523 (vs), 509 (vs), 496 (vs), 469 (s), 456 (s), 443 (m), 426 (vs), 416 (s), 401 (s), 387 (s) cm$^{-1}$.

**HRMS (EI):** *m/z* calcd. for $C_{22}H_{20}N_4O_2$ [M], 372.1581; found, 372.1579.

**UV/Vis (MeCN):** $\lambda_{max}$ = 265, 271, 397 nm.

**UV/Vis (DMSO):** $\lambda_{max}$ = 268, 274, 413 nm.

**Fluorescence (DMSO):** $\lambda_{em}$= 543 nm (excited with $\lambda$ = 400 nm).

***Φ*~F~ (DMSO):** 0.008.

### 5.6.3  NMR Spectra
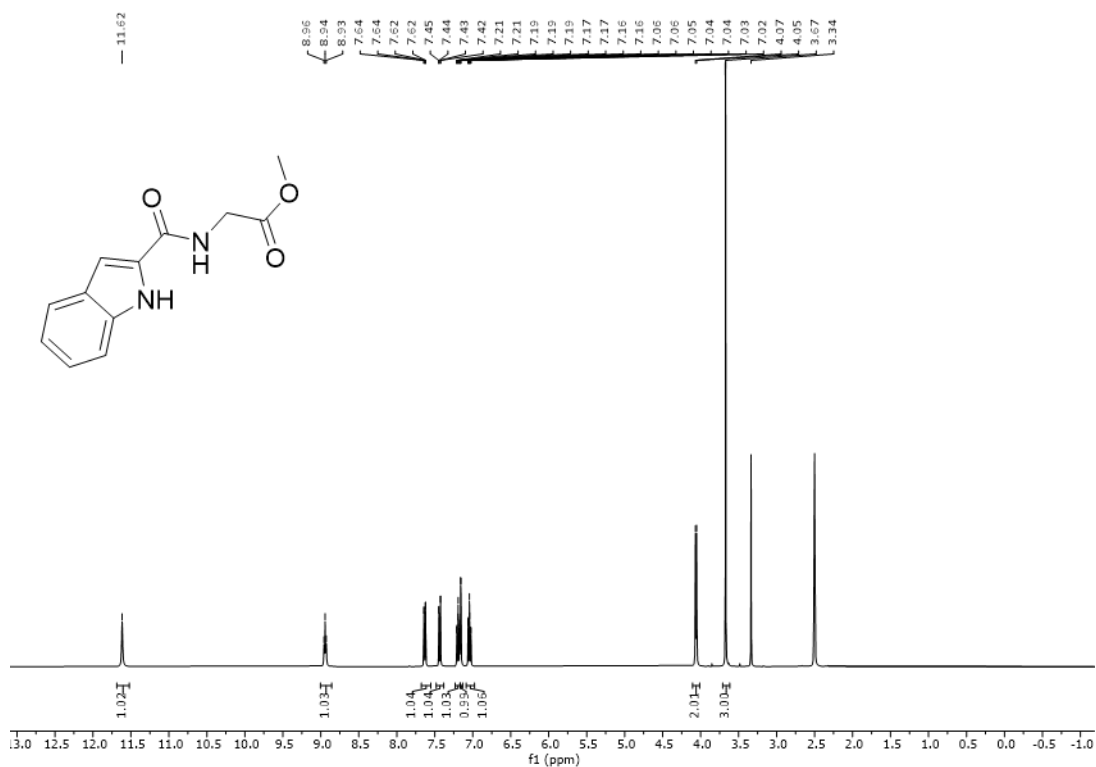


**Figure 273:** $^1$H NMR spectrum (400 MHz, DMSO-$d_6$) of compound *Z*-**43**.
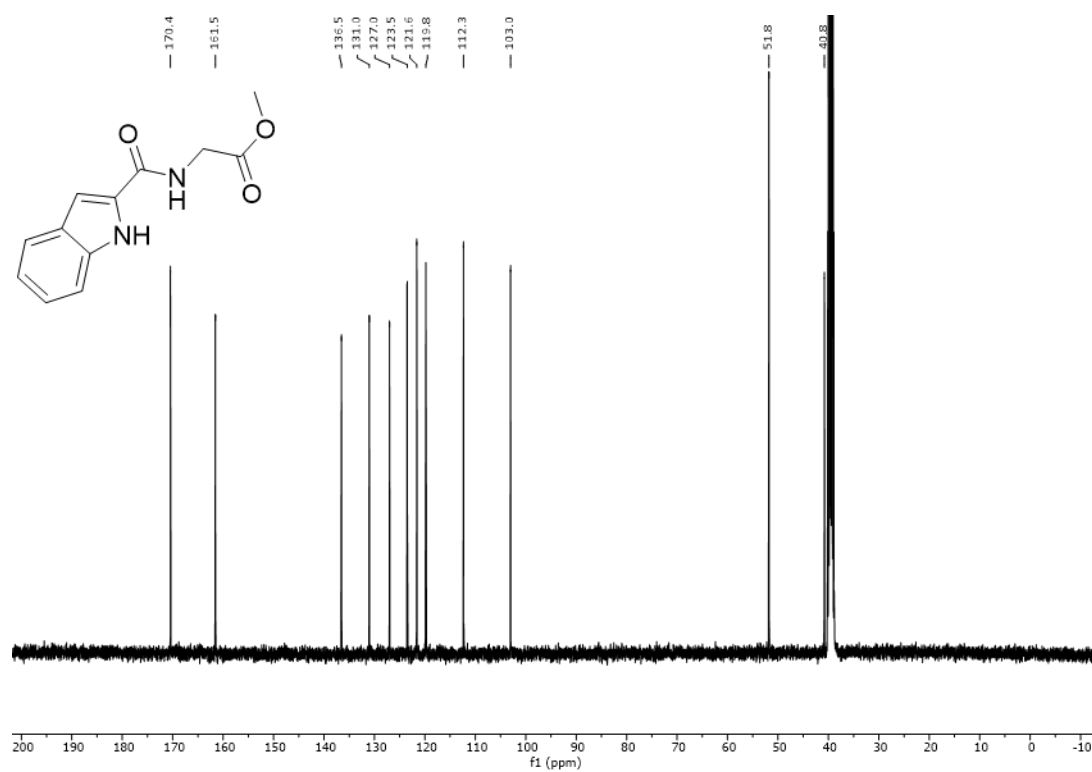
**Figure 274:** $^{13}$C NMR spectrum (101 MHz, DMSO-$d_6$) of compound Z-**43**.
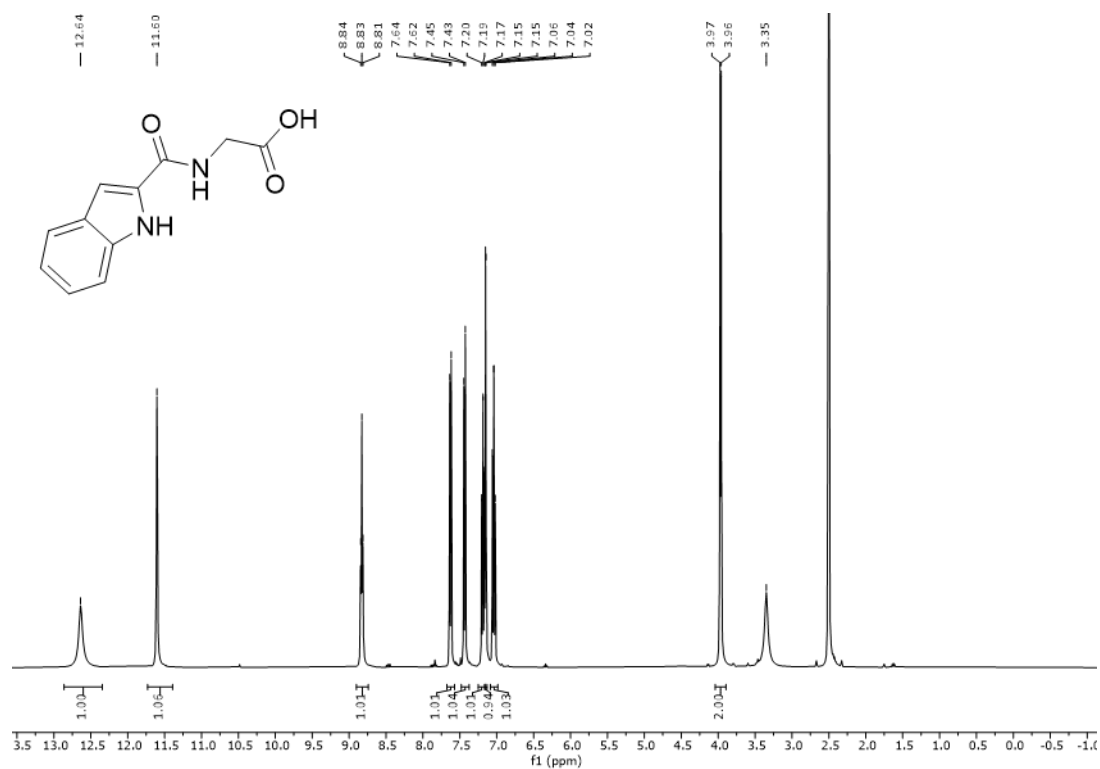


**Figure 275:** $^{1}$H NMR spectrum (400 MHz, DMSO-$d_6$) of compound Z-**44**.
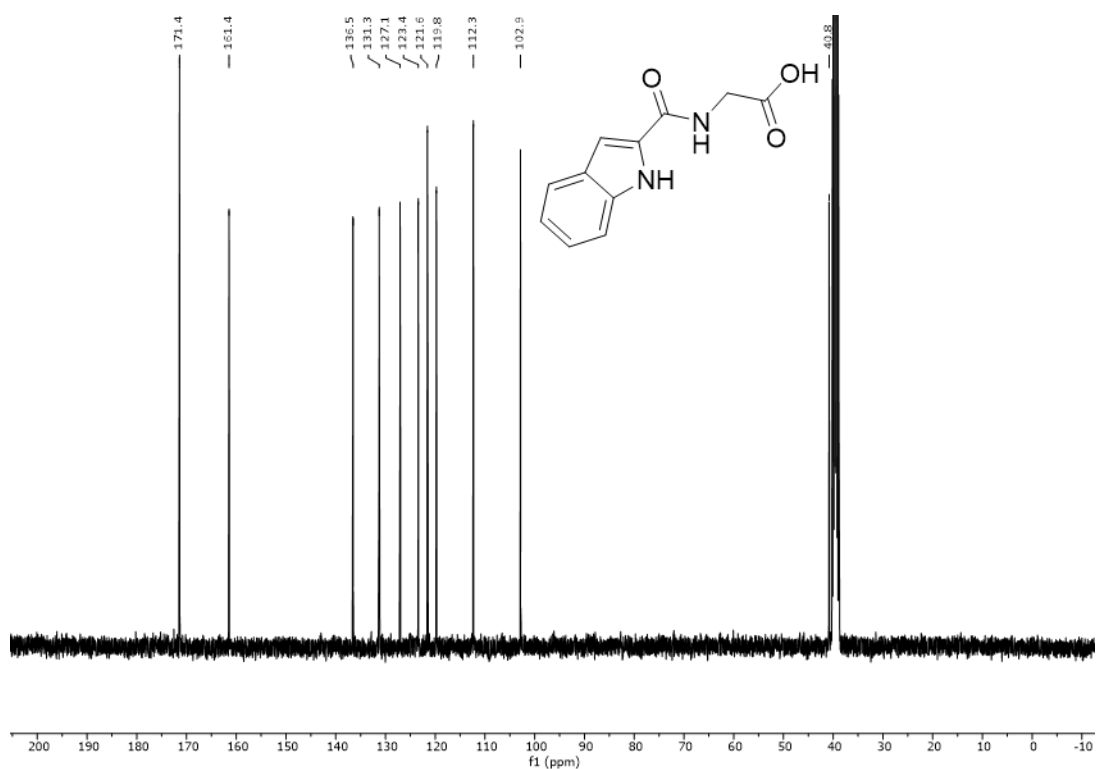
**Figure 276:** $^{13}$C NMR spectrum (101 MHz, DMSO-$d_6$) of compound Z-**44**.
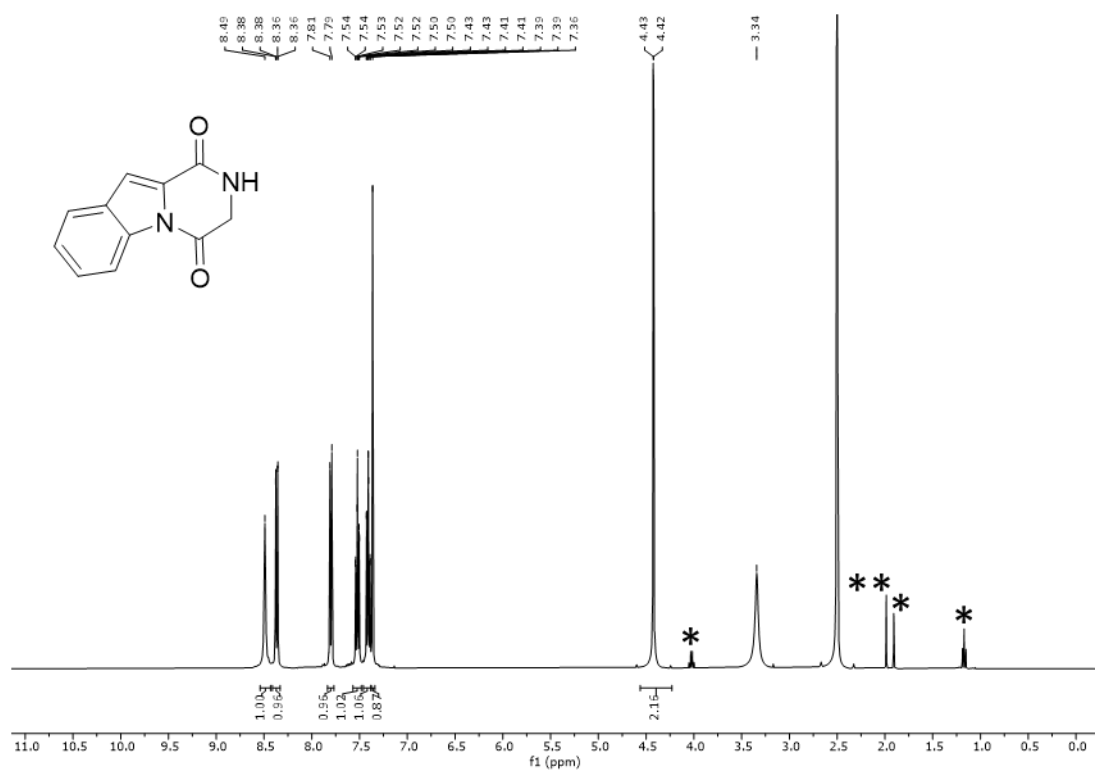


**Figure 277:** $^1$H NMR spectrum (400 MHz, DMSO-$d_6$) of compound Z-**45**. *ethyl acetate, **acetone.
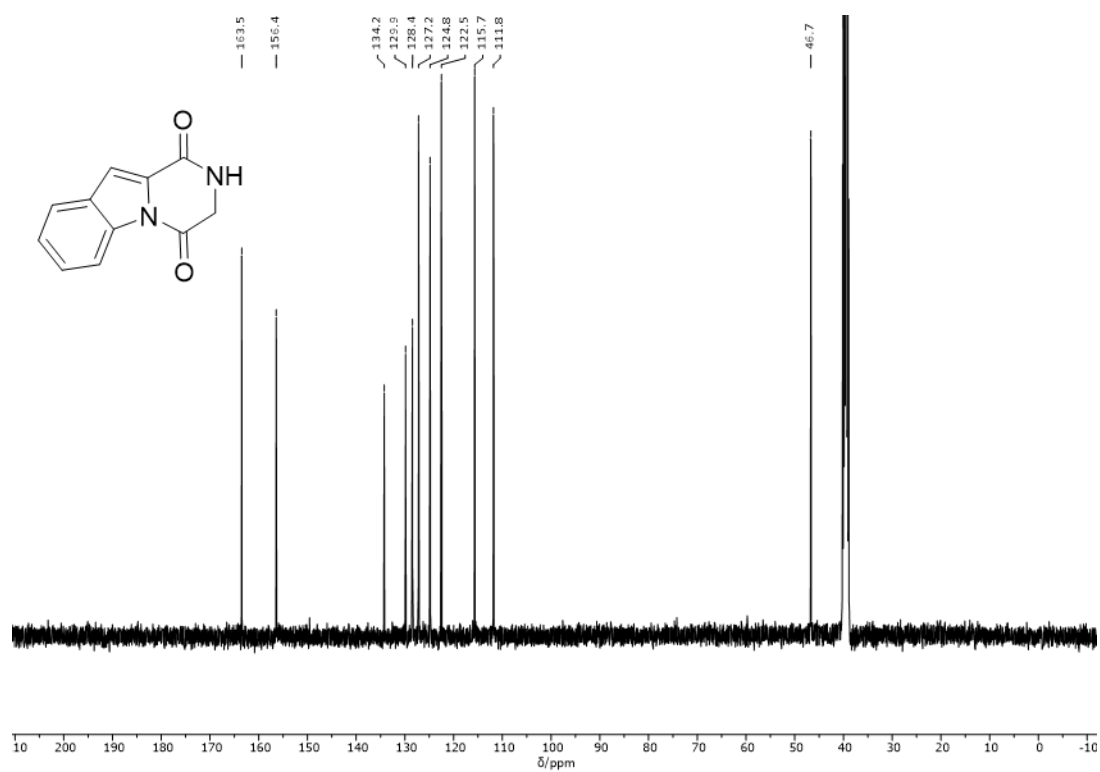
**Figure 278:** $^{13}$C NMR spectrum (101 MHz, DMSO-$d_6$) of compound Z-**45**.
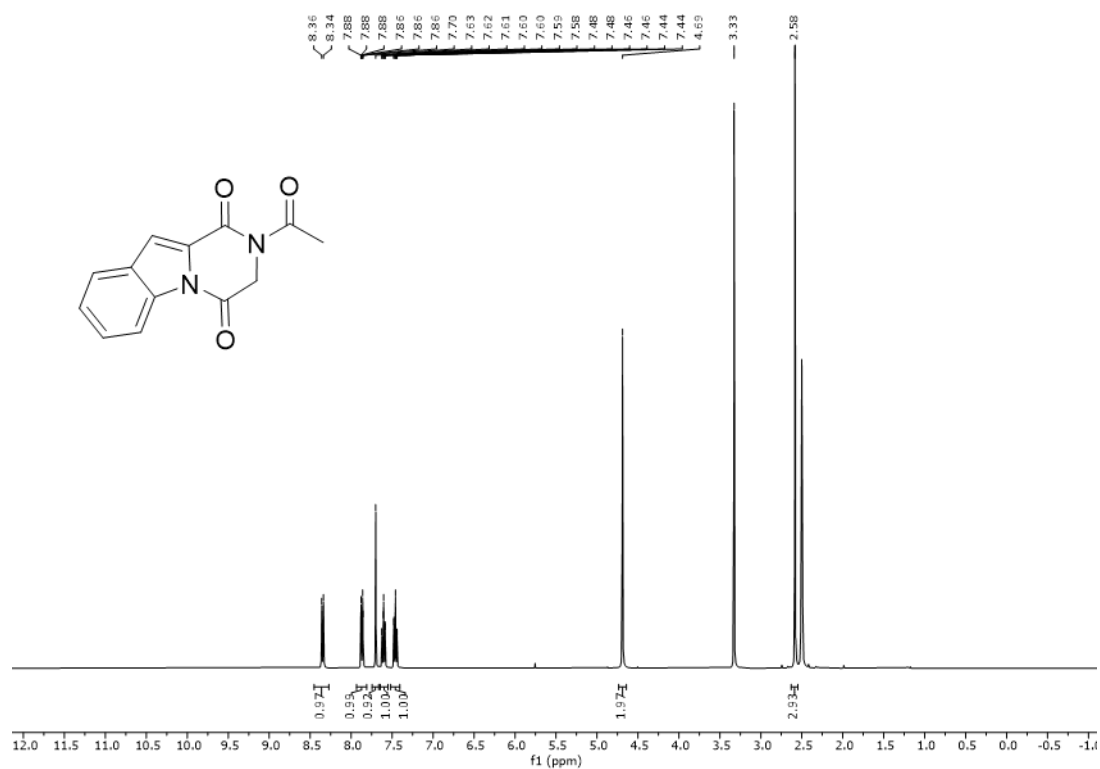


**Figure 279:** $^1$H NMR spectrum (400 MHz, DMSO-$d_6$) of compound Z-**39**.
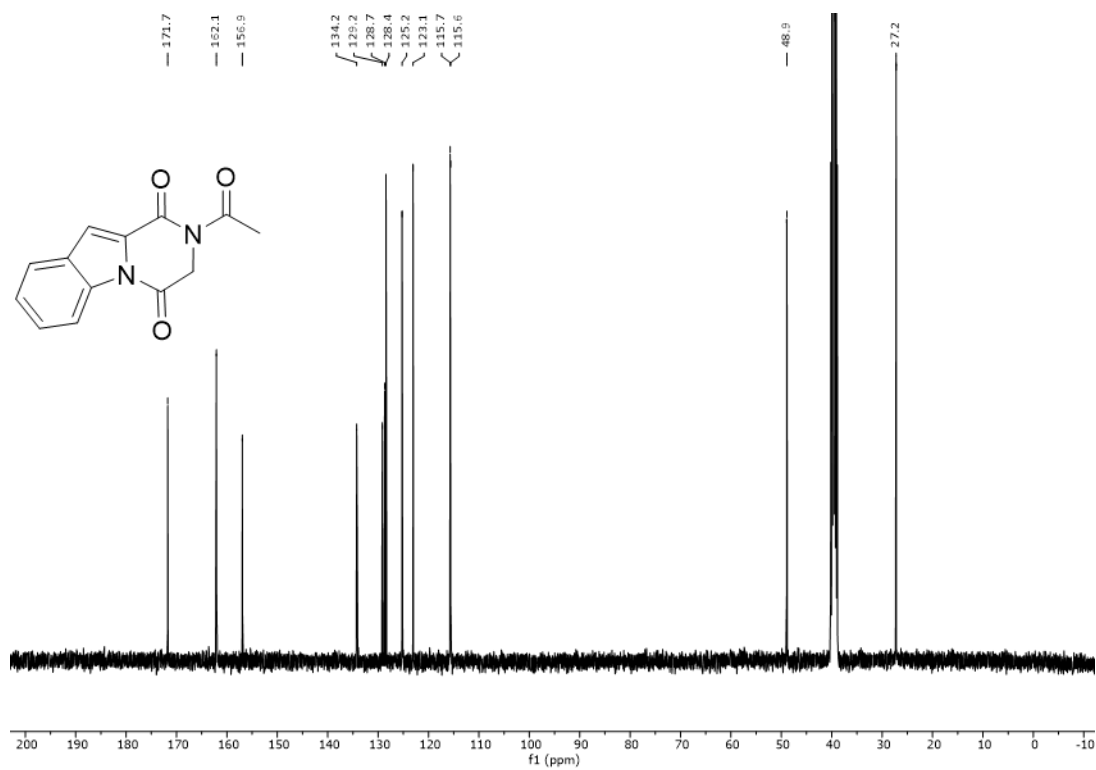
**Figure 280:** $^{13}$C NMR spectrum (101 MHz, DMSO-$d_6$) of compound Z-**39**.
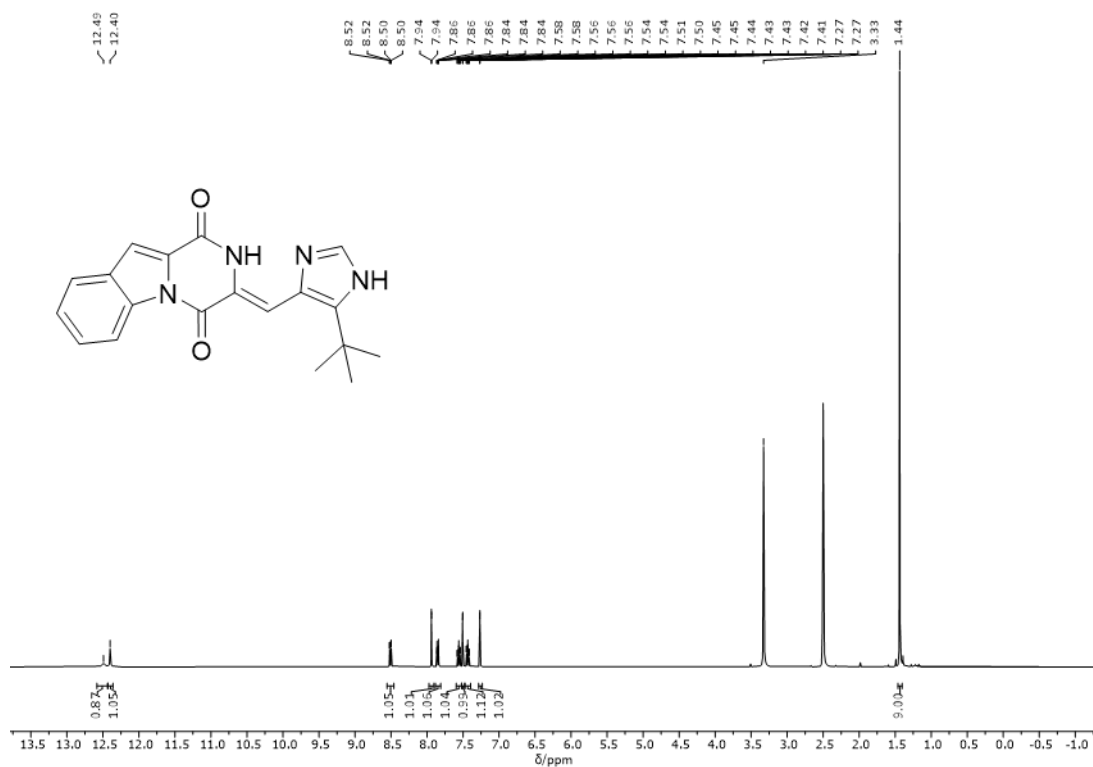


**Figure 281:** $^{1}$H NMR spectrum (400 MHz, DMSO-$d_6$) of compound Z-**40**.
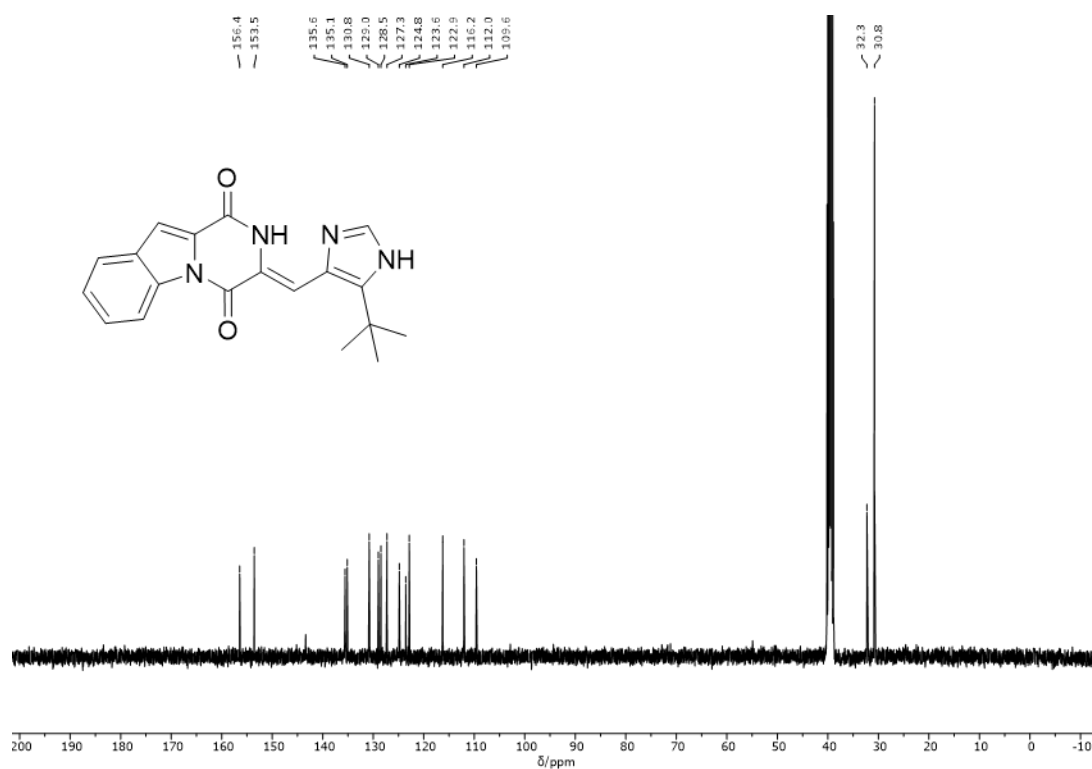
**Figure 282:** $^{13}C$ NMR spectrum (101 MHz, DMSO-$d_6$) of compound Z-**40**.
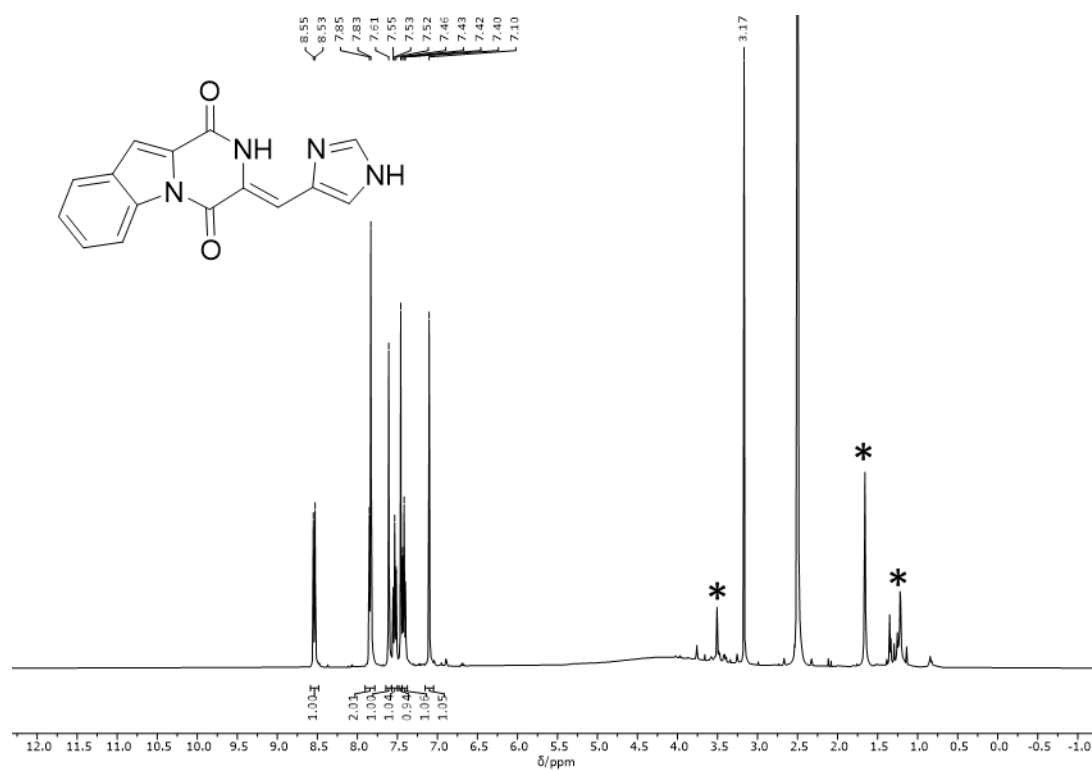


**Figure 283:** $^1H$ NMR spectrum (400 MHz, DMSO-$d_6$) of compound Z-**46**. *unidentified impurities.
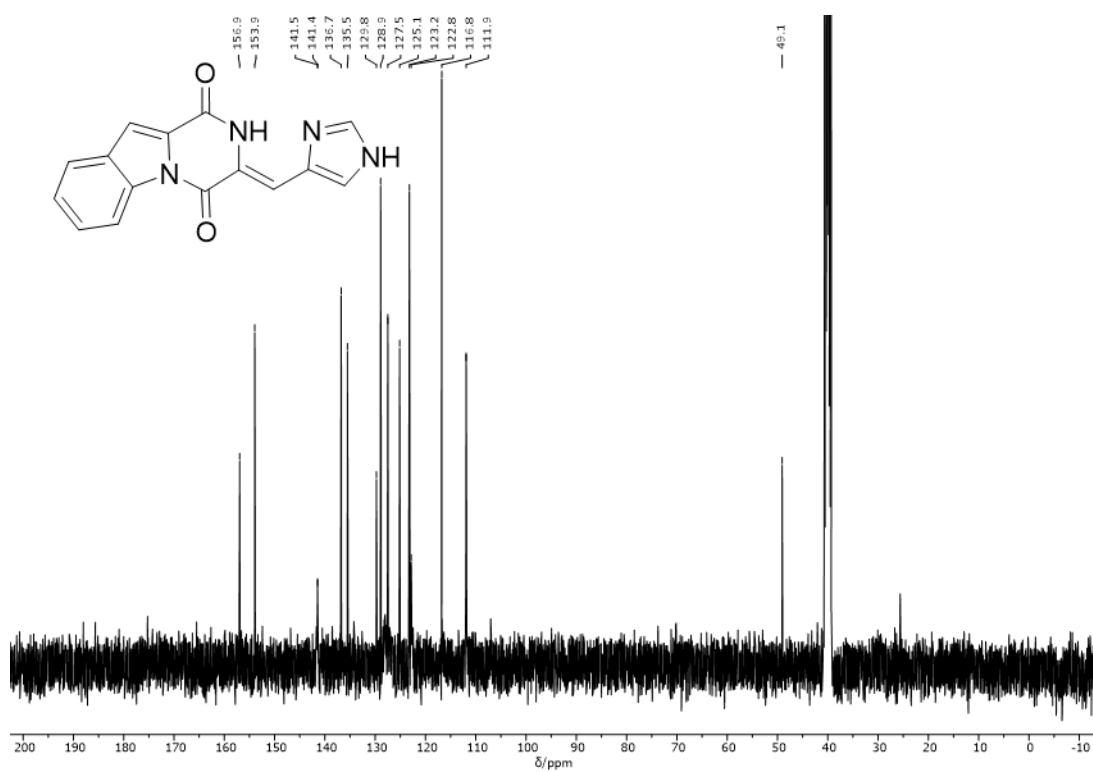
**Figure 284:** $^{13}C$ NMR spectrum (101 MHz, DMSO-$d_6$) of compound Z-**46**.
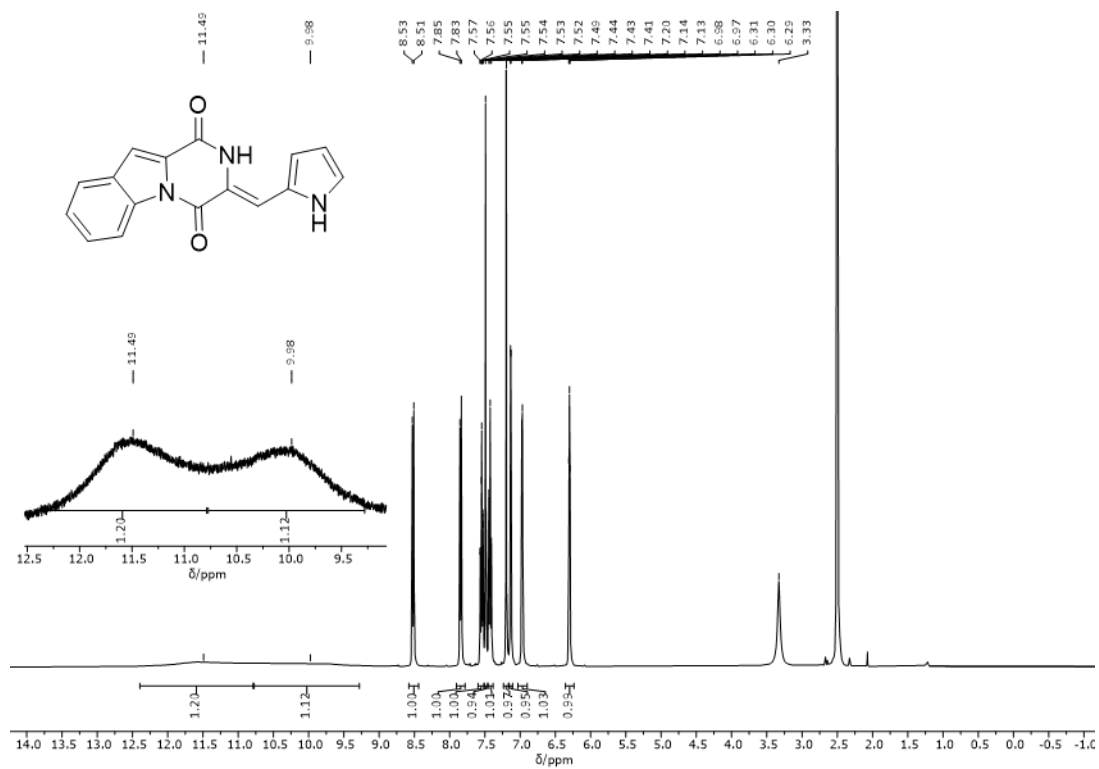


**Figure 285:** $^{1}H$ NMR spectrum (400 MHz, DMSO-$d_6$) of compound Z-**57**.
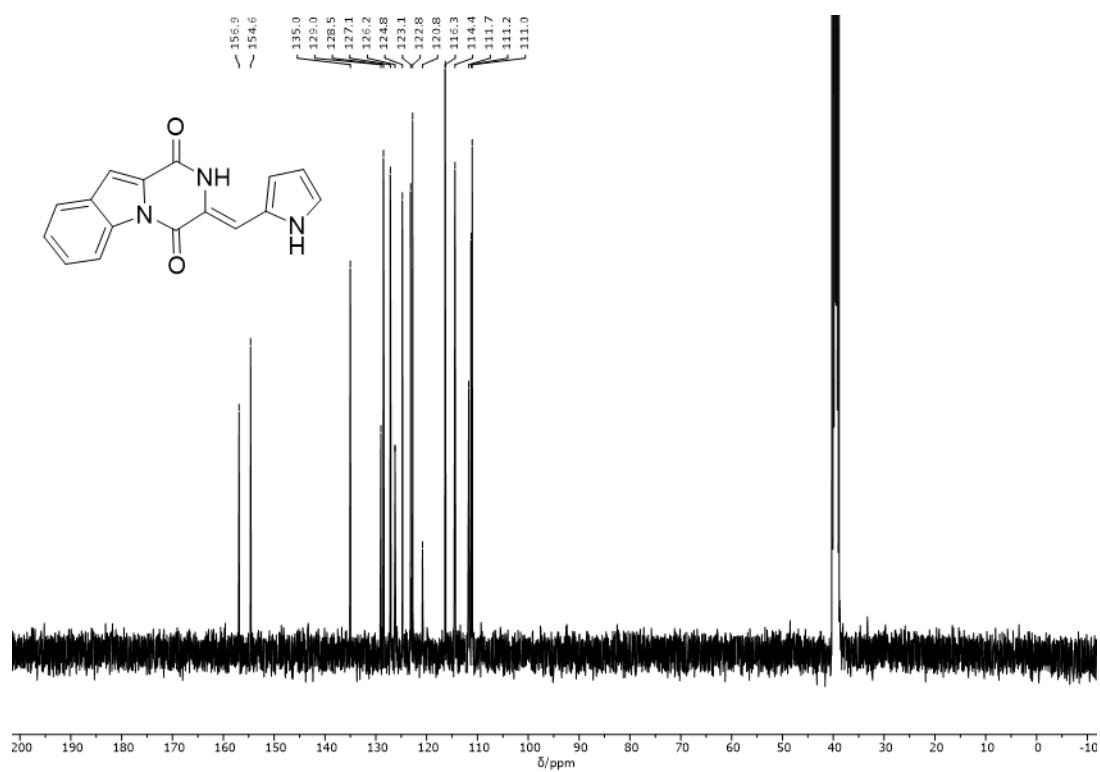
**Figure 286:** $^{13}$C NMR spectrum (101 MHz, DMSO-$d_6$) of compound Z-**57**.
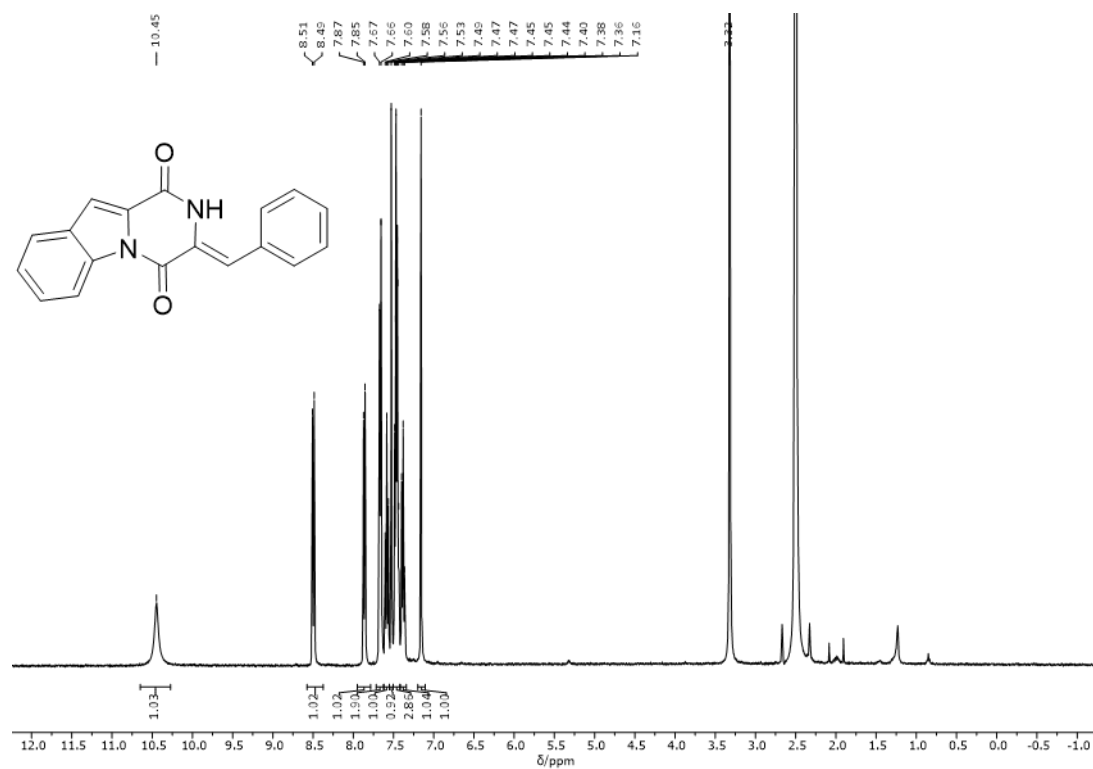


**Figure 287:** $^1$H NMR spectrum (400 MHz, DMSO-$d_6$) of compound Z-**48**.
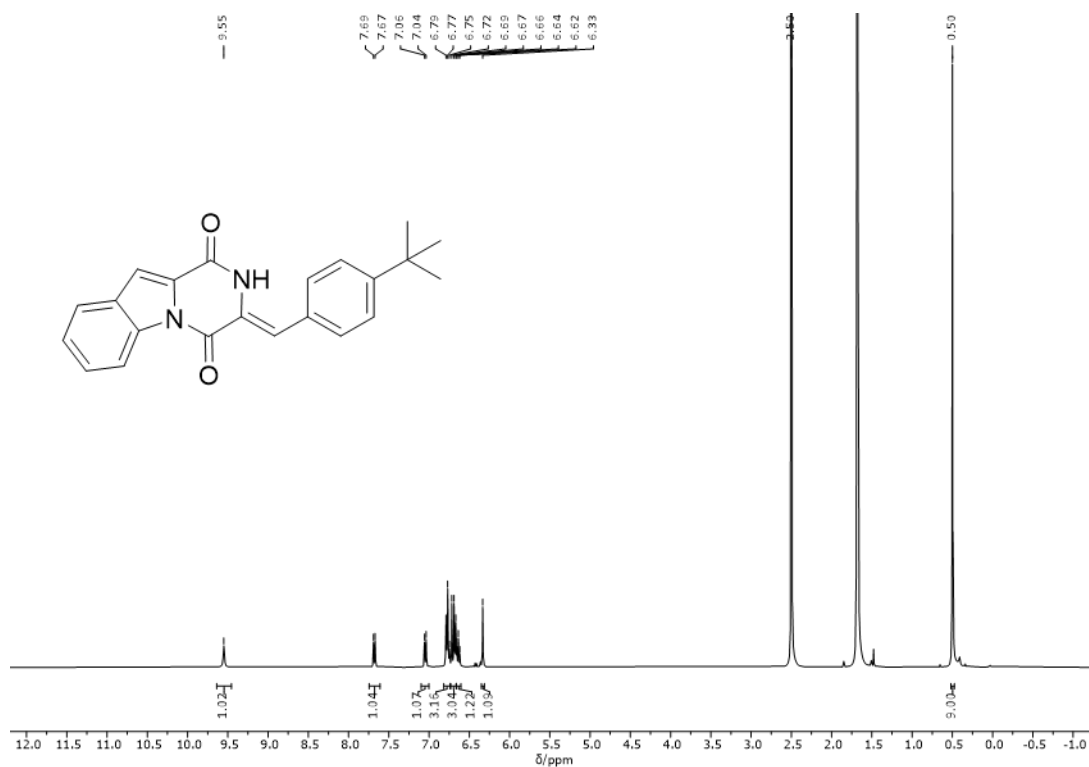
**Figure 288:** $^1$H NMR spectrum (400 MHz, DMSO-$d_6$) of compound *Z*-**47**.



**Figure 289:** $^1$H NMR spectrum (400 MHz, DMSO-$d_6$) of compound *Z*-**49**.
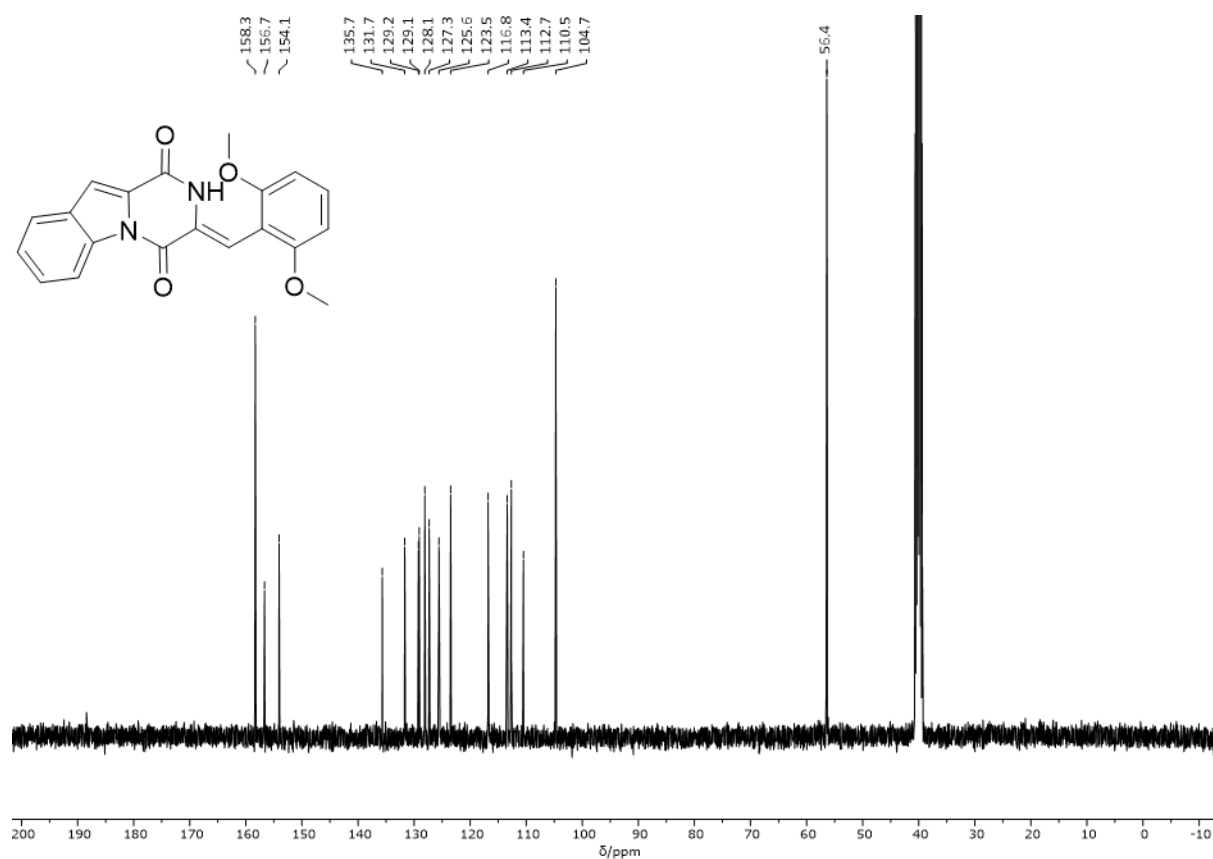
**Figure 290:** $^{13}$C NMR spectrum (101 MHz, DMSO-$d_6$) of compound Z-**49**.
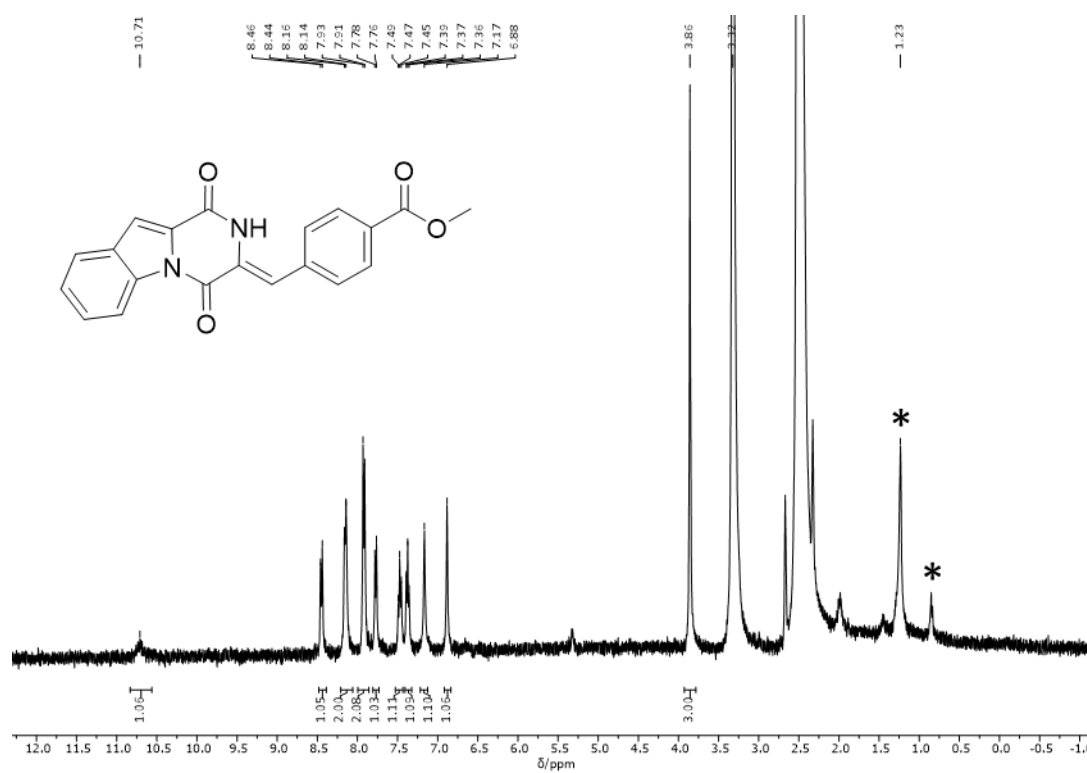


**Figure 291:** $^1$H NMR spectrum (400 MHz, DMSO-$d_6$) of compound Z-**50**. *unidentified impurities.
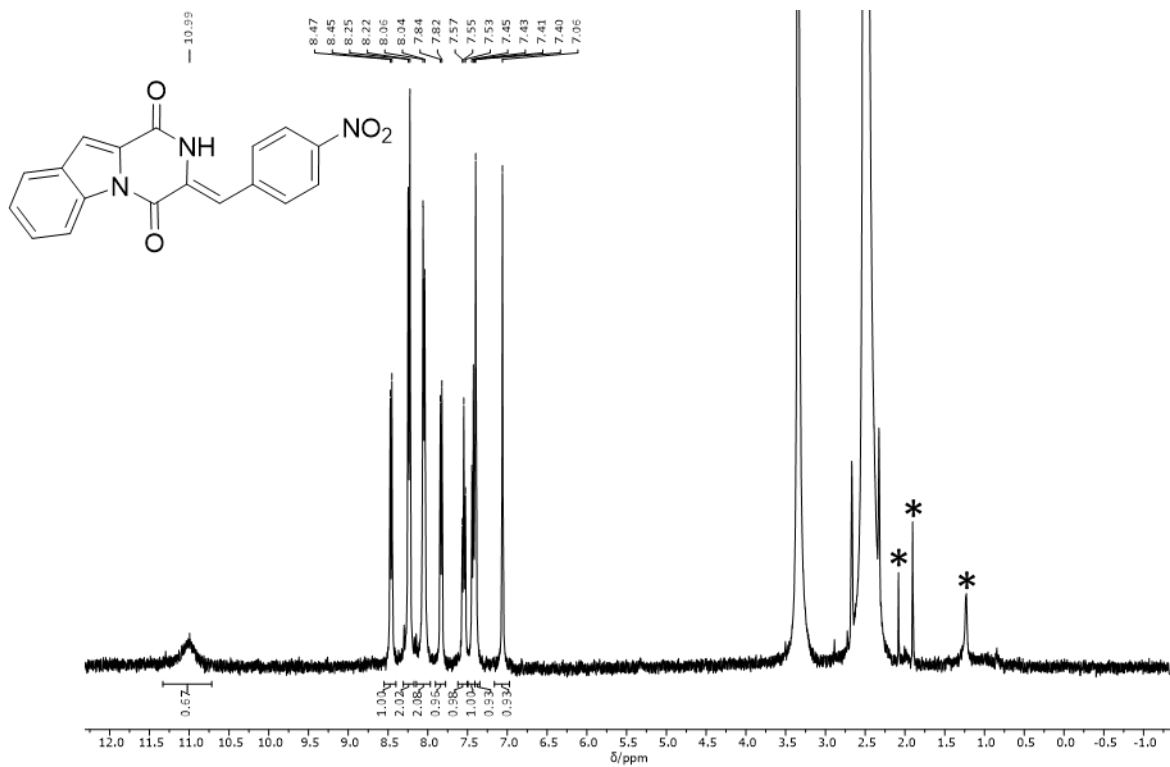
**Figure 292:** $^1$H NMR spectrum (400 MHz, DMSO-$d_6$) of compound $Z$-**51**. *unidentified impurities.
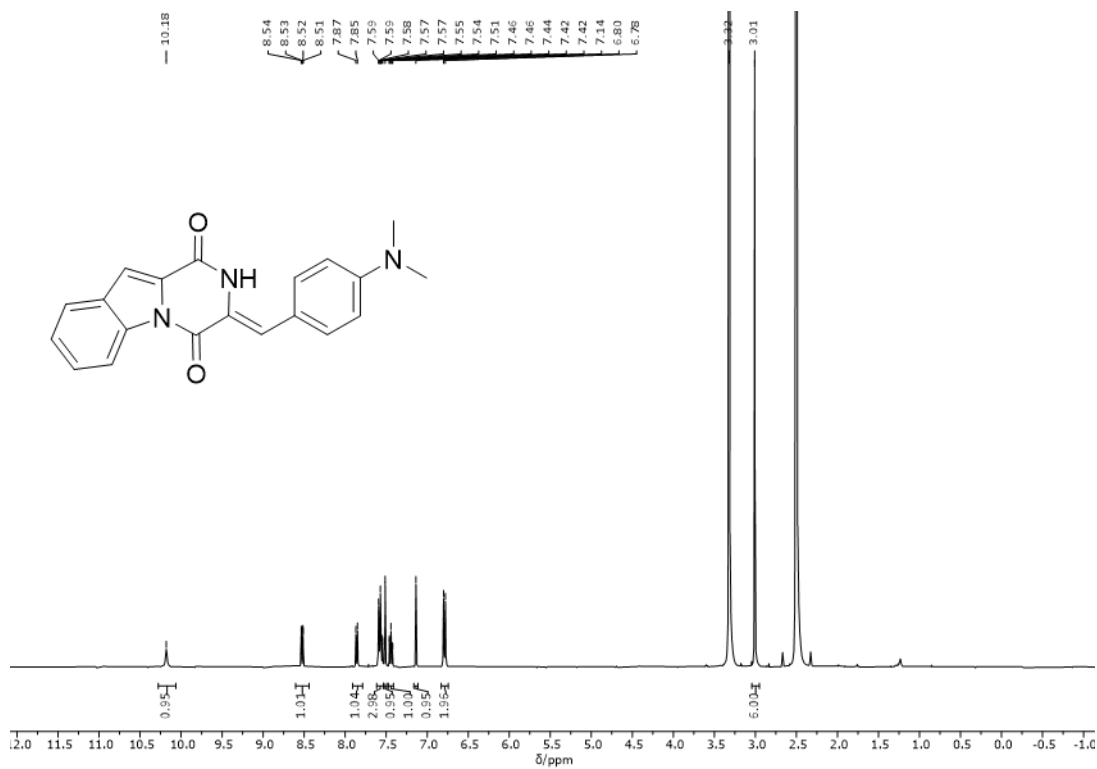


**Figure 293:** $^1$H NMR spectrum (400 MHz, DMSO-$d_6$) of compound $Z$-**52**.
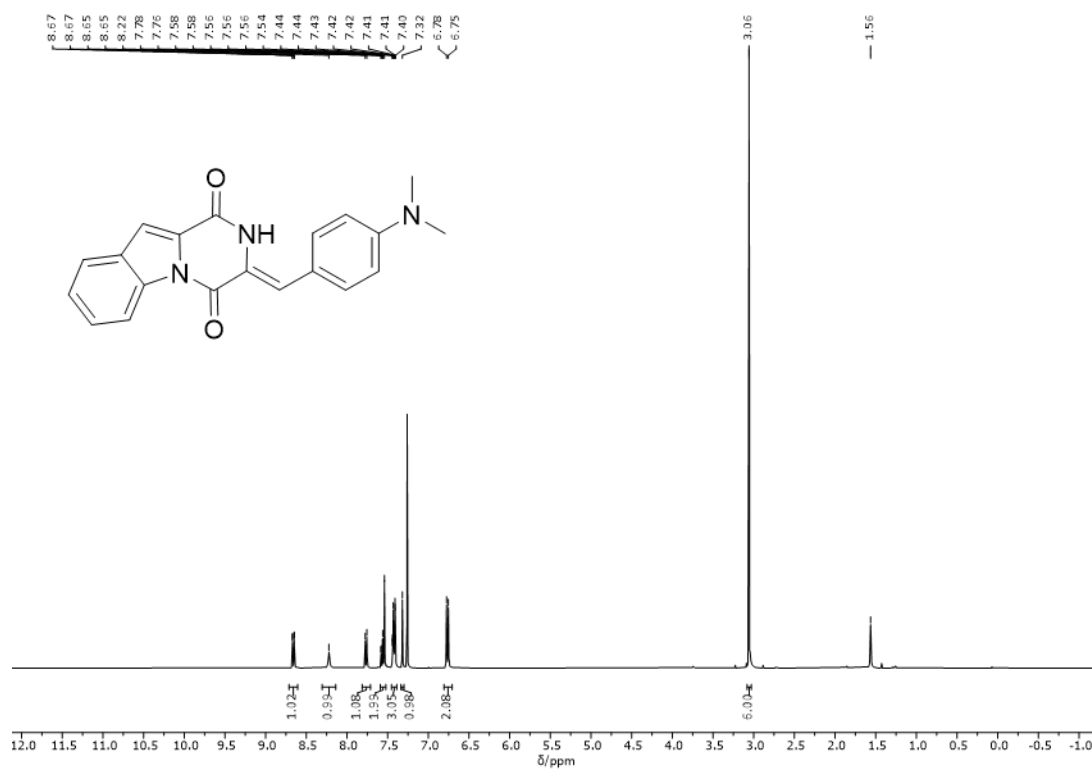
**Figure 294:** $^1$H NMR spectrum (400 MHz, CDCl$_3$) of compound Z-**52**.
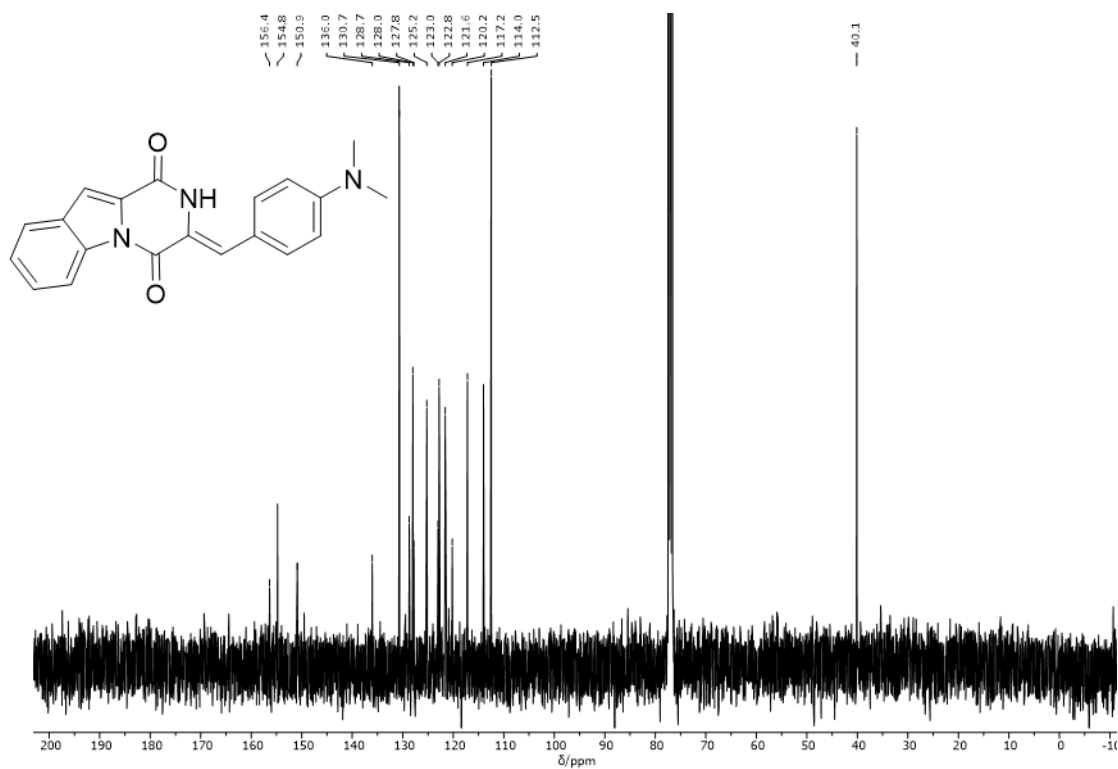


**Figure 295:** $^{13}$C NMR spectrum (101 MHz, CDCl$_3$) of compound Z-**52**.
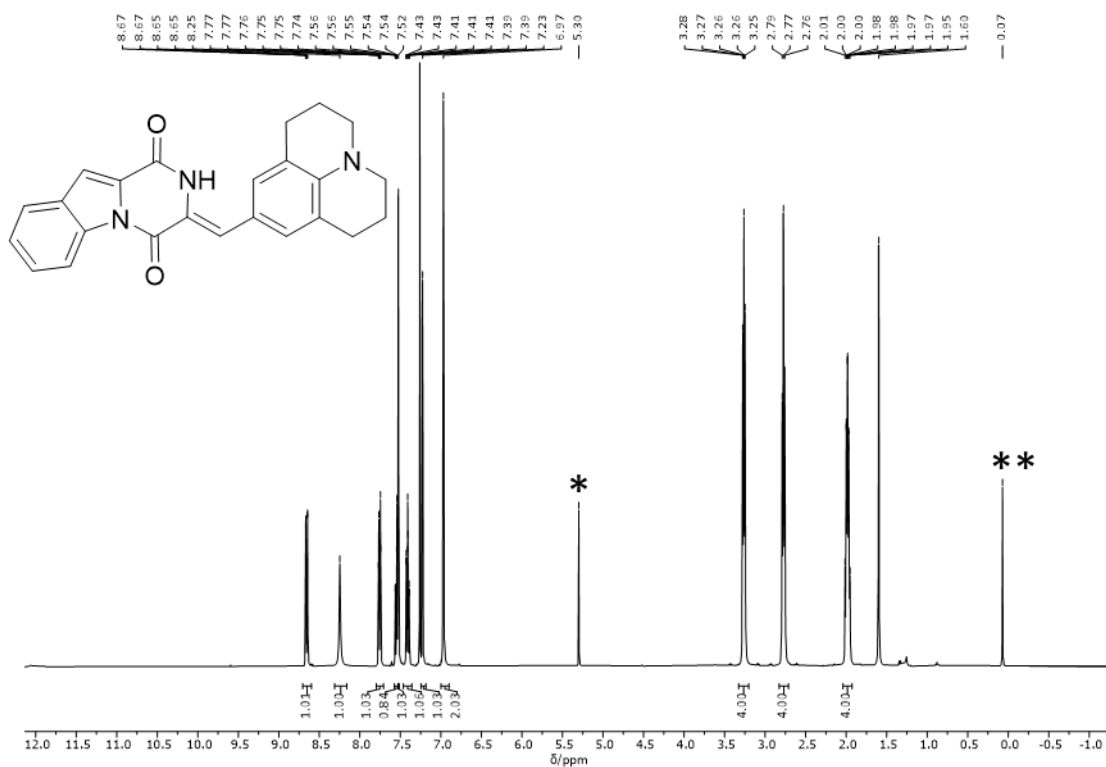
**Figure 296:** $^1$H NMR spectrum (400 MHz, CDCl$_3$) of compound Z-**53**. *DCM, **silicon grease.
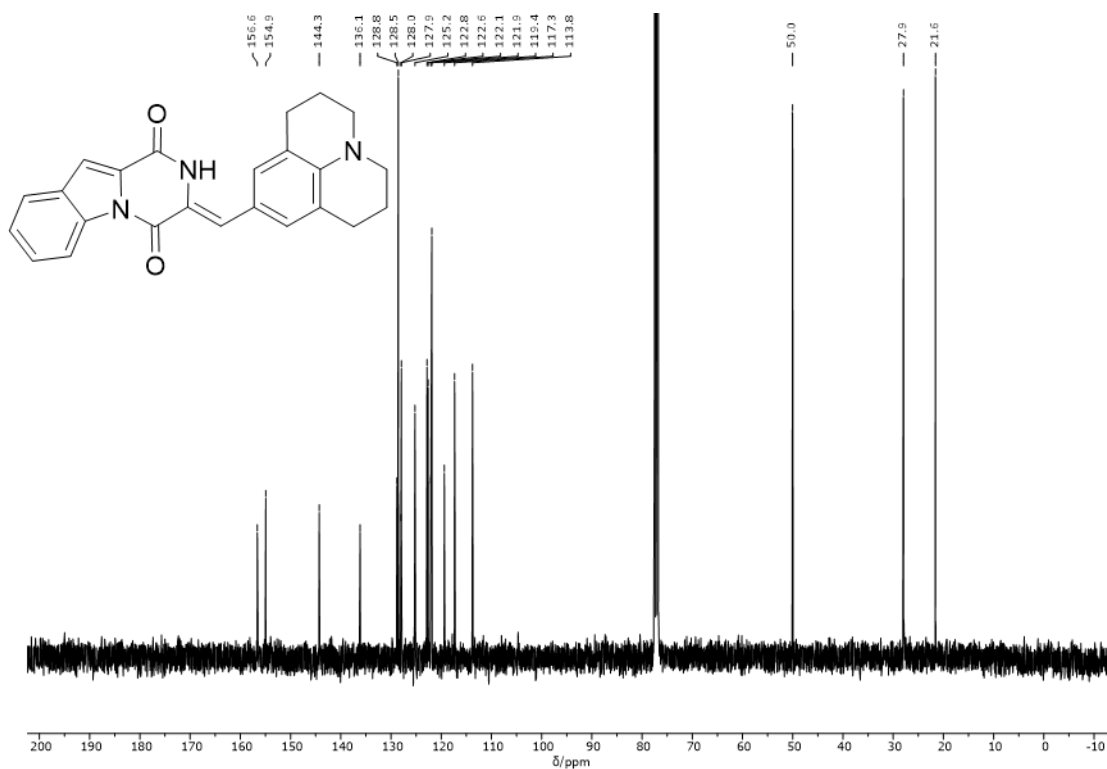


**Figure 297:** $^{13}$C NMR spectrum (101 MHz, CDCl$_3$) of compound Z-**53**.
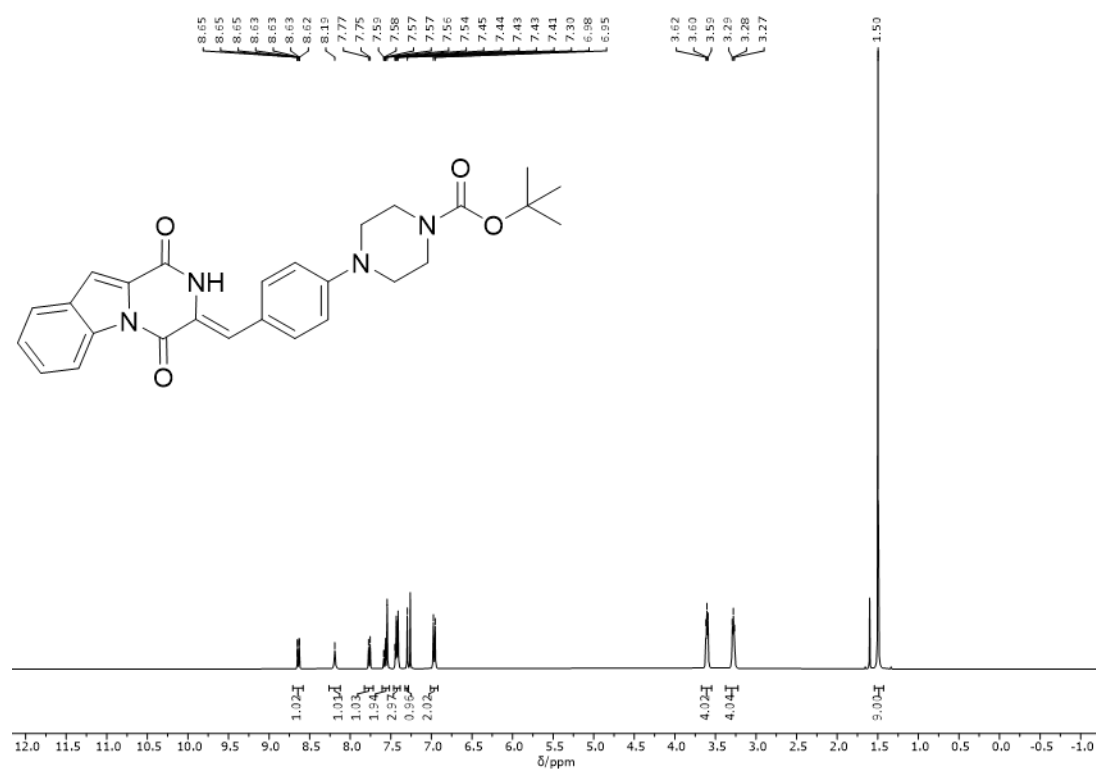
**Figure 298:** $^1$H NMR spectrum (400 MHz, CDCl$_3$) of compound *Z*-**54**.
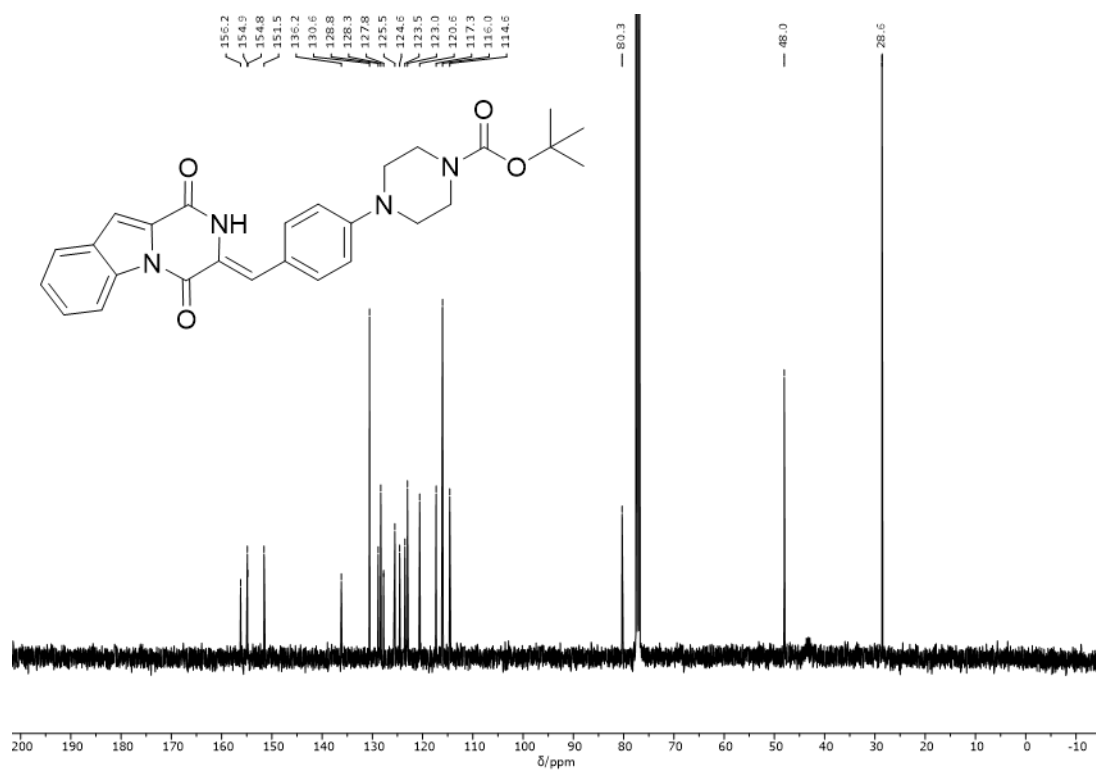


**Figure 299:** $^{13}$C NMR spectrum (101 MHz, CDCl$_3$) of compound *Z*-**54**.
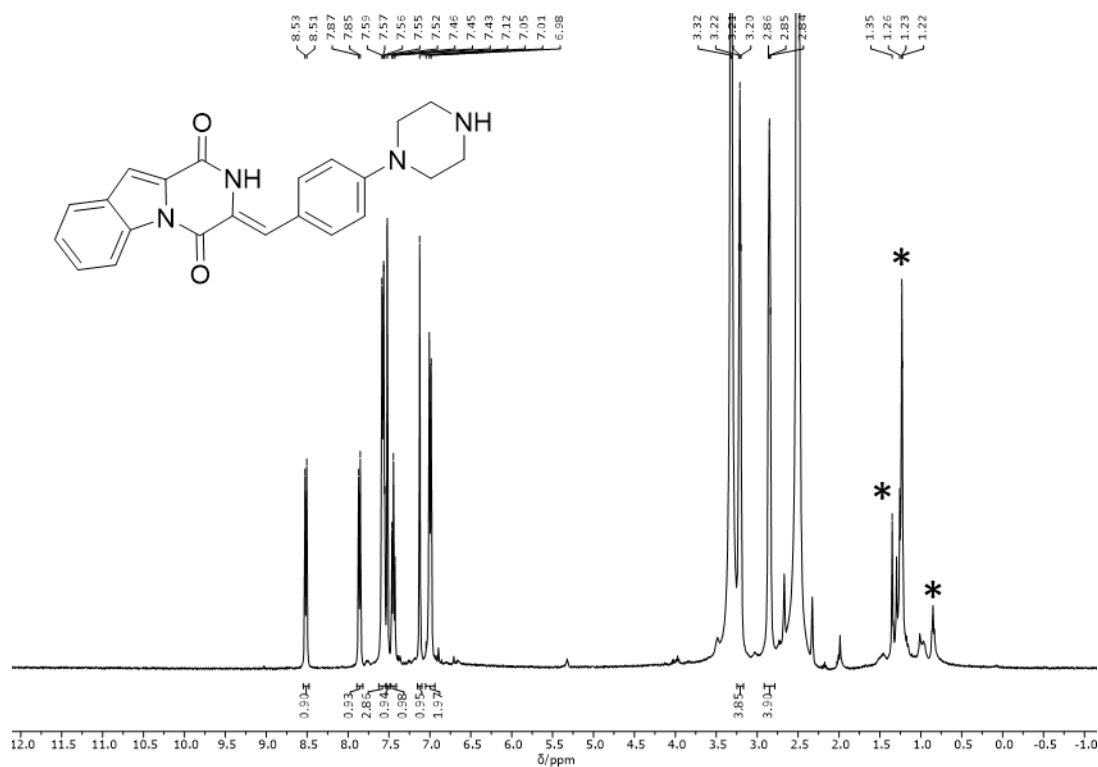
**Figure 300:** $^1$H NMR spectrum (400 MHz, DMSO-$d_6$) of compound *Z*-**55**. *unidentified impurities.
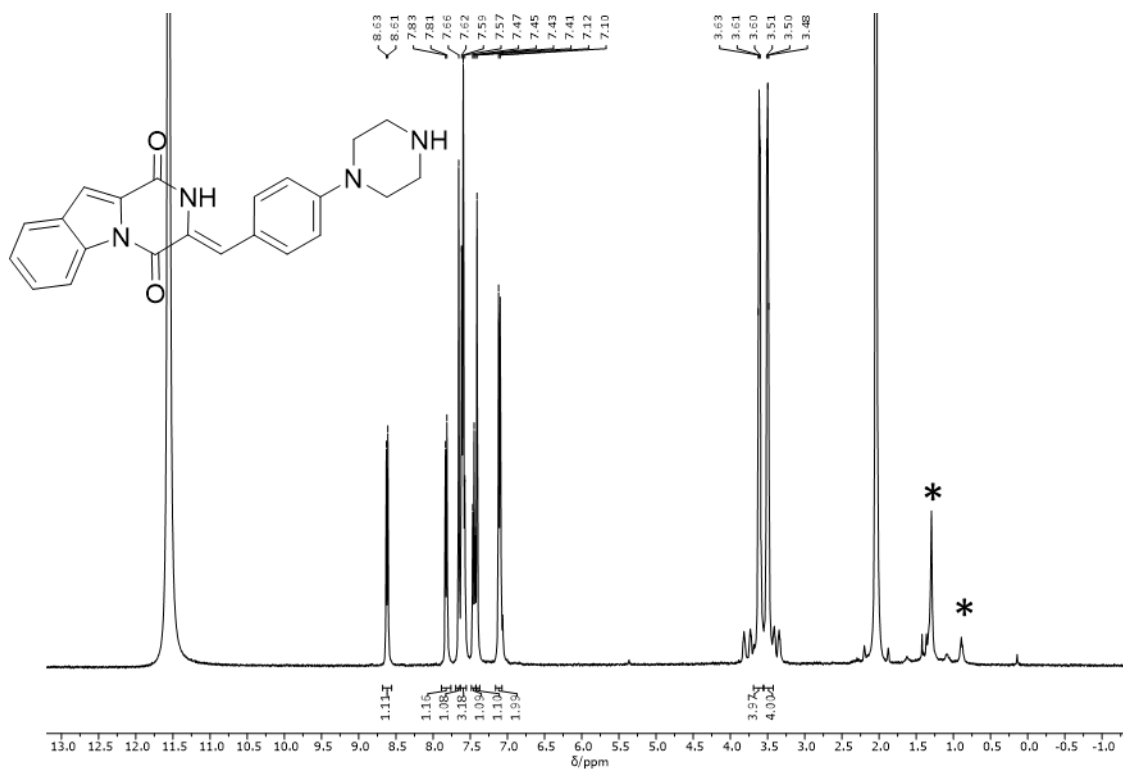


**Figure 301:** $^1$H NMR spectrum (400 MHz, acetic acid-$d_4$) of compound *Z*-**55**. *unidentified impurities.

### 5.6.4    Absorption Spectra of Non-Irradiated Samples
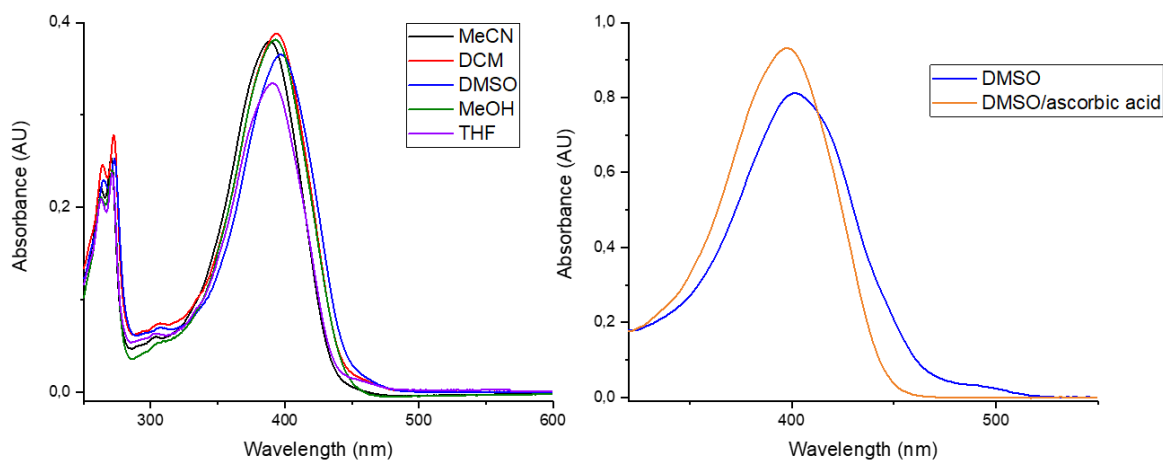


**Figure 302:** Compound *Z*-**40** was dissolved in different solvents (80 μM), respectively. Absorption spectra were measured in the dark (d = 2 mm). The spectra are assigned to the respective solvents *via* color code. In the mixture of DMSO/ascorbic acid a saturated solution of ascorbic acid in DMSO was used.
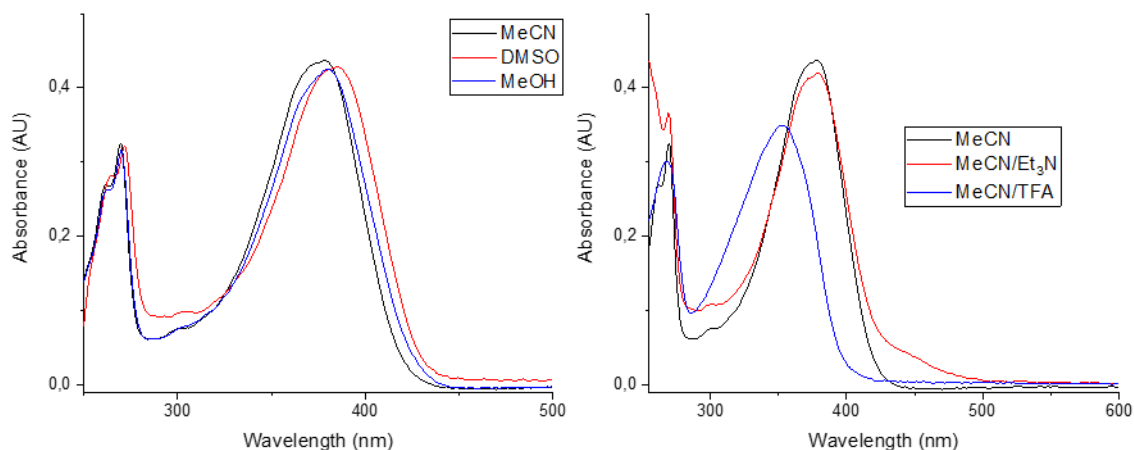


**Figure 303:** Compound *Z*-**46** was dissolved in different solvents (160 μM) and in mixtures of 1% (v/v) TFA in MeCN and 1% (v/v) Et$_3$N in MeCN, respectively. Absorption spectra were measured in the dark (d = 2 mm). The spectra are assigned to the respective solvents *via* color code.
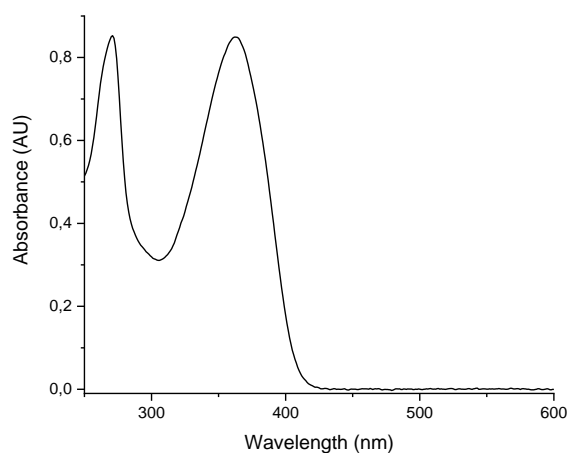
**Figure 304:** Absorption spectrum of compound *Z*-**48** (160 μM) in DMSO (d = 2 mm).
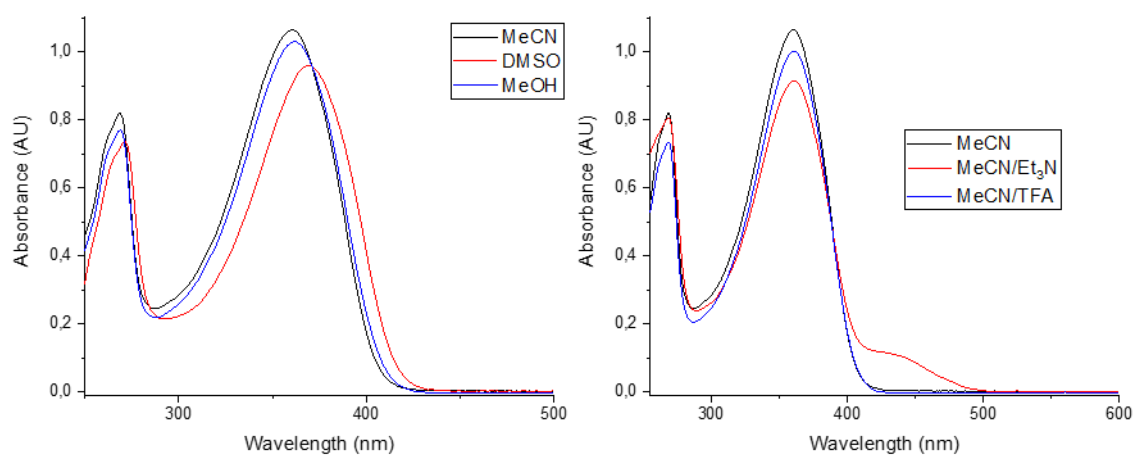


**Figure 305:** Compound *Z*-**47** was dissolved in different solvents (160 μM) and in mixtures of 1% (v/v) TFA in MeCN and 1% (v/v) Et₃N in MeCN, respectively. Absorption spectra were measured in the dark (d = 2 mm). The spectra are assigned to the respective solvents *via* color code.
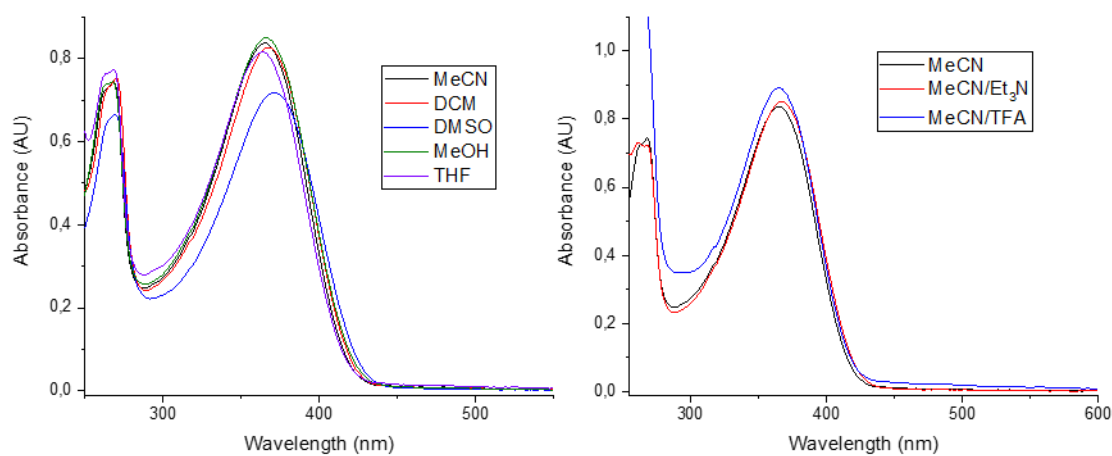


**Figure 306:** Compound *Z*-**49** was dissolved in different solvents (160 μM) and in mixtures of 1% (v/v) TFA in MeCN and 1% (v/v) Et₃N in MeCN, respectively. Absorption spectra were measured in the dark (d = 2 mm). The spectra are assigned to the respective solvents *via* color code.
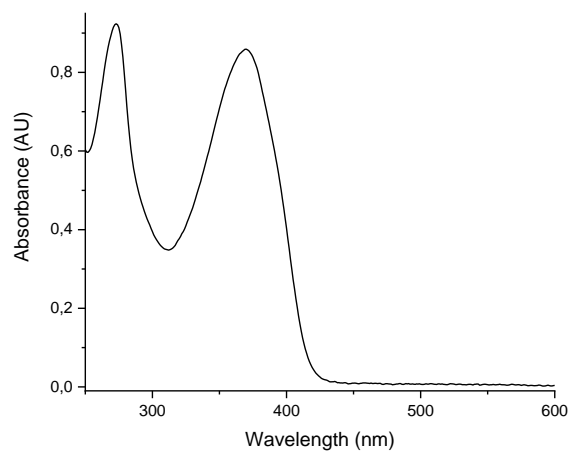
**Figure 307:** Absorption spectrum of compound *Z*-**50** (160 μM) in DMSO (d = 2 mm).
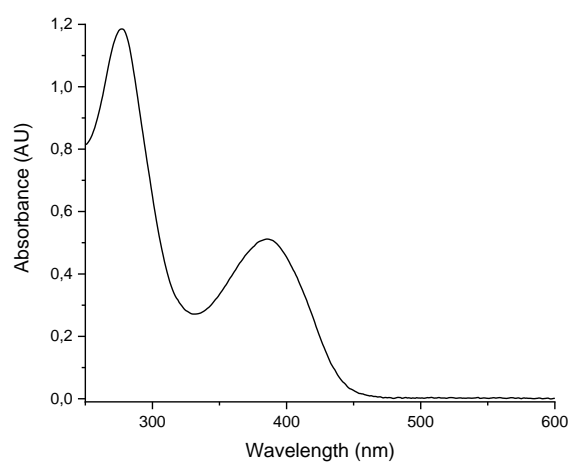


**Figure 308:** Absorption spectrum of compound *Z*-**51** (160 μM) in DMSO (d = 2 mm).
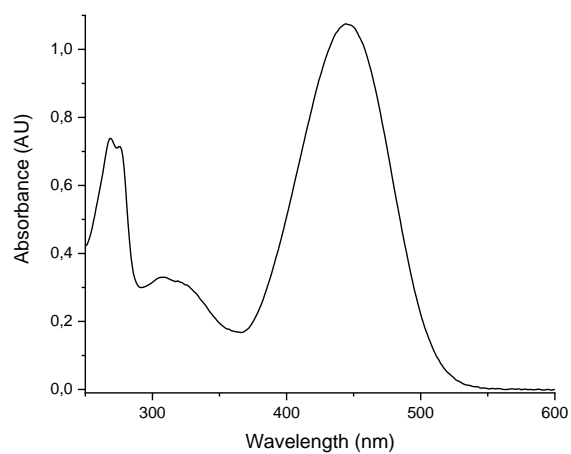


**Figure 309:** Absorption spectrum of compound *Z*-**52** (160 μM) in DMSO (d = 2 mm).
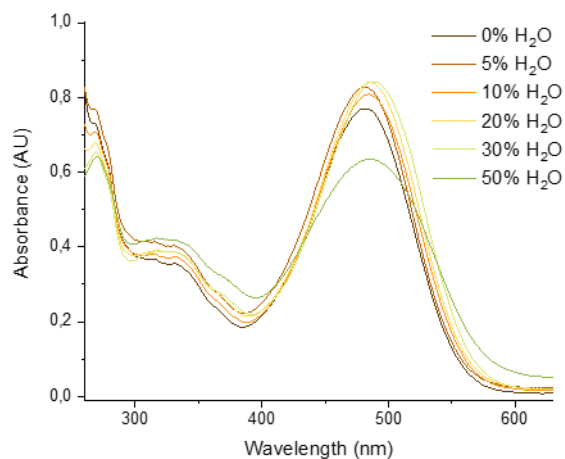
**Figure 310:** Absorption spectrum of compound *Z*-**53** (160 μM) in DMSO and different mixtures of water and DMSO (d = 2 mm).
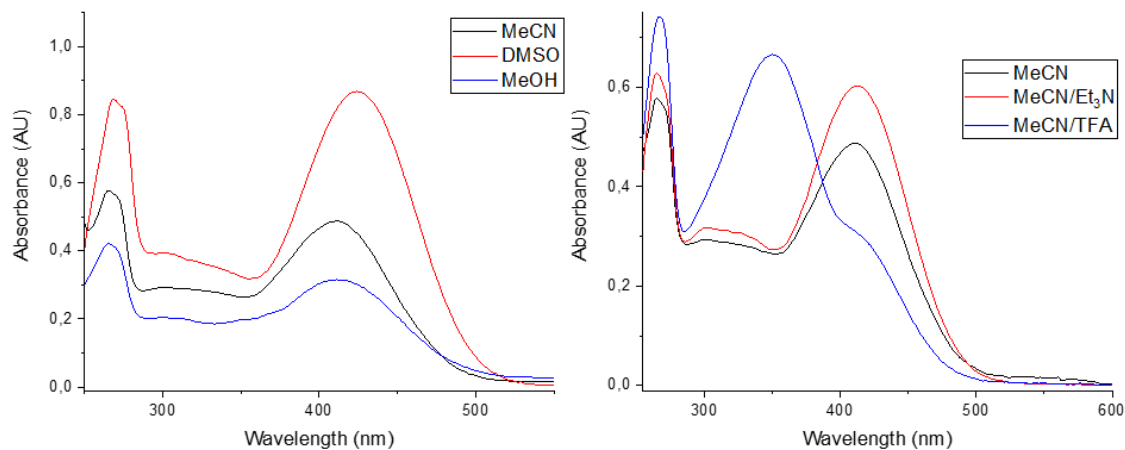


**Figure 311:** Compound *Z*-**54** was dissolved in different solvents (160 μM) and in mixtures of 1% (v/v) TFA in MeCN and 1% (v/v) Et₃N in MeCN, respectively. Absorption spectra were measured in the dark (d = 2 mm). The spectra are assigned to the respective solvents *via* color code.
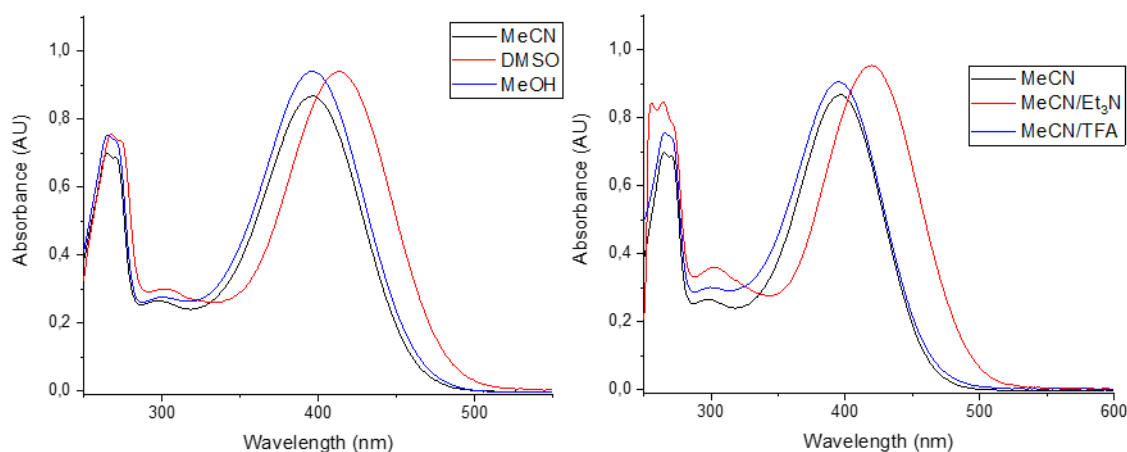
**Figure 312:** The TFA salt of compound *Z*-**55** was dissolved in different solvents (160 µM) and in mixtures of 1% (v/v) TFA in MeCN and 1% (v/v) Et₃N in MeCN, respectively. Absorption spectra were measured in the dark (d = 2 mm). The spectra are assigned to the respective solvents *via* color code.

### 5.6.5   Absorption Spectra of Irradiated Samples
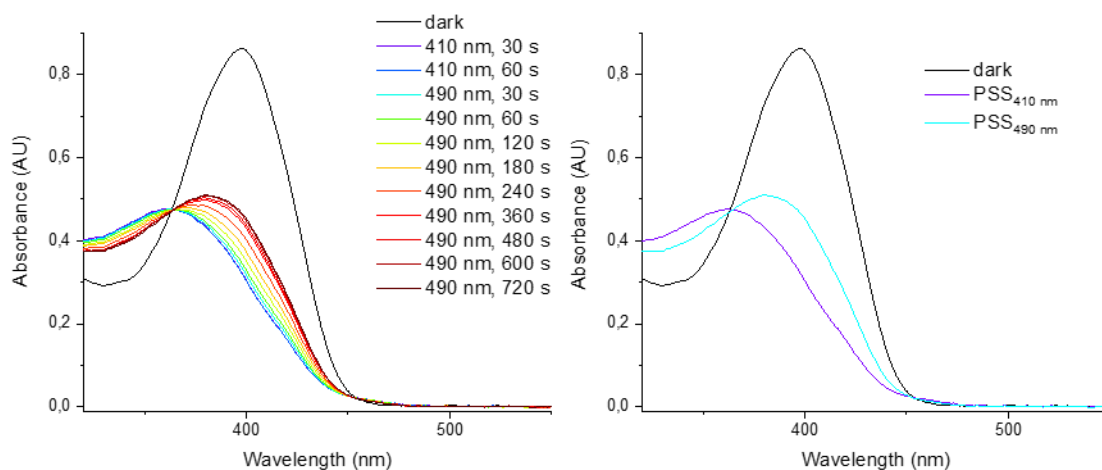


**Figure 313:** Compound **40** in saturated solution of ascorbic acid in DMSO (200 µM) was irradiated and an absorption spectrum (d = 2 mm) was measured after each irradiation step until the PSS was reached, respectively.
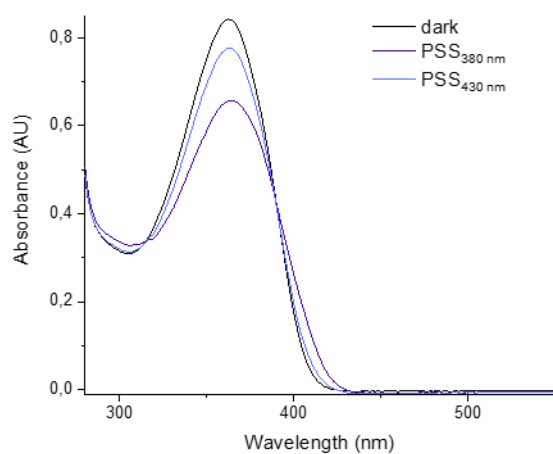
**Figure 314:** Compound **48** was dissolved in DMSO (160 µM) and an absorption spectrum (d = 2 mm) was first measured in the dark. The sample was then irradiated and an absorption spectrum was measured after each irradiation step until the PSS was reached, respectively.
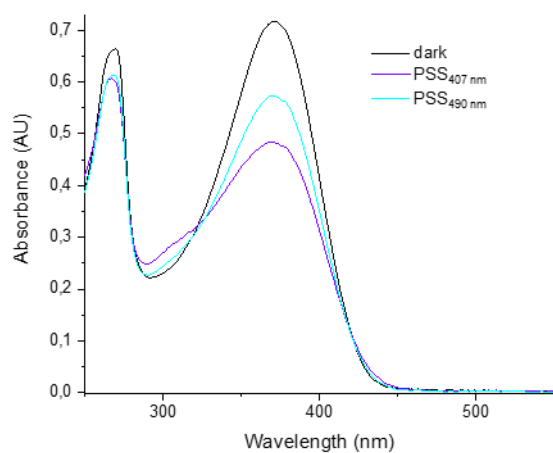


**Figure 315:** Compound **49** was dissolved in DMSO (160 µM) and an absorption spectrum (d = 2 mm) was first measured in the dark. The sample was then irradiated and an absorption spectrum was measured after each irradiation step until the PSS was reached, respectively.
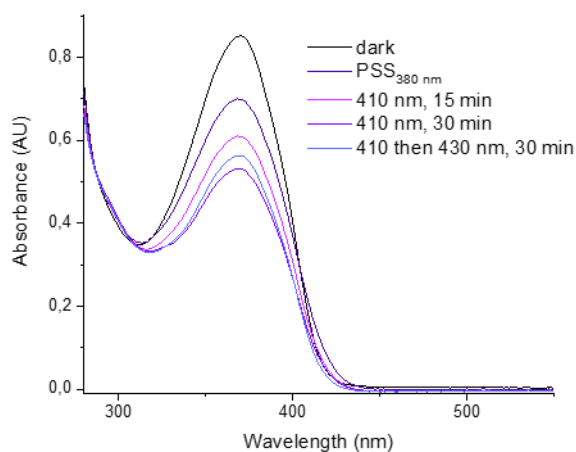
**Figure 316:** Compound **50** was dissolved in DMSO (160 µM) and an absorption spectrum (d = 2 mm) was first measured in the dark. The sample was then irradiated and an absorption spectrum was measured after each irradiation step until the PSS was reached, respectively. Upon irradiation with 410 nm no PSS was reached.
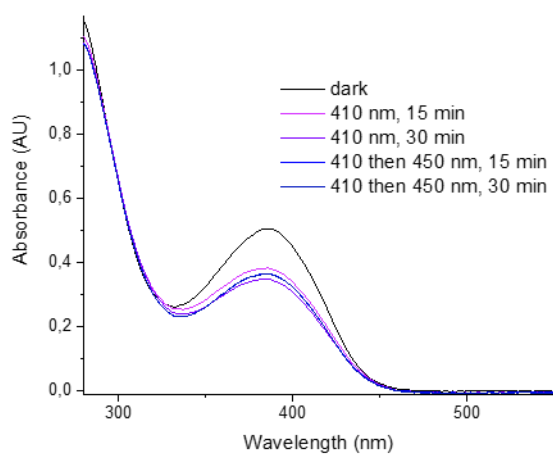


**Figure 317:** Compound **51** was dissolved in DMSO (160 µM) and an absorption spectrum (d = 2 mm) was first measured in the dark. The sample was then irradiated and an absorption spectrum was measured after each irradiation step. No PSS was reached.
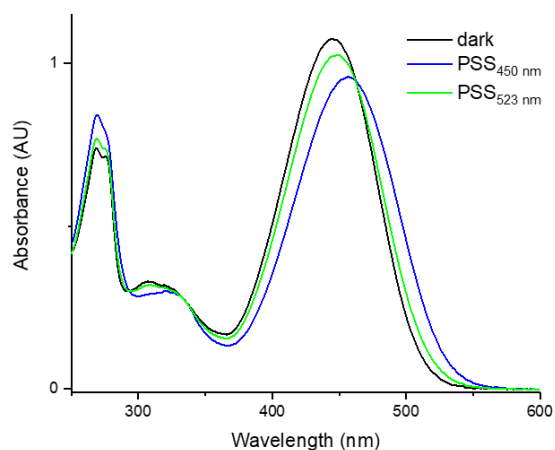
**Figure 318:** Compound **52** was dissolved in DMSO ($160\,\mu M$) and an absorption spectrum ($d = 2\,mm$) was first measured in the dark. The sample was then irradiated and an absorption spectrum was measured after each irradiation step until the PSS was reached, respectively.
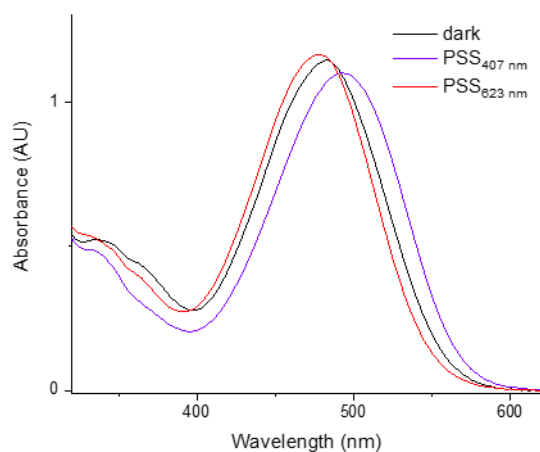


**Figure 319:** Compound **53** was dissolved in DMSO ($80\,\mu M$) and an absorption spectrum ($d = 2\,mm$) was first measured in the dark. The sample was then irradiated and an absorption spectrum was measured after each irradiation step until the PSS was reached, respectively.
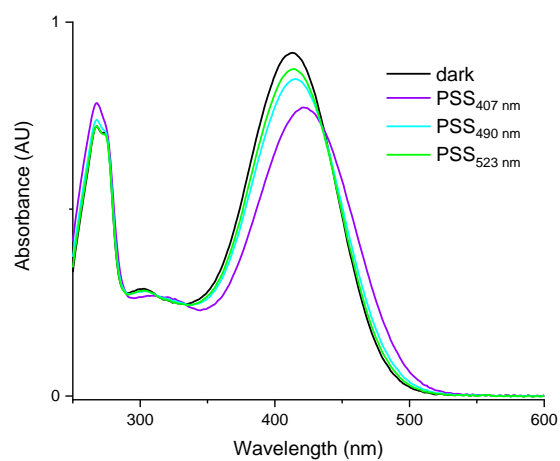
**Figure 320:** The TFA salt of compound **55** was dissolved in DMSO (160 µM) and an absorption spectrum (d = 2 mm) was first measured in the dark. The sample was then irradiated and an absorption spectrum was measured after each irradiation step until the PSS was reached, respectively.

### 5.6.6   Emission Spectra
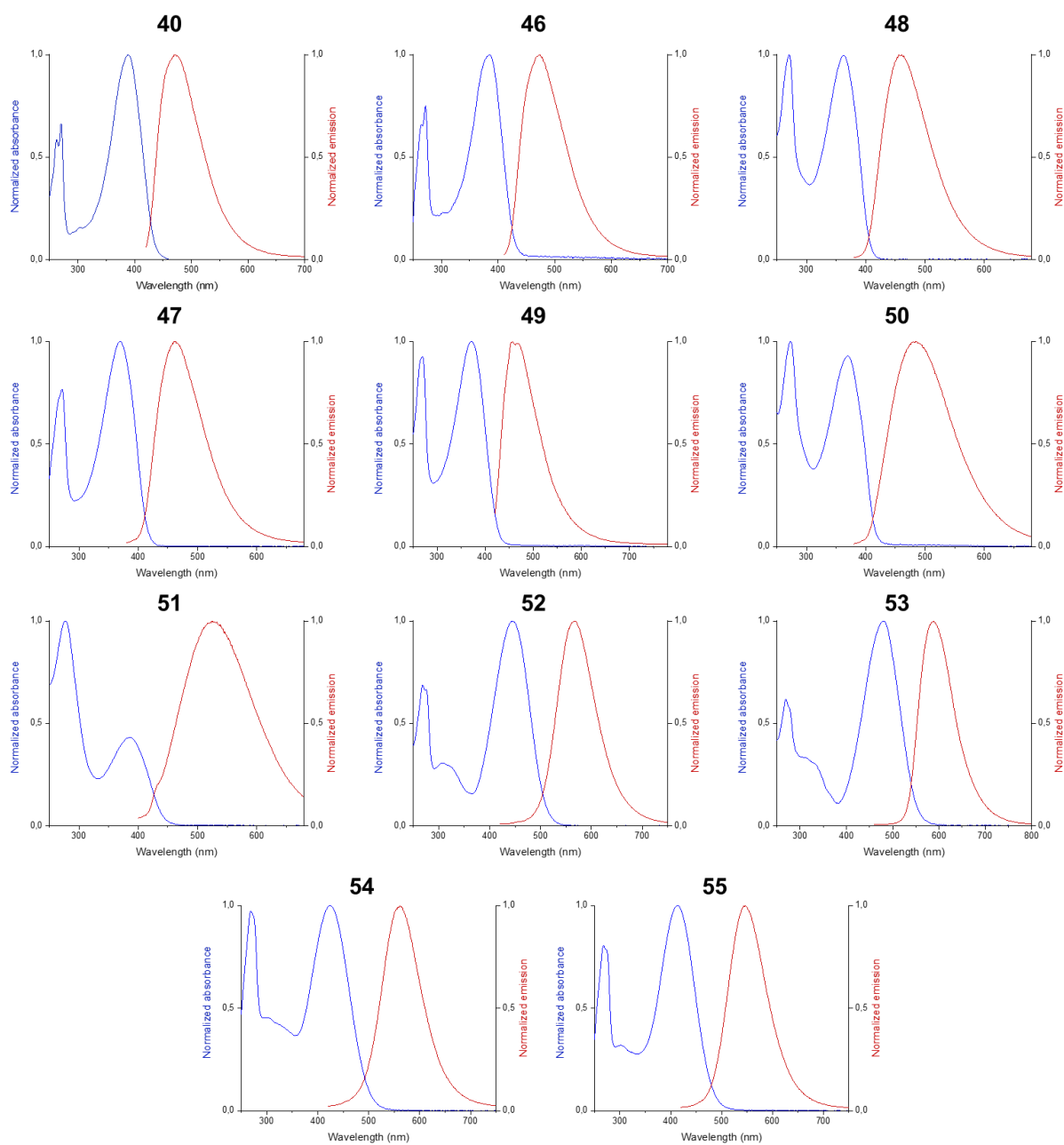


**Figure 321:** Normalized absorption (blue) and emission (red) spectra of solutions of the respective Z-isomers of **40** in MeCN and **46**-**55** in DMSO.
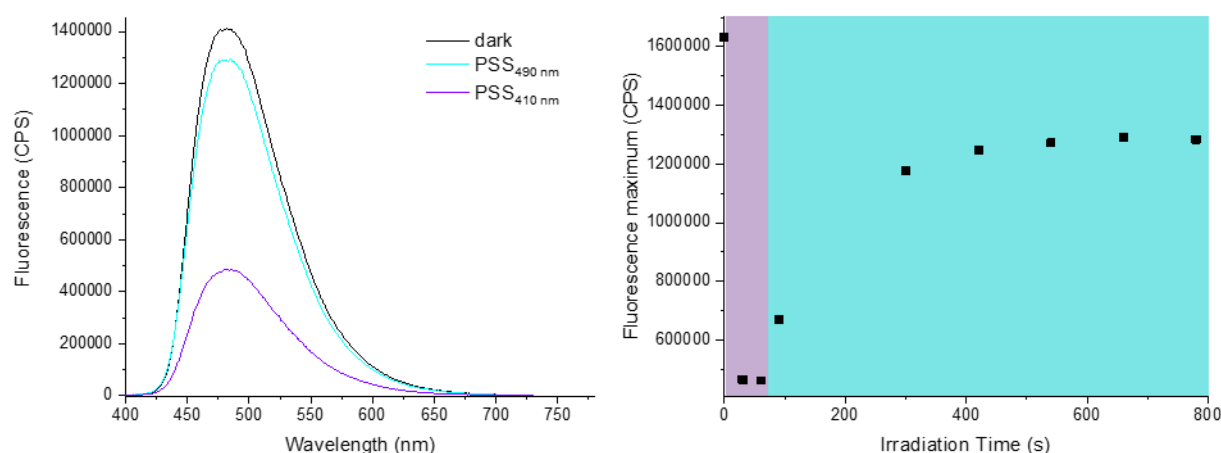
**Figure 322:** Left: Fluorescence spectra of compound **40** (200 µM) in saturated solution of ascorbic acid in DMSO before and after irradiation (excitation at 380 nm) The spectra are assigned to the respective mixture *via* color code. Right: Compound **40** (200 µM) in saturated solution of ascorbic acid was analyzed *via* fluorescence spectroscopy before and after irradiation with first 410 nm and subsequently 490 nm (indicated by the color of the background). The maximal fluorescence was plotted against the irradiation time.

### 5.6.7   Composition of the Photostationary States (PSSs)

*Compound **40**: Via analytical HPLC*

The PSS composition was determined by analyzing 1 mM solutions of compound **40** in DMSO after irradiation *via* analytical HPLC. The PSS values in have been achieved within 10 min (365, 410, 450 nm) or 20 min (490 nm). Triplicates were obtained by including two samples that were irradiated further after the PSS was reached. The signals assigned to the *Z*-isomer were integrated and divided by the signal area determined before irradiation:

% *Z*-isomer = $I_{after\ irradiation}$ /$I_{dark}$*100% (% *E*-isomer = 100% - % of *Z*-isomer).

**Table 15:** PSS composition in DMSO determined by analytical HPLC measurements performed with samples of **40** before and after irradiation.

| 365 nm (% of *E*-isomer) | 410 nm (% of *E*-isomer) | 450 nm (% of *E*-isomer) | 470 nm (% of *E*-isomer) | 490 nm (% of *E*-isomer) |
|---|---|---|---|---|
| 75 | 93 | 85 | 70 | 67 |
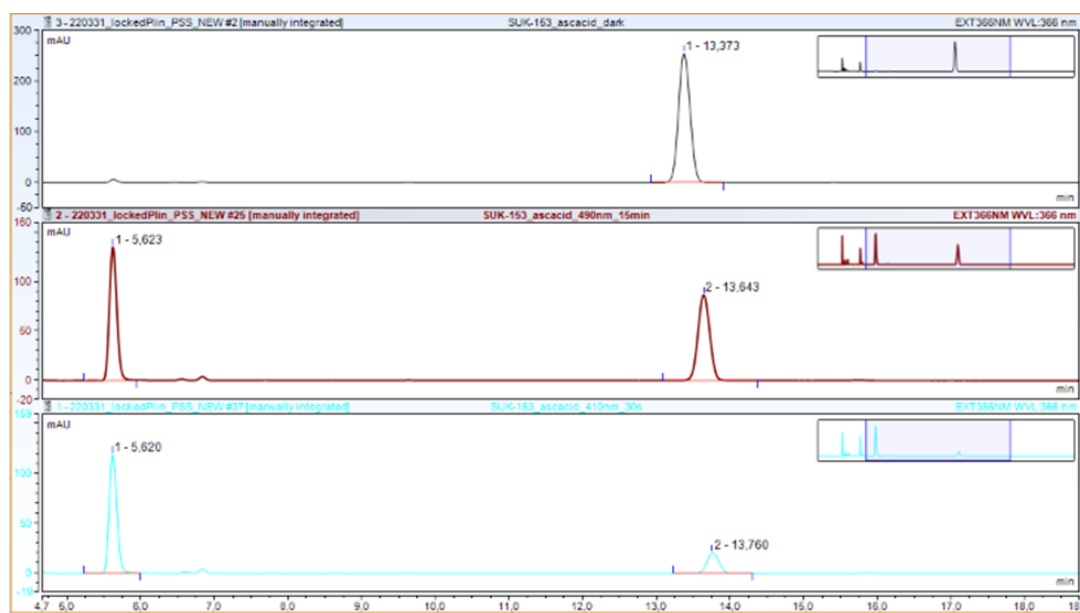
**Figure 323:** HPLC trace of 1 mM solutions of **40** in DMSO before irradiation (top) and after reaching the PSS upon irradiation with 490 nm (middle) and 410 nm (bottom).

*Compound **52**: Via NMR spectroscopy*

The PSS composition was determined by measuring $^1$H NMR spectra of **52** before and after irradiation. The PSS values in the NMR tube (0.5 mL of the 30-60 mM solution in DMSO-$d_6$) have been achieved within 1 h (523 nm) or 2 h (430, 470 nm). Signal pairs were determined for each compound: two signals assigned to the same proton for the respective photoisomers were integrated and the % of *E*-isomer $= I_E/(I_E+I_Z)*100\%$ was determined. The final *E/Z* ratios result from the average value determined from three signal pairs.

**Table 16:** PSS composition in DMSO-$d_6$ determined by measuring $^1$H NMR spectra of the respective compounds after irradiation.

| Compound | 430 nm (% of *E*-isomer) | 470 nm (% of *E*-isomer) | 523 nm (% of *E*-isomer) |
|---|---|---|---|
| **52** | 64 | 51 | 17 |
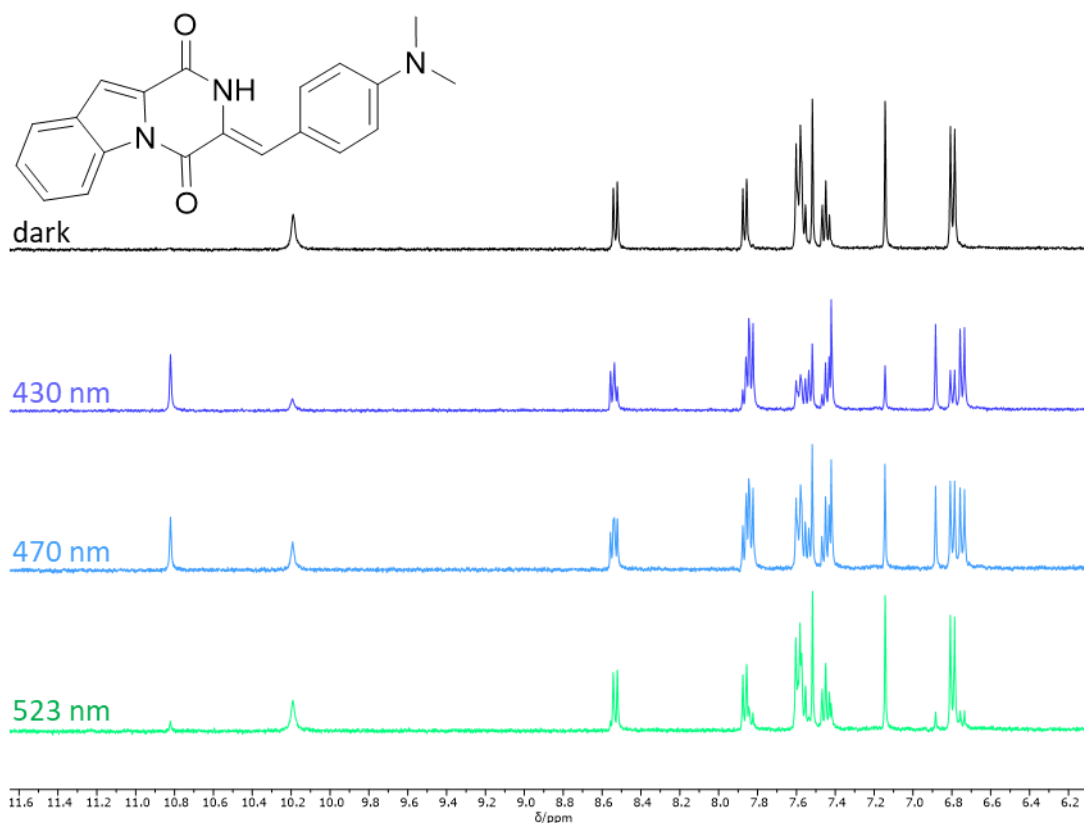
**Figure 324:** Sections of ${}^1$H NMR spectra (400 MHz, DMSO-$d_6$) of compound **52** in the dark (top) and after reaching the PSS upon irradiation with 430 nm, 470 nm and 523 nm.

### 5.6.8 Thermal Relaxation of *E*-Isomers
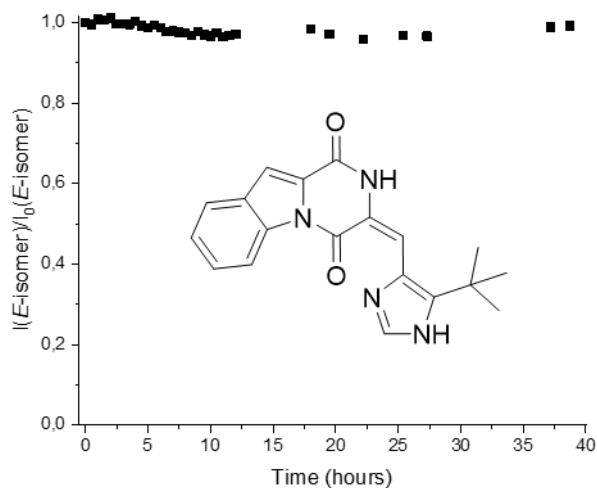


**Figure 325:** The thermal relaxation of *E*-**40** in DMSO (1:1) at 25 °C was monitored *via* analytical HPLC. The integrals of the signals assigned to the respective *E*-isomer were determined at 330 nm: $I_0$ = initial integral, I = integral at given time point.
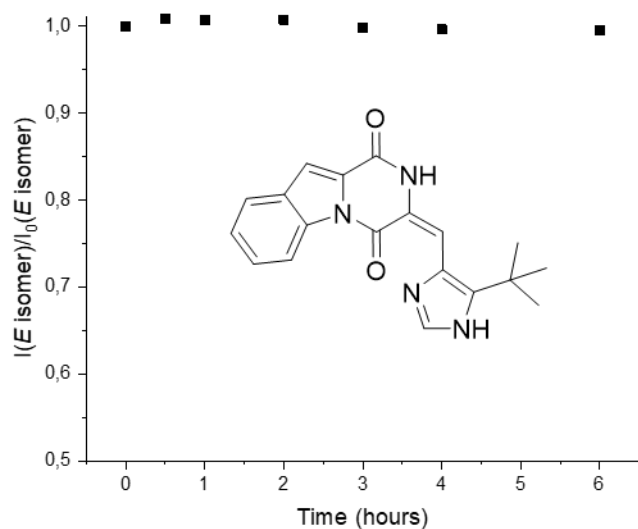
**Figure 326:** The thermal relaxation of *E*-**40** in H₂O/DMSO (1:1) at 37 °C was monitored *via* analytical HPLC. The integrals of the signals assigned to the respective *E*-isomer were determined at 330 nm: $I_0$ = initial integral, I = integral at given time point.

## 5.6.9 Switching Stability
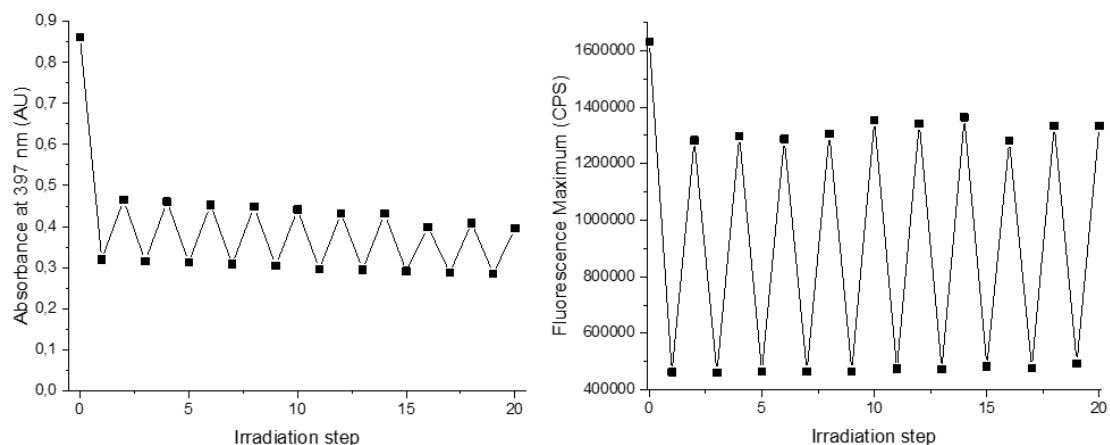


**Figure 327:** A solution of pure *Z*-**40** in a saturated solution of ascorbic acid in DMSO (200 µM) was irradiated with 410 nm for 30 s and with 490 nm for 12 min, respectively. The irradiation cycle was repeated ten times and after every irradiation step the solution was analyzed *via* absorbance (left) and fluorescence (right) spectroscopy.

**5.6.10  Cell Penetration Assays**
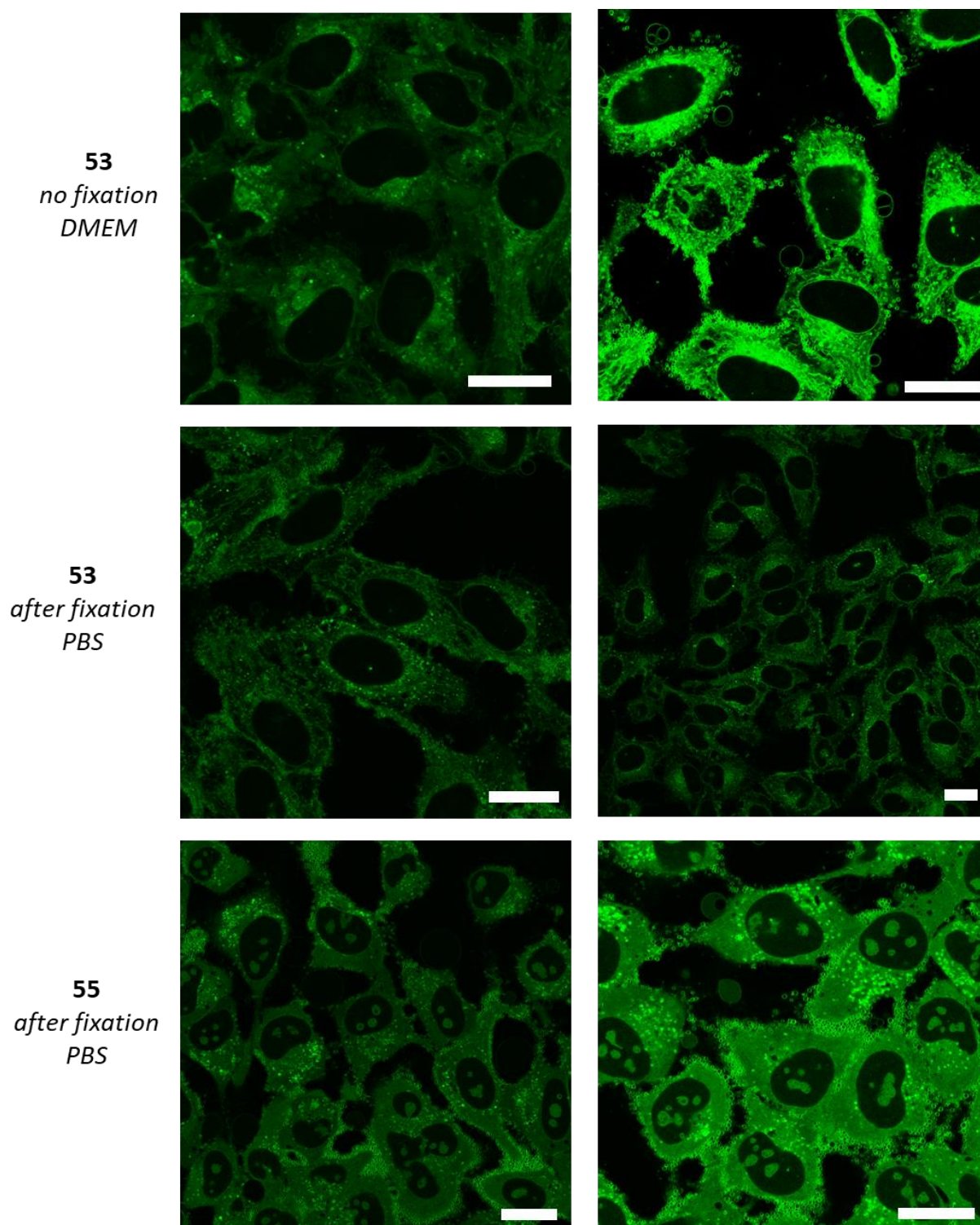


**Figure 328:** Imaging of compounds **53** and **55** in HeLa cells *via* confocal microscopy after 15 h treatment with the respective compounds (8.0 µM) (scale bars 20 µm). The results were processed and visualized with LEICA Application Suite X 3.7.4.23463 from LEICA Microsystems CMS GmbH.

## 5.6.11 Crystal Structure Determinations

Crystal structures in this section were measured and solved by Dr. Martin Nieger at the University of Helsinki (Finland).

**Table 17:** Overview of the numbering and sample code of crystal structures solved by Dr. Martin Nieger.

| Entry | Compound Number | Code Assigned by Dr. Martin Nieger | CCDC Number |
|:---:|:---:|:---:|:---:|
| 1 | 39 | SB1376_HY | - |
| 2 | 40 | SB1368_HY | - |
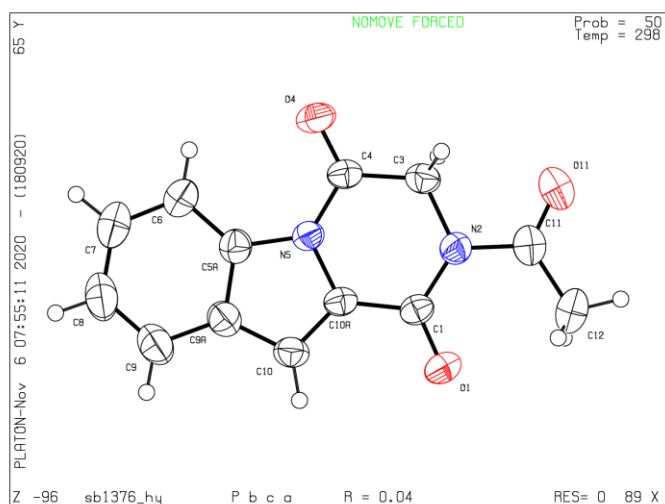
## 2-Acetyl-2,3-dihydropyrazino[1,2-*a*]indole-1,4-dione – SB1376_HY

*Crystal data*

| | |
|---|---|
| $C_{13}H_{10}N_2O_3$ | $D_x = 1.423$ Mg m$^{-3}$ |
| $M_r = 242.23$ | Cu $K\alpha$ radiation, $\lambda = 1.54178$ Å |
| Orthorhombic, *Pbca* (*no.61*) | Cell parameters from 9904 reflections |
| $a = 15.4147$ (2) Å | $\theta = 3.7$–$72.1°$ |
| $b = 6.1889$ (1) Å | $\mu = 0.86$ mm$^{-1}$ |
| $c = 23.7010$ (3) Å | $T = 298$ K |
| $V = 2261.08$ (5)  Å$^3$ | Plates, colourless |
| $Z = 8$ | $0.18 \times 0.12 \times 0.02$ mm |
| $F(000) = 1008$ | |

*Data collection*

| | |
|---|---|
| Bruker D8 VENTURE diffractometer with PhotonII CPAD detector | 1986 reflections with $I > 2\sigma(I)$ |
| Radiation source: INCOATEC microfocus sealed tube | $R_{int} = 0.039$ |
| rotation in $\phi$ and $\omega$, 1°, shutterless scans | $\theta_{max} = 72.1°$, $\theta_{min} = 4.7°$ |
| Absorption correction: multi-scan *SADABS* (Sheldrick, 2014) | $h = -19 \rightarrow 19$ |
| $T_{min} = 0.849$, $T_{max} = 0.971$ | $k = -7 \rightarrow 7$ |
| 36062 measured reflections | $l = -29 \rightarrow 29$ |
| 2223 independent reflections | |

*Refinement*

| | |
|---|---|
| Refinement on $F^2$ | Primary atom site location: dual |
| Least-squares matrix: full | Secondary atom site location: difference Fourier map |
| $R[F^2 > 2\sigma(F^2)] = 0.038$ | Hydrogen site location: inferred from neighbouring sites |
| $wR(F^2) = 0.103$ | H-atom parameters constrained |
| $S = 1.05$ | $w = 1/[\sigma^2(F_o^2) + (0.0459P)^2 + 0.6582P]$ where $P = (F_o^2 + 2F_c^2)/3$ |
| 2223 reflections | $(\Delta/\sigma)_{max} < 0.001$ |
| 164 parameters | $\Delta\rangle_{max} = 0.15$ e Å$^{-3}$ |
| 0 restraints | $\Delta\rangle_{min} = -0.17$ e Å$^{-3}$ |
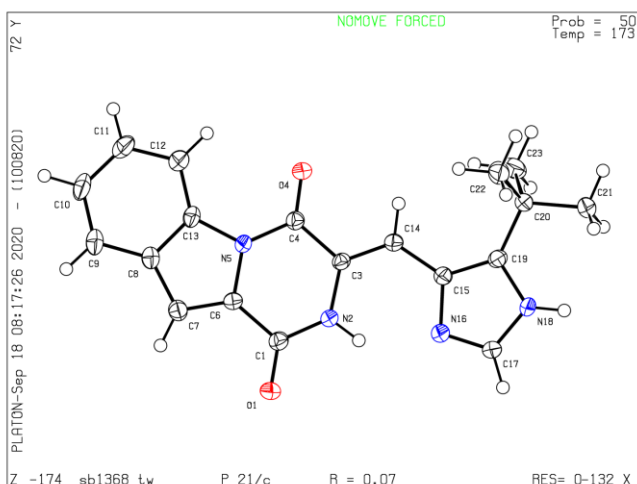
# SB1368_HY

## SUK-153

*non-merohedral twin*



(Z)-3-((5-(*tert*-Butyl)-1*H*-imidazol-4-yl)methylene)-2,3-dihydropyrazino[1,2-a]indole-1,4-dione – SB1368_HY

### Crystal data

| | |
|---|---|
| $C_{19}H_{18}N_4O_2$ | $F(000) = 704$ |
| $M_r = 334.37$ | $D_x = 1.392$ Mg m$^{-3}$ |
| Monoclinic, $P2_1/c$ *(no.14)* | Cu $K\alpha$ radiation, $\lambda = 1.54178$ Å |
| $a = 7.1588$ (3) Å | Cell parameters from 7631 reflections |
| $b = 15.0290$ (6) Å | $\theta = 4.1–72.3°$ |
| $c = 14.9109$ (6) Å | $\mu = 0.76$ mm$^{-1}$ |
| $\beta = 95.951$ (2)° | $T = 173$ K |
| $V = 1595.61$ (11) Å$^3$ | Plates, yellow |
| $Z = 4$ | $0.18 \times 0.04 \times 0.02$ mm |

### Data collection

| | |
|---|---|
| Bruker D8 VENTURE diffractometer with PhotonII CPAD detector | 3119 independent reflections |
| Radiation source: INCOATEC microfocus sealed tube | 2743 reflections with $I > 2\sigma(I)$ |
| rotation in $\phi$ and $\omega$, 1°, shutterless scans | $\theta_{max} = 72.3°$, $\theta_{min} = 4.2°$ |
| Absorption correction: multi-scan *SADABS* (Sheldrick, 2014) | $h = -8\rightarrow8$ |
| $T_{min} = 0.784$, $T_{max} = 0.971$ | $k = -18\rightarrow18$ |
| 3119 measured reflections | $l = -2\rightarrow18$ |

### Refinement

| | |
|---|---|
| Refinement on $F^2$ | Primary atom site location: dual |
| Least-squares matrix: full | Secondary atom site location: difference Fourier map |
| $R[F^2 > 2\sigma(F^2)] = 0.068$ | Hydrogen site location: difference Fourier map |
| $wR(F^2) = 0.163$ | H atoms treated by a mixture of independent and constrained refinement |
| $S = 1.18$ | $w = 1/[\sigma^2(F_o^2) + (0.015P)^2 + 3.480P]$ where $P = (F_o^2 + 2F_c^2)/3$ |
| 3119 reflections | $(\Delta/\sigma)_{max} < 0.001$ |
| 233 parameters | $\Delta\rangle_{max} = 0.28$ e Å$^{-3}$ |
| 2 restraints | $\Delta\rangle_{min} = -0.35$ e Å$^{-3}$ |

# 6   Abbrevation Index

| | |
|---|---|
| % | percent |
| ° | degree (unit of angle measurement) |
| Å | Angström ($10^{-10}$ m) |
| Ac | acetyl |
| ATR | attenuated total reflection (IR) |
| ° | degree (unit of angle measurement) |
| Boc | *tert*-Butyloxycarbonyl |
| °C | degree Celsius (unit of temperature ) |
| CA4 | combretastatin A-4 |
| cm | centimeter |
| conc. | concentrated |
| δ | chemical shift (in ppm) |
| d | doublet (NMR) |
| DCM | dichloromethane |
| dd | doublet of doublets (NMR) |
| ddd | doublet of doublets of doublets (NMR) |
| DFT | density functional theory |
| DMF | *N,N*-dimethylformamide |
| DMSO | dimethylsulfoxid |
| DMSO-$d_6$ | deuterated dimethylsulfoxide |
| E | energy |
| EA | elemental analysis |
| EDC | 1-ethyl-3-(3-dimethylaminopropyl)carbodiimide |
| EI | electron ionization |
| ESI | electrospray ionization |
| *et al.* | *et alia* |
| eV | electronvolt |
| FAB | fast atom bombardment |
| g | grams |
| GDP | guanosine diphosphate |
| GTP | guanosine triphosphate |
| h | hours |
| HITub | hemithioindigo-based indanone-like tubulin inhibitors |
| HOMO | highest occupied molecular orbital |
| HOTub | hemithioindigo-colchicinoid tubulin binders |
| HPI | hemipiperazine |
| HPLC | high pressure liquid chromatography |
| HRMS | high resolution mass spectrometry (NMR) |
| Hz | Hertz |
| I | integral |
| IR | infrared |
| *J* | coupling constant (NMR) |

| | |
|---|---|
| K | kelvin |
| KHYS | Karlsruhe House of Young Scientists |
| KIT | Karlsruhe Institute of Technology |
| L | liter |
| λ | wavelength |
| LED | light-emitting diode |
| LUMO | lowest unoccupied molecular orbital |
| M | Molar concentration |
| m | mass, multiplett (NMR), medium (IR) |
| MAP | microtubule-associated proteins |
| max. | maximal |
| MDA | microtubule destabilizing agent |
| Me | methyl |
| MeCN | acetonitrile |
| mg | milligram |
| MHz | megahertz |
| µm | mikrometer |
| µM | micromolar concentration |
| µs | microsecond |
| min | minutes |
| mL | millilitre |
| mm | millimetre |
| mM | millimolar concentration |
| mmol | millimole |
| MS | mass spectrometry |
| MSA | microtubule stabilizing agent |
| *m/z* | mass to charge ratio |
| *n*BuLi | *n*-butyllithium |
| nm | nanometer |
| NMR | nuclear magnetic resonance |
| NOESY | nuclear overhauser effect spectroscopy |
| OD | Optical Density |
| Ph | phenyl |
| PHT | pyrrole hemithioindigo |
| PHTub | PHT-based photopharmaceuticals |
| ppm | parts per million, $10^{-6}$ |
| PSS | photostationary state |
| PST | photostatin |
| quant. | quantitative |
| R | not defined substituents |
| $R_f$ | retention factor |
| ROS | reactive oxygen species |
| s | singlet (NMR), strong (IR), seconds |
| SBT | styrylbenzothiazole |
| SBTax | SBT-taxane |

| | |
|---|---|
| SBTub | SBT-based tubulin inhibitors |
| ST | styrylthiazole |
| STEpo | epothilone-based microtubule stabilisers |
| T | temperature |
| t | triplet (NMR) |
| *t*Bu | *tert*-butyl |
| td | triplet of doublets (NMR) |
| TD-DFT | time-dependent density functional theory |
| TFA | trifluoroacetic acid |
| THF | tetrahydrofurane |
| TIPS | triisopropylsilyl |
| TLC | thin-layer chromatography |
| Tol | toluene |
| UV | ultraviolet |
| *v* | wavenumber [$cm^{-1}$] |
| V | volt |
| vis | visible |
| vs | very strong (IR) |
| vs. | versus |
| vw | very weak (IR) |
| W | watt |
| w | weak (IR) |

# 7   References

1    Lerch, M. M., Hansen, M. J., van Dam, G. M., Szymanski, W. & Feringa, B. L. Emerging Targets in Photopharmacology. *Angew. Chem. Int. Ed.* **55**, 10978-10999, doi:10.1002/anie.201601931 (2016).

2    Sharma, M. & Friedman, S. H. The Issue of Tissue: Approaches and Challenges to the Light Control of Drug Activity. *ChemPhotoChem* **5**, 594-594, doi:10.1002/cptc.202100134 (2021).

3    Petermayer, C. & Dube, H. Indigoid Photoswitches: Visible Light Responsive Molecular Tools. *Acc. Chem. Res.* **51**, 1153-1163, doi:10.1021/acs.accounts.7b00638 (2018).

4    Szymanski, W., Beierle, J. M., Kistemaker, H. A., Velema, W. A. & Feringa, B. L. Reversible photocontrol of biological systems by the incorporation of molecular photoswitches. *Chem. Rev.* **113**, 6114-6178, doi:10.1021/cr300179f (2013).

5    Hull, K., Morstein, J. & Trauner, D. In Vivo Photopharmacology. *Chem Rev* **118**, 10710-10747, doi:10.1021/acs.chemrev.8b00037 (2018).

6    Sailer, A. *et al.* Hemithioindigos for Cellular Photopharmacology: Desymmetrised Molecular Switch Scaffolds Enabling Design Control over the Isomer-Dependency of Potent Antimitotic Bioactivity. *Chembiochem* **20**, 1305-1314, doi:10.1002/cbic.201800752 (2019).

7    Borowiak, M. *et al.* Photoswitchable Inhibitors of Microtubule Dynamics Optically Control Mitosis and Cell Death. *Cell* **162**, 403-411, doi:10.1016/j.cell.2015.06.049 (2015).

8    Redmond, R. W. & Kochevar, I. E. Spatially resolved cellular responses to singlet oxygen. *Photochem. Photobiol.* **82**, 1178-1186, doi:10.1562/2006-04-14-Ir-874 (2006).

9    Klan, P. *et al.* Photoremovable Protecting Groups in Chemistry and Biology: Reaction Mechanisms and Efficacy. *Chem. Rev.* **113**, 119-191, doi:10.1021/cr300177k (2013).

10   Velema, W. A., Szymanski, W. & Feringa, B. L. Photopharmacology: Beyond Proof of Principle. *J. Am. Chem. Soc.* **136**, 2178-2191, doi:10.1021/ja413063e (2014).

11   Stein, M. *et al.* Azo-Propofols: Photochromic Potentiators of GABAA Receptors. *Angew. Chem. Int. Ed.* **51**, 10500-10504, doi:10.1002/anie.201205475 (2012).

12   Mourot, A. *et al.* Rapid optical control of nociception with an ion-channel photoswitch. *Nat. Methods* **9**, 396-U114, doi:10.1038/Nmeth.1897 (2012).

13   Stein, M., Breit, A., Fehrentz, T., Gudermann, T. & Trauner, D. Optical Control of TRPV1 Channels. *Angew. Chem. Int. Ed.* **52**, 9845-9848, doi:10.1002/anie.201302530 (2013).

14   Frank, J. A. *et al.* Photoswitchable fatty acids enable optical control of TRPV1. *Nat. Commun.* **6**, doi:10.1038/ncomms8118 (2015).

15   Velema, W. A. *et al.* Optical control of antibacterial activity. *Nat. Chem.* **5**, 924-928, doi:10.1038/nchem.1750 (2013).

16   Velema, W. A. *et al.* Ciprofloxacin-Photoswitch Conjugates: A Facile Strategy for Photopharmacology. *Bioconjug. Chem.* **26**, 2592-2597, doi:10.1021/acs.bioconjchem.5b00591 (2015).

17   Johnston, N. R. *et al.* Beta Cell Hubs Dictate Pancreatic Islet Responses to Glucose. *Cell Metab.* **24**, 389-401, doi:10.1016/j.cmet.2016.06.020 (2016).

18   Broichhagen, J. *et al.* Optical control of insulin release using a photoswitchable sulfonylurea. *Nat. Commun.* **5**, doi:10.1038/ncomms6116 (2014).

19   Broichhagen, J. *et al.* Optical Control of Insulin Secretion Using an Incretin Switch. *Angew. Chem. Int. Ed.* **54**, 15565-15569, doi:10.1002/anie.201506384 (2015).

20   Broichhagen, J. *et al.* A red-shifted photochromic sulfonylurea for the remote control of pancreatic beta cell function. *Chem. Commun.* **51**, 6018-6021, doi:10.1039/c5cc01224d (2015).

21   Mehta, Z. B. *et al.* Remote control of glucose homeostasis in vivo using photopharmacology. *Sci. Rep.* **7**, doi:10.1038/s41598-017-00397-0 (2017).

22    Engdahl, A. J. *et al.* Synthesis, Characterization, and Bioactivity of the Photoisomerizable Tubulin Polymerization Inhibitor azo-Combretastatin A4. *Org. Lett.* **17**, 4546-4549, doi:10.1021/acs.orglett.5b02262 (2015).

23    Sheldon, J. E., Dcona, M. M., Lyons, C. E., Hackett, J. C. & Hartman, M. C. T. Photoswitchable anticancer activity via trans–cis isomerization of a combretastatin A-4 analog. *Org. Biomol. Chem.* **14**, 40-49, doi:10.1039/C5OB02005K (2016).

24    Rastogi, S. K. *et al.* Photoresponsive azo-combretastatin A-4 analogues. *Eur. J. Med. Chem.* **143**, 1-7, doi:10.1016/j.ejmech.2017.11.012 (2018).

25    Sailer, A. *et al.* Potent hemithioindigo-based antimitotics photocontrol the microtubule cytoskeleton in cellulo. *Beilstein J. Org. Chem.* **16**, 125-134, doi:10.3762/bjoc.16.14 (2020).

26    Müller-Deku, A. *et al.* Photoswitchable paclitaxel-based microtubule stabilisers allow optical control over the microtubule cytoskeleton. *Nat. Commun.* **11**, 4640, doi:10.1038/s41467-020-18389-6 (2020).

27    Gao, L. *et al.* A Robust, GFP-Orthogonal Photoswitchable Inhibitor Scaffold Extends Optical Control over the Microtubule Cytoskeleton. *Cell Chem. Biol.* **28**, 228-241.e226, doi:10.1016/j.chembiol.2020.11.007 (2021).

28    Sailer, A. *et al.* Pyrrole Hemithioindigo Antimitotics with Near-Quantitative Bidirectional Photoswitching that Photocontrol Cellular Microtubule Dynamics with Single-Cell Precision. *Angew. Chem. Int. Ed.* **60**, 23695-23704, doi:10.1002/anie.202104794 (2021).

29    Gao, L. *et al.* In Vivo Photocontrol of Microtubule Dynamics and Integrity, Migration and Mitosis, by the Potent GFP-Imaging-Compatible Photoswitchable Reagents SBTubA4P and SBTub2M. *J. Am. Chem. Soc.* **144**, 5614-5628, doi:10.1021/jacs.2c01020 (2022).

30    Gao, L. *et al.* Photoswitchable Epothilone-Based Microtubule Stabilisers Allow GFP-Imaging-Compatible, Optical Control over the Microtubule Cytoskeleton. *Angew. Chem. Int. Ed.* **61**, e202114614, doi:10.1002/anie.202114614 (2022).

31    Hull, K., Morstein, J. & Trauner, D. In Vivo Photopharmacology. *Chem. Rev.*, doi:10.1021/acs.chemrev.8b00037 (2018).

32    Fuchter, M. J. On the Promise of Photopharmacology Using Photoswitches: A Medicinal Chemist's Perspective. *J. Med. Chem.* **63**, 11436-11447, doi:10.1021/acs.jmedchem.0c00629 (2020).

33    Pianowski, Z. L. Recent Implementations of Molecular Photoswitches into Smart Materials and Biological Systems. *Chem. Eur. J.* **25**, 5128-5144, doi:10.1002/chem.201805814 (2019).

34    Cembran, A., Bernardi, F., Garavelli, M., Gagliardi, L. & Orlandi, G. On the mechanism of the cis-trans isomerization in the lowest electronic states of azobenzene: S0, S1, and T1. *J. Am. Chem. Soc.* **126**, 3234-3243, doi:10.1021/ja038327y (2004).

35    Heinz, B. *et al.* Comparing a photoinduced pericyclic ring opening and closure: differences in the excited state pathways. *J. Am. Chem. Soc.* **129**, 8577-8584, doi:10.1021/ja071396i (2007).

36    Aiken, S., Edgar, R. J. L., Gabbutt, C. D., Heron, B. M. & Hobson, P. A. Negatively photochromic organic compounds: Exploring the dark side. *Dyes Pigm.* **149**, 92-121, doi:10.1016/j.dyepig.2017.09.057 (2018).

37    Broichhagen, J., Frank, J. A. & Trauner, D. A Roadmap to Success in Photopharmacology. *Acc. Chem. Res.* **48**, 1947-1960, doi:10.1021/acs.accounts.5b00129 (2015).

38    Toth, B. Actual new cancer-causing hydrazines, hydrazides, and hydrazones. *J. Cancer Res. Clin. Oncol.* **97**, 97-108, doi:10.1007/BF00409895 (1980).

39    Mostafavi, S. H. *et al.* Photoinduced Deadhesion of a Polymer Film Using a Photochromic Donor–Acceptor Stenhouse Adduct. *Macromolecules* **52**, 6311-6317, doi:10.1021/acs.macromol.9b00882 (2019).

40    Kamarajan, P. & Chao, C. C. UV-induced apoptosis in resistant HeLa cells. *Biosci. Rep.* **20**, 99-108, doi:10.1023/a:1005515400285 (2000).

41    Knie, C. *et al.* ortho-Fluoroazobenzenes: Visible Light Switches with Very Long-Lived Z Isomers. *Chem. Eur. J.* **20**, 16492-16501, doi:10.1002/chem.201404649 (2014).

42    Bleger, D., Schwarz, J., Brouwer, A. M. & Hecht, S. o-Fluoroazobenzenes as Readily Synthesized Photoswitches Offering Nearly Quantitative Two-Way Isomerization with Visible Light. *J. Am. Chem. Soc.* **134**, 20597-20600, doi:10.1021/ja310323y (2012).

43    Samanta, S. *et al.* Photoswitching Azo Compounds in Vivo with Red Light. *J. Am. Chem. Soc.* **135**, 9777-9784, doi:10.1021/ja402220t (2013).

44    Leistner, A. L. *et al.* Fluorinated Azobenzenes Switchable with Red Light. *Chem. Eur. J.* **27**, 8094-8099, doi:10.1002/chem.202005486 (2021).

45    Leistner, A.-L. & Pianowski, Z. L. Smart Photochromic Materials Triggered with Visible Light. *Eur. J. Org. Chem.* **n/a**, e202101271, doi:10.1002/ejoc.202101271.

46    Hrozhyk, U. A. *et al.* Systematic Study of Absorption Spectra of Donor–Acceptor Azobenzene Mesogenic Structures. *Mol. Cryst. Liq.* **489**, 257/[583]-272/[598], doi:10.1080/15421400802218959 (2011).

47    García-Amorós, J. & Velasco, D. Recent advances towards azobenzene-based light-driven real-time information-transmitting materials. *Beilstein J. Org. Chem.* **8**, 1003-1017 (2012).

48    Beharry, A. A., Sadovski, O. & Woolley, G. A. Azobenzene photoswitching without ultraviolet light. *J. Am. Chem. Soc.* **133**, 19684-19687, doi:10.1021/ja209239m (2011).

49    Konrad, D. B. *et al.* Computational Design and Synthesis of a Deeply Red-Shifted and Bistable Azobenzene. *J. Am. Chem. Soc.* **142**, 6538-6547, doi:10.1021/jacs.9b10430 (2020).

50    Dong, M. *et al.* Near-infrared photoswitching of azobenzenes under physiological conditions. *J. Am. Chem. Soc.* **139**, 13483-13486, doi:10.1021/jacs.7b06471 (2017).

51    Kennedy, A. D., Sandler, I., Andréasson, J., Ho, J. & Beves, J. E. Visible-Light Photoswitching by Azobenzazoles. *Chem. Eur. J.* **26**, 1103-1110, doi:10.1002/chem.201904309 (2020).

52    Siewertsen, R. *et al.* Highly efficient reversible Z− E photoisomerization of a bridged azobenzene with visible light through resolved S1 (nπ*) absorption bands. *J. Am. Chem. Soc.* **131**, 15594-15595, doi:10.1021/ja906547d (2009).

53    Lentes, P. *et al.* Nitrogen bridged diazocines: Photochromes switching within the near-infrared region with high quantum yields in organic solvents and in water. *J. Am. Chem. Soc.* **141**, 13592-13600, doi:10.1021/jacs.9b06104 (2019).

54    Paul, R., Blackburn, R. S. & Bechtold, T. in *Ullmann's Encyclopedia of Industrial Chemistry*   1-16.

55    Ikegami, M. & Arai, T. Photoisomerization and Fluorescence Properties of Hemiindigo Compounds Having Intramolecular Hydrogen Bonding. *Bull. Chem. Soc. Jpn.* **76**, 1783-1792, doi:10.1246/bcsj.76.1783 (2003).

56    Huang, C. Y. *et al.* N,N'-Disubstituted Indigos as Readily Available Red-Light Photoswitches with Tunable Thermal Half-Lives. *J. Am. Chem. Soc.* **139**, 15205-15211, doi:10.1021/jacs.7b08726 (2017).

57    Tatsuo, A. & Masashi, I. Novel Photochromic Dye Based on Hydrogen Bonding. *Chem.* **28**, 965-966, doi:10.1246/cl.1999.965 (1999).

58    Cordes, T., Schadendorf, T., Priewisch, B., Rück-Braun, K. & Zinth, W. The Hammett Relationship and Reactions in the Excited Electronic State: Hemithioindigo Z/E-Photoisomerization. *J. Phys. Chem. A* **112**, 581-588, doi:10.1021/jp077472l (2008).

59    Nenov, A., Cordes, T., Herzog, T. T., Zinth, W. & de Vivie-Riedle, R. Molecular Driving Forces for Z/E Isomerization Mediated by Heteroatoms: The Example Hemithioindigo. *J. Phys. Chem. A* **114**, 13016-13030, doi:10.1021/jp107899g (2010).

60    Zweig, J. E. & Newhouse, T. R. Isomer-Specific Hydrogen Bonding as a Design Principle for Bidirectionally Quantitative and Redshifted Hemithioindigo Photoswitches. *J. Am. Chem. Soc.* **139**, 10956-10959, doi:10.1021/jacs.7b04448 (2017).

61    Kink, F., Collado, M. P., Wiedbrauk, S., Mayer, P. & Dube, H. Bistable Photoswitching of Hemithioindigo with Green and Red Light: Entry Point to Advanced Molecular Digital Information Processing. *Chem. Eur. J.* **23**, 6237-6243, doi:10.1002/chem.201700826 (2017).

62    Li, Z., He, C., Lu, Z., Li, P. & Zhu, Y.-P. Recent progress in all-visible-light-triggered diarylethenes. *Dyes Pigm.* **182**, doi:10.1016/j.dyepig.2020.108623 (2020).

63    Tsivgoulis, G. M. & Lehn, J.-M. Multiplexing optical systems: Multicolor-bifluorescent-biredox photochromic mixtures. *Adv. Mater.* **9**, 627-630, doi:10.1002/adma.19970090806 (1997).

64    Tosic, O., Altenhöner, K. & Mattay, J. Photochromic dithienylethenes with extended π-systems. *Photochem. Photobiol. Sci.* **9**, 128-130, doi:10.1039/B9PP00100J (2010).

65    Fukaminato, T. *et al.* Molecular Design Strategy toward Diarylethenes That Photoswitch with Visible Light. *J. Am. Chem. Soc.* **136**, 17145-17154, doi:10.1021/ja5090749 (2014).

66    Wu, N. M.-W., Ng, M., Lam, W. H., Wong, H.-L. & Yam, V. W.-W. Photochromic Heterocycle-Fused Thieno[3,2-b]phosphole Oxides as Visible Light Switches without Sacrificing Photoswitching Efficiency. *J. Am. Chem. Soc.* **139**, 15142-15150, doi:10.1021/jacs.7b08333 (2017).

67    Kortekaas, L. & Browne, W. R. The evolution of spiropyran: fundamentals and progress of an extraordinarily versatile photochrome. *Chem. Soc. Rev.* **48**, 3406-3424, doi:10.1039/C9CS00203K (2019).

68    Klaue, K. *et al.* Donor-Acceptor Dihydropyrenes Switchable with Near-Infrared Light. *J. Am. Chem. Soc.* **142**, 11857-11864, doi:10.1021/jacs.0c04219 (2020).

69    Maruyama, K., Terada, K. & Yamamoto, Y. Highly Efficient Valence Isomerization between Norbornadiene and Quadricyclane Derivatives under Sunlight. *Chem.* **10**, 839-842, doi:10.1246/cl.1981.839 (1981).

70    Gray, V., Lennartson, A., Ratanalert, P., Borjesson, K. & Moth-Poulsen, K. Diaryl-substituted norbornadienes with red-shifted absorption for molecular solar thermal energy storage. *Chem. Commun.* **50**, 5330-5332, doi:10.1039/c3cc47517d (2014).

71    Mansø, M., Tebikachew, B. E., Moth-Poulsen, K. & Nielsen, M. B. Heteroaryl-linked norbornadiene dimers with redshifted absorptions. *Org. Biomol. Chem.* **16**, 5585-5590, doi:10.1039/C8OB01470A (2018).

72    Hemmer, J. R. *et al.* Tunable Visible and Near Infrared Photoswitches. *J. Am. Chem. Soc.* **138**, 13960-13966, doi:10.1021/jacs.6b07434 (2016).

73    Mallo, N. *et al.* Photochromic switching behaviour of donor–acceptor Stenhouse adducts in organic solvents. *Chem. Commun.* **52**, 13576-13579, doi:10.1039/C6CC08079K (2016).

74    Hemmer, J. R. *et al.* Controlling Dark Equilibria and Enhancing Donor–Acceptor Stenhouse Adduct Photoswitching Properties through Carbon Acid Design. *J. Am. Chem. Soc.* **140**, 10425-10429, doi:10.1021/jacs.8b06067 (2018).

75    Edwards, I. R. & Aronson, J. K. Adverse drug reactions: definitions, diagnosis, and management. *Lancet* **356**, 1255-1259, doi:0.1016/S0140-6736(00)02799-9 (2000).

76    Dumontet, C. & Jordan, M. A. Microtubule-binding agents: a dynamic field of cancer therapeutics. *Nat. Rev. Drug Discov.* **9**, 790-803, doi:10.1038/nrd3253 (2010).

77    Steinmetz, M. O. & Prota, A. E. Microtubule-Targeting Agents: Strategies To Hijack the Cytoskeleton. *Trends Cell Biol.* **28**, 776-792, doi:10.1016/j.tcb.2018.05.001 (2018).

78    Akhmanova, A. & Steinmetz, M. O. Tracking the ends: a dynamic protein network controls the fate of microtubule tips. *Nat. Rev. Mol. Cell Biol.* **9**, 309-322, doi:10.1038/nrm2369 (2008).

79      Nogales, E. Structural insights into microtubule function. *Annu. Rev. Biochem.* **69**, 277-302, doi:10.1146/annurev.biochem.69.1.277 (2000).

80      Luduena, R. F. A Hypothesis on the Origin and Evolution of Tubulin. *Int. Rev. Cell Mol. Biol.* **302**, 41-185, doi:10.1016/B978-0-12-407699-0.00002-9 (2013).

81      Fees, C. P. & Moore, J. K. Regulation of microtubule dynamic instability by the carboxy-terminal tail of beta-tubulin. *Life Sci. Alliance* **1**, e201800054, doi:10.26508/lsa.201800054 (2018).

82      Mitchison, T. & Kirschner, M. Dynamic Instability of Microtubule Growth. *Nature* **312**, 237-242, doi:10.1038/312237a0 (1984).

83      Downing, K. H. Structural basis for the interaction of tubulin with proteins and drugs that affect microtubule dynamics. *Annu. Rev. Cell Dev. Biol.* **16**, 89-111, doi:10.1146/annurev.cellbio.16.1.89 (2000).

84      van Haren, J. & Wittmann, T. Microtubule Plus End Dynamics - Do We Know How Microtubules Grow?: Cells boost microtubule growth by promoting distinct structural transitions at growing microtubule ends. *Bioessays* **41**, e1800194, doi:10.1002/bies.201800194 (2019).

85      Brouhard, G. J. & Rice, L. M. The contribution of alpha beta-tubulin curvature to microtubule dynamics. *J. Cell Biol.* **207**, 323-334, doi:10.1083/jcb.201407095 (2014).

86      Borys, F., Tobiasz, P., Poterala, M. & Krawczyk, H. Development of novel derivatives of stilbene and macrocyclic compounds as potent of anti-microtubule factors. *Biomed. Pharmacother.* **133**, 110973, doi:10.1016/j.biopha.2020.110973 (2021).

87      Peterson, J. R. & Mitchison, T. J. Small molecules, big impact: A history of chemical inhibitors and the cytoskeleton. *Chem. Biol.* **9**, 1275-1285, doi:10.1016/S1074-5521(02)00284-3 (2002).

88      Pettit, G. R. *et al.* Antineoplastic Agents. 291. Isolation and Synthesis of Combretastatins A-4, A-5, and A-6. *J. Med. Chem.* **38**, 1666–1672, doi:10.1021/jm00010a011 (1995).

89      Gaspari, R., Prota, A. E., Bargsten, K., Cavalli, A. & Steinmetz, M. O. Structural Basis of cis- and trans-Combretastatin Binding to Tubulin. *Chem* **2**, 102-113, doi:10.1016/j.chempr.2016.12.005 (2017).

90      Pianowski, Z. L. Recent Implementations of Molecular Photoswitches into Smart Materials and Biological Systems. *Chemistry* **25**, 5128-5144, doi:10.1002/chem.201805814 (2019).

91      Rastogi, S. K. *et al.* Photopharmacology of Azo-Combretastatin-A4: Utilizing Tubulin Polymerization Inhibitors and Green Chemistry as the Key Steps. *Curr. Org. Chem.* **25**, 2457-2474, doi:10.2174/1385272825666210526151222 (2021).

92      Imperatore, C. *et al.* Photo-control of cancer cell growth by benzodiazo N-substituted pyrrole derivatives. *J. Photochem. Photobiol. A* **377**, 109-118, doi:10.1016/j.jphotochem.2019.03.042 (2019).

93      Gao, L. *et al.* A Robust, GFP-Orthogonal Photoswitchable Inhibitor Scaffold Extends Optical Control over the Microtubule Cytoskeleton. *Cell Chem. Biol.* **28**, 228-241 e226, doi:10.1016/j.chembiol.2020.11.007 (2021).

94      Nicholson, B. *et al.* NPI-2358 is a tubulin-depolymerizing agent: in-vitro evidence for activity as a tumor vascular-disrupting agent. *Anticancer Drugs* **17**, 25-31, doi:10.1097/01.cad.0000182745.01612.8a (2006).

95      Kanoh, K., Kohno, S., Katada, J., Takahashi, J. & Uno, I. (-)-Phenylahistin arrests cells in mitosis by inhibiting tubulin polymerization. *J. Antibiot.* **52**, 134-141, doi:10.7164/antibiotics.52.134 (1999).

96      Mita, M. M. *et al.* Phase 1 First-in-Human Trial of the Vascular Disrupting Agent Plinabulin (NPI-2358) in Patients with Solid Tumors or Lymphomas. *Clin. Cancer. Res.* **16**, 5892-5899, doi:10.1158/1078-0432.Ccr-10-1096 (2010).

97      Tian, Z. *et al.* Biological activity and interaction mechanism of the diketopiperazine derivatives as tubulin polymerization inhibitors. *RSC Adv.* **8**, 1055-1064, doi:10.1039/C7RA12173C (2018).

98      Kanoh, K. *et al.* (−)-Phenylahistin: A new mammalian cell cycle inhibitor produced by aspergillus ustus. *Bioorganic Med. Chem. Lett.* **7**, 2847-2852, doi:10.1016/s0960-894x(97)10104-4 (1997).

99      Kanoh, K. *et al.* Antitumor Activity of Phenylahistin in Vitro and in Vivo. *Biosci. Biotechnol. Biochem.* **63**, 1130-1133, doi:10.1271/bbb.63.1130 (1999).

100     Yamazaki, Y. *et al.* Synthesis and Structure-Activity Relationship Study of Antimicrotubule Agents Phenylahistin Derivatives with a Didehydropiperazine-2,5-dione Structure. *J. Med. Chem.* **55**, 1056-1071, doi:10.1021/jm2009088 (2012).

101     Kanoh, K. *et al.* Synthesis and biological activities of phenylahistin derivatives. *Bioorg. Med. Chem.* **7**, 1451-1457, doi:10.1016/S0968-0896(99)00059-0 (1999).

102     La Sala, G. *et al.* Structure, Thermodynamics, and Kinetics of Plinabulin Binding to Two Tubulin Isotypes. *Chem* **5**, 2969-2986, doi:10.1016/j.chempr.2019.08.022 (2019).

103     Karcher, J. *et al.* Selective release of a potent anticancer agent from a supramolecular hydrogel using green light. *RSC Adv.* **11**, 8546-8551, doi:10.1039/d0ra08893e (2021).

104     Vallejos, S. *et al.* A selective and highly sensitive fluorescent probe of Hg2+ in organic and aqueous media: The role of a polymer network in extending the sensing phenomena to water environments. *Sens. Actuators B Chem.* **157**, 686-690, doi:10.1016/j.snb.2011.05.041 (2011).

105     Suzuki, M., Iwasaki, T., Miyoshi, M., Okumura, K. & Matsumoto, K. New convenient syntheses of alpha-C-acylamino acids and alpha-amino ketones. *J. Org. Chem.* **38**, 3571-3575, doi:10.1021/jo00960a028 (1973).

106     Ding, Z. *et al.* Development of MBRI-001, a deuterium-substituted plinabulin derivative as a potent anti-cancer agent. *Bioorg. Med. Chem. Lett.* **27**, 1416-1419, doi:10.1016/j.bmcl.2017.01.096 (2017).

107     Gallina, C. & Liberatori, A. Condensation of 1,4-Diacetylpiperazine-2,5-Dione with Aldehydes. *Tetrahedron* **30**, 667-673, doi:10.1016/S0040-4020(01)97062-0 (1974).

108     Shin, C.-g., Hayakawa, M., Mikami, K. & Yoshimura, J. Synthesis and configurational assignments of albonoursin and its three geometric isomers. *Tetrahedron Lett.* **18**, 863-866, doi:10.1016/S0040-4039(01)92776-5 (1977).

109     Kelley, E. W., Norman, S. G. & Scheerer, J. R. Synthesis of monoalkylidene diketopiperazines and application to the synthesis of barettin. *Org. Biomol. Chem.* **15**, 8634-8640, doi:10.1039/c7ob02297b (2017).

110     Borthwick, A. D. 2,5-Diketopiperazines: Synthesis, Reactions, Medicinal Chemistry, and Bioactive Natural Products. *Chem. Rev.* **112**, 3641-3716, doi:10.1021/cr200398y (2012).

111     Asiri, A. M. New conjugated systems derived from piperazine-2,5-dione. *Molecules* **5**, 629-636, doi:10.3390/50300629 (2000).

112     Gonzalez, J. F., de la Cuesta, E. & Avendano, C. Improvements in aldol reactions with diketopiperazines. *Synthetic Commun.* **34**, 1589-1597, doi:10.1081/Scc-120030746 (2004).

113     Ho, J., Easton, C. J. & Coote, M. L. The Distal Effect of Electron-Withdrawing Groups and Hydrogen Bonding on the Stability of Peptide Enolates. *J. Am. Chem. Soc.* **132**, 5515-5521, doi:10.1021/ja100996z (2010).

114     Balducci, D., Conway, P. A., Sapuppo, G., Müller-Bunz, H. & Paradisi, F. Novel approach to the synthesis of aliphatic and aromatic α-keto acids. *Tetrahedron* **68**, 7374-7379, doi:10.1016/j.tet.2012.06.078 (2012).

115     Petermayer, C. & Dube, H. Indigoid Photoswitches: Visible Light Responsive Molecular Tools. *Acc. Chem. Res.* **51**, 1153-1163, doi:10.1021/acs.accounts.7b00638 (2018).

116 Martínez-López, D. *et al.* Hydantoin-Based Molecular Photoswitches. *J. Org. Chem.* **80**, 3929-3939, doi:10.1021/acs.joc.5b00244 (2015).

117 Cameron, D. & Eisler, S. Photoswitchable double bonds: Synthetic strategies for tunability and versatility. *J. Phys. Org. Chem.* **31**, e3858, doi:10.1002/poc.3858 (2018).

118 Blake, K. W. & Sammes, P. G. Geometrical Isomerism and Tautomerism of 3-Arylidene-6-Methyl-Piperazine-2,5-Diones. *J. Chem. Soc. C*, 980-&, doi:10.1039/j39700000980 (1970).

119 Devys, M., Barbier, M., Kollmann, A. & Bousquet, J. F. Septorine and N-Methoxy Septorine, Substituted Pyrazines from the Fungus Septoria-Nodorum Berk. *Tetrahedron Lett.* **23**, 5409-5412, doi:10.1016/0040-4039(82)80143-3 (1982).

120 Kim, M. C. *et al.* Photopiperazines A–D, Photosensitive Interconverting Diketopiperazines with Significant and Selective Activity against U87 Glioblastoma Cells, from a Rare, Marine-Derived Actinomycete of the Family Streptomycetaceae. *J. Nat. Prod.* **82**, 2262-2267, doi:10.1021/acs.jnatprod.9b00429 (2019).

121 Slavov, C. *et al.* Connectivity matters - ultrafast isomerization dynamics of bisazobenzene photoswitches. *Phys Chem Chem Phys* **18**, 14795-14804, doi:10.1039/c6cp00603e (2016).

122 Muckerman, J. T., Skone, J. H., Ning, M. & Wasada-Tsutsui, Y. Toward the accurate calculation of pKa values in water and acetonitrile. *Biochim. Biophys. Acta Bioenerg.* **1827**, 882-891, doi:10.1016/j.bbabio.2013.03.011 (2013).

123 Tshepelevitsh, S. *et al.* On the Basicity of Organic Bases in Different Media. *Eur. J. Org. Chem.* **2019**, 6735-6748, doi:10.1002/ejoc.201900956 (2019).

124 Fukumura, H. *et al.* Effect of ascorbic acid on reactive oxygen species production in chemotherapy and hyperthermia in prostate cancer cells. *J. Physiol. Sci.* **62**, 251-257, doi:10.1007/s12576-012-0204-0 (2012).

125 Kang, P. & Foote, C. S. Photosensitized Oxidation of 13C,15N-Labeled Imidazole Derivatives. *J. Am. Chem. Soc.* **124**, 9629-9638, doi:10.1021/ja012253d (2002).

126 Harry, H., Wolff, W. M. S., Stiller, K., Saito, I. & Pickett, J. E. in *R.B. Woodward Remembered* (eds H. H. Wasserman *et al.*) 191-200 (Pergamon, 1982).

127 Köttner, L., Schildhauer, M., Wiedbrauk, S., Mayer, P. & Dube, H. Oxidized Hemithioindigo Photoswitches—Influence of Oxidation State on (Photo)physical and Photochemical Properties. *Chem. Eur. J.* **26**, 10712-10718, doi:10.1002/chem.202002176 (2020).

128 Hitzenberger, J. F. *et al.* Stability of Odd- Versus Even-Electron Gas-Phase (Quasi)Molecular Ions Derived from Pyridine-Substituted N-Heterotriangulenes. *ChemPlusChem* **82**, 204-211, doi:10.1002/cplu.201600416 (2017).

129 Shellum, C. L. & Birks, J. W. Photochemical Amplifier for Liquid-Chromatography Based on Singlet Oxygen Sensitization. *Anal. Chem.* **59**, 1834-1841, doi:10.1021/ac00141a021 (1987).

130 You, Y. Chemical tools for the generation and detection of singlet oxygen. *Org. Biomol. Chem.* **16**, 4044-4060, doi:10.1039/C8OB00504D (2018).

131 Joshi, D. R. & Adhikari, N. An Overview on Common Organic Solvents and Their Toxicity. *J. Pharm. Res. Int.* **28**, 1-18, doi:10.9734/jpri/2019/v28i330203 (2019).

132 Megerle, U., Lechner, R., Konig, B. & Riedle, E. Laboratory apparatus for the accurate, facile and rapid determination of visible light photoreaction quantum yields. *Photochem. Photobiol. Sci.* **9**, 1400-1406, doi:10.1039/c0pp00195c (2010).

133 Maerz, B. *et al.* Making Fast Photoswitches Faster—Using Hammett Analysis to Understand the Limit of Donor–Acceptor Approaches for Faster Hemithioindigo Photoswitches. *Chem. Eur. J.* **20**, 13984-13992, doi:10.1002/chem.201403661 (2014).

134 Rõõm, E.-I. *et al.* Brønsted Basicities of Diamines in the Gas Phase, Acetonitrile, and Tetrahydrofuran. *Chem. Eur. J.* **13**, 7631-7643, doi:10.1002/chem.200700097 (2007).

135    Petermayer, C., Thumser, S., Kink, F., Mayer, P. & Dube, H. Hemiindigo: Highly Bistable Photoswitching at the Biooptical Window. *J. Am. Chem. Soc.* **139**, 15060-15067, doi:10.1021/jacs.7b07531 (2017).

136    Pigulla, J. & Roder, E. Azepinoindoles .3. Cyclization of N-(2-Indolylcarbonyl)-Beta-Amino Acids to Azepino[3,4-B]Indolediones. *Liebigs Ann. Chem.*, 1390-1398, doi:10.1002/jlac.197819780905 (1978).

137    Hammett, L. P. The Effect of Structure upon the Reactions of Organic Compounds. Benzene Derivatives. *J. Am. Chem. Soc.* **59**, 96-103, doi:10.1021/ja01280a022 (1937).

138    Hansch, C., Leo, A. & Taft, R. W. A survey of Hammett substituent constants and resonance and field parameters. *Chem. Rev.* **91**, 165-195, doi:10.1021/cr00002a004 (1991).

139    Karcher, J. & Pianowski, Z. L. Photocontrol of Drug Release from Supramolecular Hydrogels with Green Light. *Chem. Eur. J.* **24**, 11605-11610, doi:10.1002/chem.201802205 (2018).

140    Pianowski, Z. L., Karcher, J. & Schneider, K. Photoresponsive self-healing supramolecular hydrogels for light-induced release of DNA and doxorubicin. *Chem. Commun.* **52**, 3143-3146, doi:10.1039/c5cc09633b (2016).

141    Karcher, J. *et al.* Selective release of a potent anticancer agent from a supramolecular hydrogel using green light. *RSC Adv.* **11**, 8546-8551, doi:10.1039/D0RA08893E (2021).

142    Gottlieb, H. E., Kotlyar, V. & Nudelman, A. NMR chemical shifts of common laboratory solvents as trace impurities. *J. Org. Chem.* **62**, 7512-7515, doi:DOI 10.1021/jo971176v (1997).

143    Sheldrick, G. M. SHELXT - integrated space-group and crystal-structure determination. *Acta Crystallogr. A Found. Adv.* **71**, 3-8, doi:10.1107/S2053273314026370 (2015).

144    Sheldrick, G. M. Crystal structure refinement with SHELXL. *Acta Crystallogr. C Struct. Chem.* **71**, 3-8, doi:10.1107/S2053229614024218 (2015).

145    Gaussian 16 Rev. C.01 (Wallingford, CT, 2016).

146    Pollard, M. M. & Vederas, J. C. A convenient preparation of thioether functionalized porphyrins. *Tetrahedron* **62**, 11908-11915, doi:10.1016/j.tet.2006.09.091 (2006).

147    Basaric, N., Mitchell, D. & Wan, P. Substituent effects in the intramolecular photoredox reactions of benzophenones in aqueous solution. *Can. J. Chem.* **85**, 561-571, doi:10.1139/V07-081 (2007).

148    Beecher, J. E. & Tirrell, D. A. Synthesis of protected derivatives of 3-pyrrolylalanine. *Tetrahedron Lett.* **39**, 3927-3930, doi:10.1016/S0040-4039(98)00722-9 (1998).

149    Parsons, S., Flack, H. D. & Wagner, T. Use of intensity quotients and differences in absolute structure refinement. *Acta Crystallogr. B Struct. Sci. Cryst. Eng. Mater.* **69**, 249-259, doi:10.1107/S2052519213010014 (2013).

150    Reiss, B., Hu, Q., Riedle, E. & Wagenknecht, H. A. The Dependence of Chemical Quantum Yields of Visible Light Photoredox Catalysis on the Irradiation Power. *ChemPhotoChem* **5**, 1009-1019, doi:10.1002/cptc.202100090 (2021).

# 8 Appendix

## 8.1 Curriculum Vitae

**Susanne Kirchner**

22.06.1991, Tübingen, Germany

+4917661307610, kirchnersusanne@web.de

**Education**

| | |
|---|---|
| 10/2018 – 07/2022 | **Doctoral work**, Karlsruhe Institute of Technology (KIT), Karlsruhe Institute of Organic Chemistry, Priv.-Doz. Dr. Zbigniew Pianowski *„Hemipiperazines - Novel Photochromic Cyclic Dipeptides for Bioactivity Photomodulation"* |
| 09/2014 – 08/2018 | **M.Sc. – Chemistry** (Ø 1.3), Heidelberg University, Heidelberg Master Thesis, Karlsruhe Institute of Technology, Karlsruhe. *„Photochromic 2,5-Diketopiperazines and Peptides for Photomodulation of Biological Systems with Visible Light"* |
| 09/2011 – 08/2014 | **B.Sc. – Chemistry** (Ø 2.3), Heidelberg University, Heidelberg Bachelor Thesis, Biochemistry Center Heidelberg (BZH), Heidelberg. *„Lipidanalytik Sphingosin-1-Phosphat-Lyase defizienter Zellen"* |
| 09/2001 – 06/2010 | **General higher education entrance qualification** (Ø 1.6), Carlo-Schmid-Gymnasium, Tübingen Specialized courses: Chemistry & Social studies |

**Further experience & qualifications**

| | |
|---|---|
| 11/2019 – 07/2022 | **Qualification program**, Research Training Group GRK 2039 |
| 10/2019 – 11/2021 | **Board member**, Faculty of Chemistry and Biosciences, KIT, Karlsruhe |
| 10/2018 – 07/2022 | **Supervision & teaching** at KIT, Bachelor & Master students, interns, seminars & practical courses |

## 8.2 Publications

- M. J. Gerl, V. Bittl, S. Kirchner, T. Sachsenheimer, H. L. Brunner, C. Lüchtenborg, C. Özbalci, H. Wiedemann, S. Wegehingel, W. Nickel, P. Haberkant, C. Schultz, M. Krüger, B. Brügger, *PLoS ONE* **2016**, *11*(4): e0153009. *Sphingosine-1-Phosphate Lyase Deficient Cells as a Tool to Study Protein Lipid Interactions*.

- Z. L. Pianowski, A.-L. Leistner, S. Kirchner, S. Weber, A. Seliwjorstow, J. Karcher, German Patent Office **2019**, Germany. Patent: DE 10 2019 005 005 A1. *Diketopiperazine mit lichtaktivierter Zytotoxizität*.

- J. Karcher, S. Kirchner, A.-L. Leistner, C. Hald, P. Geng, T. Bantle, P. Gödtel, J. Pfeifer, Z. L. Pianowski, *RSC Adv.* **2021**, *11*(15), 8546-8551. *Selective Release of a potent Anticancer Agent from a Supramolecular Hydrogel using Green Light*.

- A.-L. Leistner, S. Kirchner, J. Karcher, T. Bantle, M. L. Schulte, P. Gödtel, C. Fengler and Z. L. Pianowski, *Chem. Eur. J.* **2021**, *27*(31), 8094-8099. *Fluorinated Azobenzenes Switchable with Red Light*.

- S. Kirchner, A.-L. Leistner, Z. L. Pianowski, *Molecular Photoswitches: Chemistry, Properties, and Applications*, Ed.: Z. L. Pianowski, Wiley-VHC, **2022**. *Photoswitchable Peptides and Proteins*.

- S. Kirchner, Z. Pianowski, *Int. J. Mol. Sci.* **2022**, *23*(10), 5657. *Photopharmacology of Antimitotic Agents*.

- S. Kirchner, A.-L. Leistner, P. Gödtel, A. Seliwjorstow, S. Weber, J. Karcher, M. Nieger, Z. Pianowski, *submitted. Hemipiperazines – novel molecular Photoswitches with low-nanomolar Cytotoxicity*.

## 8.3 Conference Contributions

- S. Kirchner, J. Karcher. Z. L. Pianowski, *Chemical Biology*, EMBL Heidelberg, Germany, 29th August – 01st September **2018**. *Novel halogenated azobenzene derivatives for photocontrol of peptide-based systems.* (Poster)

- S. Kirchner, J. Karcher. Z. L. Pianowski, *ESOC*, Vienna, Austria, 14th – 18th July **2019**. *Photochromic Peptides for light-triggered Drug Delivery and beyond.* (Poster)

- S. Kirchner, J. Karcher. Z. L. Pianowski, *POPs Satellite Meeting*, Karlsruhe, Germany, 13th September **2019**. *Photochromic Peptides for light-triggered Drug Delivery and beyond.* (Poster)

- S. Kirchner, *I, Scientist*, virtual conference, 16th – 19th September **2020**. (Attendance)

- S. Kirchner, A.-L. Leistner, J. Karcher. Z. L. Pianowski, *RICT*, virtual conference, 7th – 9th July **2021**. *Photochromic Peptides for light-triggered Drug Delivery.* (Poster)

- S. Kirchner, J. Karcher. Z. L. Pianowski, *Photopharmacology III*, virtual conference, 29th – 30th November **2021**. *Photochromic Peptides for light-triggered Drug Delivery.* (Poster)

## 8.4   Additional Contributions & Training

- S. Kirchner, *GRK 2039 Qualification Program*, Karlsruhe, Germany, 4<sup>th</sup> – 6<sup>th</sup> February **2020**. *Annual Retreat.* (Presentation & Poster)

- S. Kirchner, *KHYS Further Education Program for Doctoral Researchers*, Karlsruhe, Germany, 11<sup>th</sup> February **2020**. *Workshop: Good Scientific Practice.* (Attendance)

- S. Kirchner, *Knigge-Reich*, Speyer, Germany, 27<sup>th</sup> – 28<sup>th</sup> May **2020**. *Workshop: Business-Knigge-Seminar.* (Attendance)

- S. Kirchner, *GRK 2039 Qualification Program*, Karlsruhe, Germany, 8<sup>th</sup> October **2020**. *Seminar Day: Zebrafish – from Introduction as a Model System to latest Research Results.* (Attendance)

- S. Kirchner, *GRK 2039 Qualification Program*, Karlsruhe, Germany, 15<sup>th</sup> February **2021**. *Merck Virtual Site Experience.* (Attendance)

- S. Kirchner, *In-visible Berlin*, virtual workshop, Germany, 07<sup>th</sup> – 08<sup>th</sup> April **2021**. *Workshop: Unconscious Bias Training.* (Attendance)

- S. Kirchner, *Sheboss,* virtual workshop, Germany, 11<sup>th</sup> June **2021**. *Workshop: The Game of Power.* (Attendance)

- S. Kirchner, *GRK 2039 Qualification Program*, Karlsruhe, Germany, 3<sup>rd</sup> – 5<sup>th</sup> November **2021**. *Annual Retreat.* (Presentation & Poster)

- S. Kirchner, *KHYS Further Education Program for Doctoral Researchers*, Karlsruhe, Germany, 12<sup>th</sup> April **2022**. *Ethics in the Lab.* (Attendance)

- S. Kirchner, *GRK 2039 Qualification Program*, Karlsruhe, Germany, 30<sup>th</sup> May **2022**. *Seminar Day: Time resolved Spectroscopy.* (Attendance)

## 8.5 Acknowledgements